STRESS CORROSION—
NEW APPROACHES

H. L. CRAIG, Jr., *editor*

STP 610

AMERICAN SOCIETY FOR TESTING AND MATERIALS

STRESS CORROSION— NEW APPROACHES

A symposium
presented at the
Seventy-eighth Annual Meeting
AMERICAN SOCIETY FOR
TESTING AND MATERIALS
Montreal, Canada, 22–27 June 1975

ASTM SPECIAL TECHNICAL PUBLICATION 610
H. L. Craig, Jr., editor
University of Miami

List price $43.00
04-610000-27

AMERICAN SOCIETY FOR TESTING AND MATERIALS
1916 Race Street, Philadelpia, Pa. 19103

Library of Congress Catalog Card Number: 76-12835

Printed in Lutherville-Timonium, Md.
November 1976

Foreword

The symposium on New Approaches to Stress Corrosion was presented at the Seventy-eighth Annual Meeting of the American Society for Testing and Materials held in Montreal, Canada, 22–27 June 1975. Committee G-1 on Corrosion of Metals sponsored the symposium. H. L. Craig, Jr., University of Miami, presided as symposium chairman and editor of this publication.

Related
ASTM Publications

Corrosion in Natural Environments, STP 558 (1974), $29.75, 04-558000-27

Manual of Industrial Corrosion Standards and Control, STP 534 (1974), $16.75, 04-534000-27

Stress Corrosion Cracking of Metals—A State of the Art, STP 518 (1972), $11.75, 04-518000-27

A Note of Appreciation to Reviewers

This publication is made possible by the authors and, also, the unheralded efforts of the reviewers. This body of technical experts whose dedication, sacrifice of time and effort, and collective wisdom in reviewing the papers must be acknowledged. The quality level of ASTM publications is a direct function of their respected opinions. On behalf of ASTM we acknowledge with appreciation their contribution.

ASTM Committee on Publications

Editorial Staff

Contents

Introduction

Introduction

The problems of technology have become front page news, editorial subjects, ballot box issues, and decision points behind hard budget items. No longer do engineering choices remain solely in the domain of the drafting board and conference room. Scientists, engineers, and technical managers are faced with the political and economic overtones of their day-to-day activities.

A highway bridge collapses and many people are killed, drawing attention to the dangerous conditions of all aging structures. A high pressure gas pipeline explodes, killing townspeople and causing serious property damage. A tank truck splits open, spilling hazardous chemicals that snuff out the lives of nearby workers. Cracks appear in main structural elements of first line defense fighter planes. Hydrofoil struts and deck plates of ships deteriorate by cracking. Tanks and guns are found to contain materials susceptible to premature failure. Space rocket launchings are delayed by stress corrosion cracks in critical components. Nuclear power plants are shut down, with tube failures and other sensitive parts in jeopardy due to environmental attack. The list could be extended easily, to touch the life of nearly every American citizen.

Nearly half the articles published in journals devoted to corrosion science and engineering deal with the problems of stress corrosion. In this light, ASTM Subcommittee G.01.06, concerned with Stress Corrosion and Corrosion Fatigue, sponsored an international symposium where the broadest available talent could be assembled to focus on new developments in the evaluation of materials for their stress corrosion behavior. This volume is the permanent record of the information presented at the 1975 conference, in Montreal, Canada. It is the direct successor to *ASTM STP 425, Stress Corrosion Testing* (now out of print), which reported the latest technical approaches that were announced to its audience at the Atlantic City, New Jersey meeting in 1966. Doubtless, there will be continuing volumes in this sequence, as research development and testing continues unabated in this area.

The Symposium Committee chose the papers to reflect in the authors, the diversity of the audience to which this message is directed. Consumers, producers, fabricators, academic interests, government, and industrial and nonprofit laboratories are each represented. Some papers reflect the workings of the Society, to produce consensus standards, based on data, tests, and interpretations laboriously debated and refined. Others report material performance-guides to designers and managers. New test methods are introduced, such as the constant strain rate technique. This promises to be the newcomer to the field, as was the use of precracked specimens and the case of linear elastic fracture mechanics concepts in 1966. This latter methodology has reached full bloom, being represented in over half the papers.

Increasing sophistication in laboratory techniques include delicate hydrogen analyses along crack fronts, the determination of activation energies, and the application of advanced electrochemical kinetic theories to the problem of crack growth. Some of these findings must be confirmed by later investigators—but then, that is exactly the way science advances. The committee has attempted to provide a forum where new ideas meet old challenges, where new procedures withstand the examination of skilled workers and all may benefit from these exchanges. None of this would have been possible without the many dedicated reviewers who have given of their time and talent, to hone these offerings to the finest technical edge. The committee, on behalf of the society and the readers of this volume, gratefully acknowledge their debt to them. The Editor would also like to thank the members of the symposium committee and the session chairman who labored hard and long hours to make this event a worthy one. Members of the committee and chairmen were: Mel. F. Bleum, Sheldon Dean, Michael Henthorne, W. Barry Lisagor, David S. Neill, and Donald O. Sprowls. The authors are to be commended on their efforts. No publication of this nature would be possible without constant attention and expert guidance of Jane B. Wheeler and her staff at ASTM Headquarters. The Editor would also like to acknowledge his support by the National Aeronautics and Space Administration, which has made possible his continued interest and participation in stress corrosion testing.

H. Lee Craig, Jr.
School of Marine and Atmospheric Science, University of Miami, Miami, Fla. 33149; symposium chairman and editor of this publication.

D. O. Sprowls,[1] *T. J. Summerson,*[2] *G. M. Ugiansky,*[3]
S. G. Epstein,[4] *and H. L. Craig, Jr.*[5]

Evaluation of a Proposed Standard Method of Testing for Susceptibility to Stress-Corrosion Cracking of High-Strength 7XXX Series Aluminum Alloy Products

REFERENCE: Sprowls, D. O., Summerson, T. J., Ugiansky, G. M., Epstein, S. G., and Craig, H. L., Jr., **"Evaluation of a Proposed Standard Method of Testing for Susceptibility to Stress-Corrosion Cracking of High-Strength 7XXX Series Aluminum Alloy Products,"** *Stress Corrosion—New Approaches, ASTM STP 610,* American Society for Testing and Materials, 1976, pp. 3–31.

ABSTRACT: A task group sponsored jointly by The Aluminum Association and the ASTM has recommended a standard method of test for susceptibility to stress-corrosion cracking (SCC) of 7XXX aluminum alloy products (ASTM G 47-76). The proposed standard is a comprehensive method that specifies the corrosive environment and period of exposure, type of test specimen and method of loading, procedures for sampling various manufactured product forms, and guidelines for interpretation of test results. Final selection of test procedures was based on round robin tests performed in nine different laboratories and 3-year exposures to the atmosphere in both seacoast and inland industrial locations. A summary of test results is given to illustrate how the relative performance of three different tempers of 7075 alloy plate can be influenced by the choice of a test specimen, differences in the outdoor atmosphere, and interlaboratory variations in performing the standard 3.5 percent sodium chloride alternate immersion test.

KEY WORDS: stress corrosion, cracking (fracturing), tests, accelerated tests, outdoor atmospheres, aluminum alloys, interlaboratory program, sodium chloride, synthetic seawater

---

[1] Section head, Stress Corrosion Section, Alcoa Laboratories, Aluminum Company of America, Alcoa Center, Pa. 15069.

[2] Head, Corrosion Section, Kaiser Aluminum and Chemical Corp., Center for Technology, Pleasanton, Calif. 94566.

[3] Metallurgist, National Bureau of Standards, Washington, D. C. 20234.

[4] Staff metallurgist, Aluminum Association, New York, N. Y. 10017.

[5] Professor, School of Marine and Atmospheric Science, University of Miami, Fla. 33149.

In April 1971, The Aluminum Association held an ad hoc meeting of aluminum producers to discuss problems in stress-corrosion testing high-strength aluminum alloys. Subsequently on 3 June 1971, the situation was reviewed in a conference at the Air Force Materials Laboratory with representatives of the Air Force, the Naval Air Systems Command, and the Frankford Arsenal (Army). These meetings directed attention to two specific needs: (1) the need for a standard test method for products of the new high-strength 7XXX series alloys and tempers with intermediate resistance to stress-corrosion cracking (SCC) and (2) the need for an improved rating system for classifying the relative resistance to SCC of alloys and tempers. With the encouragement of the military agencies, a joint Aluminum Association-American Society for Testing and Materials task group (ASTM G-1.06.91) was organized at the annual meeting of the ASTM later in June, and a comprehensive interlaboratory (round robin) testing program was developed.

Specific objectives for the test program involving materials of known resistance to SCC were to: (1) observe the degree of variability of test results obtained with the 3.5 percent sodium chloride (NaCl) alternate immersion test (Federal Method 823) and search for possible refinements, (2) determine the effect of specimen configuration on the test performance of materials with inherently different resistances to SCC, (3) compare the test performance in the preceding alternate immersion test with that in outdoor atmospheric environments, and (4) investigate other less corrosive accelerated test media.

Interlaboratory Test Program

Participating Laboratories

The following laboratories participated in this test program in various ways:

Air Force Materials Laboratory
Alcan International Limited, Canada
Aluminum Company of America
Frankford Arsenal, Department of the Army
Kaiser Aluminum and Chemical Corporation
Marshall Space Flight Center, NASA
Martin-Marietta Aluminum
McDonnell-Douglas Company, Long Beach
National Bureau of Standards
Naval Air Development Center, Department of the Navy
Pechiney Aluminium, France
Reynolds Metals Company
Rockwell International Science Center

Test Materials

Commercially fabricated 2.5-in. (63-mm) thick plate was selected to ensure a uniform grain structure and resistance to SCC among the large number of replicate specimens needed. Plates of 7075 alloy were obtained in three tempers to provide a wide range of resistance to SCC when stressed in the short-transverse direction: high (T7351), low (T651), and intermediate (T7X51). The T7X51 temper was produced by artificially aging T651 temper plate to achieve a combination of mechanical properties and electrical conductivity intermediate between that of the T651 and T7351 tempers. The properties of the test materials are given in Table 1.

Test Specimens

Three specimen configurations commonly used for making short-transverse SCC tests were used; namely, two sizes of tension specimens and a C-ring (Fig. 1). All specimens of a given type were machined in one shop to avoid variations in machined finishes. The specimens were then ran-

TABLE 1—*Properties of 2.5-in. (63-mm) thick 7075 alloy plate for round robin tests.*[a]

				Tensile Properties				
Temper[b]	Electrical Conductivity, % IACS[c]		Test Direction	Tensile Strength, ksi	(MPa)	Yield Strength, ksi	(MPa)	Elongation, % in 4D
T651	surface	32.2	longitudinal	81.6	(563)	72.9	(503)	11.0
	T/10	31.5	long transverse	80.9	(558)	70.1	(483)	8.0
	T/2	32.6	short transverse	72.1	(497)	63.3	(436)	4.0
T7X51	surface	37.5	longitudinal	77.8	(536)	65.7	(453)	12.0
	T/10	37.1	long transverse	73.9	(510)	63.3	(436)	10.0
	T/2	38.7	short transverse	70.4	(485)	60.8	(419)	4.0
T7351	surface	41.0	longitudinal	67.0	(462)	55.1	(380)	10.0
	T/10	40.6	long transverse	66.0	(455)	54.5	(376)	10.0
	T/2	41.0	short transverse	59.1	(407)	51.7	(356)	4.0

	Weight Percent									
	Si	Fe	Cu	Mn	Mg	Cr	Ni	Zn	Ti	Be
T651	0.10	0.31	1.58	0.04	2.36	0.18	0.00	5.63	0.03	0.002
T7X51	0.10	0.24	1.80	0.03	2.44	0.18	0.00	5.87	0.04	0.002
T7351	0.11	0.32	1.66	0.04	2.44	0.18	0.00	5.71	0.03	0.002

[a] Composition (quantometric analysis of remelt specimen of plate).

[b] The T651 and T7351 tempers were fabricated, heat treated, and aged at the Alcoa Davenport Works. The T7X51 temper was laboratory aged from other T651 temper plate [9.5 h at 325°F (163°C)].

[c] IACS = International Annealed Copper Standard.

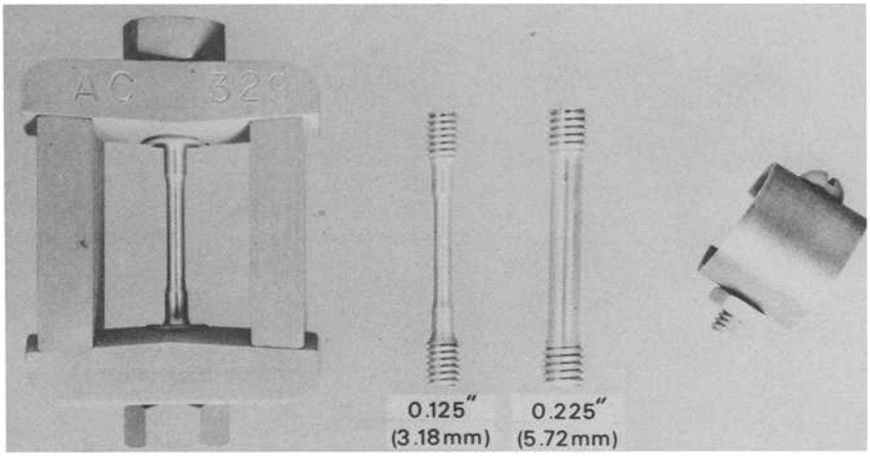

FIG. 1—*Three specimen configurations and the methods of stressing used in this investigation.*

domized and distributed to the participating laboratories for stressing and exposure.

The threaded-end tension specimens were stressed in "constant strain" type frames (Fig. 1) that develop essentially uniaxial tensile stress in the specimen [*1*].[6] The desired stress level was obtained by strain measurement on each specimen during its loading. The C-rings were stressed with the loading bolts to produce deflections calculated in accordance with ASTM Recommended Practices for Making and Using The C-Ring SCC Test Specimen (G 38-73). The stressing frames for the tension specimens and the stressing bolts for the C-rings were coated to prevent any electrochemical interaction between the specimens and the stressing components during exposure.

Three stress levels were selected for specimens in the T651 and T7X51 tempers to increase the range of SCC performance. A single stress of 43 ksi (300 MPa) was used for the T7351 temper as this represents the specified capability in a 30-day alternate immersion test for 7075-T7351 plate (Federal Specification QQ-A-250/12E). For all stress levels and all environments, quintuplicate specimens were exposed. A limited number of control specimens with no applied stress also were exposed in each corrosive environment.

Corrosive Environments

1. *Alternate Immersion in 3.5 percent NaCl Solution*—The 3.5 percent NaCl alternate immersion test described in Method 823 of Federal Stand-

---

[6] The italic numbers in brackets refer to the list of references appended to this paper.

ard 151b is specified for verification of the resistance to SCC of various T7-type tempers in specifications of 7XXX series alloy products. It is also used widely for testing other aluminum alloys.

The alternate immersion cycle is 1 h consisting of 10 min immersion in the solution followed by 50 min drying in air. The following test conditions were specified:

Sodium chloride	Reagent Grade
Water purity	ASTM D 1193-70, Type II (Specification for Reagent Water)
ph of solution	6.4 to 7.2
Temperature of solution	75 ± 2°F (24 ± 1°C)
Volume of solution/total specimens surface, min	30 ml/cm^2
Temperature of surrounding air	80 ± 2°F (27 ± 1°C)
Relative humidity of surrounding air	45 ± 6 percent

Evaporation losses were replenished by daily additions of water of the same purity, and the solution was replaced weekly. There was no requirement as to the size of the test chamber and the solution tank or the method of immersion. A summary of the specific conditions used in the various laboratories is given in Table 2.

Two test runs were made with the second run started 30 to 40 days after the first run. Specimens were inspected daily for evidence of cracking and were removed from test whenever cracking was observed. The exposures were terminated at 90 days.

2. *Other Accelerated Test Media*—A disadvantage of the Method 823 alternate immersion test in 3.5 percent NaCl solution is the severe pitting that occurs in high-strength aluminum alloy specimens. Therefore, three other less corrosive test media were investigated, (1) continuous immersion for 96 h in boiling 6 percent NaCl solution [*2*], (2) continuous immersion for 168 h in 1 percent NaCl + 2 percent potassium dichromate ($K_2Cr_2O_7$) solution at 140°F (60°C) [*3*], and (3) alternate immersion in synthetic ocean water [per ASTM Specification for Substitute Ocean Water D 1141-52 (1971)] in place of 3.5 percent NaCl solution in the Method 823 alternate immersion test. For tests in the NaCl-$K_2Cr_2O_7$ solution, specimens were chemically etched for 30 s in 5 percent sodium hydroxide (NaOH) solution at 75°C, desmutted in cold concentrated nitric acid (HNO_3) for 15 to 30 s, and rinsed in hot tap water. For all other tests, the specimens were simply degreased before exposure.

3. *Atmospheric Exposures*—Specimens were also exposed to the seacoast atmosphere at Cape Canaveral, Florida, and to the inland industrial atmosphere in Philadelphia, Pennsylvania, for reference to service-type environments. Cape Canaveral has a semitropical climate with moderately

TABLE 2—*Comparison of 3.5 percent NaCl alternate immersion (Method 823) test procedures used in round robin program.*

	Alcoa	Martin Marietta	Kaiser	MSFC	NADC	Pechiney	Reynolds	Alcan	Frankford
Room Size, m	(9 x 21 x 5)	(2 x 3.4 x 3.7)	(14 x 10 x 3)	(0.7 x 1 x 1.2)[d]	(1.8 x 1.8 x 1.8)[d]	(9 x 8 x 3)	(5 x 3 x 2)	(3 x 1 x 0.6)[d]	(6.5 x 5 x 2.5)
Tank size, m	0.8 x 1.8	0.7 x 1.3	0.9 x 0.9	0.6 x 0.8		0.3 x 0.6	0.4 x 0.9	0.5 x 0.8	0.9 x 0.9
Method of immersion	lift	lift	pump	pump	lift	lift	lift	pump	pump
V/A ratio, ml/cm^2[a]	450	185	75	23	63	770	890	700	125
3.5% NaCl solution									
pH range	6.4 to 7.2	6.5 to 7.0	. . .	6.4 to 7.2	. . .	6.4 to 7.2	6.4 to 7.2	6.5 to 7.0	6.7 to 7.0
Temperature range, °C	23 to 26	. . .	24 ± 1	23 to 24	. . .	23 to 26	23	23 to 26	22 to 25
Air conditions									
Temperature, °C	27 ± 1[b]	27 ± 1	27 ± 1	27 ± 1	27 ± 1	27 ± 1	27 ± 1	27 ± 1	27 ± 1
Relative humidity, %	45 ± 6	45 ± 6	45 ± 5	45 ± 2	45 ± 5	45 ± 6	45 ± 6	45 ± 6	45 ± 6[c]

Evaporation rate[e]	9 to 13	12 to 15	4 to 15	19 to 23	12 to 27	4 to 9	12 to 19	19 to 31	10 to 12
Time until specimens appear dry, min									
Tension specimens	20 to 30	25	10 to 20	10 to 15	10 to 25	20 to 50	20 to 35	. . .	. . .
C-rings	30 to 45	30	30 to 50	10 to 15	35 to 50	20 to 50	20 to 35	30 to 40	25 to 45
Makeup water									
Type	deionized	. . .	distilled	distilled	. . .	deionized	distilled	distilled	distilled
Total matter, ppm	1.0	1.5 to 2.5	. . .	2.0	. . .	0.5	0.2	. . .	0.2 to 1.5
Electrical conductivity, mho/cm	1.3	3.0 to 4.0	. . .	5.0	. . .	0.7 to 1.0	3.8	2.0 to 4.0	0.15 to 0.29
Passed color test	yes	no	. . .	yes	. . .	no	yes	. . .	no

---

[a] Ratio of volume of solution to total area of specimens at start of test.

[b] Except 3 percent of total test time when the range was 76 to 78°F because of mechanical difficulties.

[c] Except 6 percent of total test time. Of this 6 percent of the relative humidity was on the low (32 to 36 percent min) side for 5.2 percent and on the high (56 percent max) side for 0.8 percent.

[d] Closed cabinet.

[e] Average weight loss of water per square centimeter in 24 h from a 9-cm-diameter Petri dish placed as close as possible to the position of the specimens during exposure.

high temperature and humidity. The highest maximum daily temperatures occur in August (average 87°F) and the lowest minimum daily temperatures occur in January (average 54°F). Humidity is generally high throughout the year with an average relative humidity of 77 percent. Average rainfall is about 45 in. per year with the greatest amount generally in September (average 8 in.). The specimens were exposed on open racks located on the beach just south of the cape, 300 ft (90 m) from the mean tide line, and facing the Atlantic Ocean to the south (Fig. 2). Prevailing breezes are from the ocean.

Philadelphia has a climate somewhat more temperate than that at Cape Canaveral. The highest maximum daily temperatures, which occur in July and August, are about the same as at Cape Canaveral, but the lowest minimum daily temperatures, which occur in January and February, average about 24°F. The relative humidity has an average daily range of 55 to 81 percent during summer months and about 55 to 71 percent during the winter months. Average rainfall is about 42 in. per year with the greatest amounts in June, July, and August (average 4 in.) [*4*]. The exposure racks were located on the roof of a three-story building in an industrial-residential region, one-half mile west of the Delaware River where prevailing breezes are from the west and southwest.

To investigate the possible effect of weather conditions at the time of the initial exposure, duplicate sets of specimens were exposed in both the spring (May) and fall (November) at both test sites.

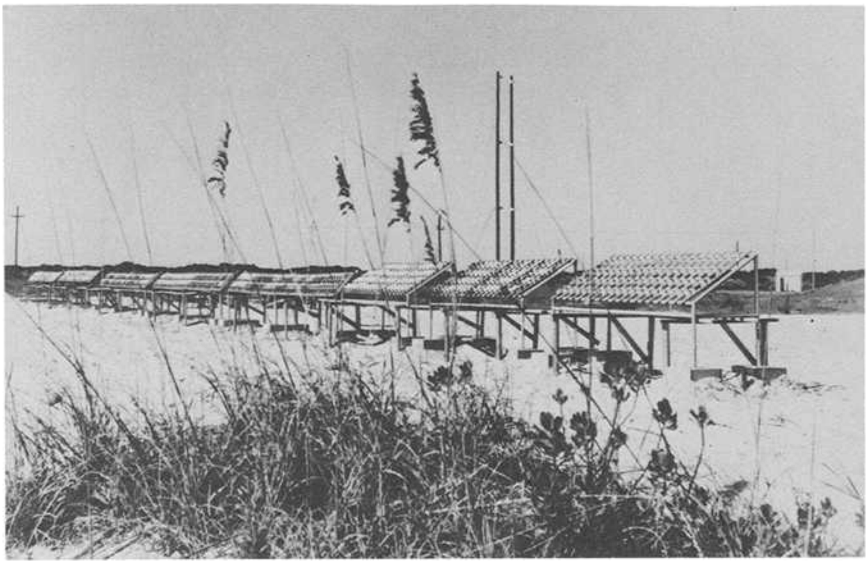

FIG. 2—*Cape Canaveral exposure test site.*

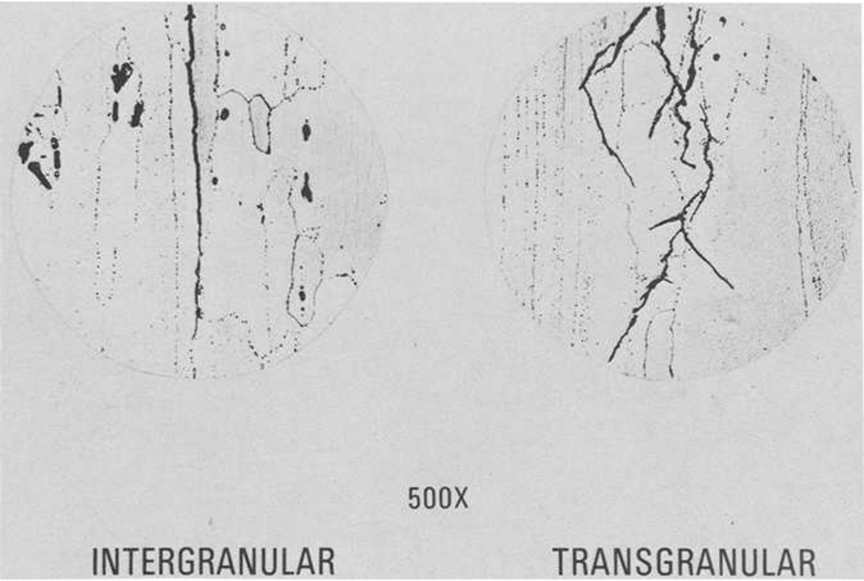

FIG. 3—*Comparison of crack tips of intergranular and transgranular modes.*

Evaluation of Test Results

The occurrence of SCC was determined by visual inspection and the number of days until discovery of cracking was recorded. Detection of cracking in the tension specimens was easy because the growth of only a very small crack (or cracks) causes this type of specimen to fracture. With C-rings, however, a similar small crack (or cracks) may not be detected because of pitting and the accumulation of corrosion product. Therefore, fairly extensive use was made of metallographic examinations to: (1) verify that SCC was the cause of fracture of tension specimens and (2) determine whether SCC was present in C-rings that visually did not appear to be cracked. The following guidelines were applied to secondary cracks and corrosion stringers: (1) cracks that followed an intergranular path or mixed intergranular-transgranular path were considered as SCC; (2) exclusively transgranular cracks that initiated in corrosion pits were not considered as SCC;[7] (3) intergranular fissures that were no deeper than the width of localized areas of intergranular corrosion or, in the case of C-rings, not deeper than those in the compressively stressed surface were not considered as SCC. A comparison of the intergranular and transgranular cracking modes is shown in Fig. 3.

---

[7] Transgranular cracking has been observed only in accelerated tests of highly stressed specimens that become severely pitted; hence, it is regarded generally as a laboratory phenomenon and a nuisance in tests to determine susceptibility to the intergranular SCC involved in service problems with aluminum alloys. Transgranular cracking was not detected in specimens that failed in the atmospheric exposures.

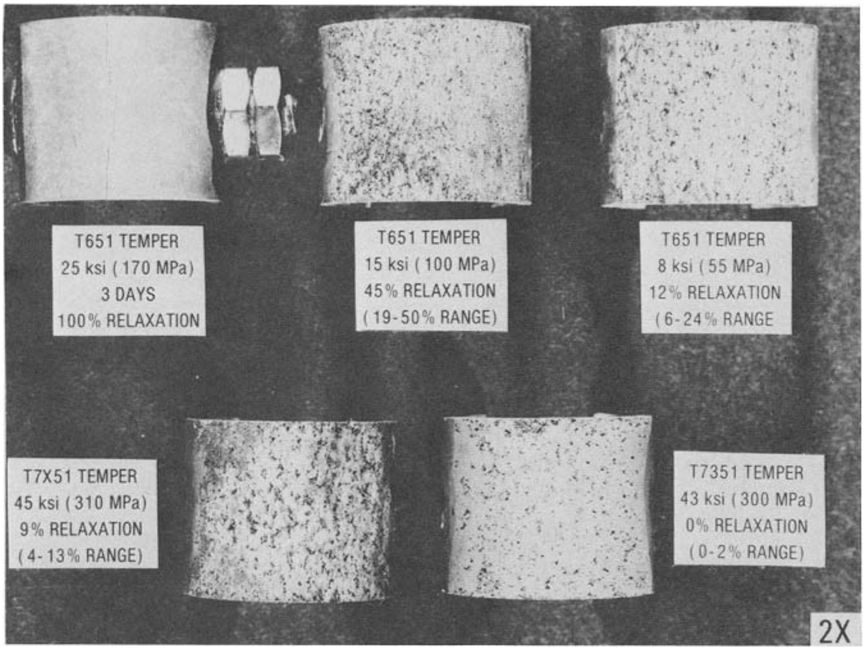

FIG. 4—*C-rings cleaned with concentrated HNO_3 to facilitate inspection after termination of exposures at 90 days. Rings with over 10 percent relaxation were likely to contain minute stress-corrosion cracks.*

Because of the difficulty in determining from visual examination alone whether SCC was present in C-rings, determination of relaxation of the applied load (strain) was used in some laboratories as an additional criterion. The relaxation was calculated from the difference between initial and final unstressed outside diameter divided by the applied deflection. The photograph in Fig. 4 illustrates the appearance of representative C-rings from the Alcoa test and the range of percent relaxations observed. This criterion is not ideal, however, because relaxation of the load also can be caused by severe pitting.

The relative corrosivities of the test environments were determined by tension tests of tension specimens exposed with no applied stress. The percent reduction in load-carrying ability of a corroded specimen was calculated from the difference in its breaking strength (breaking load divided by cross-section area before exposure) and the tensile strength of the plate.

Results and Discussion

Atmospheric Exposures

The outdoor exposures are continuing, but a number of significant observations can be made from the results obtained during the 3-year exposures to date (Table 3). Metallographic examination of representative failed specimens showed that general pitting was mild and the fractures resulted from intergranular SCC (Fig. 5).

1. *Comparison of Test Materials*—The expected differences in the three test materials were evident: (1) no SCC of any of the T7351 temper specimens; (2) limited susceptibility to SCC of the T7X51 temper depending to a striking degree upon the stress level, the specimen configura-

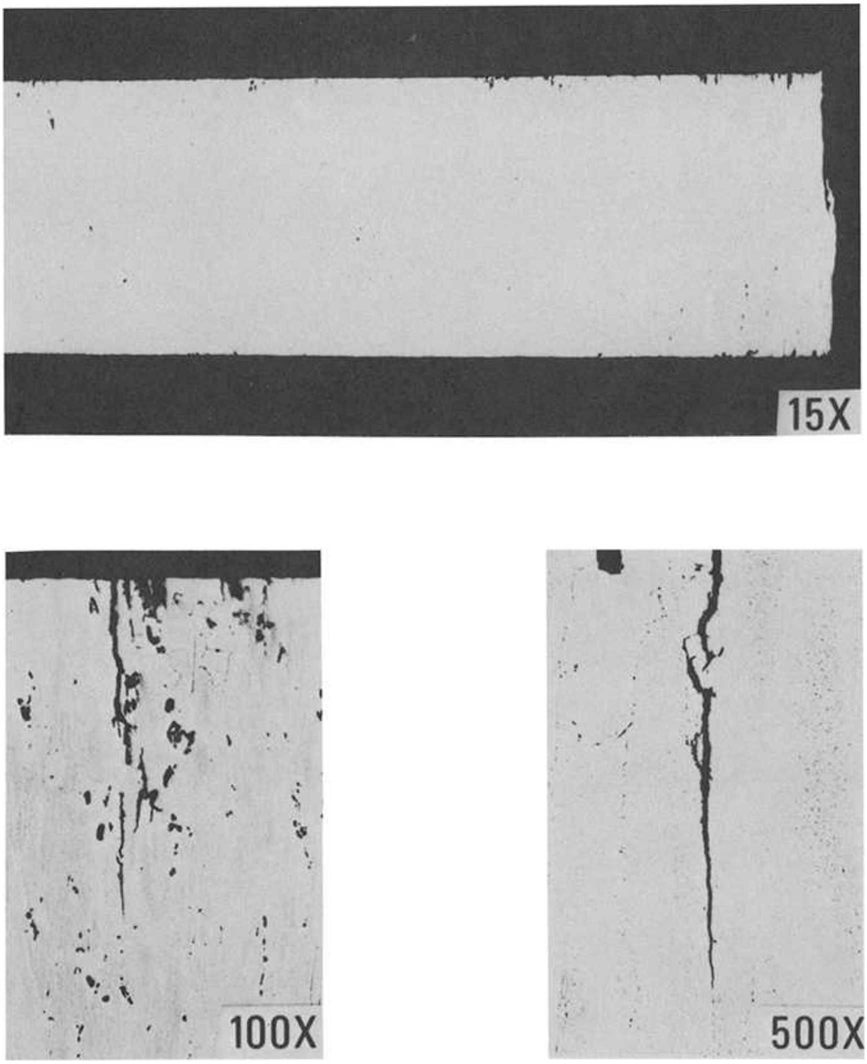

FIG. 5—*Intergranular SCC in an 0.125-in. (3.18-mm) tension specimen of 7075-T7X51 stressed 35 ksi (240 MPa) and exposed 282 days to seacoast atmosphere at Cape Canaveral.*

TABLE 3—*Summary of atmospheric stress-corrosion tests of 7075 alloy plate, short transverse stress.*

			Seacoast Atmosphere (Cape Canaveral)				Industrial Atmosphere (Philadelphia, Pa.)			
			Exposed 3 Nov. 1971		Exposed 3 May 1972		Exposed 12 Nov. 1971		Exposed 2 May 1972	
Plate Temper	Applied Stress, ksi	Specimen Configuration	F/N	Days to Failure	F/N	Days to Failure	F/N	Days to Failure	F/N	Days to Failure
T651	25	0.125 in. tension (3.18 mm)	5/5	5,5,7,7,7	5/5	1,2,2,2,5	5/5	130,163,204,208,229	5/5	37,37,42,50,66
	(170 MPa)	0.225 in. tension (5.72 mm)	5/5	7,9,12,12,14	5/5	5,5,5,5,6	5/5	86,117,168,187,247	5/5	48,48,69,88,121
		C-ring	5/5	16,16,30,30,30	4/5	77,77,77,377	5/5	228,307,382,445,615	5/5	211,211,211,211,444
	15	0.125 in. tension (3.18 mm)	5/5	5,7,9,12,22	5/5	5,5,5,6,27	5/5	155,229,242,499,649	5/5	*71*,466*,487*,487*,408**
	(100 MPa)	0.225 in. tension (5.72 mm)	5/5	7,15,16,18,23	5/5	5,6,6,6,5	5/5	217,297,653,700,853	5/5	*118*,459*,472*,481*,487*
		C-ring	3/5	30,77,153[a]	3/5	71,77,273	0/5		0/5	
	8	0.125 in. tension (3.18 mm)	4/5	18,26,90,93	4/5	6,6,6,27	1/5	149	0/5	
	(55 MPa)	0.225 in. tension (5.72 mm)	5/5	12,30,35,730, <1300	4/5	27,71,605,639	1/5	715	0/5	
		C-ring	1/5	30[a]	1/5	71	0/5		0/5	
T7X51	45	0.125 in. tension (3.18 mm)	5/5	30,37,37,55,70	5/5	5,9,27,76,76	2/5	966,1039	2/5	543,670
	(310 MPa)	0.225 in. tension (5.72 mm)	2/5	91,91	0/5		1/5	631	0/5	
		C-ring	0/5	. . .[a]	0/5		0/5		0/5	
	35	0.125 in. tension (3.18 mm)	4/5	37,545, <730,*855*	2/5	*282*,342	1/5	*566*	0/5	
	(240 MPa)	0.225 in. tension (5.72 mm)	1/5	<730	0/5		0/5		0/5	
		C-ring	0/5	. . .[a]	0/5		0/5		0/5	
	25	0.125 in. tension (3.18 mm)	2/5	30,107	0/5		0/5		0/5	
	(170 MPa)	0.225 in. tension (5.72 mm)	0/5		0/5		0/5		0/5	
		C-ring	0/5	. . .[a]	0/5		0/5		0/5	
T7351	43	0.125 in. tension (3.18 mm)	0/5		0/5		0/5		0/5	
	(300 MPa)	0.225 in. tension (5.72 mm)	0/5		0/5		0/5		0/5	
		C-ring	0/5	. . .[a]	0/5		0/5		0/5	

NOTES—1. Intended inspection schedule: <30 days, daily
30–60 days, twice a week
60–365 days, weekly
>365 days, monthly

2. Status of tests updated June 1975.

3. *Removed at 408 days and reloaded. **Broke during reloading.

4. Italicized specimens were examined metallographically; failures confirmed as SCC.

[a] All surviving C-rings were removed at 153 days for laboratory inspection and reexposed 29 Oct. 1973.

tion and the environment; and (3) marked susceptibility to SCC of the T651 temper, with less dependence upon the specimen configuration and the environment except at low stress levels.

The relative resistance of the three tempers to corrosion in the absence of applied stress is illustrated by the results of tension tests performed on duplicate control specimens exposed at Cape Canaveral from November 1971 to August 1972 (9 months).

Percent Reduction in Load-Carrying Ability

Temper	0.125 in. (3.18 mm)	0.225 in. (5.72 mm)
T651	30	12
T7X51	16	9
T7351	6	1

2. *Effect of Environment*—Judging from the times to failure listed in Table 3, SCC initiated at lower applied stresses and propagated more rapidly at Cape Canaveral than at Philadelphia. Under the semitropical conditions at Cape Canaveral, there was no difference in time to failure for specimens exposed in May and those exposed in November, probably because the temperature and humidity were relatively uniform throughout the year. On the other hand, under the seasonal climatic conditions at Philadelphia, failures of the more susceptible specimens occurred in shorter times when exposed in May than when exposed in November. Weather records [*4*] for Philadelphia showed that, for the first 60 days of the spring exposure, the average daily mean temperature was 66°F with rainfall on 31 days compared to the 38°F average daily mean temperature and 18 days with rainfall during the first 60 days for the exposure started in November. The lesser corrosivity of the industrial atmosphere is shown by the relatively small percent reduction of 9 percent for 0.125-in. (3.18-mm) diameter specimens of 7075-T651 exposed for eight months as compared to 30 percent after nine months at Cape Canaveral.

3. *Effect of Specimen Configuration*—A marked effect of specimen size and configuration was observed for the tempers and stress levels with intermediate resistance to SCC. The 0.125-in. (3.18-mm) diameter tension specimens had the highest percentage of failures and the shortest times to failures, while the C-rings had the lowest percentage and required the longest exposure times. The most striking comparison of percentage failures is shown by the results for the medium resistance T7X51 specimens stressed at 45 ksi (310 MPa).

For the most susceptible material [T651 temper specimens stressed at 25 ksi (170 MPa)], there was no appreciable effect of specimen size or

Percentage of T7X51 Specimens Failed at 45 ksi (310 MPa)

	Tension Specimens		
	0.125 in. (3.18 mm)	0.225 in. (5.72 mm)	C-Rings
Seacoast	100	20	0
Industrial	40	10	0

configuration on the percentage failures, although times to failure for the C-rings tended to be longer. While all three specimen configurations stressed at 25 ksi (170 MPa) showed a clear difference between the T651 and T7X51 tempers, only the tension specimens stressed at 43 to 45 ksi (300 to 310 MPa) provided a distinction between the T7X51 and the T7351 tempers.

3.5 Percent NaCl Alternate Immersion Tests

1. *Mode of Cracking*—The type of corrosive attack in the T651 temper specimens was a combination of intergranular corrosion and directional pitting with deeply penetrating intergranular SCC in the more highly stressed specimens. With the lowest stress [8 ksi (55 MPa)], the C-rings generally did not show visual evidence of cracking, and metallographically it was difficult to distinguish between networks of intergranular corrosion and incipient SCC.

Corrosion of the T7X51 temper specimens was directional pitting with occasional small patches of intergranular attack. Intergranular SCC was the predominant mode of cracking in specimens stressed at 45 ksi (310 MPa) similar to that in the atmosphere (Fig. 5). At the lower stresses, cracking was a mixed mode with transgranular cracking generally predominant (Fig. 6).

In T7351 temper specimens the corrosion was pitting; any cracking emanated from corrosion pits and propagated along a path that was exclusively transgranular (Fig. 7).

2. *Effect of Specimen Configuration*—Just as in the atmospheric exposures, the influence of specimen size and configuration varied with temper of the test material and magnitude of the applied stress. For example, with the T651 temper, the effect was negligible at the highest stress used [25 ksi (170 MPa)], but it was appreciable at the lower stresses. On the other hand, with the more resistant T7X51 temper, the effect was appreciable at all stress levels used (Fig. 8).

The duration of exposure also influenced the relative performance of the various specimen configurations. Within an exposure period of 20 to 30 days, C-rings and 0.225-in. (5.72-mm) tension specimens of the

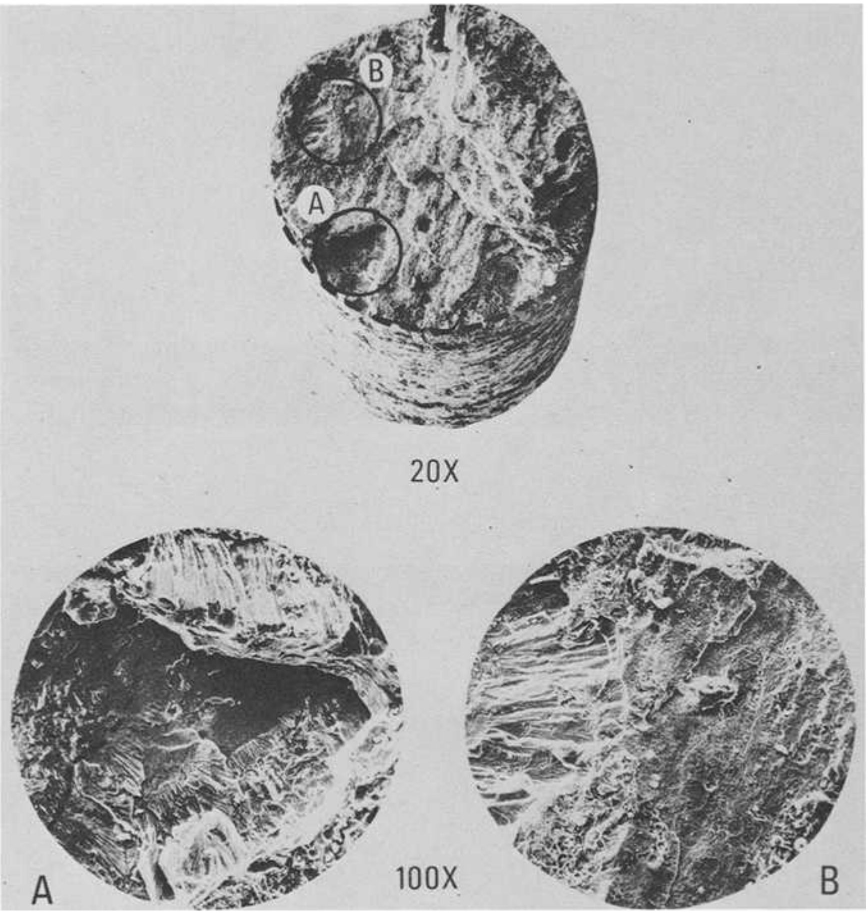

FIG. 6—*Scanning electron microscope fractographs illustrating mixed-mode cracking in an 0.125-in. (3.18-mm) tension specimen of 7075-T7X51 stressed to 35 ksi (240 MPa) and exposed 78 days to the Alcoa 3.5 percent NaCl alternate immersion test. At top is a view of the whole fracture face. Region A shows corrosion extending from the specimen surface to the dashed line and many sites of transgranular cracking indicated by the feather pattern. Region B shows a change from transgranular cracking (at left) to a flat area of intergranular cracking.*

T7X51 temper had a similar and considerably higher percent survival than the 0.125-in. (3.18-mm) tension specimens. This relationship changed with extended exposure as the performance of the 0.225-in. (5.72-mm) tension specimen tended to approach that of the smaller tension specimen (Fig. 9). A similar pattern for the T351 specimens is evident in Fig. 10 although longer exposures were required to initiate the transgranular mode of cracking. To avoid this extraneous mode of cracking in small specimens,

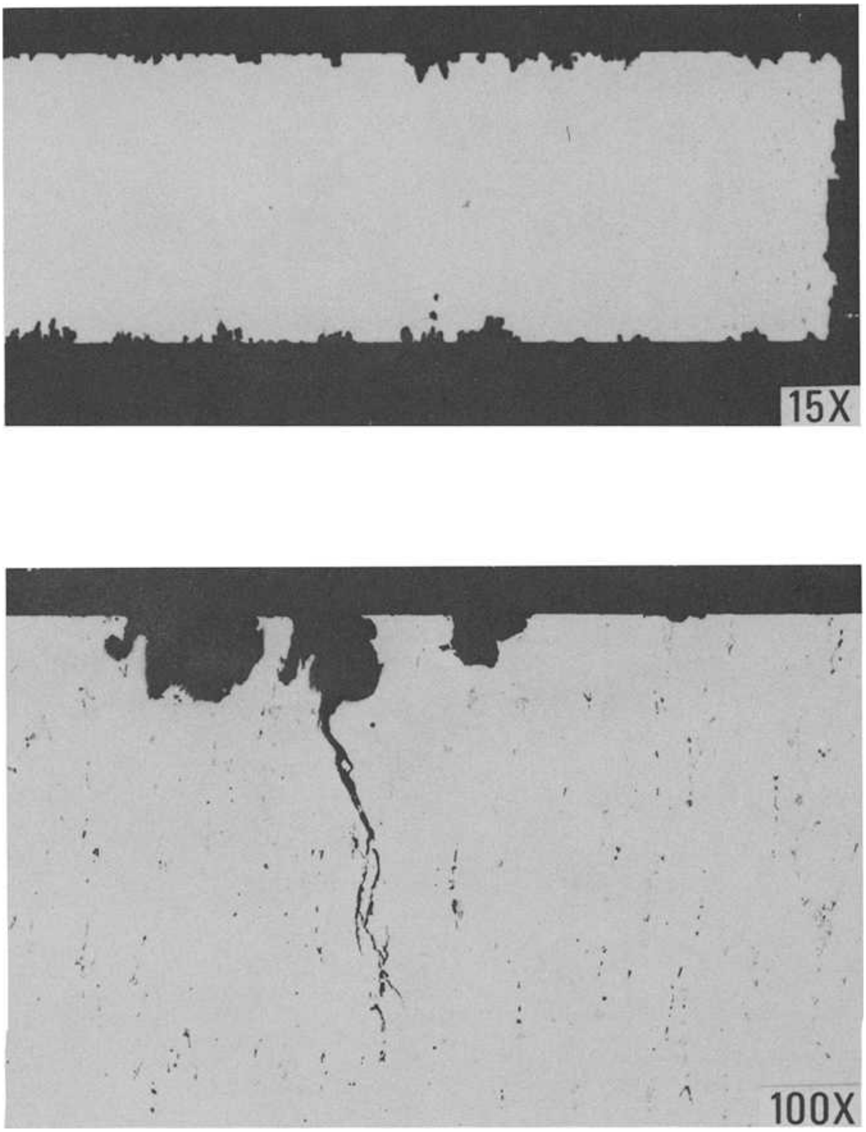

FIG. 7—*Pitting and transgranular cracking in an 0.125-in. (3.18-mm) tension specimen of 7075-T7351 stressed 43 ksi (300 MPa) that fractured after 80 days exposure to 3.5 percent NaCl alternate immersion.*

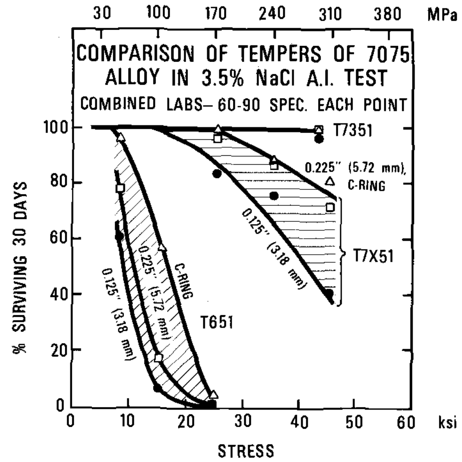

FIG. 8—*Influence of specimen configuration on test performance.*

it is necessary to use either a relatively short exposure period, such as 20 days for the 0.125-in. (3.18-mm) tension specimen, or a larger specimen.

To perform a test that would distinguish between the T7X51 and T7351 tempers and avoid extraneous failures, it appears from a comparison of Figs. 9 and 10 that the chances would be best with a 20-day exposure of 0.125-in. (3.18-mm) diameter tension specimens stressed at a high stress, such as 43 to 45 ksi (300 to 310 MPa). Under these conditions, the percent survival was 100 percent for the T7351 temper com-

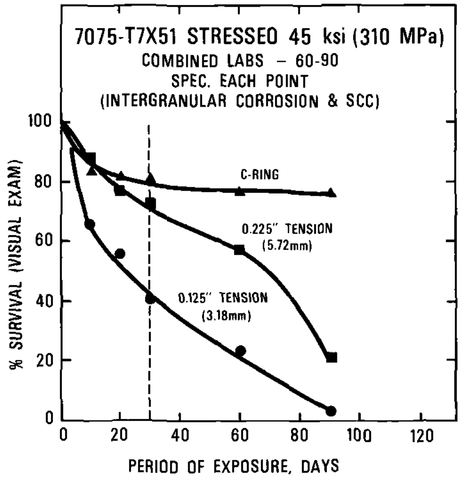

FIG. 9—*Influence of specimen configuration on test performance.*

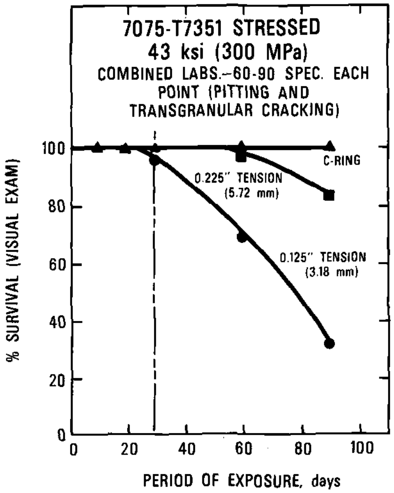

FIG. 10—*Influence of specimen configuration on test performance.*

pared to only 56 percent for the T7X51 temper. Based on the combined tests of 60 to 90 specimens for each type, the 90 percent confidence limits for the probability of three replicate specimens surviving a 20-day test would be as follows:

	0.125 in. (3.18 mm)	0.225 in. (5.72 mm)	C-Rings
T7351	88 to 100%	86 to 100%	90 to 100%
T7X51	9 to 29%	33 to 68%	41 to 69%

The relatively high percentage survivals of C-rings of the T7X51 material gives a reflection of the difficulty in identifying "failures" by visual examination.

To distinguish between the T7X51 and T651 tempers, a 20-day test at a low stress, such as 25 ksi (170 MPa), should be used. In this case, the 90 percent confidence limits for the probability of triplicate specimens surviving the test would be:

	0.125 in. (3.18 mm)	0.225 in. (5.72 mm)	C-Rings
T7X51	52 to 84%	79 to 100%	90 to 100%
T651	0 to 0.01%	0 to 0.01%	0 to 0.1%

3. *Comparison with Three-Year Atmospheric Exposures*—The alternate immersion test results closely paralleled the results of the atmospheric exposures, especially at the seacoast; but specific comparison varied, as shown by the summary of percentage failures in Table 4. Specimens with a *low resistance* to SCC [T651 stressed at 25 ksi (170 MPa)] had very high percentages of failure (93 to 100 percent) in both atmospheres and in the

TABLE 4—*Comparison of percentage failures in 3.5 percent NaCl alternate immersion*[a] *versus atmospheric exposures.*[b]

			Percentage Failures		
			Tension Specimens		
Applied Stress, ksi (MPa)	Plate Temper	Environment	0.125 in. (3.18 mm)	0.225 in. (5.72 mm)	C-Rings
25 (170)	T651	20 days 3.5% NaCl AI[c]	100	100	93
		30 days 3.5% NaCl AI	100	100	96
		seacoast atmosphere	100	100	90
		industrial atmosphere	100	100	100
25 (170)	T7X51	20 days 3.5% NaCl AI	11	2	0
		30 days 3.5% NaCl AI	16	3	0
		seacoast atmosphere	20	0	0
		industrial atmosphere	0	0	0
45 (310)	T7X51	20 days 3.5% NaCl AI	44	22	20
		30 days 3.5% NaCl AI	59	25	20
		90 days 3.5% NaCl AI	100	78	22
		seacoast atmosphere	100	20	0
		industrial atmosphere	40	10	0
43 (300)	T7351	20 days 3.5% NaCl AI	0	0	0
		30 days 3.5% NaCl AI	3[d]	0	0
		90 days 3.5% NaCl AI	77[d]	17[d]	0
		seacoast atmosphere	0	0	0
		industrial atmosphere	0	0	0

[a] Combined laboratories: 60 to 90 specimens at each stress level.
[b] Exposed 3 years; 10 specimens at each stress level.
[c] AI = alternate immersion.
[d] "Nuisance" failures caused by pitting and transgranular cracking.

20-day alternate immersion test, while specimens with a *high resistance* to SCC [T7351 stressed at 43 ksi (300 MPa) and T7X51 stressed at 25 ksi (170 MPa)] had low percentages of failure (0 to 20 percent). Specimens with a *medium resistance* to SCC [T7X51 stressed at 45 ksi (310 MPa)] had variable percentages of failure depending upon specimen configuration, type of atmosphere, and period of exposure in the alternate immersion test. The best correlation with the atmospheric exposures was for a 20-day alternate immersion exposure of 0.225-in. (5.72-mm) tension specimens.

4. *Interlaboratory Variation*—The 3.5 percent NaCl alternate immersion SCC test data were relatively uniform for specimens with a low resistance to SCC. For example, 7075-T651 specimens of all configurations stressed at 25 ksi (170 MPa) failed in short times ranging from one to seven days in all laboratories (Fig. 11). At lower stress levels, however, the range of times to failure was relatively large, and there was appreciable variation between laboratories. Appreciable variation was observed for tests of the T7X51 temper specimens, as shown in Fig. 12. Other comparisons can be made with the data in Tables 5, 6, and 7.

TABLE 5—*Summary of 3.5 percent NaCl alternate immersion tests of 7075-T651.*

Laboratory	Test Run	Stress, ksi[c]	Visual Failures[a,b]					
			0.125 in. Tension (3.18 mm)		0.225 in. Tension (5.72 mm)		C-Rings	
			F/N	Days	F/N	Days	F/N	Days
Alcoa	1	25	5/5	2,2,2,3,3	5/5	3,4,4,4,6	5/5	3,3,3,3,3
		15	5/5	3,6,9,46,*65*	5/5	4,4,6,9,*65*	1/5*	3(*30*)(*90*)(90)(90)
		8	1/5	*90*,(90)(90)(90)(90)	0/5	(*90*)(90)(90)(90)(90)	0/5*	(*60*)(*90*)(90)(90)(90)
	2	25	5/5	2,2,2,3,4	5/5	3,4,4,4,5	5/5	4,4,4,4,4
		15	5/5	3,4,4,5,5	5/5	3,4,5,28,*43*	0/5*	(*30*)(*90*)(90)(90)(90)
		8	2/5	*28*,*43*,(90)(90)(90)	0/5	(*90*)(90)(90)(90)(90)	0/5*	(*90*)(90)(90)(90)(90)
Kaiser	1	25	5/5	1,2,2,2,2	5/5	2,2,2,2,3	5/5	2,2,2,2,3
		15	5/5	2,2,7,7,10	5/5	4,4,4,6,6	0/5	(90)(90)(90)(90)(90)
		8	1/5	4,(90)(90)(90)(90)	0/5	(90)(90)(90)(90)(90)	0/5	(90)(90)(90)(90)(90)
	2	25	5/5	1,2,2,2,2	5/5	2,2,3,3,3	5/5	2,2,2,2,2
		15	5/5	2,2,2,3,5	5/5	5,6,8,39,41	2/5	2,2,(90)(90)(90)
		8	4/5	8,27,62,85,(90)	0/5	(90)(90)(90)(90)(90)	0/5	(90)(90)(90)(90)(90)
Martin Marietta	1	25	5/5	2,2,2,3,3	5/5	3,3,3,3,4	5/5	3,3,3,3,3
		15	5/5	2,2,3,3,61	5/5	4,4,5,5,5	1/5*	3,(*90*)(*90*)(90)(90)
		8	5/5	3,3,4,4,64	0/5	(90)(90)(90)(90)(90)	0/5*	(*74*)(*90*)(90)(90)(90)
	2	25	5/5	3,3,3,3,3	5/5	3,3,3,3,3	5/5	3,3,3,3,3
		15	5/5	3,3,3,4,4	5/5	3,3,3,3,6	2/5*	3,3,(*45*)(*90*)(90)
		8	5/5	3,3,3,4,5	5/5	5,7,12,13,31	0/5*	(*45*)(*90*)(90)(90)(90)
MSFC	1	25	5/5	1,2,2,2,2	5/5	1,*2*,2,2,3	5/5	2,3,3,3,3
		15	5/5	2,2,2,2,2	5/5	2,2,2,3,3	2/5	3,3,(90)(90)(90)
		8	4/5	2,*3*,9,9,(90)	5/5	*4*,4,6,9,9	0/5	(*90*)(*90*)(*90*)(90)(90)
	2	25	5/5	1,1,2,2,2	5/5	1,1,2,2,2	5/5	2,2,2,2,2
		15	5/5	1,2,2,3,4	5/5	2,2,2,3,3	0/5*	(*9*)(90)(90)(90)(90)
		8	5/5	3,3,3,4,56	5/5	3,*4*,4,4,21	0/5	(90)(90)(90)(90)(90)

NADC	1	25	5/5	1,4,4,4,4	. . .	. . .	4/5*	2,31,(*54*),60,60
		15	5/5	4,6,6,6,12	. . .	. . .	4/5*	17,21,31,(*31*),65
		8	1/5	12,(*90*)(90)(90)(90)	. . .	. . .	1/5*	(*20*)(*31*)60,(60)(65)
	2	25	5/5	2,2,5,5,5	. . .	. . .	5/5	4,4,10,25,25
		15	5/5	5,5,7,10,10	. . .	. . .	2/5*	3,32,(*90*)(90)(90)
		8	0/5	(90)(90)(90)(90)(90)	. . .	. . .	1/5*	4,(32)(*32*)(*90*)(*90*)
Pechiney	1	25	5/5	*1*,*1*,1,*2*,*2*	5/5	*1*,*2*,*2*,*2*,*3*	5/5	3,4,4,4,4
		15	5/5	*3*,*3*,*3*,*3*,*3*	0/5	*4*,17,*29*,*30*,*45*	0/5*	(*30*)(*30*)(*61*)(*90*)(*90*)
		8	3/5	*66*,*70*,*70*,(90)(90)	0/5	(90)(90)(90)(90)(90)	0/5	(*90*)(*90*)(*90*)(90)(90)
	2	25	5/5	*1*,1,1,2,3	5/5	5,*5*,6,6,7	5/5	*2*,2,2,2,2
		15	5/5	2,*3*,*3*,4,7	5/5	6,7,9,*42*,*78*	1/5*	*5*,(*90*)(*90*)(90)(90)
		8	3/5	*38*,*78*,*83*,(90)(90)	0/5	(90)(90)(90)(90)(90)	0/5*	(*90*)(*90*)(*90*)(90)(90)
Reynolds	1	25	5/5	1,1,1,2,*2*	5/5	2,2,2,2,3	5/5	1,1,2,2,2
		15	5/5	2,2,2,2,*3*	5/5	3,4,4,4,*5*	2/5*	*10*,11,(*90*)(90)(90)
		8	2/5	2,*4*,(*90*)(90)(90)	0/5	(*90*)(90)(90)(90)(90)	1/5*	*12*,(*90*)(90)(90)(90)
	2	25	5/5	1,2,2,2,2	5/5	3,3,3,3,*3*	5/5	*1*,1,2,2,2
		15	5/5	1,2,3,3,*87*	5/5	4,*5*,46,*46*,*64*	5/5	*2*,2,2,2,5
		8	4/5	2,2,*2*,*88*,(90)	0/5	(*90*)(90)(90)(90)(90)	0/5*	(*90*)(90)(90)(90)(90)
Alcan	1	25	. . .	. . .	. . .	. . .	5/5	*3*,3,3,3,3
		15	. . .	. . .	. . .	. . .	5/5	*8*,*8*,*8*,8,8
		8	. . .	. . .	. . .	. . .	0/5	(*90*)(*90*)(90)(90)(90)
	2	25	. . .	. . .	. . .	. . .	5/5	*2*,2,2,2,2
		15	. . .	. . .	. . .	. . .	5/5	*7*,*7*,*7*,*7*,7
		8	. . .	. . .	. . .	. . .	0/5	(*90*)(*90*)(*90*)(*90*)(90)
Frankford	1	25	. . .	. . .	. . .	. . .	5/5	*2*,2,2,2,2
		15	. . .	. . .	. . .	. . .	5/5	6,7,8,12,*13*
		8	. . .	. . .	. . .	. . .	0/5	(90)(90)(90)(90)(90)
	2	25	. . .	. . .	. . .	. . .	5/5	2,2,2,2,2
		15	. . .	. . .	. . .	. . .	5/5	*2*,7,11,13,*19*
		8	. . .	. . .	. . .	. . .	1/5*	*19*,(*90*)(*90*)(*90*)(90)

---

[a] Specimens enclosed in parentheses were found not to be cracked when visually examined after nitric acid cleaning.

[b] Italicized specimens were metallographically examined; * denotes that intergranular SCC was present.

[c] Stress conversions: 25 ksi = 170 MPa, 15 ksi = 100 MPa, 8 ksi = 55 MPa.

TABLE 6—*Summary of 3.5 percent NaCl alternate immersion tests of 7075-T7X51.*

			Visual Failures[a,b]					
			0.125 in. Tension (3.18 mm)		0.225 in. Tension (5.72 mm)		C-Rings	
Laboratory	Test Run	Stress, ksi[c]	F/N	Days	F/N	Days	F/N	Days
Alcoa	1	45	5/5	8,*42*,50,69,*72*	1/5*	*65*,(*90*)(*90*)(90)(90)	0/5*	(*30*)(*90*)(*90*)(90)(90)
		35	2/5	*69*,*78*,(*90*)(90)(90)	0/5	(*90*)(*90*)(90)(90)(90)	0/5	(*60*)(*90*)(*90*)(90)(90)
		25	0/5	(*90*)(90)(90)(90)(90)	0/5	(*90*)(90)(90)(90)(90)	0/5	(*60*)(*90*)(90)(90)(90)
	2	45	5/5*	*26*,53,63,64,*69*	5/5*	*33*,51,66,79,*87*	0/5*	(*30*)(*90*)(90)(90)(90)
		35	2/5*	63,*63*,(90)(90)(90)	0/5	(*90*)(90)(90)(90)(90)	0/5	(*90*)(90)(90)(90)(90)
		25	0/5	(*90*)(90)(90)(90)(90)	0/5	(*90*)(90)(90)(90)(90)	0/5	(*90*)(90)(90)(90)(90)
Kaiser	1	45	5/5	23,27,33,33,40	5/5	28,38,44,56,88	0/5	(90)(90)(90)(90)(90)
		35	4/5	44,48,52,81,(90	0/5	(90)(90)(90)(90)(90)	0/5	(90)(90)(90)(90)(90)
		25	1/5	74,(90)(90)(90)(90)	0/5	(90)(90)(90)(90)(90)	0/5	(90)(90)(90)(90)(90)
	2	45	5/5	20,39,41,48,69	4/5	61,62,86,89,(90)	0/5	(90)(90)(90)(90)(90)
		35	4/5	42,55,67,71,(90)	0/5	(90)(90)(90)(90)(90)	0/5	(90)(90)(90)(90)(90)
		25	1/5	76,(90)(90)(90)(90)	0/5	(90)(90)(90)(90)(90)	0/5	(90)(90)(90)(90)(90)
Martin Marietta	1	45	5/5	9,*17*,*28*,38,40	3/5	*68*,80,87,(90)(90)	0/5*	(*74*)(*90*)(90)(90)(90)
		35	3/5	*57*,80,80,(90)(90)	2/5	*67*,81,(90)(90)(90)	0/5	(90)(90)(90)(90)(90)
		25	0/5	(90)(90)(90)(90)(90)	0/5	(90)(90)(90)(90)(90)	0/5	(*90*)(90)(90)(90)(90)
	2	45	5/5	*3*,3,4,4,4	4/5	5,*6*,*52*,88,(90)	0/5	(*45*)(90)(90)(90)(90)
		35	5/5	*3*,4,4,4,5	1/5	5,(90)(90)(90)(90)	0/5	(*45*)(90)(90)(90)(90)
		25	5/5	*20*,22,27,39,*47*	0/5	(90)(90)(90)(90)(90)	0/5	(*45*)(90)(90)(90)(90)
MSFC	1	45	5/5	2,2,3,4,4	4/4	12,13,16,22	0/5	(*90*)(*90*)(90)(90)(90)
		35	5/5	2,2,3,3,4	5/5	*5*,*7*,14,27,30	0/5	(*90*)(90)(90)(90)(90)
		25	5/5	*5*,*6*,16,*20*,21	5/5	27,36,*47*,51,57	0/5	(*90*)(90)(90)(90)(90)
	2	45	5/5	3,3,3,3,3	5/5	4,4,12,15,35	0/5	(90)(90)(90)(90)(90)
		35	5/5	2,2,3,3,3	5/5	5,30,36,38,45	0/5	(90)(90)(90)(90)(90)
		25	5/5	*3*,*15*,18,57,63	5/5	7,50,53,58,63	0/5	(90)(90)(90)(90)(90)

NADC	1	45	4/5	5,17,*36*,*56*,(90)	. . .	. . .	0/5*	(*32*)(*32*)(*32*)(32)(*62*)
		35	4/5	10,*34*,*56*,*69*,(90)	. . .	. . .	0/5*	(*21*)(*32*)(*62*)(90)(90)
		25	2/5	82,89,(90)(90)(90)	. . .	. . .	0/5	(*62*)(90)(90)(90)(90)
	2	45	4/5	14,24,32,50,(90)	. . .	. . .	0/5*	(*33*)(*33*)(*51*)(*90*)(90)
		35	3/5	70,*74*,*83*,(90)(90)	. . .	. . .	0/5*	(*33*)(*51*)(*90*)(90)(90)
		25	1/5	70,(90)(90)(90)(90)	. . .	. . .	0/5	(56)(85)(90)(90)(90)
Pechiney	1	45	5/5	*13*,*14*,*28*,*29*,*66*	1/5	*49*,(90)(90)(90)(90)	1/5*	*60*,(*90*)(*90*)(*90*)(*90*)
		35	0/5	(90)(90)(90)(90)(90)	0/5	(90)(90)(90)(90)(90)	0/5*	(*90*)(*90*)(*90*)(*90*)(*90*)
		25	0/5	(90)(90)(90)(90)(90)	0/5	(90)(90)(90)(90)(90)	0/5	(*90*)(*90*)(*90*)(90)(90)
	2	45	5/5	*7*,*16*,22,*23*,*48*	4/5	*2*,*2*,*6*,*36*,(90)	2/5*	*5*,*5*,(*90*)(*90*)(*90*)
		35	2/5	*70*,*87*,(90)(90)(90)	0/5	(90)(90)(90)(90)(90)	0/5*	(*90*)(*90*)(*90*)(*90*)(*90*)
		25	0/5	(90)(90)(90)(90)(90)	0/5	(90)(90)(90)(90)(90)	0/5	(*90*)(*90*)(90)(90)(90)
Reynolds	1	45	5/5	*3*,5,*8*,24,*35*	5/5	*62*,62,*80*,87,*87*	5/5	3,5,5,6,6
		35	5/5	*26*,38,*40*,67,*73*	1/5	*48*,(*90*)(90)(90)(90)	5/5*	*8*,11,11,12,*12*
		25	0/5	(*90*)(90)(90)(90)(90)	0/5	(*90*)(90)(90)(90)(90)	0/5	(*90*)(90)(90)(90)(90)
	2	45	5/5	5,6,*32*,38,*40*	5/5	*19*,64,*64*,67,*73*	5/5	*3*,*3*,3,4,4
		35	5/5	*42*,45,*52*,*76*,90	2/5	*86*,90,(90)(90)(90)	5/5	*3*,*3*,3,3,6
		25	0/5	(*90*)(90)(90)(90)(90)	0/5	(*90*)(90)(90)(90)(90)	0/5	(*90*)(90)(90)(90)(90)
Alcan	1	45	. . .	. . .	. . .	. . .	0/5*	(*90*)(90)(90)(90)(90)
		35	. . .	. . .	. . .	. . .	0/5*	(*90*)(90)(90)(90)(90)
		25	. . .	. . .	. . .	. . .	0/5	(*90*)(90)(90)(90)(90)
	2	45	. . .	. . .	. . .	. . .	0/5*	(*90*)(*90*)(*90*)(*90*)(90)
		35	. . .	. . .	. . .	. . .	0/5*	(*90*)(*90*)(*90*)(*90*)(90)
		25	. . .	. . .	. . .	. . .	0/5	(*90*)(*90*)(*90*)(*90*)(90)
Frankford	1	45	. . .	. . .	. . .	. . .	4/5*	*5*,*5*,*30*,*45*,(*90*)
		35	. . .	. . .	. . .	. . .	0/5*	(*90*)(90)(90)(90)(90)
		25	. . .	. . .	. . .	. . .	0/5	(90)(90)(90)(90)(90)
	2	45	. . .	. . .	. . .	. . .	2/5*	*3*,*3*,(*90*)(*90*)(*90*)
		35	. . .	. . .	. . .	. . .	1/5*	*3*,(*90*)(*90*)(*90*)(*90*)
		25	. . .	. . .	. . .	. . .	0/5*	(*90*)(*90*)(*90*)(*90*)(*90*)

---

[a] Specimens enclosed in parentheses were found not to be cracked when visually examined after nitric acid cleaning.

[b] Italicized specimens were metallographically examined; * denotes that intergranular SCC was present.

[c] Stress conversions: 45 ksi = 310 MPa, 35 ksi = 240 MPa, 25 ksi = 170 MPa.

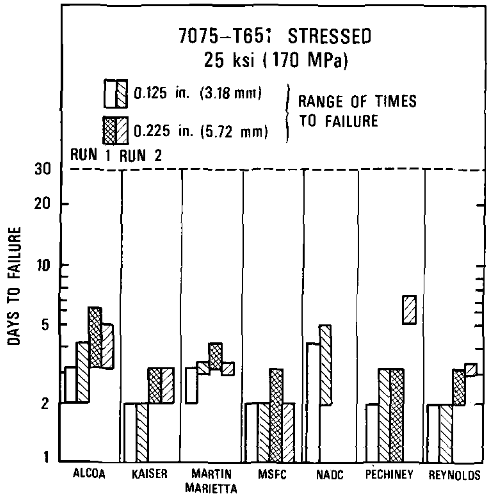

FIG. 11—*Variability in 3.5 percent NaCl alternate immersion test results.*

The results of tension tests made on control specimens exposed for 30 days with no applied stress showed only small interlaboratory differences (Table 8). Although the generally higher losses in strength in the Marshall Space Flight Center tests tended to parallel the more rapid SCC effects in that laboratory, other comparisons were not consistent. For example, the

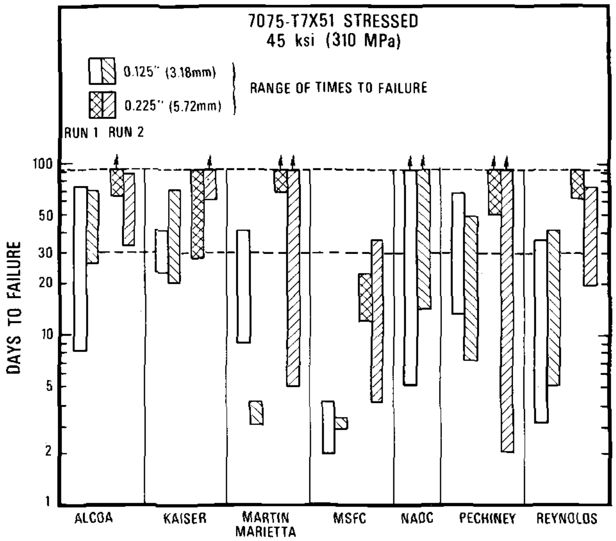

FIG. 12—*Variability in 3.5 percent NaCl alternate immersion test results.*

TABLE 7—*Summary of 3.5 percent NaCl alternate immersion tests of 7075-T7351.*

Laboratory	Test Run	Stress, ksi	Visual Failures[a,b] 0.125 in. Tension (3.18 mm) F/N	Days	0.225 in. Tension (5.72 mm) F/N	Days	C-Rings F/N	Days
Alcoa	1	43	2/5	*71*,*82*,(*90*)(90)(90)	0/5	(*90*)(*90*)(90)(90)(90)	0/5	(*60*)(*90*)(90)(90)(90)
	2	(300 MPa)	3/5	*79*,*80*,*89*,(90)(90)	0/5	(*90*)(90)(90)(90)(90)	0/5	(*90*)(90)(90)(90)(90)
Kaiser	1	43	4/5	53,57,74,77,(90)	1/5	88,(90)(90)(90)(90)	0/5	(90)(90)(90)(90)(90)
	2	(300 MPa)	4/5	60,74,80,81,(90)	0/5	(90)(90)(90)(90)(90)	0/5	(90)(90)(90)(90)(90)
Martin Marietta	1	43	5/5	*69*,73,75,80,*84*	1/5	*87*,(90)(90)(90)(90)	0/5	(*74*)(*90*)(90)(90)(90)
	2	(300 MPa)	5/5	*46*,47,49,52,*60*	1/5	80,(90)(90)(90)(90)	0/5	(*90*)(90)(90)(90)(90)
MSFC	1	43	5/5	*23*,24,31,*34*,52	5/5	56,66,69,73,83	0/5	(*90*)(90)(90)(90)(90)
	2	(300 MPa)	5/5	44,52,56,59,80	1/5	70,(90)(90)(90)(90)	0/5	(90)(90)(90)(90)(90)
NADC	1	43	0/5	(90)(90)(90)(90)(90)	. . .	. . .	0/5	(*90*)(90)(90)(90)(90)
	2	(300 MPa)	2/5	*87*,*88*,(90)(90)(90)	. . .	. . .	0/5	(90)(90)(90)(90)(90)
Pechiney	1	43	4/5	*45*,*64*,*76*,*83*,(90)	0/5	(90)(90)(90)(90)(90)	0/5	(*90*)(*90*)(90)(90)(90)
	2	(300 MPa)	3/5	*48*,*57*,*87*,(90)(90)	0/5	(90)(90)(90)(90)(90)	0/5	(*90*)(*90*)(90)(90)(90)
Reynolds	1	43	3/5	*48*,63,*69*,(*90*)(90)	0/5	(90)(90)(90)(90)(90)	0/5	(*90*)(90)(90)(90)(90)
	2	(300 MPa)	3/5	*40*,87,*88*,(*90*)(90)	1/5	*87*,(*90*)(90)(90)(90)	0/5	(*90*)(90)(90)(90)(90)
Alcan	1	43	. . .	. . .	. . .	. . .	0/5	(*90*)(90)(90)(90)(90)
	2	(300 MPa)	. . .	. . .	. . .	. . .	0/5	(*90*)(*90*)(*90*)(*90*)(90)
Frankford	1	43	. . .	. . .	. . .	. . .	0/5	(90)(90)(90)(90)(90)
	2	(300 MPa)	. . .	. . .	. . .	. . .	0/5	(*90*)(90)(90)(90)(90)

[a] Specimens enclosed in parentheses were found not to be cracked when visually examined after nitric acid cleaning.

[b] Italicized specimens were metallographically examined; no intergranular SCC present.

TABLE 8—*Percent reduction in load-carrying ability of unstressed tension specimens exposed 30 days to 3.5 percent NaCl by alternate immersion in various laboratories.*[a]

Laboratory	Test Run	0.125 in. Tension (3.18 mm) T651	T7X51	T7351	0.225 in. Tension (5.72 mm) T651	T7X51	T7351
Alcoa	1	24	16[b]	1	7[c]	10	3
	2	25	24	11	12	13	3
Kaiser	1	36	27	16	24	15	6
	2	32	25	10	21	13	3
Martin Marietta	1	23	23	14	14	14	6
	2	23	26	16	13	15	7
MSFC	1	34	28	14	20	17	9
	2	34	28	13	24	27	9
NADC	1	38	26	13		no test	
	2	25	26	13			
Pechiney	1	28	22	11	17	15	7
	2	34	23	10	20	16	5
Reynolds	1	27	24	14	14	12	5
	2	21	25	14	12	14	3

[a] Averages of duplicate tests; test values were close except where noted otherwise.
[b] Test values averaged were 9 and 22 percent.
[c] Test values averaged were 3 and 11 percent.

losses in strength obtained in the Kaiser and Naval Air Development Center tests were almost as high as those at Marshall Space Flight Center, but the SCC effects were much less.

In general, the variation between the two test runs in a given laboratory were in good agreement. The principal exceptions were at Martin Marietta and Pechiney; this is shown by the data for the T7X51 temper (Table 6).

In spite of the considerable attention directed to the specific practices used in each laboratory (Table 2), no conclusion was reached concerning the cause of the variability noted in the SCC test results among the various laboratories. It is thought that the differences are related to the period and degree of wetness experienced by the specimens during the drying cycle, but this variable is inherent in an alternate immersion type of test and is difficult to control.

5. *Substitution of Synthetic Seawater*—The results of these tests performed in four of the laboratories are given in Table 9 in comparison with the results of previous tests with 3.5 percent NaCl. While these data are relatively limited and there was a marked interlaboratory variability, particularly for the T7X51 temper specimens, the results are promising. The combined data presented graphically in Fig. 13 indicate the possibility of a better distinction between the T7X51 and T7351 tempers. Also, pitting

TABLE 9—*Summary of alternate immersion tests in substitute ocean water [ASTM D 1141-52 (1971), Formula A].*[a]

			MSFC		Kaiser		Frankford		Alcoa		Frankford–C-Rings	
Temper	Stress, ksi	Corrodent	F/N	Days to Failure	F/N	Days to Failure	F/N	Days to Failure	F/N	Days to Failure	F/N	Days to Failure
T651	25	sea salt	5/5	3,3,3,3,4	5/5	1,2,2,2,2	5/5	2,2,2,2,3	3/3	3,5,7	5/5	3,3,3,3,4
T651	(170 MPa)	3.5% NaCl	5/5	1,2,2,2,2	5/5	1,2,2,2,2	...	...	5/5	2,2,2,3,3	5/5	2,2,2,2,2
T651		3.5% NaCl	5/5	1,1,2,2,2	5/5	1,2,2,2,2	...	...	5/5	2,2,2,3,4	5/5	2,2,2,2,2
T651	15	sea salt	5/5	3,3,4,8,86	5/5	2,2,2,4,4	5/5	2,2,3,4,4	3/3	5,7,9	5/5	4,4,4,4,4
T651	(100 MPa)	3.5% NaCl	5/5	2,2,2,2,2	5/5	2,2,7,7,10	...	...	5/5	3,6,9,46,65	5/5	6,7,8,12,13
T651		3.5% NaCl	5/5	1,2,2,3,4	5/5	2,2,2,3,5	...	...	5/5	3,4,4,5,5	5/5	2,7,11,13,19
T651	8	sea salt	3/5	7,7,8,2OK90	5/5	5,25,25,84,90	3/5	8,8,24,2OK90	3/3	9,11,11	0/5	5OK90
T651	(55 MPa)	3.5% NaCl	4/5	2,3,9,9,OK90	1/5	4,4OK90	...	...	1/5	90,4OK90	0/5	OK90
T651		3.5% NaCl	5/5	3,3,3,4,56	4/5	8,27,62,85,OK90	...	...	2/5	28,43,3OK90	1/5	19,4OK90
T7X51	45	sea salt	4/5	7,10,10,14,OK90	5/5	4,4,4,4,4	5/5	8,8,14,17,18	3/3	6,10,10	5/5	8,8,10,10,10
T7X51	(310 MPa)	3.5% NaCl	5/5	2,2,3,4,4	5/5	23,27,33,33,40	...	...	5/5	8,42,50,69,72	4/5	5,5,30,49,OK90
T7X51		3.5% NaCl	5/5	3,3,3,3,3	5/5	20,39,41,48,69	...	...	5/5	26,53,63,64,69	2/5	3,3,3OK90
T7X51	35	sea salt	2/5	14,28,3OK90	5/5	4,5,7,9,29	5/5	14,17,17,18,18	1/3	10,2OK90	5/5	8,8,8,11,24
T7X51	(240 MPa)	3.5% NaCl	5/5	2,2,3,3,4	4/5	44,48,52,81,OK90	...	...	2/5	69,78,3OK90	0/5	5OK90
T7X51		3.5% NaCl	5/5	2,2,3,3,3	4/5	42,55,67,71,OK90	...	...	2/5	63,63,3OK90	1/5	3,4OK90
T7X51	25	sea salt	0/5	5OK90	5/5	5,7,7,26,33	5/5	17,18,18,23,28	0/3	3OK90	5/5	8,10,14,16,80
T7X51	(170 MPa)	3.5% NaCl	5/5	5,6,16,20,21	1/5	74,4OK90	...	...	0/5	5OK90	0/5	5OK90
T7X51		3.5% NaCl	5/5	3,15,18,57,63	1/5	76,4OK90	...	...	0/5	5OK90	0/5	5OK90
T7351	43	sea salt	0/5	5OK90	0/5	5OK90	0/5	5OK90	0/3	3OK90	0/5	5OK90
T7351	(350 MPa)	3.5% NaCl	5/5	23,24,31,34,52	4/5	53,59,74,77,OK90	...	...	2/5	71,82,3OK90	0/5	5OK90
T7351		3.5% NaCl	5/5	44,52,56,59,80	4/5	60,74,80,81,OK90	...	...	3/5	79,80,89,2OK90	0/5	5OK90

---

[a] Tests made with 0.125-in. (3.18-mm) tension specimens except where noted otherwise.

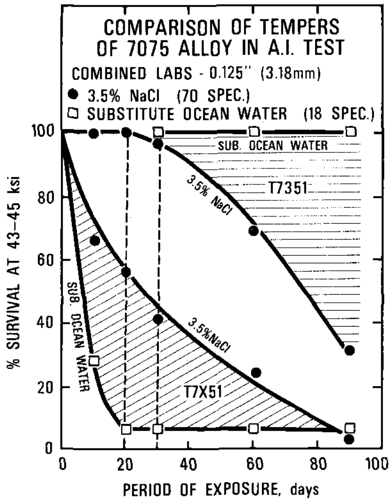

FIG. 13—*Influence of type of salt solution on test performance.*

of the specimens in the synthetic seawater was reduced markedly, thereby eliminating the extraneous failures of the highly SCC resistant materials and making visual examination of C-ring specimens easier. Further investigation of this corrodent is being carried out by the Task Group.

Other Accelerated Test Media

The results of the exploratory SCC tests with the two total immersion-type tests in nonpitting corrodents were disappointing, and they are not included in this report. The data were erratic and did not show the expected trends as were obtained in the other exposures.

Summary and Conclusions

This interlaboratory program of SCC testing was successful in demonstrating the high degree of variability that can be obtained in stress-corrosion test results for a given material depending on the test procedure. It was shown clearly that while the test performance of a material with low resistance to SCC, such as 7075-T651, may not be influenced appreciably by the test procedure, the test results for material with improved resistance to SCC, exemplified by the T7X51 and T7351 tempers, can be markedly influenced by testing methods. The type of specimen, C-ring versus tension specimen, and small changes in section size or diameter are significant factors.

The 3.5 percent NaCl alternate immersion test defined in Federal Method 823 and in the new ASTM Recommended Practice for Alternate Immersion Stress Corrosion Testing for 3.5% Sodium Chloride Solution (G 44-75) may indicate various degrees of SCC in aluminum-zinc-magnesium-copper type specimens. Additional investigation is needed to determine the necessary controls to produce more uniform test results. The test nevertheless is a useful test because it can be related with outdoor exposure, especially in seacoast environments. Selection of the proper exposure period for optimum correlation with a particular environment requires experience at that site with the alloy in question. It is expected that these test data will be an aid for selecting test conditions for alloys of this type to relate with general categories of atmospheric exposures, such as: seacoast, tropical, highly industrial, semi-industrial, rural, etc.

One problem with the alternate immersion test in a solution of 3.5 percent reagent grade NaCl in high-purity water is the severe pitting that develops in high-strength aluminum alloys. The substitution of synthetic seawater [ASTM Method D 1141-52 (1971), Formula A] shows considerable promise in minimizing this problem.

Acknowledgments

In addition to the authors, the following individuals have served on this task group and have had an active part in the various phases of the interlaboratory test program: R. H. Gassner, F. E. Loftin, D. L. Mellem, F. H. Meyer, B. R. Pathak, M. Reboul, J. V. Rinnovatore, Wayne Robertson, and I. S. Shaffer.

References

[1] Craig, H. L., Jr., Sprowls, D. O., and Piper, D. E. in *Handbook on Corrosion Testing and Evaluation,* W. H. Ailor, Ed., Wiley, New York, 1971, p. 231.

[2] Lifka, B. W. and Sprowls, D. O. in *Stress Corrosion Testing, ASTM STP 425,* American Society for Testing and Materials, 1967, p. 342.

[3] Helfrich, W. J., "Development of a Rapid Stress Corrosion Test for Aluminum Alloys," Final Summary Report Contract No. NAS 8-20285, 15 May 1968, for the George C. Marshall Space Flight Center.

[4] *Local Climatological Data,* Annual Summary with Comparative Data for Philadelphia, 1973, published by the U.S. Department of Commerce National Oceanic and Atmospheric Administration Environmental Data Service.

F. H. Haynie[1]

Air Pollution Effects on Stress Induced Intergranular Corrosion of 7005-T53 Aluminum Alloy

REFERENCE: Haynie, F. H., "**Air Pollution Effects on Stress Induced Intergranular Corrosion of 7005-T53 Aluminum Alloy,**" *Stress Corrosion—New Approaches, ASTM STP 610,* American Society for Testing and Materials, 1976, pp. 32–43.

ABSTRACT: Through a statistically designed, controlled environment experiment, it was found that atmospheric levels of sulfur dioxide induce a type of stress-accelerated intergranular corrosion in 7005-T53 aluminum alloy extruded tube material. Varying levels of nitrogen dioxide, ozone, relative humidity, and their interactions (including those with sulfur dioxide) did not cause statistically significant damage in this particular experiment. Some level of stress was necessary to cause this type of attack.

KEY WORDS: stress corrosion, crack propagation, intergranular corrosion, aluminum alloys, experimental design, air pollution, sulfur dioxide

For the past several years the Environmental Protection Agency has been conducting field and laboratory investigations to assess the detrimental effects of air pollution on materials [*1–5*].[2] The ultimate objective of these studies has been to develop dose-response relationships for various classes of materials. This information serves as input for cost-benefit analysis and as criteria for developing secondary air quality standards.

The catastrophic failure of metals caused by stress-corrosion cracking (SCC) is of concern because air pollutants may contribute to such failures. The results could be loss of life as well as increased costs. The 7000 series of high-strength aluminum alloys, which contain little or no copper, is more susceptible to SCC in industrial environments than along the seacoast [*6*]. Since air pollution is synonymous with industrial environments and is, therefore, a likely cause of failure, an alloy from this series was selected as a representative metal for assessing SCC.

[1] Environmental engineer, Environmental Protection Agency, Environmental Research Center, Research Triangle Park, N. C. 27711.

[2] The italic numbers in brackets refer to the list of references appended to this paper.

Accelerated degradation of materials by pollutants can be measured by conducting controlled environment laboratory exposures with varying levels of pollutants and comparing the observed effects. Thus, a statistically designed study involving the exposure of economically significant materials to controlled environments containing pollutants (sulfur dioxide (SO_2), nitrogen dioxide (NO_2), and ozone (O_3)) as well as clean air was conducted. Over 20 000 h of exposure time, which includes 4000 h of clean exposure were accumulated.

Experimental Procedure

Facility

This exposure study was conducted in five environmental chambers that were designed to operate continuously with each chamber having independent control of input temperature and humidity, lighting intensity, and concentrations of pollutant gases [7]. Before initiating this study, differences in chamber lighting and pollutant distribution, as well as the control capability of the environmental variables within the five chambers, were adjusted to less than 10 percent variation for 95 percent of the measurements.

Each environmental chamber was equipped with a cap that housed a xenon arc lamp for simulating sunlight. The chambers also contained chill racks upon which material specimens were mounted to enhance dew formation. Diurnal conditions were simulated using a programmed dew/light cycle. The temperature and relative humidity of the air flowing to the chambers were maintained at desired levels. However, the temperature of the specimens continually varied during the dew/light cycle, thus changing the local relative humidity. Moisture condensed on the specimens when the temperature was below the dew point. This mode of exposure allowed the surfaces of test materials to absorb and concentrate gaseous pollutants as they do in real-world environments.

Material

A 7005-T53 alloy tubing was selected for this experiment because the supplier had observed SCC in C-rings made from this material when they were exposed to an industrial atmosphere and the specimens are economically produced.

The purchased extruded tubing had an outside diameter of approximately 5.7 cm with a wall thickness of approximately 0.23 cm. The chemical analysis of the material is given in Table 1.

TABLE 1—*Elemental analysis of 7005-T53 tubing.*

Percent										
Si	Fe	Cu	Mn	Mg	Cr	Ni	Zn	Ti	Zr	Al
0.09	0.22	0.04	0.40	1.58	0.09	<0.01	4.61	0.03	0.13	remainder

Preparations

The tubing was machined into 1.9-cm-wide C-ring specimens leaving the inside and outside surfaces in the as-received condition.

C-ring specimens were stressed according to ASTM recommendations; actual dimensions were measured to within 10 μm. Two levels of stress were used: 2.07 × 10^8 N/m^2 (30 ksi) and 2.76 × 10^8 N/m^2 (40 ksi). Figure 1 shows the design of a stressed C-ring specimen. To measure time of failure, each specimen was spring loaded and electrically connected to a recorder. An insulated wire was attached across the compressed spring. Failure of a C-ring specimen caused the wire to break, thus signaling the time of failure.

To simplify the electrical wiring scheme, a group of three equally stressed C-ring specimens were mounted on a metal (aluminum alloy 6061-T6) plate that was then placed at random on a chamber exposure rack. For each exposure condition, two groups (one at each stress level) of three specimens were exposed.

Each group of three specimens was wired according to Fig. 2 so that time of failure for each specimen could be determined by recording step changes in voltages on a ten channel multipoint recorder. The resistance R in Fig. 2 was varied from one group to another to separate voltage traces on the recorder. Resistance values ranged from 0 to 35 Ω. When a specimen breaks, the recorder voltage increases and thus marks the time of failure.

For those specimens that did not completely fail within the 1000 h of exposure, a 5.1-cm cord across the stressed area was cut from each and

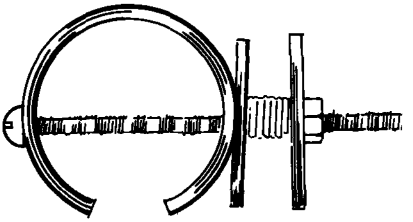

FIG. 1—*Method of stressing C-ring specimens.*

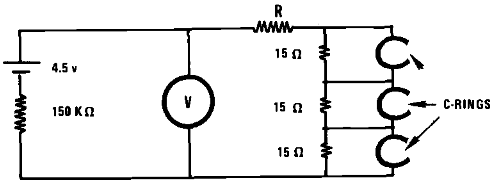

FIG. 2—*Wiring of specimens to record times of failure.*

compressed to failure by bending in a tensile-compression testing instrument. The maximum load required to bend the specimen was assumed to be a function of the remaining uncracked cross sectional thickness and was recorded as the response to the controlled environmental factors. A typical compression curve on these specimens had two maxima (Fig. 3). The first represented buckling and the second bending; the second maximum was used as the response.

Experimental Design

Environmental factors that were likely to have a detrimental effect on the stressed specimens were incorporated into a statistically designed study. Table 2 presents these factors and exposure levels selected for this study.

A two level factorial design was selected for identifying the environmental factors or combination of factors or both that have significant effects on materials. The low levels selected for the three gaseous pollutants represent primary ambient air quality standards, whereas the high levels represent concentrations that may be found at industrial sites. Since there are four factors at two levels (Table 2) the complete study design requires 16 (2^4) different exposures, one at each combination of factor

TABLE 2—*Environmental factors and levels selected for the experiment.*

	Levels	
Environmental Factors	Low	High
Sulfur dioxide, μg/m^3	79 (0.03 ppm)	1310 (0.50 ppm)
Nitrogen dioxide, μg/m^3	94 (0.05 ppm)	940 (0.50 ppm)
Ozone, μg/m^3	157 (0.08 ppm)	980 (0.50 ppm)
Relative humidity,[a] %	50	89

[a] Two levels of relative humidity were maintained at a temperature of 35°C for the air entering the environmental chambers. During the dew/light cycle, the temperature and relative humidity were allowed to fluctuate within each chamber.

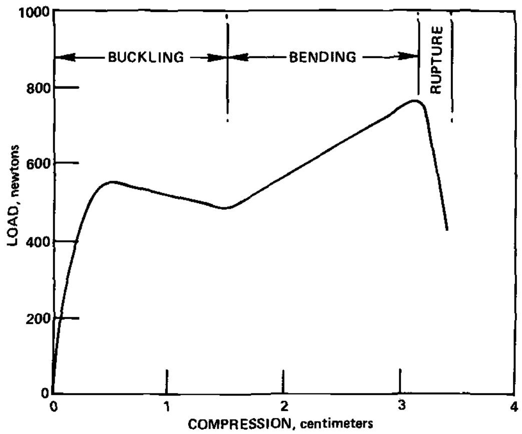

FIG. 3—*Typical C-ring cord compression-load curve showing maxima when buckling and bending.*

and level, and does not include replication. For this study only one level of temperature (35°C) was investigated. According to reaction kinetics, it is unlikely that environmental factors that are statistically insignificant at high temperatures will show significant interactions with temperature. Thus, in the polluted exposures a temperature lower than 35°C was not necessary in order to identify environmental factors (pollutants) that cause significant effects.

In addition to these polluted experiments, clean air exposures were investigated to determine effects in a simulated clean environment. For these exposures, two levels of temperature (13 and 35°C) and relative humidity (50 and 90 percent) were selected. For each set of conditions, both clean and polluted, the duration of exposure was 1000 h consisting of 40 min dew/light cycles. Two sets of specimens (one at each stress level) were exposed at each set of conditions.

Results and Analysis

None of the specimens exposed 1000 h to the 16 polluted environment conditions completely failed; thus, time to failure could not be used as a response.

Specimens exposed to the polluted conditions developed small intergranular cracks perpendicular to the stress direction (Fig. 4). The number and lengths of these cracks appeared to be a function of the exposure time, the severity of the environment, and the level of stress. No cracks developed in the unstressed portion of each specimen nor in specimens exposed 1000 h in the clean environments.

FIG. 4—*Stress induced intergranular cracks in 7005-T53 after 1000 h exposure to air containing* SO_2 *(mark = 1 mm).*

Selected specimens were examined by both light and scanning electron microscopy. The cracks were intergranular and microprobe analysis revealed sulfur on the fracture faces (Fig. 5).

The second maximum in the C-ring cord load-compression curve was used as the response for each specimen. Results for the polluted conditions are given in Table 3. Values ranged from a low of 288 N to a high of 804 N. Low values represent cross sections reduced by stress-induced intergranular corrosion. The best estimate of the standard deviation on any one set of data was ±108 N.

Bias may have been introduced into this experiment because of the method used to expose the C-ring specimens. From the standpoint of experimental design, a better method would have been to expose individual specimens randomly placed on a chamber rack, rather than to expose three equally stressed specimens as a group and randomly place the group

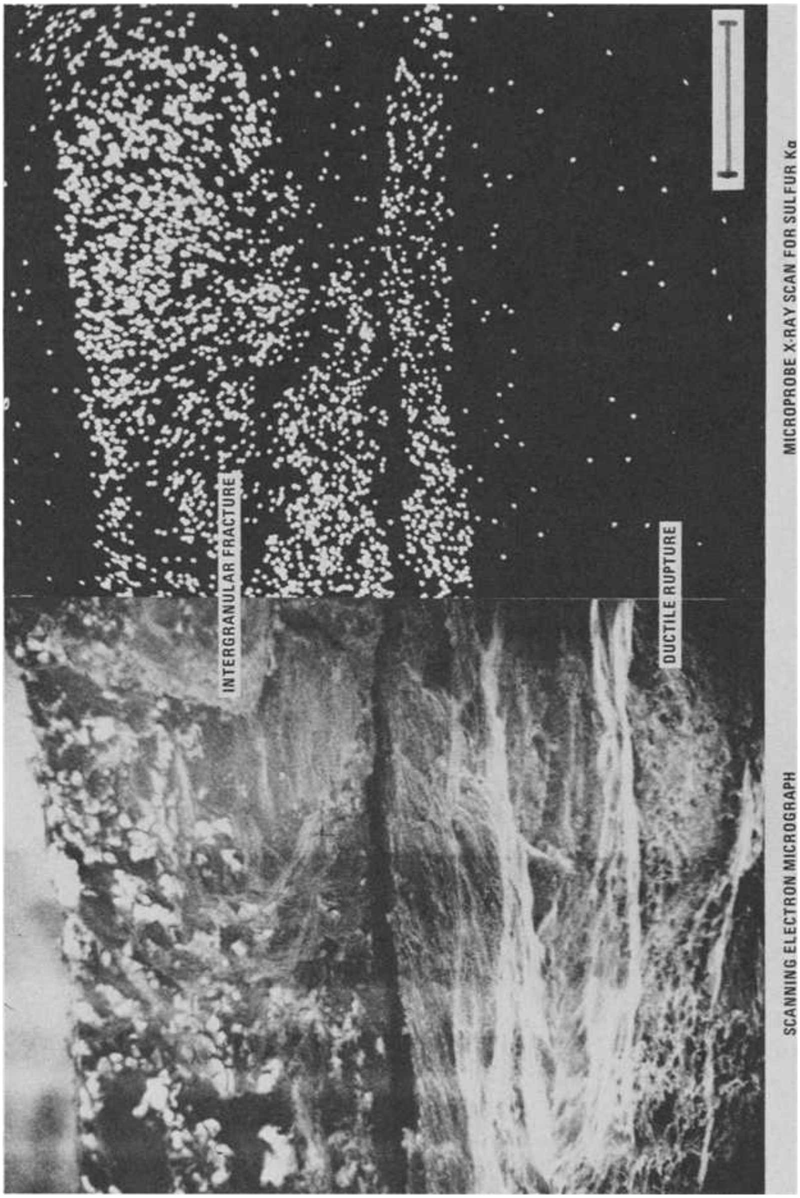

FIG. 5—*Fracture face of aluminum alloy specimens ruptured by bending after intergranular cracks were formed during exposure to* SO_2 *containing air (mark = 100 μm).*

TABLE 3—*Bending strength of aluminum alloy stress-corrosion specimens after exposure to designated controlled polluted air environmental conditions for 1000 h.*

	Bending Strength and Standard Deviation, N					
	High Relative Humidity		Low Relative Humidity			
Stress, kN/m^2	High SO_2	Low SO_2	High SO_2	Low SO_2	Exposure Condition	
276	522 ± 107	524 ± 173	503 ± 249	780 ± 185	High O_3	High NO_2
207	693 ± 137	725 ± 31	690 ± 148	760 ± 77		
276	288 ± 175	740 ± 72	570 ± 118	777 ± 14	Low O_3	
207	482 ± 32	764 ± 69	611 ± 115	705 ± 20		
276	632 ± 66	804 ± 58	396 ± 189	657 ± 58	High O_3	Low NO_2
207	512 ± 105	791 ± 30	529 ± 34	685 ± 73		
276	534 ± 32	486 ± 127	591 ± 35	681 ± 176	Low O_3	
207	690 ± 6	712 ± 71	669 ± 123	728 ± 66		

NOTE—Bending strength values based on three data sets per exposure condition.

on the chamber rack. Thus, because of grouping, a possible position effect could be confounded with some tested effects. In analyzing variance, the possibility of arriving at erroneous conclusions of statistical significance for some variables was minimized by assuming that all triple and higher interaction effects were caused by error and using the values of those effects to calculate the error mean square. The resulting *F* test for significance, therefore, was much more stringent than would have occurred by assuming that the only error was associated to within sample variance.

Table 4 gives the analysis of variance for the mean bending strengths of specimens exposed to the polluted conditions.

Differences in mean bending strengths were associated statistically with SO_2 concentrations at the 99 percent confidence level and with stress at the 95 percent confidence level. These two factors account for 47 percent of the variability in the mean bending strengths.

There were no visible signs of corrosion or cracking in any of the specimens exposed to the clean environment conditions for 1000 h. Microscopic examination of random specimens revealed no microscopic cracks.

The results of the bending strength tests are given in Table 5. Analysis of variance indicated that none of the factors were associated statistically with the data variability. The mean bending strength and standard deviation on the mean were 717 N ± 36 N. This contrasts with 774 N ± 28 N for 11 unstressed, unexposed control specimens. A *t*-test for significance

TABLE 4—*Analyses of variance of polluted exposure data.*

Factor[a]	Degrees of Freedom	Mean Square	*F*
SO_2	1	181 052	16.74[b]
O_3	1	957	0.09
NO_2	1	43	0.00
Relative humidity (RH)	1	5 859	0.54
Stress (ST)	1	49 691	4.59[c]
$SO_2 \times O_3$	1	259	0.02
$SO_2 \times NO_2$	1	8 750	0.81
$SO_2 \times$ RH	1	14	0.00
$SO_2 \times$ ST	1	5 486	0.51
$O_3 \times NO_2$	1	3 720	0.34
$O_3 \times$ RH	1	21 998	2.03
$O_3 \times$ ST	1	504	0.05
$NO_2 \times$ RH	1	31 407	2.90
$NO_2 \times$ ST	1	1 140	0.10
RH × ST	1	5 430	0.50
Residual	16	10 814	

[a] × = interaction between main factors.
[b] Significant at 99 percent confidence level.
[c] Significant at 95 percent confidence level.

indicated an approximate 70 percent probability that the two means are different.

Most of the within sample variability is caused by extremely low bending strength values for four specimens exposed to the high relative humidity conditions (303 N, 387 N, 401 N, 516 N). All of these values are below the two standard deviations lower limit for the control specimen results, and three of them are below the three standard deviations limit. If the three lowest values are excluded from the clean exposure data, the mean and standard deviation on the mean are 768 N ± 25 N, which has less than a 20 percent probability that it is different from the mean for the control specimens. Thus, it is very likely that at least three of the specimens were weakened significantly by stressed exposure to the high humidity clean environment conditions.

TABLE 5—*Average bending strength and standard deviation (N) of aluminum alloy specimens exposed 1000 h to designated clean air conditions.*

Stress, kN/M²	90% Relative Humidity		50% Relative Humidity	
	35°C	13°C	35°C	13°C
276	697 ± 187	633 ± 259	700 ± 24	882 ± 61
207	730 ± 79	507 ± 284	822 ± 87	770 ± 101

NOTE—Values based on three data sets per exposure condition.

It is possible that these specimens contained cracks not visible to the naked eye and were not examined microscopically.

Additional evidence for SCC of this material in clean environments was obtained. During this experimental program both low- and high-stressed specimens that were stored in a laboratory drawer were found completely failed by single intergranular stress-corrosion cracks with no other visible signs of damage. This suggested that our exposures were not long enough to observe similar complete failures and possibly the mechanism of damage under the polluted conditions was not the same as for clean conditions.

A statistically designed orthogonal square experiment consisting of SO_2, temperature, relative humidity, and time as variables each at five levels was initiated. The same two levels of stress were applied to the aluminum alloy specimens. The results of these exposures were to be used to establish dose-response relationships for other materials as well as for the aluminum stress-corrosion specimens. The longest exposures were to be 4000 h.

For budgetary reasons the experiment was terminated after approximately 2000 h of exposure in each of five chambers. Because of the statistical nature of the experiment, no comparisons between exposures could be made (the levels of all variables including time were different).

The longest exposure was a little over 2000 h with clean air at an input relative humidity of 80 percent and an input temperature at 29°C. The stress levels were the same as in the original experiment. None of the specimens completely failed, but all three of the high-stressed and one of the low-stressed specimens had a single primary crack similar to that in Fig. 6. There were no other visible signs of corrosion or small cracks as was observed with the polluted exposures.

Discussion

Characteristic SCC of 7005-T53 tubing can occur in clean air at high relative humidities. A damage mechanism that by some definitions could be called SCC is enhanced by SO_2 in air. This mechanism differs from that observed in the clean environment in that many small cracks are formed perpendicular to the applied stress rather than a single primary crack. They are the same in that in both cases intergranular cracks do not form in the absence of tensile stress. The pollution damage mechanism may be better described as stress-induced intergranular corrosion.

If the two mechanisms are different, the processes could occur simultaneously in the polluted exposures. The formation of many small cracks should reduce the stress intensity in any one crack on a C-ring specimen and thus reduce the likelihood that a single large crack will grow to failure. Because SCC is associated with an incubation period during which little,

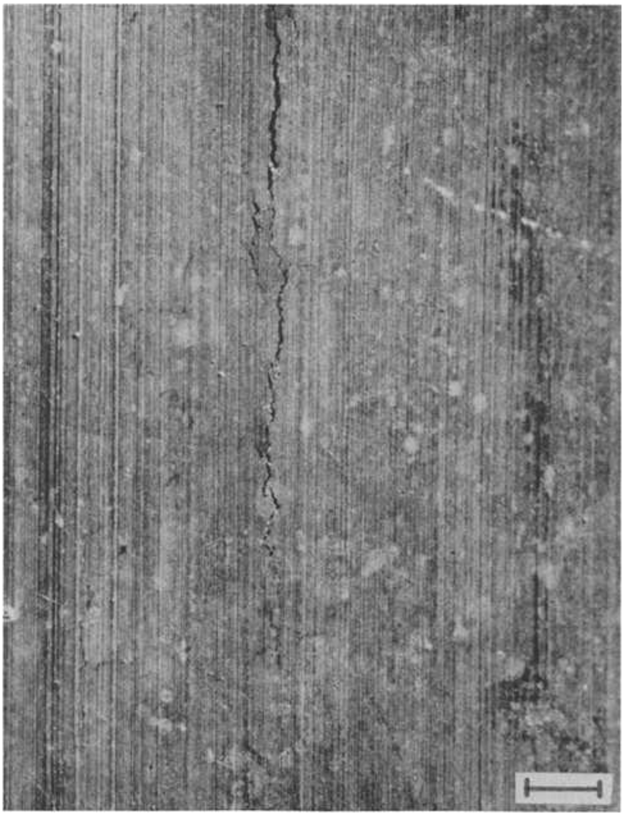

FIG. 6—*Stress-corrosion crack after 2000 h exposure to clean air (mark = 1 mm).*

if any, damage occurs, the pollution damage mechanism could obviate or mask characteristic SCC by the early initiation of many small cracks.

Tensile stress must be present before either mechanism will reduce the bending strength of these specimens. SO_2 will enhance the stress induced intergranular corrosion and exposure time is required. Thus, the data can be approximated by an empirical expression of the form

$$S_B = a_0 \exp -a_1(1 + a_2\mathrm{SO_2})\mathrm{ST} \times t$$

where

S_B = bending strength in newtons (N),
a_0 = coefficient representing undamaged bending strength,
SO_2 = μg/m^3,
ST = applied tensile stress in kN/m^2,
t = exposure time in days, and
a_1 and a_2 = regression coefficients.

A least squares fit of all the data including the clean air exposures and the controls gives the relationship

$$S_B = 808 \exp -1.346 \times 10^{-5}(1 + 0.001692\mathrm{SO_2})\mathrm{ST} \times t$$

Because all the exposure data were obtained at one exposure time, the time relationship has less validity than the other two variables.

This expression accounts for 27.6 percent of the total variability in the data. Within sample variability accounts for 38.9 percent leaving 33.5 percent variability associated with experimental error and lack of fit to the model. The high variability between replicate specimens makes the lack of fit variability statistically insignificant. Thus, the empirical expression is as good model as can be fitted to this particular set of data.

Conclusions

It is concluded from the results of this laboratory controlled environment experiment that:

1. SO_2 and tensile stress cause a type of stress induced intergranular corrosion in 7005-T53 extruded tubing.
2. At the levels selected for this experiment, NO_2, O_3, relative humidity, and their interactions (including those with SO_2 and stress) caused no statistically significant damage to the stress-corrosion specimens.
3. Characteristic SCC of this alloy can occur in ultraclean air under simulated diurnal conditions of sunlight, temperature, and relative humidity.
4. The damage mechanisms observed in the polluted and clean environments are possibly different and may occur simultaneously under polluted conditions.

References

[1] Campbell, G. G., Schurr, G. G., Slawikowski, D. E., and Spence, J. W., *Journal of Paint Technology,* Vol. 46, No. 593, June 1974, pp. 59–71.
[2] Beloin, N. J., *Textile Chemist and Colorist,* Vol. 4, No. 3, March 1972, pp. 77–82.
[3] Beloin, N. J., *Textile Chemist and Colorist,* Vol. 5, No. 7, July 1973, pp. 128–133.
[4] Haynie, F. H. and Upham, J. B., *Materials Protection and Performance,* Vol. 9, No. 8, Aug. 1970, pp. 35–40.
[5] Haynie, F. H. and Upham, J. B., *Materials Protection and Performance,* Vol. 10, Nov. 1971, pp. 18–21.
[6] Lifka, B. W. and Sprowls, D. O. in *Stress Corrosion Testing, ASTM STP 425,* American Society for Testing and Materials, 1967, p. 342.
[7] Spence, J. W. and Haynie, F. H. in *Corrosion in Natural Environments, ASTM STP 558,* American Society for Testing and Materials, 1974, pp. 279–291.

J. E. Finnegan[1] *and W. H. Hartt*[2]

Stress-Intensity Dependence of Stress-Corrosion Crack-Growth Rate in 7079-T651 Aluminum

REFERENCE: Finnegan, J. E. and Hartt, W. H., **"Stress-Intensity Dependence of Stress-Corrosion Crack-Growth Rate in 7079-T651 Aluminum,"** *Stress Corrosion—New Approaches, ASTM STP 610,* American Society for Testing and Materials, 1976, pp. 44–60.

ABSTRACT: Stress-corrosion cracking experiments have been performed on double-cantilever-beam specimens of 7079-T651 aluminum in 3 percent sodium chloride in distilled water and in seawater. At relatively low-stress intensities (Region I of the crack-growth rate/stress-intensity plot) crack length versus exposure time curves were comprised of steps, plateaus, and straight-line segments. These could not be related to any variations in the stress-intensity parameter; so, where such behavior was encountered, no unique relationship between stress intensity and crack-growth rate was apparent. On the other hand, crack-growth rate did vary inversely with exposure time for the range 25 to 200 h. Such an observation was interpreted to mean that properties of the local environment within a crack control extension rate.

KEY WORDS: stress corrosion, cracking (fracturing), crack propagation, aluminum, stress intensity, cantilever beams, salt water, seawater, solubility

Nomenclature

a	Crack length
b	Specimen width
c	Compliance
da/dt	Stress-corrosion crack-growth rate
E	Young's modulus
h	Specimen half height
K_I	Plane-strain stress intensity

---

[1] Formerly, graduate student of Ocean Engineering, Florida Atlantic University, Boca Raton, Fla. 33431; presently, research engineer, Dow Chemical Company, Freeport, Tex. 77541.

[2] Associate professor of Ocean Engineering, Florida Atlantic University, Boca Raton, Fla. 33431.

K_{Ii}	Initial plane-strain stress intensity
K_{Ic}	Plane-strain fracture toughness
K_{Iscc}	Plane-strain stress-intensity threshold for stress-corrosion cracking
v	Deflection of crack faces measured at bolt centerline
t	Exposure time
ys	Yield strength

Advent of linear elastic fracture mechanics and its application to environmental cracking of high-strength materials [*1,2*][3] have contributed significantly to characterizing and quantifying stress-corrosion crack-growth rates [*3*]. In this regard it has been found that, for a particular alloy-environment combination, stress-corrosion crack-growth rate *da/dt* depends uniquely upon plane-strain stress-intensity K_I [*3*], with the generalized relationship between the two as projected schematically in Fig. 1. This is characterized by three Regions, I and III being strongly stress-intensity dependent and II being K_I independent.

The stress corrosion cracking (SCC) behavior of high-strength aluminum alloys (particularly 7xxx and special purity aluminum-zinc-magnesium (Al-Zn-Mg) alloys) has been extensively investigated [*3,4*]. While the mechanism or mechanisms is (are) still unclear, variables considered important include (1) nature of slip processes in the alloy [*5–11*], probably as determined by alloy composition or microstructure or both, and (2) environment [*12,13*] and electrochemical factors [*14,15*]. With regard to

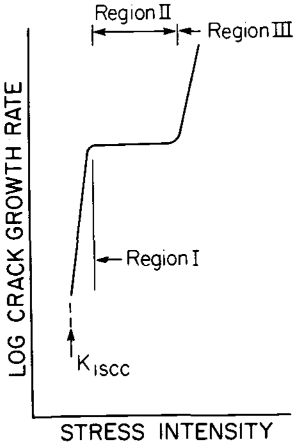

FIG. 1—*Schematic illustration of the generalized relationship between stress intensity and stress-corrosion crack-growth rate.*

[3] The italic numbers in brackets refer to the list of references appended to this paper.

Fig. 1 only Regions I and II have been noted for commercial 7xxx aluminum alloys. While a threshold stress intensity for SCC K_{Iscc} is indicated in Fig. 1, existence of such for aluminum alloys has been questioned.

The objective of the experiments described here was to better characterize stress-corrosion crack-growth rates of a high-strength aluminum alloy in the low stress-intensity range (Region I).

Procedure

The present experiments employed double-cantilever-beam (DCB) specimens obtained from a 3.24-cm (1.275-in.) thick plate of 7079-T651 aluminum. Chemical analysis of this is presented as Table 1. Metallographic observation of polished and etched sections revealed a grain structure elongated in the rolling direction and similar in appearance to what has been reported by others for commercial 7xxx stock [*3,16*]. Specimens of the DCB type were sectioned from the plate and machined to final dimensions of 12.7 by 3.24 by 3.24 cm (5.00 by 1.275 by 1.275 in.) and notched parallel to the rolling plane to obtain a short transverse stress orientation. The completed specimen geometry is as illustrated in Fig. 2. Notch lengths were either 1.27 cm (0.500 in.) or 3.81 cm (1.500 in.) both measured from the point of loading (bolt centerline). The former (1.27 cm notch depth) are subsequently termed short notch and the latter long notch specimens. Reference lines spaced 0.254 cm (0.100 in.) apart were scribed on the specimen faces across which the stress-corrosion crack was to propagate.

Two corrosive environments were employed, the first being a 3 percent sodium chloride (NaCl) distilled water solution and, second, seawater as available at the Florida Atlantic University Marine Materials and Corrosion Laboratory. The latter water is delivered to the laboratory via an all plastic pumping system through a well point positioned at the mean water line and 5 ft below the sand. Thus, the seawater was filtered and free of fouling organisms; salinity, conductivity, and pH readings indicated that the environment was indeed representative seawater (neglecting the biological component). For all experiments the test cell was of approximately 0.8 litre capacity. Some of the NaCl distilled water experiments were with the solution unstirred, while for others it was recirculated

TABLE 1—*Chemical analysis for 7079-T651 plate.*

Element	Zn	Mg	Cu	Cr	Mn	Si	Fe	Ti	Ni	Al
Weight, %	4.48	3.22	0.62	0.16	0.21	0.08	0.14	0.04	0.02	balance

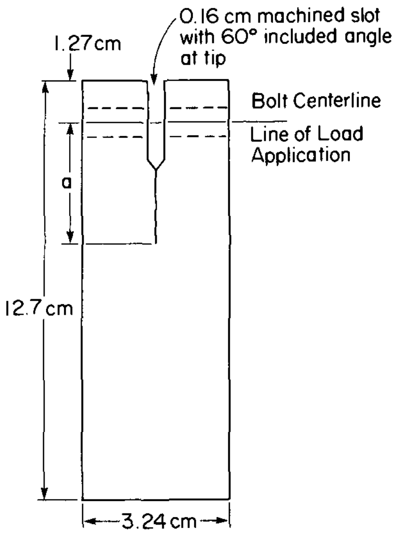

FIG. 2—*Geometry of 7079-T651 aluminum specimens.*

through a 10 litre reservoir. For the latter environment (recirculated salt water) and also for seawater tests a flow rate of 0.3 litre/min was employed.[4]

Prior to immersion a number of specimens were precracked by tightening one of the bolts until stress intensity at the notch tip exceeded the fracture toughness. Stress intensity at the resultant crack tip was then modified for some specimens by reducing deflection (backing off on the bolt) to the range 0.6 to 1.0 K_{Ic}. As an alternate test procedure other specimens were deflected to the range 0.3 to 0.85 K_{Ic}, such that no precrack formed. Upon exposure in the test environment, crack length was recorded as a function of exposure time using a low power microscope (×30) and micrometer eyepiece.[5] For tests in the NaCl distilled water solution corrosion product buildup was such that the specimen face at the crack tip vicinity had to be wiped off prior to measurement. Specimens in seawater experienced lesser surface deterioration and product accumulation, and these were generally viewed without wiping. Crack-growth rate as a function of stress intensity was computed in all cases by graphically determining the slope of the crack length-time curve at various crack lengths [*17*].

---

[4] The seawater pumping system did have occasional periods of shutdown; however, no anomalies in the experimental data could be related to these.

[5] For tests on specimens not precracked crack extension was preceded by an initiation period. It is considered here that the experiment commenced when crack growth began, and so initiation time has been disregarded.

Results and Discussion

Crack Extension Data

In Table 2 data are listed with regard to test conditions for individual specimens, including dimensions (notch depth), initial deflection, initial stress-intensity K_{Ii},[6] environment, and exposure time. Figure 3 describes crack length as a function of time for representative specimens. A noteworthy aspect of these crack extension curves is occurrence in numerous instances of inflections or steps or both. For all short notch specimens crack extension can be conveniently described in three distinct steps or stages, which are: (1) an initial, rapid decay in rate of crack extension (exposure time <200 h), (2) a plateau (zero crack growth rate) or near-plateau after approximately 200 h exposure, and (3) staircase or stepwise crack growth (alternate periods of dormancy and extension) for exposure times beyond 200 h. Long-notch specimens exhibited similar behavior, provided the initial stress-intensity K_{Ii} was less than about 0.5 K_{Ic}. For long-notch specimens with K_{Ii} in the range 0.5 to 1.0 K_{Ic} the first two steps of short-notch crack extension (1 and 2 just mentioned) were also evidenced, but, here the crack subsequently repropagated until it traversed the entire specimen. The resultant curve (see Fig. 3) was of an S-shape, similar to that observed by Dahlberg [*18*]. That the preceding steps are

TABLE 2—*Summation of specimens and exposure variables for SCC tests.*

Specimen Number	Notch Type	Deflection, cm	Initial Stress Intensity, MN/m$^{3/2}$	Environment	Exposure Time, h
B	short	0.036	21.4	NaCl/DW (recirculated)	1 234[a]
C	long	0.071	14.3	NaCl/DW (recirculated)	1 076[a]
E	long	0.036	7.2	NaCl/DW (recirculated)	5 088
F	short	0.018	14.9	NaCl/DW (recirculated	3 679
G	long	0.097	16.1	NaCl/DW (not recirculated)	530[a]
8	long	0.058	10.1	seawater	13 945
9	long	0.051	8.9	seawater	12 612
10	long	0.069	14.0	seawater	1 053[a]
11	long	0.046	9.2	seawater	8 188
12	short	0.036	17.5	seawater	8 186
13	long	0.112	16.0	seawater	361[a]
14	short	0.028	19.2	seawater	5 328
15	long	0.135	14.7	seawater	188[a]

[a] Mean value for the initial stress intensity of precracked specimens was 19.3 MN·m$^{-3/2}$ (22.0 ksi·in.$^{1/2}$). This was taken to be the plane-strain fracture toughness, K_{Ic}.

---

[6] Procedures for determining these stress-intensity values are presented subsequently.

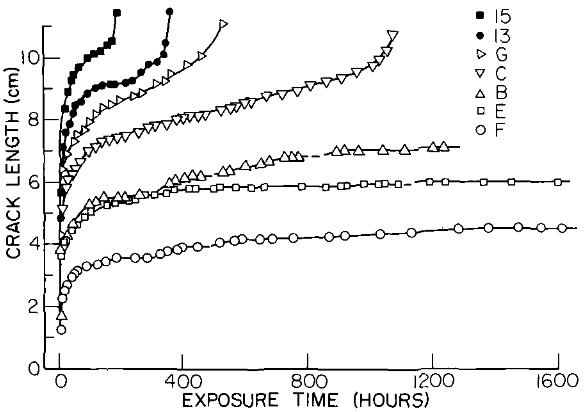

FIG. 3—*Crack extension curves for typical specimens over a range of initial stress-intensity values. Solid data points are for seawater tests and open points for NaCl distilled water.*

characteristic of the cracking process itself rather than experimental scatter or random, periodic arrestment and advance, is suggested by Fig. 4 which presents data from opposite faces of the same specimen. This shows that, while the crack does not grow with exact correspondence on the two faces, still occurrence of the plateau and subsequent steps correlate well from one side to the other. For engineering purposes of projecting structure life it would be acceptable to place a smooth curve through the data in Figs. 3 and 4, thereby disregarding plateaus and steps; but if the cracking mechanism *per se* is of interest, then these individual features (plateaus and steps) must be considered. These data (Fig. 3) revealed no major differences in crack extension behavior for seawater tests, as compared to

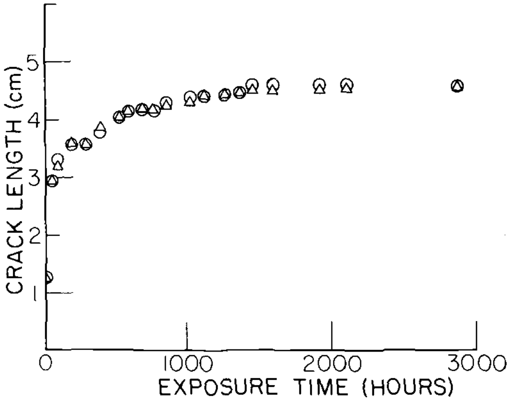

FIG. 4—*Crack extension data from opposite faces of Specimen F.*

NaCl distilled water. This aspect of the present experiments, along with a rationalization of the stepwise growth at long exposure times (see item 3 previously mentioned) is discussed in detail elsewhere [*19*].

Stress-Intensity Determinations

In several past experiments [*3*] the equation of Mostovoy et al [*20*] has been used to calculate plane-strain stress intensity of DCB specimens. This expression is

$$K_I = \frac{vEh(3h(a + 0.6h)^2 + h^3)^{1/2}}{4((a + 0.6h)^3 + h^2a)} \quad (1)$$

where

v = crack or notch opening displacement at the point of load application,
E = Young's modulus (7.10×10^{10} MN/m^2),
a = crack length, and
$2h$ = the specimen height (3.24 cm).

Because the data in Fig. 3 exhibits complex trends (plateaus and steps), which were not anticipated based upon Eq 1, it was considered necessary to either confirm applicability of the Eq 1 or to develop an alternative technique for evaluating K_I. This latter technique was accomplished by experimental determination of compliance based upon the relation [*21*]

$$K_I = \frac{v}{c}\left(\frac{E}{2b}\right)^{1/2}\left(\frac{dc}{da}\right)^{1/2} \quad (2)$$

where

c = compliance and
b = specimen thickness.

Compliance was determined by deflecting long-notch DCB specimens in an Instron testing machine and monitoring deflection v as a function of applied load. Various crack lengths for compliance specimens were affected by three techniques: (*a*) precracking, (*b*) jeweler's saw cut, and (*c*) 1.59 mm (0.063 in.) band saw cut. Resultant data as a function of crack or saw cut length are presented as Fig. 5, and it is apparent that no significant variation for the three specimen types (mechanical precrack, jeweler's saw cut, or band saw cut) is evident. Thus, removal of material by band or jeweler's saw (or, alternately, by machining a notch) did not alter the moment of inertia of the specimens to a degree detectible by the present analysis. Plane-strain stress intensity, as evaluated from this and Eq 2, is plotted versus crack length in Fig. 6. Also included is a K_I versus a curve based upon Eq 1. These show that for long-notch specimens with crack

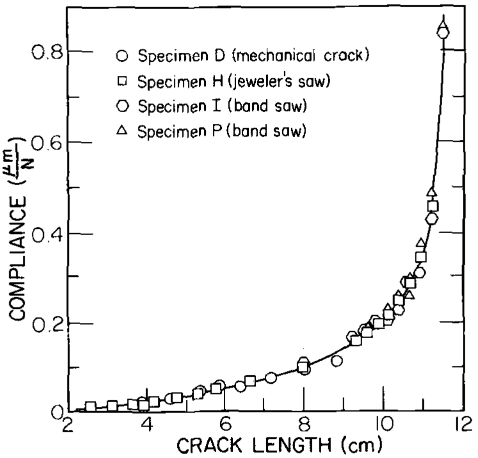

FIG. 5—*Compliance data as a function of crack (or saw cut) length.*

lengths less than about 8 cm differences between the two techniques are less than about 10 percent. As a crack extends beyond this length, however, experimental compliance data decrease less rapidly than predicted from Eq 1. At a crack length of approximately 10.5 cm, analysis in terms of experimental data and Eq 2 projects that K_I increases sharply with further crack extension. Experimental compliance determinations on DCB specimens by Dahlberg [*18*] have revealed this same trend (increasing stress intensity as the crack approaches the back specimen face), and his rationalization has been in terms of a "ligament dependent state," as projected originally by Srawley and Gross [*22*].

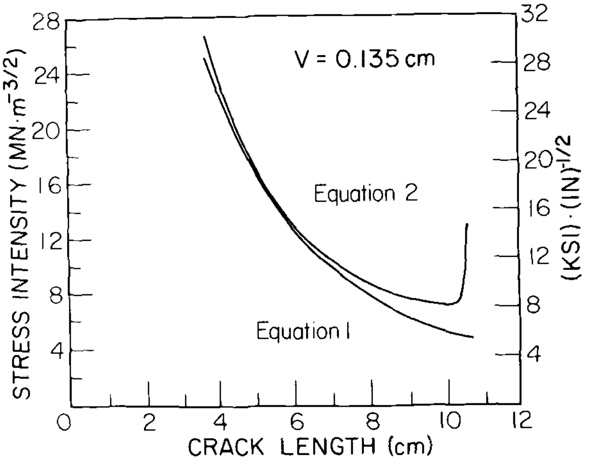

FIG. 6—*Stress intensity as a function of crack length as determined by Eq 1 and by Eq 2.*

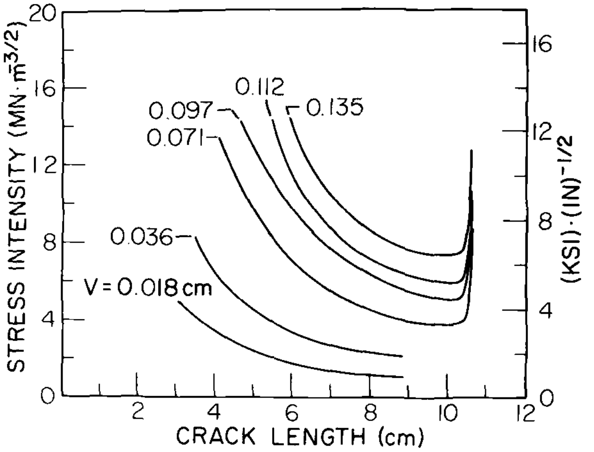

FIG. 7—*Stress intensity as a function of crack length for deflections discussed in text (Table 2).*

Compliance data as a function of crack length for each specimen deflection employed in the present tests are presented as Fig. 7. Curves applicable to long-notch specimens (Table 2) were calculated from Eq 2, whereas those for short-notch specimens are based upon Eq 1. From these the stress intensity corresponding to any crack length for any specimen in Fig. 3 can be readily determined. Figure 7 projects, however, that the plateaus and steps evident in Fig. 3 cannot be related to anomalous or unexpected stress-intensity trends.

Crack Velocity Characteristics

Figure 8 shows typical crack length-time curves for the first 300 h of each test and for a range of initial stress intensity (Table 2). This points up that initial crack-growth rate (exposure time <25 h) in most specimens was high and varied in proportion to K_{Ii}. It is within this initial phase of tests that the Region II or stress independent mode of growth probably occurred for those specimens stressed to sufficiently high K_{I} values. Subsequent to about 25 h exposure, however, crack extension for all specimens appears similar, and the various curves are but displaced relative to one another along the vertical axis. This suggests that crack-growth rate in this range may be influenced more by exposure time t than by stress intensity. This latter point is also illustrated by the K_{I} values listed in Fig. 8, which correspond to the plateau crack length of each specimen. Further, Fig. 9 projects crack-growth rate/stress-intensity curves, based upon the data in Fig. 8, and this indicates that for exposure times between about 25 and 200 h crack-growth rate of long-notch specimens is a function of K_{Ii}. A

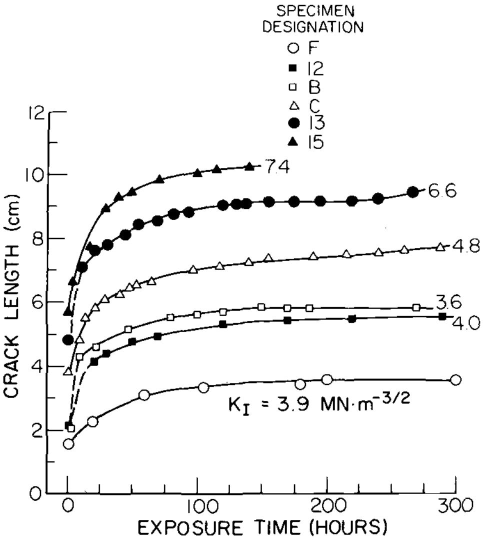

FIG. 8—*Crack extension curves for typical specimens and for a range of initial stress intensity (Table 2).* K_I *values on figure represent the stress intensity corresponding to the plateau crack length.*

unique $(da/dt) - K_I$ relation is observed for short-notch specimens, irrespective of initial stress intensity, and this is the same as for long-notch specimens of small $K_{Ii}(K_{Ii} \lesssim 0.45\ K_{Ic})$. For comparison purposes data of Speidel et al [*3*] are also shown.

From SCC experiments upon 4340 steel, Landes and Wei [*23*] observed initial values of crack growth rate to depend upon K_{Ii} as well as K_I. Their specimens were of an increasing stress-intensity type, however, and the initial transients they noted were related probably to a start-up time for the crack-growth process. Wei et al [*24*] have discussed decreasing stress-intensity specimens and pointed up that a small stress-intensity gradient is desirable if transients are to be avoided. However, for the present tests, plateaus were noted even in the crack length range 9 to 10 cm (see specimens 13 and 15 in Fig. 3). Analysis of K_I for these specimens (Fig. 7) projects that, at least to a first approximation, stress intensity is relatively independent of crack length in this range (9 to 10 cm). Thus, factors other than the transients discussed by Wei et al [*24*] were probably responsible.

An alternative point just made is that for $25 \lesssim t \lesssim 200$ h crack extension curves were all of the same general form (Fig. 8). Thus, Fig. 10 is a plot of log da/dt versus t, and this shows crack-growth rate for all specimens to differ by no more than a factor of two or three over the range $25 \lesssim t \lesssim 150$ h. Subsequent to 150 h crack length either remained un-

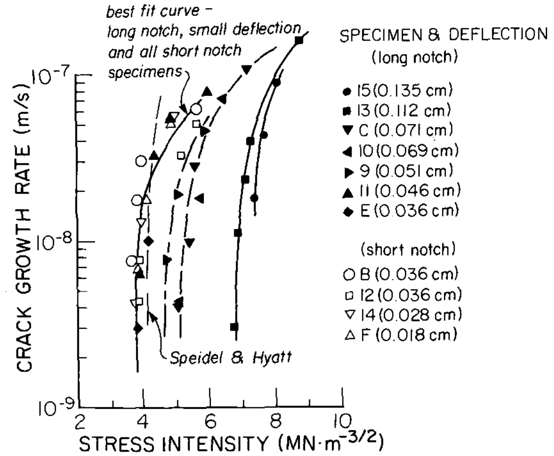

FIG. 9—*Crack-growth rate versus stress intensity for typical specimens.*

changed, corresponding to the lower bounding line in Fig. 10, or increased at an approximately constant rate (upper line). The apparent dependence of crack-growth rate upon K_{Ii} (Fig. 9) can be related to exposure time. In this regard a vertical line in Fig. 9 corresponding to constant stress intensity intersects the crack-growth curves in an order inversely proportional to *t,* that is, lowest crack-growth rate corresponds to greatest exposure time.

The observation that crack-growth rate for the present alloy and test conditions was not singularly related to stress intensity is significant. That previous investigators have projected such a relationship is probably a consequence of their employing a single K_{Ii} and but one specimen geom-

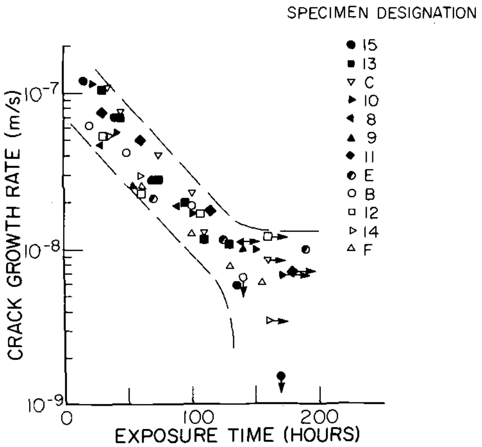

FIG. 10—*Crack-growth rate as a function of exposure time.*

etry. For the present tests the fact that two notch lengths and a range of initial stress intensities were used permitted the time dependence (alternately, stress-intensity independence) of crack-growth rate to be recognized.

It has been considered that corrosion product wedging [*17,25*] and resultant, enhanced crack face displacements with increasing t could result in exposure time-dependent crack growth. No experiments to determine definitively if this was the case in the present tests were performed; however, periodic measurement of deflection v for several specimens showed this parameter to remain unchanged, even for the longest tests. It is perhaps significant that upon fracturing specimens tested in NaCl distilled water considerable corrosion product was noted within the crack. For specimens tested in seawater, however, presence of such corrosion product was much less apparent from visual observation.

A second possibility is that stress-intensity independent crack-growth rate may be due to variations in electrochemical potential in the crack-tip vicinity; however, no attempt was undertaken in the present investigation to determine potential in this region. Occasional measurement of potential with a reference electrode positioned several centimetres from specimens revealed values in the range −0.88 to −0.79 V (saturated calomel electrode (SCE)), and no trend with regard to exposure time was evident.

Also considered was that crack front bowing or differences in crack-growth rate at the specimen center and external surface may be important. At least one previous study [*26*] has shown this can be highly significant. To investigate this, crack front profile for each specimen was examined subsequent to testing. Additionally, several specimens were stressed and exposed for times ranging from 50 to 200 h. These were then fractured and examined also. Resultant data are presented as Table 3, revealing that the crack tip at the free surface lagged that at the specimen center by from 0.20 to 0.69 cm. While there is evident here that a trend for crack-tip bowing is more pronounced at greater exposure times, still nothing is apparent from Table 3 to suggest that plateaus or K_I independent crack growth ($25 \lesssim t \lesssim 150$ h) are anomolies of specimen or crack-front geometry.

TABLE 3—*Crack front profile dimensions for SCC specimens.*

Specimen Number	Exposure Time, h	Crack Length, Specimen Edge, cm	Crack Length, Specimen Centerline, cm	Crack Length Differential, cm
B	1 234	7.11	7.52	0.41
E	5 088	6.22	6.91	0.69
8	13 945	8.15	8.70	0.55
9	12 612	8.32	8.79	0.47
R	50	5.59	5.33	0.26
S	75	5.04	5.24	0.20
T	100	4.96	5.33	0.37
U	202	5.35	5.69	0.34

Although it has been reported that crack-growth rate at low-stress intensities is independent of chloride ion concentration, within Region II of (da/dt) versus K_I plots this parameter varies in direct proportion to halide concentration of the electrolyte [*3*]. This has prompted a mass-transport-kinetics (MTK) explanation of cracking rate, whereby crack extension is controlled by diffusion rate of chloride ions to the crack-tip region. To determine if plateau segments of the present crack extension curves were sensitive to Cl^- concentration tests were conducted using two NaCl concentrations other than the 3 percent specified earlier. As noted in Fig. 11 crack-growth rate in the pre-25 h range did vary in direct proportion to Cl^- concentration, but beyond this no effect from salt concentration was apparent. Thus, sensitivity of Region II crack-growth rate to salt concentration does not extend to the present range of stress-intensity independent behavior. It cannot be ruled out, however, that transport kinetics of an ion other than chloride were controlling.

The fact that the present specimen geometry and material properties were well within established limits for plane-strain testing, as specified by the relationship in ASTM Test for Plane-Strain Fracture Toughness of Metallic Materials (ASTM E 399)

$$b = 2.5\left(\frac{K_{Ic}}{ys}\right)^2 \tag{3}$$

suggests that there should be no anomalous crack extension due to mixed or variable fracture mode [*1,26*].

A more realistic possibility is that SCC rate is controlled by some limiting aspect of the dissolution process. In this regard Poulose et al [*27*] proposed that galvanic effects from intergranular $MgZn_2$ control cracking rate within a K_I independent region for a high-purity Al-5.5Zn-2.5Mg alloy. Also, Sedriks et al [*28*] have considered that stress-corrosion crack-growth rate of a special purity Al-5.35Zn-2.52Mg alloy is under cathodic reac-

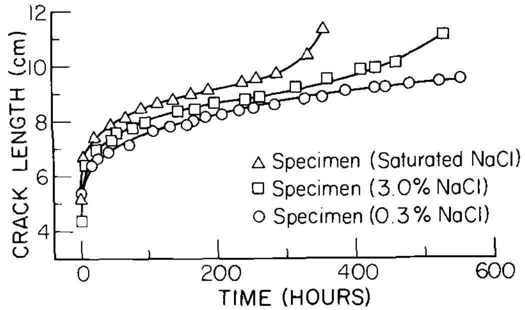

FIG. 11—*Crack extension curves for three concentrations of NaCl. Deflection* v *for each was 0.097 cm.*

tion control. An interesting observation with regard to fracture faces of the present specimens is the appearance of bright regions [*29*], two examples of which are pictured in Fig. 12. Thus, the bulk of the fracture face across which the stress-corrosion crack has propagated was heavily corroded, but within the region indicated corrosion appeared very slight, and the boundary between the two is quite distinct. It is not unrealistic that these bright regions were sites for cathodic reactions that occurred in conjunction with an anodic one at the crack tip. Supporting this is the finding that the bright region surface area varied directly with crack velocity. For example, Fig. 12*a* corresponds to a crack-growth rate of 2.6×10^{-8} m/s, while in Fig. 12b da/dt is zero. Arguing that corrosion has simply not had time to develop on these portions of the fracture faces is inappropriate, since such areas were evident even where cracks had arrested for several thousand hours.

In a confined region such as a stress-corrosion crack pH is influenced by solubility of corrosion products [*30,31*], and both theoretical and experimental considerations have concluded this to be about 3.5 in the case of aluminum [*32*]. It is recognized that reaction products from corroding aluminum transform with time, proceeding from the initial, least stable aluminum hydroxide ($Al(OH)_3$) to the most stable hydrargillite ($Al_2O_33H_2O$). This process is commonly referred to as "aging." At least one investigation has considered that this may be significant with regard to SCC [*33*]. It is also possible that the bright areas just described are related to aging of corrosion products and associated pH changes. The change in crack growth from stress-intensity dependent to time dependent after approximately 25-h exposure or occurrence of the plateau or near-plateau at approximately 200 h may be coupled to this. Further experiments are necessary, of course, to deduce the full significance of corrosion products and crack-tip pH to the cracking process.

Additional possible mechanisms such as stress sorption, film rupture and repair, and hydrogen embrittlement are viewed generally as stress-intensity dependent and, as such, should not be applicable to the present tests for exposure times between 25 and 200 h. It may be argued, however, that if cracking rate is governed by interaction of environment with defect structure of the plastic zone and if occurrence of this is insensitive to dislocation density and plastic zone size, then the preceding processes (stress sorption or others) could apply.

Conclusions

1. Within Region I of the crack-growth rate/stress-intensity plot 7079-T651 aluminum in 3 percent NaCl distilled water or seawater exhibited crack extension behavior characterized by plateaus, linear segments, and steps.

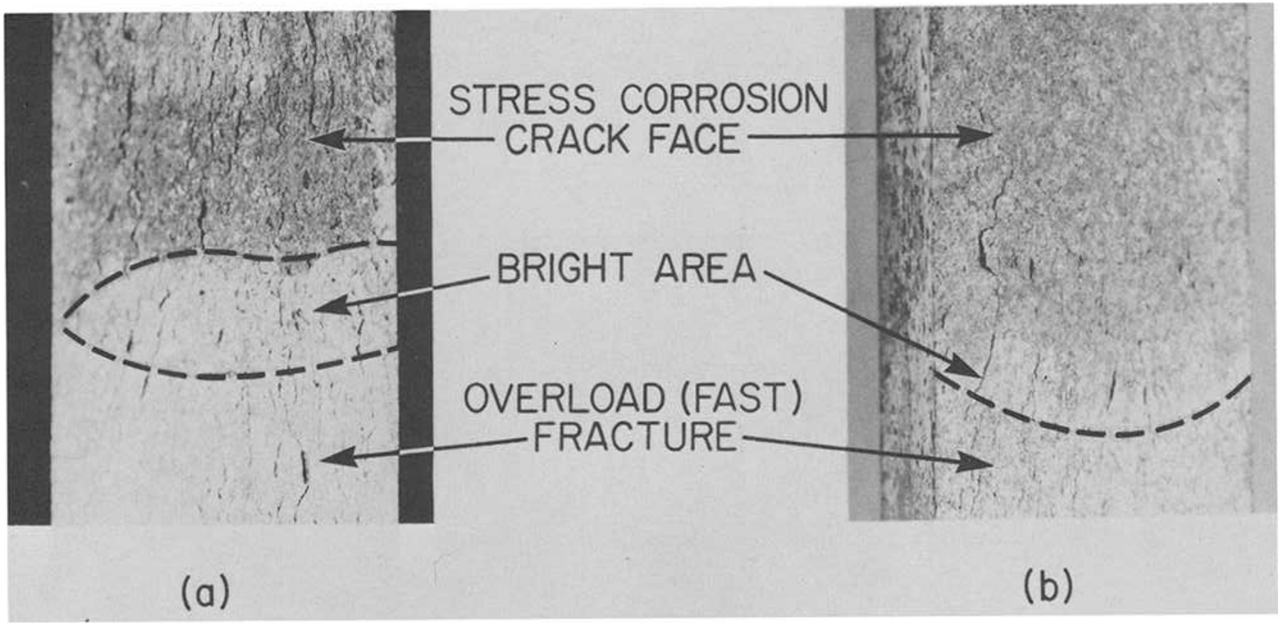

FIG. 12—*Two examples of specimen fracture faces illustrating crack front bowing and "bright region" adjacent to the crack tip.*

2. All short-notch specimens and long-notch specimens with initial stress intensity below approximately 0.5 K_{Ic} exhibited a singular (da/dt) versus K_I relation. No such correlation was apparent for long-notch specimens with initial stress intensity greater than 0.5 K_{Ic} however, and so for these tests no unique correspondence of crack-growth rate to stress intensity was evident.
3. Stress-corrosion crack-growth rate in 7079-T651 aluminum for $25 \lesssim t \lesssim 200$ h varied inversely with exposure time.
4. Occurrence of time dependent (stress-intensity independent) crack growth is consistent with a model whereby the nature of the local crack environment exerts a controlling influence.

Acknowledgment

The authors wish to express gratitude to the Florida Atlantic University Division of Sponsored Research for partial financial support and to John Yeend for assistance with the experiments.

References

[*1*] Johnson, H. H. and Paris, P. C., *Journal of Engineering Fracture Mechanics,* Vol. 1, 1968, p. 3.
[*2*] Brown, B. F., *Metallurgical Reviews,* Review 129, 1968, p. 171.
[*3*] Speidel, M. O. and Hyatt, M. V. in *Advances in Corrosion Science and Technology,* Vol. 2, M. G. Fontana and R. W. Staehle, Eds., Plenum Press, New York, 1972, p. 115.
[*4*] Sprowls, D. O. and Brown, R. H. in *Proceedings Fundamental Aspects of Stress Corrosion Cracking,* R. W. Staehle, A. J. Forty, and D. van Rooyen, Eds., National Association of Corrosion Engineers, Houston, Tex., 1969, p. 489.
[*5*] Thomas, G. and Nutting, J., *Journal of the Institute of Metals,* Vol. 88, 1959–1960, p. 81.
[*6*] Pugh, E. N. and Jones, W. R. D., *Metallurgia,* Vol. 63, 1961, p. 3.
[*7*] McEvily, A. J., Jr., Clark, J. B., and Bond, A. P., *Transactions Quarterly,* American Society for Metals, Vol. 60, 1967, p. 661.
[*8*] Sedriks, A. J., Slattery, P. W., and Pugh, E. N., *Transactions Quarterly,* American Society for Metals, Vol. 62, 1969, p. 238.
[*9*] Holl, H. A., *Corrosion,* Vol. 23, 1967, p. 173.
[*10*] Speidel, M. O. in *Proceedings Fundamental Aspects of Stress Corrosion Cracking,* R. W. Staehle, A. J. Forty, and D. van Rooyen, Eds., National Association of Corrosion Engineers, Houston, Tex., 1969, p. 561.
[*11*] DeArdo, A. J., Jr., and Townsend, R. D., *Metallurgical Transactions,* Vol. 1, 1970, p. 2573.
[*12*] Lifka, B. W. and Sprowls, D. O. in *Stress Corrosion Testing, ASTM STP 425,* American Society for Testing and Materials, 1967, p. 342.
[*13*] Romans, H. B. and Craig, H. L., Jr., in *Stress Corrosion Testing, ASTM STP 425,* American Society for Testing and Materials, 1967, p. 363.
[*14*] English, G. C. and Hollingsworth, E. H., "Investigation of the Mechanism of Stress Corrosion of Aluminum Alloys," U. S. Navy, Bureau of Naval Weapons Contract NOW 64-0170c, Final Report, 1965.
[*15*] McHardy, J. and Hollingsworth, E. H., "Investigation of the Mechanism of Stress Corrosion of Aluminum Alloys," U. S. Navy, Bureau of Naval Weapons Contract NOW 65-0327f, Final Report, 1966.

[*16*] Mulherin, J. H. and Rosenthal, H., *Metallurgical Transactions,* Vol. 2, 1971, p. 427.

[*17*] Hyatt, M. V., *Corrosion,* Vol. 26, 1970, p. 487.

[*18*] Dahlberg, E. P., "Stress and Corrosion Environments (characterizing Stress-Corrosion Cracking in a 7079-T651 Aluminum Alloy by Using a Self-Stressed Double Cantilever Beam Specimen)," Report of NRL Progress, National Research Laboratory, Washington, D.C., Aug. 1968, p. 25.

[*19*] Finnegan, J. E. and Hartt, W. H., to be submitted to *Corrosion.*

[*20*] Mostovoy, S., Crosley, P. B., and Ripling, E. J., *Journal of Materials,* Vol. 2, 1967, p. 661.

[*21*] Irwin, G. R. in *Handbook der Physik,* Springer, Berlin, Vol. VI, 1958, p. 551.

[*22*] Strawley, J. E. and Gross, B., *Materials Research and Standards,* Vol. 7, 1967, p. 155.

[*23*] Landes, J. D. and Wei, R. P., to be published.

[*24*] Wei, R. P., Novak, S. R., and Williams, D. P., *Materials Research and Standards,* Vol. 12, 1972, p. 25.

[*25*] Pickering, H. W., Beck, F. H., and Fontana, M. G., *Corrosion,* Vol. 18, 1962, p. 230t.

[*26*] Williams, D. N., *Metallurgical Transactions,* Vol. 5, 1974, p. 2351.

[*27*] Poulose, P. K., Morral, J. E., and McEvily, A. J., *Metallurgical Transactions,* Vol. 5, 1974, p. 1393.

[*28*] Sedriks, A. J., Green, J. A. S., and Novak, D. L., *Metallurgical Transactions,* Vol. 1, 1970, p. 1815.

[*29*] Speidel, M. O., "Stress Corrosion Crack Growth in Aluminum Alloys," presented at NATO Conference on Stress Corrosion Cracking in Alloys, Portugal, 1971.

[*30*] Edeleanu, C. and Evans, U. R., *Transactions of the Faraday Society,* Vol. 47, 1951, p. 1121.

[*31*] Pourbaix, M., *Atlas of Electrochemical Equilibria in Aqueous Solutions,* Pergamon Press, New York, 1966, p. 186.

[*32*] Rosenfeld, I. L. and Marshakov, I. K., *Zhurnal Fiziccheskoi Khimii,* Vol. 31, 1957, p. 2328.

[*33*] Sedriks, A. J., Green, J. A. S., and Novak, D. L., *Corrosion,* Vol. 27, 1971, p. 198.

B. Cina[1] *and T. Kaatz*[1]

Learning from Experience of the Stress-Corrosion Failure of High-Strength Aluminum Alloy Forgings

REFERENCE: Cina, B. and Kaatz, T., **"Learning from Experience of the Stress-Corrosion Failure of High-Strength Aluminum Alloy Forgings,"** *Stress Corrosion—New Approaches, ASTM STP 610,* American Society for Testing and Materials, 1976, pp. 61–71.

ABSTRACT: Despite the extensive literature on the subject and the known methods for preventing stress corrosion, the users of high-strength aluminum alloys are still on occasion faced with this problem particularly in wrought components. Examples from actual experience with aircraft forgings are cited to emphasize the susceptibility of the transverse direction, particularly at parting lines, and the complex and often unpredictable role of residual stresses. Despite the absence of a specific short transverse direction, cylindrical forgings can show considerable susceptibility in their single transverse direction. Attention is drawn to the possibly dangerous combination of stresses resulting from heat treatment, machining, and interference assemblies.

It is shown that the mere presence at the surface of a forging of residual compressive stresses resulting from heat treatment is no guarantee that stress-corrosion failure will not initiate from such a surface.

Residual stresses developed along the inside diameter of a blind hole on quenching are a major unknown, and methods for obviating such difficulties are discussed.

In addition to the factors known to affect stress-corrosion susceptibility, there would also seem to be a batch factor whereby some apparently small and temporary modification in manufacturing procedure can increase the susceptibility to stress corrosion significantly.

An example is quoted of the minute amount of moisture found sufficient to initiate a stress-corrosion failure.

The necessity is discussed and emphasized for determining the nature and gradient of residual stresses adjacent to potentially critical surfaces as a stage in the qualification of prototype forgings.

KEY WORDS: stress corrosion, cracking (fracturing), aluminum alloys, forgings, residual stress, quenching, assembly stresses, machining, blind holes, corrosive medium

---

[1] Chief metallurgist and senior physicist, respectively, Materials and Process Engineering, Engineering Division, Israel Aircraft Industries Ltd., Lod, Israel.

Our knowledge and understanding of stress corrosion, particularly of high-strength aluminum alloys, has considerably advanced in the past ten years as attested in a-state-of-the-art symposium [*1*].[2] Even in a symposium held in 1966 [*2*], confidence was expressed that designers were by then able to deal with the shortcomings of these alloys. Nevertheless, their users are still plagued occasionally by stress-corrosion failures. It is suggested that there are two principal reasons for this: the inevitable interval in getting laboratory results into practice through designers and manufacturers and the predominantly qualitative manner in which the role of residual stresses has been treated. This paper will be concerned with the latter topic, since it has largely been neglected at least from the quantitative aspect, and our experience has shown that it can be a major factor in causing stress-corrosion failure. Details will be given of three specific stress-corrosion failures of high-strength aluminum alloys with particular attention being paid to the role played by residual stresses, both tensile and compressive.

Procedure

Standard optical and scanning electron microscope techniques were used to identify the cracks in the stress-corrosion failures.

A quantitative assessment of residual stresses was made by X-ray diffraction employing copper $K\alpha$ X-radiation and a standard two exposures technique [*3*]. Silver powder was used to determine specimen-film distance. The accuracy of the residual stress measurements is estimated to be ±2 kpsi (±13.8 MN/m^2).

Specific Stress-Corrosion Failures

Failure Initiating from a Zone of Residual Compressive Stress

A flap actuator in the form of a cylinder of inside diameter 1⅜ in. and wall thickness ⅛ in. failed after 63 h of service. The cylinder was made from a 7075-T6 aluminum forging. The flap was hydraulically operated, and oil was found leaking out of a crack extending over almost the full length of the cylinder, the crack being located in the parting line of the forging. The cylinder was sectioned longitudinally so as to expose the crack which is shown in Fig. 1. The zone in which the failure initiated is shown arrowed. It was found that this zone contained several cracks all of which originated at the outside diameter of the component, and extended to a depth of up to 1⁄10 in. and over a distance of just over 1½ in.

---

[2] The italic numbers in brackets refer to the list of references appended to this paper.

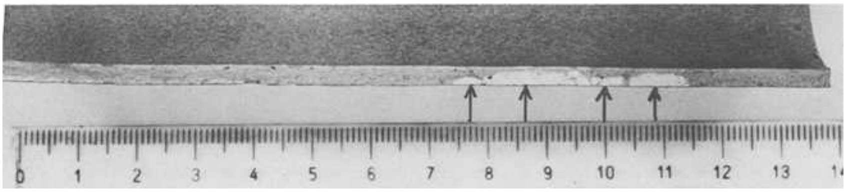

FIG. 1—*Stress-corrosion cracks visible on the fracture surface of a flap actuator cylinder of 7075-T6 aluminum. Dimensions are in centimetres.*

Metallographic examination showed the initiating cracks to be intergranular, a feature subsequently confirmed by scanning electron microscopy. The latter likewise showed the grains in these cracks to be very thin and plate-like as would be expected in the region of the parting line of the forging. A scanning electron micrograph of the fracture is shown in Fig. 2.

Since the parting line region on the outside diameter of the forging had not been machined, compressive residual stresses should have been present at the surface so that stress corrosion had presumably not been anticipated.

X-ray diffraction examination carried out on another identical but intact cylinder showed a residual compressive hoop stress present of only 2 kpsi (13.8 MN/m^2). Calculation showed that the hydraulic pressure operating in the cylinder would have developed a hoop tensile stress of about 15.3 kpsi (105.8 MN/m^2) on the outside surface. The net tensile hoop stress experienced on the outer diameter of the cylinder therefore, would, have been about 13 kpsi (89.7 MN/m^2) which is above the threshold value of 7 kpsi (48.3 MN/m^2) for stress-corrosion cracking in this alloy [*4*].

The level of the residual compressive stress observed was much smaller than expected. Since precise details of method of manufacture of the cylinder were not available, an attempt was made to establish this experimentally. A solid bar of 7075 aluminum of the same outside diameter as that of the cylinder was heat treated to bring it to the T6 temper. Quenching from the solution treatment temperature was carried out in water at ambient temperature. In the T6 condition, a residual compressive hoop stress of 24 kpsi (165.6 MN/m^2) was determined by X-ray diffraction on the unmachined outer diameter of the bar. This bar was then bored to form a cylinder with a blind hole and a wall thickness of ⅛ in. in simulation of the cylinder which failed in service. Reexamination by X-ray diffraction of the outer diameter of the cylinder showed a residual compressive hoop stress of only 3 kpsi (20.7 MN/m^2). These results would suggest that the cylinder which failed had been machined from a solid forging after final heat treatment. The relative merits of machining prior to and after heat treatment, with respect to residual stresses, will be dealt with in the discussion.

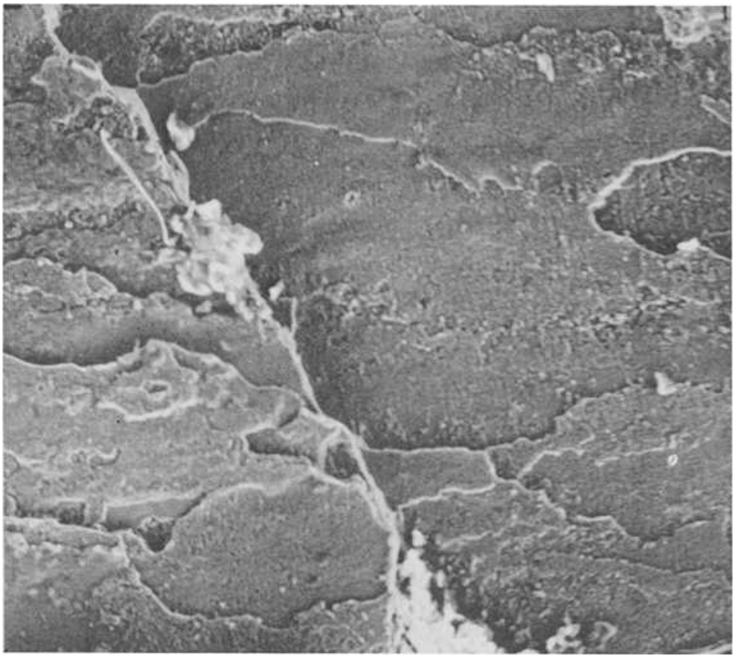

FIG. 2—*A scanning electron micrograph of the surface of one of the stress-corrosion cracks visible in Fig. 1, showing plate-like grains and intergranular cracking (×2000).*

There remains the question of the corrosive medium. The part in question is anodized and painted prior to being put into service. Although the part is not exposed to rain, it is exposed to the atmosphere and particularly to fairly heavy dew conditions which occur during the night and early morning. Furthermore, it was found that the paintwork in service parts was often locally damaged on the parting line which is a zone raised somewhat above the rest of the forging. Accordingly it would seem that minor damage due to handling during maintenance was responsible for locally removing the protective paintwork on the parting line and so exposing bare metal to atmospheric humidity. Since few regions in Israel are far from the coast, there may well have been a relatively high salt content in the atmosphere which would have accelerated the stress corrosion.

Failure Initiating from the Inner Diameter of a Landing Gear Cylinder with a Blind Hole

Classical intergranular stress-corrosion failures occurred along the parting line of several tubular forgings intended for a landing gear. The part was made of 7079-T6 aluminum of 72 kpsi (497 MN/m^2) minimum tensile strength. It had a bore mainly of 2.5 in. diameter and 15 in. length, and a wall thickness of 0.28 in. The bore was closed at one end with no vent hole. Rough machining was carried out prior to heat treatment, and quenching from the solution heat treatment temperature was carried out with the tube lying horizontally. Quenching was in water at 140°F (60°C).

Cracking occurred several months after heat treatment and final machining, while the parts were lying in stores. The crack in several cases extended through the full wall thickness of the forging and was up to 7 in. in length. Cracks were never obtained at the ends of the forging. The reason for this became apparent later.

A view of the greater part of the length of the crack in a more extreme case is shown in Fig. 3. The fracture had a scaly appearance typical of stress-corrosion cracks occurring along the parting line of a forging, the scaliness being due to the pack structure of very thin grains in this region. Whereas in one instance cracking may have been nucleated by fine long scratches introduced inadvertently during the final machining and dimensioning of the bore, cracking was also observed without such scratches.

Barker and Turnbull [5] have determined the residual stresses in the 2.9 in. diameter bore of a 7079-T6 aluminum tubular forging, of wall thickness 0.45 in. and bore length 25½ in., that is, akin to the one under consideration. Their forging was likewise rough machined before solution treatment, quenching was carried out in water, and again there was no vent hole. Circumferential tensile stresses of 10.3 and 18.1 kpsi (73.1 and 124.9 MN/m^2) were determined at two separate points in the half of the bore furthest from its open end. In view of the similarity of the two cases, it is reasonable to assume that stresses of similar type and magnitude were present in the case under investigation.

Using X-ray diffraction technique, we determined the circumferential residual stress on the outer surface of the cylinder and in the inner diameter of the bore at points about 0.25 in. from its open end, that is, where cracking was never experienced. Residual compressive stresses of 25 and 21 kpsi (172.5 and 144.9 MN/m^2) were observed. The presence of a residual compressive stress in the bore would be due to the ability to ob-

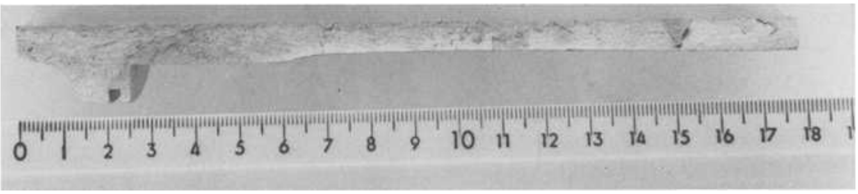

FIG. 3—*Stress-corrosion cracking through the full-wall thickness of a landing gear cylinder of 7079-T6 aluminum. Dimensions are in centimetres.*

tain efficient quenching at a point close to its open end, whereas residual tensile stresses would be formed further in the bore due to the difficulty of obtaining water circulation at these locations. In fact, the level of the residual compressive stress formed on quenching may well have been somewhat higher than that measured, since the bore was final machined after heat treatment. The presence of a high-residual compressive stress in the bore close to its open end would explain why stress-corrosion cracks never extended to this point but were always confined to the innermost and more central regions of the bore.

With regard to the corrosive medium in the present instance, since the cracks were discovered in stores after shipment from the United States, it must be presumed that the medium was the atmosphere prior to shipment since full protective measures were taken to prevent corrosion during sea transportation. This point is discussed further in the next section.

Batch Factor

In the latter case described, reference was made to the fact that several forgings were found to have cracked. It is of interest to examine the actual number of parts involved. Over 100 forgings have been produced and put into service without any report of stress-corrosion cracking. Of a subsequent batch of six forgings, three were found to be cracked, as described, while still in stores. Almost a year later the remaining three forgings were still found to be sound.

Several months after the first incident, of a further batch of ten forgings, four were found to be cracked due to stress corrosion.

We were informed by the manufacturer of the forgings that all had been produced in a standard manner. Chemical analyses did not vary from the requirements of Federal Specification QQ-A-367,[3] and heat treatment conformed to Military Specification H-6088E.[4] Since all the forgings would have been produced with a similar relatively high level of residual circumferential tensile stress in the innermost regions of the bore, the possibilities for stress corrosion occurring therefore, would, seem to be as follows:

1. There may be, as yet, an unrecognized batch factor, possibly representing some adverse combination of variations in manufacturing parameters. Each such variation would be permissible in itself, but when several operate together they may be sufficient to affect adversely the stress-corrosion resistance of the alloy.
2. There may have been an inadvertently long exposure to the atmosphere of a freshly machined surface, possibly combined with high humidity

---

[3] U.S. Federal Specification QQ-A-367; Aluminum Alloy Forgings, 1968.

[4] U.S. Military Specification MIL-H-6088E; Heat Treatment of Aluminum Alloys, 1972.

FIG. 4—*Stress-corrosion crack in the parting line and through the full-wall thickness of a 7079-T6 aluminum forged landing gear (×0.8).*

and atmospheric contamination, prior to such surface being protected by approved corrosion preventative compounds as per requirements of Specification MIL-STD-649.[5] Since assurances were obtained from the manufacturer that inadvertently long exposures to the atmosphere did not occur, it would seem that the batch factor was responsible for the failures observed.

Case of Combined Residual Stresses

A crack was detected in the trunnion boss of several landing gears while still in storage prior to assembly on an aircraft. The crank extended through the full wall thickness of the trunnion boss, about $\frac{9}{16}$ in. (1.35 cm), as shown in Fig. 4, was over 3 in. (7.5 cm) long, and was located in the parting line of the forging. The part is made from 7079-T6 aluminum. A steel sleeve, shrunk fit into the trunnion boss, serves to hold a steel trunnion pin. Both sleeve and pin are visible in Fig. 4. On deliberate exposure of the fracture surface for examination, it was found that cracking commenced from the inner diameter of the trunnion boss, from two or three origins as shown in Fig. 5. The planes of the several cracks were separated from one another by only a few degrees, as measured radially

---

[5] U.S. Military Standard MIL-STD-649; Aluminum and Magnesium Products, Preparation for Shipment and Storage, 1969.

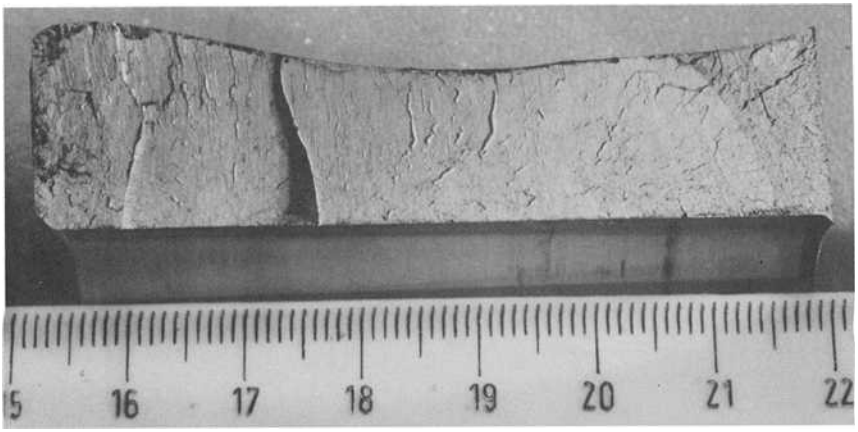

FIG. 5—*The surfaces of three stress corrosion cracks initiating from the inside diameter of a 7079-T6 aluminum landing gear forging* (the lower edge in the photograph) *and extending through its full-wall thickness. The flat scaly appearance is due to the thin plate-like structure of the grains in the parting lines. Dimensions are in centimetres.*

from the geometric center of the trunnion boss. The extreme flatness of the crack surfaces will again be noted. In explanation of this flatness, Fig. 6 shows the macrostructure of a transverse section of a trunnion boss in the region of the parting line. It will be seen that in the latter region the grains are very thin and elongated in the direction of the flow of metal during forging. The cracking was found to be intergranular. The evidence pointed to stress corrosion as the cause of the failure.

From an analysis of the manufacturing conditions it became apparent that the stresses required to cause the failure could have three combined causes: heat treatment, machining, and assembly of the gear.

The trunnion boss was machined after heat treatment. Barker and Turnbull [5] have shown that for a cylinder of 2.9 in. (7.4 cm) inside diameter, 3.8 in. (9.6 cm) outside diameter, and 0.45 in. (1.14 cm) wall thickness, machined after heat treatment, tensile hoop stresses up to over 6000 psi can be present on the bore surface. The dimensions of their cylinder are not so far removed from those in our investigation [1.75 in. (4.4 cm) inside diameter, 2.88 in. (7.3 cm) outside diameter, and 0.57 in. (1.44 cm) wall thickness], as to disqualify using their residual stress measurement as a guide to the situation present in our case.

The steel bushing was shrunk fit into the trunnion boss with tolerances on its outside diameter and on the inside diameter of the trunnion boss such that, in the extreme case, an additional tensile hoop stress of 9800 psi could have been developed in the bore of the trunnion boss.

FIG. 6—*Macrostructure of a transverse section through the parting line of a 7079-T6 aluminum landing gear forging showing the long thin grains in the immediate vicinity of the parting line (×3).*

Finally a probable small residual tensile stress may have been induced in the surface layers of the bore of the trunnion boss by machining, but since precise details of machining were not available, this can not be estimated.

In summary then, residual tensile hoop stresses may have been present in the bore of the trunnion boss up to a level of about 16 000 psi after insertion of the bushing. This figure is significantly above the threshold value of 7000 psi required for stress corrosion.

There remains the identification of the nature and source of the corrosive medium if the case for stress-corrosion failure is to be substantiated. The steel bushing, which was cadmium plated, was shrunk fit into the trunnion boss by a dual operation; cooling the steel bushing in liquid nitrogen to at least −120°F (−84°C), and heating the aluminum forging to 250°F (121°C). On removal of the bushing from the coolant and prior to its insertion into the trunnion boss, some condensation of moisture from the atmosphere on the bushing would be unavoidable. This moisture would be carried into the trunnion boss. On removal of the aluminum forging from the oven, the inner surface of the trunnion boss was painted with zinc chromate primer as a protection against galvanic corrosion from contact with the steel bushing. This compound contains molecules of water of crystallization, and there is the possibility that, at a temperature of 250°F (121°C), some decomposition of the primer occurred releasing some of the water molecules. In either case we are concerned with minute quantities of water being entrapped between the bushing and the trunnion boss.

After insertion of the bushing in the trunnion boss there is no possibility of a corrosive medium entering between the two surfaces.

The case for stress-corrosion cracking of the trunnion boss would seem to have been established.

Discussion

The fact that residual tensile or compressive stresses were found on the surfaces of heat treated aluminum forgings which failed by stress corrosion is not surprising or disturbing. What is disturbing is that the parts had to fail before apparently any attempt was made to determine whether residual stresses were present in the forgings and, if so, the type and level of these stresses.

In the first instance described stress corrosion initiated at an external surface having a residual compressive hoop stress of 2 to 3 kpsi (13.8 to 20.7 MN/m^2). The cylinder in question had apparently been bored after heat treatment so reducing the residual compressive hoop stress on the outside diameter from 24 kpsi (165.6 MN/m^2) to only 3 kpsi (20.7 MN/m^2). The latter was inadequate to counteract the service tensile hoop stress of 15.3 kpsi (105.8 MN/m^2). Had the part been bored prior to heat treatment a much higher residual compressive stress would have been left on the outer diameter and stress-corrosion failure would probably have been avoided.

In the second case quoted, stress corrosion initiated from the bore of a cylinder which had been bored prior to heat treatment. Here the correct action would have seemed to be taken, yet failure ensued. The reason for this was twofold; residual tensile hoop stresses were formed on the bore of the cylinder due to the bore being blind and therefore not permitting efficient flushing of the bore wall on water quenching from the solution heat treatment temperature. The second possible reason for failure of this cylinder may have been what was termed a "batch factor" for the particular alloy in question, 7079-T6 aluminum. Possibly little can be done about the batch factor, but more efficient quenching of bores can be achieved by the provision of suitably located and dimensioned vent holes, by the use of vent tubes, or by fountain quenching.. In the latter case a quenching fixture inserted into the bore allows water under pressure to flow over the entire surface of the bore, as described by Barker and Turnbull [5]. If none of the solutions proffered is practicable and the presence of residual tensile stresses in the bore is unavoidable, there should at least be recognition of the fact, and steps should be taken during manufacture to ensure that such surfaces are never left unprotected against moisture or contaminants (gaseous or otherwise) in the atmosphere.

In the particular case of stress-corrosion failure resulting from combined residual tensile stresses, not only was the total level of residual stress relatively high with respect to the threshold stress required for stress corrosion, 16 and 7 kpsi (110.4 and 48.3 MN/m^2), but it was apparently not realized that the minute amount of moisture entrapped between the aluminum alloy bore and the steel bushing would be sufficient to initiate stress corrosion.

Conclusions

There are three main conclusions to be drawn from the present work.

1. As much attention should be, henceforward, paid to determining the location, type, and level of residual stresses as is paid to determining mechanical properties in high-strength aluminum alloy components of the 2000 and 7000 types. This is particularly important for alloys whose tempers have a threshold value for stress corrosion of only 7 kpsi (48.3 MN/m^2) in tension. Such determinations should be made in the region of critical surfaces. Such information would be invaluable where fatigue is also a problem.

It is suggested tentatively that the ASTM Committee G-1 on Corrosion of Metals encourage a study of the possibility of such residual stress determination becoming a prerequisite in the qualification, for example, of prototype forgings. The intention would be that appropriate requirements would be eventually incorporated into military and other specifications for such hardware.

2. Clearly, as more precise quantitative data become available as to the total level of tensile stresses liable to be encountered by a part in service, they may necessitate the selection of a more stress-corrosion resistant alloy or temper.

3. Since only minute amounts of moisture are needed to initiate stress corrosion, care should be exercised that the surfaces bearing residual tensile stresses are never left unprotected whether during manufacture, shipment, or service.

Acknowledgments

The authors wish to thank M. Meron, manager, Materials and Process Engineering, for his suggestions and encouragement in preparing this report.

References

[*1*] Sprowls, D. O., Brown, R. H., and Shumaker, M. B. in *Stress Corrosion Cracking of Metals—A State of the Art, ASTM STP 518, A*merican Society for Testing and Materials, 1972, pp. 87–118.

[*2*] Craig, H. L., Jr. in *Stress Corrosion Testing, ASTM STP 425,* American Society for Testing and Materials, 1967, p. 2.

[*3*] Barrett, C. S. and Massalski, T. B. in *Structure of Metals,* McGraw-Hill, New York, 1966, pp. 472–474.

[*4*] Sprowls, D. O. and Brown, R. H., "Resistance of Wrought High Strength Aluminum Alloys to Stress Corrosion," Technical Paper No. 17, Aluminum Company of America, Pittsburgh, Pa., 1962.

[*5*] Barker, R. S. and Turnbull, C. K., *Metal Progress,* Nov. 1966, pp. 60–65.

R. W. Judy, Jr.,[1] *and R. J. Goode*[1]

Crack Growth in Heavy Section Titanium

REFERENCE: Judy, R. W., Jr., and Goode, R. J., **"Crack Growth in Heavy Section Titanium,"** *Stress Corrosion—New Approaches, ASTM STP 610,* American Society for Testing and Materials, 1976, pp. 72–81.

ABSTRACT: The integrity of structures that operate in the marine environment depends on both the resistance to the propagation of cracks and the resistance to fracture that are inherent to the structural material. Diagrammatic procedures have been established to analyze systematically the material thickness-stress level-defect size interactions that are implied by the basic characterizations and their relation to various types of structures. In the case of titanium alloys, the extremely rapid growth of stress-corrosion cracks in salt water effectively precludes the possibility of design use of the crack-growth rates; for this reason the design problem reduces to selection of materials to prevent stress-corrosion cracking (SCC) and to minimize corrosion-fatigue crack growth. In this paper, the results of experiments conducted for structural integrity analyses of two 2-in.-thick titanium alloys are presented to illustrate the procedures currently used to measure the basic properties of structural titanium alloys and to interpret these characterizations for structural behavior. One of the test materials was highly sensitive to salt water SCC and the other was immune. Use of the SCC Ratio Analysis Diagram concept as a framework for interpretation of the fracture resistance and SCC resistance of these materials is also illustrated.

KEY WORDS: stress corrosion, crack propagation, titanium alloys, fracture properties, environments, corrosion fatigue

The increasing use of high-strength metals for modern high-performance structures and the recent proliferation of formal requirements for design to ensure maximum structural integrity have created the need for a systems-type approach for analysis of potential crack growth and fracture in these structures. Fracture problems are more simple than slow crack growth, and several methods of designing to prevent catastrophic failure exist and are being used. Subcritical crack growth in a structure designed to be fracture-safe necessitates extensive maintenance and repair, which can be as severe a problem as fracture. For structures which must operate in seawater or in other corrosive environments, prevention of crack growth, as well as general corrosion, is a primary design factor.

---

[1] Head, Structural Mechanics Section, and head, Strength of Metals Branch, respectively, Naval Research Laboratory, Washington, D. C. 20375.

The most fundamental requirement in any analysis of structure performance is an accurate characterization of the appropriate material property that governs the phenomenon being considered. In the case of failure by fracture, test methods and analyses that enable designers to predict structural performance under given circumstances are available [*1*,*2*].[2] Similarly, the utilization of linear-elastic fracture mechanics for defining the threshold stress intensities for crack growth in aqueous environments is well documented and is advanced to the point where design procedures for analysis of potential crack growth exist [*3*], and standardization of test procedures is imminent. In the proposed requirements for stress-corrosion cracking (SCC) specimen design, two of the most important items are minimum dimensions of specimens and positive evidence that crack growth is present. It is obvious that the largest specimen that can be used is the most representative of material performance in heavy section applications and, at the same time, is the most likely to meet minimum specimen dimensional requirements. To demonstrate the methods of test and interpretation of the results in terms of the effect of crack growth on structural performance, the properties of two samples of heavy section titanium are presented in this report.

Materials and Procedures

The test materials were two samples (Coded A and B) of a commercially available titanium alloy in 2-in.-thick rolled plate form. Both samples were reduced to plate from the same ingot, but were processed and heat treated by different procedures to produce a sample of nominally 115 ksi yield strength that was sensitive to salt water SCC (Sample A) and one of nominally 100 ksi yield strength that was immune to SCC (Sample B). Standard 1-in. dynamic tear (DT) tests [*4*] were conducted for materials at each surface and at the center of the plate for both samples. Full-thickness cantilever-type [*5*] specimens 2 by 4 by 14 in. oriented in the T-L crack propagation direction were machined from each plate (Fig. 1). The specimens had chevron notches and were prefatigued to crack depths of approximately 2 in. by procedures conforming to the requirements of ASTM Test for Plane-Strain Fracture Toughness of Metallic Material (E 399-72) for determining K_{Ic}. Tests were conducted in hydraulic loading machines in an environment consisting of 3½ weight percent salt in distilled water. The environment was contained in a corrosion cell and was changed daily. After the threshold value of K was determined, a single specimen of each sample was tested in an air environment at applied K levels approximately 5 ksi$\sqrt{\text{in.}}$ below and 5 ksi$\sqrt{\text{in.}}$ above the threshold K.

---

[2] The italic numbers in brackets refer to the list of references appended to this paper.

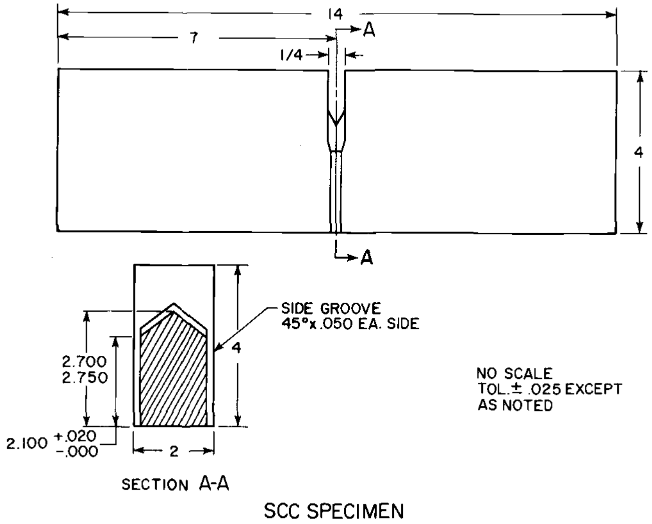

FIG. 1—*Specimen configuration for SCC tests of 2-in.-thick titanium plate materials.*

Results

The results of the DT and K_{Iscc} tests are shown in Tables 1 and 2 and in Figs. 2-5. The DT test results were averaged for each sample and then were used to extrapolate a value of K_{Ic} that the material might be expected to display if the thickness were sufficient to maintain plane-strain constraint. In neither material was the fracture resistance low enough to measure valid K_{Ic} for 2 in. thickness, and, therefore, the values of K_{Ic} extrapolated from the K_{Ic}-DT correlation derived for 3-in. plate [*6*] may not represent the true plane-strain fracture toughness of the material accurately. The intent of the extrapolation is to provide a general reference value of K for fracture to compare with K_{Iscc}; these values are included in Table 1.

A complete display of the test data used to define the sensitivity of Sample A to SCC is shown in Fig. 2. There are two important points on the scale of applied K. The first reference point is the maximum value of K that can be defined under purely plane-strain conditions, according to

TABLE 1—*Fracture resistance properties of 2-in.-thick Ti-6Al-2Cb-1Ta-0.8Mo plates.*

Alloy	1-in. DT Energy, ft·lb	K_{Ic} (extrapolated), ksi$\sqrt{\text{in.}}$	Max K for 2 in., ksi$\sqrt{\text{in.}}$
A	1650	138	103
B	1900	150	90

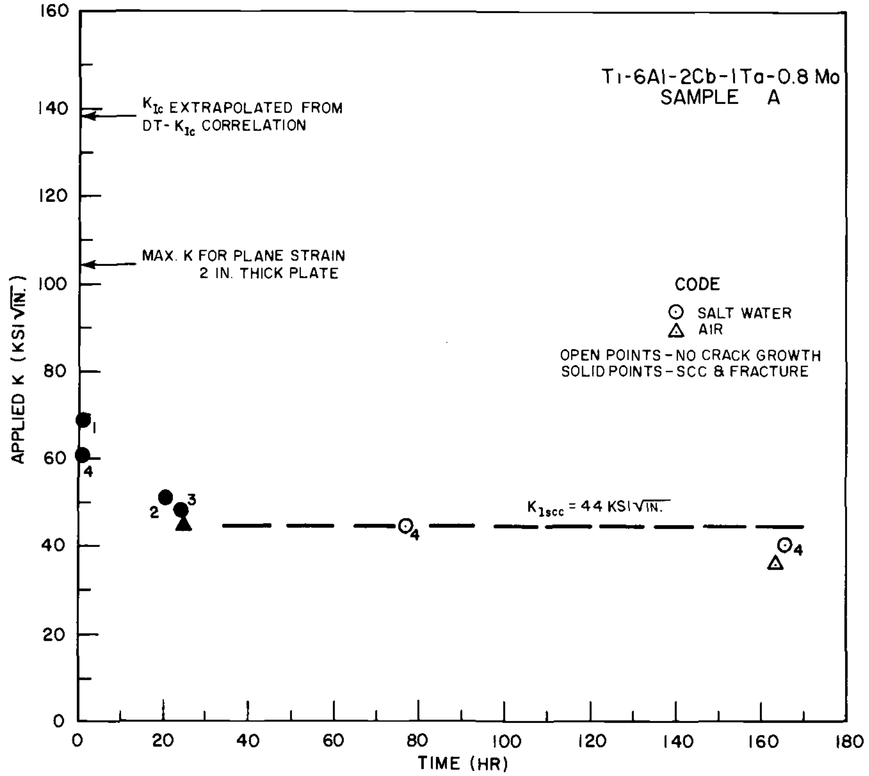

FIG. 2—*Test results for Sample A. The small numbers refer to the sequence in which the specimens were tested.*

TABLE 2—*SCC properties of 2-in.-thick Ti-6Al-2Cb-1Ta-0.8Mo plates.*

Speci-men No.	Environ-ment	No Failure		Failure		Remarks
		K, ksi$\sqrt{\text{in.}}$	Time, h	K, ksi$\sqrt{\text{in.}}$	Time, h	
A-1	SW	...	...	69	0.3	crack growth observed
A-2	SW	...	...	51.5	21.3	crack growth observed
A-3	SW	...	...	48	23.5	crack growth observed
A-4	SW	40	166	61	6.3	crack growth observed
A-5	air	37	160	46	25	crack growth observed
B-1	SW	66	150	134	0.4	no crack growth
B-2	SW	112	165	134	0.05	no crack growth
B-3	SW	100	162	132	0.1	no crack growth
B-4	SW	...	...	119	0.02	no crack growth
B-5	air	110	164	145	...	no crack growth

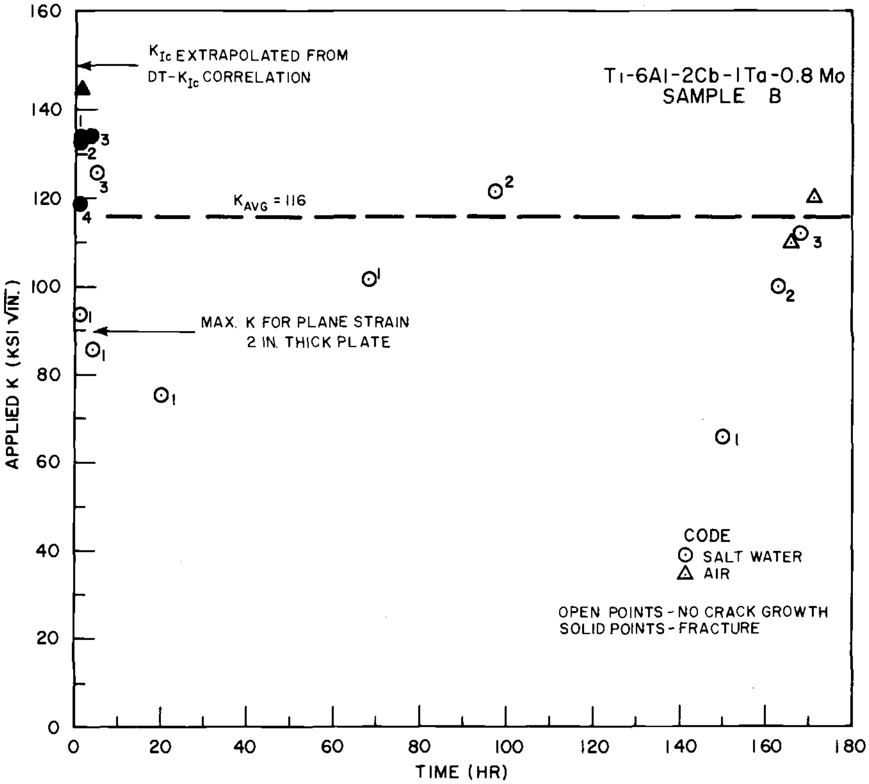

FIG. 3—*Test results for Sample B. The small numbers refer to the sequence in which the specimens were tested. Data points obtained by step loading were not used to define* K_{Iscc}.

criteria defined in ASTM Method E 399-72; the second reference point is the extrapolated value of K_{Ic}, which is 138 ksi$\sqrt{\text{in.}}$ for Sample A. The K_{Iscc} value was found by bracketing between specimens where crack growth was observed (solid points) and those where no growth was observed (open points). The small numbers refer to the order in which specimens were tested, and where a given number appears more than once, the load was adjusted to increase the applied K to sequentially higher levels. When the first specimen was loaded to an applied K of 69 ksi$\sqrt{\text{in.}}$, the crack began to grow immediately, and the specimen failed after 0.3 h. The second specimen was loaded to an initial K value of 52 ksi$\sqrt{\text{in.}}$; crack growth was not detected until the specimen failed after 21.3 h. Because the failure time of 21 h for specimen number 2 was extremely long for titanium and was therefore expected to be very near K_{Iscc}, the third specimen was loaded to an applied K of 48 ksi$\sqrt{\text{in.}}$ with the intent of getting a "runout" point, that is, a no-crack-growth point for 150 h; however, the

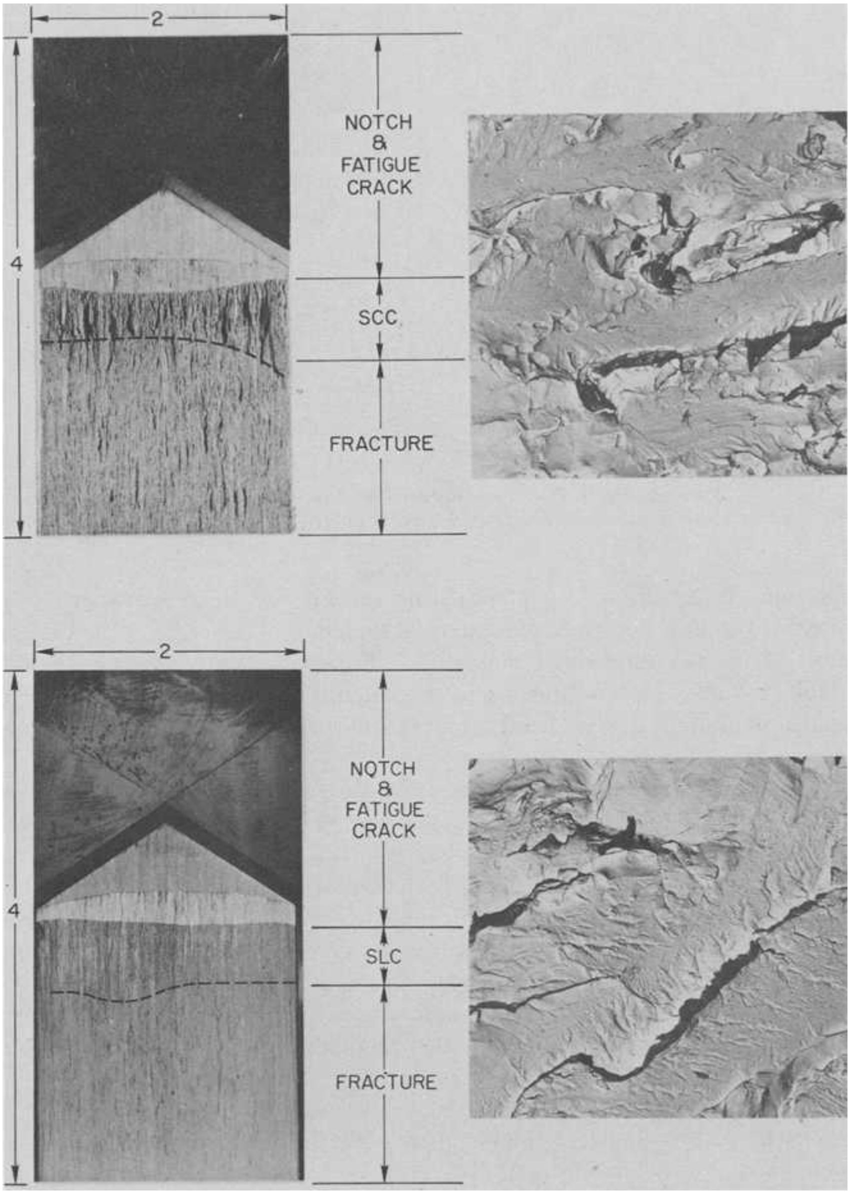

FIG. 4—*Specimens of Sample A tested in salt water* (top) *and air* (bottom) *showing similarity of macro- and microappearance of crack growth regions.*

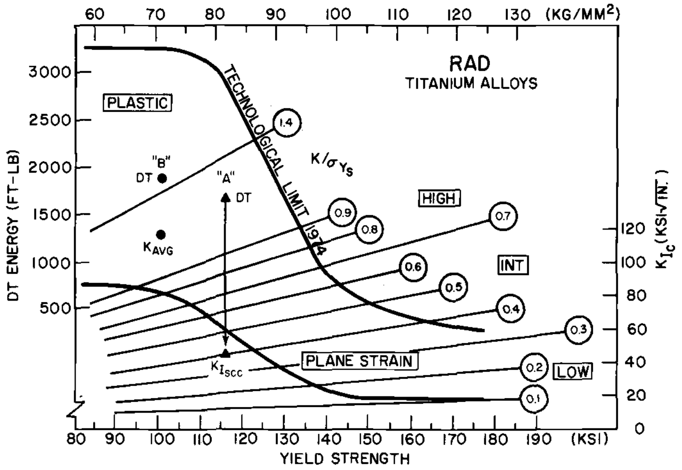

FIG. 5—*Ratio Analysis Diagram (RAD) for 2-in.-thick titanium alloys showing the data defining fracture resistance and SCC properties of both samples of material.*

specimen failed after 23.5 h. Both the second and third specimen spent most of the test time with no external evidence of crack growth, that is, most of the test time was "incubation." Following the incubation period, crack growth began and the specimens failed. Each of the first three specimens exhibited a significant amount of crack growth prior to final separation.

The fourth specimen was loaded at 40 ksi$\sqrt{\text{in.}}$, which was a runout for 165.5 h. The load was increased to 44.5 ksi$\sqrt{\text{in.}}$ and was maintained for 76.6 h; following this, the applied K was raised to well above the level necessary to initiate crack growth, so that immediate crack growth and specimen failure followed. The threshold K_{Iscc} was defined as 44 ksi$\sqrt{\text{in.}}$ by taking the average of the highest "no-crack-growth" point on initial loading of the specimen and lowest "crack-growth" point, again on the initial loading of the specimen. These correspond to specimen number 3 (48 ksi$\sqrt{\text{in.}}$ with crack growth) and specimen number 4 (40 ksi$\sqrt{\text{in.}}$ with no crack growth). Except for use in narrowing the range of K values that could include K_{Iscc}, the step-load test results were not utilized. Both of the points used to define K_{Iscc} involved only the initial loading of the specimen, so that step loading is not a factor.

As a final step, one specimen was tested in air to confirm that the crack growth was due to the salt water. The procedure was to apply a load intended to be 5 ksi$\sqrt{\text{in.}}$ below K_{Iscc} (44 ksi$\sqrt{\text{in.}}$), hold for 150 h min, and raise to approximately 5 ksi$\sqrt{\text{in.}}$ above K_{Iscc}. The actual values were 37 and 46 ksi$\sqrt{\text{in.}}$ for initial and stepped loads, respectively. The result was a runout at initial load and a considerable amount of crack growth followed by complete failure of the specimen at the stepped load. The tests were conducted in an air-conditioned room, so that excessive humidity was not present.

Sample B, which was immune to SCC, presented an entirely different problem. The maximum plane-strain K value was 90 ksi$\sqrt{\text{in.}}$ for this material, while the extrapolated K_{Ic} value was 150 ksi$\sqrt{\text{in.}}$ The first specimen was tested at 66 ksi$\sqrt{\text{in.}}$ for 150 h with no crack growth; subsequent to this the load was increased in steps as shown in Fig. 3 until the specimen failed at 134 ksi$\sqrt{\text{in.}}$, with no evidence of slow crack growth. Two additional specimens were tested with the same result, starting from initial K values of 100 and 112 ksi$\sqrt{\text{in.}}$ and failing at 132 and 134 ksi$\sqrt{\text{in.}}$, respectively. The fourth specimen failed 1 min after an initial load of 119 ksi$\sqrt{\text{in.}}$; the average threshold value of K was rounded off to 116 ksi$\sqrt{\text{in.}}$ (average of 112 and 119).

No evidence of slow crack propagation could be found from examination of the fracture surfaces. The air environment specimen sustained 110 ksi$\sqrt{\text{in.}}$ for 164 h with no failure; it was necessary to increase the load to 144.5 ksi$\sqrt{\text{in.}}$ to cause fracture of this specimen.

The most significant finding of this investigation was that in Sample A, the salt water environment was not necessary to cause crack growth, as evidenced by crack growth in the normal air environment for a specimen loaded to an applied K level just above the salt water K_{Iscc}. Examination of the fracture surfaces by electron microfractography revealed no dramatic difference in the crack propagation mechanism between a specimen tested in salt water and the specimen tested in air. Figure 4 shows the macro- and microappearances of the two specimens. In general the macroappearance of the specimens was identical; the microfracture mode was mixed cleavage and microvoid coalescence in approximately the same proportions for the slow crack propagation region of each specimen. A more detailed investigation might reveal some factors that are not readily apparent; however, the conclusion reached from the studies to date indicate that there are no effective differences between SCC and sustained load cracking (SLC) for these materials that would significantly influence structural performance.

The two alloys of this study represent typical behavior for titanium alloys in that crack growth, if present, proceeds very rapidly and at K levels well below the fracture resistance property. The significance of the test results are best judged by comparing the K_{Iscc} value with a valid measure of the fracture resistance. The case of Sample A involves a low K_{Iscc}, a high fracture resistance, and therefore a very large amount of crack growth. The case of Sample B involves no apparent crack growth, and both fracture resistance and an average K for failure in the SCC test well in excess of the maximum allowable for plane-strain conditions in 2-in. plate. Thus the structural use of these materials would require (*a*) very careful consideration of environmental effects for Sample A and (*b*) no detailed analysis of potential environmental crack growth for Sample B. It should be noted that on the K versus time plots for Sample A no real significance for structural design can be drawn from the time scale. The cracks proceed at a very rapid rate and are preceded by a rather long incubation period. The total time includes both the time for incubation and the time for failure of a particular specimen. A change of specimen geometry would alter the shape of the curve, so that use of da/dt data would require direct modeling of the part in question.

The foregoing conclusions could be very quickly reached by engineering methods involving the Stress-Corrosion Ratio Analysis Diagram (SCC-RAD) [*3*]. The titanium SCC-RAD (Fig. 5 is designed to facilitate analysis of the combined effects of materials properties and effects of section thickness for fracture and SCC. Fracture resistance properties are plotted as DT energy, and K_{Iscc} or K_{avg} are plotted from the K_{Ic} scale. The zone between K/σ_{ys} ratio values of 0.9 to 1.4 is the elastic-plastic fracture zone for 2-in.-thick materials; this zone forms the transition from plane-strain, or brittle behavior (below ratio 0.9), to fully ductile behavior (above ratio 1.4). The lines of K/σ_{ys} ratio can be used as a reference to various fracture mechanics equations which define combinations of stress level-defect size that can cause fracture or the initiation of SCC under plane-strain conditions. An arbitrary separation of the SCC-RAD into three regions (high, intermediate, and low) according to the approximate flaw sizes and stress levels that are tolerable is made by $K_{\mathrm{Iscc}}/\sigma_{\mathrm{ys}}$ lines of 0.3 and 0.7, as shown. These separations are made on the basis of experience with flaw detection in marine structures and the general range of properties of structural materials and performance. The primary function of the SCC-RAD is to provide a display of both fracture resistance and SCC resistance so that the K_{Iscc} parameter can be evaluated on a comparative basis. For Sample B both DT and K_{avg} reside quite close together in the plastic region for 2 in. thickness; this implies that there is little or no effect of the environment. Sample A has plastic fracture resistance, but the K_{Iscc} value is in the plane-strain region; the wide separation between the two values is a measure of the environmental effect.

The impact of SCC resistance on structural performance is usually in the area of maintenance problems. For heavy-section titanium, however, SCC growth is so rapid that a sensitivity to SCC can effectively preclude its use. There are many difficulties in using these K_{Iscc} values directly in structural design. Crack-growth rates are very rapid for titanium and are dependent on the geometry of the specimen or the part or structure being designed or both. One of the primary values of the K_{Iscc} test is as an indicator that crack growth is accelerated by the presence of the environment. In most structures, particularly military structures, service-induced crack growth is most often due to fatigue loading in the low-cycle range; a low K_{Iscc} value is thus a red flag that rapid corrosion-fatigue crack growth is predicted for the structure in the environment of interest. Thus Sample A should be excluded from use on large, heavy-section structures because of potential fatigue/corrosion-fatigue problems, while Sample B would not be expected to exhibit any effect of environment in service.

References

[*1*] Pellini, W. S., "Criteria for Fracture Control Plans," NRL Report 7406, Naval Research Laboratory, Washington, D. C., May 1972.

[*2*] Goode, R. J. and Judy, R. W., Jr., *Welding Journal Research Supplement,* Vol. 53, No. 3, March 1974, pp. 135s–143s.

[*3*] Judy, R. W., Jr., and Goode, R. J., "Prevention and Control of Subcritical Crack Growth in High-Strength Metals," NRL Report 7780, Naval Research Laboratory, Washington, D. C., 2 Aug. 1974.

[*4*] Puzak, P. P. and Lange E. A., "Standard Method for the 1-Inch Dynamic Tear Test," NRL Report 6851, Naval Research Laboratory, Washington, D. C., 13 Feb. 1969.

[*5*] Brown, B. F., Jr., *Materials Research and Standards,* Vol. 6, No. 3, 1966, pp. 129–133.

[*6*] Judy, R. W., Jr., Freed, C. N., and Goode, R. J., "A Characterization of the Fracture Resistance of Thick-Section Titanium Alloys," *Titanium Science and Technology,* Vol. 2, R. I. Jaffee and H. M. Burte, Eds., Plenum, New York, 1974.

J. H. Payer,[1] W. E. Berry,[1] and W. K. Boyd[1]

Constant Strain Rate Technique for Assessing Stress-Corrosion Susceptibility

---

REFERENCE: Payer, J. H., Berry, W. E., and Boyd, W. K., **"Constant Strain Rate Technique for Assessing Stress-Corrosion Susceptibility,"** *Stress Corrosion—New Approaches, ASTM STP 610,* American Society for Testing and Materials, 1976, pp. 82–93.

ABSTRACT: The constant strain rate technique is a rapid laboratory method to assess susceptibility of metals and alloys to stress-corrosion cracking (SCC). Positive results are obtained since specimen failure occurs, either in a ductile manner or prematurely in a brittle mode if SCC occurs. Experimental apparatus, methods to interpret results, and important experimental parameters are discussed.

KEY WORDS: stress corrosion, cracking (fracturing), strain rate, failure, ductility, brittleness

The constant strain rate technique is a method to assess the susceptibility of metals and alloys to stress-corrosion cracking (SCC). Much of the development of this technique to its present state can be credited to Parkins and his co-workers at University of Newcastle upon Tyne. The study of SCC of mild steel in hydroxide solutions [*1*][2] demonstrates the primary advantage of the constant strain rate test. It provides a rapid laboratory method to determine the SCC susceptibility of ductile materials in solutions in which other SCC tests do not readily promote SCC. The results are positive in that failure occurs either in a ductile manner or prematurely in a brittle mode if SCC occurs. A general discussion of the technique was presented previously by Reinoehl and Boyd [*2*]. The relative merits of constant strain, constant load, and constant strain rate techniques have been presented and compared by Parkins [*3*]. The purpose of this paper is to describe the equipment used in constant strain rate studies, to present methods to measure severity of SCC, and to identify important experimental parameters.

---

[1] Research metallurgist, associate section manager, and section manager, respectively, Columbus Laboratories, Battelle Memorial Institute, Columbus, Ohio 43201.

[2] The italic numbers in brackets refer to the list of references appended to this paper.

In essence, the constant strain rate technique comprises straining a specimen at a slow, constant strain rate under controlled environmental conditions. Typical strain rates range from 10^{-4} to 10^{-8}/s. Strain rates in the critical range to promote SCC maintain the delicate balance at the crack tip between deformation, dissolution, film formations, and diffusion.

Description of Equipment

Constant Strain Rate Apparatus

The essential requirements of a constant strain rate apparatus are (1) sufficient stiffness to resist significant deformation under loads required to deform specimens, (2) a system to provide reproducible, constant strain rates over the range of 10^{-4} to 10^{-8}/s, and (3) a cell to contain the test solution and maintain the desired experimental conditions throughout the test. Other ancillary equipment is used to control environmental conditions and record data.

A schematic diagram of a constant strain rate unit is presented in Fig. 1. A movable carriage is lowered at a constant speed through a screw-drive mechanism. The specimen is fixed between the top of the frame and the lower beam of a movable carriage. A container made of inert material holds the solution. Electrodes to measure and control potential, stirrers, gas dispersion tubes, etc., can be included. A load cell measures the applied load on the specimen. Ancillary controls can be used to maintain constant temperature, potential, pressure, and gas flow. The solution can be circulated if desired. Elapsed time, applied load, potential, and current can be recorded.

Both mechanical and electrical speed control units have been used. In the former, a constant speed motor is geared-down to the desired speed through a combination of gears and gear reducers. Strain rate is selected by engaging the appropriate set of gears. Alternatively in the latter, a variable speed motor is linked to a gear train, and the desired strain rate is maintained by setting the motor speed. The essential requirement of either system is that the desired speed can be reproducibly selected and maintained constant during each experiment.

In addition to uniaxial tensile units as just described, cantilever constant strain rate apparatus also have been used. An extension arm attached to a cantilever beam specimen is lowered at a constant rate. Although the calculation of strain rate at the root of a notch or at a crack tip is complex, this technique has been applied successfully in the study of SCC of mild steel in carbonate-bicarbonate environments to determine crack velocity, critical strain rates, and inhibitor effectiveness [*4,5*]. The results correlate with those from uniaxial tension, strain rate tests in the same environment.

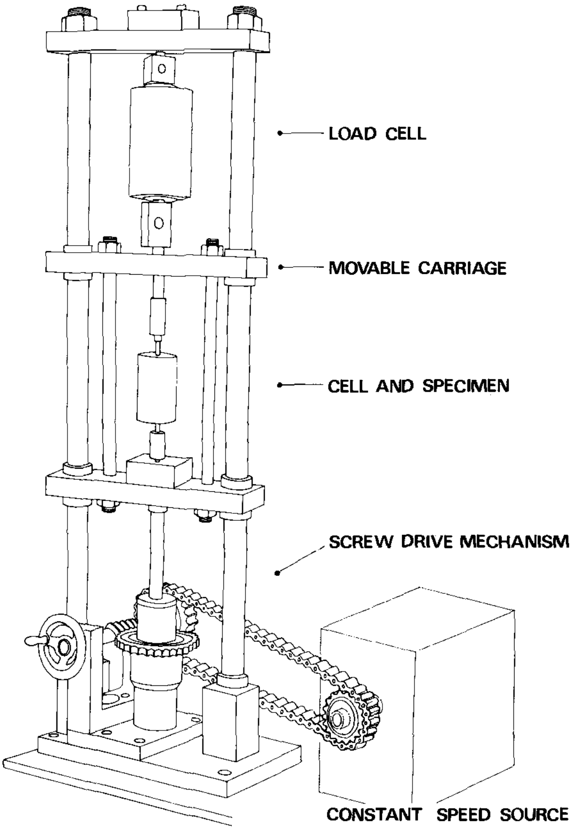

FIG. 1—*Schematic diagram of constant strain rate apparatus.*

Constant Strain Rate Specimens

Specimen configuration can be selected to suit the form of the material. Round specimens approximately 3 mm diameter are convenient, although sheet and wire specimens have been used. A reduced test section facilitates uniform deformation and allows complete immersion which negates problems associated with the liquid-vapor interface and cell seals. Specimens and mounting fixtures should be designed to provide pure tensile loads with no bending or twisting imparted to the specimen. Spherical joints and universal joints have been used to accomplish this.

Smooth and notched specimens have been tested successfully. Cantilever beam specimens are of conventional design, that is, notched with a fatigue precrack.

Interpretation of Results

Several properties are used to define and compare the severity of SCC of materials and aggressiveness of environments. Generally, a measure of the reduction of area, time to failure, or elongation in a test solution is compared to the behavior in an environment which does not promote SCC, for example, oil or air. While such comparisons provide a quantitative expression of SCC severity, none is universally valid, and the parameter chosen must be justified for use with the material-solution system being studied. Only metallographic examination of the fractured specimen determines unequivocally the presence or absence of SCC.

Photomacrographs of two carbon steel specimens after constant strain rate tests are presented in Fig. 2. Data presented in this paper were determined with ASTM A381 steel. The specimen on the right was tested in a carbonate solution under conditions which promote SCC, while the specimen on the left was tested in hot oil. Both tests were run at a strain rate of 2.5×10^{-6}/s and 180°F. A large number of secondary cracks and reduced ductility at failure is evident for the stress corroded specimen. A photomicrograph of the specimen showing a secondary intergranular crack is presented in Fig. 3. Reductions of area were 55 and 41 percent for the mechanical and SCC failure, respectively.

Increased severity of SCC is indicated by shorter times to failure, reduced ductility, for example, less reduction of area or less elongation, smaller maximum load prior to failure, and smaller true stress at failure. Results of metallographic examination can be presented quantitatively by comparing the number of secondary stress corrosion cracks or length of cracks.

Experimental Parameters Which Affect SCC

Experimental parameters which affect SCC behavior include environment, potential, metal composition and structure, strain rate, and temperature. The effects of these parameters are demonstrated in the remainder of this section.

Potential

There is a critical potential range for a material in an environment which promotes SCC, and exposure within this range is necessary for cracking to occur. As demonstrated in the study mild steel in caustic solutions [*6*], SCC is promoted by either adjusting the solution composition to render the free-corrosion potential (FCP) in the critical potential range or applying an imposed potential in the cracking range. Mild steel does not

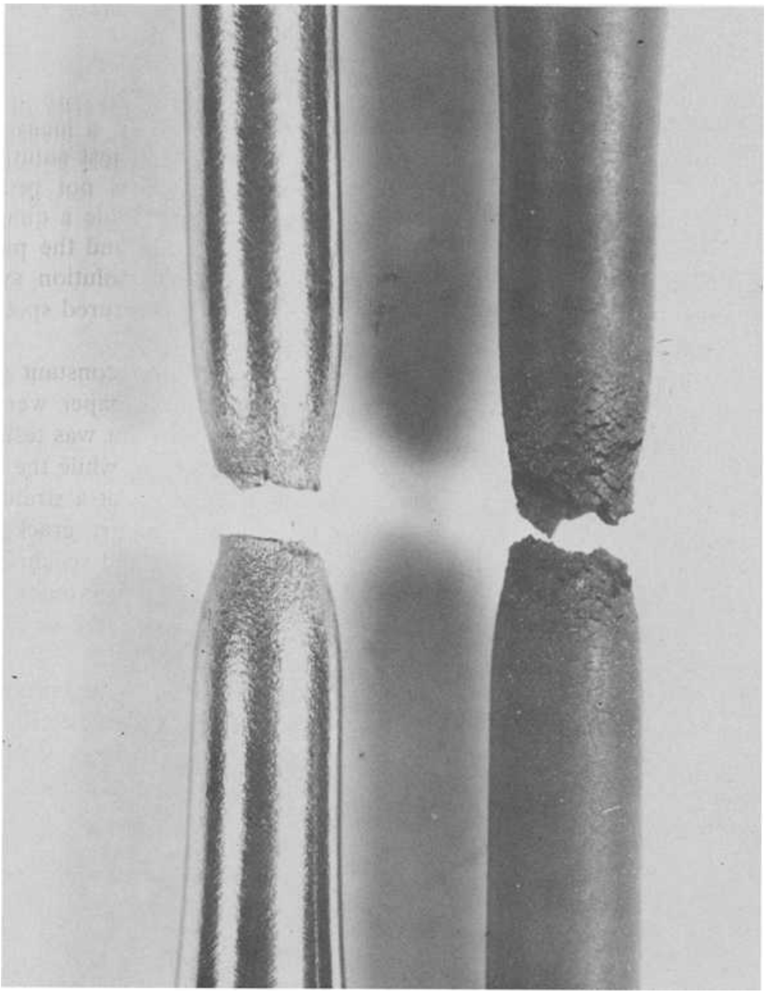

FIG. 2—*Photomacrographs of specimens after constant strain rate experiment: ductile failure in oil, SCC in carbonate solution (original diameter 2.5 mm).*

exhibit SCC at its FCP, approximately −1.10 V [copper-copper sulfate (Cu-$CuSO_4$)], in 33 weight percent sodium hydroxide ($NaOH$). However, the addition of 0.1 weight percent lead dioxide (PbO_2) raises the FCP approximately to −1.0 V (Cu-$CuSO_4$) and SCC occurs without application of imposed potential [*6*]. Galvanic effects of coupling dissimilar metals or contact with thick oxides can also result in a potential shift into the cracking range.

Results of constant strain rate tests of carbon steel in 33 weight percent NaOH at 180°F are presented in Fig. 4. Reduction of area of specimens

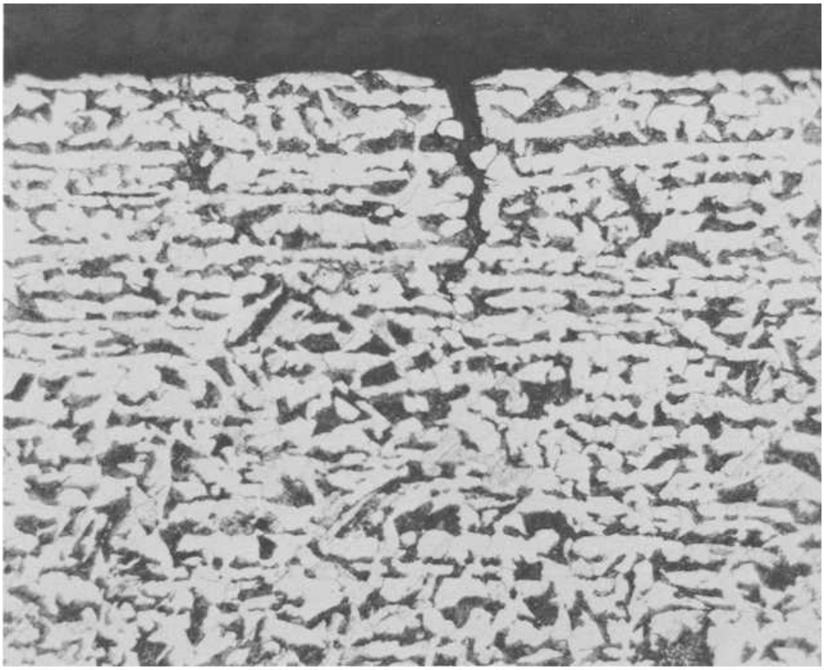

FIG. 3—*Photomicrograph of carbon steel after constant strain rate test in an environment which promotes SCC (×250).*

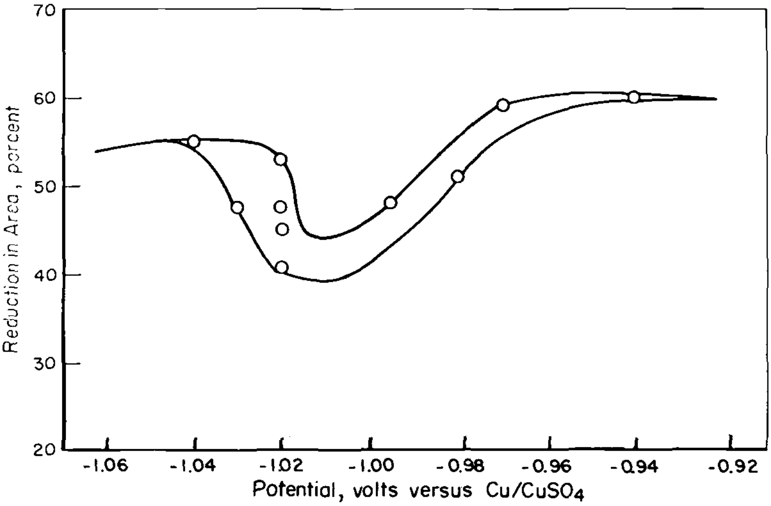

FIG. 4—*Reduction of area as a function of applied potential for carbon steel in 33 weight percent NaOH at 180°F.*

strained at 2.5 × 10^{-6}/s is plotted as a function of applied potential. The two lines delineate a scatterband of experimental results. SCC was observed for applied potentials from approximately −1.015 to −0.097 V (Cu-$CuSO_4$). Cracking was most severe at −1.000 V (Cu-$CuSO_4$).

The location and extent of a critical potential range are a function of the material and the environment. Critical potential ranges for SCC of mild steel in caustic, carbonate-bicarbonate, and nitrate solutions are shown in Fig. 5. Corrosion potentials in each of these environments are indicated. A specific range is found for each steel-solution combination [*5*].

Environment

The specificity of environments which promote SCC has long been recognized. Constant strain rate tests provide a technique to investigate the effects of solution composition or additions to a base solution on severity of SCC. A good example of the latter is taken from a study in which effective inhibitors to decrease SCC severity for carbon steel in sodium hydroxide solutions and carbonate-bicarbonate solutions were identified using this technique [*5*]. The inhibiting effect of 1 weight percent potassium dichromate ($K_2Cr_2O_7$) in carbonate-bicarbonate solution at 180°F and strain rate of 2.5 × 10^{-6}/s is presented in Fig. 6. Results for solutions with inhibitor addition are compared with behavior in solutions with no addition designated by the region bound by solid lines. With no addition, severe SCC was observed in the potential range extending from approximately

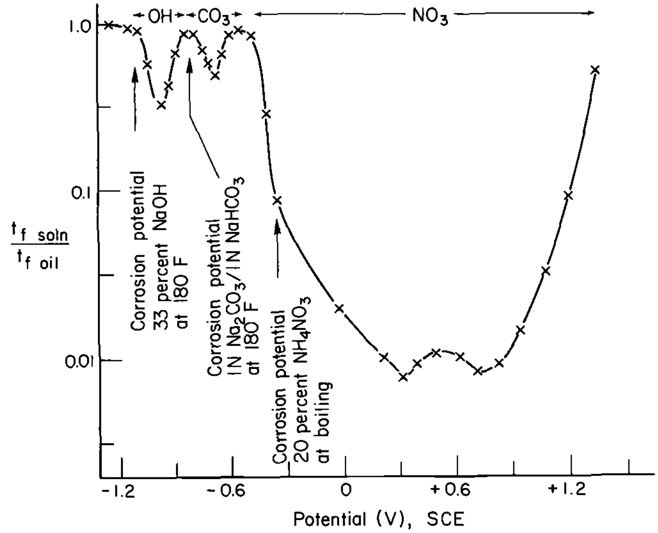

FIG. 5—*Potential ranges for SCC of carbon steel in caustic, carbonate/bicarbonate, and nitrate solutions.*

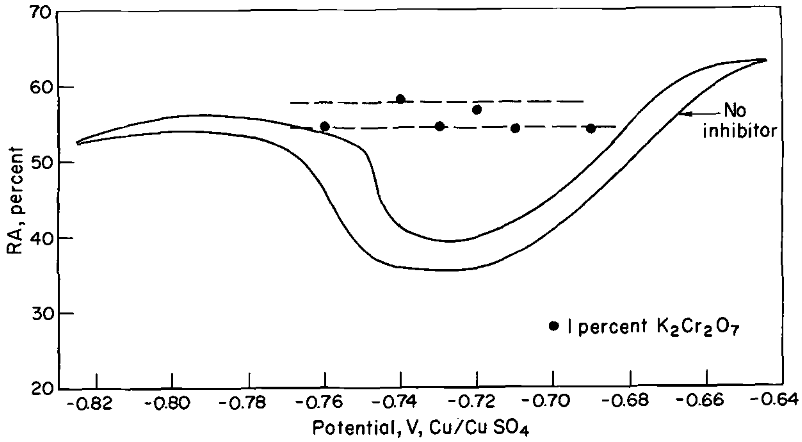

FIG. 6—*Inhibiting effect of 1 weight percent $K_2Cr_2O_7$ on SCC of carbon steel in carbonate/bicarbonate solution at 175°F.*

−0.70 to −0.76 V (Cu-$CuSO_4$). Whereas, SCC was eliminated over this entire potential range by the inhibitor.

It is important to determine the effect of candidate inhibitors at several potentials, since the beneficial effect of some additions result from a potential shift out of the cracking range. These inhibitors are unsafe in many applications because conditions are such that a shift back into the critical SCC range might occur with minor changes in the environment. Other inhibitors, as in the case just cited, are effective over a broad potential range [*5*].

Metal Composition and Structure

Constant strain rate technique provides a useful tool to investigate the effects of chemical composition and metallurgical structure on severity of SCC. The effect of alloy additions of aluminum, chromium, copper, molybdenum, nickel, silicon, and titanium to carbon steel has been studied in nitrate, caustic, and carbonate solutions [*4*]. Not surprisingly, the alloy effects were found to differ in each environment, for example, molybdenum was beneficial in carbonate solution but detrimental in both hydroxide and nitrate solutions. Composition of the base steel, for example, carbon content, was also found to alter the effect of alloy additions. Generalities can be misleading and should be substantiated by data covering the range of conditions of interest.

The effect of metallurgical structure and composition of alloys in high-temperature, high-pressure water has been investigated at Battelle. Results of experiments in water with 100-ppm dissolved oxygen at 550°F are

TABLE 1—*Constant strain rate results in high-purity water with 100-ppm O_2 at 550°F.*

Materials	Condition	Failure, h	Reduction in Area, %	Comment
SS-304	mill annealed	62.4	61	no SCC
	4 h/1250°F	26.4	15	SCC
	7 h/1150°F	56.3	60	SCC
SS-304L	24 h/1150°F	26.2	28	SCC
INC-600	mill annealed	77.9	59	no SCC
	7 h/1150°F	81.8	62	no SCC

presented in Table 1. A strain rate of 3 × 10^{-6}/s was used for all experiments. Heat treatment of mill annealed Type 304 stainless steel in the 1150 to 1250°F range resulted in sensitization and the onset of SCC. A low-carbon stainless steel, Type 304L, exhibited sensitization after 24 h at 1150°F and was found to be susceptible to SCC, while Inconel 600 did not stress corrode in either the mill annealed or sensitized condition. A means was thus provided to determine the effects on SCC susceptibility of alloy composition and structural changes brought about by intentional heat treatment or fabrication practice.

Strain Rate

In general, the severity of SCC is a function of strain rate. Maximum severity is observed over a critical range, and the susceptibility decreases at faster and slower strain rates. Maximum severity of SCC is observed for strain rates of the order of 10^{-6}/s for many material-solution systems. A too rapid strain rate results in ductile failure of the specimen before significant SCC occurs. Alternatively, a very slow strain rate allows repassivation at the crack tip and suppresses SCC. For example, transgranular SCC of titanium in 3 percent sodium chloride (NaCl) occurred only over a narrow range of strain rates, and ductile failure was observed at higher and lower rates [*8*]. The absence of SCC at slow rates was attributed to film repair at the crack tip which suppressed crack growth.

The effect of strain rate on stress-corrosion susceptibility of carbon steel in carbonate-bicarbonate solution at 175°F and three applied potentials is shown in Fig. 7. Severity of SCC increases with decreasing strain rates from 10^{-5}/s [*5*]. At two potentials severity of SCC decreases again at lower strain rates. The most severe strain rate is a function of the metal-solution system, potential, and temperature and must be determined for each instance.

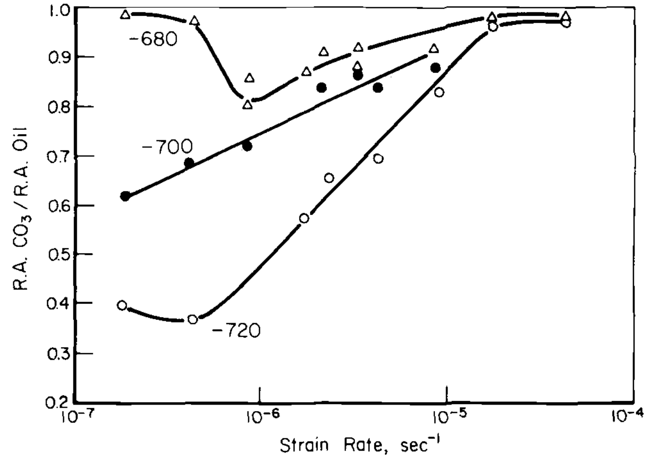

FIG. 7—*Effect of strain rate on SCC of carbon steel in carbonate/bicarbonate solution at 175°F.*

The effect of strain rate on average crack velocity is shown in Fig. 8. Carbon steel specimens exposed to caustic solution at 180°F and −1.010 V (Cu-CuSO$_4$) were removed prior to the onset of necking and metallagraphically examined [5]. The average crack velocity was calculated from average crack length and exposure time from the onset of yielding to the termination of the experiment. No SCC was observed at strain rates above 3×10^{-6}/s. The average crack velocity was approximately 10^{-6} mm/s for strain rates of 2.5×10^{-6} to 1×10^{-7}/s and did not vary greatly over this range.

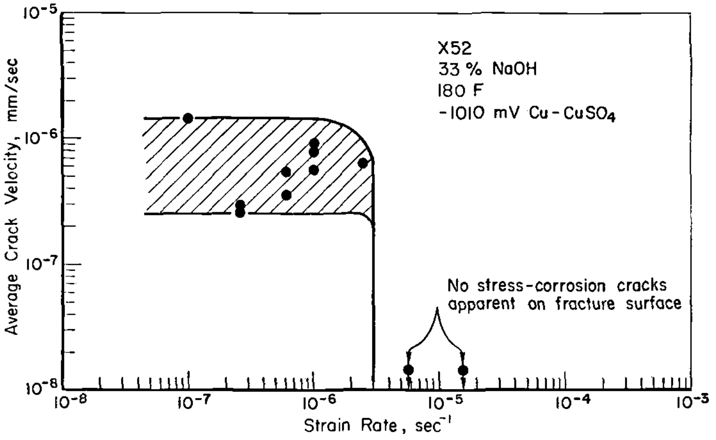

FIG. 8—*Effect of strain rate on crack velocity of carbon steel in caustic solution at 180°F.*

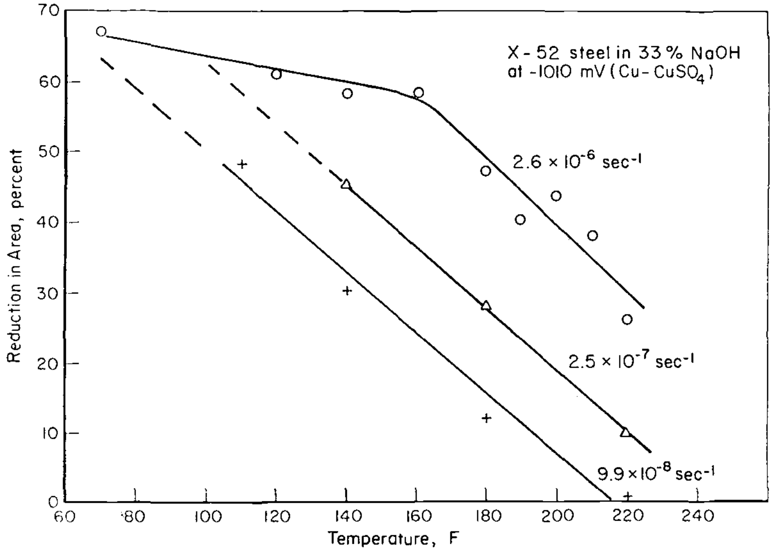

FIG. 9—*Effect of temperature and strain rate on SCC of carbon steel in caustic solution.*

Temperature

The effect of temperature on severity of SCC of carbon steel in caustic solution at three strain rates is shown in Fig. 9. As indicated by lower reduction of area, SCC is more severe as temperature increases and strain rate decreases [5]. The break in the curve for 2.6×10^{-6}/s indicates the transition temperature between a region of SCC, 180°F and above, and a region of no SCC, 160°F and below. A maximum in SCC severity at approximately 190°F is observed for carbon steel in carbonate-bicarbonate solutions. The rapid decrease in SCC above 190°F is due to the breakdown of the carbonate-bicarbonate solution.

Conclusion

Constant strain rate technique provides a rapid laboratory method to assess susceptibility of metals and alloys to SCC. Absolute results are obtained because failure occurs either in a ductile manner or prematurely by a brittle mode when SCC occurs. Absence of SCC assures that the material can be safely used under the conditions examined. Judgment is necessary if SCC is observed, since the material often can provide sufficient useful life in service.

Several parameters are available to compare the severity of SCC of materials and to compare the aggressiveness of environments. Metallographic examination provides the most positive determination of SCC.

The validity of other measures of SCC severity (reduction of area, time to failure, elongation) must be justified for each instance.

The constant strain rate technique has been applied to a wide variety of metal-solution systems and has provided a useful measure of SCC susceptibility. Data obtained are useful for materials selection on a sound engineering basis and provide a basis for better understanding of stress-corrosion cracking mechanisms.

References

[*1*] Humphries, M. J. and Parkins, R. N., *Corrosion Science,* Vol. 7, 1967, p. 747.

[*2*] Reinoehl, J. E. and Boyd, W. K., Proceedings of Specialists Meeting on Stress Corrosion Testing Methods, NATO Advisory Group for Aerospace Research and Development, Brussels, Belgium, Oct. 1971.

[*3*] Parkins, R. N., Proceedings of Specialists Meeting on Stress Corrosion Testing Methods, NATO Advisory Group for Aerospace Research and Development, Brussels, Belgium, Oct. 1971.

[*4*] Parkins, R. N., Fifth Symposium on Line Pipe Research, American Gas Association, Inc., Houston, Tex., Nov. 1974, Paper V, pp. 1–40.

[*5*] Berry, W. E., Fifth Symposium on Line Pipe Research, American Gas Association, Inc., Houston, Tex., Nov. 1974, Paper V, pp. 1–40.

[*6*] Reinoehl, J. E. and Berry, W. E., *Corrosion,* Vol. 28, 1972, p. 151.

[*7*] Sutcliffe, J. F., Fessler, R. R., Boyd, W. K., and Parkins, R. N., *Corrosion,* Vol. 28, 1972, p. 313.

[*8*] Powell, D. T. and Scully, J. C., *Corrosion,* Vol. 24, 1968, p. 1515.

J. G. Kaufman,[1] *J. W. Coursen,*[1] *and D. O. Sprowls*[1]

An Automated Method for Evaluating Resistance to Stress-Corrosion Cracking with Ring-Loaded Precracked Specimens

---

REFERENCE: Kaufman, J. G., Coursen, J. W., and Sprowls, D. O., "**An Automated Method for Evaluating Resistance to Stress-Corrosion Cracking with Ring-Loaded Precracked Specimens,**" *Stress Corrosion—New Approaches, ASTM STP 610,* American Society for Testing and Materials, 1976, pp. 94–107.

ABSTRACT: This paper describes a ring-loading method for evaluating stress-corrosion resistance with precracked specimens and presents representative data for compact specimens of some high-strength aluminum alloys. The deflection of the ring was large relative to that of the specimen, simulating deadweight loading. This method provides several advantages over techniques previously used. Unlike most constant-displacement loading systems, the load and crack length and thus the stress intensity are known accurately throughout the life of each test, and the initiation and growth of stress-corrosion cracking (SCC) lead to a definitive end point (failure). Also, the effects of corrosion product wedging are minimal. The ring loading system is more compact than most deadweight systems, and because it is readily automated, data can be collected with the expenditure of few manhours.

KEY WORDS: stress corrosion, crack propagation, automated test methods, ring loading, threshold, stress intensity, aluminum alloys

Fracture mechanics principles and precracked specimens have been used to advantage in recent years in evaluating the stress-corrosion resistance of metallic alloys [*11*].[2] Although the presence of the mechanical precrack does not necessarily eliminate the incubation period as first thought, the fracture mechanics approach does provide some additional screening and design tools such as crack-growth rate (da/dt) data and threshold stress intensity (K_{Ith}) values.

The specimens used by various investigators include the compact-tension, cantilever beam, double cantilever beam, and center slot. Either one

---

[1] Senior engineering associate, research engineer, and section head, Stress Corrosion Section, Alcoa Laboratories, Aluminum Company of America, Alcoa Center, Pa. 15069.

[2] The italic numbers in brackets refer to the list of references appended to this paper.

of two methods of loading are used: constant displacement or constant load (deadweight). Constant displacement loading provided by bolts or wedges is useful both for accelerated screening tests or atmospheric environments. Systems employing this technique are compact and self-contained, and, theoretically at least, each specimen can provide an arrest or threshold stress intensity value in addition to crack-growth rate (da/dt) data. However, without instrumentation of the bolts the applied load and stress intensity are inferred and are not known precisely even at arrest. An additional problem is the wedging effect caused by corrosion products which can prevent arrest [*2*]. The deadweight loading systems are usually bulky and better suited to research testing. Also, several tests at different applied stress intensities are required to establish threshold values. However, the applied loads, and therefore stress intensities, are known more precisely, and corrosion product wedging is not a significant problem.

The ring-loading method described in this paper provides a bridge between the extremes of deadweight and constant displacement loadings. For instance, with proper design of the specimen and ring, a constant stress-intensity test can be conducted. Or, as was the case in this investigation, the spring constant of the ring can be made large in comparison with that of the compact specimens, thus simulating a deadweight loading with considerably more compactness than in cantilever bending. The ring-loading system, however, is much more compact than most deadweight loading systems, and with the ability for direct recording of both load (from ring stress) and crack opening displacement (COD), offers advantages over all of the other systems.[3] It is the purpose of this paper to describe this automated method of evaluating resistance to stress-corrosion cracking (SCC) utilizing the ring-load method.

Procedure

All of the specimens tested were 2.0 or 2.5-in.-thick aluminum alloy plate. The tensile properties were determined in the long-transverse and short-transverse directions in accordance with ASTM Methods of Tension Testing of Metallic Materials (E 8-69) and ASTM Methods of Testing Wrought and Cast Aluminum and Magnesium Alloy Products (B 557-73) and are shown in Table 1.

Fracture toughness tests were conducted with standard ($a = B = 0.5W$) 0.75 (2219 alloy) or 1.0-in. (all other alloys) thick short-transverse (S-L) compact specimens in accordance with ASTM Method of Test for Plane-Strain Fracture Toughness of Metallic Materials (E 399-74). The results of these tests are also shown in Table 1.

---

[3] Some ring-loading-type tests were made by E. P. Dahlberg in the ARPA Coupling Program on Stress-Corrosion Cracking [*1*], but without the automated features described in this paper.

TABLE 1—*Results of tension and fracture toughness tests of some aluminum alloy plate.*

	Long Transverse[a]			Short Transverse[b]			Short Transverse (S-L)		
Alloy and Temper	Tensile Strength, ksi[c]	Yield Strength, ksi[c]	Elongation in 4D, %	Tensile Strength, ksi[c]	Yield Strength, ksi[c]	Elongation in 4D, %	Specimen Thickness, in.[d]	K_Q, ksi$\sqrt{\text{in.}}$[e]	Valid K_{Ic}
2021-T81	68.8	59.5	4.8	68.6	59.1	5.0	1.00	19.6	yes
2024-T351	67.5	47.1	17.0	55.4	42.4	3.5	1.00	21.0	yes
2024-T851	68.6	62.2	7.5	63.9	61.8	1.0	1.00	16.7	yes
2219-T37	58.7	42.5	17.5	57.9	42.1	12.0	0.75	27.1	no[f]
2219-T87	71.6	58.2	9.5	69.1	57.7	5.5	0.75	19.6	yes
7039-T6351	64.4	55.1	12.0	62.6	54.2	6.0	1.00	20.4	yes
7075-T651	81.9	71.9	8.5	75.3	66.7	2.0	1.00	19.5	yes
7075-T7351	69.7	58.6	10.0	65.0	55.1	4.0	1.00	21.0	yes

[a] Duplicate 0.500-in.-diameter specimens taken at quarter-plane per ASTM standards.

[b] Duplicate 0.125-in.-diameter specimens centered in plate thickness.

[c] 1 ksi = 6.89 MPa.

[d] 1 in. = 2.54 cm. Specimen thickness = $B = a = 0.5W$.

[e] 1 ksi$\sqrt{\text{in.}}$ = 1.10 MPa$\sqrt{\text{m}}$.

[f] Did not meet ASTM criteria for specimen thickness or plastic deformation.

All of the ring-load tests were conducted with fatigue precracked short-transverse (S-L) compact specimens similar to those used for the fracture toughness tests. The crack length after precracking was estimated from measurements made on the sides of the specimens. The loads required to provide the desired initial stress-intensity (K_{Ii}) levels were calculated using the equation for the compact specimen shown in ASTM Method E 399–74.

Load-deflection calibration data were obtained for the compact specimens over a crack length-to-specimen width (a/W) range of 0.45 to 0.80. This was accomplished by making successively longer saw cuts in a series of specimens, and with each length, loading the specimen in a testing machine utilizing a clip gage in integrally machined knife edges in the crack opening to measure displacement. Using a least squares analysis, the following equation was fit to these data

$$a = W\left[0.18728 + 8.0737 \times 10^{-3}\left(\frac{VEB}{P}\right) - 4.8716 \times 10^{-5}\left(\frac{VEB}{P}\right)^2 + 1.4100 \times 10^{-7}\left(\frac{VEB}{P}\right)^3 - 1.5267 \times 10^{-10}\left(\frac{VEB}{P}\right)^4\right] \quad (1)$$

where

a = crack length, in.;
W = specimen width, in.;
V = crack opening displacement (COD), in.;
E = modulus of elasticity, psi;
B = specimen thickness, in.; and
P = load, lb.

A typical ring-load setup is shown in Fig. 1. The rings and tension bolts are constructed from high-strength aluminum alloys. The nuts on the ends of the tension bolts are seated spherically to provide self-alignment. The clip gage is a single piece keyhole-shape construction. Both the load rings and the clip gages are instrumented with strain gages, and the readings are monitored with a multichannel digital strain indicator.

In the loading procedure, the clip gage is mounted on the specimen, and the load is applied by tightening one of the spherically seated nuts. The applied load is read from the meter on the multichannel strain indicator, and the specimens are immersed immediately in the corrodant. The corrodant used was a corrosion inhibited and buffered 3.5 percent sodium chloride (NaCl) solution of the formula: 0.6 M NaCl + 0.2 M sodium dichromate ($Na_2Cr_2O_7$) + 0.07 M sodium acetate ($NaC_2H_3O_2$) + acetic acid ($HC_2H_3O_2$) to a pH of 4. This solution was used because it causes more rapid growth of SCC and less rapid corrosion of the surfaces of the precrack than plain 3.5 percent NaCl solution [2]. It is realized that the

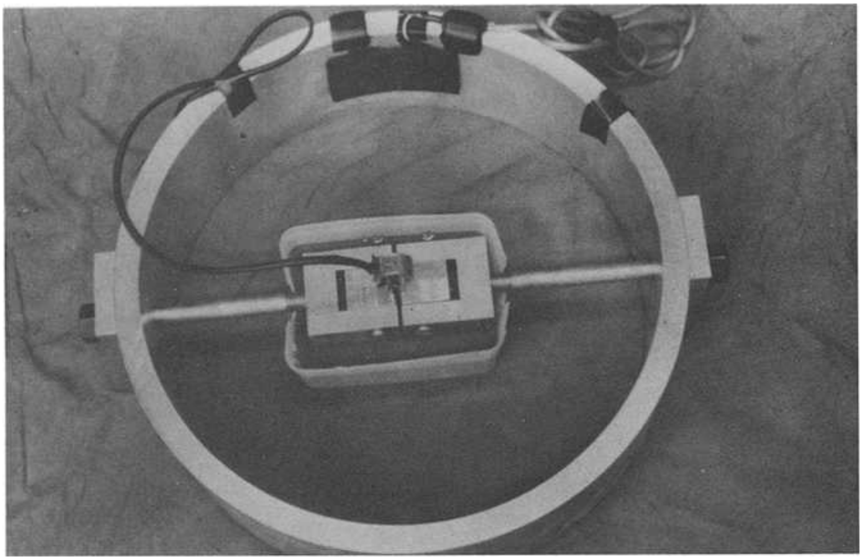

FIG. 1—*Ring loaded compact specimen.*

determination of a threshold stress-intensity factor in an accelerated test is subject to validation by comparison with data obtained in the intended service environment.

Load and COD readings from up to 15 tests can be monitored simultaneously with the data logging equipment used for these tests. The load and COD readings are taken automatically every 8 h (the reading interval can be varied), and these readings are printed on a teletype and punched on paper tape for subsequent computer analysis.

Computer programs were developed to sort the data by test, plot the load and COD data against time, and fit polynomial equations to these data. A typical plot of the data and best fit curves is shown in Fig. 2. Using these best fit equations, Eq 1, and the equation for stress intensity for the compact specimens, the crack lengths and stress intensities were evaluated at selected time intervals throughout the life of each test. The crack-growth rate was also determined by differentiating the equation developed for crack length versus time. A typical computer printout of these data is shown in Table 2.

Results and Discussion

The results of the ring-load stress-corrosion tests are summarized in Table 3. The applied loads were calculated based on the target stress-intensity values and the crack lengths measured on the sides of the specimens. When the loads were applied, the crack lengths calculated from the

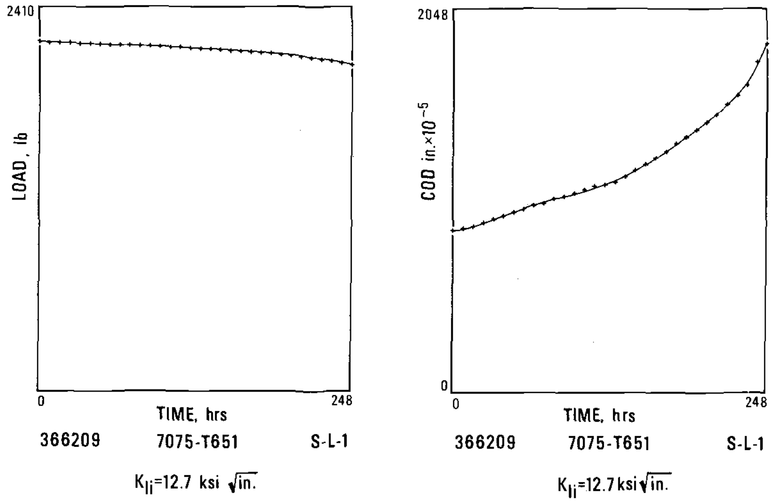

FIG. 2—*Typical computer plot of load and COD data with best-fit curves.*

load and COD measurements often differed from those measured on the sides of the specimens. Thus, the calculated initial stress intensities differed somewhat from the target values. The initial crack lengths calculated from load and COD measurements provide an integrated average crack length as opposed to an estimated value based on side measurements and were found to be more accurate. General corrosion of the crack faces usually destroys the definition of the end of the fatigue crack, but in the few instances where the precrack lengths could be discerned after fracture, the initial crack lengths were very close to the calculated values. The crack lengths at fracture, which would normally be the end of environmental crack growth, were also reasonably close to the calculated values in most instances.

A decided advantage of the ring-load test is that the initial load and crack length, and thus stress intensity, are known accurately. The load can be adjusted to provide the desired initial stress intensity, as was done in two of these tests, but in most instances it seemed sufficient to know the initial values without making minor load adjustments.

Many of the tests demonstrated a period of incubation before the initiation of environmental crack growth. As might be expected, the length of the incubation time generally increased with decreasing initial stress intensity. Also, some of the 2000 series alloys, particularly alloy 2219-T37, demonstrated temporary arrest during the test. This is illustrated by the data for one of the specimens of 2219-T37 shown in Fig. 3. The specimen experienced a short incubation period, followed by rapid crack growth and then an arrest of about 100 h duration before accelerated crack growth to failure. Metallographic examinations revealed that the probable cause of

TABLE 2—*Stress-corrosion fracture toughness data for ring loaded compact tension specimens.*

Alloy-temper: 7075-T651
Sample number: 366209
Specimen thickness: 1.000 in.
Ring constant: 0.500 in./h
Product: plate
Specimen number: S-L-1
Specimen width: 2.000 in.
Gage constant: 100 000. in./in.

Size: 2.5 in. thick
Mechanical test number: 092768A
Initial crack length: 0.990 in.
Modulus: 10.0 × 10^3 ksi
Spec. loaded: 03-23-71
Type test: TI
Type precrack: FC
Initial K_I: 14.7 ksi $\sqrt{\text{in.}}$

Time, h	Load(P), lb	COD(V), in.	Crack Length (a), in.	Crack-Growth Rate (ADDT), in./h	Stress Intensity Factor(KI), ksi $\sqrt{\text{in.}}$	Remarks Crack Growth Rate Difference
0	2191	0.00864	0.888	0.1216E-03	12.7	0.0000E-00
10	2190	0.00877	0.893	0.7000E-03	12.8	0.5784E-03
20	2188	0.00895	0.902	0.1011E-02	12.9	0.3116E-03
30	2185	0.00918	0.912	0.1131E-02	13.1	0.1199E-03
40	2181	0.00942	0.923	0.1125E-02	13.3	−0.5765E-05
50	2178	0.00966	0.934	0.1050E-02	13.5	−0.7545E-04
60	2175	0.00989	0.945	0.9507E-03	13.6	−0.9970E-04
70	2171	0.01011	0.954	0.8614E-03	13.8	−0.8933E-04
80	2168	0.01030	0.962	0.8063E-03	13.9	−0.5503E-04
90	2165	0.01048	0.970	0.7993E-03	14.1	−0.7024E-05
100	2161	0.01067	0.978	0.8446E-03	14.2	0.4527E-04
110	2157	0.01087	0.987	0.9382E-03	14.4	0.9362E-04
120	2153	0.01110	0.997	0.1069E-02	14.6	0.1312E-03
130	2148	0.01138	1.008	0.1222E-02	14.8	0.1534E-03
140	2144	0.01170	1.021	0.1380E-02	15.0	0.1573E-03
150	2138	0.01208	1.036	0.1523E-02	15.3	0.1428E-03
160	2133	0.01250	1.052	0.1636E-02	15.7	0.1129E-03
170	2127	0.01295	1.069	0.1709E-02	16.1	0.7361E-04
180	2121	0.01344	1.086	0.1744E-02	16.5	0.3448E-04
190	2114	0.01394	1.103	0.1753E-02	16.9	0.9201E-05
200	2106	0.01445	1.121	0.1769E-02	17.4	0.1569E-04
210	2097	0.01499	1.139	0.1845E-02	17.9	0.7654E-04
220	2086	0.01560	1.158	0.2064E-02	18.4	0.2193E-03
230	2074	0.01638	1.181	0.2541E-02	19.2	0.4769E-03
240	2059	0.01745	1.211	0.3429E-02	20.2	0.8880E-03
248	2045	0.01868	1.242	0.4567E-02	21.4	0.1137E-02
Calculated SIF based on measured (a) after fracture			1.278		23 089	

NOTE—Standard error = 0.4214052.

Load = 0.1095E 04+ 0.3124E-01T+ −0.7680E-02T**2+ 0.1433E-03T**3+
−0.1393E-05T**4+ 0.7107E-08T**5 + −0.1822E-10T**6+ 0.1815E-13**7+

COD = 0.8648E 03+ 0.8799E 00T+ 0.3715E-01T**2+ −0.9484E-04T**3+
−0.7191E-05T**4+ 0.8756E-07T**5 + −0.3743E-09T**6+ 0.5561E-12T**7+

a = 0.8882E 00+ 0.1216E-03T+ 0.3694E-04T**2+ −0.5819E-06T**3+
0.3601E-08T**4+ −0.5193E-11T**5 + −0.2498E-13T**6+ 0.6918E-16T**7+

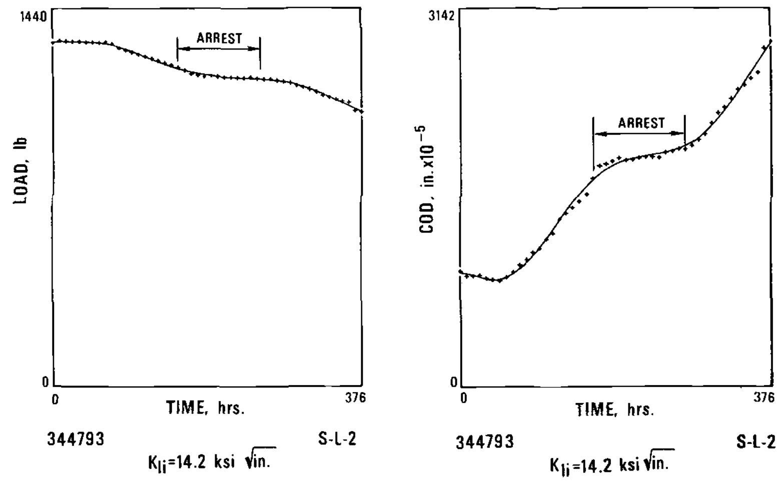

FIG. 3—*Ring loaded compact specimen of 2219-T37 exposed in a salt-dichromate-acetate solution.*

these temporary arrests was crack branching, which may delay the forward progress of the crack on its final path to failure.

One method of analyzing these data and comparing different alloys is by considering crack-growth rates (*da*/*dt*) as a function of instantaneous stress intensity. A plot of such data for 7075-T651 is shown in Fig. 4. A

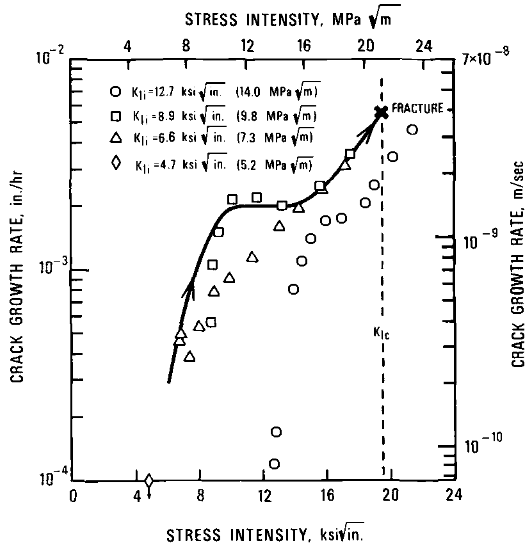

FIG. 4—*Crack-growth rate versus stress-intensity for compact specimens of 7075-T651 plate exposed in a salt-dichromate-acetate solutions.*

TABLE 3—*Results of tests of ring-loaded short transverse (S-L) compact specimens from some aluminum alloy plate.*

Alloy and Temper	Target		Initial Values			Final Values			Incubation Time, h	Time to Failure, h
	K_{Ii},[a] ksi$\sqrt{\text{in.}}$	% K_{Ic}	Crack Length,[b] in.	Load,[c] lb	K_{Ii},[a] ksi$\sqrt{\text{in.}}$	Crack Length,[b] in.	Load,[c] lb	K_{If},[a] ksi$\sqrt{\text{in.}}$		
					High-Resistance Alloys					
2021-T87	17.7	90	1.030	2490	17.7	1.141	2440	20.9	200[h]	392
	15.0	76	1.054	2210	16.3	1.112[d]	2200	17.9[d]	...	OK 2328
2024-T851	15.0	90	0.962	2270	14.6	1.137	2190	18.6	80	240
	12.0	72	0.939	1810	11.3	0.979[d]	1810	11.9[d]	...	OK 2400
2219-T87	19.0	97	0.782	1820	20.4	0.840	1790	22.7	0	16
	18.6	95	0.809	1800	21.3	0.871	1760	24.1	0[h]	504
	17.7	90	0.758	1730	18.4	0.803[d]	1720	20.1[d]	...	OK 1816
7075-T7351	21.0	100	0.909	3180	18.7	0.926	3120	19.1	...	OK 2780
					Low-Resistance Alloys					
2024-T351	15.8	75	0.882	2360	13.6	1.323	2140	26.8	50	664
	12.0	57	0.958	1900	12.1	...[e]	1865	...[e]	150	1192
	10.5	50	0.870	1570	8.9	...[e]	...	...[e]	...	OK 3980

2219-T37	13.5	50	0.767	1311	14.2	1.118	1040	31.1	50[h]	376
	13.5	50	0.760	1330	14.2	1.199	900	36.5	200[h]	1280
	12.0	44	0.779	1160	12.9	1.201	810	33.3	0[h]	560
7039-T6351	15.3	75	0.886	2300	13.3	1.286	2110	24.2	0	320
	10.2	50	0.972	1470	9.6	1.438	1250	21.0	0	600
	8.2	40	1.000	1190	8.2	...[f]	660	...[f]	1300	1872
	7.0	34	0.888	1200	7.0[g]	...[f]	870	...[f]	0	2376
7075-T651	14.7	75	0.888	2190	12.7	1.242	2040	21.4	0	248
	9.8	50	0.910	1490	8.9	1.338	1350	17.5	200	400
	7.0	36	0.852	1200	6.6[g]	1.456	980	17.2	350	824
	5.9	30	0.826	880	4.7	0.865	870	4.9	...	OK 2208

---

[a] 1 ksi$\sqrt{\text{in.}}$ = 1.1 MPa$\sqrt{\text{m}}$.

[b] 1 in. = 2.54 cm.

[c] 1 lb = 4.45 N.

[d] Apparent increase in crack length and stress intensity due to long-term drift in clip gage. There was no significant decrease in load.

[e] Clip gage failed during test.

[f] Rapid fracture. Cracks too long for meaningful calculation.

[g] Load was adjusted at beginning of test to obtain target K_{Ii} level.

[h] Temporary arrest occurred during the test.

close look at the data points indicates that a family of curves could be developed showing low *da/dt* rates at the initial stress-intensity level (regardless of what that level is) but with a tendency for the *da/dt* rates to converge somewhat at stress-intensity levels approaching K_{Ic} [*3*]. Also, it may be observed that two of the individual tests demonstrate an intermediate period of constant crack-growth rate (or plateau value) and one test demonstrates a steadily increasing crack-growth rate.

It appears that the most useful method of representing the data for several tests of a given alloy is a curve through the upper limit of crack-growth rates developed by all of the tests, as shown by the line in Fig. 4. The upper boundary lines for several alloys are shown in Fig. 5. This comparison of crack-growth rates indicates that alloys 7075-T651 and 7039-T6351 are clearly the most susceptible to SCC, and alloys 2024-T81, 2219-T87, and 7075-T7351 are very resistant to SCC. Alloys of low and intermediate resistance to SCC develop a "plateau velocity" which has often been observed in constant displacement (bolt load) type tests. Alloys of relatively high resistance to SCC, such as 2024-T851 and 2021-T81, experience crack growth only at K_I levels close to their K_{Ic} values and do not demonstrate a clearly defined plateau value [*1*].

Data for alloys 2219-T87 and 7075-T7351 are shown as points on axes of Fig. 5. Two specimens of 2219-T87 failed, but at levels above the ambient K_{Ic} value, and metallographic examination indicated that the fractures were of a tensile nature and not SCC. Creep may be responsible for

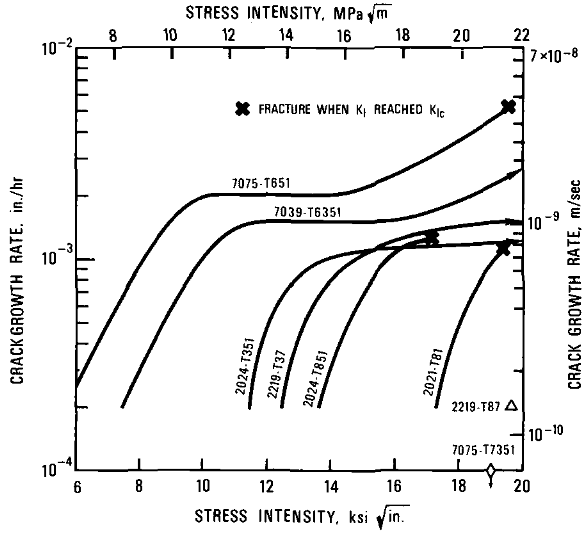

FIG. 5—*Crack-growth rate versus stress intensity for S-L compact specimens of some aluminum alloys exposed in a salt-dichromate-acetate solution.*

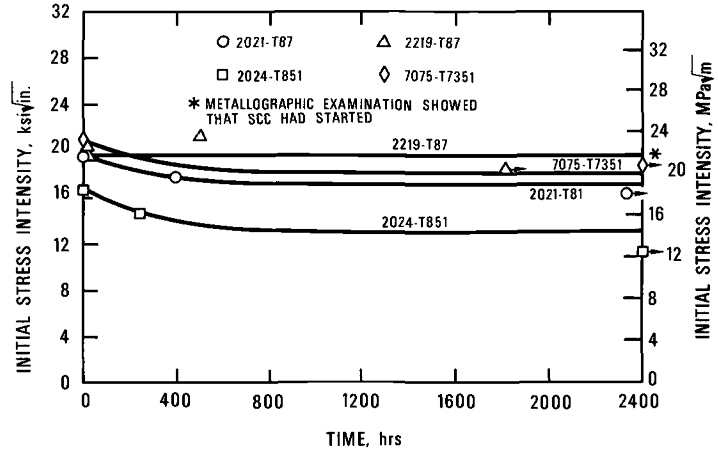

FIG. 6—*Initial stress intensity versus time to failure for some S-L compact specimens of resistant aluminum alloys exposed in a salt-dichromate-acetate solution.*

the failure of these specimens. Some slight crack growth was detected in the specimen of 7075-T7351, but it was so small that the growth rate is below the limits of Fig. 5.

Crack-growth rate data may be used to compare the relative resistance of various alloys, and, theoretically, these curves could be extrapolated to an arbitrarily chosen low rate to establish a threshold stress-intensity factor (K_{Ith}). However, a more straightforward method of determining threshold values with ring-load test data that does not involve an arbitrarily chosen *da*/*dt* is to plot initial or applied stress intensity versus time to failure as shown in Figs. 6 and 7. (The data points shown on the zero time axis are ambient K_{Ic} values.) For both high- and low-resistance alloys, a near threshold level was reached within 1000 h of exposure in this accelerated test environment. An exposure of about 2000 h with no significant indication of crack growth or drop in load, was considered sufficient to establish threshold values. Metallographic examinations of the "run-out" specimens showed no evidence of SCC except in those of 7075-T651 and T7351. The data in Figs. 6 and 7, tempered by the metallographic evidence, were used to establish the threshold stress-intensity levels shown in Table 4.

Summary and Conclusions

The ring-loading method used in conjunction with automatic data logging equipment has proven to be a useful method of determining stress-corrosion resistance using a fracture mechanics approach. Alloy rankings developed with ring-load data are about the same as those developed with

TABLE 4—*Estimated threshold stress-intensity factors for some aluminum alloy plate.*[a]

Alloy and Temper	K_{Ith} ksi$\sqrt{in.}$	K_{Ith} MPa$\sqrt{m}$	K_{Ith} $\%K_{Ic}$
	RESISTANT ALLOYS		
2219-T87	>20	22	100
2021-T81	17	19	85
7075-T7351	18	20	85
2024-T851	13	14	80
	SUSCEPTIBLE ALLOYS		
2024-T351	11	12	50
2219-T37	12	13	45
7039-T6351	6	7	30
7075-T651	4	4	20

[a] In a salt-dichromate-acetate solution.

smooth tension specimen data, and a proposal has been made for combining these two types of data for design purposes [2].

The ring-loading method has the following advantages over other techniques used for tests for precracked specimens:

1. The applied load, initial crack length, and the applied stress intensity are known more accurately than in most constant displacement type tests.
2. The progress of the test is monitored automatically with the data

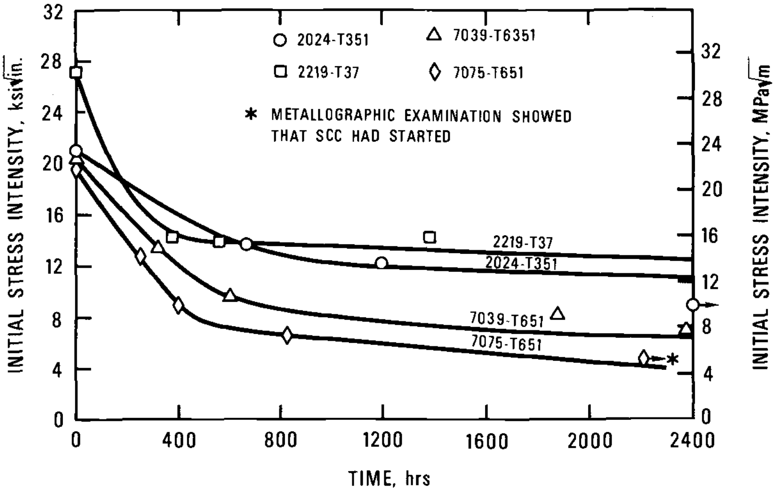

FIG. 7—*Initial stress intensity versus time to failure for some S-L compact specimens of low-resistance aluminum alloys exposed in a salt-dichromate-acetate solution.*

logging equipment and is in a form amenable to computer analysis. Thus more data can be collected with the expenditure of fewer manhours. This facilitates the determination of incubation periods and temporary arrests and can indicate instances in which metallographic examination may provide more information.

3. Because the stress intensity increases if crack growth develops, the test has a definite end point (fracture), and since the crack is opening, there are no apparent problems with corrosion product wedging effects.

4. The ring-load system is more compact and less cumbersome to operate than most deadweight systems.

Acknowledgment

The data presented in this paper were developed with the support of a U. S. Government contract [2].

References

[1] Brown, B. F., *Stress Corrosion Cracking in High Strength Steels and in Titanium and Aluminum Alloys*, Naval Research Laboratory, Washington, D. C., 1972. (Sponsored by the Advanced-Research Projects Agency, ARPA Order No. 878).

[2] Sprowls, D. O., Shumaker, M. B., Walsh, J. D., and Coursen, J. W., "Evaluation of Stress-Corrosion Cracking Susceptibility Using Fracture Mechanics Techniques," Final Report of Government Contract NAS 8-21487-Part I, prepared for George C. Marshall Space Flight Center, 31 May 1973.

[3] Wei, R. P., Novak, S. R., and Williams, D. P., *AGARD Conference Proceedings*, No. 98, Advisory group for Aeronautical Research and Development, 4-8 Oct. 1971.

W. G. Clark, Jr.,[1] *and J. D. Landes*[1]

An Evaluation of Rising Load K_{Iscc} Testing

REFERENCE: Clark, W. G., Jr., and Landes, J. D., "**An Evaluation of Rising Load K_{Iscc} Testing,**" *Stress Corrosion—New Approaches, ASTM STP 610,* American Society for Testing and Materials, 1976, pp. 108–127.

ABSTRACT: This report presents a detailed evaluation of the rising load, accelerated K_{Iscc} testing procedure proposed by McIntyre and Priest. Conventional long hold-time "bolt loaded" K_{Iscc} tests were conducted with 160 and 180-ksi yield-strength Type 4340 steel exposed to seawater, hydrogen, and hydrogen sulfide gas environments, and the results of these tests compared with similar data generated under rising load conditions. The results show that rising load K_{Iscc} testing in hydrogen sulfide gas can be used as a valuable technique for rapidly screening structural alloys with regard to their susceptibility to environment induced cracking in hydrogen bearing environments. However, this testing procedure cannot always be used to develop a quantitative measure of K_{Iscc}. Specifically, it is shown that for steels below about 200 ksi in yield strength, the K_{Iscc} measured in hydrogen sulfide gas is not the same as that measured in other hydrogen bearing environments (hydrogen and seawater). In addition, it is shown that gas pressure and loading rate can have a significant effect on the apparent K_{Iscc} measured under rising load conditions.

KEY WORDS: stress corrosion, environments, crack propagation, seawater, toughness, mechanical properties, gases, hydrogen, hydrogen sulfide

Currently, the accepted methods of determining the fracture mechanics stress-corrosion threshold parameter, K_{Iscc} (the value of the plane-strain stress-intensity factor below which an existing crack will not grow due to stress corrosion), for structural metals involve either the constant-load cantilever bend test or the constant-displacement "bolt loaded" compact toughness test [*1,2*].[2] Although each of these procedures have distinct advantages and limitations with regard to K_{Iscc} testing, they both have the same major limitation—testing times of the order of hundred to thousands of hours are required normally to establish a meaningful K_{Iscc} value [*3,5*].

In 1972, McIntyre and Priest reported that the K_{Iscc} values determined for a series of high-strength steels (200 to 400 ksi yield strength) exposed

---

[1] Fellow engineers, Mechanics Department, Westinghouse Research Laboratories, Pittsburgh, Pa. 15235.

[2] The italic numbers in brackets refer to the list of references appended to this paper.

to seawater, hydrogen (H_2) gas, and hydrogen sulfide (H_2S) gas environments were essentially independent of the test environment [*6*]. In addition, they noted that the corresponding crack-growth rates in the H_2S gas environment were of the order of three to four orders of magnitude faster than that encountered in either seawater or H_2 gas. On the basis of these observations, McIntyre and Priest have proposed that K_{Iscc} testing in H_2S gas can be used as an accelerated test procedure for evaluating a material's stress-corrosion threshold in other hydrogen bearing environments. More specifically, the proposed test procedure involves conventional rising load K_{Ic} fracture-toughness testing in a H_2S environment. The stress-intensity level associated with the onset of crack growth encountered in such a test is interpreted as the material's K_{Iscc}. Preliminary results involving this accelerated test method show that the time required to determine K_{Iscc} values can be reduced from many hours to a few minutes.

In view of the potential advantages associated with the accelerated K_{Iscc} test proposed by McIntyre and Priest, an extensive program was undertaken at Westinghouse Research to further evaluate the technique and to establish the limitations. Among the specific aspects of the test procedure investigated in this program were the determination of the applicability of the technique to lower strength steels ($<$200 ksi yield strength), and the evaluation of the effect of loading rate and H_2S gas pressure on the apparent K_{Iscc}. Conventional long hold-time K_{Iscc} tests were conducted with 160 and 180-ksi yield-strength Type 4340 steel specimens exposed to seawater, H_2, and H_2S gas environments, and the results of these tests compared with the results of accelerated K_{Iscc} tests. This report presents a detailed discussion of the test program and results. A modified rising load (slow loading rate) K_{Iscc} test procedure which involves the use of a displacement gage to monitor crack initiation and growth behavior is described. A limited number of tests were also conducted to evaluate the effect of precracking technique (environment induced static load crack growth versus fatigue precracking in air) on rising load K_{Iscc} measurements. A preliminary evaluation of the effect of air additions on the K_{Iscc} measured in H_2S gas is also described.

Material

The material involved in this investigation consisted of quenched and tempered AISI Type 4340 steel (ASTM A288-CL-8) supplied as 3-in.-thick forged plate. Materials heat treated to both 160 and 180 ksi yield-strength levels were included. The nominal chemical composition, heat treatment, and room-temperature mechanical properties of the forgings are summarized in Table 1.

TABLE 1—*Chemical composition, heat treatment, and room-temperature mechanical properties of materials investigated.*

Chemical Composition, weight percent

Material Identification	C	Si	P	S	Mn	Ni	Cr	Mo	V
No. 160	0.31	0.27	0.006	0.014	0.63	2.29	0.87	0.39	0.067
No. 180	0.36	0.25	0.010	0.010	0.76	2.54	0.86	0.39	0.093

Heat Treatment

No. 160	austenitized 4 h at 1560°F, water quenched; double tempered 4 h at 1080°F and furnace cooled
No. 180	austenitized 4 h at 1560°F, water quenched; tempered 4 h at 1040°F and water quenched to room temperature

Mechanical Properties at 76°F

	0.2% Yield Strength, ksi	Tensile Strength, ksi	Elongation in 2 in., %	Reduction in Area, %	Charpy Impact Energy, ft·lb
No. 160	159.5	171	16.5	51.5	50
No. 180	179	194	14	46	30

Experimental Procedure

Long-Time K_{Iscc} *Testing*

Most of the long-time K_{Iscc} tests were conducted with 1-in.-thick wedge-opening-loading (WOL) type compact toughness specimens of the geometry shown in Fig. 1. A limited number of tests involving 2-in.-thick specimens were also included. The specimens were removed from the 3-in. thick forgings such that the plane of the machined notch was parallel to the long-transverse direction and perpendicular to the major axis of the forging (L-T crack plane orientation). Prior to K_{Iscc} testing, all specimens were fatigue precracked in air approximately 0.300 in. beyond the notch tip. The stress-intensity range associated with the precracking operation did not exceed 15 ksi$\sqrt{\text{in.}}$ ($R = 0.1$).

The long-time K_{Iscc} tests were conducted in accordance with the bolt loading constant displacement stress-corrosion test procedure described by Novak and Rolfe [2]. Figure 2 presents a schematic illustration of the loading technique and instrumentation involved. The bolt loaded specimens were loaded initially to relatively high stress-intensity levels (K_{Ii}), exposed to the environment of interest for a predetermined length of time, unloaded, fatigue marked, and subsequently pulled to failure. The fatigue marking procedure was used to produce a "bench mark" which clearly

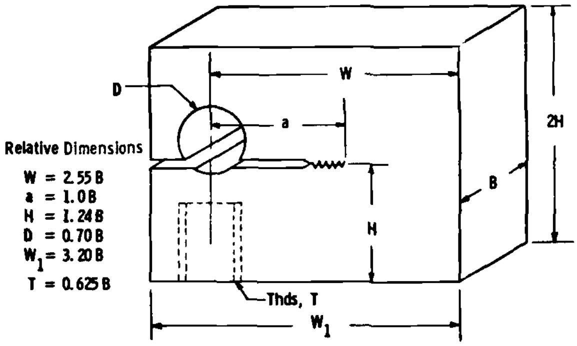

FIG. 1—*WOL type compact fracture-toughness specimen (relative dimensions in terms of thickness* B*).*

defines the extent of any prior environment induced crack growth. Since the test is conducted under constant displacement conditions, the load on the specimen and, consequently, the nominal stress intensity factor decreases as the crack grows, leading to crack arrest as the decreasing K_I level approaches the threshold for cracking, K_{Iscc}. From knowledge of the initial loading conditions and the final crack length at the end of the test, the stress-intensity level associated with crack arrest can be computed [2]. For a given type material and specimen geometry the stress intensity developed as the result of bolt loading can be expressed directly as a function of the displacement across the machined slot and crack length. This relationship involves the stress-intensity expression and compliance characteristic of the specimen involved. The stress-intensity expression for the

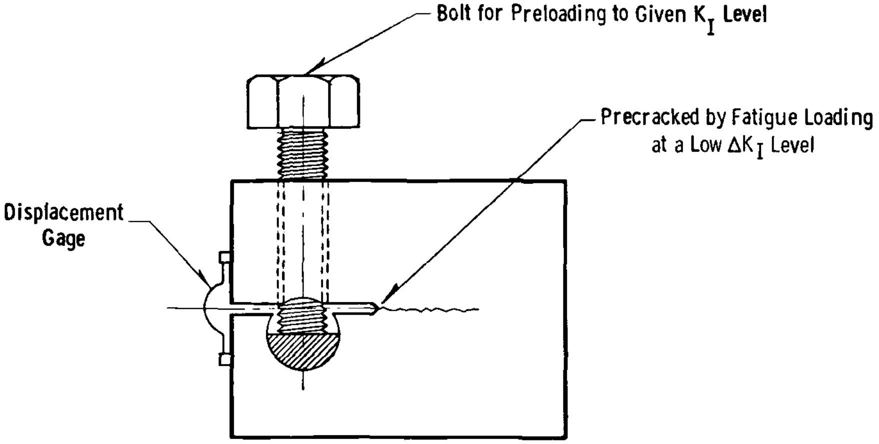

FIG. 2—*WOL specimen modified for use as a stress-corrosion susceptibility specimen.*

1-in.-thick WOL type compact tension specimen involved here is given by [7]

$$K_{\mathrm{I}} = Y\frac{P\sqrt{a}}{BW} \tag{1}$$

where

a = crack length measured from the centerline of loading,
P = applied load,
B = specimen thickness (1 in.),
W = specimen width measured from the centerline of loading (2.55 in.), and
Y = a constant which depends upon the relative crack length a/W

$$\left[Y = 30.96 - 195.8\left(\frac{a}{W}\right) + 730.6\left(\frac{a}{W}\right)^2 - 1186.3\left(\frac{a}{W}\right)^3 + 754.6\left(\frac{a}{W}\right)^4\right]$$

The appropriate compliance calibration expression for the WOL specimen is

$$EB\left(\frac{V_i}{P}\right) = C \tag{2}$$

where

C = compliance constant dependent upon a/W,
E = modulus of elasticity,
V_i = displacement across the machined slot measured at the centerline of loading, and
P, a, and W = applied load, crack length, and specimen width, respectively, as described for Eq 1.

The compliance expression can be combined with the stress-intensity expression to yield the relationship between K_{I}, V_i, and a, specifically

$$\frac{K_{\mathrm{I}}}{V_i} = \frac{YE\sqrt{a}}{CW} \tag{3}$$

This expression provides a convenient method of computing K_{I} for various combinations of crack length and displacement values. Note that the value of displacement, V_i, refers to the displacement measured at the centerline of loading. Since most displacements are measured near the front of the specimen rather than at the centerline of loading, Eq 3 must be corrected for the point at which displacement measurements are made. This correction involves a trigonometric manipulation [*2*]. Figure 3 shows the K_{I}/V versus crack length calibration for the 1-in.-thick steel specimens involved in this investigation. Note that the displacement, V (in mils, 0.001 in.),

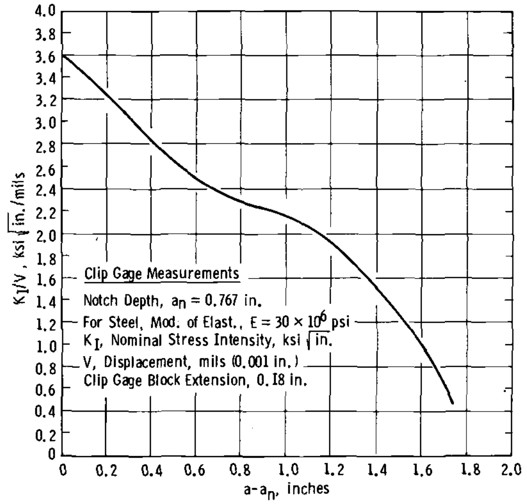

FIG. 3—K_I/V *calibration curve for steel 1T WOL specimens.*

refers to displacement measurements made at gage points which extend 0.180 in. beyond the front face of the specimen. Also note that the crack length $a - a_n$ refers to the crack length measured beyond the tip of the machined slot. The calibration curve shown in Fig. 3 was used to compute both the stress-intensity factor associated with the initial loading of the specimens (K_{II}) and the stress intensity at crack arrest (K_{Iscc}).

Bolt loaded K_{Iscc} tests were conducted at 75°F in synthetic seawater (ASTM Specification for Substitute Ocean Water (D 1141-52 (1971) Formula A)), high purity, dry H_2 gas[3] at 80 psig, and high purity H_2S gas[4] at 50 psig. In all tests, the loading bolts and split pins (Fig. 2) were made of Type 4340 steel. The seawater tests were conducted in a plastic container, and the specimens were bolt loaded with the specimen notch and precrack exposed to the seawater environment. The specimens exposed to the H_2 and H_2S environments were loaded initially in air and then placed in a Type 304 stainless steel pressure chamber which was evacuated to 10^{-2} torr and back filled with the gas of interest. The seawater tests were exposed to the environment for hold times ranging from 170 to 15 000 h. The gaseous environment tests involved hold times ranging from as short as 10 min to as long as 2000 h. Crack-length versus elapsed-time measurements were made with the seawater tests, and these results converted to crack-growth rate data. The crack lengths were monitored visually. No crack-growth rate data were generated with the bolt loaded specimens exposed to the gaseous environments.

---

[3] 99.95 volume percent H_2, dew point −70°F (−60°C).

[4] 99.6 volume percent (liquid phase) H_2S, typically 31-ppm water.

Rising Load K_{Iscc} *Testing*

The rising load K_{Iscc} testing procedure involved in this study varies from that originally proposed by McIntyre and Priest primarily in that a load-displacement record is used to determine the onset of subcritical crack growth rather than an electrical potential crack monitoring system [*6*]. Figure 4 presents a schematic illustration of the rising load K_{Iscc} testing concept involving the use of displacement measurements to monitor crack-growth behavior. The testing technique is essentially identical to the procedure used for K_{Ic} fracture-toughness testing (ASTM Test for Plane-Strain Fracture Toughness of Metallic Materials E 399-72) except that a slower rate of loading is involved normally, and the specimen is exposed to the environment while being loaded. A typical gaseous environment test set up is illustrated in Fig. 5. As noted in Fig. 4, if subcritical crack extension occurs during the rising load test, the load corresponding to crack initiation can be determined from the point of nonlinear deviation on the load-displacement record. The corresponding crack length and ultimately, the stress-intensity level associated with the onset of crack growth can be determined from the relationship between the stress-intensity expression and compliance characteristics of the specimen (Eq 3). Figure 6 shows the displacement/load (V/P) versus crack-length calibration for the 1-in.-thick steel WOL specimens involved here. This curve can be used to determine the crack length corresponding to the point of deviation on the load-displacement record. From this crack length and the corresponding displacement value, the stress-intensity level associated with the onset of subcritical crack growth can be determined using the curve shown in Fig. 3. A comparison of actual crack-length measurements made on broken specimens with the crack length determined from the V/P calibration shown in Fig. 6 indicates a crack-length measurement accuracy of about ±0.02 in. for cracks 0.50 in. in length ($a - a_N$) or less. The accuracy of

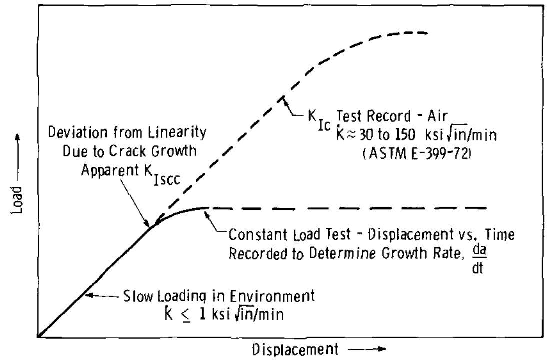

FIG. 4—*Schematic of rising load* K_{Iscc} *testing.*

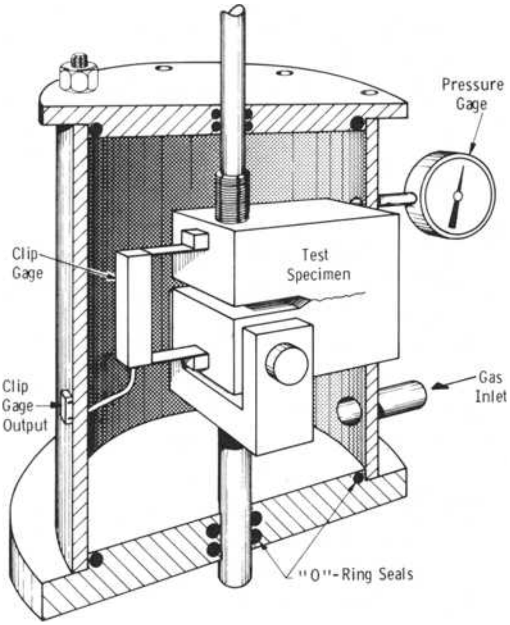

FIG. 5—*Slow loading rate* K_{Iscc} *test.*

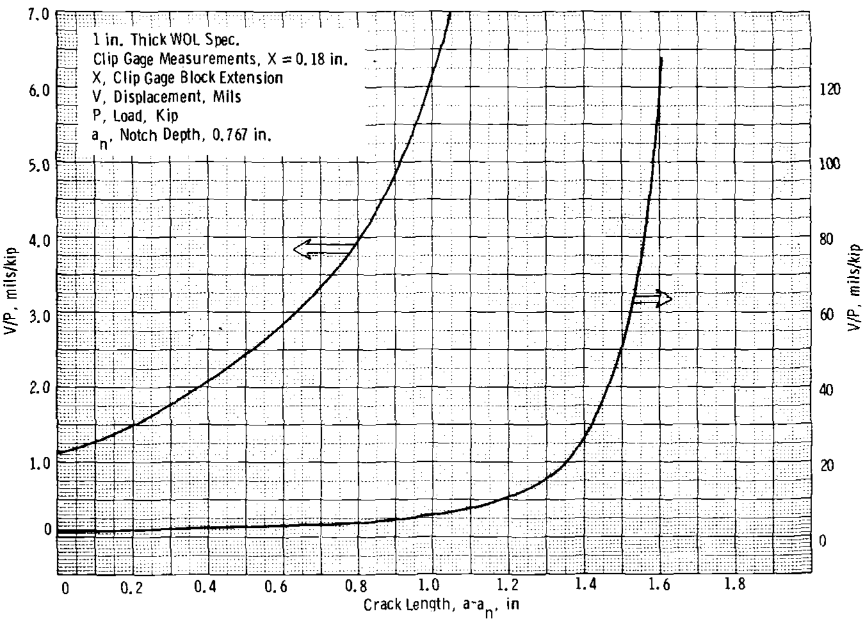

FIG. 6—V/P *calibration for steel 1T WOL specimens.*

the V/P versus crack-length calibration increases to about ±0.010 in. for larger cracks.

Once the onset of crack growth has occurred, crack-growth rate data can be developed by maintaining the load constant and monitoring the displacement as a function of elapsed time. These results can be converted to crack-growth rate data by means of the calibration curve shown in Fig. 6.

In order to standardize the technique used to establish the point of deviation on the load-displacement record associated with the onset of subcritical crack growth, a 5 percent secant offset procedure similar to that used for K_{Ic} testing (ASTM Method E 399-72) was employed. Specifically, a line with a slope 5 percent less than the slope of the linear load-displacement record is drawn through the origin of the test record, and the point at which the test record curve crosses the 5 percent offset line is used to define the load and displacement at the onset of crack extension.

All of the slow loading rate K_{Iscc} tests involved in this investigation were conducted with 1-in.-thick WOL specimens (Fig. 1) in accordance with the test procedure just described. The specimens were fatigue precracked in air prior to loading in the environment. Tests were conducted at loading rates ranging from 20 to 5000 lb/min. For the crack lengths involved in this study, these loading rates correspond to $\dot{K}_I$ (rate of change in K_I) values of 0.1 to 45 ksi$\sqrt{\text{in.}}$/min. Rising load K_{Iscc} tests were conducted at 75°F in air, synthetic seawater, and both H_2 and H_2S gas at various pressures. Crack-growth rate data were also generated in these environments.

Test Results

Long-Time K_{Iscc} Testing

Tables 2 and 3 present the results of the long-time bolt loaded K_{Iscc} tests for the 180 and 160-ksi yield-strength Type 4340 steels, respectively. Note that no subcritical crack growth was encountered in the 54 percent relative humidity air tests conducted with the 180-ksi yield-strength material. Note also that for a given environment, there is no significant difference in the K_{Iscc} values obtained for the 180-ksi yield-strength material at the various hold times and K_{Ii} levels involved. The fact that there are no hold-time effects within a relatively wide range of hold times at the same K_{Ii} level is usually a clear indication that the K_{Iscc} has been adequately identified. Although there is considerable scatter in the K_{Iscc} data reported in Table 2, particularly for the H_2 gas environment tests, it is apparent that there is a significant difference between the K_{Iscc} values obtained in seawater and those measured in the gaseous environments ($K_{Iscc} \approx 37$ ksi$\sqrt{\text{in.}}$ versus $K_{Iscc} \approx 30$ ksi$\sqrt{\text{in.}}$, respectively). There does not appear to be a significant difference between the K_{Iscc} values obtained for the 180-ksi yield-strength material in H_2 gas at 80 psig or H_2S gas at 50 psig.

TABLE 2—*Summary of long-time* K_{Iscc} *test results for 180-ksi yield-strength Type 4340 steel (all tests 1T WOL specimens, 75°F).*

Specimen Identification	Environment	Hold Time, h	K_{Ii}, ksi$\sqrt{\text{in.}}$	K_{Iscc}, ksi$\sqrt{\text{in.}}$
T-11	54% RH[a] air	336	105	no growth
T-14	54% RH air	336	85	no growth
A2-27	synthetic seawater	600	45	40
A2-28	synthetic seawater	600	63	39
3-28	synthetic seawater	10 920	80	34
3-22[b]	synthetic seawater	10 980	60	33
3-14	synthetic seawater	5 200	60	40
			(avg 37 ± 34)	
T2-4[c]	80-psig H_2 gas	10 (min)	53	27
T2-1	80-psig H_2 gas	24	73	28
A2-31	80-psig H_2 gas	24	81	35
A2-32	80-psig H_2 gas	24	68	26
A2-34	80-psig H_2 gas	110	61	28
T2-2	80-psig H_2 gas	180	56	36
			(avg 30 ± 5)	
3-17	50-psig H_2S gas	24	60	31
3-19	50-psig H_2S gas	24	60	24
3-27	50-psig H_2S gas	1 130	60	27
			(avg 27 ± 4)	

[a] RH = relative humidity.
[b] Stress-corrosion precrack.
[c] Loaded in H_2 environment.

TABLE 3—*Summary of long-time* K_{Iscc} *test results for 160-ksi yield-strength Type 4340 steel.*

Specimen Identification	Environment, 75°F	Hold Time, h	K_{Ii}, ksi$\sqrt{\text{in.}}$	K_{Iscc}, ksi$\sqrt{\text{in}}$.
9336-7	synthetic seawater	170	104	97
5-24[a]	synthetic seawater	10 980	100	81
5-16	synthetic seawater	15 200	85	82
5-2[b]	synthetic seawater	10 000	75	no growth
			(avg 87)	
5-5[b]	80-psig H_2 gas	160	80	54
5-6[b]	80-psig H_2 gas	2 856	80	55
5-11[b]	80-psig H_2 gas	435	80	68
			(avg 59)	
5-13	50-psig H_2S gas	24	100	60
5-23	50-psig H_2S gas	1 130	100	no growth
			(avg 60)	

[a] Stress-corrosion precrack.
[b] 2T WOL specimens all other tests conducted with 1T WOL specimens.

The K_{Iscc} data generated for the 160-ksi yield-strength material (Table 3) show that the K_{Iscc} measured in the seawater environment is approximately 87 ksi$\sqrt{\text{in.}}$ versus about 55 ksi$\sqrt{\text{in.}}$ in the H_2 and H_2S environments. Comparison of the K_{Iscc} data generated for the 160 and 180-ksi yield-strength materials clearly indicates a very significant variation in the susceptibility to cracking with a relatively small change in yield-strength level. Specifically, a 20 ksi decrease in yield-strength level essentially yields a twofold increase in K_{Iscc} for the environments studied here.

Rising Load K_{Iscc} *Tests*

Figure 7 presents three typical load-displacement records representative of the rising load K_{Iscc} tests involved in this investigation. In each case, the loading rate was held constant at 20 lb/min ($\dot{K} = 0.1$ ksi$\sqrt{\text{in.}}$/min for the linear portion of the curves) until specimen failure occurred. Note that the deviation from linearity encountered in the H_2S environment is characterized by a very sharp break in the load-displacement record, and no significant increase in the load occurs prior to failure. In the H_2 environment, the deviation from linearity is more gradual, and there is about a 1000 lb increase in load prior to the development of rapid unstable crack growth. In air, the first deviation from linearity encountered on the load-displacement record occurs at about 20 000 lb, and the load continues to increase up to 28 000 lb before fast fracture occurs. The difference in the load-displacement records obtained in the H_2 and H_2S environments can be interpreted to reflect a difference in unstable crack-growth rate. In the case of the H_2S test, when crack growth first occurs the corresponding crack-growth rate is so fast that no significant increase in load occurs prior

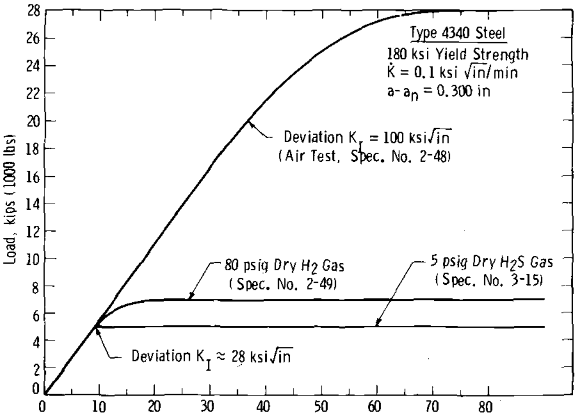

FIG. 7—*Effect of environment on load-displacement behavior.*

to failure. In H_2 the initial crack-growth rate is not quite as fast as that encountered in H_2S, and some increase in load occurs prior to the development of rapid unstable crack growth. Thus, it is apparent that the shape of the load-displacement record and, in particular, the extent of deviation from the linear portion of the curve is controlled by the interrelationship between the loading rate used in the test and the crack-growth rate properties of the material-environment system being studied. Specifically, the slower the rate of crack growth encountered in a given material-environment system the slower the loading rate required to detect the initiation of crack growth. Because of the high K_I levels associated with the air test shown in Fig. 7, the deviation from linearity may be the result of either subcritical crack growth, plastic yielding, or a combination of both mechanisms.

Table 4 presents the results of the rising load K_{Iscc} tests for the various conditions involved in this investigation. In all cases, the apparent K_{Iscc} values reported in Table 4 were determined on the basis of a 5 percent secant analysis of the respective load-displacement record as described previously. Note that in some cases, a single specimen was used to generate several data points (Specimens 3-12, 3-18, 3-22, 5-17, and 5-18). When this procedure was used, care was taken to ensure that the test conditions were altered such that the prior loading would not influence the subsequent test. For example, in those cases involving the use of a single specimen to evaluate the effect of gas pressure on apparent K_{Iscc}, the pressure was decreased progressively for each test such that the corresponding K_{Iscc} values increased. Comparison of the multiple specimen results with single tests indicate that there was no significant load history effects associated with any of the multiple test results presented here. In all cases involving multiple specimens, the crack was extended at least 0.100 in. under one set of loading conditions prior to testing at the next set of loading conditions. This procedure was used to ensure a relatively straight precrack for the subsequent test. Comparison of results generated with specimens containing fatigue precracks versus specimens containing stress-corrosion precracks (Table 4) does not reflect a significant effect of precracking technique on the apparent K_{Iscc} results.

The reproducibility and absence of a significant prior history effect on the apparent K_{Iscc} values measured with the multiple test procedure used in this investigation is clearly apparent in the results generated with Specimen 3-12. Note that at a $\dot{K}$ of 45 ksi$\sqrt{\text{in.}}$/min the apparent K_{Iscc} level is 70 ksi$\sqrt{\text{in.}}$; yet, when the test is subsequently repeated at a $\dot{K}$ of 0.2 ksi$\sqrt{\text{in.}}$/min, the apparent K_{Iscc} value is 35 ksi$\sqrt{\text{in.}}$, essentially the same as that measured originally. The tests conducted with Specimens 3-18 and 3-22 also illustrate the reproducibility of this technique.

Examination of the data presented in Table 4 shows that for the 180-ksi yield-strength material tested in both air and H_2 gas, there is a significant

TABLE 4—*Summary of rising load* K_{Iscc} *tests.*

Specimen Identification	Environment	Loading Rate, ksi$\sqrt{in.}$/min	Apparent K_{Iscc}, ksi$\sqrt{in.}$
180-KSI YIELD-STRENGTH TYPE 4340 STEEL			
2-47	54% RH[a] air	0.1	100
2-45	54% RH air	0.3	105
2-46	54% RH air	0.7	120
3-14	synthetic seawater	0.1	no growth to 60
2-49	H_2 gas 80 psig	0.1	30
2-52	H_2 gas 80 psig	0.1	34
3-26	H_2 gas 80 psig	0.1	28
4-23	H_2 gas 80 psig	0.7	38
4-24	H_2 gas 80 psig	0.35	36
3-12	H_2 gas 80 psig	0.1	32
3-12	H_2 gas 80 psig	0.35	35
3-12	H_2 gas 80 psig	0.7	40
3-12	H_2 gas 80 psig	1.1	42
3-12	H_2 gas 80 psig	3.4	44
3-12	H_2 gas 80 psig	7.4	53
3-12	H_2 gas 80 psig	16.0	58
3-12	H_2 gas 80 psig	45	70
3-12	H_2 gas 80 psig	0.20	35
3-17	H_2S gas 5 psig	0.1	27
3-18[b]	H_2S gas 5 psig	4.0	29
3-18	H_2S gas 5 psig	42	27
3-22[b]	H_2S gas 18 psig	0.1	24
3-22	H_2S gas 50 psig	0.1	22
3-18[b]	H_2S gas 50 psig	3.3	24
3-18	H_2S gas 50 psig	30	24
3-22[b]	H_2S gas 18 psig	0.1	26
3-22[b]	plus 5 volume % air	0.1	26
3-22[b]	plus 5 volume % air	0.1	26
160-KSI YIELD-STRENGTH TYPE 4340 STEEL			
5-20	H_2 gas 80 psig	0.1	66
5-22	H_2 gas 80 psig	0.1	54
5-14	H_2S gas 5 psig	0.1	90
5-18[b]	H_2S gas 5 psig	0.1	86
5-17[b]	H_2S gas 18 psig	0.1	68
5-18[b]	H_2S gas 18 psig	0.1	70
5-17	H_2S gas 50 psig	0.1	52
5-18	H_2S gas 50 psig	0.1	57
5-24	H_2S gas 50 psig	2.8	52
5-24	H_2S gas 50 psig	12	55
5-24	H_2S gas 50 psig	32	54

[a] RH = relative humidity.

[b] Environment induced precrack.

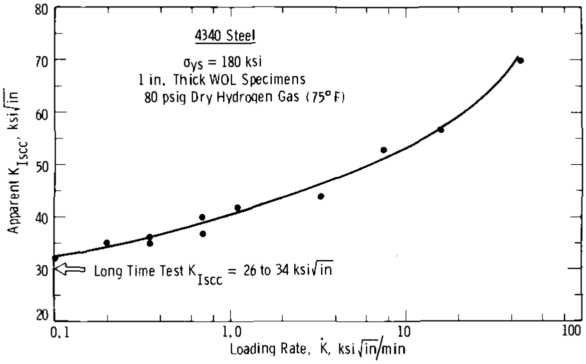

FIG. 8—*Effect of loading rate on apparent* K_{Iscc}.

effect of loading rate on apparent K_{Iscc}. In both cases, the apparent K_{Iscc} increases as the loading rate increases. Figure 8 presents the effect of loading rate on the apparent K_{Iscc} measured for the 180-ksi yield-strength material in 80-psig H_2 gas. Similar data generated with the 180 and 160-ksi yield-strength steels exposed to the H_2S gas, do not reveal a significant loading rate effect. These results are presented in Fig. 9.

Figure 10 presents the effect of H_2S gas pressure on the apparent K_{Iscc} values measured for both the 160 and 180-ksi yield-strength materials. Note that the gas pressure has a more significant effect on the apparent K_{Iscc} values associated with the lower strength material than on the higher strength steel.

Further examination of the data summarized in Table 4 shows that rising load K_{Iscc} testing (at $\dot{K} = 0.1$ ksi$\sqrt{\text{in.}}$/min) of the 180-ksi yield-strength material in a synthetic seawater environment does not yield subcritical crack growth up to a K_I level of 60 ksi$\sqrt{\text{in.}}$ In addition, note that

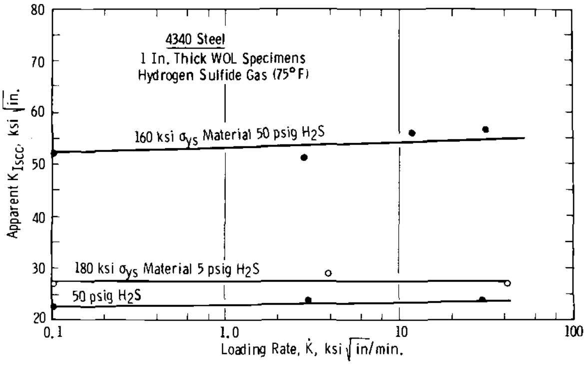

FIG. 9—*Effect of loading rate on apparent* K_{Iscc} *in* H_2S.

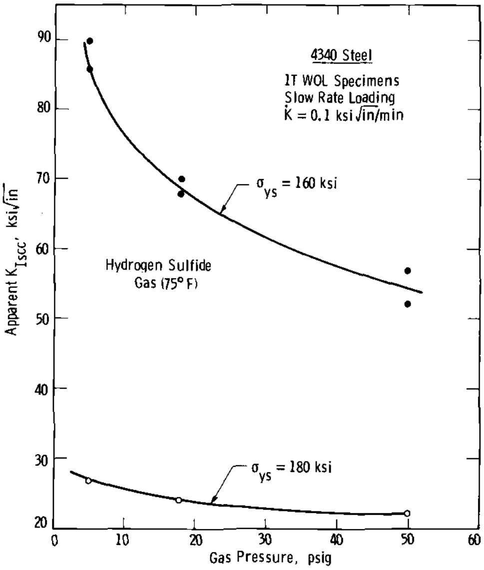

FIG. 10—*Effect of* H_2S *gas pressure on the apparent* K_{Iscc} *of Type 4340 steel.*

there is no significant difference between the apparent K_{Iscc} values measured for the 180-ksi yield-strength material exposed to pure H_2S gas and H_2S gas containing 5 volume percent air.

Table 5 presents a comparison of the K_{Iscc} data generated as the result of both the long time bolt loaded and rising load K_{Iscc} tests. Note that for a given yield strength level the K_{Iscc} values measured in either H_2 or H_2S gas are not dependent upon the specific testing procedure. However, note that in seawater the long-time K_{Iscc} value obtained for the 180-ksi yield-strength material is about 37 ksi$\sqrt{\text{in.}}$; yet, no crack growth was encountered in the rising load test to a K_I level of 60 ksi$\sqrt{\text{in.}}$ Table 5 also shows that the K_{Iscc} values determined in either H_2 or H_2S gas are not the same as that determined in seawater.

Figure 11 presents the results of the crack-growth rate data generated for the 180-ksi yield-strength material exposed to various environments. In all cases, these data were developed under constant load conditions.[5] Note that the crack-growth rate behavior encountered in the H_2 and H_2S environments is of the order of 3 to 5 orders of magnitude faster than that encountered in the synthetic seawater. Note also that unstable crack growth was encountered in air. A limited amount of crack-growth rate data generated for the 160-ksi yield-strength material indicates a crack-growth rate of the order of 1 in./min of K_I levels between 60 and 100 ksi$\sqrt{\text{in.}}$ in the 50-psig H_2S environment.

---

[5] Following the onset of crack growth in the rising load test, the load was held constant until failure occurred.

TABLE 5—*Summary of stress-corrosion threshold data generated in this investigation.*

Environment	K_{Iscc}, ksi$\sqrt{\text{in.}}$, (long time bolt loaded tests)	Apparent K_{Iscc}, ksi$\sqrt{\text{in.}}$, (rising load tests)
180-KSI YIELD-STRENGTH TYPE 4340 STEEL[a]		
54% RH[b] air	no growth to K_I = 105	100
Synthetic seawater	37	no growth to 60
H_2 gas, 80 psig	30	32
H_2S gas, 5 psig	26	27
H_2S gas, 18 psig	...	24
H_2S gas, 50 psig	27	23
H_2S gas plus 5 volume % air	...	26
160-KSI YIELD-STRENGTH TYPE 4340 STEEL		
Synthetic seawater	87	...
H_2 gas, 80 psig	59	60
H_2S gas, 5 psig	...	88
H_2S gas, 18 psig	...	69
H_2S gas, 50 psig	60	54

[a] $\dot{K} \approx 0.1$ ksi$\sqrt{\text{min}}$

[b] RH = relative humidity.

With regard to the crack growth encountered in the air environment, note that unlike the rising load air test data shown in Fig. 7, the crack-growth rate data were developed under constant load conditions. Specifically, the rising load portion of the test was terminated at a K_I level of 105 ksi$\sqrt{\text{in.}}$ and the corresponding load held constant for the duration of

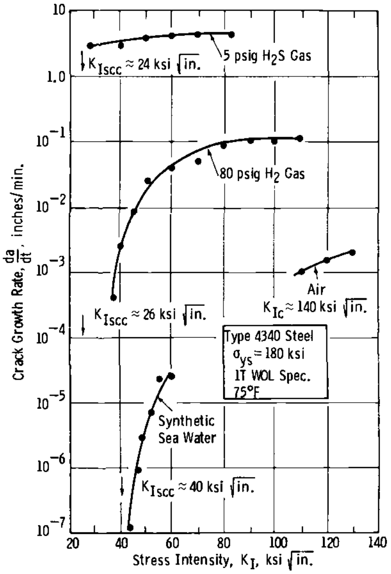

FIG. 11—*Effect of environment on static load crack growth rate (180-ksi yield-strength Type 4340 steel).*

the test. Since crack growth to failure did occur under these conditions, it is apparent that the possibility of subcritical crack growth in air should be a primary consideration in the evaluation of this material.

Discussion

The data generated in this investigation clearly indicate that the rising load K_{Iscc} testing procedure proposed by McIntyre and Priest includes several very significant limitations. The most important limitation is the fact that the H_2S gas pressure can have a pronounced effect on the apparent K_{Iscc} value. Although the H_2S gas pressure was not found to be a significant factor in the tests involving the high-strength material, gas pressure was a very important variable in the tests conducted with the 160-ksi yield-strength steel (Fig. 10). Specifically, increasing the H_2S gas pressure from 5 to 50 psig produced almost a 50 percent decrease in apparent K_{Iscc} (88 to 54 $\text{ksi}\sqrt{\text{in.}}$). In addition, the tests conducted in this investigation do not show that the same K_{Iscc} value is obtained for a given material in the three H_2 bearing environments studied here. Examination of the data summarized in Table 5 shows that there is a significant difference between the K_{Iscc} values measured in the three environments. It is also apparent from these data that the lower the yield strength of the material the larger the difference in K_{Iscc} values obtained for the environments studied. Based on this observation, it is not surprising that the high-strength steels initially studied by McIntyre and Priest (196 to 237 ksi yield strength) yielded essentially the same K_{Iscc} values in different environments.

In general, the K_{Iscc} values measured in the H_2 and H_2S gas environments were the same for both the long-time bolt loaded tests and the rising load tests. This behavior is to be expected in view of the relatively fast crack-growth rates associated with these environments (Fig. 11). However, the rising load K_{Iscc} testing procedure did not yield adequate results for the seawater environment tests. Two factors limited the use of the slow loading rate tests in seawater. First, because of the relatively slow rate of crack growth in seawater, sufficient time is not available in the rising load test to permit the development of significant crack growth. Secondly, K_{Iscc} tests conducted in aqueous environments usually involve a crack incubation period which may be several days or more.

The significant effect of loading rate on apparent K_{Iscc} illustrated in Fig. 8 is the result of the interaction between the rate of crack growth, the time involved in the test, and the ability to resolve and detect crack extension. Obviously, the test must be conducted at a loading rate slow enough to allow the detection of crack growth before the rising load increases a significant amount beyond the onset of crack initiation. The faster the rate of crack growth associated with a given material environment system the less effect loading rate has on the apparent K_{Iscc} value measured in the rising load test. This observation accounts for the absence of a loading rate effect in the H_2S gas tests shown in Fig. 9. For a crack-growth detection system of given resolution it is possible to determine the interrelationship between loading rate and crack-growth rate and ultimately, to evaluate the accuracy of the rising load K_{Iscc} test. The relationship between the rate of crack growth (da/dt), loading rate (dP/dt), and accuracy (ΔK_{Iscc} = apparent K_{Iscc} − actual K_{Iscc}) of the rising load K_{Iscc} test procedure described in this report can be expressed as

$$\text{apparent } K_{Iscc} - \text{actual } K_{Iscc} = \frac{dP}{dt} D Y \tau \sqrt{a} \Big/ B \frac{d\tau}{d(a/W)} \frac{da}{dt} \tag{4}$$

where

$$Y\left(\frac{a}{W}\right) = \frac{KBW}{P\sqrt{a}},$$

$$\tau\left(\frac{a}{W}\right) = \frac{BEV}{P}, \quad \text{and}$$

D = percent deviation from linearity on the load displacement record (secant offset).

Equation 4 essentially defines the amount by which the apparent K_{Iscc} value will exceed the actual K_{Iscc} (the K_I level associated with the onset of crack growth) at given values of da/dt, dP/dt, and for a given secant offset. Thus, for the 5 percent secant offset procedure used to define the onset of crack initiation in this investigation

$$\Delta K_{Iscc} = \frac{0.16(dP/dt)}{da/dt} \text{ when } a/W \approx 0.4 \text{ and } D = 0.05 \tag{5}$$

On the basis of Eq 5, it is apparent that a crack-growth rate of the order of 3×10^{-3} in./min is required to measure the onset of crack initiation within 1 ksi$\sqrt{\text{in.}}$ at a loading rate of 20 lb/min. This estimate of accuracy is consistent with the loading rate effect data (Fig. 8) and crack-growth rate data (Fig. 11) generated for the 180-ksi yield-strength material tested in 80-psig dry H_2 gas.

The fact that subcritical crack growth was noted for the 180-ksi yield-strength Type 4340 steel in 54 percent relative humidity air at a K_I level substantially lower that the K_{Ic} fracture toughness of the material (100 versus 140 ksi$\sqrt{\text{in.}}$) is very significant. This behavior clearly indicates that the K_{Ic} fracture-toughness parameter determined under relatively high loading rates in air may not always adequately define the critical conditions required to cause failure in air. The results of this investigation indicate that K_{Iscc} testing in air environments should be an important consideration in the evaluation of the fracture properties of relatively high-strength steels.

Although this investigation has shown that there are several significant limitations associated with rising load K_{Iscc} testing in H_2S gas, it is also apparent that this test procedure can be used as an extremely valuable technique for rapidly screening alloys with regard to their susceptibility to stress corrosion cracking in H_2 bearing environments. In addition, because of the short testing times involved as well as the ability to conduct several tests with a given specimen, this technique should be extremely useful in the study of the basic mechanisms associated with environment induced subcritical crack growth.

Conclusions

1. Rising load K_{Iscc} testing in H_2S gas can be used as a valuable technique for rapidly screening ferrous alloys with regard to their susceptibility to environment induced cracking in H_2 bearing environments.
2. Rising load K_{Iscc} testing in H_2S gas cannot be arbitrarily used to develop a quantitative measure of K_{Iscc} in other environments such as H_2 gas and seawater.
3. The gas pressure and loading rate associated with rising load K_{Iscc} testing in H_2S gas can have a significant effect on the apparent K_{Iscc} measured in such a test.
4. The accuracy and, ultimately, the applicability of rising load K_{Iscc} testing depends directly upon the crack-growth rate associated with the material-environment system being studied. The slower the rate of crack growth the less accurate the rising load K_{Iscc} testing procedure.
5. The K_{Iscc} for the 180-ksi yield-strength Type 4340 steel evaluated in this program was found to be 37, 30, and 27 ksi$\sqrt{\text{in.}}$ in the seawater, 80-psig H_2 gas, and 50-psig H_2S gas environments, respectively.
6. The K_{Iscc} values determined for the 160-ksi yield-strength material exposed to the seawater, 80-psig H_2 gas, and 50-psig H_2S gas environments were 87, 59, and 60 ksi$\sqrt{\text{in.}}$, respectively.
7. Environment induced subcritical crack growth was encountered for the 180-ksi yield-strength material in a 54 percent relative humidity air environment. The apparent K_{Iscc} level in air is approximately 105 ksi$\sqrt{\text{in.}}$
8. Precracking technique (fatigue precracking or environment induced static load cracking) did not have a significant effect on the rising load K_{Iscc} values determined for Type 4340 steel exposed to H_2 and H_2S gas environments.
9. Prior load history does not appear to have a significant effect on K_{Iscc} values determined for Type 4340 steel under rising load conditions in H_2 and H_2S gas.

References

[*1*] Brown, B. F., *Materials Research and Standards,* Vol. 6, No. 3, March 1966, pp. 129–133.

[*2*] Novak, S. R. and Rolfe, S. T., *Journal of Materials,* Vol. 4, No. 3, Sept. 1969, pp. 701–728.

[*3*] Ceschini, L. J. and Clark, W. G., Jr., "An Apparatus for Stress-Corrosion Testing with Large Precracked WOL Specimens," Proceedings of the AGARD Specialists Meeting on Stress Corrosion Testing Methods, Advisory Group for Aeronautical Research and Development, 1972.

[*4*] Clark, W. G., Jr. and Kim, D. S., *Engineering Fracture Mechanics,* Vol. 4, 1972.

[*5*] Wei, R. P., Novak, S. R., and Williams, D. P., *Materials Research and Standards,* Vol. 12, No. 9, 1972, pp. 25–30.

[*6*] McIntyre, P. and Priest, A. H., "Accelerated Test Technique for the Determination of K_{Iscc} in Steels," British Steel Corporation Report MG/31/72, 1972.

[*7*] Wilson, W. K., "Stress Intensity Factors for Compact Tension Specimens," Westinghouse Research Memo 67-1D6-BTLFR-M1, June 1967.

P. Shahinian[1] *and R. W. Judy, Jr.*[1]

Stress-Corrosion Crack Growth in Surface-Cracked Panels of High-Strength Steels

---

REFERENCE: Shahinian, P. and Judy, R. W., Jr., "**Stress-Corrosion Crack Growth in Surface-Cracked Panels of High-Strength Steels,**" *Stress Corrosion—New Approaches, ASTM STP 610,* American Society for Testing and Materials, 1976, pp. 128–142.

ABSTRACT: Stress-corrosion crack growth in 17-4PH and 4340 steels in 3.5 percent sodium chloride solution was examined over a wide range of K_{Iscc}/σ_{ys} values by electrochemically coupling the 17-4PH steel to aluminum, zinc, magnesium, and open circuit and by testing the 4340 steel at three strength levels in open circuit.

It was demonstrated that the parameter, K_{Iscc}, determined from small cantilever bend specimens can be used to predict the flaw size/stress level combinations required for the onset of crack growth in large surface-cracked tensile panels. For this purpose the stress-intensity values for the surface-cracked panels were calculated from the basic surface-flaw equation.

The microfracture processes in the stress-corrosion cracking included intergranular, cleavage, and microvoid coalescence, the proportion of intergranular became greater with increase in negative electrochemical potential.

KEY WORDS: stress corrosion, high strength steels, crack propagation, electrochemical coupling, mechanical properties, fractography

The usefulness of fracture mechanics for defining stress-corrosion cracking (SCC) tendencies of high-strength metals is derived from the ability to use the parameter K_{Iscc} for calculation of stress/flaw size combinations necessary for the initiation of crack growth. It has been assumed that K_{Iscc} can be substituted in the fracture stress-intensity equations governing various crack configurations, even though there is not sufficient experimental evidence to support the assumption adequately. Consequently, acceptance of the approach for design has been slow. The parameter however has been used successfully as an index of material sensitivity to SCC and thus serves as an aid in material screening and selection. Applicability of the parameter for design and life prediction of large structures has not been, as

---

[1] Consultant and head, respectively, Structural Mechanics Section, Engineering Materials Division, Naval Research Laboratory, Washington, D. C. 20375.

yet, demonstrated. Furthermore, only limited evidence of the generality of the parameter for various crack sizes and specimen geometries has been obtained.

A number of investigations have been made of the effect of specimen thickness on the initiation of stress-corrosion crack growth, but the results do not appear to be entirely consistent and in any case the effect is not simple. In these studies, as thickness was increased, the apparent K_{Iscc} was either lowered [*1,2*],[2] raised [*3*], or remained unaffected [*4,5*]. The apparent discrepancies probably are related to the K_{Iscc} level of the material and whether plane-strain conditions prevailed.

Where comparisons among K_{Iscc} values obtained from different specimen types have been made, the agreement has been good. Beachem and Brown [*6*] observed general agreement among K_{Iscc} values obtained from cantilever beam, center-cracked, and surface-cracked specimens of AISI 4340 steel in 3.5 percent sodium chloride (NaCl) solution. Positive results were also obtained by Judy and Dahlberg [*7*] who showed that K_{Iscc} values determined with surface-cracked specimens of a titanium alloy in 3.5 percent NaCl solution were essentially identical to those from cantilever beam specimens. However, these data were limited in range with respect to material strength level, crack size, and electrochemical potential.

This study was undertaken to examine the validity over a broad range of conditions of the premise that K_{Iscc} values determined by tests of bend-type specimens can be utilized to predict crack growth in large surface-cracked panels which are representative of structural components. AISI 4340 steel and 17-4PH stainless steel were used as test materials in 3.5 percent NaCl solution. To obtain a wide range of K_{Iscc} values, the heat treatment was varied for the 4340 steel, and, for the 17-4PH steel, the electrochemical potential was varied. Further, specimen configurations were selected to give a wide variation of stress levels and flaw sizes to allow validation of the concept over as large a range as possible. In the analysis, comparisons were made between the K_I required for the onset of crack growth in tensile panels and characteristic K_{Iscc} values determined from small cantilever beam specimens. Graphical fracture mechanics plots were constructed to illustrate the applicability of the concept in terms of flaw sizes and stress levels.

Materials and Procedures

The materials used for the investigation were vacuum-melted 17-4PH stainless steel plate in the H1050 temper and AISI 4340 steel plate heat treated to three strength levels; the mechanical properties are given in Table 1. For the SCC tests, the specimens had the configurations and

---

[2] The italic numbers in brackets refer to the list of references appended to this paper.

TABLE 1—*Tensile properties of steels.*

Materials	Thickness, in.	Yield Strength, 0.2%, ksi	Tensile Strength, ksi	Reduction of Area, %	Elongation, %
17-4PH					
H	⅝	159.6	165.2	59	17
I	1	161.7	167.2	62	15
D	⅜	158.3	163.5	60	16
4340					
V-1	1	206.7	228.2	20	7
V-2	½	204.1	227.6	28	9
V-4	1	158.6	171.3	31	12
V-3 and V-5	1	128.6	141.9	39	15

NOTE—1 in. = 0.0254 m.
1 ksi = 6.89 MPa.

dimensions shown in Fig. 1 and Table 2 with orientation transverse-short (T-S) for the cantilever type and transverse-short and transverse-long (T-S and T-L) combination for the surface-cracked tensile panels [*8*]. Part-through semiellipitical flaws were machined in each tensile panel by the electrical-discharge-machining (EDM) process, and all specimens were precracked by fatiguing in bending; the flaw dimensions are given in Table 2.

TABLE 2—*Specimen and flaw dimensions.*

Specimen	B, in.	W, in.	L, in.	a, in.	l, in.	a/l
17-4PH						
H-1	0.65	1.5	14	0.085	0.212	0.40
H-2	0.65	1.5	14	0.147	0.659	0.22
H-3	0.65	1.5	14	0.073	0.161	0.45
H-4	0.66	1.5	14	0.124	0.421	0.29
H-5	0.65	1.5	14	0.096	0.253	0.38
I-1	1.0	2.0	18	0.151	0.384	0.39
I-2	1.0	2.0	18	0.178	0.640	0.28
I-3	1.0	4.0	18	0.294	1.69	0.17
I-4	1.0	4.0	18	0.372	1.97	0.19
D-1	0.37	4.0	18	0.222	1.69	0.13
4340						
V-1	1.0	8.0	36	0.400	1.972	0.20
V-2	0.5	8.0	36	0.141	0.531	0.27
V-3	1.0	8.0	36	0.368	2.143	0.17
V-4	1.0	8.0	36	0.241	0.793	0.30
V-5	1.0	6.0	36	0.259	0.581	0.45

NOTE—1 in. = 0.0254 m.

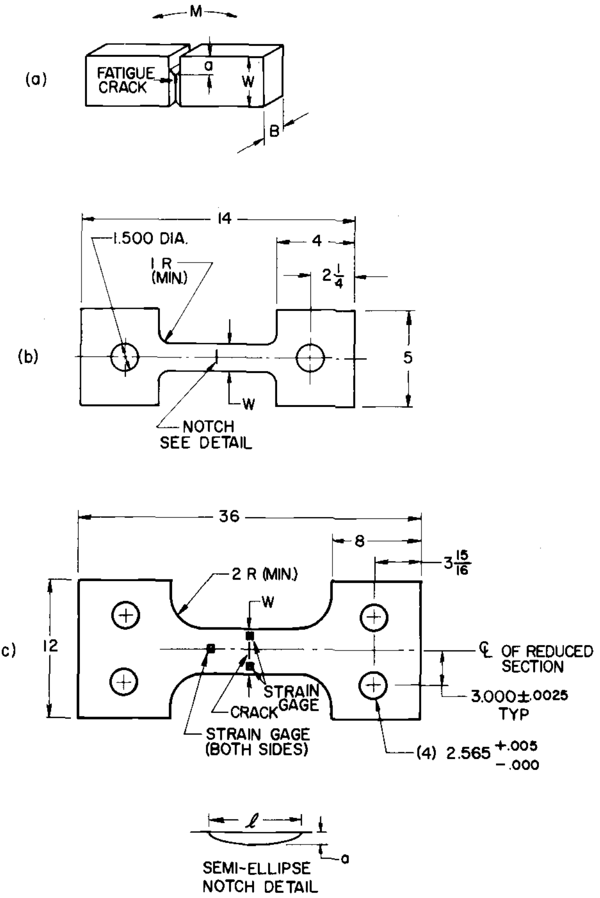

FIG. 1—*Stress corrosion cracking test specimen configurations,* (a) *cantilever,* (b) *17-4PH steel panels, and* (c) *4340 steel panels. Dimensions in inches (1 in. = 0.0254 m).*

Characteristic K_{Iscc} values were determined by testing the cantilever specimens in a dead-load test frame, which is described elsewhere [*9*]. In the test frame the specimen with the notch positioned up is clamped rigidly at one end, and the other end is attached to a lever arm on which weights are added. The specimens were step loaded, the number of steps being kept to a minimum by relying on prior knowledge of K_{Iscc} values for comparable materials and electrochemical conditions. The duration of each step usually was approximately 150 h.

A 400 000 lb capacity hydraulic tensile machine was used for the 17-PH steel tests, and a 1.5 million lb capacity screw-type machine was used for the 4340 steel tests. Both machines permitted long-term tests of hundreds of hours without significant changes of load during sizable amounts of crack growth. The stresses on the 17-4PH steel specimens were determined from the machine load indicator and on the 4340 steel specimens from strain gages mounted midway between the specimen fillet and crack plane, as indicated in Fig. 1*c*.

A plastic container was placed around the crack region to hold the 3.5 percent NaCl solution, which was changed frequently during the tests. All tests of 4340 steel were run in the freely corroding condition, whereas those of the 17-4PH steel were, in addition, cathodically coupled to aluminum (5086 alloy), zinc, or magnesium. In the cathodically coupled tests, the electrode size was chosen so that the wetted areas of specimen and electrode were approximately equal.

The test procedure for the large tensile panels having a known surface crack size was designed to demonstrate the accuracy of K_{Iscc} in predicting growth in surface cracks. The first step was to apply a stress intensity just below that predicted to be necessary for crack growth, K_{Iscc}, for a reasonable time period, usually a minimum of about 150 h, to establish that no crack growth would occur. Following this, the stress intensity was raised a small amount to a value just above that required to cause crack growth. If crack growth did not occur at this stress-intensity level, the load was raised an additional increment. Crack growth was monitored by strain gages placed near the tip of the original crack and, in addition for the larger 4340 steel specimens, by a strain-gaged beam clip gage. The occurrence of stress-corrosion crack growth, or the lack of it, was verified by electron microscopy of the crack surfaces after termination of the test and fracture of the specimen.

The stress-intensity factor, K_{I}, values for the cantilever specimen tests were calculated from the Kies equation [*10*]

$$K_{\mathrm{I}} = \frac{4.12M(1/\alpha^3 - \alpha^3)^{1/2}}{(BB_N)^{1/2}W^{3/2}} \tag{1}$$

where

M = bending moment,
B = specimen thickness,
B_N = net thickness at grooves,
W = specimen width, and
$\alpha = 1 - a/W$, where a is the crack depth.

For the surface-cracked (or part-through crack) specimen the K_{I} was calculated from the surface flaw equation developed by Irwin [*11*]

$$K_{\mathrm{I}} = 1.1\sigma\sqrt{\pi a/Q} \tag{2}$$

where

σ = nominal stress,

a = crack depth, and

Q = constant dependent on flaw shape and σ/σ_{ys} ratio [12].

Calculations for test purposes were made with the best estimate of crack depth. Final calculations of K_I were made with the original crack dimensions (machined notch plus fatigue crack) measured on the fracture surface after completion of the test.

Results and Discussion

K_{Iscc} *Determinations*

The K_{Iscc} values for the 17-4PH steel which were determined from the cantilever tests ranged from 27 ksi$\sqrt{\text{in.}}$ (30 MN/$m^{3/2}$) for the steel cathodically coupled to magnesium to 103 ksi$\sqrt{\text{in.}}$ (113 MN/$m^{3/2}$) for the open circuit (freely corroding) condition, Table 3. As the system was changed by anode substitution to increase negatively the electrochemical potential (open circuit, −0.3 V; aluminum −0.8 V; zinc, −1.0 V; and magnesium, −1.3 V) the experimentally determined K_{Iscc} value was lowered; the potentials of the specimens were measured against a silver/silver chloride (Ag/AgCl) reference electrode. The substantial effect of electrochemical potential on K_{Iscc} of 17-4PH steel is shown in Fig. 2. Slight variations in K_{Iscc} were observed for the two 17-4PH plates tested under the same electrochemical conditions, but these did not alter the general trend of K_{Iscc} with potential. The values for plate I were obtained from a previous study of the same material, Ref *13*. In contrast to the sensitivity of K_{Iscc} to potential exhibited by the 17-4PH steel, K_{Iscc} of 4340 steel has been reported [*14*] to be relatively insensitive to potential.

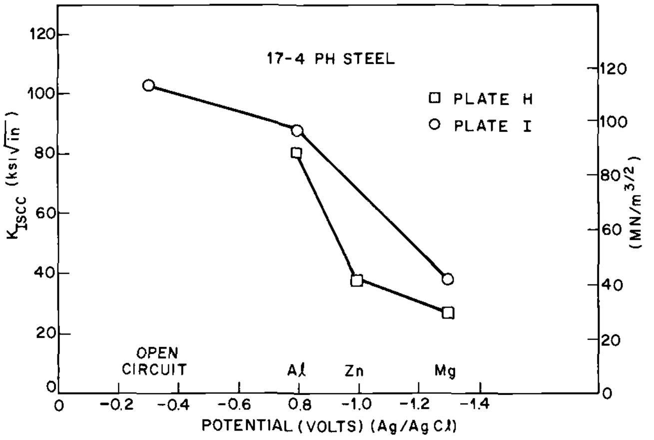

FIG. 2—*Variation of* K_{Iscc} *with electrochemical potential for 17-4PH steel in 3.5 percent NaCl solution.*

TABLE 3—*Tensile panel SCC test results.*

Specimen	a/Q	Coupled To	K_{Iscc},[a] ksi$\sqrt{in.}$	σ_N/σ_{ys}	σ_G/σ_{ys}, G	K_N, ksi$\sqrt{in.}$	K_G, ksi$\sqrt{in.}$	K_N/σ_{ys}, $\sqrt{in.}$	K_G/σ_{ys}, $\sqrt{in.}$	K_{Iscc}/σ_{ys}, $\sqrt{in.}$
17-4PH										
H-1	0.044	Zn	38 ± 4	0.60	0.69	39	45	0.24	0.28	0.24
H-2	0.12	Al	81 ± 6	0.72	0.81	76	86	0.48	0.54	0.51
H-3	0.034	Zn	38 ± 4	...	0.71	...	40	...	0.25	0.24
H-4	0.080	Zn	38 ± 4	0.45	0.62	39	54	0.24	0.34	0.24
H-5	0.050	Mg	27 ± 3	...	0.47	...	33	...	0.21	0.17
I-1	0.083	Al	88 ± 5	0.92	...	84	...	0.52	...	0.54
I-2	0.13	Al	88 ± 5	0.75	0.85	84	95	0.52	0.59	0.54
I-3	0.25	open	103 ± 5	0.54	0.65	84	106	0.52	0.65	0.64
I-4	0.30	Al	88 ± 5	0.41	...	70	...	0.43	...	0.54
I-4	0.30	Mg	38 ± 5	0.23	0.28	42	52	0.26	0.32	0.24
D-1	0.13	Mg		...	0.32	...	50	...	0.31	
4340										
V-1	0.31	open	18 ± 3	...	0.09	...	19	...	0.09	0.09
V-2	0.094		18 ± 3	0.12	0.17	15	20	0.07	0.10	0.09
V-3	0.30		68 ± 5	0.45	...	62	...	0.48	...	0.53
V-4	0.15		51 ± 4	0.58	0.66	70	80	0.44	0.51	0.32
V-5	0.13		85 ± 5	0.86	...	77	...	0.60	...	0.66

[a] Determined by cantilever beam tests.

NOTE—K_{Iscc} values for plate I from Ref *13*.

G = crack growth.

N = no growth.

1 in. = 0.0254 m.

1 ksi$\sqrt{in.}$ = 1.098 MN/$m^{3/2}$.

For the 4340 steel, K_{Iscc} values from cantilever tests for the freely corroding condition (−0.6 V) ranged from 18 ksi$\sqrt{\text{in.}}$ (20 MN/$m^{3/2}$) for the high-strength material to 85 ksi$\sqrt{\text{in.}}$ (94 MN/$m^{3/2}$) for the low-strength material. A rather large discrepancy between K_{Iscc} values for material taken from the two low-strength tensile panels was indicated, which is not entirely accountable. While the hardness of the V-3 panel was about 2 HRC points higher than that of the V-5 panel, this would not be expected to cause the observed difference in K_{Iscc} values. As will be noted later, the correspondence between the apparent K_{Iscc} of edge-notch cantilever and panel tests indicates that the discrepancy is due to a material factor and not test procedure.

A comparison of the 17-4PH and 4340 steels at the 160 ksi (1102 MPa) strength level shows that the 4340 steel is more sensitive to SCC (lower K_{Iscc}) in the freely corroding condition and also on an equivalent potential (−0.6 V) basis. Inasmuch as K_{Iscc} of 4340 steel is insensitive to potential, this difference in SCC resistance would be expected to greatly diminish at higher negative potentials.

SCC of Tensile Panels

To demonstrate that the onset of SCC in surface-cracked panels can be predicted, the Flaw Size Analysis Diagram, Fig. 3, which is based on Eq 2 is used. On the diagram the scales are K_I/σ_{ys} versus a/Q, which is the normalized flaw parameter, and vertical lines represent the characteristic K_{Iscc}/σ_{ys} ratio for specific electrochemical conditions. The vertical scales at the right of the diagram give the absolute critical flaw depths for long, thin flaws (depth-to-length ratio of 0.1) and for short flaws (ratio of 0.25). Curves are drawn for the noted relative applied stress levels, σ/σ_{ys}.

In the analysis of the data, the K_I/σ_{ys} values calculated from the surface flaw equation for the no crack growth and crack growth conditions were compared with the appropriate K_{Iscc}/σ_{ys} values. The data for each test are plotted for a constant a/Q, since the term is fixed to flaw size and shape and hence is a constant for each test. In some tests a K_I value was not obtained for either no crack growth or growth owing to experimental uncertainties.

The results for the 17-4PH steel, Figs. 3 and 4, demonstrate clearly that for the regions of applied stress, flaw sizes, and electrochemical potentials considered the initiation of crack growth can be predicted by the surface flaw equation. For the small flaw data of plate I, Fig. 3, the K_I/σ_{ys} values for no crack growth and for growth in a given test essentially bracket the characteristic K_{Iscc}/σ_{ys} value. In tests where only data for crack growth were obtained, the K_I/σ_{ys} value fell above the critical value, as predicted. It should be noted that the K_{Iscc} is not a precise value but represents a range with boundaries as indicated on the diagrams. Consequently, evi-

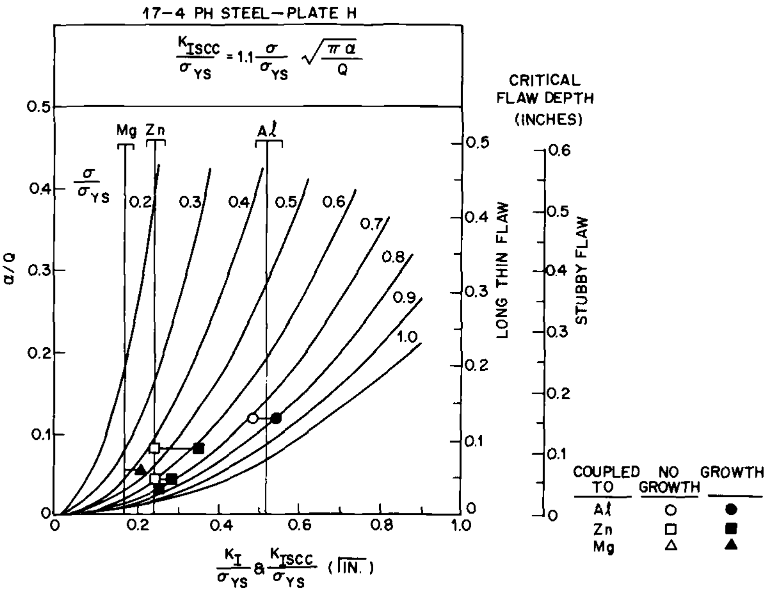

FIG. 3—*Flaw size analysis diagram showing that results of tensile tests of surface-cracked 17-4PH steel panels (plate H) coupled to aluminum, zinc and magnesium in 3.5 percent NaCl solution are in agreement with predictions of* K_{Iscc} *values measured in cantilever tests.*

dence of either crack growth or no growth at stresses within this range is not inconsistent with the predictions of the parameter.

Data indicating the performance of 17-4PH steel panels containing large flaws are shown in Fig. 4. The experimentally determined K_I values required for the onset of crack growth in the panel under these conditions conform to the predictions of the diagram. These data and those in Fig. 3 demonstrate the applicability of the diagram for 17-4PH steel over the stress range of 0.3 to 0.9 σ_{ys} and for flaw depths of 0.073 to 0.372 in. (1.85 to 9.45 mm).

Also consistent with the preceding results was the observation in the magnesium-coupled test D-1 (not included in the diagrams) that crack growth occurred at a K_I of 50 ksi$\sqrt{\text{in.}}$ (55 MN/$m^{3/2}$). This would be in agreement if its K_{Iscc} is assumed to be comparable to those for plates H and I and published values [*15*] for this steel.

In these panel tests it appeared that crack growth was fastest in magnesium-coupled specimens, intermediate in zinc-coupled, and slowest in aluminum-coupled specimens. Actual growth rates were not measured, but estimates were based on rates of change of sensor readings and on final crack size and duration. The influence of the electrochemical potential on

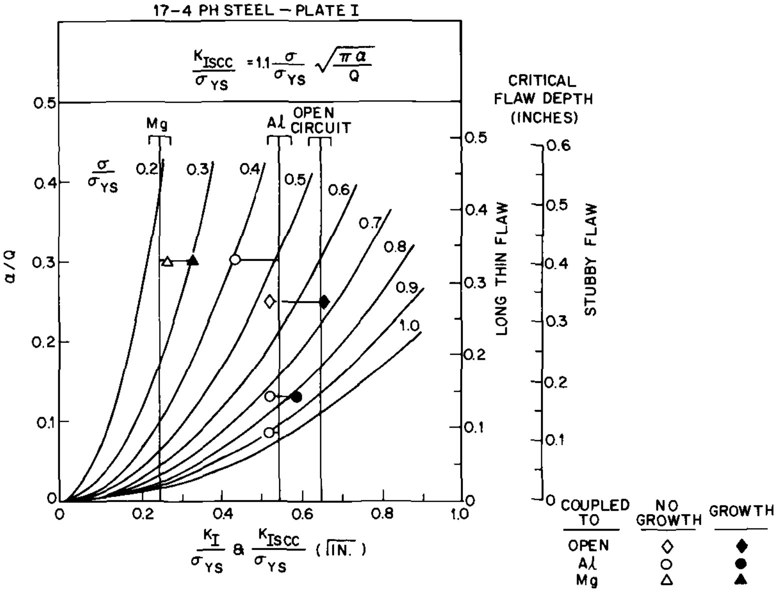

FIG. 4—*Flaw size analysis diagram for surface-cracked 17-4PH steel panels (plate I) coupled to aluminum and magnesium and freely corroding in 3.5 percent NaCl solution.*

growth rate appeared to be greater along the specimen surface than in the through-thickness direction.

Further confirmation of the validity of the approach was obtained with the 4340 steel panel tests although the data were sparse and in several respects inconclusive. The results for the low-strength (129 ksi, 889 MPa) panels, Fig. 5, were consistent in that crack growth did not occur when held for 400 h at K_I levels slightly below their characteristic K_{Iscc}. As mentioned earlier, the K_{Iscc} values for the two test panels were not the same, perhaps due to a slight variation in heat treatment. Stresses above the critical level for crack growth were not applied to these panels.

The behavior of the intermediate strength (159 ksi, 1096 MPa) panel did not conform to prediction in that crack growth did not occur in 300 h at a K_I/σ_{ys} of 0.44 $\sqrt{\text{in.}}$ (0.070 $\sqrt{\text{m}}$) which is higher than the K_{Iscc}/σ_{ys} value of (0.32 $\sqrt{\text{in.}}$, 0.051 $\sqrt{\text{m}}$). Growth did take place, however, at a K_I/σ_{ys} of 0.51 $\sqrt{\text{in.}}$ (0.082 m). This behavior may be due to the step loading procedure, that is, time at stress below the K_{Iscc}, having an effect, corrosion, or inadequate performance of the growth detectors, but there is no direct evidence of this. In any event the result is considered to be inconclusive.

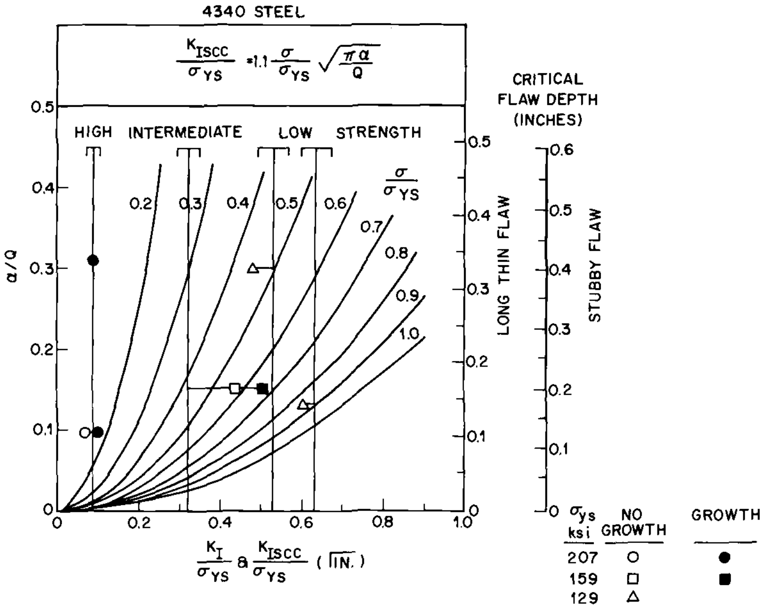

FIG. 5—*Flaw size analysis diagram showing results of freely corroding tests of surface-cracked 4340 steel panels at three strength levels in 3.5 percent NaCl solution in relation to characteristic* K_{Iscc} *values.*

For the high-strength (207 ksi, 1426 MPa) panel, the K_{Iscc} from the cantilever test accurately predicted the initiation of crack growth. In this material the threshold for growth is easily detectable. Crack growth was very rapid, leading to fracture of the specimens only several hours after load application at stresses below 0.2 σ_{ys}.

The results from both the 17-4PH and 4340 steel tests show that the K_I calculated from the surface flaw equation can be used to predict growth of surface cracks in tensile panels. Valid K_{Iscc} values determined from cantilever tests of small specimens provided the reference threshold for initiation of crack growth.

Fractographic Analysis

The microfracture processes in the 17-4PH and 4340 steels were observed to be sensitive to the conditions of the tests and reflected changes in electrochemical potential and stress intensity.

Stress-corrosion crack growth in the 17-4PH steel coupled to aluminum occurred at approximately the same rate everywhere along the crack periphery, as indicated by the uniform width of the SCC band, Fig. 6. In contrast, when the 17-4PH steel was coupled to zinc or magnesium the

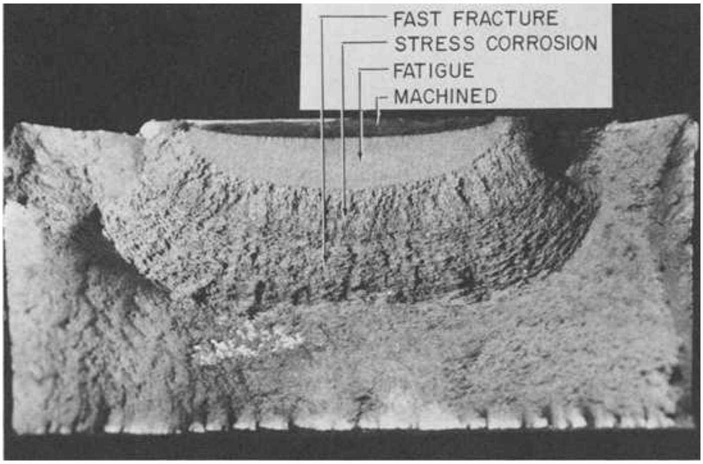

FIG. 6—*Fracture surface of surface-cracked 17-4PH steel panel (H-2) coupled to aluminum in 3.5 percent NaCl showing regions of fatigue, stress corrosion, and fast fracture.*

rate of crack growth was apparently faster along the specimen surface than in the through-thickness direction. That is, more growth occurred along the major axis of the ellipse than along the minor axis. This effect may be deduced from the crack-front geometry and the nonuniform SCC regions in the zinc-coupled specimens, Fig. 7, and the magnesium-coupled speci-

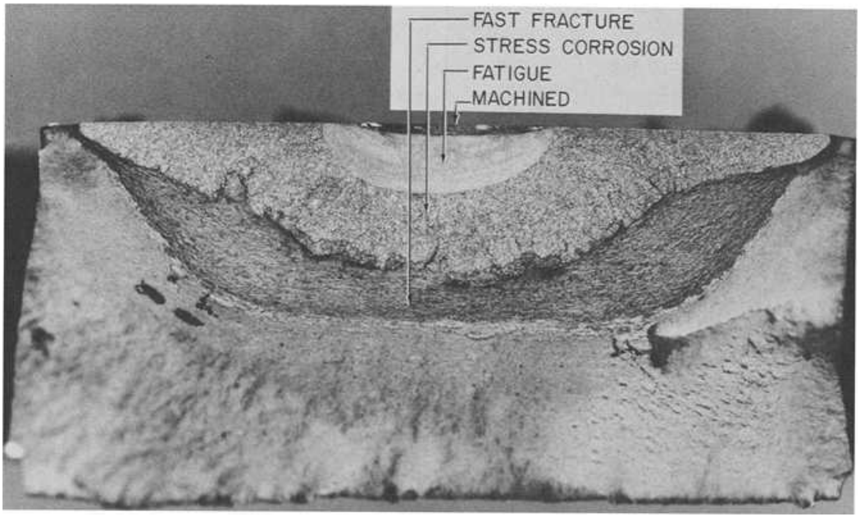

FIG. 7—*Fracture surface of surface-cracked 17-4PH steel panel (H-4) coupled to zinc in 3.5 percent NaCl showing large SCC region.*

men. The width of the SCC band at the surface was about three to four times larger than that at the deepest part of the crack. Growth rates appear to be inversely proportional to distance of the crack from the specimen surface. This effect occurred despite the fact that the stress-intensity factor is a maximum at the minor axis of the ellipse and a minimum at the major axis [*16*].

The enhanced crack growth at and near the surface would appear to be related to the greater hydrogen activity of the zinc- and magnesium-coupled systems and the reduced availability of hydrogen at the deeper recesses of the crack relative to the surface. As a result of the electropotential field between the anode and crack surfaces, the rate of hydrogen generation may not be uniform over the crack surfaces, being particularly less at the deeper regions.

SCC of the 17-4PH steel took place by several microseparation processes, intergranular, cleavage, and microvoid coalescence, the relative amounts being dependent on the electrochemical conditions. Fast fracture occurred by microvoid coalescence.

In comparisons of the SCC regions of the 17-4PH specimens at comparable distances from the fatigue-SCC interface, it was observed that the fracture modes, in order of decreasing percentages, were:

(*a*) for the aluminum coupled—cleavage, slightly less intergranular, and microvoid coalescence,

(*b*) for the zinc coupled—intergranular, slightly less cleavage, and minor amount of microvoid coalescence, and

(*c*) for the magnesium coupled—predominantly intergranular, cleavage, and small amount of microvoid coalescence.

In general, the amount of intergranular separation increased progressively as the coupling was changed from aluminum to zinc to magnesium. In this sequence as the electrochemical potential is increased negatively, more hydrogen becomes available and tends to promote intergranular cracking. These results are consistent with the trend of fracture modes in relation to hydrogen concentration presented by Meyn [*17*] for 17-4PH steel.

In the high-strength 4340 steel test panel (V-1), the SCC separation mode adjacent to the fatigue zone was intergranular. As the crack grew, cleavage began to appear in increasing, though small, amounts. At approximately ⅛ in. (3 mm) from the fatigue-SCC interface, separation modes were estimated to be 90 percent intergranular and 10 percent cleavage. The increasing amounts of cleavage probably results from the increase in K that occurs with the growing crack. As the crack approached the back face of the specimen, the fracture also included microvoid coalescence.

In the intermediate-strength 4340 steel, SCC occurred by predominantly microvoid coalescence. For this material the stress intensity required for crack growth is much higher than for the higher strength steel.

Summary

This investigation was undertaken to validate the premise that K_{Iscc} determined by tests of small bend-type specimens can be utilized to predict crack growth in large surface-cracked panels which are typical of structural components. A wide range of $K_{\mathrm{Iscc}}/\sigma_{\mathrm{ys}}$ values was examined by using 17-4PH stainless steel electrochemically coupled to aluminum, zinc, and magnesium as well as freely corroding in 3.5 percent NaCl and with 4340 steel at three strength levels. The K_{Iscc} of 17-4PH steel was found to be very sensitive to electrochemical potential, and the K_{Iscc} of 4340 steel was sensitive to strength level.

The test results showed that the initiation of crack growth can be predicted for surface-cracked tensile panels with a high degree of confidence. For this purpose the surface-flaw equation, $K_{\mathrm{Iscc}}/\sigma_{\mathrm{ys}} = 1.1\ \sigma/\sigma_{\mathrm{y}}\sqrt{\pi a/Q}$, accurately predicted stress level/flaw size combinations required for crack growth under a wide range of conditions. Valid K_{Iscc} values determined from cantilever bend tests served as the reference and reflected the SCC behavior of the tensile panels.

Examination of the panel fracture surfaces by transmission electron microscopy revealed the separation processes in the SCC region of the 17-4PH panels to be intergranular, cleavage, and microvoid coalescence. As the electrochemical potential of the system was increased negatively, resulting in more hydrogen generation at the specimen, the proportion of the intergranular mode increased while the other modes decreased. The shape of the SCC region indicates that the growth rate of the crack was uniform around its periphery in the aluminum-coupled panel but in the zinc- and magnesium-coupled panels the rate was higher along the surface than in the through-thickness direction.

The results of this investigation confirm that there is a predictive capability for stress-corrosion growth of surface cracks typical of common flaws in structures.

Acknowledgments

The authors appreciate the substantial contributions of W. E. King, Jr., R. F. Bryner, M. L. Cigledy, and W. M. Elwell in the testing phase and of S. M. McCoy in the fractographic examination. Also they are grateful to C. T. Fujii and C. D. Beachem for advice on several aspects of the study. This investigation was provided financial support by the Naval Material Command, Code 0342.

References

[*1*] Piper, D. E., Smith, S. H., and Carter, R. V., *Metals Engineering Quarterly*, Vol. 8, No. 3, 1968, pp. 50–63.

[*2*] Beachem, C. D. and Meyn, D. A., "The Effect of Thickness Upon Sustained Load Crack Propagation in Ti-6Al-4V Alloy Tested in 3½% NaCl Solution," NRL Report 7449, Naval Research Laboratory, Washington, D. C., 8 Aug. 1972.

[*3*] Novak, S. R., *Journal of Engineering Fracture Mechanics,* Vol. 5, 1973, pp. 727–763.

[*4*] Piper, D. E. and Feeney, J. A., "Titanium, ARPA Coupling Program on Stress Corrosion Cracking," Eleventh Quarterly Report, NRL Memorandum Report 2028, Naval Research Laboratory, Washington, D. C., July 1969.

[*5*] Sandoz, G. in *Proceedings,* Conference on Fundamental Aspects of Stress Corrosion Cracking, National Association of Corrosion Engineers, Houston, Tex., 1969, pp. 684–690.

[*6*] Beachem, C. D. and Brown, B. F. in *Stress Corrosion Testing, ASTM STP 425,* American Society for Testing and Materials, 1967, pp. 31–40.

[*7*] Judy, R. W., Jr., and Dahlberg, E. P., "Stress-Corrosion Cracking Tests of Surface-Flawed Specimens of Ti-7Al-2Cb-1Ta," Report of NRL Progress, Naval Research Laboratory, Washington, D. C., May 1968, pp. 30–31.

[*8*] Goode, R. J., *Materials Research and Standards,* Vol. 12, No. 9, Sept. 1972, pp. 31–32.

[*9*] Brown, B. F., *Materials Research and Standards,* Vol. 6, No. 3, March 1966, pp. 129–133.

[*10*] Kies, J. A. et al in *Fracture Toughness Testing and Its Applications, ASTM STP 381,* American Society for Testing and Materials, 1965, pp. 328–356.

[*11*] Irwin, G. R., *Transactions,* American Society of Mechanical Engineers, Series E, Vol. 29, No. 4, 1962, pp. 651–654.

[*12*] Tiffany, C. F. and Masters, J. N. in *Fracture Toughness Testing and Its Applications, ASTM STP 381,* American Society for Testing and Materials, 1965, pp. 249–277.

[*13*] Fujii, C. T., Jr., this publication, pp. 213–225.

[*14*] Brown, B. F., "Stress-Corrosion Cracking in High Strength Steels and in Titanium and Aluminum Alloys," Naval Research Laboratory, Washington, D. C., 1972.

[*15*] Judy, R. W., Jr., Fujii, C. T., and Goode, R. J., "Properties of 17-4PH Steel," NRL Report 7639, Naval Research Laboratory, Washington, D. C., 18 Dec. 1973.

[*16*] Brown, W. F., Jr., and Srawley, J. E., *Plain Strain Crack Toughness Testing of High Strength Metallic Materials, ASTM STP 410,* American Society for Testing and Materials, 1967, pp. 109–115.

[*17*] Meyn, D. A., "Influence of Stress Intensity Level and Hydrogen Activity on Sustained Load Cracking Mechanism in 17-4PH Stainless Steel," Report of NRL Progress, Naval Research Laboratory, Washington, D. C., Dec. 1974, pp. 22–24.

D. O. Sprowls,[1] *J. W. Coursen,*[1] *and J. D. Walsh*[1]

Evaluating Stress-Corrosion Crack-Propagation Rates in High-Strength Aluminum Alloys with Bolt Loaded Precracked Double-Cantilever-Beam Specimens

---

REFERENCE: Sprowls, D. O., Coursen, J. W., and Walsh, J. D., **"Evaluating Stress-Corrosion Crack-Propagation Rates in High-Strength Aluminum Alloys with Bolt Loaded Precracked Double-Cantilever-Beam Specimens,"** *Stress Corrosion—New Approaches, ASTM STP 610,* American Society for Testing and Materials, 1976, pp. 143–156.

ABSTRACT: Propagation rates for stress-corrosion cracking (SCC) of high-strength aluminum alloys determined with mechanically precracked double-cantilever-beam (DCB) specimens provide a quantitative means of comparing the resistance to SCC of alloys and tempers. For relatively resistant materials however, the rates can be markedly influenced by test conditions and interpretation of the crack-growth data. This paper describes a relatively simple, accelerated testing method for determining SCC velocities that rank the SCC behavior of aluminum alloys in the same order as SCC propagation rates in a seacoast or industrial atmosphere. Practical difficulties associated with this test method, however, warrant further evaluation to justify this as a primary method of testing.

KEY WORDS: stress corrosion, cantilever beams, crack propagation, stress intensity, plateau velocity, threshold, environments, test methods, aluminum alloys

The primary objective in performing a stress-corrosion test with fracture mechanics type precracked specimens is to determine the threshold stress intensity below which stress-corrosion cracking (SCC) will not occur for a specific material and test orientation in a specific environment [*1*].[2] Another objective is to determine the rate of SCC propagation, *da*/*dt*, as a func-

---

[1] Section head, Stress Corrosion Section, research engineer, and technician, respectively, Alcoa Laboratories, Aluminum Company of America, Alcoa Center, Pa. 15069.

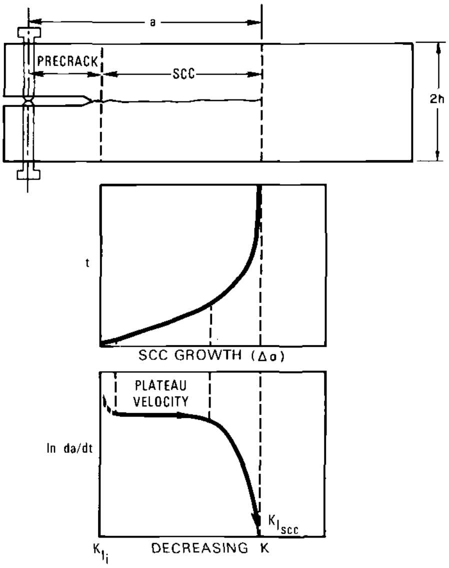

FIG. 1—*Schematic illustration of SCC growth and the relationship between the SCC propagation rate and the decreasing stress intensity in a bolt loaded DCB specimen.*

tion of the mechanical crack driving force, K_I, under controlled test conditions [*2*]. It is generally agreed that in order to fully characterize the resistance to SCC by this test method, it is preferable to obtain the complete curve of K_I versus da/dt.

A convenient type of specimen for determining SCC propagation rate is a double-cantilever-beam (DCB) loaded by constant displacement to a stress intensity at or just below the critical stress intensity required for mechanical fracture. With such extremely high stress intensity, SCC will start quickly in highly susceptible materials and proceed for a time at a fairly constant rate before it slows down to approach an arrest as the crack lengthens and K_I decreases. When (and if) the crack growth comes to an "arrest," the stress intensity can be said to be at the threshold for SCC (K_{Iscc}). A typical SCC crack-growth curve and the relationship of the SCC propagation rate with the decreasing stress intensity is shown for a relatively susceptible material in Fig. 1. (Note that the graphs are plotted in a rather unorthodox manner in order to relate the performance with the crack growth shown in the specimen.) The purpose of the present paper is to consider the use of SCC "plateau velocities," as illustrated in Fig. 1, for comparing the resistance to SCC of aluminum alloys and to describe a

---

[2] The italic numbers in brackets refer to the list of references appended to this paper.

simple test procedure for obtaining such data. The significance of the plateau velocity is that it is the highest SCC propagation rate that a material will sustain for an appreciable crack extension under the controlled test.

Experimental Procedure and Test Results

A bolt-loaded, 90-deg chevron-notched, DCB specimen was used for most of the experiments described next. The DCB length, 5.0 in. (130 mm), and thickness, 1.0 in. (25 mm), were not varied although in some cases the chevron was omitted or other dimensions changed as subsequently noted. The specimen orientation (S-L) was such that stress was applied in the short transverse direction to the grain structure, and the SCC growth was in the longitudinal direction. The precrack was produced by loading with either one or two bolts until fracture (popin) occurred and the crack was advanced until it was about 0.1 in. (2.5 mm) long on the sides of the specimen. A few drops of 3.5 percent sodium chloride (NaCl) solution (reagent grade NaCl and deionized water) were added to the notch during popin. Loaded specimens were placed in a vertical position with the notched end up, and a few drops of 3.5 percent NaCl solution were added to the notch three times daily (once daily on weekends). Crack lengths were measured every one or two days to the nearest 0.01 in. (0.25 mm) on both sides of the specimen and the measurements averaged. Upon termination of exposure after 30 or 40 days, the specimens were broken open to examine the fracture surfaces; in some cases specimens were sawed in half lengthwise so that one half could be broken open and the other half sectioned for metallographic examination of the crack tip.

Effect of Environmental Factors

SCC propagation rates, like the threshold stress or stress intensity, depend upon the conditions of test. The effect of the corrosive environment is illustrated by the test results shown in Figs. 2 and 3 for specimens of alloy 7079-T651 exposed to the atmosphere under various conditions. The SCC growth curves in Fig. 2 show that the crack growth was relatively rapid at first but, in the laboratory atmosphere and in the outdoor industrial atmosphere, the crack growth increased only very slightly after about 250 days. Although these curves were plotted only to 365 days, the exposures were continued for at least another year, and the extended curves were used for the derivations of K_I and da/dt in Fig. 3. Wide variations both in the plateau velocities and the apparent K_{Iscc} values were observed, depending upon the atmospheric conditions. Corrosion of the crack faces with the formation of wedges of corrosion product prevented crack arrest and the estimation of K_{Iscc} values for the seacoast atmosphere and the 3.5 percent NaCl solution tests. Although there were no data points

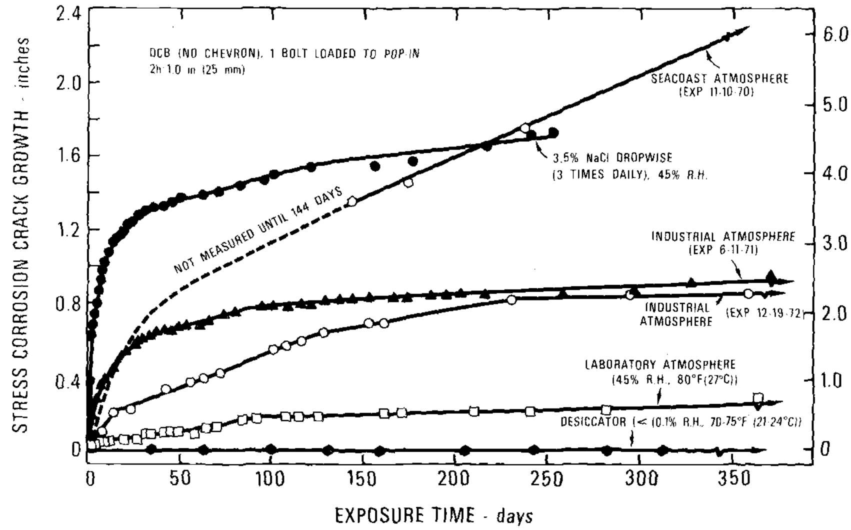

FIG. 2—*Effect of corrosive environment on SCC propagation in 7079-T651 aluminum alloy plate (2.5 in. (64 mm) thick).*

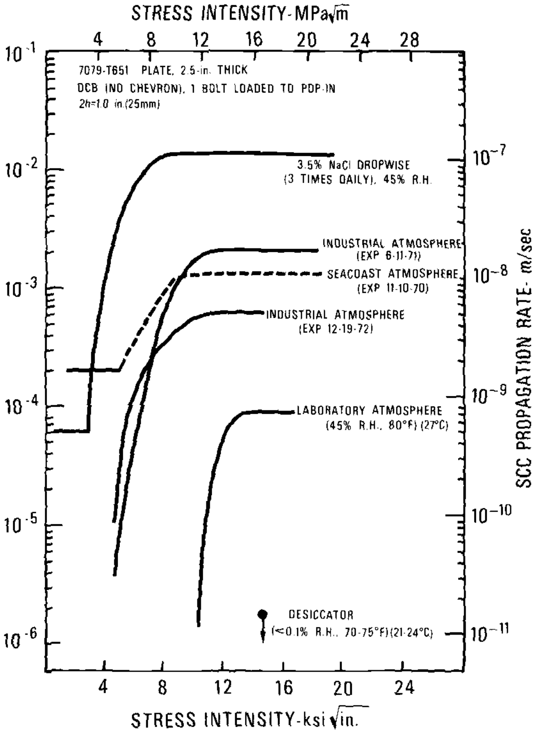

FIG. 3—*Effect of corrosive environment on SCC propagation rate in 7079-T651 alloy plate (2.5 in. (64 mm) thick).*

from which to calculate a plateau velocity in the seacoast atmosphere, its approximate position was estimated from expected relationships with the other curves. It is noteworthy, also, that in the dry air in the desiccator no SCC growth occurred within a period of over three years; this was confirmed by breaking the specimen open and examining the fracture surface.

It is easy to determine plateau velocities in corrosive environments for materials with a relatively low resistance to SCC, such as 7079-T651 alloy plate when stressed in the short-transverse direction; however, it is not so easy for situations in which there is very little crack growth. For the more SCC resistant materials the initial SCC crack growth is likely to be erratic because the extremely high local stress concentration at the crack tip may cause a sudden, small, initial burst of cracking, or, conversely, localized plastic deformation can have a crack-blunting effect that will delay the initiation of SCC. Consequently, estimates of the initial crack velocity can be misleading.

Examples of the variation encountered in the environmental crack-growth curves of materials with relatively high resistance to SCC are shown in Fig. 4 (7075-T651 was included as a point of reference). Various approaches were tried for determining meaningful plateau velocities, and it was concluded that the simplest procedure that is subject to the least error in interpretation is to calculate an average velocity by dividing the total crack growth by the total exposure time for a specified period. The period should be long enough to ensure an opportunity for SCC to initiate and to include the initial sustained crack growth, yet not so long as to include excessive crack growth caused by corrosion product wedging. This method will not only identify the materials with relatively low resistance to SCC (such as the 7075-T651) but will also provide useful values for the highly resistant materials that may not develop a K_I versus *da*/*dt* curve with a definite plateau.

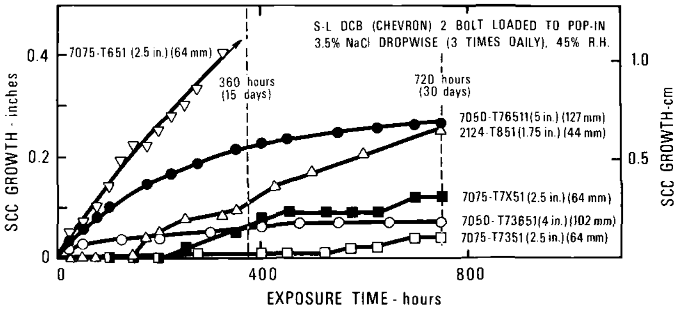

FIG. 4—*Example of SCC crack growth in various materials with relatively high resistance to SCC.*

A comparison of average velocities calculated by this method (*c*) with two other procedures (*a* and *b*) is shown next (estimates of an average velocity believed to be more realistic are marked with an *):

Average Velocities, in./h (m/s)

	(*a*) First Growth		(*b*) Growth Breaks		(*c*) Average Growth (15 Days)	
7075-T651	160×10^{-5}*	(113×10^{-10})	...		110×10^{-5}	(78×10^{-10})
7050-T76511	90*	(64)	...		60*	(42)
2124-T851	100	(71)	40×10^{-5}*	(28×10^{-10})	30*	(21)
7075-T7X51	30	(21)	12*	(8)	19*	(13)
7050-T73651	60	(42)	...	...	20*	(14)
7075-T7351	10	(7)	6	(4)	3*	(2)

(*a*) Average slope of the initial portion of the crack growth curve beginning at the time when growth starts and extending until the curve starts to bend over.

(*b*) Slope of a straight line drawn tangent to the crack growth curve at successive breaks in the growth curve as exemplified by the curve for 7075-T7X51 in Fig. 4.

(*c*) Slope of straight line from zero time to the amount of growth at 15 days.

The propagation rate calculated from the slope of the first growth (Procedure (*a*)) appears to be meaningful for the alloys having lower resistance to SCC but are too high for the more resistant alloys. Procedure (*b*) is not applicable to all growth curves. The 15-day average rates determined by Procedure (*c*) are the most generally applicable, and the procedure is not subject to interpretation. A 15-day period is recommended instead of a longer period, such as 30 days, because it provides a more realistic distinction between alloys similar to that obtained from exposures of smooth specimens in a seacoast atmosphere [*3*].

Effect of Variations in Test Procedure

A series of experiments was performed to determine whether the SCC growth would be affected by several variations that would simplify or increase the flexibility of the test procedure. For example, it would be advantageous to be able to compare the results from tests of DCB specimens of different heights (2*h*) because of the necessity of testing S-L orientation specimens from materials of various thicknesses. Therefore, tests were performed on specimens with beam heights of 0.5 in. (13 mm), 1.0 in. (25 mm), and 2.0 in. (51 mm). A comparison also was made of a straight notch versus the chevron notch in the 1.0 in. (25 mm) high specimen because considerable data in the literature have been obtained with the straight notch [*3,4*]. The chevron notch and higher (stiffer) beams have the advantage of causing less plastic deformation during the precracking of specimens of tougher alloys and tempers. In a further effort to minimize plasticity effects during tension precracking, a deeper notch (1.5 in. (38 mm) versus 0.625 in. (15.9 mm), was tested also with the 1.0 in. (25 mm) high specimen. One other experiment was carried out in which drops of the 3.5 percent NaCl solution were added to the specimens only once a day instead of three times. For all of the above experiments, tests were made on single specimens of each of three tempers of 7075 alloy plate artificially aged to provide a range in mechanical properties and different SCC performances (Table 1 and Ref *7*). It was assumed that trends in performance shown by these materials would apply also for others with similar resistance to SCC.

The average velocities based on 15-day exposures are summarized in Table 2, and certain comparisons are illustrated graphically in Figs. 5 and 6. Varying the beam height did not appreciably affect the average SCC velocities for any of the three tempers. However, the other variations in specimen configuration (straight notch or increased notch depth) and the reduced frequency of wetting with 3.5 percent NaCl solution did reduce the SCC propagation rates for 7075-T7X51 and T7351—although not for

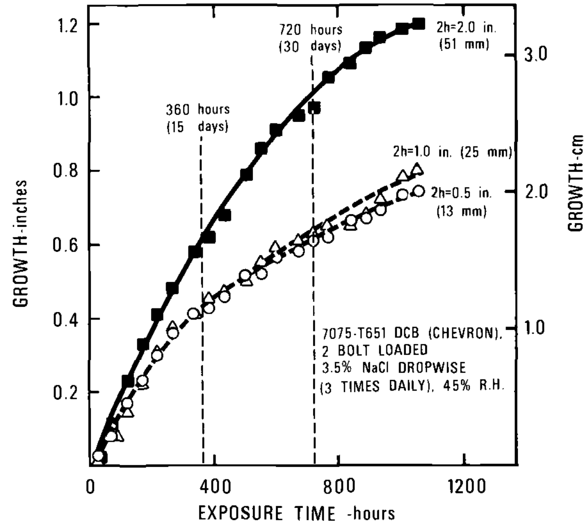

FIG. 5—*Effect of beam height (2*h*) on environmental crack growth in S-L specimens from 7075-T651 alloy plate.*

TABLE 1—*Characteristics of 2.5-in. (64-mm) thick 7075 alloy plate used to evaluate variations in test procedure.*

		Long Transverse			Short Transverse			
Temper	Electrical Conductivity, % IACS[a]	Tensile Strength, ksi (MPa)	Yield Strength, ksi (MPa)	Elongation, % in 4D	Tensile Strength, ksi (MPa)	Yield Strength, ksi (MPa)	Elongation, % in 4D	K_{Ic}, ksi$\sqrt{\text{in.}}$ (MPa$\sqrt{\text{m}}$)
T651	33.5	80.2 (553)	71.7 (494)	8.0 ...	74.8 (516)	66.6 (459)	2.0 ...	15.7[b] (17.4)[b]
T7X51	38.7	73.9 (510)	63.3 (436)	10.0 ...	70.4 (485)	60.8 (419)	4.0 ...	19.9 (22.0)
T7351	41.0	68.0 (469)	56.6 (390)	9.5 ...	65.0 (448)	54.4 (375)	4.0 ...	19.2 (21.3)

CHEMICAL COMPOSITION—PERCENT (REMELT ANALYSES)

Temper	Si	Fe	Cu	Mn	Mg	Zn	Cr	Ni	Ti	Be
T651, T7351	0.08	0.31	1.80	0.02	2.38	6.02	0.19	0.00	0.03	0.002
T7X51	0.10	0.24	1.80	0.03	2.44	5.87	0.18	0.00	0.04	0.002

[a] IACS = International Annealed Copper Standard.

[b] Value meaningful, although not technically valid according to ASTM criteria (E 399).

TABLE 2—*Effect of variations in test procedure on SCC propagation rates in DCB specimens of 7075 alloy in various tempers.*

Temper	Beam Height (2 h),		Notch,			Frequency of 3.5% NaCl Application	Average Velocity[a]	
	in.	(mm)	Type	Depth, in.	(mm)		in./h	(m/s)
T651	0.5	(13)	chevron	0.625	(15.9)	3 times/day	110 × 10^{-5}	(78 × 10^{-10})
	1.0	(25)	chevron	0.625	(15.9)	3 times/day	110	(78)
	2.0	(51)	chevron	0.900	(22.9)	3 times/day	170	(120)
	1.0	(25)	straight	0.625	(15.9)	3 times/day	125	(88)
	1.0	(25)	chevron	1.500	(38.1)	3 times/day	100	(71)
	1.0	(25)	chevron	0.625	(15.9)	1 time/day	110	(78)
T7X51	0.5	(13)	chevron	0.625	(15.9)	3 times/day	14	(10)
	1.0	(25)	chevron	0.625	(15.9)	3 times/day	20	(14)
	2.0	(51)	chevron	0.900	(22.9)	3 times/day	14	(10)
	1.0	(25)	straight	0.625	(15.9)	3 times/day	8	(6)
	1.0	(25)	chevron	1.500	(38.1)	3 times/day	8	(6)
	1.0	(25)	chevron	0.625	(15.9)	1 time/day	6	(4)
T7351	0.5	(13)	chevron	0.625	(15.9)	3 times/day	6	(4)
	1.0	(25)	chevron	0.625	(15.9)	3 times/day	3	(2)
	2.0	(51)	chevron	0.900	(22.9)	3 times/day	4	(3)
	1.0	(25)	straight	0.625	(15.9)	3 times/day	<3[b]	(<2)
	1.0	(25)	chevron	1.500	(38.1)	3 times/day	<3[b]	(<2)
	1.0	(25)	chevron	0.625	(15.9)	1 time/day	<3[b]	(<2)

[a] Based on an exposure period of 15 days.
[b] No SCC growth until 16 to 32 days.

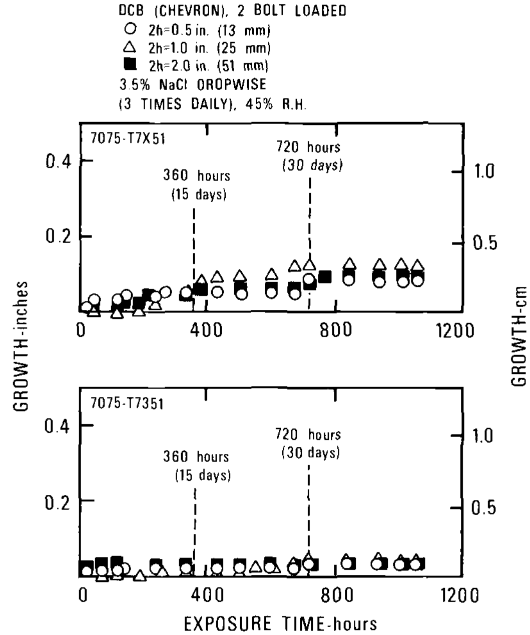

FIG. 6—*Effect of beam height (*2h*) on environmental crack growth in S-L specimens from 7075-T7X51 and 7075-T7351 alloy plate.*

the T651 temper. The relative extent of SCC crack growth in the three different tempers is shown in the photograph of fracture surfaces in Fig. 7.

SCC Velocities in Natural Environments

Average SCC velocities in the 3.5 percent NaCl test for a variety of alloys and tempers are compared in Table 3 with similarly obtained maximum sustained velocities observed in the seacoast atmosphere at Point Judith, Rhode Island, and in an inland industrial atmosphere at New Kensington, Pennsylvania [*3*]. It is significant that a ranking of these materials by the 3.5 percent NaCl test places them in the same general categories as SCC propagation rates in outdoor atmospheric exposures. Although some discrepancies were noted, such as the relatively low value for 5456-sensitized. In the industrial atmosphere, this is believed to be inherent to the different behavior of this alloy in different environments, and it is not a reflection on the test method. The velocities in the accelerated test were about five to ten times greater than the velocities in the atmosphere, and velocities tended to be equal or about twice as great in the seacoast atmosphere as in the industrial atmosphere, depending upon the alloy. The more corrosive conditions at the seacoast also caused more

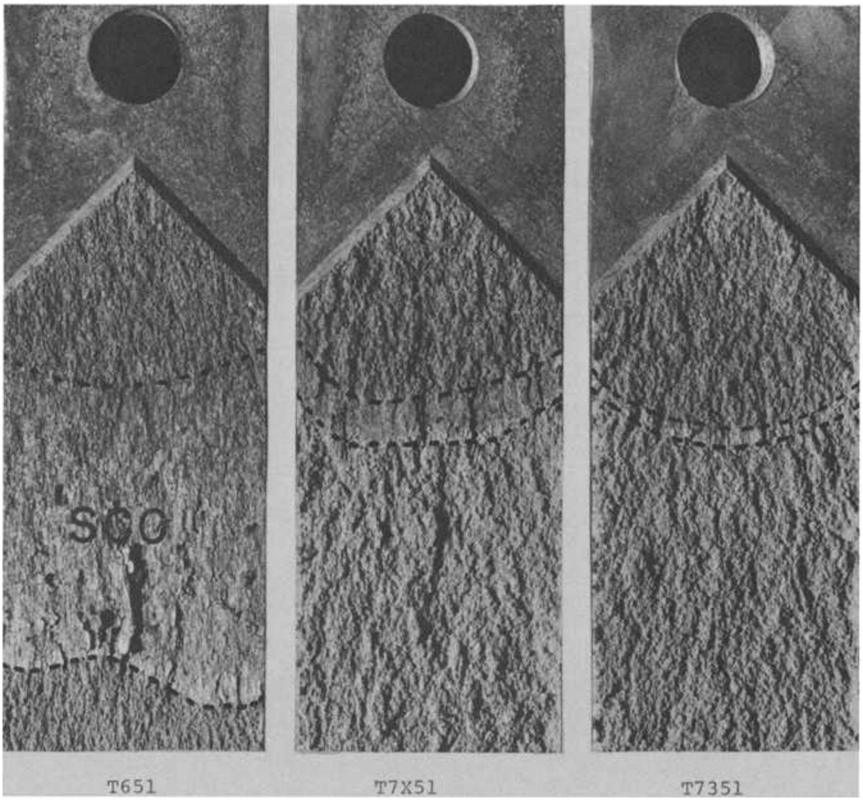

FIG. 7—*Fracture surfaces of DCB specimens showing relative SCC growth for several tempers of 7075 alloy plate.*

rapid mechanical fracturing of the highly resistant 2XXX alloys as a result of corrosion product wedging. A comparison of micrographs is shown in Fig. 8 of typical intergranular SCC and transgranular mechanical cracking similar to the tension precrack in two different lots of 2124-T851 alloy plate.

Summary

The method described previously for estimating average sustained SCC velocities at stress intensities at or just below the critical stress intensity has several advantages for screening tests of alloys and tempers. The test is fairly rapid; it is sensitive to various degrees of susceptibility to SCC; it does not require determination of stress intensities, and it simplifies the interpretation of the crack-growth curves. It is essential, however, for materials that show only small amounts of environmental crack growth, espe-

TABLE 3—*Comparison of SCC propagation rates in the 3.5 percent NaCl accelerated test and in outdoor atmospheres.*[a]

Alloy and Temper	Average Velocity, in./h (m/s)					
	3.5% NaCl (15 days)		Seacoast (6 months)		Industrial (6 months)	
7079-T651	320×10^{-5}	(226×10^{-10})	35×10^{-5}	(25×10^{-10})	25×10^{-5}	(18×10^{-10})
7039-T6351	220	(155)	30	(21)	25	(18)
5456-sensitized	210	(148)	40	(28)	2	(1)
2219-T37	210	(148)	35	(25)	20	(14)
2014-T651	120	(85)	15	(11)	10	(7)
2024-T351	100	(71)	20	(14)	10	(7)
7075-T651	100	(71)	20	(14)	10	(7)
2021-T81	30[b]	(21)	6[b]	(4)	2[b]	(1)
2219-T87	20[b]	(14)	4[b]	(3)	1[b]	(0.7)
2024-T851	20[b]	(14)	2[b]	(1)	0.5[b]	(0.4)
5456-H117	6[b]	(4)	<0.2	(<0.1)	<0.2	(<0.1)
6061-T651	6[b]	(4)	<0.2	(<0.1)	<0.2	(<0.1)
7075-T7351	3	(2)	<0.2	(<0.1)	0.4	(0.3)

[a] Tests on 1 in. (25 mm) high, straight-notch DCB specimens machined from 2.0 in. (51 mm) or 2.5 in. (64 mm) plate (Ref *4*).

[b] Mechanical fracture rather than SCC.

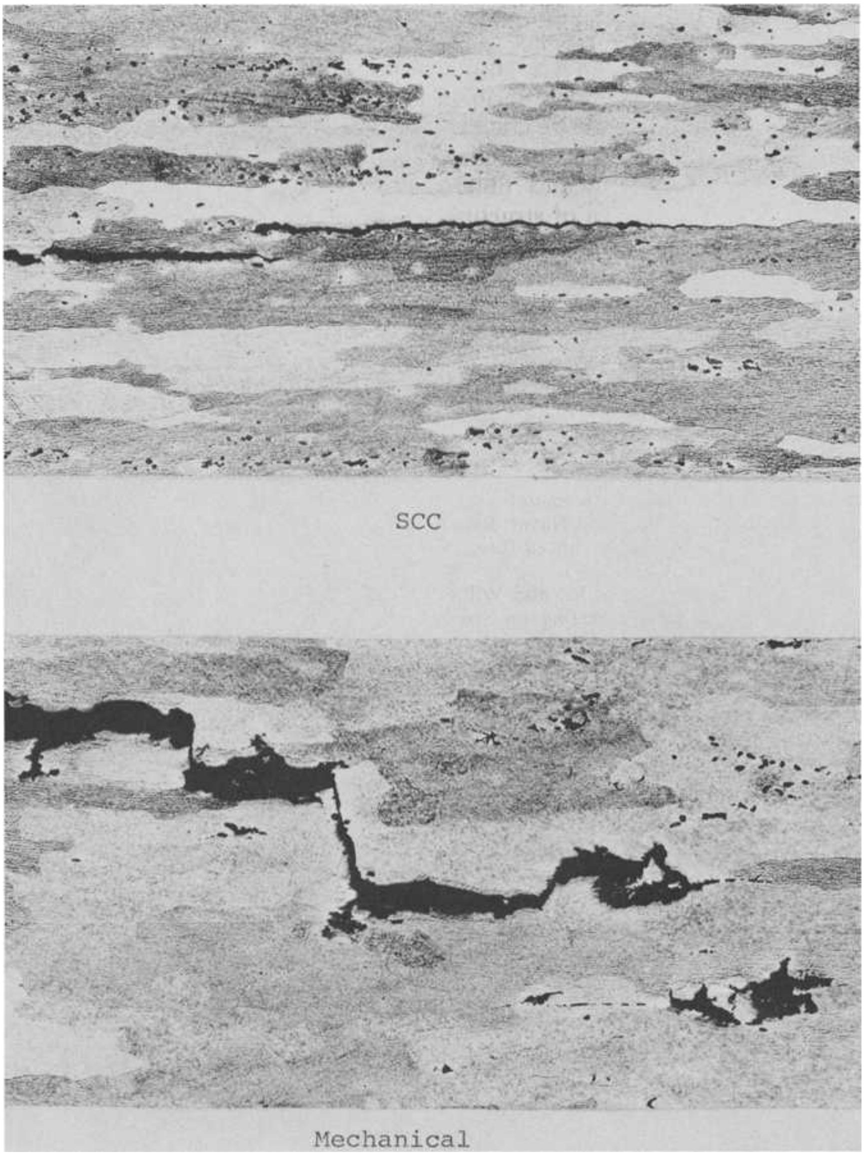

FIG. 8—*Micrographs (X100) of tip of environmental crack in DCB specimens of 2124-T851 alloy plate (Keller's etch).*

cially in the case of 2XXX alloys, to establish that the crack growth is really SCC and not simply mechanical fracture caused by corrosion product wedging. The mode of cracking can be readily determined either by fractographic examination or metallographic examination of the crack tip.

Although SCC velocities obtained by this method are not directly applicable in the design of structures, knowledge of relative SCC propagation rates can be useful in special situations for appraising the hazard of SCC and determining suitable inspection intervals.

Practical difficulties involved in measuring small amounts of SCC growth, however, warrant further evaluation to justify this as a primary method of testing.

References

[*1*] Brown, B. F., *Stress Corrosion Cracking in High Strength Steels and in Titanium and Aluminum Alloys*, Naval Research Laboratory, Washington, D. C., 1972. (Sponsored by the Advanced-Research Projects Agency ARPA Order No. 878), pp. 1–16 (Fundamentals).

[*2*] Wei, R. P., Novak, S. R., and Williams D. P., *AGARD Conference Proceedings No. 98*, Specialists Meeting on Stress Corrosion Testing Methods, Brussels, Belguim, 5 and 6 Oct. 1971, pp. 5–1 through 8.

[*3*] Sprowls, D. O., Shumaker, M. B., Walsh, J. D. and Coursen, J. W., Final Report-Part I of Contract No. NAS 8-21487; prepared for George C. Marshall Flight Center, 31 May 1973.

[*4*] Speidel, M O. and Hyatt, M. V., *Advance in Corrosion Science and Technology*, Vol. 2, M. G. Fontana and R. W. Staehle Eds., Plenum Press, New York, 1972, p. 158.

[*5*] Babilon, C. F., Wygonik, R. H., Nordmark, G. E., and Lifka, B. W., Technical Report AFML-TR-73-83, April 1973, USAF Contract No. F33615-71-C-1571, Air Force Materials Laboratory, Dayton, Ohio.

[*6*] Davies, R. E., Nordmark, G. E., and Walsh, J. D., Final Report, NASC Contract No. N00019-72-C-0512, prepared for Naval Air Systems Command, Washington, D. C., July 1975.

[*7*] "Standard Method for Stress Corrosion Testing and an Improved System for Rating the Relative Resistance to Stress-Corrosion Cracking of High Strength 7XXX Aluminum Alloys Products," Report of AA/ASTM Task Group G01.06.91 by D. O. Sprowls, Chairman, et al. Also in this publication.

P. J. Bania[1] *and S. D. Antolovich*[2]

Activation Energy Dependence on Stress Intensity in Stress-Corrosion Cracking and Corrosion Fatigue

---

REFERENCE: Bania, P. J. and Antolovich, S. D., "**Activation Energy Dependence on Stress Intensity in Stress-Corrosion Cracking and Corrosion Fatigue,**" *Stress Corrosion—New Approaches, ASTM STP 610,* American Society for Testing and Materials, 1976, pp. 157–175.

ABSTRACT: The phenomena of stress-corrosion cracking and corrosion fatigue have been investigated assuming that a thermally activated process (diffusion) acts in conjunction with mechanical energy to produce subcritical extension of a flaw. Associated with this diffusion process is an apparent activation energy which is shown to be dependent on the stress-intensity level indicating that the rate limiting diffusion step is associated with the material rather than the environment. A characteristic activation energy associated with the diffusion process is obtained by plotting apparent activation energy versus mechanical energy input required for crack extension and extrapolating to zero mechanical energy input. The characteristic activation energy associated with the stress-corrosion differs fram that associated with the corrosion-fatigue process. Thus, a linear superposition model for corrosion fatigue employing stress-corrosion data is not valid for the material studied. Also from this plot it can be seen that the toughness of the material at the crack tip is inherently degraded by the diffusion process.

KEY WORDS: titanium alloy, stress corrosion, cracking (fracturing), corrosion fatigue, activation energy, stress intensity, hydrogen embrittlement

The phenomena of stress-corrosion cracking (SCC) and corrosion fatigue (CF) have been the subject of extensive investigation over the past decade. One conclusion to be drawn from these studies is that in order to prevent or curtail these processes from occurring, a more basic understanding of the mechanisms involved is mandatory. While it is clear that both the SCC and CF processes occur under conditions of stress and an aggressive envi-

---

[1] Formerly, graduate student, University of Cincinnati, presently, metallurgist, Wright-Patterson Air Force Base, Ohio 45433. This work was submitted in partial fulfillment for M.S. degree.

[2] Professor, Department of Materials Science, University of Cincinnati, Cincinnati, Ohio 45219.

ronment, it is not clear whether both processes occur by the same mechanisms. However, due to their similarities in nature, SCC and CF are frequently considered to incorporate the same basic corrosion processes [*1–3*].[3] (It should be noted that the use of the term "aggressive" environment when considering SCC or CF does not necessarily refer to an environment which alone results in significant chemical attack but rather any environment which in conjunction with stress produces subcritical extension of a flaw below a critical stress level which is determined in an inert environment.)

Generally it is accepted that the SCC process, and hence the CF process, occurs through the combination of a mechanical effect coupled with a thermally activated chemical effect. The thermally activated chemical effect frequently is assumed to be diffusion controlled, and, accordingly, experiments have been conducted [*4,5*] aimed at determining an activation energy, Q, associated with the thermally activated process in order to identify a critical diffusing species. Since in a series process the slowest step is rate controlling, the activation energy may be characteristic of diffusion of the critical species within the plastic zone region or diffusion in the environment to the crack tip. If this activation energy could be shown to be dependent on the stress-intensity factor K (which has no effect on the environment) this would then provide strong evidence that the rate controlling diffusion step takes place either on the surface or in the bulk of the solid. This concept of Q being dependent on K is predicated on the fact that since the dilatation field at the crack tip changes with K, so too should the thermal energy required for any thermally activated process in the crack tip change.

The hypothesis of Q being dependent on K gives rise to another interesting situation. It would mean that there is no unique value of activation energy associated with the SCC or CF processes. This result has been demonstrated experimentally [*6*]. Thus, a single value for the activation energy should only correspond to a single dilatation or stress-intensity state. Since an increase in the stress-intensity factor also increases the dilatation at the crack tip, it seems likely that it would thus be easier for diffusion to occur in this region. Therefore, assuming a constant failure mechanism, the activation energy should be correspondingly less and should decrease with increasing stress intensity.

With this information in mind, the following program was undertaken in order to evaluate the dependency of the activation energy on the stress-intensity factor. It will be assumed throughout this report that in either the SCC or CF process the total energy available for crack extension (E_{tot}) may be supplied either mechanically (E_{mech}) or thermally (E_{th}). Thus

$$E_{\text{tot}} = E_{\text{mech}} + E_{\text{th}} \tag{1}$$

---

[3] The italic numbers in brackets refer to the list of references appended to this paper.

where the thermal energy contribution is taken to be equal to the experimentally determined activation energy Q (apparent activation energy). A plot of E_{mech} versus E_{th} and extrapolation to zero E_{mech} should yield a characteristic activation energy, Q', associated with the diffusion process in the unstressed or zero mechanical energy state. This characteristic activation energy value can now be compared to the readily available activation energies for diffusion in unstressed material in order to identify the diffusion species. Thus, the similarities between the SCC and CF processes may be evaluated by simply comparing their characteristic activation energies. Also with this characteristic activation energy, the validity of the linear superposition model for corrosion fatigue [*7,8*] will be evaluated. Typically, by this model

$$(da/dn)_{\text{CF}} = (da/dn)_{\text{AIR}} + (\alpha/f)(da/dt)_{\text{SCC}} \tag{2}$$

where

(da/dn) = crack growth rate per cycle;
(da/dt) = crack growth rate per unit time;
f = frequency, and
α = the fraction of the loading cycle that the SCC process is operating.

If the characteristic activation energy for SCC is seen to differ from that for the CF value, then it would not be valid to combine the two processes in such a manner.

Experimental Procedure

Material and Specimens

The material studied in this program was ½-in. gage Ti-6Al-4V plate (normal grade) in the mill annealed condition—rolled from 1700°F, annealed for 8 h at 1350°F, and furnace cooled. The chemical analysis and mechanical properties as supplied by the vendor are listed in Table 1. The directionality of the properties gives an indication that the material is not textured uniformly. The microstructure of the material shown in Fig. 1 displays a typical mill annealed rolled texture. This texture proved to be the overriding factor in determining the orientation to be tested for the SCC and CF conditions. This will be discussed further in a later section.

Three common specimen designs were used in the program. The single-edge notch (SEN) specimen was used to determine the fatigue crack-growth rates in laboratory air, and the standard compact tension specimen was used to determine the fracture toughness. All SCC and CF tests were performed in a 3.5 percent sodium chloride (NaCl) solution with side-grooved tapered double cantilever beam (DCB) specimens, as shown in

TABLE 1—*Chemical analyses and mechanical properties as supplied by the vendor.*

ALLOY COMPOSITION						
C	Fe	N	Al	V	H	Ti
0.026	0.17	0.012	6.5	4.3	0.005	balance

MECHANICAL PROPERTIES				
Gage	Yield Strength, psi	Tensile Strength, psi	Elongation, %	Reduction in Area, %
0.500 in.	L 143 300	150 400	16.0	33.1
	T 147 200	176 600	16.0	38.8

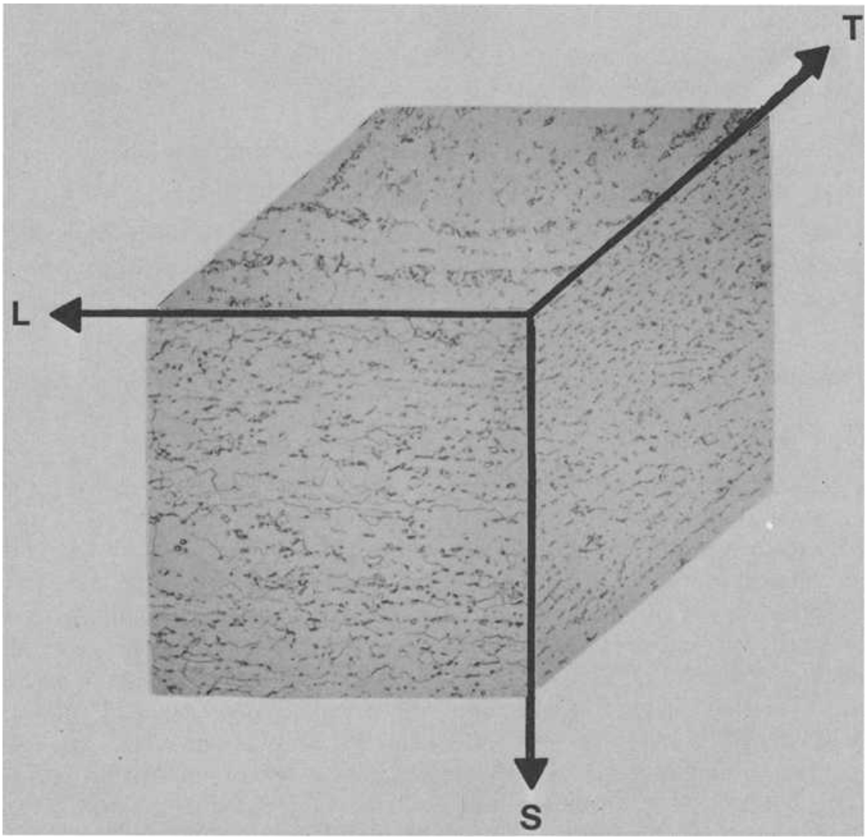

FIG. 1—*Microstructure of the Ti-6Al-4V plate showing a typical rolled texture with a high percentage of primary alpha.*

Fig. 2. Stress-intensity solutions for these specimens have been published elsewhere [*9,10*]. The solution was prepared from distilled water and chemical grade NaCl, and air was continuously bubbled through the solution during the tests. Tapered DCB specimens for preliminary tests were machined in the transverse (L-T) orientation. However, in both the SCC and CF preliminary tests, the crack would only propagate in the rolling direction, thus inducing failure along the tensile axis. No significant growth could be induced prependicular to the rolling direction even when the side-groove was machined to a depth of half the specimen thickness. As a result of this highly textured behavior, all specimens for the remainder of the program were machined in the longitudinal (T-L) orientation so the mate-

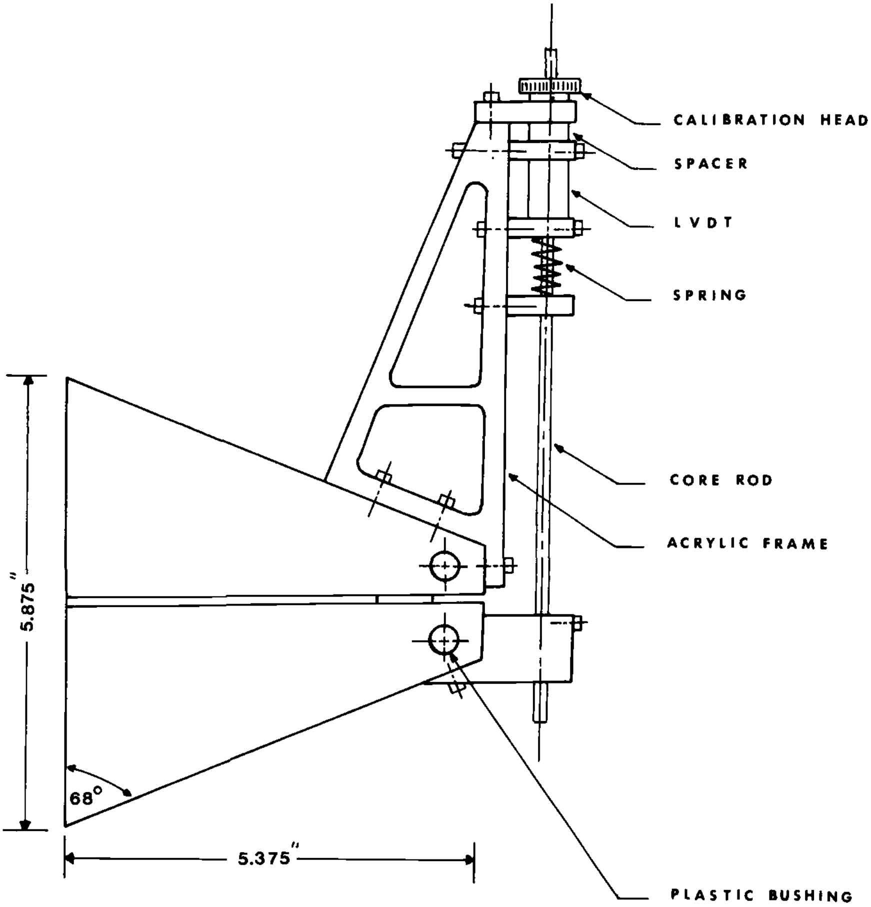

FIG. 2—*Schematic illustration of the tapered DCB specimen with the extensometer used in the SCC and CF tests.*

rial could be tested in this highly preferred crack path direction. These preliminary tests indicated that the plate material was not sufficiently cross-rolled during fabrication to prevent anisotropic behavior.

Apparatus for SCC and CF Tests

The same apparatus was used in both the SCC and CF tests. The setup is shown in Fig. 3. Since the compliance technique was used to measure crack lengths, the extensometer design shown in Fig. 2 was used to measure the remote crack opening displacements. This design provided the advantage of keeping the displacement measuring device out of the corrosive environment, thus improving its overall life and maintainability. Also, this extensometer has the advantage of *in situ* calibration at any time during the tests. An linear variable differential transformer (LVDT) was used on the extensometer as the displacement measuring device. In order to prevent any undesirable corrosion reactions with the specimen, the extensometer frame was constructed from an acrylic sheet material. The environmental chamber was also constructed from the acrylic material in order to prevent any undesirable corrosion products from contaminating the solution. The chamber was free to slide along the Teflon sleeve on the

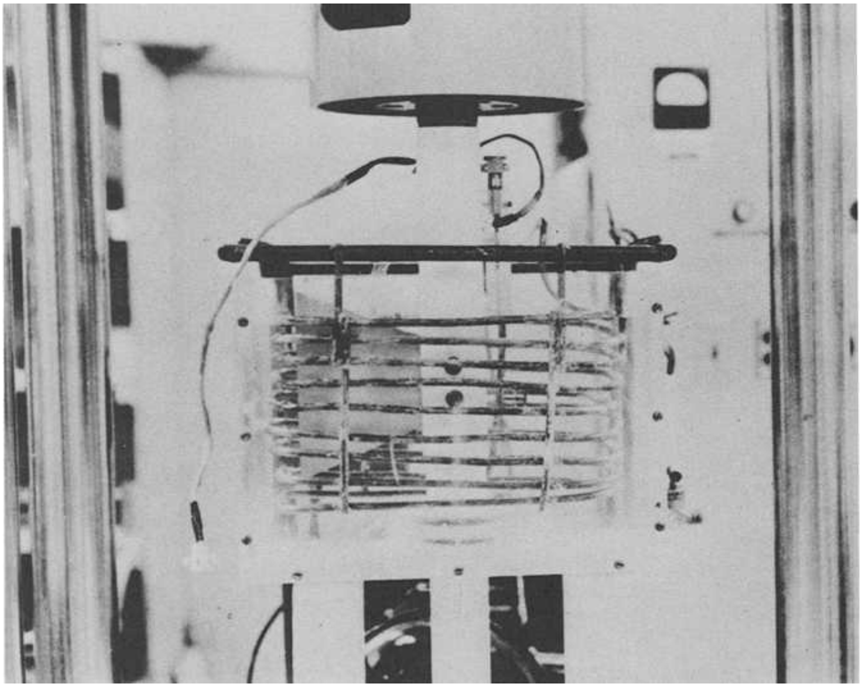

FIG. 3—*Experimental setup displaying chamber, cooling coils, grips, and specimen with extensometer.*

bottom grip by means of a compression O-ring seal. This provided easy access to the specimen and extensometer. Also, to eliminate undesirable corrosion products, the exposed surfaces of the loading pins were coated with a silicone rubber, and the grips and cooling coils were coated with an epoxy lacquer. Finally, to minimize any galvanic coupling between the specimen and grips, a plastic bushing with a 0.125 in. wall thickness was press-fitted into the pin loading holes of the grips and specimens. As a result of these precautions, the specimens were insulated completely from any extraneous coupling reactions.

Crack Length Measurements

The compliance technique was used to monitor the crack length of the tapered DCB specimens during SCC and CF testing accurately. This method was chosen for two primary reasons. First, it appeared to be the most practical means in light of the experimental setup. Second, it was felt that the compliance technique was more suitable for detecting any crack tunneling than any surface monitoring technique. Also, the compliance technique provided the added advantage of eliminating much of the human error associated with surface measurement techniques.

The calibration procedure for the compliance measurements was as follows: a tapered DCB specimen with an accurately measured machined notch length (simulated crack length) was slowly loaded between 50 and 350 lb, while an x-y recorder simultaneously plotted displacement as measured by the LVDT (V) versus load (P). This procedure was repeated several times for a series of machined notch lengths which were increased incrementally by roughly a tenth of an inch. The slope of this displacement versus load diagram is the compliance (λ) of the specimen and is a function of the notch length. From such a series of tests, a relationship between compliance and notch length can be established. For the linear portion of this relationship, in which all tests were conducted, the following relationship holds

$$\lambda = k_1(a) + k_2 \tag{3}$$

where

a = crack length (notch length) and
k_1 and k_2 = constants.

This relationship was used to measure crack length during the CF tests by simply monitoring displacement versus load on any cycle during the test. For the SCC tests, since it was desired to maintain a constant load at all times, the relationship $\lambda = V/P$ was substituted into Eq 3 to obtain the following relationship

$$\frac{\Delta V}{P} = k_1(\Delta a) \tag{4}$$

Thus, the crack length was monitored continuously at all times.

Testing

Room temperature crack growth rates were measured on three SEN specimens. Data were recorded at growth intervals of 0.010 in. All tests were conducted in laboratory air at a frequency of 1 Hz with an *R* ratio of 0.1. The CF tests were conducted at a frequency of 0.33 Hz and an *R* ratio of 0.1. Data were recorded for the SCC and CF tests at growth intervals of between 0.050 to 0.100 in. The extensometer was calibrated repeatedly throughout the testing program. Finally, the fracture toughness tests were conducted according to ASTM Test for Plane-Strain Fracture Toughness of Metallic Materials (E 399-72) requirements.

Results

Fracture and Air Fatigue

The results of the fracture toughness tests yielded an average fracture toughness of 34 ksi$\sqrt{\text{in.}}$ (37 MPa$\sqrt{\text{m}}$) in the T-L orientation. All tests qualified as valid plane-strain fracture toughness tests according to the ASTM specifications. The results of the air fatigue tests conducted on the SEN specimens are shown in Fig. 4. The points shown represent the average of the three tests. These data are in good agreement with the data found in the literature for similar material [*11*].

Diminishing Rate SCC Tests

In the earlier SCC tests conducted at low-stress intensity levels, crack growth was detected which was seen to be decreasing in rate with increasing time. After a sufficient length of time, crack extension was stopped completely. A similar effect was seen by Hancock and Johnson [*12*] for H-11 steel. They attributed this behavior to the formation of an oxide film which restricted the SCC process. Green and Sedricks [*13*] showed that for high aluminum content (greater than 5 percent) titanium alloys, surface film formation was definitely a competing process to SCC. Thus, it seems reasonable that at slow enough rates of crack extension, the film formation process may slow down and eventually halt the diffusion process necessary for further subcritical crack extension. If this were the situation, the film would seem to be very brittle as evidenced by the following results. When the specimen was loaded, a small amount of crack extension would occur and eventually stop. If the specimen was then unloaded and immediately reloaded to the original load, again a small amount of crack extension would result with a similar decreasing rate. Thus, the film would seem to be very brittle and hence very susceptible to cracking as a result of load fluctuations. This effect may play an important role in the corrosion fatigue process.

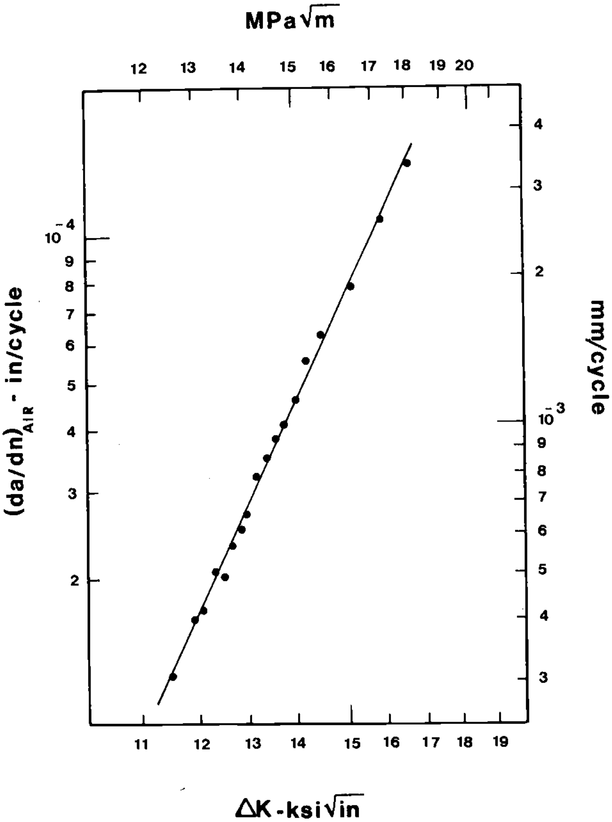

FIG. 4—*Air fatigue crack propagation rate as a function of stress intensity range.*

It should be noted at this point that if these SCC tests had been conducted on specimens for which the stress intensity increased with increasing crack length at constant load, (for example, compact tension specimens), this behavior might not have been recorded. No data are reported in this section due to the lack of steady-state crack extension rates.

Constant Rate SCC Tests

The results of the SCC tests which yielded constant rates for given levels of stress intensity are summarized in Table 2 and plotted in Fig. 5. All points in this figure refer to steady crack-growth rates in which no change was detected with increasing time. These results can be used to determine the apparent activation energy for the SCC process. Since the SCC data show the process to be activated thermally, we may write

$$(da/dt)_{SCC} = Ae^{-(Q_{SCC}/RT)} \tag{5}$$

TABLE 2—*SCC and CF test results.*

	SCC Tests		CF Tests	
	da/dt (in./s)	*K* (ksi$\sqrt{\text{in.}}$)	*da/dn* (in./cycle)	Δ*K* (ksi$\sqrt{\text{in.}}$)
2°C	4.62 × 10^{-4}	18	1.0 × 10^{-4}	11
	6.58 × 10^{-4}	19	4.3 × 10^{-4}	13
	10.46 × 10^{-4}	20	9.9 × 10^{-4}	14
	13.54 × 10^{-4}	21	15.8 × 10^{-4}	16
25°C	4.44 × 10^{-4}	17	1.9 × 10^{-4}	11
	9.04 × 10^{-4}	18	4.1 × 10^{-4}	13
	9.87 × 10^{-4}	18	11.3 × 10^{-4}	14
	14.13 × 10^{-4}	19	24.6 × 10^{-4}	16
65°C	11.89 × 10^{-4}	14	3.2 × 10^{-4}	11
	21.92 × 10^{-4}	16	7.5 × 10^{-4}	13
	25.80 × 10^{-4}	16	21.3 × 10^{-4}	14
	35.12 × 10^{-4}	17	42.0 × 10^{-4}	16

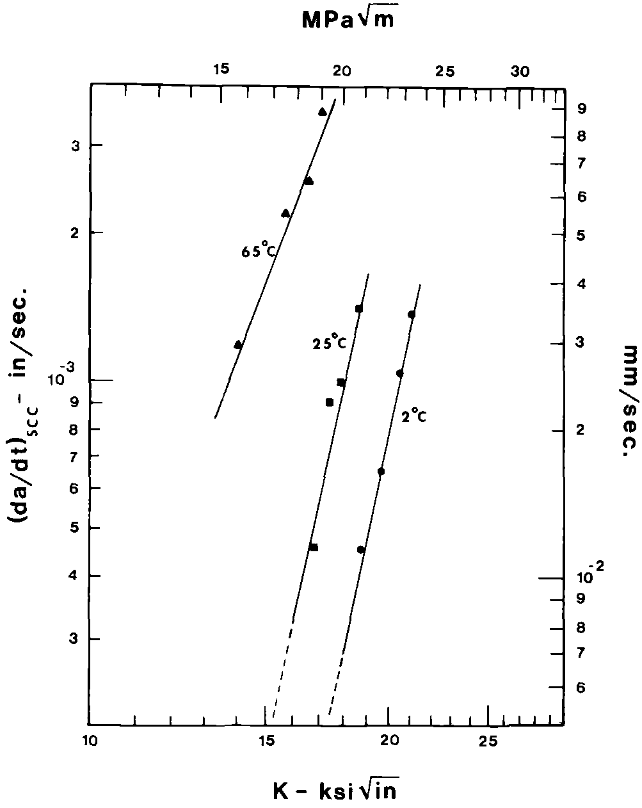

FIG. 5—*SCC-test results.*

where

$(da/dt)_{\text{SCC}}$ = crack extension rate,
A = a constant, and
Q_{SCC} = is the apparent activation energy. Thus

$$\ln (da/dt)_{\text{SCC}} = \ln (\text{rate})_{\text{SCC}} = \ln A - Q_{\text{SCC}}/\text{RT} \tag{6}$$

From Eq 6 it can be seen that from a plot of ln $(\text{rate})_{\text{SCC}}$ versus $1/T$, both of which are measured experimentally, the apparent activation energy can be determined from the slope of the line. Such a plot is shown in Fig. 6, with the slope of each line proportional to the Q_{SCC} associated with the indicated K level for each line. The value of Q_{SCC} is the thermal energy (E_{th}) contribution to the total energy required for crack extension as indicated by Eq 1. As for the mechanical energy contribution, (E_{mech}), Paris and Sih [*14*] show that the energy available for crack extension per unit

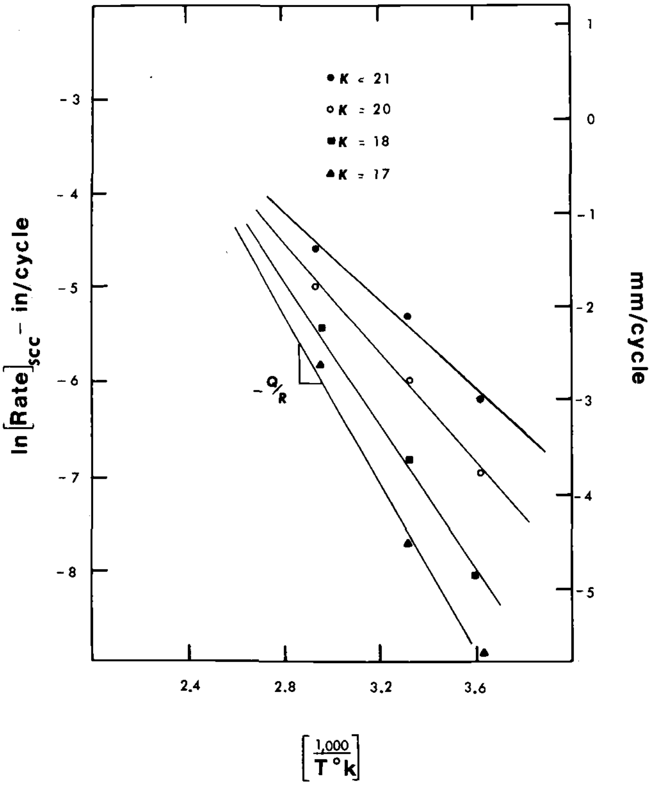

FIG. 6—*Plot of ln* $(rate)_{SCC}$ *versus* $1/T$ *used to determine the apparent activation energy,* Q_{SCC}.

area of new crack generated can be expressed as (K^2/E) for Mode I type loading. (The factor $(1 - \nu^2)$ will be neglected.) Now the effect of stress intensity on the apparent activation energy can be evaluated as shown in Fig. 7. Besides showing the dependency of Q_{SCC} on K, this plot can yield valuable insights with respect to the actual diffusion process and its effects on the material.

As expected, the plot in Fig. 7 shows that there is a definite dependence of the apparent activation energy on the stress-intensity factor. The activation energy decreases with increasing stress intensity. As previously indicated, this behavior is attributed to the dilatation field created by the stress amplification in the crack-tip region allowing for greater ease of diffusion and a lower activation energy [*15,16*].

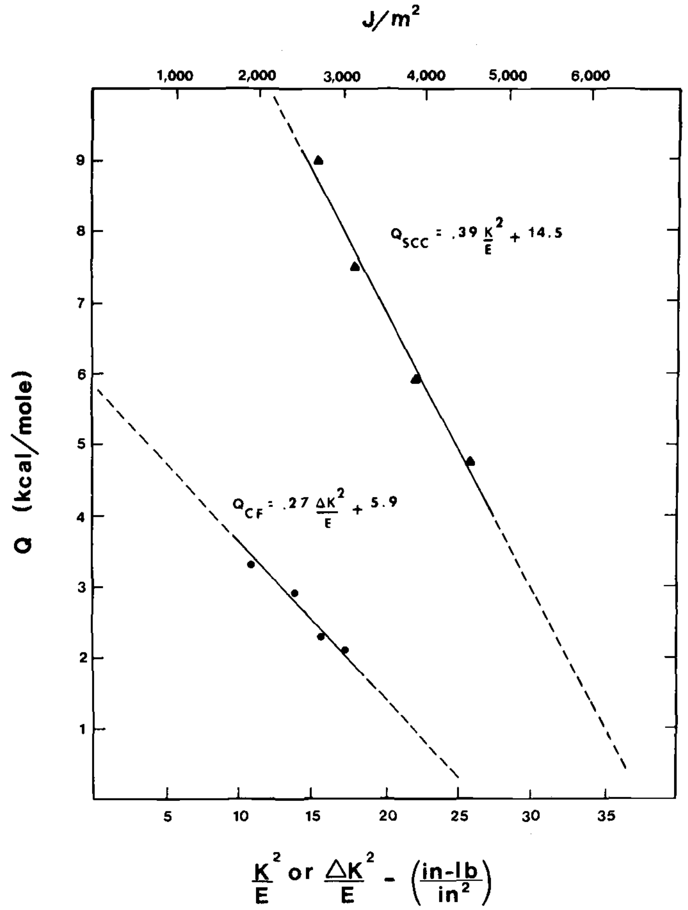

FIG. 7—*Apparent activation energy as a function of stress intensity (range) for SCC and CF.*

At first glance, one might expect an extrapolation of the plot in Fig. 7 to zero thermal activation energy to yield a value of ($K_{Ic}{}^2/E$) which would correspond to roughly 60 (in · lb)/in.^{2} or 10 500 J/m^2. This is to be expected since this extrapolation should closely resemble a test in air in which no thermally activated chemical process is assumed to occur. However, it can be seen that the extrapolation yields a value of approximately 37 (in · lb)/in.^{2} or 6 500 J/m^2. Thus, it would appear that the material had been degraded as a result of the interaction with the environment, rendering a more brittle material with a lower fracture toughness value at the crack-tip region. This degradation of the material at the crack tip can be expected if diffusion—especially hydrogen diffusion—is occurring at the crack tip. Since most investigators assume that hydrogen is the diffusing species, [*17,18*] then hydrogen embrittlement either by chemical interaction or pressure void formation would appear to be likely candidates for the degradation process. However, other processes such as crack initiation due to brittle film formation may also be strong contributing factors as previously mentioned.

Another interesting result obtained from Fig. 7 comes from an extrapolation of the plot to zero mechanical energy. Such a procedure should yield a value of the characteristic activation energy, Q', associated with the diffusion process in the material. From this characteristic activation energy we should be able to identify the critical diffusion species in the SCC process. The value obtained by such a procedure for the SCC tests in this program is 14.5 kcal/mol. This value is somewhat higher than the reported values for activation energies for SCC in titanium alloys, but this is expected since the values reported are for specific stress-intensity levels. Katz [*19*] however indicated a difference in activation energies for two stress-intensity levels for the highly susceptible Ti-8Al-1Mo-1V alloy, with the same trend as indicated in this study. The value of 14.5 kcal/mol obtained in this investigation is close to the range of values reported for diffusion of hydrogen in alpha-titanium [*20,21*]. This value was chosen for comparison purposes since alpha is the more susceptible phase, as indicated by increasing alloy susceptibility with alpha-content and the less forgiving nature of the alpha-phase with respect to hydrogen embrittlement. Also, other investigators have identified alpha as the more susceptible phase in SCC [*22,23*]. Thus, with the characteristic activation energy determination and comparison, we can identify the most probable diffusion species associated with the most sensitive microstructure feature.

Corrosion Fatigue Tests

By a procedure similar to that used in the SCC tests, an apparent activation energy was determined for the CF process. The data are plotted in Fig. 8, and ln $(\text{rate})_{\text{CF}}$ versus $1/T$ is plotted in Fig. 9. Again, the apparent activation energy is determined from the slope of each line in Fig. 9 asso-

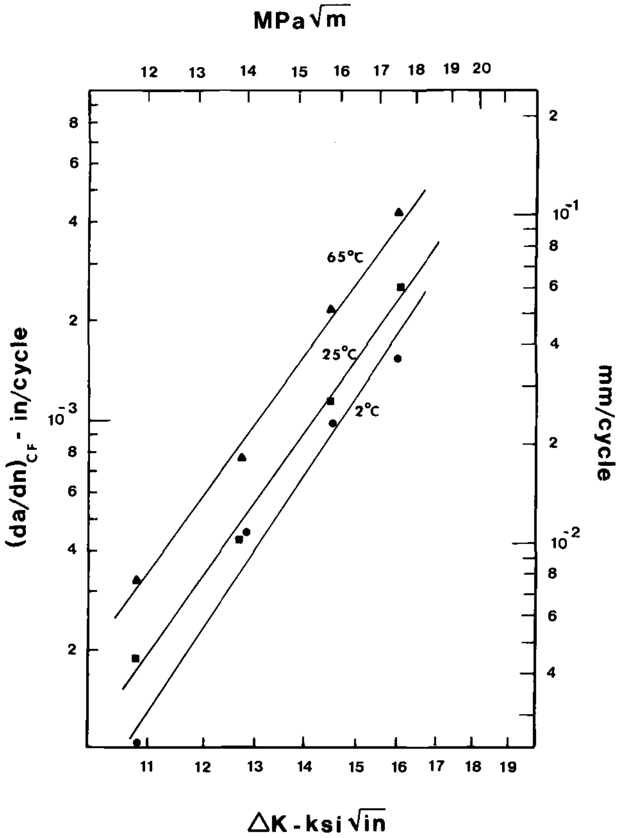

FIG. 8—*CF test results.*

ciated with the indicated stress-intensity range. A plot of Q_{CF} versus $(\Delta K^2/E)$ is shown in Fig. 7. As in the SCC case, the apparent activation energy for the CF process is shown to be dependent on the stress-intensity factor. It can be seen, however, that the characteristic activation energy for the CF process is only 5.9 kcal/mol. This is less than one half the value obtained for the SCC process. There are a number of possible explanations for this lower value. First, since there should be a higher defect density in a plastic zone formed by cyclic loading, increased ease of diffusion could result from this situation. It is well established that diffusion occurs more readily along grain boundaries, dislocations, high vacancy areas, and so on. Another factor contributing to the lower characteristic activation energy for the CF process may be locally high hydrostatic pressures resulting from trapped solution during the loading cycle. Finally, the repeated breaking of a continuous film which may be hindering the diffusion process may be a significant factor. All of these factors could sig-

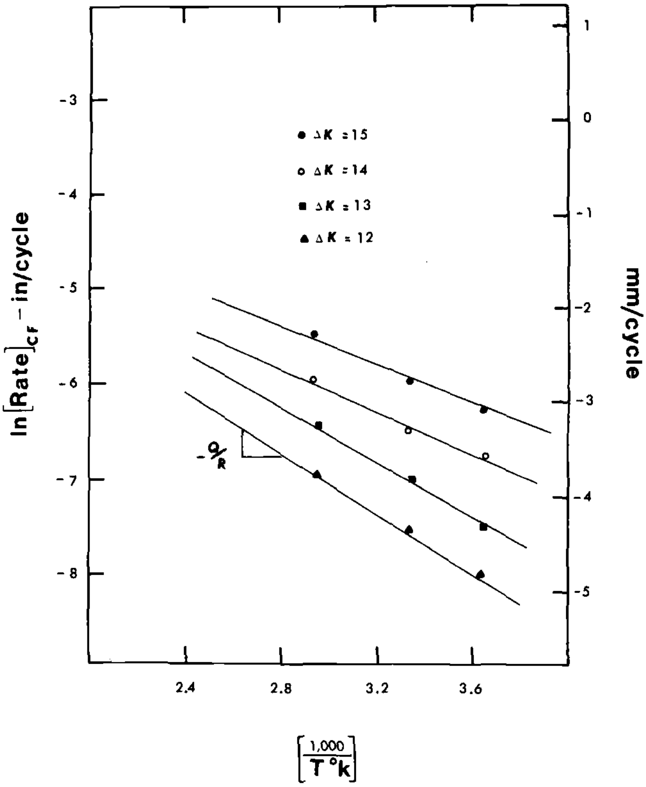

FIG. 9—*Plot of ln (rate)*$_{CF}$ *versus 1/*T *used to determine the apparent activation energy,* Q$_{CF}$.

nificantly lower the activation energy and thus aid the crack extension process.

It should be noted at this point that the difference in characteristic activation energies obtained for the SCC and CF tests should not be construed as an indication of different *failure mechanisms*. The fracture surfaces shown in Fig. 10 indicate that a similar cleavage type failure mode predominated in both the SCC and CF tests. Thus, the difference in the characteristic activation energies is taken more properly as an indication of different diffusion processes, both of which result in the same fracture mechanism.

Conclusions

Since the characteristic activation energy for the CF process is significantly lower than that obtained for the SCC process, it would appear that

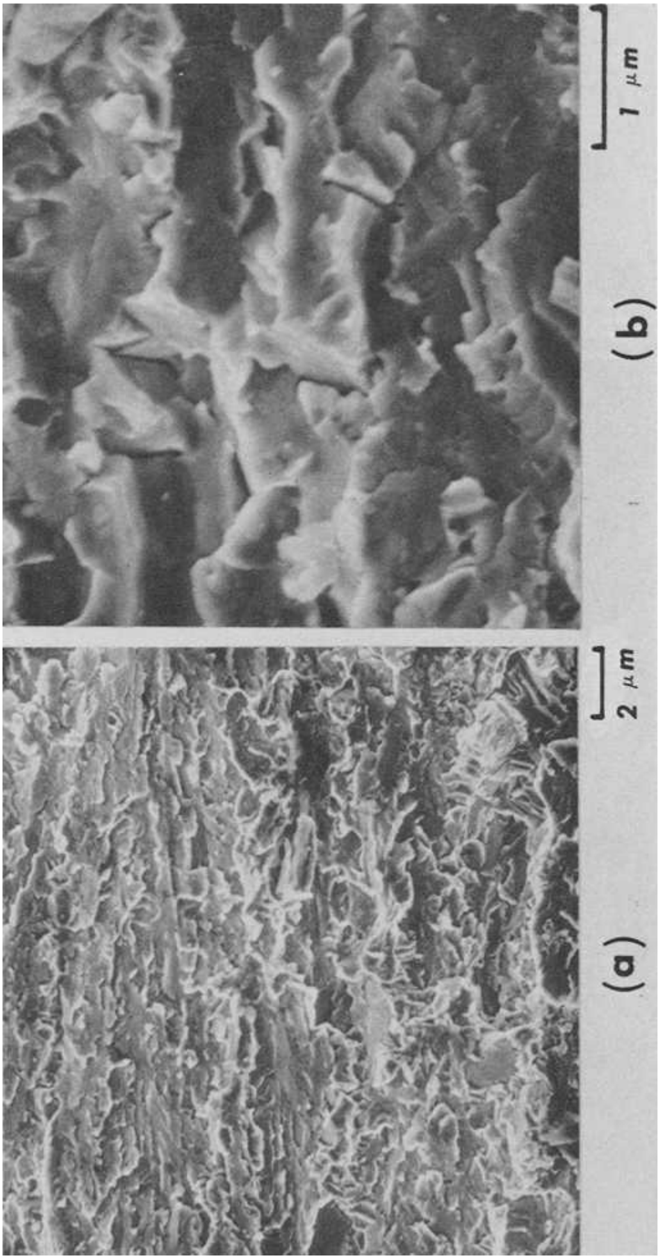
(a)
2 μm
(b)
1 μm

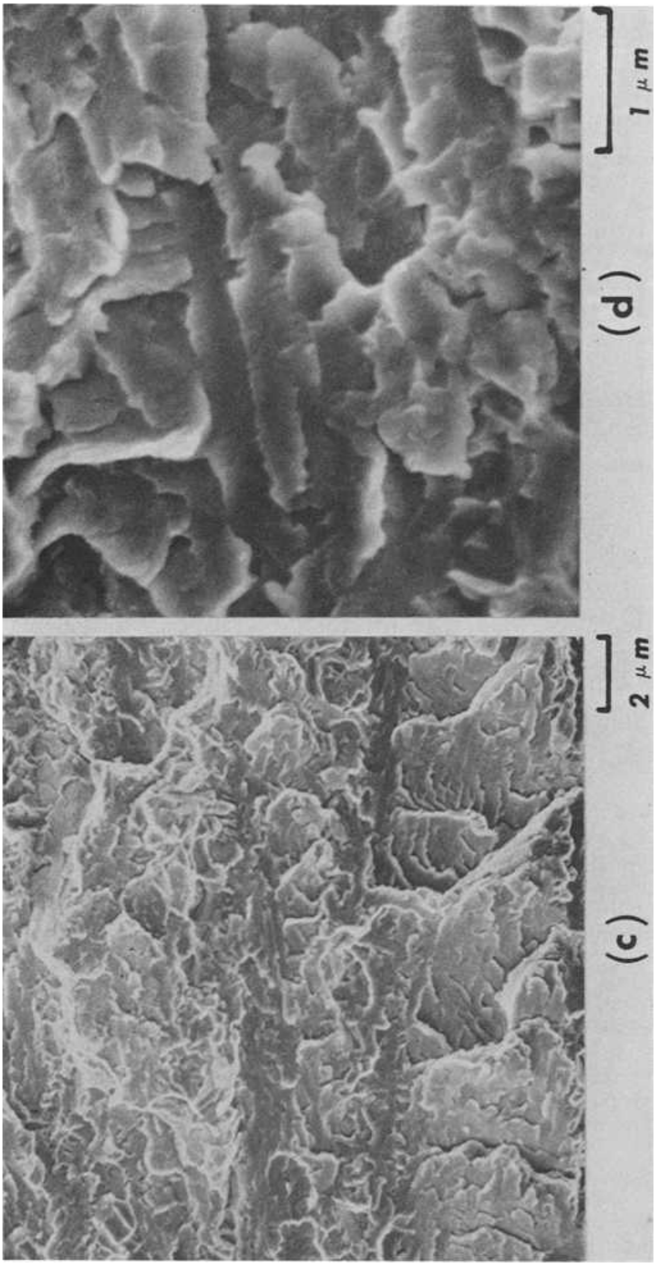

FIG. 10—*SEM micrographs of failed surfaces:* (a) + (b) *Typical fracture features of SCC specimens;* (c) *and* (d) *typical features of CF specimens. Crack propagation direction is from left to right.*

the CF process is potentially more dangerous than the SCC process, Also, since there are different diffusion processes occurring, the linear superposition model fails indicating that using independently obtained SCC data to predict CF behavior can be very dangerous—at least for the alloy studied. As indicated in the previous paragraph, the use of SCC data for CF calculations by the linear superposition model may yield much slower crack growth rates than actually occur in CF situations.

Summary

1. The apparent activation energy associated with the SCC and CF processes is shown to be dependent on the stress-intensity factor.
2. The process associated with the SCC and CF processes is deduced to depend on diffusion within the material rather than within the environment.
3. The material itself is shown to be inherently degraded by an embrittlement process as a result of interacion with the environment.
4. The value of 14.5 kcal/mol as the characteristic activation energy for SCC suggests that hydrogen diffusion in the material is the rate controlling mechanism.
5. The characteristic activation energy for CF, 5.9 kcal/mol, is significantly lower than that for the SCC process suggesting a different mechanism.
6. The linear superposition model does not apply for the Ti-6Al-4V alloy studied in this program.

References

[1] Meyn, D. A., *Metallurgical Transactions*, Vol. 2, March 1971, pp. 853–865.

[2] Crooker, T. W., Judy, R. W., and Lange, E. A., *Transactions*, American Society for Metals, Vol. 59, 1966, pp. 195–207.

[3] Dahlberg, E. P., *Transactions*, American Society for Metals, Vol. 58, 1965, pp. 46–53.

[4] Johnson, H. H. and Willner, A. M., *Applied Materials Research*, Vol. 4, No. 1, 1965, pp. 34–40.

[5] VanDer Sluys, W. A., *Engineering Fracture Mechanics*, Vol. 1, No. 3, 1969.

[6] Wei, R. P., *Proceedings of Conference, Fundamental Aspects of Stress Corrosion Cracking*, Ohio State University, Columbus, Ohio, 1969, pp. 104–111.

[7] Gerberich, W. W., Birat, J. P., and Zackay, V. F., "A Superposition Model for Environmentally Assisted Fatigue Crack Propagation," UCRL Report No. 20538, University of California, Berkeley, Calif., 1971.

[8] Wei, R. P. and Landes, J. D., *Materials Research and Standards*, Vol. 9, No. 7, 1969, pp. 25–27.

[9] Mostovoy, S., Crosley, P. B., and Ripling, E. J., *Journal of Metals*, Vol. 2, No. 3, Sept. 1967 pp. 661–681.

[10] *Stress Analysis and Growth in Crack, ASTM STP 513*, American Society for Testing and Materials, 1971.

[11] *Damage Tolerant Design Handbook*, MCIC-HB-01, Battelle Columbus Laboratories and AFML/AFFDL Wright-Patterson Air Force Base, 1972, Section 8.4.

[*12*] Hancock, G. G. and Johnson, H. H., *Transactions of the Metallurgical Society*, American Institute of Mining, Metallurgical, and Petroleum Engineers, Vol. 236, No. 4, 1966, pp. 513–516.
[*13*] Green, J. A. S. and Sedricks, A. J., *Metallurgical Transactions*, Vol. 2, No. 7, 1971, pp. 1807–1812.
[*14*] Paris, P. C. and Sih, G. C., *Fracture Toughness Testing and Its Applications, ASTM STP 381*, American Society for Testing and Materials, 1965, pp. 30–81.
[*15*] Shewmon, P. G., *Diffusion in Solids*, McGraw-Hill, New York, 1963, pp. 23–28.
[*16*] Cottrell, A. H., *Theoretical Structural Metallurgy*, St. Martins Press Inc., New York, 1955, pp. 188–190.
[*17*] Green, J. A. S. and Sedriks, A. J., *Corrosion*, Vol. 18, No. 6, June 1972, pp. 226–230.
[*18*] Powell, D. T. and Scully, J. C., *Corrosion*, National Association of Corrosion Engineers, Vol. 24, No. 6, 1968, pp. 151–158.
[*19*] Katz, Y., "Micromechanical Approach to Stress Corrosion Cracking in Titanium Alloys," Ph.D. thesis, University of California, Berkeley, 1969.
[*20*] Syschikov, V. I., *Metal Science and Heat Treatment*, May-June 1970, pp. 433–435.
[*21*] Wasilewski, R. J. and Kehl, G. L., *Metallurgia*, Vol. 1, No. 301, 1954, pp. 225–230.
[*22*] Fager, D. N. and Spurr, W. F., *Transactions Quarterly*, American Society for Metals, Vol. 61, No. 2, 1968, pp. 283–292.
[*23*] Curtis, R. E., Boyer, R. R., and Williams, J. C., *Transactions Quarterly*, American Society for Metals, Vol. 62, No. 2, 1969, pp. 457–469.

W. P. Gilbreath[1] *and M. J. Adamson*[1]

Aqueous Stress-Corrosion Cracking of High-Toughness D6AC Steel

---

REFERENCE: Gilbreath, W. P. and Adamson, M. J., "**Aqueous Stress-Corrosion Cracking of High-Toughness D6AC Steel,**" *Stress-Corrosion—New Approaches, ASTM STP 610,* American Society for Testing and Materials, 1976, pp. 176–187.

ABSTRACT: The crack growth behavior of D6AC steel as a function of stress intensity, stress and corrosion history, and test technique, under sustained load in filtered natural seawater, 3.3 percent sodium chloride solution, and distilled water, was investigated. Reported investigations of D6AC were considered in terms of the present study with emphasis on thermal treatment, specimen configuration, fracture toughness, crack-growth rates, initiation period, and threshold. Both threshold and growth kinetics were found to be relatively insensitive to these test parameters. The apparent incubation period was dependent on technique, both detection sensitivity and precracking stress intensity level.

KEY WORDS: stress corrosion, D6AC steel, high strength steel, toughness, seawater, failure, test method

D6AC steel has been extensively utilized in the aerospace industry because of its strength and good toughness coupled with its relatively low cost. Major components on the F111 aircraft and on the Titan IIIC missile have been fabricated from D6AC, and current plans call for use of the alloy for the solid rocket booster (SRB) cases to be used in the Space Shuttle program. In the Shuttle program, the plans are to recover the used cases from the ocean after launch and to return them to the launch site for cleaning, refurbishment, and reuse. This program calls for a 10 to 20 launch reuse capability for each of the cases. Because these applications require long-term exposure to various aqueous environments, a number of investigations [*1–6*][2] have examined the stress-corrosion susceptibility of D6AC steel under aqueous conditions.

---

[1] Research scientist and chemical engineering technician, respectively, Ames Research Center, National Aeronautics and Space Administration, Moffett Field, Calif. 94035.

[2] The italic numbers in brackets refer to the list of references appended to this paper.

It has been generally recognized within the last few years that in order to characterize the stress-corrosion susceptibility of a particular alloy adequately, it is necessary to determine at least the subcritical crack-growth kinetics and the threshold stress intensity for the initiation of subcritical growth (K_{Iscc}). Also important, although less often studied, is the incubation period before crack-growth commences. When possibilities of variable heat treatments might exist either in design selection or in service, the effect of this factor must be adequately simulated in susceptibility testing. To ensure useful design data, the effects of various test parameters must also be defined; of particular concern and controversy are selection of a proper test method (no ASTM standard method yet exists for stress-corrosion testing) and proper simulation of the service environment.

The purposes of the present paper are threefold: (1) to present new data on the stress-corrosion susceptibility of D6AC steel in one heat-treated condition that compares behavior in several aqueous environments; (2) to collate the stress-corrosion data of various investigators on D6AC to determine the influence of various test variables on the incubation characteristics, crack-growth kinetics, and threshold stress-intensity for crack initiation (K_{Iscc}); and (3) to discuss the implications of the experimental observations on the development of standard experimental procedures for examining the stress-corrosion susceptibility of high-strength steels.

Experimental

The D6AC steel used in this investigation was produced by Cameron (Heat 52663) and the analysis, supplied by the vendor was: 0.47C, 0.82Mn, 0.008P, 0.005S, 0.19Si, 1.14Cr, 0.60Ni, 1.01Mo, 0.10V, and the balance iron (all in weight percent).

Specimens were machined from D6AC plate in two orientations so that the crack-growth direction was either transverse (L-T) or longitudinal (T-L) to the rolling direction.

Two different specimen types were used for the stress-corrosion experiments. One type was the compact tension (CT) specimen specified for fracture toughness testing (ASTM Test for Plane-Strain Fracture Toughness of Metallic Materials (E 399)), and the other was a wedge-opening-loaded (WOL) specimen having the same basic dimensions of the CT specimen but modified to be loaded by an instrumented bolt in the manner suggested by Novak and Rolfe [*7*]. These two specimen configurations are shown in Figs. 1 and 2, respectively. In addition to being loaded by pins in a testing machine (the conventional procedure) a few of the standard CT specimens were loaded by a wedge which was forced into the machined notch. This will be described more completely in a later section.

Following machining, the specimens were commercially heat-treated to the following specifications [*8*]: the normalized material was vapor de-

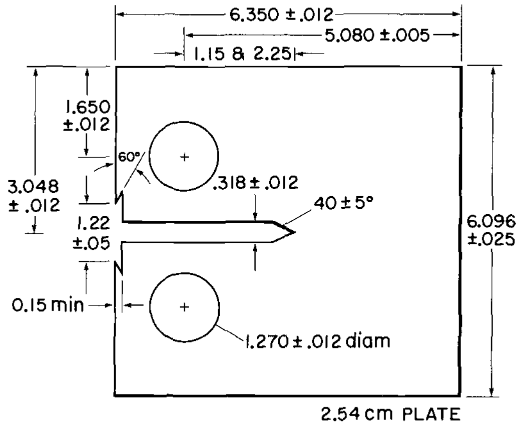

FIG. 1—*Specimen configuration for SCC study. Dimensions in centimeters.*

greased, preheated in air to 750 K (900°F); austenitized (while protected by neutral salt) at 1160 ± 10 K (1625°F) for 6000 s; then quenched in rapidly agitated salt (60 to 1 volume ratio) to 475 K (400°F) in less than 300 s and held for 1800 s. Following air cooling to 310 K (100°F), the specimens were stress relieved in agitated salt at 475 K for 3600 s, then washed in hot water to remove all salt residues before double tempering in air at 880 K (1125°F) for periods of 7000 s each. Finally, the specimens were grit blasted, and, in some cases, polished to make it easier to view the subsequent crack growth. The temperature was monitored and controlled during the heat treatment by thermocouples placed in drilled holes in two of the specimens. Tension specimens were simultaneously heat treated with the fracture specimens. Average mechanical properties produced by this heat treatment, as determined for three specimens, are listed in Table 1.

Following isopropanol and distilled water washing, the specimens were fatigued to produce a starter crack. They were cycled in a tension-tension mode for about 100 000 cycles to form a flaw from 4 to 10 mm in length. During fatiguing, the specimens were loaded to impose a maximum calculated stress intensity at the crack tip of roughly 45 $\mathrm{MNm}^{-2}\mathrm{m}^{1/2}$ (40 ksi $\mathrm{in.}^{1/2}$).[3] The initial crack length (a_0) was visually determined on both faces as the distance from the load line center to the fatigue crack tip. The specimens were then stored in a desiccator until used.

As stated earlier, the two primary indicators of a material's susceptibility to stress-corrosion cracking (SCC) are the rate of environment induced, subcritical crack growth, and the threshold stress-intensity value,

---

[3] In a few tests, somewhat different stress-intensities were used for fatiguing. The effects of these tests will be discussed in conjunction with Table 3.

TABLE 1—*Average mechanical properties of D6AC plate.*

Yield Strength		Ultimate Strength		Elongation, % in 2.5 cm	Reduction in Area, %	Hardness, R_c
MNm^{-2}	ksi	MNm^{-2}	ksi			
1400	204	1520	220	11	40	45

K_{Iscc}. The test method employed to obtain information on these two factors was to load the precracked specimens to some calculated initial stress-intensity level, and to maintain the crack mouth opening displacement, V, constant thereafter. If crack extension then occurred due to SSC, the load would decrease and cause a corresponding decrease in K. By measuring the rate of change in compliance at various K levels, it was possible to

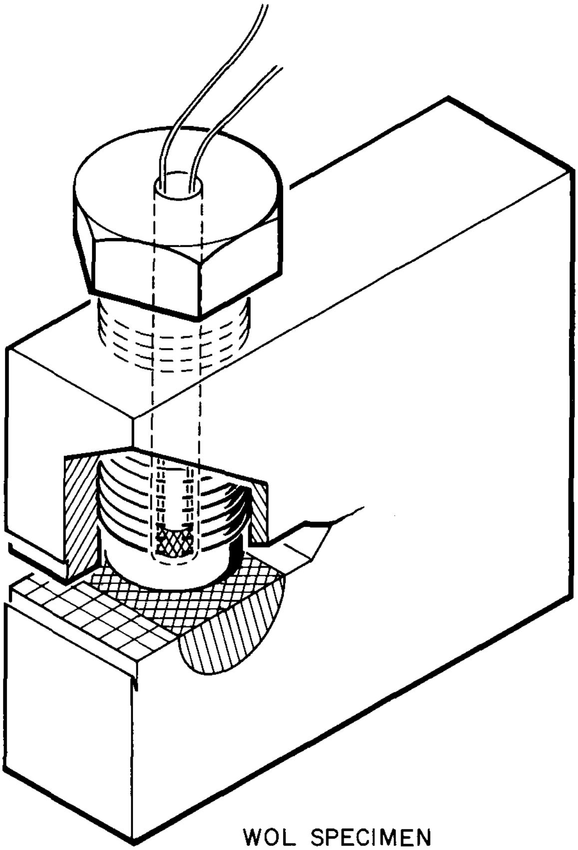

FIG. 2—*Modified wedge opening loaded specimen with instrumented bolt.*

calculate crack-growth rates as a function of K. Under these test conditions, the crack would be self arresting as K decreased below the threshold value, so that K_{Iscc} could be determined from the same test. The value of the initial stress intensity, K_{Io} , for these tests was selected to be less than the fracture toughness, K_{Ic}, but usually greater than the stress intensity used for fatigue precracking, K_{If}.

Stress intensity values for the CT specimens under various stress conditions were determined by measuring two of the three variables: a, crack length; P, load; or V. Several relations governing K as a function of these variables were used: ASTM Method E 399, boundary collocation method of Gross et al [9], and experimentally from compliance measurements on two of the D6AC specimens. The relations proved to be in substantial agreement over their applicable crack length limits. While the crack growth could be detected from either load changes or observations of crack length changes, the changes in load were the more sensitive indicator. Therefore, it was much easier to detect crack advance in those specimens loaded in a testing machine or with an instrumented bolt (for which load changes could be monitored) than it was for specimens loaded by a wedge. These latter specimens had the advantage of simplicity, however, in that their use did not tie up either a testing machine or other instrumentation for the relatively long test period required for these experiments. The instrumented bolts were designed for this program and represented a good compromise between the use of pin loading in a test machine and simple wedge loading. These bolts were calibrated easily to give reliable load values and provided essentially the same formation (albeit with somewhat less accuracy) as did the load cell of the testing machine.

Tests were conducted in three different aqueous environments: distilled water, 3.3 percent sodium chloride (NaCl) solution and filtered Pacific seawater (1.023 specific gravity). Both static and circulating environments were used. For those specimens under load in the test machine, the water was circulated continuously around the notched region of the specimen by attaching a cylindrical plastic envelope to each face of the specimen. Flow quantities were around 5 cm^3 of aqueous solution per minute, and the reservoir was renewed periodically.

For tests under static conditions with wedge- and bolt-loaded specimens, the specimens were simply immersed in the solution to above the notch tip. Specimens were either preloaded or loaded following immersion. For the bolt-loaded specimens, care was taken to avoid contact between the bolt and the water. For the wedge-loaded specimens, the wedge was made from identically heat-treated D6AC. The solutions used for the static tests usually were renewed daily. Crack extension at the specimen surface in the wedge-loaded specimens was determined optically by a cathetometer, and in the bolt-loaded specimens the average advance was determined by converting the strain output to load and solving the stress intensity relations just mentioned.

Results

Fracture Toughness Evaluation

Fracture toughness determinations were made on several CT specimens using the prescribed ASTM Method E 399 and gave the results shown in Table 2.

TABLE 2—*Fracture toughness of D6AC steel.*

Specimen	Crack Length, cm	Specimen Orientation	Fracture Toughness	
			$MNm^{-2}m^{1/2}$	ksi in.$^{1/2}$
1	1.57	L-T	124	113
2	2.77	L-T	117	106
3	1.63	T-L	121	110
4	3.91	T-L	119	108

Stress Corrosion

The data for crack growth as a function of stress intensity for the three environments—natural seawater, 3.3 percent NaCl solution, and distilled water—are shown in Fig. 3. Because of the expected exposure of the SRB material to natural seawater, most exposures were performed in this medium, and results from the other environments are related to these. Other results are described which relate to the effect of changing environments, incubation time, and load history.

The crack-growth rate versus stress-intensity results in Fig. 3 are characterized by three distinct growth rate regions. For all three environments below a stress intensity of about 20 $MNm^{-2}m^{1/2}$, crack-growth rates became vanishingly small (less than $10^{-10}ms^{-1}$ or 10 μin./h). For stress intensities above this (apparent) threshold up to 100 $MNm^{-2}m^{1/2}$, the growth rate was relatively insensitive to changes in stress intensity. In this region, the growth rates in both natural seawater and the 3.3 percent salt solution were equivalent and increased from about 5 to 20 $\times$ 10^{-9} ms^{-1} with increasing K. Although the data show considerable variance, the rates in distilled water appear to fall in the lower part of the scatterband. Additionally, an increase in rate was found in the case of several specimens in which seawater was substituted for distilled water after crack-growth initiation. Above 100 $MNm^{-2}m^{1/2}$ (as K_{Ic} was approached), the crack-growth rates in the three liquid environments became quite dependent on stress intensity and rapidly accelerated. In distilled water, the rate in this region appeared indistinguishable from the rates exhibited in the seawater solutions. Visual observation showed corrosion, as rusting, occurred a few hours after specimen immersion in both the saline and fresh water. Atomic absorption spectrographic analysis indicated that the corrosion rate in the

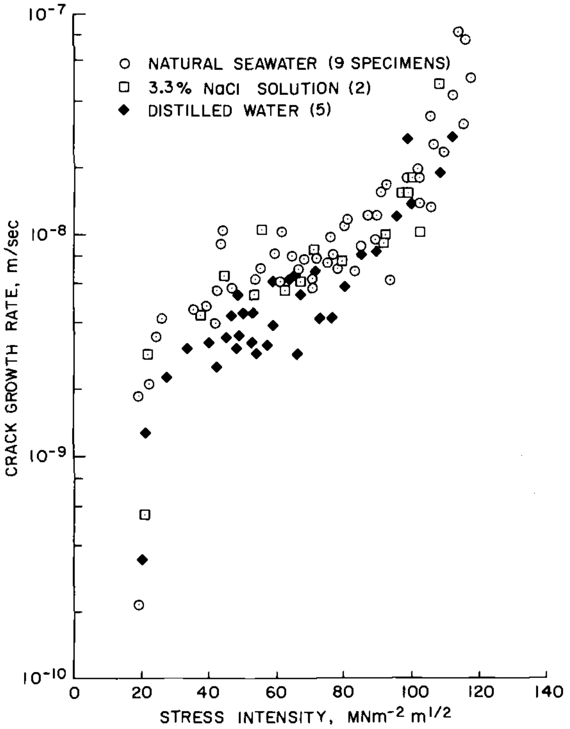

FIG. 3—*Crack growth rates as a function of stress intensity for D6AC steel in aqueous environments.*

saline environments was several times greater than in the fresh water during the initial stages. In all environments the major constituents were leached out in proportion to their fraction in the alloy, except for chromium whose rate was a factor of ten lower.

No differences in crack-growth rate were discernible, beyond experimental scatter for the three loading modes, for L-T versus T-L orientation or for the pre- versus solution loaded specimens.

Table 3 shows the elapsed time between loading in the environment and the first indication of crack growth as a function of imposed stress intensity for the specimens examined. Also tabulated are three other parameters: (1) the stress intensity ratio, defined as the imposed stress intensity divided by the maximum stress intensity during fatigue precracking (K_{Io}/K_{If}); (2) the particular aqueous environment; and (3) the loading method used. Several observations may be made from these data concerning the incubation period. These observations will be enumerated and discussed in a later section.

TABLE 3—*Crack-growth initiation periods in D6AC steel.*

Initial Stress Intensity, K_{Io}, $MNm^{-2}m^{1/2}$	K_{Io}/K_{If}	Environment	Loading Mode	Incubation Period, h
120	2.5	seawater	wedge	1
112	2.4	distilled water	wedge	20
112	2.4	seawater	bolt	0.2
110	1.8	3.3% NaCl	wedge	13
104	2.4	3.3% NaCl	wedge	5
88	1.9	seawater	testing machine	0.5
82	1.8	distilled water	testing machine	1
73	1.04	distilled water	testing machine	120
69	1.5	distilled water	wedge	180
66	1.26	distilled water	testing machine	1
62	1.36	seawater	bolt	5
55	0.92	distilled water	wedge	>340
48	0.95	seawater	bolt	>500
47	1.18	seawater	wedge	210
47	1.16	seawater	testing machine	4
41	0.93	seawater	testing machine	>105
38	1.20	seawater	bolt	13

Discussion

Although, individually, the prior investigations [*1–6*] of the stress-corrosion susceptibility of D6AC were quite limited, either in the experimental variables examined or in the number of specimens tested or both; taken as a whole some meaningful comparison with the present work may be made. Collectively, they examined the SCC behavior of D6AC from different sources and of differing compositions in fresh water and 3.5 percent salt solution. Differing thermal treatments were used giving relatively minor variations in material strength but producing toughness values from 50 to 120 $MNm^{-2}m^{1/2}$. Specimen configurations, cut from various sample orientations, were: contoured double cantilever beam, surface flawed, wedge opening loaded and compact tension, and were both standard and nonstandard for fracture toughness testing. A variety of loading modes, crack-growth detection methods and test techniques were employed.

A composite of the results from these studies along with the present results are presented in Fig. 4. The scatterbands shown on the curves representing the data of this investigation and the data of Feddersen et al [*4*], represent the maximum scatter observed in a fairly large number of tests. This scatter contains the effects of different specimen types, different environments (distilled, seawater), different loading methods, etc. The two data points representing the crack-growth rate data of Amateau and Kendall [*6*] were derived from corrosion-fatigue results. By comparing the

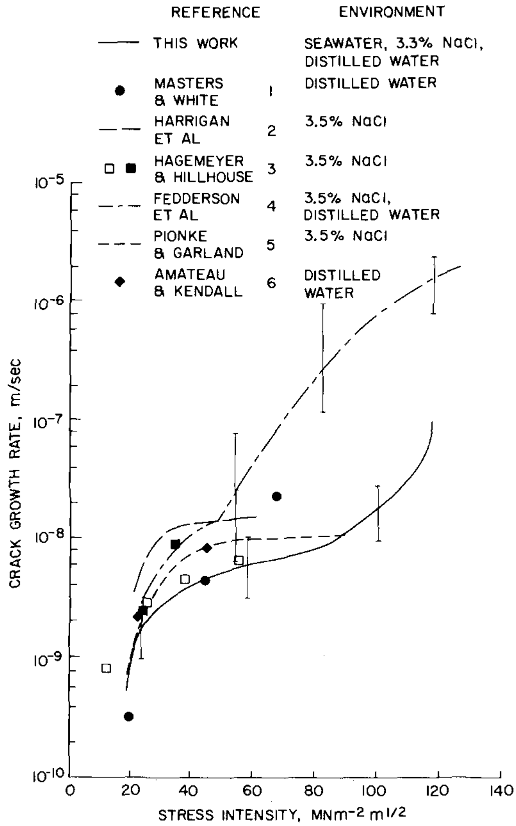

FIG. 4—*Reported crack growth rates of D6AC steel as a function of stress intensity.*

sustained-load and corrosion fatigue results of both Masters and White [*1*] and Feddersen et al [*4*], at equivalent environmental conditions, stress ratios, and cyclic frequencies, it was possible to develop a proportionality factor between corrosion-fatigue growth rates and sustained-load growth rates. This factor was used to calculate the two (equivalent) sustained-load data points shown for Amateau and Kendall. As can be seen in Fig. 4, considering the large number of material and test variables included, the kinetic data from all the investigations are in good correspondence. This is especially true of the threshold stress intensity for SCC, K_{Iscc}, for which almost all experiments give a value of 18 $MNm^{-2}m^{1/2}$. This correspondence could also be expected from the present results which showed (Fig. 3) an insensitivity of K_{Iscc} to test conditions. The agreement in kinetics is good at low-stress intensities (<50 $MNm^{-2}m^{1/2}$), where the average rates vary from one another by less than a factor of 3. At higher stress intensities, all data except those of Feddersen et al are still in good agreement, and the curves have the shape generally expected for environment-induced crack growth [*10*]. The reason for the divergence of the data of Feddersen et al at the higher stress-intensities cannot be explained at this time; however, it should be noted that these authors report crack-growth rate data for stress intensities which are greater than the reported fracture toughness values. In both the present investigation and in the study by Feddersen et al, it was noted that the average crack-growth rates in distilled water were slightly less than those in seawater. However, the differences in rate were less than the scatter of the results for crack growth in seawater alone. This observation along with the observation that there were no detectable differences in either K_{Iscc} values or growth rates in synthetic seawater (3.5 percent NaCl) as opposed to natural seawater suggests that precise simulation of the environment is not necessary in determining the sensitivity of D6AC to aqueous SSC. (This may not be true in other solutions containing additives or inhibitors, see Parrish et al, this publication.

The results shown in Table 3 indicate that an incubation period exists for the initiation of cracking of D6AC in aqueous environments. This observation has also been made by previous investigators [*1,3,4*] who have attempted to relate the length of this period to initial stress intensity, K_{Io}. The data of Table 3 show several interesting effects related to incubation. First, it is clear that the *apparent* incubation period is strongly dependent on the method of measuring crack growth. Visual inspection methods of crack extension on the exterior surfaces of the type employed for wedge-loaded specimens led to estimated times which were about 10 times longer than did the instrumented methods based on measuring compliance changes (machine loading and bolt loading) that gave information on the average advance of the crack front. Presumably, more sensitive instrumented methods such as acoustic emission would yield still shorter apparent incubation periods. Limited acoustic emission tests, although strictly qualitative, indicated some cracking did occur prior to detection of load drop off. Additionally, Hagemeyer and Hillhouse [*3*] who ran SCC tests on two specimens report a six day incubation period based on crack extension at the surface but "immediate" (less than one day, from the reported data) cracking by acoustic emission. Regardless of the detection method, the results do show the existence of either an initial no-growth or very slow growth rate period before a steady state growth rate is achieved. Second, the results show no effect of the type of environment (that is, distilled water versus seawater) on the length of the incubation period. This is consistent with a previous observation [*4*] and perhaps arises from the fact that both saline and fresh water were shown to readily attack D6AC. Finally, the length of the incubation period appears to depend strongly on the specimen history—namely, the ratio of the initial sustained stress intensity, K_{Io}, the maximum fatigue stress intensity, K_{If}. Actually, as can be seen from Fig. 5 (which plots only the test machine and instrumented bolt loading results—methods that were of comparable detection sensitivity)

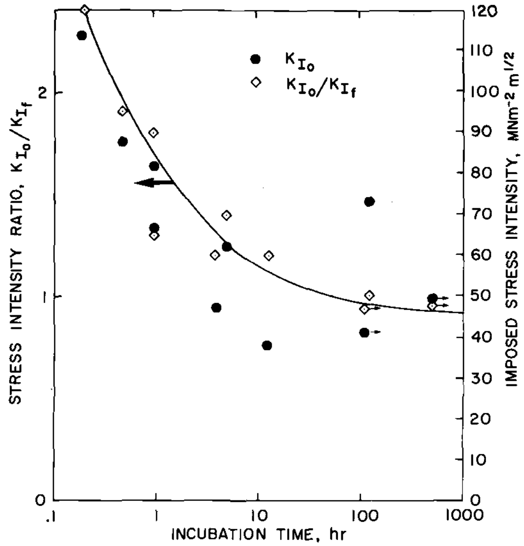

FIG. 5—*Incubation periods for crack-growth initiation of D6AC steel in aqueous environments as a function of stress intensity* (K_{Io} *and the ratio of stress intensity to fatigue stress intensity* (K_{Io}/K_{If})).

this parameter (K_{Io}/K_{If}) provides a better correlation with incubation time than does K_{Io}, raising some question as to whether incubation time is actually a direct function of K_{Io} as suggested by previous workers [*11*]. Although it might be argued from the data of Table 3 and Fig. 5 that there is a general trend toward longer incubation periods at lower stress intensities, two factors other than stress intensity probably play an important role in this lengthening. First, there is generally a decrease in stress ratio as stress intensity is decreased, thus leading to longer times. (For those cases where there is not a corresponding decrease in stress ratio, no trend is apparent.) Second, it is easier to detect crack growth at high rather than at low stress intensities because of the faster crack-growth rates at high stress intensities. Independent of these comments, the data of Table 3 and Fig. 5 do indicate that a cutoff in growth initiation occurs, at a stress ratio of about one, when the fatigue induced plastic zone is larger than that produced on initial loading. The entire question of incubation periods undoubtedly deserves further study before it can be completely resolved. The observations of the effects of stress history are particularly important to clarify, as proper understanding may lead to prestress treatments which might result in improved stress-corrosion resistance of particular D6AC components (including Shuttle SRB cases).

Conclusions

1. D6AC steel in a high-toughness condition exhibits substantially similar stress-corrosion behavior in natural seawater, 3.3 percent NaCl solu-

tion, and distilled water: a threshold at 20 $\text{MNm}^{-2}\text{m}^{1/2}$, a slow crack growth ($10^{-8}$ ms^{-1}) at moderate stress intensities, and sharply increasing rates as K_{Ic} (120 $\text{MNm}^{-2}\text{m}^{1/2}$) is approached.

2. The thermal treatment employed in the investigation produces the highest reported toughness for D6AC. Collation with results of earlier workers showed that differences in heat treatment, specimen orientation, roll direction, environment, specimen configuration, loading mode and pre- or solution loading have very little effect on threshold, flaw growth kinetics or the intrinsic incubation period for crack initiation.

3. In D6AC, stress history and corrosion history are basic to certain aspects of its stress-corrosion behavior. Incubation is closely related to prestressing or fatigue precracking effects.

4. Additionally, from this work certain implications may be drawn concerning the development of standard test procedures for examining the stress corrosion susceptibility of D6AC and possibly, other high-strength steels. Foremost, is the fact that the results proved to be rather insensitive to test conditions. Crack growth rates and threshold, within the limits examined, are virtually independent of specimen configuration (loading procedure), test technique, and aqueous environment. The coincidence of the synthetic and actual seawater results should considerably reduce the complexity of simulation necessary for viable design operation. In contrast, incubation was dependent on test technique in at least two respects. First, the stress-intensity level during test initiation must be somewhat higher than the fatigue precrack level to repress effects that arise through fatigue damage. And second, the measured incubation time is related closely to the sensitivity of the crack-growth detection technique. Since this initial phase probably combines no growth with variable low growth rates, it may be desirable to employ an extrapolation from steady-state rate method to derive relatively reproducible incubation values. Overall, if other alloy systems were to behave in a manner similar to that observed with D6AC, it might be possible to allow considerable variation of test procedure for assessing stress corrosion effects.

5. Because D6AC corrodes badly on exposure, protective agents, either coatings or galvanic means, usually are employed with it in service. Since the present (and past stress corrosion) studies consider only the bare alloy, the effectiveness of these agents in inhibiting SSC under service conditions should be examined.

References

[*1*] Masters, J. N. and White, J. L., Technical Report AFML-TR-70-310, The Boeing Company, Seattle, Wash., 1971.

[*2*] Harrigan, W. C., Dull, D. L., and Raymond, L. in *Progress in Flaw Growth and Fracture Toughness Testing, ASTM STP 536,* American Society for Testing and Materials, 1972, pp. 171–181.

[*3*] Hagemeyer, J. W. and Hillhouse, L., Research Report ERR-FW-1114, General Dynamics, Fort Worth, Tex., Dec. 1970.

[*4*] Feddersen, C. E., Moon, D. P., and Hyler, W. S., MCIC-72-04, National Technical Information Service, U. S. Department of Commerce, Jan. 1972.
[*5*] Pionke, L. J. and Garland, K. C., Contractor Report CR 120160, National Aeronautics and Space Administration, Washington, D. C., Dec. 1973.
[*6*] Amateau, M. F. and Kendall, E. G., Air Force Report No. SAMSO-TR-71-186, The Aerospace Corporation, Los Angeles, Calif., Sept. 1971.
[*7*] Novak, S. R. and Rolfe, S. T., *Journal of Materials,* 1969, Vol. 4, pp. 701–728.
[*8*] Jacobs, Samuel, United Technology Corporation, Sunnyvale, Calif., private communication.
[*9*] Gross, B., Roberts, E., Jr., and Srawley, J. E., *International Journal of Fracture,* 1966, Vol. 4, pp. 267–276.
[*10*] Williams, D. P., *International Jounrnal of Fracture,* 1973, Vol. 9, pp. 63–74.
[*11*] Dull, D. L. and Raymond, L., *Metallurgical Transactions,* 1972, Vol. 3, pp. 2943–2947.

P. A. Parrish,[1] *C. M. Chen,*[2] *and E. D. Verink, Jr.*[2]

Retardation of Crack Propagation for D6AC High-Strength, Low-Alloy Steel in Aqueous Media by Addition of Oxidizing Inhibitors

---

REFERENCE: Parrish, P. A., Chen, C. M., and Verink, E. D., Jr., **"Retardation of Crack Propagation for D6AC High-Strength, Low-Alloy Steel in Aqueous Media by Addition of Oxidizing Inhibitors,"** *Stress Corrosion—New Approaches, ASTM STP 610,* American Society for Testing and Materials, 1976, pp. 189–198.

ABSTRACT: High-strength, low-alloy, martensitic steels are known to be subject to hydrogen embrittlement. This was demonstrated by measurements of crack-tip pH and localized hydrogen content at the fracture surface, and also by observation of electrochemical behavior of simulated "crevices." The effect of certain oxidizing inhibitors was used to elucidate the mechanisms of stress-corrosion cracking (SCC) and to retard crack growth.

Hydrazine additions reduced the crack growth rate by an order of magnitude for D6AC in aqueous solutions. A 2 percent addition of hyrazine to solutions either with or without chlorides increased K_{Iscc} from 12 (without inhibitor) to 25 ksi$\sqrt{\text{in.}}$ (with inhibitor). The critical flaw size varies as the square of K_{Iscc}, so doubling K_{Iscc} is the equivalent of increasing the size of a critical flaw fourfold, which in turn makes more likely its detection nondestructively. Localized hydrogen analyses at various locations on the fracture surface of a D6AC specimen pulled to failure after exposure in hydrazine-inhibited solution (with or without chlorides) showed no hydrogen enrichment of the fracture surface (as compared to the bulk specimen remote from the fracture), hence no hydrogen embrittlement.

While sodium dichromate additions also increased K_{Iscc} and reduced the crack-growth rate in chloride-free solutions, they were not effective in 0.1 N sodium chloride solutions.

Special electrochemical measurements (with and without chlorides) showed that in the presence of the hydrazine inhibitor, the electrode potential of D6AC at the tip of an advancing corrosion fatigue crack was above (more noble than) the potential of the equilibrium hydrogen electrode. By contrast, the electrode potential at the apex of an advancing corrosion fatigue crack in D6AC exposed in dichromate-inhibited, chloride-containing solution was below (more active than) the potential of the equilibrium hydrogen electrode. Thus dichromate additions did not prevent hydrogen entry into D6AC in chloride solutions.

[1] Metallurgist, Metallurgy and Materials Science Division, U. S. Army Research Office, Department of the Army, Research Triangle Park, N. C. 27709.

[2] Visiting assistant professor; and, chairman and professor, Materials Science and Engineering, University of Florida, Gainesville, Fla. 32601.

KEY WORDS: stress corrosion, hydrogen embrittlement, crack propagation, inhibitors, fracture properties, alloy steels

Oxidizing inhibitors nitrite and chromate can be utilized to retard crack growth in high-strength, low-alloy martensitic steels in aqueous solution. Artificial crevice cell and crack-tip pH measurements show that conditions favorable for hydrogen embrittlement of the steel exist in propagating cracks. By utilizing a unique ultrasensitive hydrogen detector, localized hydrogen content measurements of fracture surfaces of the alloy which failed under tensile load in aqueous solution were carried out which showed that hydrogen was absorbed at the propagating crack tip, but, for fracture surfaces where an oxidizing inhibitor was added to the solution, no hydrogen absorption occurred at the crack tip.

Experimental

Crevice Corrosion Characteristics of D6AC

Crevice corrosion characteristics of D6AC in 0.1 *M* sodium chloride (NaCl) solution were studied as a function of bulk solution pH in a stirred, aerated solution at a temperature of 25°C. The chemical composition of D6AC is 0.45C, 1.15Cr, 0.55Ni, 1.0Mo, 0.8Mn, 0.25Si, 0.05V, and balance iron. The alloy was heat treated by the following sequence: austenizing at 1700 ± 25°F, Aus-Bay quenching, quenching into 140 ± 10°F oil, snap tempering at 375°F, and double tempering at 1025°F for 2 h. The ultimate tensile strength was in the range of 230 to 235 ksi, with K_{Ic} ranging from 90 to 95 ksi $\sqrt{\text{in.}}$ The artificial crevice cell is shown in Fig. 1 [*1*].[3] The crevice solution is separated from the bulk solution by a 4 μm porosity, fritted-glass disk. The exposed area of the bulk specimen was 16.0 cm^2 and that of the crevice specimen was 1.0 cm^2. pH and potential were measured in the crevice compartment.

K_{Iscc} *and Crack-Growth Rate Studies*

Compact tension specimens of D6AC were used to determine the K_{Iscc} and crack-growth rates in various environments. The specimen geometry satisfied ASTM requirements for plane-strain condition (ASTM Test for Plane-Strain Fracture Toughness of Metallic Materials (E 399-70)).

The specimens were stressed laterally to facilitate the immersion of the specimens into a cell containing the solution required for the test by a lateral stressing frame incorporated into a creep machine. The crack length

---

[3] The italic numbers in brackets refer to the list of references appended to this paper.

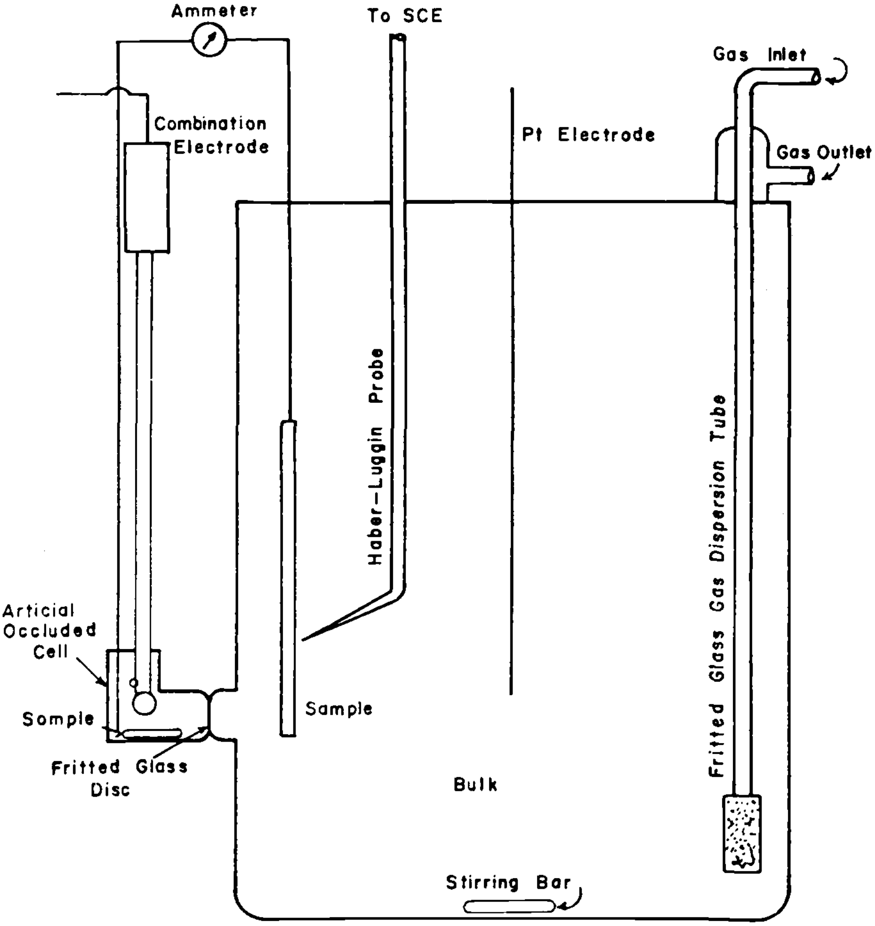

FIG. 1—*Schematic af artificial crevice cell.*

was measured by a double cantilever displacement clip gage, with strain gages cemented to the tension and compression surfaces of each beam to form a Wheatsone bridge. The crack length, *a*, was recorded as a function of time for the load, *P*. The stress-intensity factor, K_I, and the crack growth rate, da/dt, were determined by a computer.

The determination of K_{Iscc} and da/dt for D6AC in this manner gives a quantitative means of measuring the susceptibility to stress-corrosion cracking (SCC) of the alloy in various aqueous environments, and can indicate the effectiveness of the chemical addition to the bulk solution in preventing or retarding crack propagation at loads less than the critical stress intensity K_{Ic}.

Determination of pH Within a Propagating Crack

The pH at the tip of a propagating crack was measured by the indicator method of Brown et al [*2*], utilizing the same group of standard indicators, and freezing the solution contained at the crack tip by immersing the specimen in liquid nitrogen. The specimen was then broken in air by overloading, and indicator applied to the frozen fracture surface gave the determination of pH at the crack tip as thawing of the fracture surface yielded the liquid present at the crack tip.

Localized Hydrogen Concentration Measurements in Fractured Specimens

The localized concentrations of hydrogen as a function of position across the fracture surface on specimens which failed in uninhibited and in inhibited solution were compared by the unique ultrasensitive hydrogen detector system developed by Das [*3*], which works on the principle of selective permeation of hydrogen through a semipermeable palladium membrane. This membrane is attached to a continuously evacuated vacuum chamber. The specimen is heated rapidly in an induction furnace to its melting point and held at this temperature until complete extraction of hydrogen is accomplished in an argon gas atmosphere which also serves as the carrier gas; this gas directs the evolved gases past the semipermeable membrane. Only hydrogen can permeate the membrane and pass into the high vacuum chamber where the increase in pressure provides the quantitative measurement of hydrogen.

Results

Artificial Crevice Cell and Crack Tip pH Measurements

The results of artificial crevice cell (Table 1), and pH measurements within propagating cracks (Table 2) agreed with Brown et al [*4*]. In Fig. 2, specimens exposed to initial bulk pH ranging from two to eight (black circles) were superimposed on the potentiodynamically determined experimental pH potential diagram for D6AC in 0.1 *M* Cl^- solution [*5*]. For each condition of initial bulk pH and potential, the steady-state crevice conditions (black squares) were favorable for hydrogen evolution and subsequent embrittlement of the alloy.

The pH measurements at the tips of actual propagating cracks in D6AC, exposed to solutions of pH = 5.9 (distilled water) and 8.5 (0.1 *M* NaCl + 0.1 *M* sodium bicarbonate ($NaHCO_3$) buffer) agreed with the artificial crevice results. The crack tip was acidified such that the pH's measured in each case were 4.8 and 4.5, respectively.

TABLE 1—*pH-potential data, D6AC in artificial crevice cell.*

Test No.	Solution	Bulk Potential, SCE[a]	Bulk, pH	Crevice Potential, SCE[a]	Crevice, pH
1	0.01 *M* HCl 0.09 *M* NaCl	−0.536V	2.1	−0.597	2.7
2	0.09 *M* NaCl	−0.556	2.1	−0.603	2.9
3	0.001 *M* HCl 0.1 *M* NaCl	−0.415	5.5	−0.525	4.9
4	0.1 *M* NaCl	−0.375	5.5	−0.515	4.7
5	0.1 *M* NaCl	−0.270	5.5	−0.510	4.3
6	0.1 *M* NaCl 0.045 *M* NaOH 0.045 *M* $KHC_8H_4O_4$	−0.445	6.1	−0.560	3.7
7	0.045 *M* $KHC_8H_4O_4$	−0.300	6.1	−0.505	4.0
8	0.1 *M* NaCl	−0.430	8.1	−0.560	5.0
9	0.1 *M* NaCl	−0.560	8.1	−0.578	4.9
10	0.1 *M* NaCl 0.63 *M* N_2H_4	−0.142	9.9	−0.182	9.6
11	0.64 *M* N_2H_4	−0.153	9.9	−0.175	9.5
12	0.1 *M* $Na_2Cr_2O_7$	−0.100	4.0	+0.003	4.3
13	0.1 *M* $Na_2Cr_2O_7$	−0.108	4.0	+0.012	4.4
14	0.1 *M* $Na_2Cr_2O_7$ 0.1 *M* NaCl	−0.050	4.3	−0.150	4.0
15	0.1 *M* NaCl	−0.040	4.3	−0.138	4.0

[a] SCE = saturated calomel electrode.

In solutions containing oxidizing inhibitors, no significant shift of crevice conditions occurred (that is, no acidification). The measured electrode potentials were more noble than the hydrogen evolution potential. The pH measurements at the tip of a propagating crack exposed to solutions containing the oxidizing inhibitor, hydrazine, illustrate this behavior. That hydrazine, commonly used as a deoxidizer, can also act as an oxidizing inhibitor has been shown by Fontana [*6*].

K_{Iscc} *and Crack Growth Rate Studies*

K_{Iscc} and crack growth rate tests for D6AC were carried out in the following solutions:

(*a*) Distilled water.
(*b*) 0.1 *M* NaCl + 0.1 *M* $NaHCO_3$ buffer; pH = 8.5.
(*c*) 0.1 *M* NaCl + 0.1 *M* $NaHCO_3$ + 0.63 *M* hydrazine (N_2H_4).
(*d*) Crack growth in 0.1 *M* sodium dichromate ($Na_2Cr_2O_7$).

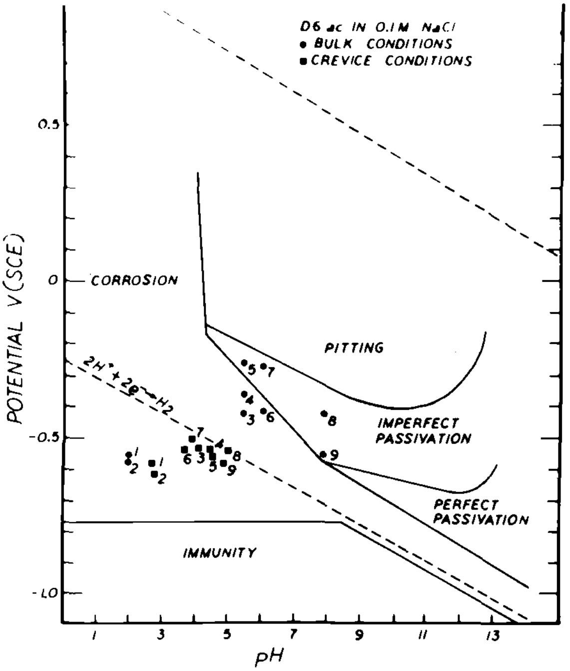

FIG. 2—*Artificial crevice cell results, pH 2.1 to 8.1.*

The results are shown in Fig. 3. The K_{Iscc} improved remarkably in 0.1 *M* $Na_2Cr_2O_7$ solution to 32 ksi $\sqrt{in.}$ The Region II (plateau region–K_I independent) was reduced to about 8×10^{-6} in./min. Thus, in chloride-free solutions chromate can be beneficial if present at this concentration.

An experiment was devised to test the ability of chromates to arrest a propagating crack in D6AC. Crack growth was initiated in chloride-free distilled water and allowed to reach steady-state crack growth (Region II). Then, by removing some of the water and replacing it with $Na_2Cr_2O_7$ so that the solution finally consisted of 0.1 *M* $Na_2Cr_2O_7$, the effect of inhibitor addition on crack growth was seen. As shown in Fig. 4, the crack-growth rate, *da/dt,* decreased and approached zero immediately after the $Na_2Cr_2O_7$ was added. After a waiting period of 48 h (during which time *da/dt* remained too small to measure), the specimen was incrementally loaded and the crack started to grow once again at $K_I = 32$ ksi $\sqrt{in.}$, identical to the value for K_{Iscc} in 0.1 *M* $Na_2Cr_2O_7$ solution (compare with Fig. 3).

Crack Growth in 0.1 M *Nacl + 0.1* M *$Na_2Cr_2O_7$*

In the presence of 0.1 *M* NaCl, the effectiveness of 0.1 *M* $Na_2Cr_2O_7$ for crack prevention was diminished. The K_{Iscc} was reduced to 19 ksi $\sqrt{in.}$, and the crack growth in Region II increased to 3×10^{-5} in./min.

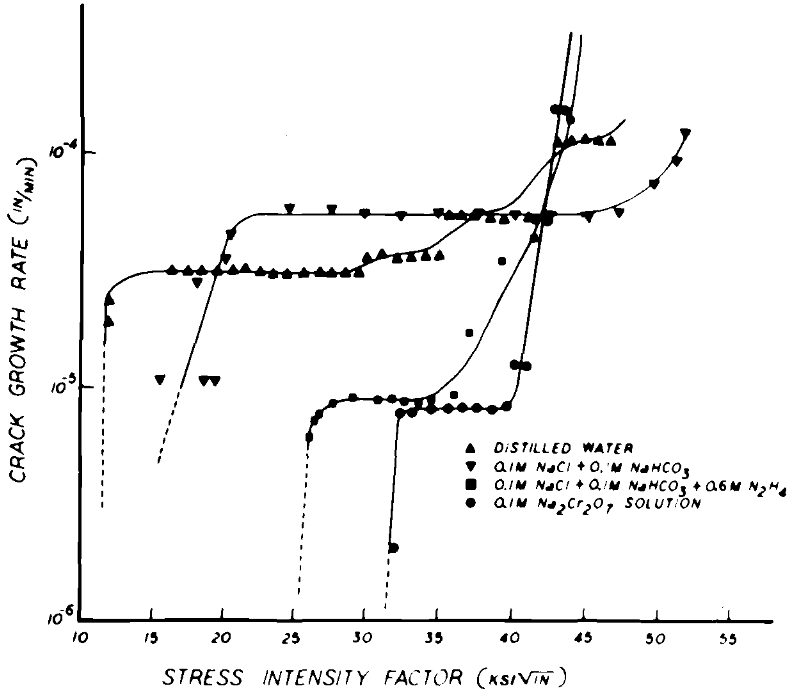

FIG. 3—*Effect of oxidizing inhibitors N_2H_4 and $Na_2Cr_2O_7$ on crack growth.*

Hydrogen Analysis of Localized Areas of Fracture Surfaces

The D6AC compact specimens were fractured in distilled water and buffered solutions of 0.1 *M* NaCl with and without inhibitor additions. Figures 5*a* and *b* show the results of local hydrogen analysis from tests conducted in distilled water and in hydrazine-inhibited distilled water, respectively. Specimens were stored at liquid nitrogen temperature until hydrogen analysis could be made. Referring to Fig. 5*a*, in the area of the fatigue-precrack zone which was exposed to distilled water environment for 8 h before crack growth began, the hydrogen content was the highest (23.88 ppm). During Region II crack growth, in which the crack propagated at a faster rate, the hydrogen content showed a considerable gradient. In the shear-lip area, which underwent fracture due to specimen overload, the hydrogen content was 8.25 ppm. At the end of fracture, and in the region of the machined notch (where no SCC occurred), the hydrogen level was 1.45 to 3.36 ppm, which should be taken as the "baseline" hydrogen content of the specimen before exposure.

For the specimen fractured in distilled water containing 0.63 *M* N_2H_4, Fig. 5*b*, the influence of N_2H_4 on the amount of distribution of hydrogen is shown dramatically. Nowhere on the specimen surface is the hydrogen content above the baseline range.

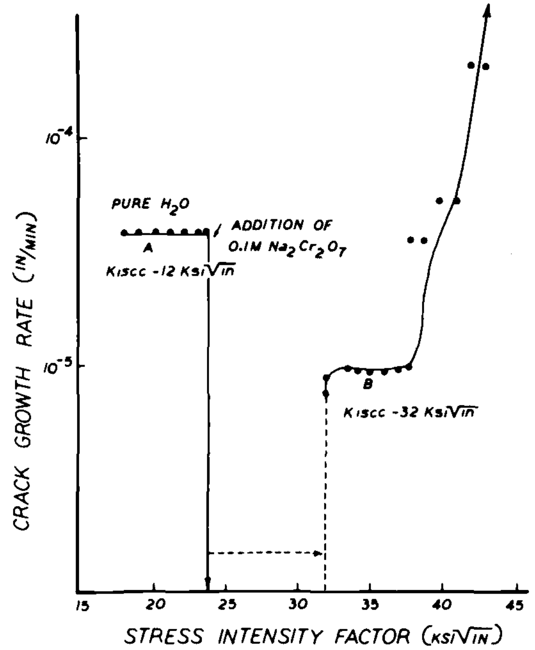

FIG. 4—*Effect of oxidizing inhibitor addition to aqueous solution on active crack growth.*

Discussion

Without use of an oxidizing inhibitor, K_{Iscc} and cracking rate for D6AC (in distilled water) in Region II were 12 to 15 ksi $\sqrt{in.}$ and 4 to 7 × 10^{-5} in./min, respectively. The pH and potential at the crack tip shifts to conditions favorable for hydrogen evolution under all conditions of aqueous exposure tested. Localized hydrogen analyses on the fracture surfaces indicated that failure was by hydrogen embrittlement. However, when an oxidizing inhibitor such as N_2H_4 was added to the solution, K_{Iscc} increased and crack growth rate decreased to 25 ksi $\sqrt{in.}$ and 7 × 10^{-6} in./min, respectively. In this case, the pH and potential at the crack tip remained almost the same as in the bulk solutions and were, therefore, unfavorable for hydrogen evolution. The absence of hydrogen enrichment (as shown by localized hydrogen analysis) explains the freedom from hydrogen embrittlement. $Na_2Cr_2O_7$ is an effective inhibitor in chloride free solutions but not in the presence of chlorides [7]. The strong oxidizing capability of $Na_2Cr_2O_7$ oxidizes the D6AC surface to ferric oxide (Fe_2O_3) in the absence of chlorides [*8*]. In the presence of chloride ion in the solution, the passive film undergoes attack at the crack apex. This induces a reduced pH and electrode potential at the crack tip. As the data indicate in Table 1,

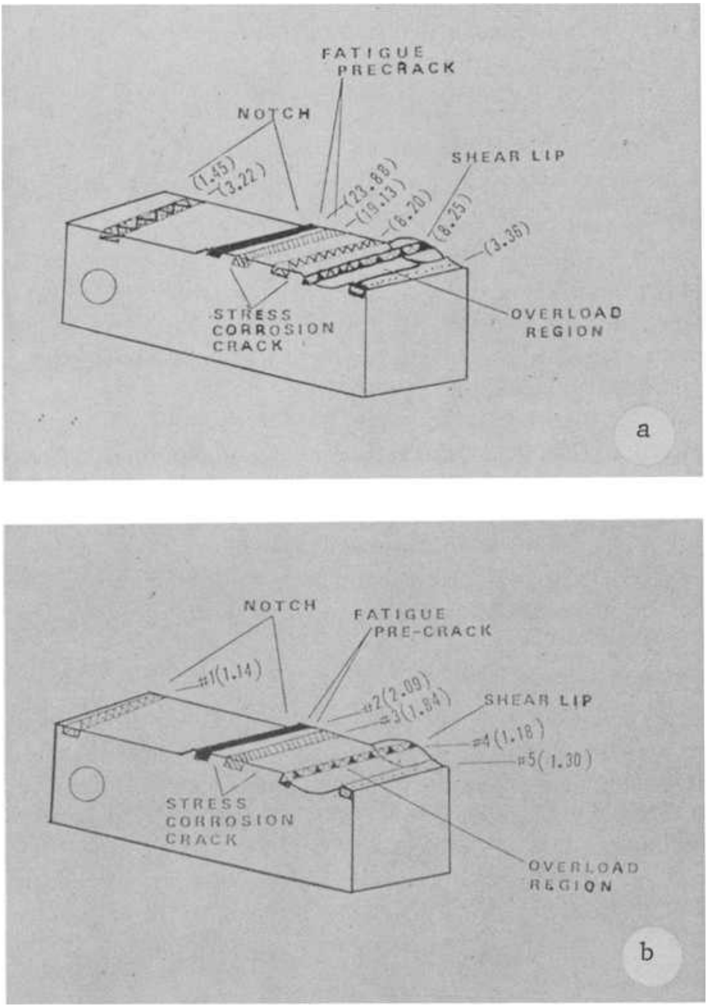

FIG. 5—(a) *Localized hydrogen analysis: D6AC fractured in distilled water and frozen in liquid* N_2. (b) *Localized hydrogen analysis: D6AC fractured in 0.1* M *NaCl + 0.1* M $NaHCO_3$ *+ 0.6* M N_2H_4 *inhibitor.*

the electrochemical potential shifts to below hydrogen evolution line, thereby causing hydrogen embrittlement.

The addition of N_2H_4 to alkaline solution (in this investigation, to 0.1 *M* NaCl + 0.1 *M* $NaHCO_3$, pH = 8.5) yields the reaction [*8*]

$$N_2H_4 + OH^- = NH_3 + \tfrac{1}{2}N_2 + H_2O + \bar{e}\ E_0 = -2.42V_{SHE}$$

Nitrite ion was observed in the bulk and crevice compartments of the artificial crevice cell, in agreement with Latimer [*9*], who reported that ammonium hydroxide is readily oxidized on various metal anodes to nitrite. The overall reaction would be

$$NH_4OH + 7OH^- = NO_2^- + 6H_2O + 6\bar{e}.$$

It thus appears that N_2H_4 inhibits crack growth by the formation of nitrite, which is a strong oxidizer. The passive γ-Fe_2O_3 film is formed by the reaction

$$Fe + NaNO_2 + H_2O \rightarrow \gamma\text{-}Fe_2O_3 + NaOH + NH_3$$

Preliminary crack growth measurements for D6AC in 0.1 *M* $NaNO_2$ aqueous solution show good effectiveness of nitrite in retarding crack growth with K_{Iscc} raised to 45 ksi $\sqrt{\text{in.}}$ and Region II crack growth velocity measured at 10^{-6} in./min.

It should be noted that, while the K_{Iscc} was improved remarkably by these oxidizing inhibitors, failure of crack-growth specimens did occur at stress-intensity levels less than K_{Ic}. This could indicate that the passive layer formed at the crack tip is imperfect in its protection of the crack tip. The reduced effectiveness of dichromate with chloride present in the solution may be the extreme case of the imperfection of the passive layer. However, this explanation should be taken as speculation at this point.

Conclusions

Oxidizing inhibitors may be used to retard crack propagation for high-strength, low-alloy steels. For D6AC the use of such inhibitors gives promise of being able to avoid hydrogen embrittlement. The critical stress-intensity factor K_{Iscc}, apparently also may be manipulated by use of oxidizing inhibitors. This is of great practical importance since the critical flow size varies directly as the square of K_{Iscc}, and any procedure which leads to increasing the critical flaw size into a range of easy detection by nondestructive methods will be of immense engineering value.

References

[1] Efird, K. D., M.S. thesis, University of Florida, Gainesville, Fla., 1970.
[2] Brown, B. F., Fuji, C. T., and Dahlberg, E. P., *Journal of the Electrochemical Society* Vol. 116, 1969, p. 218.
[3] Das, K. B., Air Force Materials Laboratory TR-73-244, Wright-Patterson Air Force Base, Ohio, 1973.
[4] Smith, J. A., Peterson, M. H., and Brown, B. F., *Corrosion,* Vol. 26, No. 12, 1970.
[5] Verink, E. D., Jr., and Johnson, J. M., Annual Report, Air Force Materials Laboratory Contract F33(615)-73-C-5007.
[6] Fontana, M. G., Air Force Materials Laboratory TR-72-102, Wright-Patterson Air Force Base, Ohio, Aug. 1972.
[7] Evans, U. R., *The Corrosion and Oxidation of Metals,* Arnold, London, 1960.
[8] Jolly, W. L., *The Inorganic Chemistry of Nitrogen,* W. A. Benjamin, Inc., Menlo Park, Calif., 1964, p. 60.
[9] Latimer, W. M., *The Oxidation States of the Elements and Their Potentials in Aqueous Solutions,* second edition, Prentice-Hall, Edgewood Cliffs, N. J., 1952, p. 101.

G. M. Waid[1] *and R. T. Ault*[1]

Effects of Composition on Stress-Corrosion Cracking Resistance of Ultrahigh-Strength Steels

---

REFERENCE: Waid, G. M. and Ault, R. T., "**Effects of Composition on Stress-Corrosion Cracking Resistance of Ultrahigh-Strength Steels,**" *Stress Corrosion—New Approaches, ASTM STP 610,* 1976, pp. 199–212.

ABSTRACT: An investigation was made to evaluate the effects of various alloying and impurity elements on the stress-corrosion cracking (SCC) resistance of ultrahigh-strength steels. The influence of phosphorus and sulfur on the SCC threshold parameter, K_{Iscc}, of HP 9-4-45 steel heat treated to both bainitic and martensitic microstructures was measured. The bainitic microstructure was consistently more resistant to SCC than was the martensitic structure, and neither phosphorus nor sulfur had a pronounced effect on the K_{Iscc} value. However, impurities, especially sulfur, had an adverse effect on fracture toughness. A systematic examination of silicon, chromium, and molybdenum compositional effects on the SCC behavior of 0.40C low-alloy martensitic steels also was included in this study. SCC as measured by the K_{Iscc} parameter of these low-alloy steels heat treated to strength levels in the neighborhood of 300 000 psi was, essentially, independent of composition; however, increasing amounts of silicon and possibly chromium decreased the crack-growth rates. The fracture-toughness levels of these alloy steels, however, were highly dependent on compositional variations.

KEY WORDS: stress corrosion, crack propagation, toughness, fracture strength, microstructure, compositions, ultrahigh strength steels

It was the purpose of this investigation to determine the influence of various alloying and impurity elements on the stress-corrosion cracking (SCC) resistance of martensitic and bainitic ultrahigh-strength steels. Other investigators [*1*][2] have studied the influence of impurity elements on the SCC resistance of 18Ni (300) grade maraging steels. Proctor and Paxton [*2*] investigated the effect of prior-austenite grain size on the SSC susceptibility of AISI 4340 steel, and determined that grain refinement

---

[1] Research metallurgist and section chief, respectively, Bar, Plate, and Tubular Products Section, Metallurgy Division, Research Center, Republic Steel Corporation, Cleveland, Ohio 44131.

[2] The italic numbers in brackets refer to the list of references appended to this paper.

had little influence on the K_{Iscc} level, but that crack-growth rates were decreased as prior-austenite grain size decreased. It has also been found that crack-growth rates decrease with increased silicon contents [*3*]. May and Priest [*4*] determined the effects of silicon, phosphorus, and sulfur on the fracture toughness and SCC resistance of a high-strength martensitic steel; however, their K_{Iscc} levels were determined after runout times of only 25 h, which is insufficient time for valid K_{Iscc} determinations. Work by Sandoz [*5*] determined the influence of alloying elements on the SCC resistance of 4340 type steels at tensile strength levels of 190 to 250 ksi.

The work presented in this paper demonstrates the influence of alloying elements on the SCC resistance and fracture-toughness behavior of medium carbon martensitic steels at tensile strength levels in excess of 300 ksi, and the effect of impurity elements on the fracture-toughness and SCC behavior or both martensitic and bainitic microstructures in a 9Ni-4Co steel.

Materials

To investigate the effects of varying levels of phosphorus and sulfur on the SCC resistance of 9Ni-4Co-0.45C steel, six 35-lb (15.9-kg) vacuum-induction melted heats were made. The compositions of these heats are shown in Table 1. To study the effects of silicon, chromium, and molybdenum on the SCC resistance of 0.40C martensitic, ultrahigh-strength steels, fifteen 50-lb (22.7-kg) vacuum-induction melted heats with varying amounts of silicon, chromium, and molybdenum were made. These compositions also are listed in Table 1. The fifteen low-alloy martensitic steels were designed statistically so that the compositional dependence of the elements silicon, chromium, and molybdenum on strength, toughness, and SCC could be evaluated. Both the 35-lb (15.9-kg) and 50-lb (22.7-kg) VIM heats were forged and rolled to ½-in. (12.7-mm) thick plates, from which standard 0.252-in. (6.40-mm) diameter tensile, Charpy V-notch, fracture toughness, and stress-corrosion coupons were obtained. All tensile and Charpy V-notch specimens were of longitudinal (L-T) orientation with respect to the rolling direction of the plate. The fracture toughness and stress-corrosion specimens were of the longitudinal (L-T) orientation.

The 9Ni-4Co-0.45C steels were heat treated to a bainitic structure as follows: normalize 1625°F (885°C), 1 h, air cool; austenitize 1475°F (802°C), ½ h, transfer to salt bath at 465°F (241°C) for 6 h, air cool; and a martensitic structure with the following heat treatment: normalize 1625°F (885°C), 1 h, air cool; austenitize 1475°F (802°C), ½ h, oil quench; refrigerate −110°F (−79°C), 2 h, air warm; temper 500°F (260°C) for 2 + 2 h, air cool. The low-alloy martensite steels were heat treated as follows: normalize 1750°F (954°C), 1 h, air cool; austenitize 1650°F (899°C), 1 h, oil quench; refrigerate −110°F (−79°C), 1 h, air warm; temper 600°F (316°C) for 2 + 2 h, air cool.

TABLE 1—*Chemical compositions of steels investigated.*

Heat No.	C	Mn	Si	P	S	Ni	Cr	Mo	V	Co
					9Ni-4Co Steels					
V723	0.41	0.27	0.10	0.003	0.002	8.55	0.28	0.33	0.095	4.36
V724	0.42	0.23	0.09	0.013	0.020	8.41	0.36	0.40	0.090	4.30
V725	0.44	0.27	0.05	0.022	0.025	8.34	0.30	0.34	0.084	4.30
V726	0.42	0.27	0.09	0.004	0.025	8.30	0.30	0.33	0.087	4.22
V727	0.42	0.25	0.08	0.020	0.009	8.20	0.28	0.40	0.090	4.17
V746	0.44	0.27	0.06	0.004	0.010	7.97	0.31	0.32	0.070	4.20
					Low-Alloy Martensitic Steels					
R 1	0.39	0.36	1.82	0.002	0.005	2.00	1.00	0.43	0.22	
R 2	0.41	0.36	1.78	0.002	0.005	2.00	1.01	0.84	0.22	
R 3	0.42	0.37	1.81	0.002	0.005	2.00	1.77	0.43	0.22	
R 4	0.41	0.37	1.80	0.002	0.005	2.00	1.58	0.78	0.22	
R 5	0.42	0.38	2.50	0.002	0.005	2.15	1.05	0.45	0.23	
R 6	0.41	0.37	2.50	0.002	0.005	2.15	1.05	0.80	0.23	
R 7	0.40	0.32	2.20	0.006	0.005	2.15	1.65	0.45	0.18	
R 8	0.40	0.31	2.20	0.002	0.005	2.00	1.55	0.80	0.18	
9	0.44	0.38	1.48	0.002	0.005	2.02	1.40	0.64	0.20	
10	0.42	0.38	2.75	0.002	0.005	2.05	1.38	0.68	0.20	
11	0.43	0.35	2.11	0.006	0.008	2.05	1.75	0.68	0.21	
12	0.40	0.35	2.15	0.006	0.007	2.07	0.80	0.68	0.21	
13	0.39	0.33	2.02	0.002	0.005	1.97	1.34	0.26	0.21	
14	0.40	0.33	2.02	0.002	0.007	2.00	1.35	1.02	0.21	
15	0.39	0.32	2.05	0.002	0.007	2.07	1.37	0.66	0.22	

Experimental Procedure

The fracture-toughness and stress-corrosion specimens were the bend specimen type (ASTM Test for Plane-Strain Fracture Toughness of Metallic Materials (E 399-72)) and were finish machined to dimensions of 0.400 by 0.800 by 5.0 in. (10.16 by 20.32 by 127.0 mm) after heat treatment. The plane-strain fracture-toughness tests met all requirements of validity as specified in ASTM Method E 399-72. All tests were conducted at room temperature. The stress-corrosion specimens were fatigue cracked according to ASTM Method E 399-72 (K_f maximum $\leq$ 0.6 K_Q); prior to cantilever beam loading and the filling of a plastic reservoir surrounding the fatigue crack with a 3½ percent sodium chloride (NaCl) solution. The salt solution was changed daily except on weekends and the K_{Iscc} levels were determined after a runout time of 500 h for the 9Ni-4Co steels and 200 h for the low-alloy martensitic steels.

Results and Discussion

Phosphorus and Sulfur Effects in 9Ni-4Co-0.45C Steels

The tensile, Charpy impact, fracture toughness, and SCC properties for the 9Ni-4Co-0.45C steels with varying phosphorus and sulfur levels are presented in Table 2. These results reveal that for each heat, independent of phosphorus and sulfur levels, the bainitic microstructure yields both superior toughness, and SCC resistance characteristics compared to the martensitic structure. A typical delayed failure curve for these steels is illustrated in Fig. 1 for Heat V746. The superior SCC resistance characteristics of the bainitic microstructure is evident. Other investigators [*6,7,8*] also demonstrated the superior fracture-toughness properties of the lower bainite microstructure in 9Ni-4Co-0.45C steel.

The data in Table 2 for steels V727 and V746 illustrate that both K_{Ic} and K_{Iscc} are essentially independent of phosphorus content at the levels of 0.004 and 0.020 percent phosphorus. The effect of sulfur content on fracture toughness and stress-corrosion resistance is shown in Fig. 2 for phosphorus contents below 0.004 percent. From this figure it can be seen that an increasing sulfur level significantly decreases the fracture toughness of both the bainitic and martensitic microstructures but has apparently no effect on the K_{Iscc} level. The effects of phosphorus and sulfur content on Charpy V-notch impact properties are presented in Fig. 3. It is apparent from these data that sulfur is far more detrimental to toughness properties than phosphorus.

Fractographic studies of both broken fracture-toughness and SCC specimens from selected heats were conducted to examine possible differences in the fracture surfaces with respect to either increasing impurity content

TABLE 2—*Tensile, Charpy, fracture-toughness, and stress-corrosion properties of 9-4-45 steel with phosphorus and sulfur additions.*[a]

Heat No.	Microstructure	Direction	Yield Strength, ksi	Ultimate Tensile Strength, ksi	Elongation, %	Reduction in Area, %	CVN, ft·lb	K_{Ic}, ksi$\sqrt{\text{in.}}$	K_{Iscc}, ksi$\sqrt{\text{in.}}$	P, %	S, %
V723	martensite	L	239	276	10	41	15	61.1	14	0.003	0.002
	martensite	T	239	271	10	40	14	...	...		
	bainite	L	216	267	15	53	25	91.1	16		
	bainite	T	216	266	12	43	22	...	...		
V724	martensite	L	246	280	9	34	12	42.3	11	0.013	0.020
	martensite	T	245	280	9	33	11	...	...		
	bainite	L	210	269	11	43	17	64.8	15		
	bainite	T	210	268	11	36	12	...	...		
V725	martensite	L	243	283	3	3	8	40.0	11	0.022	0.025
	martensite	T	243	285	2	2	5	...	...		
	bainite	L	215	269	9	34	14	54.0	13		
	bainite	T	216	266	8	29	11	...	...		
V726	martensite	L	249	288	7	22	11	43.0	12	0.004	0.025
	martensite	T	249	285	6	21	9	...	...		
	bainite	L	215	269	10	38	13	53.0	18		
	bainite	T	215	270	9	27	11	...	...		
V727	martensite	L	241	277	10	44	14	54.0	13	0.020	0.009
	martensite	T	240	277	9	41	11	...	...		
	bainite	L	215	269	12	51	21	71.5	16		
	bainite	T	214	268	11	47	18	...	...		
V746	martensite	L	244	277	10	47	14	55.0	11	0.004	0.010
	martensite	T	243	282	9	37	12	...	...		
	bainite	L	215	267	13	50	22	77.0	17		
	bainite	T	213	268	11	41	20	...	...		

[a] Average room temperature properties.

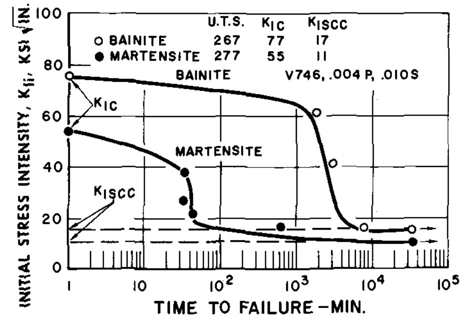

FIG. 1—*Delayed failure behavior of 9-4-45 steel with 0.004 percent phosphorus and 0.010 percent sulfur.*

or microstructural changes. No dependence of the fracture surface morphology on either of these two parameters was found. The examination of the fracture surfaces from K_{Ic} specimens revealed no unusual features. The fractographic studies of SCC specimens showed that the SCC region had varying amounts of intergranular fracture, with most specimens having 50 percent or greater intergranular fracture. The fast fracture regions varied from mostly dimpled rupture to domains with large flat areas and very smooth dimpled rupture.

Silicon, Chromium, and Molybdenum Effects on 0.40 Carbon, Low-Alloy Martensitic Steels

The tensile, Charpy impact, fracture toughness, and SCC results for a number of specially prepared heats are presented in Table 3. These heats were designed statistically using a 2^3 factorial experiment, augmented by star and center points, which enabled mechanical property-composition

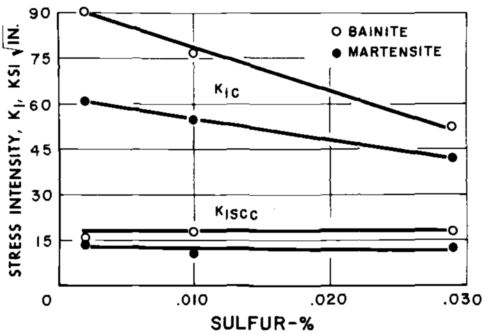

FIG. 2—*Effect of sulfur content on* K_{Ic} *and* K_{Iscc} *for 9-4-45 steel.*

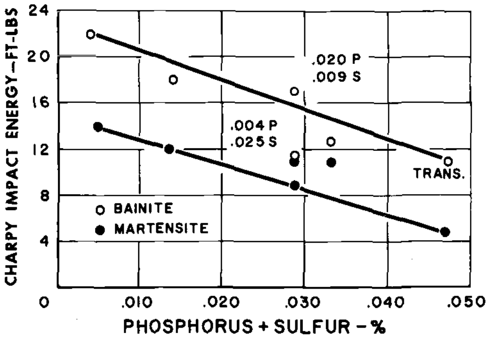

FIG. 3—*Impact properties of 9-4-45 steel as a function of phosphorus plus sulfur content.*

prediction equations to be developed. The prediction equations for ultimate tensile strength and plane-strain fracture toughness tested at 70°F (21°C) and −65°F (−54°C) were obtained from the regression analysis of the compositions and mechanical properties given in Tables 1 and 3, respectively; whose equations are:

1. K_{Ic}, ksi$\sqrt{\text{in.}}$ at +70°F $= -35.7 + 119.9\,(\%\,\text{Si}) - 39.1\,(\%\,\text{Cr}) + 31.5\,(\%\,\text{Mo}) - 29.6\,(\%\,\text{Si}^2) - 19.8\,(\%\,\text{Mo}^2) - 19.8\,(\%\,\text{Cr} \times \%\,\text{Mo}) + 16.1\,(\%\,\text{Cr}^2)$

   $R^2 = 0.97$

   Standard error $= 1.51$ ksi$\sqrt{\text{in.}}$

2. K_{Ic}, ksi$\sqrt{\text{in.}}$ at −65°F $= 20.46 + 58.0\,(\%\,\text{Si}) - 36.75\,(\%\,\text{Cr}) - 11.95\,(\%\,\text{Mo}) - 14.78\,(\%\,\text{Si}^2) + 10.67\,(\%\,\text{Cr}^2)$

   $R^2 = 0.94$

   Standard error $= 1.4$ ksi$\sqrt{\text{in.}}$

3. Ultimate tensile strength, ksi $= 322.5 - 90.2\,(\%\,\text{Si}) + 76.6\,(\%\,\text{Cr}) + 24.6\,(\%\,\text{Si}^2) - 23.1\,(\%\,\text{Cr}^2) + 12.8\,(\%\,\text{Mo})$

   $R^2 = 0.93$

   Standard error $= 2.9$ ksi

The multiple correlation coefficient (R^2) and the standard error of estimate are statistical measurements of the predictability of a regression equation. The multiple correlation coefficient is a measure of the fraction of total variation about the average of the dependent variable which is explained by the regression. The standard error of estimate or standard error is a measure of the accuracy of fit of the regression equation. The smaller the value, the better the regression equation predictions fit the data.

TABLE 3—*Mechanical properties of Ni-Cr-Mo-Si-V martensitic steels.*

Heat No.	Yield Strength, ksi	Ultimate Tensile Strength, ksi	Elongation, %	Reduction in Area, %	CVN, ft·lb		K_{Ic}, ksi$\sqrt{\text{in.}}$		K_{Iscc}, ksi$\sqrt{\text{in.}}$
					+70°F	−65°F	+70°F	−65°F	
R 1	261	299	11	47	18.5	18	59.8	45.4	18
	256	296	11	44	22	21	62.7	46.2	
					20.5	19	64.3		
R 2	266	307	11	39	16.5	15.5	55.6	42.2	17
	261	303	11	40	15.5	16	60.0	39.0	
					14.5	17	58.9		
R 3	263	309	11	41	18	20.5	61.4	40.3	16
	261	306	11	39	19	19.5	60.0	40.7	
					20	17.5	62.4		
R 4	269	316	9	31	15.5	17	49.6	36.3	16
	268	312	8	25	17	14.5	48.2	37.8	
					17	15.5	49.9		
R 5	269	311	10	36	17	17.5	58.8	42.6	18
	261	301	11	38	20.5	15	59.3	40.7	
					19.5	17.5	58.7		
R 6	271	315	11	36	15	16	49.8	35.5	18
	267	311	11	35	18	15	50.7	35.5	
					16	15	50.5		

R 7	266	315	8	28	16	16.5	58.9	36.0	18
	264	313	10	40	17	13	57.6	38.1	
					19	14.5	. . .		
R 8	272	312	12	37	17	17	52.6	36.0	17
	274	321	9	26	18	15.5	49.7	32.2	
					17	14	52.0		
9	273	314	10	29	15	13.5	48.0	35.0	16
	270	312	8	23	16.5	15.5	47.6	35.0	
					14.5	12	48.0		
10	284	333	8	34	16	12	40.5	31.4	16
	286	332	9	31	15.5	11	40.4	29.6	
					15.5	9	40.1		
11	265	311	11	40	14	16.5	54.7	37.6	18
	257	309	9	25	14	17.5	54.2	40.2	
					16.5	16	57.8		
12	263	300	10	42	22	21	66.0	46.3	18
	261	299	10	37	22.5	20.5	64.4	46.2	
					19.5	19	65.0		
13	264	307	11	40	21	17	62.0	44.6	18
	262	307	11	42	19	18	61.4	45.1	
					20	15	60.9		
14	273	316	11	35	17	14.5	47.6	34.1	19
	268	312	10	35	18	9	46.7	36.8	
					16.5	10	46.1		
15	269	310	10	36	19.5	14.5	56.0	40.7	17
	261	306	10	34	19	16.5	56.6	39.2	
					. . .	18.5	58.8		

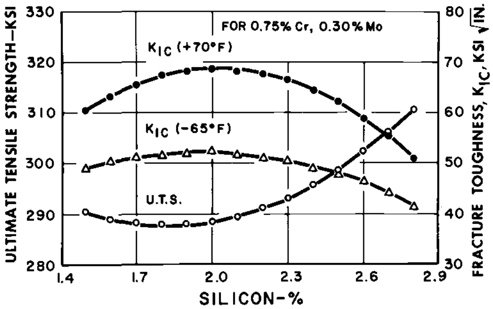

FIG. 4—*Graphically representation of mechanical property composition (silicon) prediction equations for Heats R1 through 15.*

These regression equations were used to optimize the strength and toughness properties of the alloy system as influenced by varying levels of silicon, chromium, and molybdenum. As an illustration of how these equations were utilized, the effect of varying silicon content at constant chromium and molybdenum levels on ultimate tensile strength and K_{Ic} is shown in Fig. 4. Fracture toughness increases markedly with increasing silicon to approximately 2.1 weight percent. Toughness decreases with increasing silicon above this level. The ultimate tensile strength increases rapidly at silicon contents above 2.0 percent.

Unfortunately, the results of the SCC tests showed that the threshold parameter, K_{Iscc}, was essentially independent of compositional changes. The K_{Iscc} values given in Table 3 for the 15 heats varies over a very limited range, from 16 ksi$\sqrt{\text{in.}}$ (17.6 MPa$\sqrt{\text{m}}$) to 19 ksi$\sqrt{\text{in.}}$ (20.9 MPa$\sqrt{\text{m}}$). These findings were similar to those determined by Sandoz [5]. From these data, any attempt at finding a correlation between K_{Iscc} and a toughness or a strength parameter would result in a very weak relationship, especially at these strength levels.

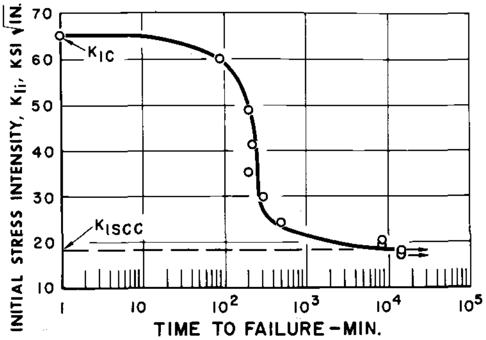

FIG. 5—*Delayed failure behavior of Heat 12.*

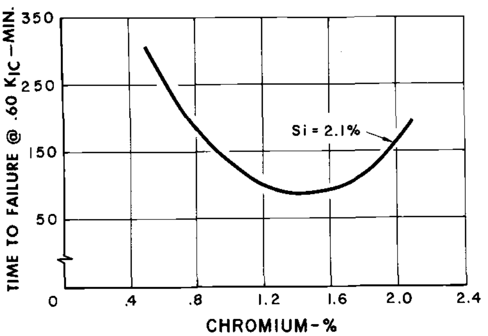

FIG. 6—*Influence of chromium content on time to failure at* $K_{Ii} = 0.60\ K_{Ic}$ *for Ni-Cr-Mo-V martensitic steels.*

Delayed failure curves were developed for each of the 15 heats and, in general, were similar in nature to the delayed failure curve shown for Heat 12 in Fig. 5. While the threshold level, K_{Iscc} value, did not vary significantly for these steels, it was found that there was a significant variation between heats in the time to the knee of the curve, where the applied stress intensity, K_{Ii}, decreases rapidly at essentially constant time (about 200 min for Heat 12). Taking the time increment required for the sudden drop in stress intensity to occur, a regression analysis was made to determine if the time increment to failure at an arbitrary chosen stress-intensity level (in this case 60 percent of K_{Ic}) was dependent significantly on compositional changes. The resulting regression equation is:

$$\text{time to failure at } K_{Ii} = 0.60\,K_{Ic}, \text{ min} = 488.8 + 60.3\,(\%\,\text{Si}) - 735.0\,(\%\,\text{Cr}) + 256.8\,(\%\,\text{Cr}^2)$$

$$R^2 = 0.73$$

$$\text{Standard error} = 24.0 \text{ min}$$

The regression equation indicates that at an applied stress-intensity level equal to 60 percent of K_{Ic}, the time to failure is independent of molybdenum content, linearly and quadratically dependent on chromium level, and linearly dependent on silicon content. This equation is expressed graphically for certain compositions in Figs. 6 and 7.

No previous work has demonstrated a chromium effect on SCC resistance in low-alloy martensitic steels; however, Carter [*3*] has shown that increasing silicon content in 4340 type steels decreases the crack growth rate in K_{Iscc} tests. His findings also showed that increasing silicon did not influence the K_{Iscc} level for these steels, which is in agreement with results presented in this paper. Benjamin and Steigerwald [*11*] also have shown that the stress-corrosion crack-growth rate changes markedly with composition, but that the lower critical limit, K_{Iscc}, does not appear to be altered.

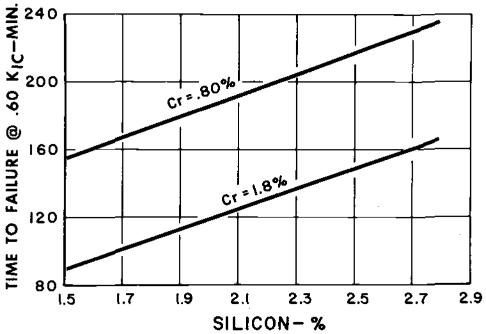

FIG. 7—*Influence of silicon content on time to failure at* K_{Ii} = *0.60* K_{Ic} *for Ni-Cr-Mo-V martensitic steels.*

These results indicate that changes in composition in 0.40C, low-alloy martensitic steels, influence the time to failure (incubation time plus crack growth) under a stress-corrosion environment even though these changes do not influence the stress-intensity level where rapid mechanical crack propagation starts. Carter [*3,12*] postulated that the stress-intensity level at which the slowly moving crack reaches a critical length under SCC conditions, and rapid mechanical crack propagation, is higher than the K_{Ic} stress-intensity value, thus indicating that some type of crack blunting is occurring. In ultrahigh-strength steels, the importance of increasing times to failure with increasing silicon and, possibly, chromium contents is minimal, because the magnitude of subcritical slow crack growth in terms of time and crack length is small.

The finding that the threshold stress-intensity parameter, K_{Iscc}, is virtually independent of compositional variations in ultrahigh-strength steels might be attributed to the role hydrogen has in the stress-corrosion mechanism. Sandoz et al [*13*] have found that the solution chemistry near a stress-corrosion crack tip always is at a constant pH value of 3.7 ± 0.1, regardless of the composition of the particular steel. This result indicates that the chemical reactions which produce hydrogen are not affected. The alloying elements, silicon and chromium, appear to influence the crack growth rate, thus, possibly affecting hydrogen diffusion; however, since the K_{Iscc} parameter is a threshold value and not time-dependent, the increase in hydrogen diffusion would not change the magnitude of K_{Iscc} for a particular group of steels. Microstructural differences have an effect on SCC resistance, though it is not known if this can be traced to their ability to effect changes in the corrosion kinetics.

The K_{Iscc} results presented in Tables 2 and 3 also reveal that the SCC resistance of the Ni-Cr-Mo-Si-V low-alloy martensitic steels is superior to that obtained for the 9Ni-4Co-0.45C medium alloy steels. The observation that the variations in silicon, chromium, and molybdenum in the low-alloy martensitic steels did not influence the K_{Iscc} values in that alloy system cannot be extended to imply that SCC resistance is independent of composition for other alloy systems, as shown previously by other investigators [*1,3,5*]. Judgments concerning the influence of composition on the SCC resistance are only valid for the range of composition investigated within a given alloy system. The lower K_{Iscc} values for the 9Ni-4Co-0.45C steels compared to the low-alloy Ni-Cr-Mo-Si-V steels can be understood in terms of higher carbon and nickel contents in the 9Ni-4Co-0.45C steels which result in a greater degree of twinned martensite compared to the low-alloy steels, and this is known to be detrimental to hydrogen embrittlement and SCC resistance [*14*]. In addition, the significantly different silicon levels in the two alloy systems would favor increased SCC resistance in the higher silicon low-alloy martensitic steels.

Conclusions

The SCC resistance of ultrahigh-strength steels is virtually independent of compositional variations. Impurity elements such as phosphorus and sulfur have little effect on the threshold stress-intensity parameter, K_{Iscc}, of 9Ni-4Co-0.45C alloy steel. Fracture toughness and Charpy impact properties are affected adversely with increasing sulfur content (up to 0.025 weight percent; however, phosphorus (ranging up to 0.022 weight percent) has little influence on either of these two toughness parameters. Microstructural differences do have pronounced effects on both fracture toughness and SCC resistance, although no differences in fracture mode could be found from fractographic studies. The lower bainitic microstructure is consistently tougher and more resistant to SCC than the martensitic structure in 9Ni-4Co-0.45C alloy steels. In low-alloy, medium-carbon, martensitic steels, the K_{Iscc} parameter is unaffected by variations of the alloying elements, silicon (1.5 to 2.7 weight percent); chromium (0.8 to 1.75 weight percent); and molybdenum (0.25 to 1.00 weight percent) within the composition ranges given with K_{Iscc} values varying from 16 to 19 ksi$\sqrt{\text{in.}}$ (17.6 to 20.9 MPa$\sqrt{\text{m}}$). Increasing silicon and chromium levels increase the times to failure in these low-alloy steels. Fracture toughness is influenced in a nonlinear way by these elements as presented in the regression equations, silicon being beneficial up to about 2.20 weight percent, with chromium and molybdenum held at minimum levels.

References

[*1*] Carter, C. S., "Evaluation of a High-Purity 18% Ni (300) Maraging Steel Forging," AFML-TR-70-139, Air Force Materials Laboratory, Dayton, Ohio, June 1970.

[2] Proctor, R. P. M. and Paxton, H. W., *Transactions Quarterly*, American Society for Metals, Vol. 62, Dec. 1969, p. 989.

[*3*] Carter, C. S., *Corrosion*, National Association of Corrosion Engineers, Vol. 25, Oct. 1967, p. 423.
[*4*] May, M. J. and Priest, A. H., "Effect of Silicon, Sulphur, and Phosphorus on the Fracture Toughness and Stress Corrosion Cracking Resistance of a High-Strength Martensitic Steel," MG/E/311/67, British Iron and Steel Research Association.
[*5*] Sandoz, G., *Metallurgical Transactions*, Vol. 2, April 1971, p. 1055.
[*6*] Pascover, J. S. and Matas, S. J. in *Structure and Properties of Ultrahigh-Strength Steels, ASTM STP 370*, American Society for Testing and Materials, 1965.
[*7*] Liu, Y. H., *Transactions Quarterly*, American Society for Metals, Vol. 62, March 1969, p. 55.
[*8*] Smith, D. W., Richardson, W., and Hehemann, R. F., "Phase Transformations and Structure-Property Relationships," Progress Report to Office of Naval Research, July 1968, Contract No. ONR No. N0014-67-A-0404-0001.
[*9*] Cottrell, C. L. M. in *High Strength Steels*, The Iron and Steel Institute, Special Report 76, 1962, p. 1.
[*10*] Birkle, A. J., Wei, R. P., and Pellissier, G. E., *Transactions Quarterly*, American Society for Metals, Vol. 59, Dec. 1966, p. 981.
[*11*] Benjamin, W. D. and Steigerwald, E. A., "Environmentally Induced Delayed Failures in Martensitic High-Strength Steels," AFML-TR-68-80, April 1968, Air Force Materials Laboratory, Dayton, Ohio.
[*12*] Carter, C. S., "Crack Extension in Several High-Strength Steels Loaded in 3.5% Sodium Chloride Solution," Boeing Document D6-19770, 1967.
[*13*] Sandoz, G., Fujii, C. T., and Brown, B. F., *Corrosion Science*, Vol. 10, Oct. 1970, p. 839.
[*14*] Boniszewski, T., Watikinson, F., Baker, R. G., and Tremleth, H. F., *British Welding Journal*, Vol. 12, Jan. 1965, p. 14.

C. T. Fujii[1]

Stress-Corrosion Cracking Properties of 17-4 PH Steel

REFERENCE: "Fujii, C. T., **"Stress-Corrosion Cracking Properties of 17-4 PH Steel,"** *Stress Corrosion—New Approaches, ASTM STP 610,* American Society for Testing and Materials, 1976, pp. 213–225.

ABSTRACT: Recent unexpected occurrences of stress-corrosion cracking (SCC) with 17-4 PH structural components indicated a need for improved characterization of the alloy and application of more advanced analytical procedures for reliably predicting structural performance. Accordingly, the purpose of the present studies was to establish systematically the SCC properties of 17-4 PH steel over a wide range of yield strengths and applied cathodic potentials. Six different heat treatments were selected for the SCC studies. The data, when analyzed in terms of ratio analysis procedures, are immediately useful for predictions of service reliability of the steel in marine structures.

The results show that 17-4 PH steel is moderately sensitive to SCC at high-strength levels, less sensitive to SCC at intermediate strength levels, and relatively insensitive to SCC in the metallurgically overaged, low yield strength condition. Increased applied cathodic potentials increase the SCC susceptibility of the alloy significantly which strongly suggests the involvement of hydrogen in the SCC mechanism. The minimum specimen thickness required for determining a thickness-independent K_{Iscc} for steels by the cantilever method appears to be considerably less than for a standard K_{Ic} test.

KEY WORDS: stress corrosion, galvanic corrosion, hydrogen, precipitation hardening steels, heat treatment, mechanical properties

The high-strength stainless steel, 17-4 PH,[2] is representative of a class of alloys that derives its strength and hardness through a combination of martensitic transformation and precipitation hardening. Because of their relatively good corrosion resistance and mechanical properties, precipitation hardenable stainless steels have long been utilized for specialized needs in aircraft and rocket components, and in certain marine applications. More recently, 17-4 PH steel has been used in hydrofoil construction for the struts and foils.

---

[1] Head, Corrosion Mechanisms Section, Strength of Metals Branch, Engineering Materials Division, Naval Research Laboratory, Washington, D. C. 20375.

[2] Registered trademark of Armco Steel Corporation.

Predictably, more incidences of stress-corrosion cracking (SCC) in high-strength stainless steel components have been experienced as demands on performance in a hostile environment increased [*1*].[3] The problems mainly stem from erroneous estimates based on prior service experiences and inadequate characterization of the SCC properties of these steels to allow rational analysis of reliability in structural applications. Clearly, proper data must be available to define limits of safe use for any alloy system.

The previous data which are available on 17-4 PH steel, though limited, suggest that its SCC properties are generally good, but results have sometimes been ambiguous and the data scatter extensive [*1–4*]. In view of the overall uncertainties and incompleteness of the documented SCC data, the studies to be reported here focussed on systematically characterizing the SCC properties of 17-4 PH over a range of yield strengths under four different electrochemical conditions. The observations and data should be useful for further understanding of the SCC mechanism and reliably predicting structural performance of the alloy.

Procedure

Material and Specimen Preparation

The materials used in the SCC studies were plates of different thicknesses produced from vacuum melted 17-4 PH steel with a nominal composition as given in Table 1. The thicknesses of the 17-4 PH plates were 1, $\frac{5}{8}$, $\frac{3}{8}$, $\frac{5}{16}$, and $\frac{3}{16}$ in. Two series of experiments were conducted. The more extensive study utilized specimens cut from 1-in.-thick plate which were subsequently heat treated to obtain a range of yield strengths. Included in this study were tension tests (0.505 in. diameter), full-thickness dynamic tear (DT) tests, and SCC tests at different applied electrochemical potentials. The cantilever specimens used to determine the critical stress-intensity factor for SCC (K_{Iscc}) were side-grooved, notched and fatigue precracked, and tempered. The different heat treatments and the corre-

TABLE 1—*Nominal composition of 17-4 PH steel.*[a]

Cr	Ni	Cu	Mn	Si	Cb + Ta	C	P	S
15.50– 17.50	3.00– 5.00	3.00– 5.00	1.00 max	1.00 max	0.15– 0.45	0.07 max	0.04 max	0.03 max

[a] Weight percent.

---

[3] The italic numbers in brackets refer to the list of references appended to this paper.

TABLE 2—*Heat treatments for 17-4 PH specimens.*

Temper	Heat Schedule
Solution treated	1900°F for 1 h, oil quench
H900, H975, H1025, H1075, H1150	solution treated material heated at specified temperature for 4 h, air cooled
H1150M	solution treated material heated at 1400°F for 2 h, air cooled, then heated at 1150°F for 4 h and air cooled

TABLE 3—*Mechanical properties of vacuum-melted 17-4 PH steel.*

Temper	DTE,[a] ft·lb	σ_{ys}, ksi	σ_{ts}, ksi	EL,[b] %	RA,[c] %
H900	320	177	196	14	50
H975	2510	162	171	15	55
H1025	3335	157	162	15	55
H1075	3175	151	157	17	55
H1150	4815	120	142	19	61
H1150M	. . .	91	125	22	64

[a] DTE = dynamic tear energy.
[b] EL = elongation.
[c] RA = reduction in area.

sponding measured mechanical properties are summarized in Tables 2 and 3, respectively.

The second set of experiments were conducted to determine the effect of specimen thickness on the measured value of K_{Iscc}. The cantilever specimen blanks were cut from the plates of different thicknesses listed previously. Finished specimens were notched and fatigue precracked, and tempered at 1050°F. No side-grooves were machined into these groups of specimens.

Stress-Corrosion Cracking Tests

Figure 1 illustrates the SCC specimen and method used in these experiments. The critical dimensions of the precracked cantilever specimen for the first series of experiments were $B = 0.75$ in., $W = 1.0$ in., and $a = 0.25$ in. (0.125-in. notch plus 0.125-in. fatigue crack) where B, W, and a are as defined in Fig. *1a*. The critical dimensions of the specimens used to study the effect of thickness of K_{Iscc} are summarized in Table 4. The cantilever test method, Fig. 1*b*—described more fully by Brown [5]—was used to determine critical stress-intensity factors in air (K_{Ix}) and in salt water (K_{Iscc}) for different strength levels (first series of experiments) and different specimen thicknesses (second series of experiments). The corrodent was a 3.5 percent sodium chloride (NaCl) solution contained in a poly-

TABLE 4—*Effect of specimen thickness*, B, *on* K_{Iscc} *of 17-4 PH steel.*[a]

Plate Thickness, in.	Dimensions, in.			K_{Iscc}, ksi$\sqrt{\text{in.}}$		
	B	*W*	*a*	FC,[b] −0.3 V	5086 Al, −0.8 V	Zn, −1.0 V
3/16	0.200	0.380	0.20	(85)	65	44
				(80)	58	40
5/16	0.305	0.630	0.34	107	86	53
				95	78	48
3/8	0.372	0.740	0.40	106	85	55
				111	85	55
5/8	0.625	1.250	0.66	113	95	49
				120	91	54
1	0.730	1.000	0.52	106	87	53
				100	89	55

[a] H1050 temper, σ_y = 158 ksi.
[b] FC = freely corroding.

ethylene reservoir around the crack. This corrodent was changed daily during the experiment which typically ran for 300 to 600 h. The SCC experiments were conducted for the freely corroding condition of the specimen and for different cathodically polarized conditions by galvanic coupling to anodes of 5086 aluminum alloy, zinc, and magnesium. In all of the SCC tests, the electrochemical potentials of the specimens were measured against a silver/silver chloride (Ag/AgCl) reference electrode. All of the experiments were conducted at room temperature of approximately 24°C.

The stress-intensity factor, K_{Ix}, measured for fast fracture in air, was used as a guide for estimating initial loads for the K_{Iscc} tests. The initial loads for K_{Iscc} tests were usually 50 percent of the measured K_{Ix} values. To determine the critical K_I value for salt water crack growth under any

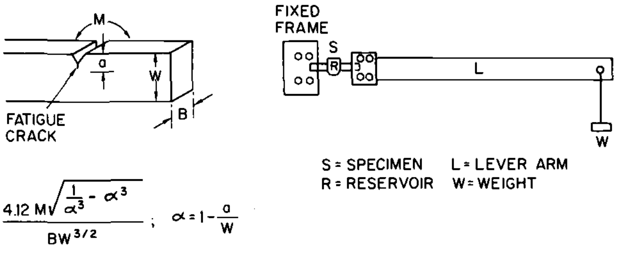

(a) (b)

FIG. 1—(a) *Schematic of fatigue-precracked cantilever specimen used to determine* K_{Iscc}, (b) *Schematic of cantilever test equipment for measuring* K_{Iscc}.

given condition, a step-loading bracketing technique was used. Loads were increased incrementally every 100 h until crack growth was observed. Indications of crack growth were obtained by noting the movement of the cantilever beam via a precision dial gage positioned near the loaded end on the beam. Upon completion of each SCC test, crack growth was verified by visual and microscopic examination of the fracture surfaces. The critical K_{Iscc} value was considered to be bracketed between the lowest K_{I} value which produced crack growth and fracture, and the highest K_{I} value which failed to cause any crack extension after 100 h.

Post-test examination included fractography of the fracture surfaces, metallography, and transmission electron microscopy of the alloy from different tempers.

Results

Effects of Yield Strength and Potential

The SCC properties of 17-4 PH steel are summarized in Table 5 for the six heat treatments. Values for the corresponding yield strengths, K_{Ix}, and K_{Iscc} for four electrochemical conditions are tabulated. The approximate electrochemical potential of the specimen measured for each experimental condition is noted below the K_{Iscc} subcolumn headings.

If the critical stress-intensity factors in air, K_{Ix}, are used as baselines, all of the K_{Iscc} data indicates that the alloy is susceptible to SCC under both freely corroding and cathodically polarized conditions, although clearly in varying degrees depending on yield strength and potential. The last column of Table 5 lists the K_{Iscc} values of specimens instrumentally

TABLE 5—*SCC properties of 17-4 PH steel.*[a]

		K_{Ix}, ksi$\sqrt{\text{in.}}$	K_{Iscc}, ksi$\sqrt{\text{in.}}$				
Temper	σ_y, ksi	Air	FC,[b] −0.3 V[c]	5086 Al, −0.8 V	Zn, −1.0 V	Mg, −1.3 V	IP,[d] −1.3 V
H900	177	113	79	54	30	26	28
H975	162	146	102	76	45	32	30
H1025	157	157	111	89	53	35	36
H1075	151	166	123	103	65	40	39
H1150	120	170	130	116	77	44	41
H1150M	91	118	97	93	100	90	...

[a] Corrodent: 3.5% NaCl solution.
[b] FC = freely corroding.
[c] Potential as measured against Ag/AgCl reference electrode.
[d] IP = instrumentally potentiostated.

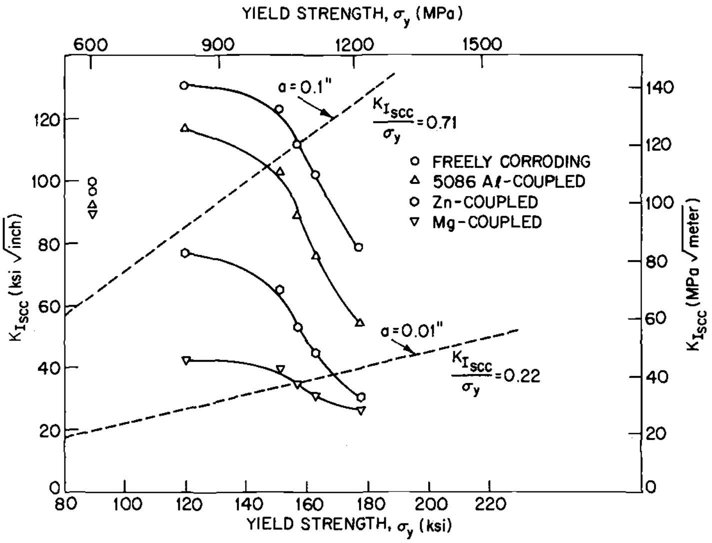

FIG. 2—K_{Iscc} *data for 17-4 PH steel of different yield strengths under four electrochemical conditions.*

potentiostated at −1.3 V which is equivalent to galvanically coupling the specimen to magnesium. The excellent agreement between the K_{Iscc} data of the potentiostated and magnesium-coupled specimens at each yield strength studied suggests that the magnesium corrosion product that unavoidably contaminates the bulk corrodent during the experiment has little influence on the measured K_{Iscc} parameter.

The effects of yield strength and potential on the SCC properties of 17-4 PH steel are compared and evaluated more easily in Figs. 2 and 3. Figure 2 shows K_{Iscc} as a function of yield strength at each of the electrochemical potential, as indicated by the four curves drawn through the data points. The shape and negative slope of each curve show that K_{Iscc} decreases progressively with increasing yield strength in the approximate range of 120 to 180 ksi under all four electrochemical conditions. The relative position of each curve shows that increasing cathodic polarization of the specimen decreases the value of K_{Iscc} at any given yield strength. The group of four points in the upper left portion of Fig. 2 represents the SCC property of the alloy in the metallurgically overaged condition (that is, H1150M temper). The alloy in this condition ($\sigma_y = 91$ ksi) is highly resistant to SCC. The dash lines in Fig. 2 are arbitrarily selected constant ratio (K_{Iscc}/σ_y) lines of 0.71 and 0.22. The indicated values of the critical length for crack growth *a* of surface flaws, 0.1 and 0.01 in. in length, respectively, were calculated on the basis of the fracture mechanics relationship, $a_{cr} = 0.2(K_{Iscc}/\sigma_y)^2$ (Ref *6*). This simple equation for a surface flaw is derived assuming plane-strain conditions and application of yield

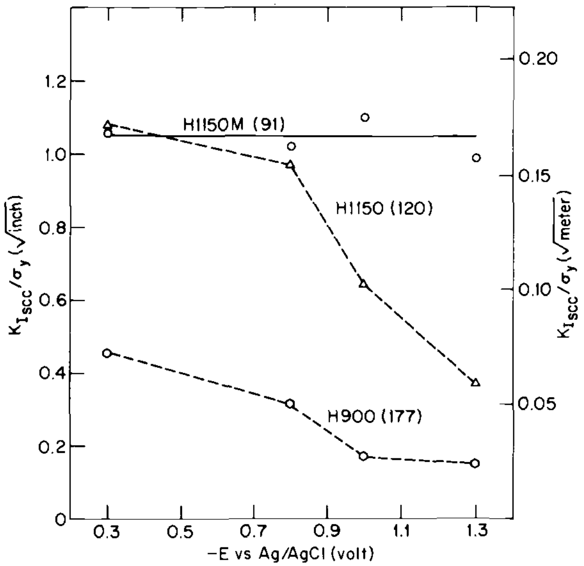

FIG. 3—*Effect of applied cathodic potentials on the* K_{Iscc}/σ_y *ratio for three different tempers of 17-4 PH steel.*

point tensile stress normal to the direction of growth of a long, elliptically shaped crack. The advantages of high-ratio material in terms of tolerating existing flaws in structural applications are thus clearly illustrated by the large difference in the value *a* for the two ratios represented by the dash lines.

In Fig. 3, the ratio K_{Iscc}/σ_y—shown to be useful for comparing the SCC properties of alloys in terms of flaw tolerance—is plotted against the electrochemical potential for three heat treatments. The numbers in parenthesis accompanying each curve are the corresponding yield strengths in ksi units. The curves for other heat treatments fall between and follow the trend of the dash curves for the H1150 and H900 tempers presented here. Figure 3 shows that the effect of potential on the SCC properties of high-ratio material (H1150) is greater than for the low-ratio (H900) material for the normally aged condition. Also illustrated is the negligible effect of potential on the SCC properties of the alloy in the H1150M temper—the metallurgically overaged condition. The superior position of the solid line for the H1150M temper relative to the dash curves indicates the beneficial effects of overaging on SCC flaw tolerance in this alloy system.

Effect of Specimen Thickness, B

The complete SCC data from the cantilever K_{Iscc} tests on specimens cut from several thin plates of 17-4 PH steel and given a H1050 temper are summarized in Table 4. The original thicknesses of these plates are given in column 1. The cantilever specimen dimensions B, W, and a—defined in Fig. 1a—are the thickness, width, and initial crack length, respectively. Experiments were duplicated for each specimen thickness and electrochemical condition, and the overlap of duplicate results, with one exception ($\frac{5}{16}$ in. freely corroding), was within the estimated experimental limits of accuracy of ±5 ksi$\sqrt{\text{in.}}$ for an individual test. SCC was confirmed by examination of all fracture surfaces for visual evidences after completion of each test. Extensive plastic yielding, particularly of the thinner specimens, occurred in the area of fast fracture, but evidences of SCC were not obscured and accurate measurements of the initial crack length a were not impaired. The only specimens for which examination of the fractures for SCC was not convincing were the two $\frac{3}{16}$-in. freely corroding specimens, and, therefore, these data are in parenthesis to indicate questionable visual evidence for SCC.

The effect of specimen thickness on the measured values of K_{Iscc} under three electrochemical conditions is illustrated graphically in Fig. 4 where the critical K_{Iscc} is plotted against B. The K_{Iscc} data from the $\frac{3}{16}$-in.-thick specimens are suppressed obviously at all three potentials. The data indicate that the minimum thickness required to measure a K_{Iscc} value which is independent of B decreases with increasing cathodic potentials. Cantilever specimens with minimum B, W, and a dimensions which are approximately 0.5, 1.0, and 0.5 in., respectively would appear to be conservatively sufficient to determine a B-independent K_{Iscc} for a 160 ksi yield strength steel up to a K_{Iscc}/σ_y ratio of approximately 0.7.

Fractography, Microstructure

Stress-corrosion cracks of 17-4 PH steel characteristically feature intergranular cracking (IGC), cleavage, and microvoid coalescence (MVC) as crack propagation modes. The proportions of each mode observed on a fracture surface produced by SCC appear to be mostly dependent on the applied stress-intensity factor, K_{I}, and potential, E. High values of K_{Iscc} generally produced increases in the proportions of cleavage and MVC; low values of K_{Iscc} associated with cathodically polarized conditions favored IGC and cleavage as preferred fracture modes. The results suggest a correlation of the fracture mode with the amount of hydrogen generated during the SCC experiment as previously discussed by Meyn [7].

The microstructure of the SCC specimens was dominated by martensite with some ferrite, and the details were in accord with previously documented work [8]. Transmission electron microscopy (TEM) of thin foils from the SCC specimens revealed that a lath structure was common to all tempers. The present TEM observations on the effect of heat treatment on precipitate size, particle distribution, dislocation density, and the lath

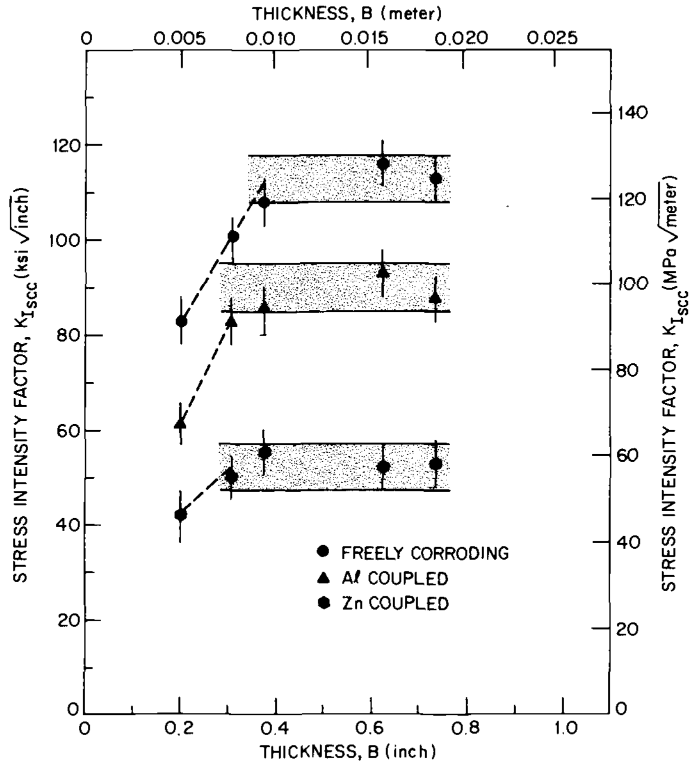

FIG. 4—*Effect of specimen thickness on the measured value of* K_{Iscc} *for the H1050 temper of 17-4 PH steel under three electrochemical conditions.*

structure are generally similar to those reported previously [9]. There is a pronounced decrease in the population but an increase in size of precipitate particles associated with the overaging H1150M temper in comparison to the H1150 heat treatment.

Discussion

The SCC properties of 17-4 PH steel are very dependent on yield strength and electrochemical potential and thus follows the general trend experienced for most other high-strength steels. For engineering or structural applications, the comparison of its relative SCC resistance with those of other high-strength steels is conveniently done in the format of a Ratio Analysis Diagram (RAD) [*10*]. Figure 5 is a RAD for SCC of steels in laboratory salt water (approximately 3.5 percent NaCl solution) where the ordinate is the critical stress-intensity factor for SCC, K_{Iscc}, and the abscissa is the yield strength, σ_y, of the steel. The SCC envelope, the shaded region, was constructed using most of the available SCC data determined for a wide variety of steels by several laboratories [*2*]. Visual confirmation of crack growth, as required in the present experiments on 17-4 PH steel, was imposed as a requirement before the K_{Iscc} data were included to define the boundary limits of the envelope. The older forging grade steels would be representative of material in the lower regions of the envelope. The newer weldable steels of improved quality would generally fall in the higher range of the envelope. The system of constant K_{Iscc}/σ_y ratio lines divides the diagram into three ratio zones—high, intermediate, and low. These zones may also be regarded as levels of resistance to SCC. The transition from high to intermediate and low SCC resistance is relatively sharp as indicated by the general slope of the envelope. As discussed earlier, the ratios are related directly to critical flaw sizes for SCC and are most useful for predicting structural performance when applied in this context. The SCC problem is much less severe for high-ratio than low-ratio material because of its inherently higher flaw tolerance. Thus, under constant applied stress conditions, high-ratio material will tolerate larger preexisting cracks before succumbing to SCC. The SCC data of Fig. 5 show that for the freely corroding condition 17-4 PH has relatively "high" SCC resistance at yield strengths below approximately 150 ksi and an "intermediate" level of SCC resistance at higher yield strengths. Cathodic polarization of the specimen to the zinc potential (−1.0 V versus Ag/AgCl) reduces the SCC resistance to "intermediate" and "low" levels for the indicated yield strength range of 120 to 180 ksi. The advantages of low yield strength and the disadvantages of zinc-coupling on the SCC properties of 17-4 PH steel in comparison to other commercial steels are thus clearly evident in Fig. 5.

The effect of increased cathodic potentials on SCC resistance, as measured by K_{Iscc} strongly implicates hydrogen in the SCC mechanism of 17-4 PH steel. The present observations are consistent with previously published experimental results and bolster a growing consensus that hydrogen exerts a primary influence on stress-corrosion crack growth of steels [*11–15*]. The exact nature of hydrogen's role in SCC continues to elude nonconjectural definition. Kim and Loginow [*16*], in studies on a quenched and tempered Ni-Cr-Mo steel, have shown that hydrogen uptake increases with yield strength of the alloy. This is attributed to the increased dislocation density, precipitate population, grain boundaries, and other hydrogen trap sites with increasing yield strength of the alloy. Moreover, the results indicate that trap-site hydrogen uptake in Ni-Cr-Mo steel becomes immeasurably small (<0.1 ppm) at a yield strength level of approximately 70 ksi. In a study aimed at explaining the effects of hydrogen on SCC properties of steels, Sandoz [*14*] showed that the critical stress-intensity factor for crack growth became nearly independent of the source or the quantity of hydrogen at a yield strength level of about 90 ksi. Because of the obvious improvement in SCC resistance of the low yield strength (91 ksi) overaged material and the trend of the SCC data with yield strength in the 17-4 PH system, it is tempting to suggest that the microstructural differences produced by the aging treatments determine hydrogen uptake and account for the differences in SCC properties observed for the alloy. However, evaluations of the microstructures do not appear to support this simple rationale. The tempered martensitic microstructures, the precipitate particle characteristics, and the dislocation patterns offer an abundance of hydrogen trap sites at all tempers, and no discernible correlation of the complex microstructures with SCC behavior is apparent. Furthermore, it is more probable that the absolute quantity of hydrogen in the steel is not crucial but, rather, the amount available in the crack-tip region (which alters the local mechanical properties) that is important to *K*-related determinations. Thus, considerations of solubilities, diffusivities, and interactions of hydrogen in the crack-tip region, as well as the size of the plastic zone, may be more pertinent. The hydrogen in the bulk steel may serve as a source of hydrogen or represent a boundary limit for diffusion of hydrogen in the region of the crack tip. The primary source of hydrogen active in SCC is the result of electrochemical reactions at the metal surface as suggested by the effects of cathodic potentials on K_{Iscc}. The explanation for relative noneffectiveness of this cathodic hydrogen source on K_{Iscc} observed for low yield strength steels (<90 ksi) requires more definitive experimental characterization than presently available of crack-tip interactions involving hydrogen, the alloy, and mechanical factors.

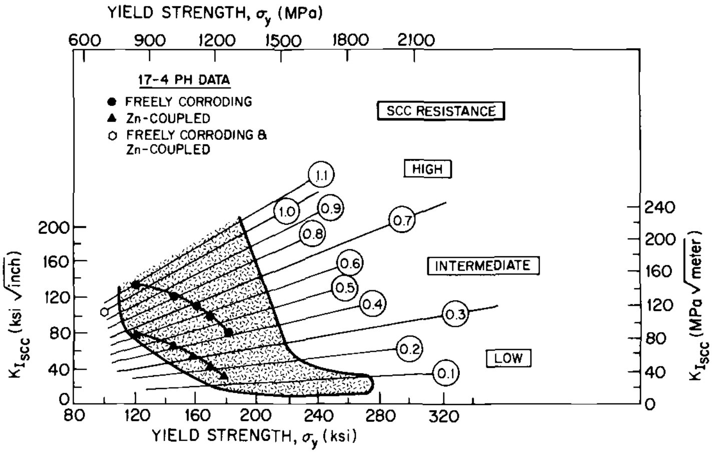

FIG. 5—*RAD for SCC of steels with ratio zoning and superposition of 17-4 PH data.*

The results of the studies on the effect of thickness on K_{Iscc} suggest that a thickness (B) independent value can be measured on a precracked cantilever bend specimen with a thickness of 0.5 in. or greater for 17-4 PH steel up to a K_{Iscc}/σ_y ratio of approximately 0.7. If the plane-strain crack toughness testing requirement for B given by $B > 2.5(K_{Ic}/\sigma_y)^2$ is adopted for SCC testing, a minimum thickness of approximately 1.2 in. would be required for a ratio of 0.7 to determine K_{Iscc} values which are considered valid by present ASTM requirements for plane strain with respect to thickness (ASTM Test for Plane-Strain Fracture Toughness Testing of Metallic Materials (E 399-74)). It would appear that this requirement may be overly restrictive for the determination of K_{Iscc} of steels. The results for 17-4 PH steel suggest that the minimum specimen thickness expressed by $B > 1.0(K_{Iscc}/\sigma_y)^2$ is adequate for determining a nonvariant K_{Iscc}. The difference in the thickness requirement for determining K_{Ic} and K_{Iscc} indicated here may again be a manifestation of the effects of hydrogen in altering the properties of the crack tip. Additional experiments are required obviously to establish the applicability of $B > 1.0(K_{Iscc}/\sigma_y)^2$ to other types of steels over a wider yield strength range. Furthermore, the minimum thickness requirements for nonferrous alloys need to be independently assessed for the establishment of any standardized K_{Iscc} test.

Conclusions

The present SCC studies on 17-4 PH steel show that:

1. Increasing yield strength decreases K_{Iscc}.
2. Increasing cathodic polarization decreases K_{Iscc}.
3. Metallurgically overaging improves the SCC resistance and flaw tolerance of the alloy, and results in a negligibly small effect of cathodic potentials on K_{Iscc}.
4. The specimen thickness required for determining thickness independent K_{Iscc} for 17-4 PH steel is considerably less than required for a standard K_{Ic} test.
5. Crack-tip hydrogen appears to be a primary factor in the SCC properties of this alloy system.

Acknowledgments

The efforts of the following contributors in their area of technical specialization is gratefully acknowledged: R. L. Newbegin (K_{Iscc} tests), T. C. Lupton (fractography), T. R. Harrison (metallography), and J. R. Reed (thin-foil TEM). Discussions with W. S. Pellini, B. F. Brown, R. W. Judy, Jr., and R. J. Goode were helpful. The research was financially supported by the Naval Material Command and the Office of Naval Research.

References

[1] Carter, C. S., Farwick, D. G., Ross, A. M., and Uchida, J. M., *Corrosion,* Vol. 27, No. 5, 1971, pp. 190–197.

[2] Sandoz, G. in *Stress-Corrosion Cracking in High Strength Steels and in Titanium and Aluminum Alloys,* B. F. Brown, Ed., U.S. Government Printing Office, Washington, D. C., Stock No. 0851-0058, 1972, pp. 80–145.

[3] Lennox, T. J., Jr., Groover, R. E., and Peterson, M. H., *Materials Protection,* Vol. 8, No. 5, 1969, pp. 41–48.

[4] Bloom, F. K., *Corrosion,* Vol. 11, No. 8, 1955, pp. 351t–361t.

[5] Brown, B. F., *Materials Research and Standards,* Vol. 6, No. 3, 1966, pp. 129–133.

[6] Beachem, C. D. and Brown, B. F. in *Stress Corrosion Testing, ASTM STP 425,* American Society for Testing and Materials, 1967, pp. 31–40.

[7] Meyn, D. A., "Influence of Stress Intensity Level and Hydrogen Activity on Sustained Load Cracking Mechanism in 17-4 PH Stainless Steel," Report of NRL Progress, Naval Research Laboratory, Washington, D. C., Dec. 1974, pp. 22–24.

[8] *Atlas of Microstructures of Industrial Alloys—Metals Handbook,* Vol. 7, American Society for Metals, Metals Park, Ohio, 1972, p. 147.

[9] Rack, H. J. and Kalish, David, *Metallurgical Transactions,* Vol. 5, July 1974, pp. 1595–1605.

[10] Pellini, W. S., "Criteria for Fracture Control Plans," NRL Report 7406, Naval Research Laboratory, Washington, D. C., 11 May 1972, pp. 46–51.

[11] Vaughan, D. A. and Phalen, D. I. in *Stress Corrosion Testing, ASTM STP 425,* American Society for Testing and Materials, 1967, pp. 209–227.

[12] Barth, C. F., Steigerwald, E. A., and Troiano, A. R., *Corrosion,* Vol. 25, No. 9, 1969, pp. 353–358.

[13] McGuire, M. F., Troiano, A. R., and Hehemann, R. F., *Corrosion,* Vol. 29, No. 7, 1973, pp. 268–271.

[14] Sandoz, G., *Metallurgical Transactions,* Vol. 3, May 1972, pp. 1169–1176.

[15] Dautovich, D. P. and Floreen, S., *Metallurgical Transactions,* Vol. 4, Nov. 1973, pp. 2627–2630.

[16] Kim, C. D. and Loginow, A. M., *Corrosion,* Vol. 24, No. 10, 1968, pp. 313–318.

R. Chait[1] *and M. D. Campbell*[2]

Corrosion Fatigue and Stress-Corrosion Cracking of High-Hardness Laminar Composite Steel

REFERENCE: Chait, R. and Campbell, M. D., "**Corrosion Fatigue and Stress-Corrosion Cracking of High-Hardness Laminar Composite Steel,**" *Stress Corrosion—New Approaches, ASTM STP 610,* American Society for Testing and Materials, 1976, pp. 226–242.

ABSTRACT: In this study both corrosion fatigue and stress-corrosion cracking behavior of a high-hardness laminar composite steel are examined in the presence of a 3.5 percent sodium chloride (NaCl) environment and compared to the behavior in air. It is shown that the susceptibility is not limited to specimens with a crack or notch. Smooth specimens with a machine ground surface tested under static as well as cyclic loading are affected adversely by the 3.5 percent NaCl environment. Using center notched panels to study crack growth behavior, it is shown that the influence of the 3.5 percent environment becomes more apparent as the maximum cyclic stress decreases. Ballistically damaged panels were also examined in a corrosive environment under the same cyclic stress conditions. Compared to the center notched panels a longer life is observed. It is suggested that this is due to the orientation of the ballistically induced cracks with respect to the loading axis. Environmental effects are also seen in the static loading of ballistically damaged panels. K_{Iscc} estimates were obtained from these panels and compared to the results of conventional specimens. Both sets of results indicate significant susceptibility of the laminar composite steel to stress corrosion.

KEY WORDS: laminates, composite materials, steels, stress corrosion, fatigue behavior, environmental effects

Based on threshold stress intensity K_{Iscc} data [*1*][3] of high-strength steel it is evident that the fracture-toughness values obtained under noncorrosive conditions can not be used as a measure of materials behavior in an aggressive environment. This is especially true of high-hardness armor steels [*2*]. The present effort focuses on one such steel, a laminar com-

---

[1] Supervisory materials engineer, Army Materials and Mechanics Research Center, Watertown, Mass. 02172.

[2] Staff scientist, Convair Division, General Dynamics Corporation, San Diego, Calif.

[3] The italic numbers in brackets refer to the list of references appended to this paper.

posite armor steel consisting of an approximately RC 60 frontal portion metallurgically bonded to a RC 50 backup portion of equal thickness. Past efforts on this material have concentrated on important baseline mechanical properties such as tensile and compressive properties, fracture toughness, fatigue strength, crack growth behavior, and temperature effects [*3–7*]. Also of interest have been the residual strength and life behavior [*4,5,8*]. The tests for most of these investigations were conducted in air. The present paper details the behavior of this material under a corrosive environment from both a stress-corrosion cracking (SCC) and corrosion fatigue standpoint.

Material and Test Procedure

Material Processing and Composition

As noted previously, the laminar composite steel consists of a hard frontal portion metallurgically bonded to a softer, approximately equal thickness backup portion by means of a rolling bonding process that takes place at 1150 to 1260°C. Preparation prior to roll bonding consists of grinding the two component plates, seam welding the periphery, and evacuating the interfacial region. Cross rolling follows to achieve the final thickness of 0.220 in. (5.6 mm). The composite is then hardened by oil quenching from about 815°C and tempered 120 to 167°C, to give the high hardness values. A schematic of the composite is shown in Fig. 1.

As a result of the foregoing heat treatment both sides exhibit a tempered martensitic microstructure. However, the difference in hardness stems mainly from a higher carbon level in the frontal portion with respect to that in the backup portion. The chemical compositions for both sides are shown in Table 1. Note that carbon content in the frontal portion is about twice that of the other side. The other alloying elements (nickel chromium, and molybdenum) are present in approximately equal amounts for both sides. Composite material of this composition given the above heat treatment possess the baseline mechanical properties shown in Table 2.

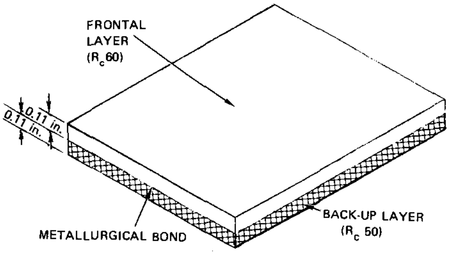

FIG. 1—*Schematic of high-hardness laminar composite steel.*

TABLE 1—*Chemistry and hardness.*

	C	Mn	P	S	Si	Ni	Cr	Mo	Al	Approximate Hardness
Hard side[a]	0.62	0.47	0.008	0.008	0.32	3.30	0.07	0.40	0.02	R_c 60
Soft side	0.28	0.48	0.008	0.010	0.29	3.33	0.11	0.42	0.03	R_c 50

[a] Both hard and soft side materials were obtained with conventional air melt practices.

TABLE 2—*Room temperature baseline mechanical properties.*[a]

0.2% yield strength (tension)	197 ksi (1358 MPa)
0.2% yield strength (compression)	239 ksi (1648 MPa)
Ultimate tensile strength	261 ksi (1800 MPa)
Notch tensile strength	242 ksi (1669 MPa)
Fracture toughness (K_Q)	45 to 60 ksi$\sqrt{\text{in.}}$ (49 to 66 MPa$\sqrt{\text{m}}$) depending on orientation

[a] Properties represent those of the composite.

Test Procedure

Baseline corrosion fatigue data in the presence of crack were obtained on a 3-in.-(76-mm) wide by 12-in.-(305-mm) center-notched panels. The through-the thickness electrically discharge machined notch, approximately 1 in. (25 mm) long with 0.002 in. (0.06 mm) radius, was oriented perpendicular to loading direction. The specimens were subjected to sinusoidal loading in a 3.5 percent sodium chloride (NaCl) environment with an Materials Testing System (MTS) closed-loop, electrohydraulic 150 000 lb (667 000 N) capacity machine. Tests were conducted at the following maximum gross section stress levels: 8 ksi (55 MPa), 10.5 ksi (72 MPa), and 13 ksi (90 MPa). The minimum gross section stress level in each case was 3 ksi (21 MPa). Crack growth was monitored on both sides of the specimen with microscopes mounted on the platen of the MTS unit. A plastic chamber, which surrounded the test section, was used to carry the 3.5 percent NaCl solution.

Using the foregoing test apparatus, corrosion fatigue tests were also conducted in 3.5 percent NaCl on 6-in. (152-mm) wide by 14-in. (356 mm) long ballistically damaged panels. The minimum and maximum gross section stress for these tests were 3 and 8 ksi, respectively. All ballistic tests were conducted at the Army Materials and Mechanics Research Center ballistic test facility using caliber 0.30 ball M2 and armor piercing (AP) M2 projectiles. Projectile velocity was in the vicinity of the V_{50} ballistic limit as defined by Abbott [9]. The ballistic damage of the panels was assessed with a wet, fluorescent magnetic particle inspection technique. The SCC resistance of ballistically damaged panels in 3.5 percent NaCl was also studied, utilizing the closed-loop, electrohydraulic test system. Tests were not conducted beyond 10 000 min. Using an hydraulic test fixture, the details of which are given in Ref *8,* some panels used for the SCC study were subjected to an applied stress during ballistic impact.

The corrosion fatigue and SCC of smooth specimens having a gage section ½ in. (13 mm) wide and 1 in. (25 mm) long was also examined. The corrosion fatigue tests were conducted on an SF-1U Sonntag fatigue machine in reversed bending (minimum : maximum stress ratio of -1.0) at a frequency of 30 Hz. Both the as-received mill surface condition, and machine ground surface condition were evaluated in air as well as in water (H_2O). Using the same apparatus, constant load tests (hard side in tension) were performed on material of both surface conditions in a 3.5 percent NaCl environment.

Results and Discussion

Corrosion Fatigue

Crack growth characteristics, as measured from centered-notched panels tested in a 3.5 percent NaCl environment are shown in Figs. 2–4 for three $\sigma_{\max}$ stress levels, 8, 10.5, and 13 ksi, respectively. For each stress level, comparison is made to the crack growth behavior in air. As shown in Fig. 2 for $\sigma_{\max} = 8$ ksi (55 MPa), the total number of cycles to failure of the composite n_f, is about 150 cycles less in 3.5 percent NaCl than it is in air. Note also that the cracks grow at a faster rate on the front or hard side and lag behind in the softer backup material. However, the effect of the corrosive environment is to reduce this crack growth rate difference between the front and the back sides. At the same $\sigma_{\max}$ level an additional tests was conducted at 15 Hz in 3.5 percent NaCl. However, the increased frequency did not significantly alter the crack growth behavior. All further testing was performed at 15 Hz.

As shown in Fig. 3, increasing $\sigma_{\max}$ from 8 ksi (55 MPa) to 10.5 ksi (72 MPa) decreases n_f in 3.5 percent NaCl from 500 to about 180 cycles, a decrease of about 65 percent. Figure 4 shows that a further increase in $\sigma_{\max}$ to 13 ksi (89 MPa) decreases n_f in 3.5 percent NaCl to 90 cycles, about an 80 percent decrease when compared to the life at 8 ksi (55 MPa). The value of $\sigma_{\max}$ also affects the difference between n_f in 3.5 percent NaCl and that in air. As shown in Fig. 5, this difference increases as the value of $\sigma_{\max}$ is lowered.

Residual life information just noted were compared to that obtained with ballistically damaged specimens. The damage pattern of the specimens chosen for cycling in 3.5 percent NaCl between $\sigma_{\max} = 8$ ksi (55 MPa) and $\sigma_{\min} = 3$ ksi (20 MPa) at 15 Hz is shown in Figs. 6 and 7 for the hard side and soft side, respectively. Plugging and radial cracking are

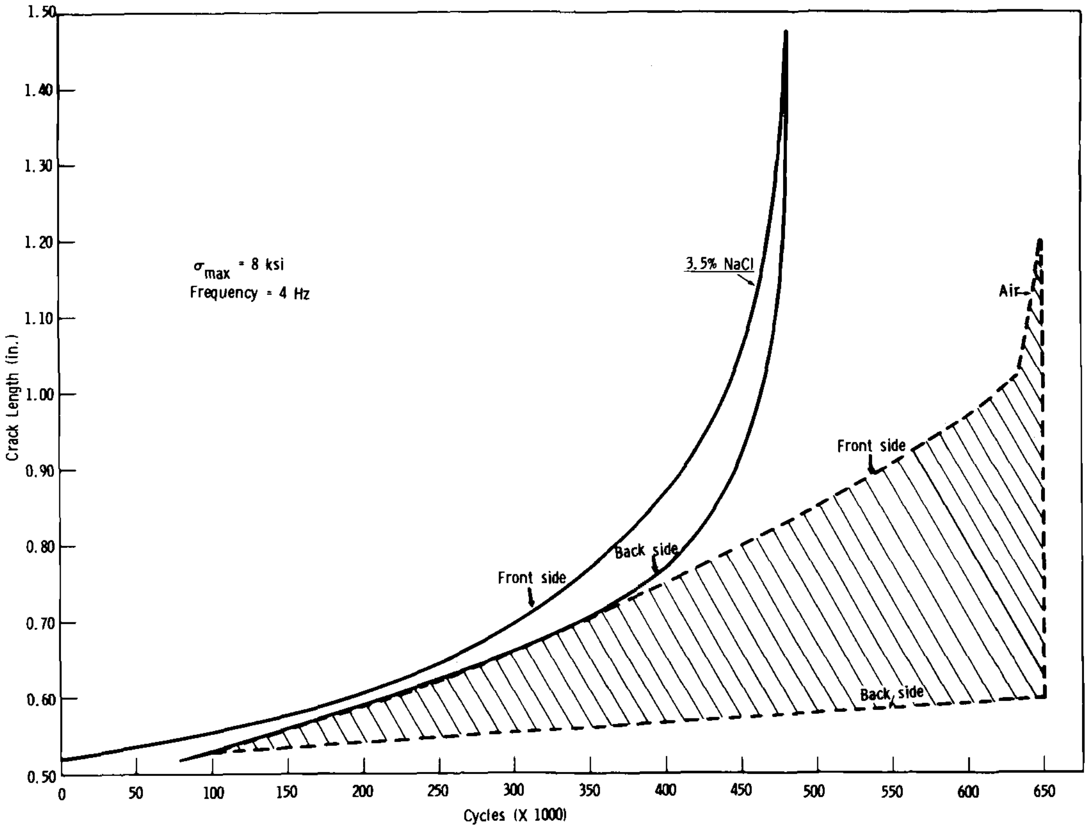

FIG. 2—*The influence of 3.5 percent NaCl environment on crack growth characteristics* (σ_{min} = *3 ksi*). *Crack growth data obtained in air taken from Ref 5.*

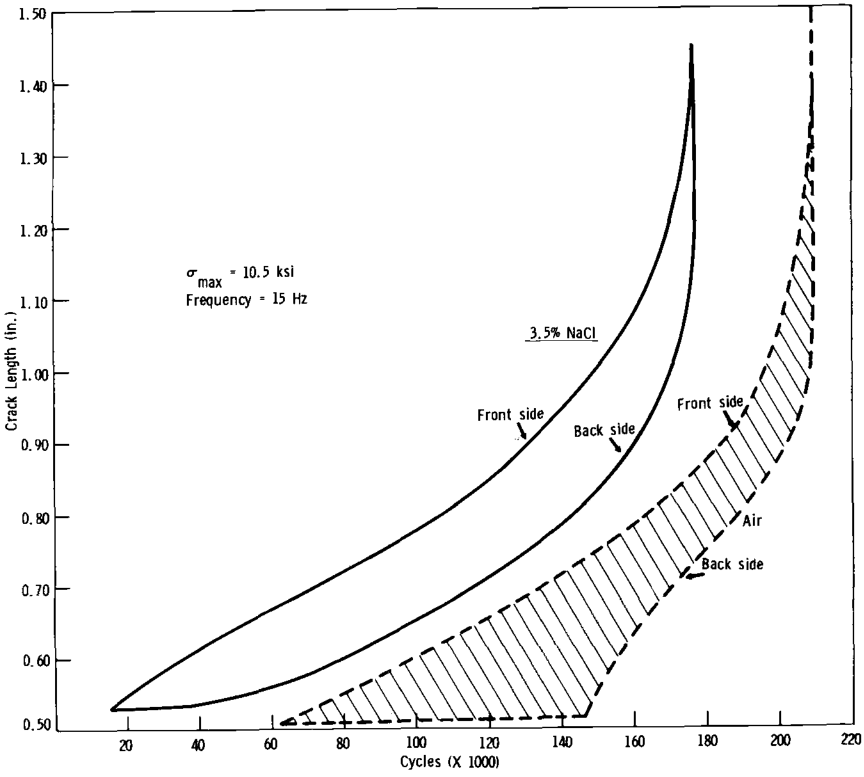

FIG. 3—*The influence of 3.5 percent NaCl environment on crack growth characteristics (σ_{min} = 3 ksi). Crack growth data obtained in air taken from Ref 5.*

seen on the hard side where the projectile first impacts, while spalling damage is present on the softer, backup side. Of the two specimens tested, one failed after 4.9 × 10^6 cycles and the other lasted 5.0 × 10^6 without failure. This is approximately 10 times the life of the center notched panel tested under the similar conditions. Examination of the specimen which sustained 5.0 × 10^6 cycles in 3.5 percent NaCl without failure reveals that additional cracks, most of them with a directional component perpendicular to the loading axis, are present on the front side as seen in Fig. 6. On the other hand, the soft side, shown in Fig. 7, exhibits no appreciable difference in crack appearance before and after testing. Therefore, with the random orientation of the original ballistically induced cracks on the front side it is not surprising to find that ballistically damaged panels exhibits greater residual life than the center-notched panel. The corrosion fatigue data obtained with the center notched panels thus represent a lower bound to the degradation in residual life due to ballistic damage.

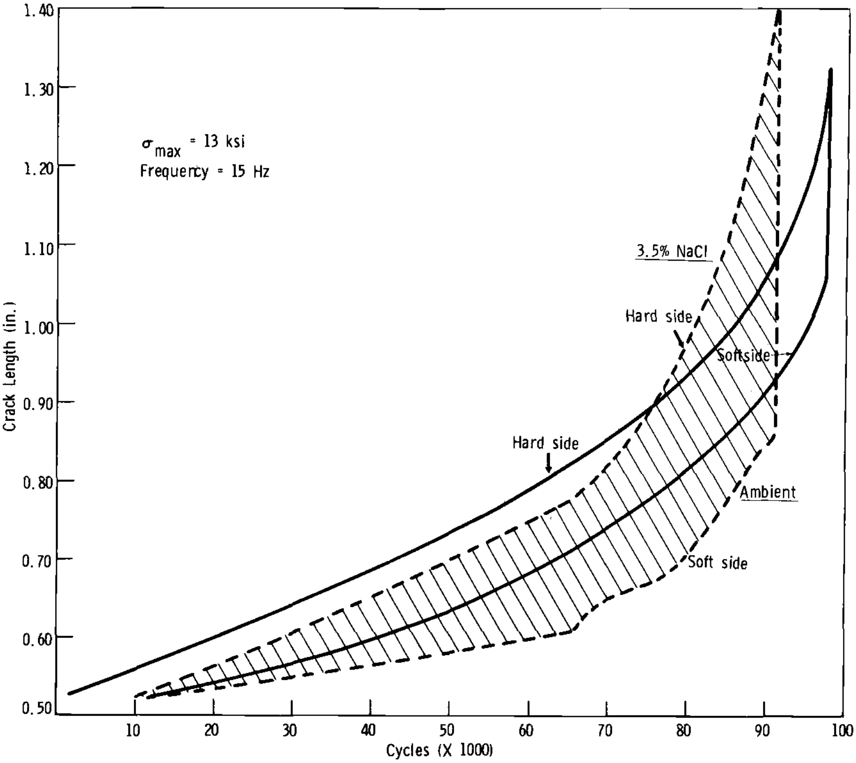

FIG. 4—*The influence of 3.5 percent NaCl environment on crack growth characteristics (σ_{min} = 3 ksi). Crack growth data obtained in air taken from Ref 5.*

Corrosion fatigue effects are also seen in the absence of a machined notch or ballistically induced cracks. *S-N* (maximum cyclic stress versus number of cycles to failure) are shown in Fig. 8 for smooth specimens possessing either the as-received mill surface condition or machine ground surface condition. The effect of testing in H_2O shows up most noticeably with material whose surface finish has been improved by machine grinding. Specifically, a fatigue strength at 10^6 cycles of about 80 ksi (551 MPa) was obtained in air for the machine ground surface, while in H_2O the fatigue strength (10^6 cycles) is about 45 ksi (310 MPa). The rough as-received mill surface condition contains crack initiation sites (Fig. 9) which by themselves lower the fatigue resistance. Therefore, the effect of an H_2O environment on the as-received mill surface condition is much less than it is with the machine ground surface condition.

Stress-Corrosion Cracking

It is also important to give consideration to the residual life of ballistically damaged panels which are subjected to sustained loading in an

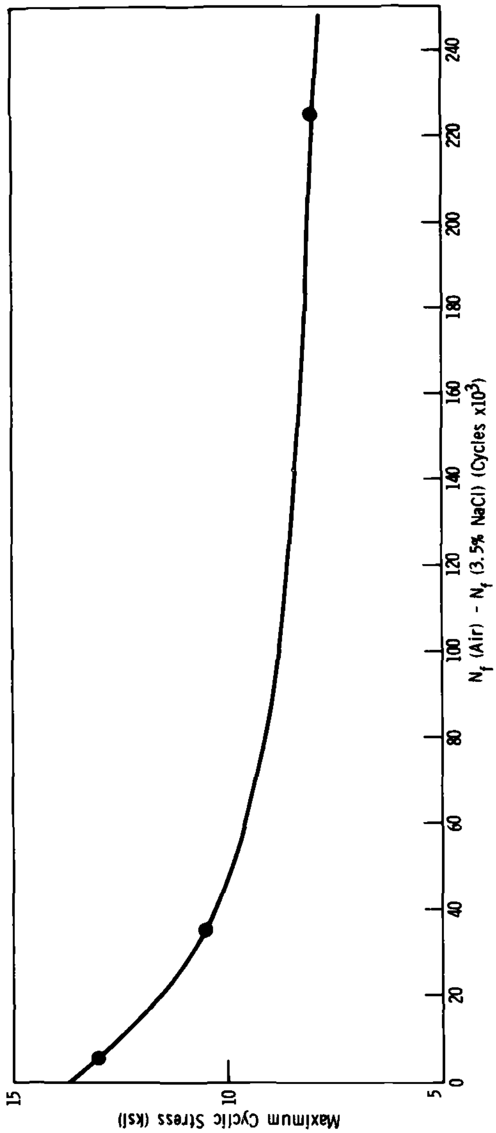

FIG. 5—*The effect of maximum cyclic stress on* N_f *(air)-*N_f *(3.5% NaCl).*

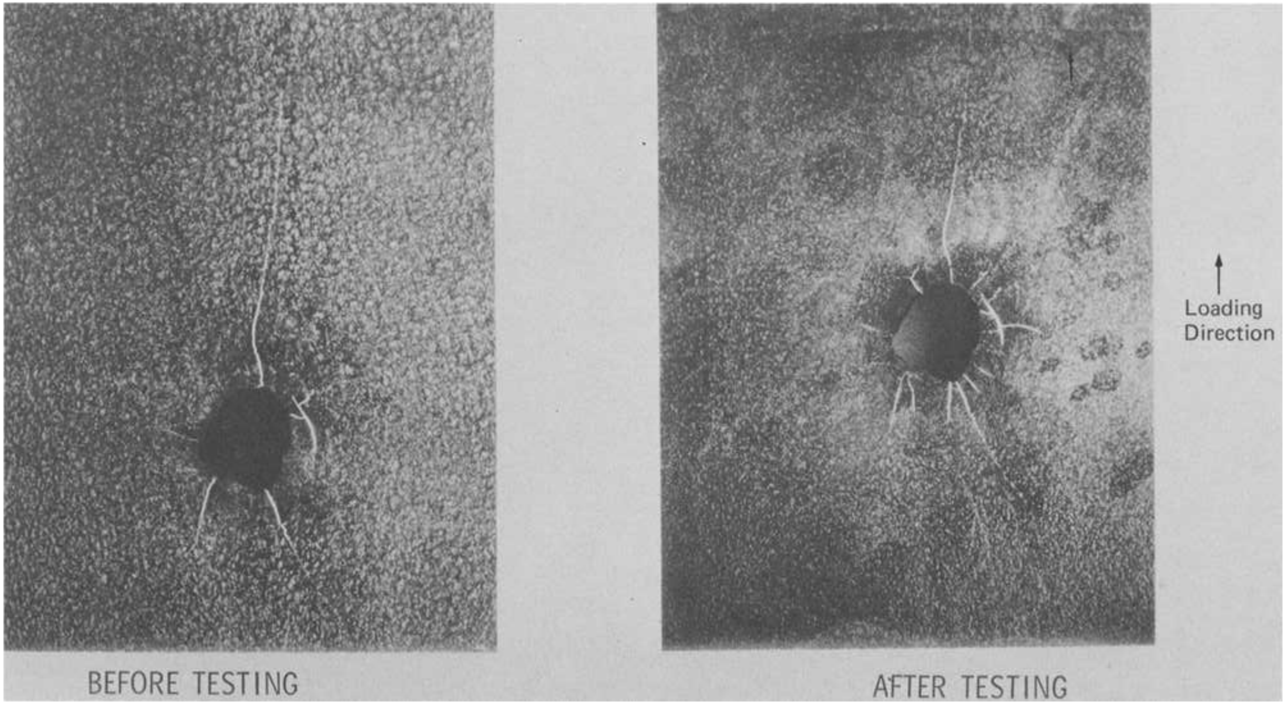

FIG. 6—*Appearance of the front side before and after cycling in 3.5 percent NaCl (approximately ×1).*

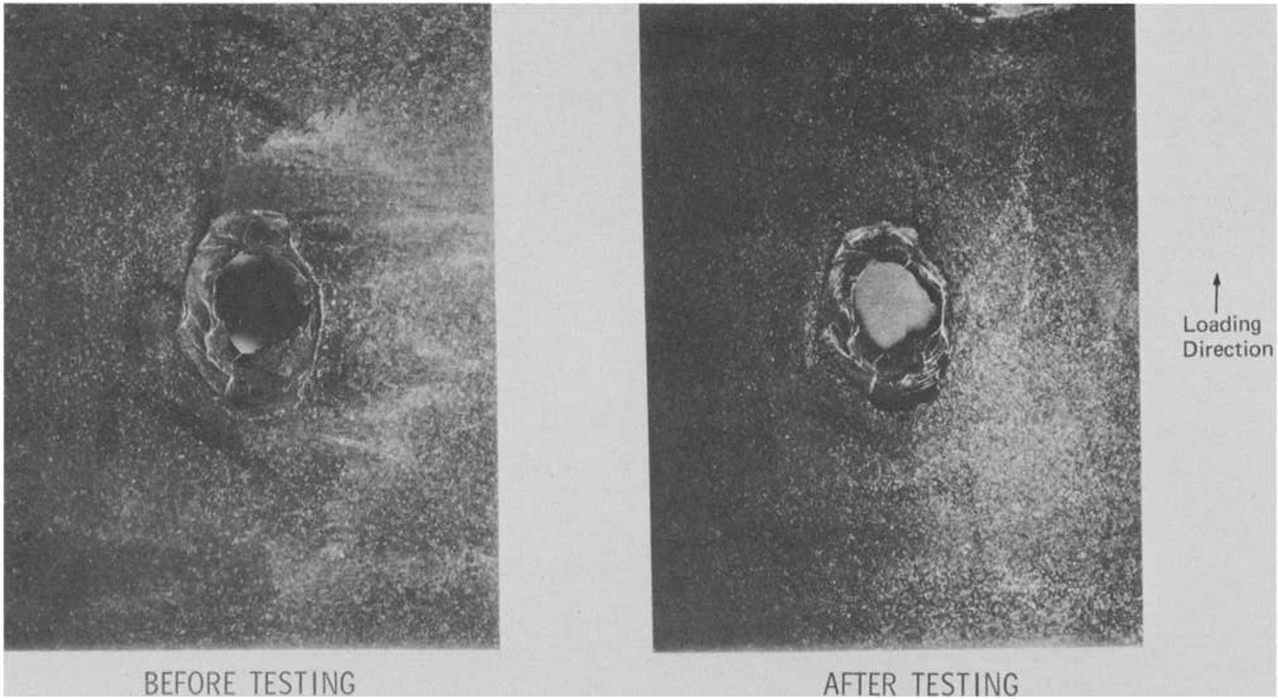

FIG. 7—*Appearance of back side before and after cycling in 3.5 percent NaCl (approximately* ×*1).*

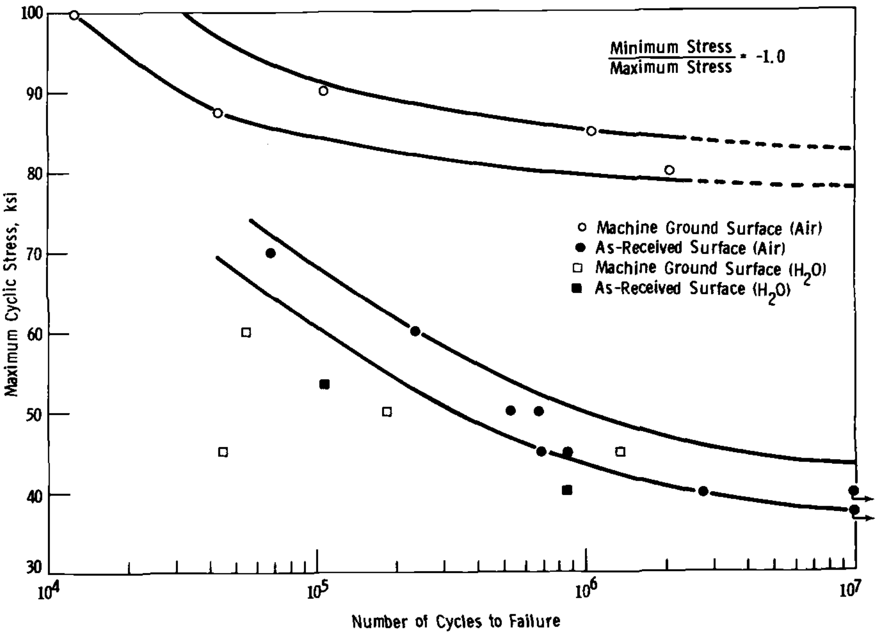

FIG. 8—S-N *fatigue curve showing effect of environment.*

aggressive environment, in this case 3.5 percent NaCl. SCC results for ballistically damaged panels are shown in Fig. 10. While there is considerable scatter in the results, certain observations can be made. First, it is seen that the panels ballistically impacted while under an applied load do not exhibit any greater tendency toward stress-corrosion effects than those impacted without an applied load. Secondly, partial penetration are as detrimental as complete penetrations provided that the projectile velocity is in the vicinity of the V_{50} ballistic limit for both cases. The damage pattern for a partial penetration is shown in Fig. 11. Apparent ballistic damage is limited to the front side where magnetic particle inspection reveals the presence of both radial cracking and logarithmic spiral type cracking. However, examination of ballistically damaged specimens with ultrasonic and acoustical holographic techniques showed the presence of internal damage (delamination) not revealed by magnetic particle inspection [*10*]. Such damage is probably present contributing to the susceptibility of the partially penetrated specimen to stress corrosion. This specimen failed at a stress level of 30 ksi (206 MPa) after 450 min. Tested at the same stress level was a specimen which had undergone complete penetration. As shown in Fig. 12, the complete penetration is accompanied by plugging

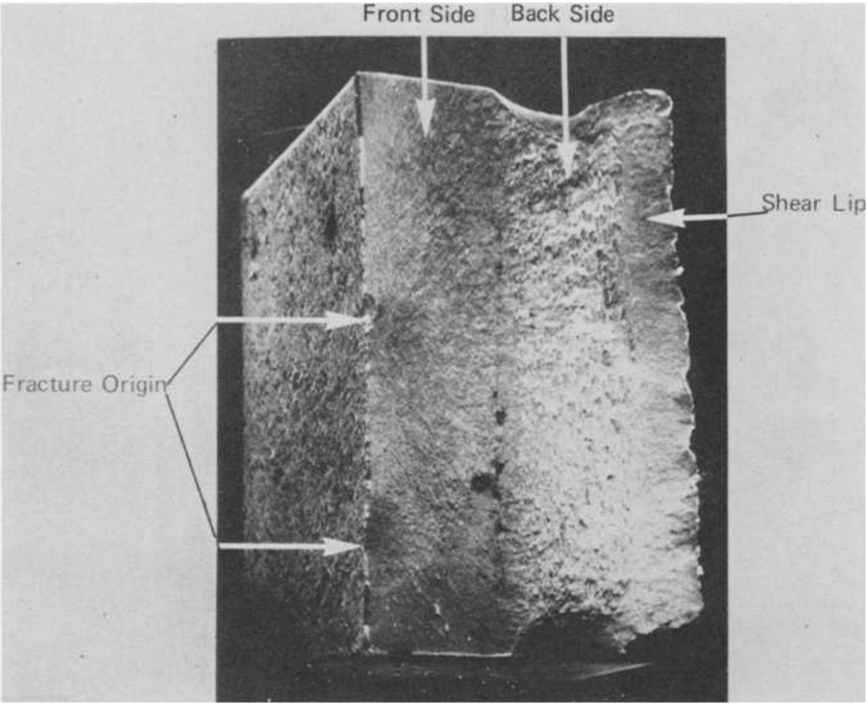

FIG. 9—*Crack initiation on front side (×5.6).*

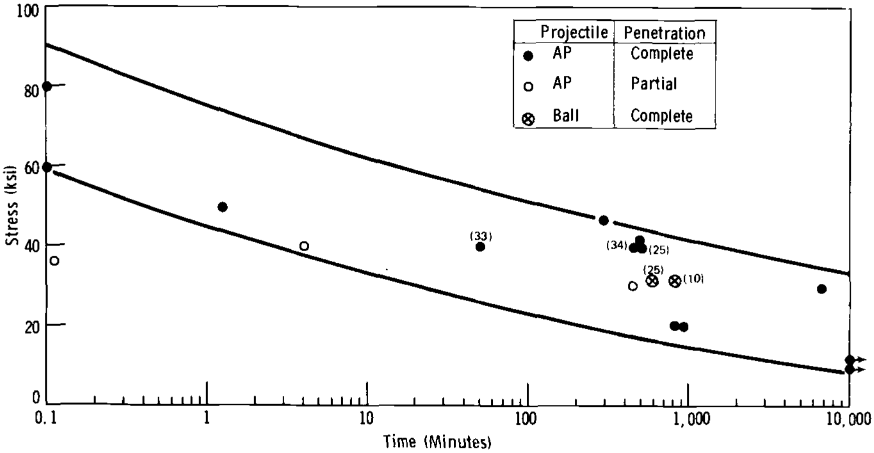

FIG. 10—*Applied stress versus time to failure in 3.5 percent NaCl solution for ballistically impacted laminar composite armor steel (numbers in parentheses refer to the applied stress level at impact).*

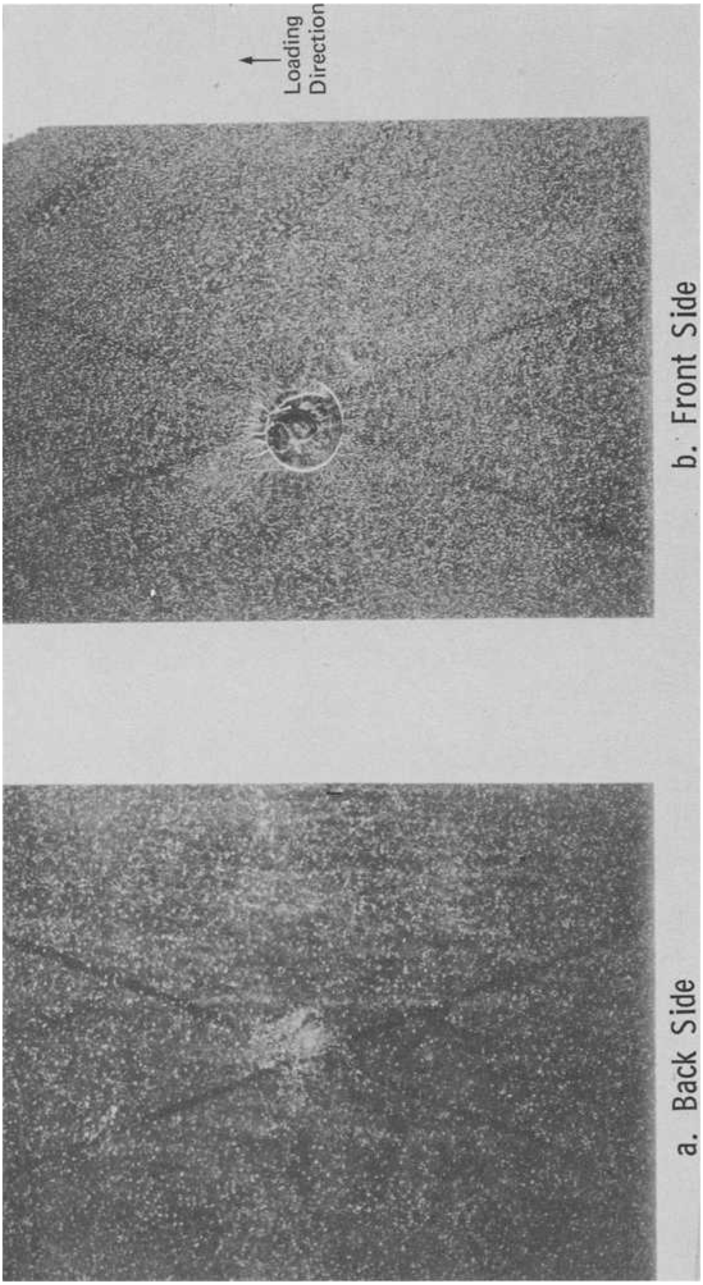

FIG. 11—*Damage due to partial penetration. With an applied stress of 30 ksi, time to failure was 450 min (×1).*

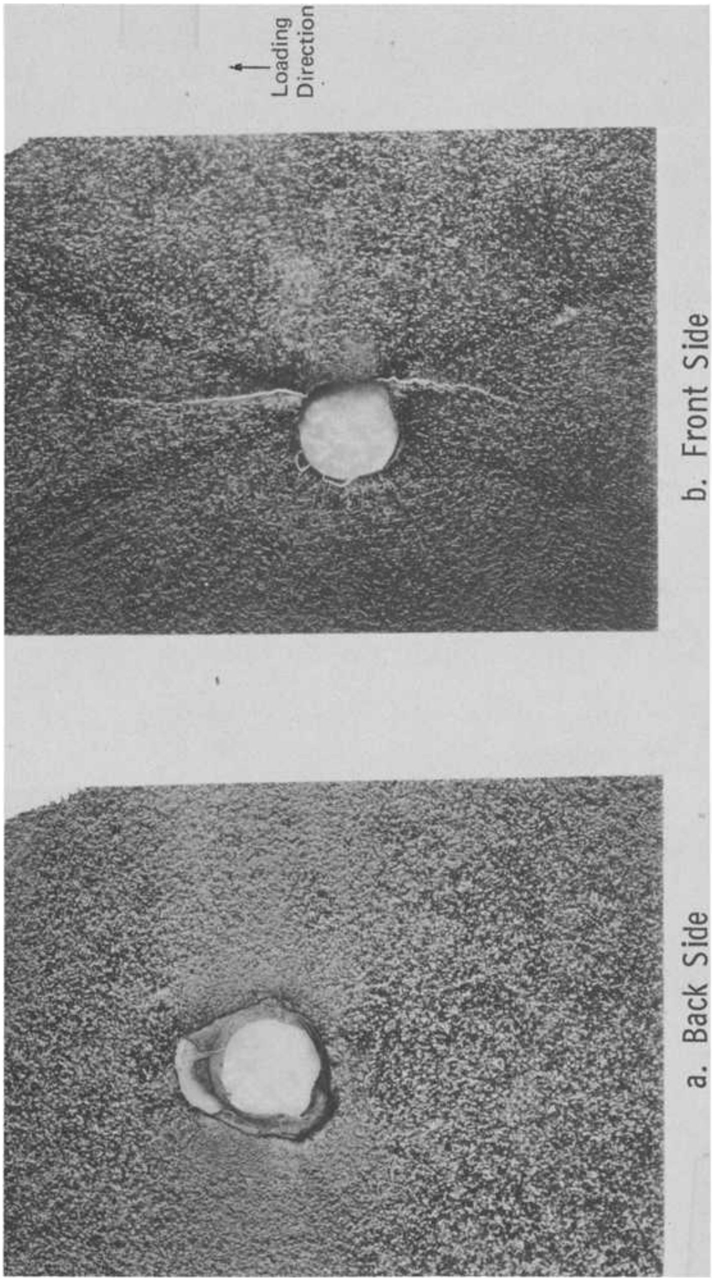

a. Back Side

b. Front Side

FIG. 12—*Damage due to complete penetration. With an applied stress of 30 ksi, time to failure as 5816 min.*

and radial cracking on the hard side while on the softer backup portion back spall is evident. This specimen failed after 5816 min at the same stress level.

It is of interest to calculate an approximate K_{Iscc} value from the data obtained on ballistically damaged panels. It is assumed that the crack that causes failure does not penetrate the thickness since most of the cracks that resulted from ballistic impact were observed on the hard side only. Therefore to obtain an approximate value for the plane-strain stress-intensity facter, K_I, the Irwin equation for a surface crack was utilized [*11*]. This expression is given by

$$K_I^2 = \frac{1.2\sigma^2 a}{\Phi^2 - 0.212(\sigma/\sigma_{ys})^2} \tag{1}$$

where σ and σ_{ys} are the applied stress and yield stress, respectively; a is the crack depth and Φ is an elliptic integral dependent on a/c where $2c$ is the crack length. To obtain c, representative photographs such as those shown in Fig. 12 were examined, and the maximum lateral damage (crack length projected perpendicular to the loading axis) was determined. The value for c was taken as half the maximum lateral damage, while a was assumed to be half the plate thickness. Tests were not conducted beyond 10 000 min, and as a result σ was taken as the maximum stress level below which there was no failure in this time period. With these approximations, K_{Iscc} from Eq 1 is about 6 ksi$\sqrt{\text{in.}}$ (7 MPa$\sqrt{\text{m}}$). This is in satisfactory agreement with K_{Iscc} = ksi$\sqrt{\text{in.}}$ (11 MPa$\sqrt{\text{m}}$) obtained with standard laboratory specimens for the same material tested in 3.5 percent NaCl [7].

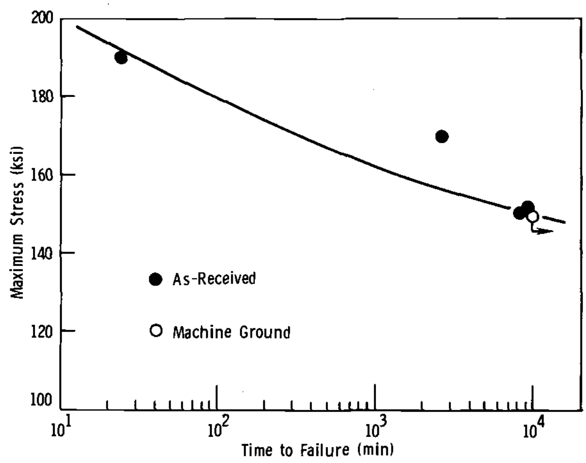

FIG. 13—*Time to failure for smooth specimens of as-received materials in 3.5 percent NaCl environment.*

Smooth specimen for both the as-received, mill surface condition and machine ground surface condition were also tested under sustained loading in 3.5 percent NaCl. The results are shown in Fig. 13. The stress level below which no fracture occurs after approximately 10 000 min is about 60 percent of the ultimate tensile strength determined in air. Although there are limited data, it appears that the machine ground surface offers little improvement in life compared to the as-received mill surface when tested in 3.5 percent NaCl surface. These results are in agreement with similar specimens tested under corrosion fatigue conditions (*cf* Fig. 8). Previous work [*8*] has shown that to improve the corrosion fatigue properties of a machine ground surface a protective coating should be used.

Conclusions

This study has examined the corrosion fatigue and SCC behavior of a high-hardness laminar composite armor steel. The following conclusions can be drawn from this study:

1. Using center-notched panels to study the crack growth behavior, it is shown that difference between total numbers of cycles to failure of the composite in air and in an aggressive environment decreases as the maximum stress increases.
2. Cyclically loaded ballistically damaged panels tested under a corrosive environment exhibited greater stress-corrosion resistance than identically tested center-notched panels. This would indicate that the latter can be used as lower bound to residual life under cyclic loading when designing with a ballistically damaged material.
3. Environmental effects are also seen in the static loading of ballistically damaged panels. Utilizing these specimens, an approximate K_{Iscc} value was obtained which was in satisfactory agreement with that obtained with standard laboratory specimens.
4. Smooth specimens tested under cyclic or static loading are also affected by corrosive environments. This is especially true of machine ground surfaces.

References

[*1*] Sandoz, G. in *Stress Corrosion Cracking in High Strength Steels and in Titanium Aluminum Alloys*, Naval Research Laboratory, Washington, D. C., 1972, p. 79.

[*2*] Mostovoy, S. and Ripling, E. J., "The Feasibility of Using Fracture Mechanics for Evaluating High Hardness Armor Steel," Technical Report No. 10580, U.S. Army Tank Automotive Command, Warren, Mich., June 1969.

[*3*] Hickey, C. F., *Journal of Metals*, Vol. 3, March 1968, p. 3.

[*4*] Anctil, A. A. et al, "Structural Properties of Dual Hardness Steel Armor," Technical Report AMMRC TR-73-6, Army Materials and Mechanics Research Center, Watertown, Mass., Feb. 1973.

[*5*] Anctil, A. A. and Kula, E. B., "Fatigue Crack Propagation in Armor Steels," Technical Report AMMRC TR-69-25, Army Materials and Mechanics Research Center, Watertown, Mass., Nov. 1969.

[*6*] Chait, R., Hickey, C. F., and Curll, C. H. in *Fatigue and Fracture Toughness—Cryogenic Behavior, ASTM STP 556,* American Society for Testing and Materials, 1974, p. 68.

[*7*] Lum, P. T., Chait, R., and Hickey, C. F., *Metallurgical Transactions,* Vol. 6A, 1975, p. 5.

[*8*] Chait, R. and Curll, C. H., "Mechanical Behavior of Ballistically Damaged and Undamaged Laminar Composite Armor Steel," Technical Report AMMRC TR-73-59, Army Materials and Mechanics Research Center, Watertown, Mass., Dec. 1973.

[*9*] Abbott, K. H., "Ballistic Acceptance Testing of Armor," Technical Report AMMRC SP-70-6, Army Materials and Mechanics Research Center, Watertown, Mass., Aug. 1970.

[*10*] Chait, R. and DerBoghosian, S., "NDT Evaluation of Ballistically Impacted Laminar Composite Armor Steel," Technical Report AMMRC TR-73-37, Army Materials and Mechanics Research Center, Watertown, Mass., Aug. 1973.

[*11*] Irwin, G. R., *Journal of Applied Mechanics,* Dec. 1962, p. 651.

Edward Taylor[1]

Stress-Corrosion Cracking Evaluation of Aerospace Bolting Alloys

---

REFERENCE: Taylor, Edward, "**Stress Corrosion Cracking Evaluation of Aerospace Bolting Alloys,**" *Stress Corrosion—New Approaches, ASTM STP 610,* American Society for Testing and Materials, 1976, pp. 243–251.

ABSTRACT: The susceptibility of aerospace bolting alloys to stress-corrosion cracking has been of continuing interest especially since strength levels have by far exceeded 200 000 psi, the threshold above which failures are much more common. The search for a stress corrosion resistant material has progressed through a number of alloys with strength levels up to 300 000 psi.

All of the high-strength steel alloys exhibted a similar trend where time to failure decreases as strength level increases. However, different levels of immunity were observed for the different alloys. Martensitic stainless steels were found to be much more resistant to stress-corrosion cracking but were very sensitive to hydrogen embrittlement from plating or galvanic corrosion reactions.

The use of a MIL-STD-1312 test procedure to evaluate coated or plated alloy steel bolts is sanctioned because of the short time to failure required, the reproducibility of results, and the duplication of service failures. The same is not true for the more resistant alloys where times to failure are in thousands of hours and results are scattered. A more aggressive test is warranted.

Crevice corrosion and pitting at interfaces are the most common initiators of stress-corrosion cracking failures for high-strength fasteners. Since this is unavoidable with fastened joints, it behooves the consumer to realize all of the advantages and disadvantages of various materials so that he may select the best one for his needs.

KEY WORDS: stress corrosion, coatings, high strength steels, bolts, environmental tests, corrosion, electroplating, pitting, crack propagation, corrosion resistant alloys

The susceptibility of aerospace bolting alloys to stress-corrosion cracking (SCC) has been of continuing interest to Standard Pressed Steel Company especially since strength levels have exceeded 200 ksi, the threshold above which failures are much more common. In the early part of 1965, an investigation began in the laboratory which resulted in many company

---

[1] Corrosion engineer, Standard Pressed Steel Co., Jenkintown, Pa. 19046.

reports, presentations, and published papers. Two previous publications by the American Society for Testing and Materials[2,3] are concerned with the test method employed, the effect of bolt processing, and the effect of protective coatings.

The search for a bolt material which is resistant to SCC has progressed through a number of different alloys with strength levels up to 300 000 psi. A search for the best protective coating system led to diffused nickel cadmium, SermeTel W, and eventually to nickel plus SermeTel W[3]. Concurrently, investigation of the martensitic precipitation hardening stainless steels was being pursued as well as the high-nickel alloys with high-strength properties. These alloys resist rusting without the need for protective coating systems. Times to failure for these alloys in an alternate immersion stress-corrosion test are measured in thousands of hours compared to the hundreds of hours reached by cadmium plated ultrahigh-strength alloy steel bolts.

Two of the alloys evaluated in this program have never exhibited failures, even after many thousands of hours of testing. These alloys seem to be immune to SCC. Some alloys exhibit failures in 100 h or less, indicating a very low tolerance to corrosion induced cracking.

Alternate Immersion Test Method

Bolt specimens were stressed by torque with nuts after passing them through fixtures such as that shown in Fig. 1, whose dimensions are specified in MIL-STD-1312, Test 9. These fixtures, called cylinders, usually were made of the same material as the bolt and were heat treated to the same strength level. In the case of corrosion resistant alloys, the cylinders are sometimes made from 6Al-4V titanium, which is generally available in diameters large enough for them. When alloy steels were tested, H-11 cylinders usually were used, but with a vinyl coating to prevent general corrosion of the exposed surfaces.

The bolts were end-drilled so that a supermicrometer could be used to measure bolt elongation as the nut was torqued to increase the load. Normally, 75 percent of the actual ultimate tensile strength is applied according to the requirements of MIL-STD-1312. Occasionally, 90 or 100 percent of the bolt's proportional limit is selected as the applied load. These values were chosen because of the susceptibility of bare H-11 bolts to cracking in a previous study.[2]

---

[2] Lin, C. S., Laurilliard, J. J., and Hood, A. C. in *Stress Corrosion Testing, ASTM STP 425,* American Society for Testing and Materials, 1967, pp. 84–98.

[3] Taylor, E. in *Stress Corrosion Cracking of Metals—A State of the Art, ASTM STP 518,* American Society for Testing and Materials, 1972, pp. 131–138.

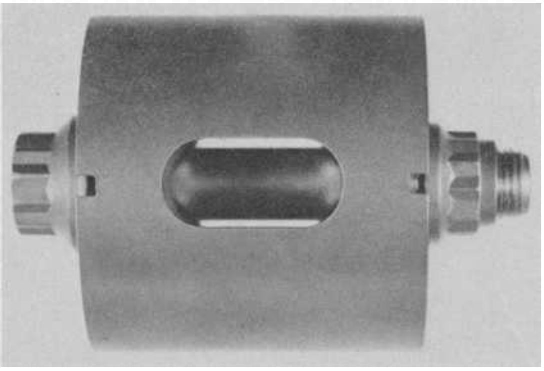

FIG. 1—*Alternate immersion specimen.*

The assembled specimens were submerged for 10 min of each hour in a 3.5 percent sodium chloride (NaCl) solution and were suspended in dry moving air the remainder of the time. This cycle was repeated until broken pieces were noticed or until the specified test period was finished. The solution was changed daily, except for weekends, and no dissimilar assemblies were exposed in the same container. A restraining enclosure was constructed with perforated expanded metal to house the test facility so that cracking bolts did not endanger nearby personnel.

Simulated Service Environment Test Method

Bolt specimens were stressed by torque with nuts after passing them through aluminum plate whose noncritical dimensions allowed a clearance fit. The bolts were end-drilled so that their elongation could be measured as a function of load. After dipping or swabbing the bolts with a 3½ percent NaCl solution, they were tightened to 75 percent of their actual ultimate tensile strength. The assembled specimen was observed over a 100-h period after which the bolt was removed, reswabbed, and reassembled to accumulate an additional 100 h of exposure at room temperature. This procedure was repeated until failure of the bolt or cessation of the test. Figure 2 shows the specimen configuration.

Results

The compositions of the alloys tested are shown in Table 1.

In the alternate immersion test, all of the high-strength steel alloys ex-

TABLE 1—*Alloy composition.*

	C	Mn	P	S	Si	Ni	Cr	Mo	V	Co	Al	Ti	B	Zr	Ca	Cu	Cb and Ta	N	Fe
Maraging 300	0.02	0.04	0.005	0.008	0.006	18.95	...	4.96	...	9.09	0.15	0.66	0.005	0.010	0.05	...	...	...	balance
8740	0.42	0.99	0.009	0.011	0.33	0.56	0.53	0.27	...	...	...	...	...	...	...	...	...	...	balance
4037	0.38	0.81	0.011	0.014	0.25	...	...	0.21	...	...	...	...	...	...	...	...	...	...	balance
4340	0.40	0.72	0.013	0.013	0.27	1.69	0.75	0.22	...	...	...	...	...	...	...	...	...	...	balance
H-11	0.40	0.29	0.006	0.012	1.00	...	5.11	1.33	0.56	...	...	...	...	...	...	...	...	...	balance
PH13-8 Mo	0.05	0.1	...	...	0.1	8.0	12.8	2.25	...	...	1.15	...	...	...	...	...	...	0.01	balance
Custom 455	0.03	0.50	...	...	0.50	7.0 10.0	11.0 13.0	...	...	...	...	0.90 1.40	0.005	...	...	1.00 3.00	0.25 0.50	...	balance
MP35N	0.025	0.15	0.015	0.010	0.15	35	20	10	...	balance	...	1.00	...	...	...	...	...	...	1.00
MP159	0.04	0.2	0.02	0.010	0.2	balance	19.0	7.0	...	35.7	0.2	3.0	...	...	...	...	0.6	...	9.0
Inconel 718	0.08	0.35	0.015	0.015	0.35	52.5	19.0	3.0	...	1.0	0.5	1.0	0.006	...	...	0.30	5.0	...	balance

NOTE—The alloys are listed in order of appearance in the report tables.

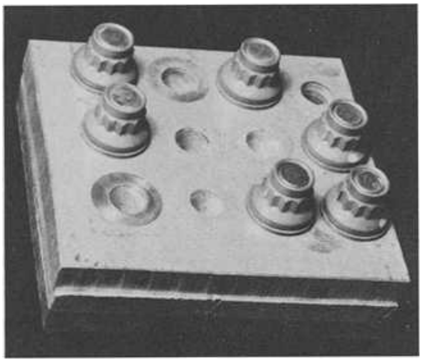

FIG. 2—*Simulated service environment specimen.*

hibited the same trend where time to failure decreases as strength level increases, as shown in Table 2. Failures were generally in the bolt shank near the cylinder window where crevice corrosion was observed.

Of the alloy steels, the Maraging 300 steel did not fail at strength levels of 260 ksi and below, whereas 8740 and 4037 steel did not fail at a strength level of 215 ksi or below. No failures of 4340 steel occurred at 205 ksi or lower, and H-11 steel did not fail at 170 ksi or below. Of the corrosion resistant alloys tested, PH13-8Mo failed after fairly short times in some tests but also exhibited long life without failure in others. Custom 455 failures occurred after fairly long times with good repeatability. MP35N[4] and MP159[4], members of the MULTIPHASE[4] alloy family showed no failures after 5000 h at 270 and 280 ksi strength levels, as shown in Table 2.

In the simulated service environment test, the failure of Maraging 300 steel bolts occurred after slightly more than 100 h with an intergranular mode of attack. Bolts made of PH13-8Mo alloy also failed by this test method after as little as 66 h.

These specimens exhibited a brittle fracture surface indicative of hydrogen embrittlement. Subsequent tests with Custom 455, Inconel 718, MP35N, and MP159 alloy bolts revealed no failures after exposures of 1000 to 2900 h in the simulated service test. These results are tabulated in Table 3.

---

[4] Trademark of Standard Pressed Steel Co.

TABLE 2—*Stress-corrosion cracking results using MIL-STD-1312 test method.*

Strength Level, ksi	MP35N	MP159	Maraging 300	PH13-8 Mo	Custom 455	8740	4037	4340	H-11
305								36 ± 52	
300			324 ± 296			19 ± 5			132 ± 53
295			1432 ± 1047						698 ± 55
290						307,1011 NF, 1967 NF	198 ± 16		
285						406 ± 193			
280	5012 NF (2 pieces)	5000 NF (5 pieces)	339 ± 179					147 ± 81	6 ± 8
275	2499 NF (5 pieces)								
270						214 ± 153		196 ± 75	216 ± 45
265									
260			1030 NF, 1054 NF 1127 NF			161 ± 146	723 ± 699	176 ± 154	215 ± 241
255									
250			2145 NF (3 pieces)			346 ± 199			123 ± 36
245							3617, 2145 NF 4834 NF		
240			1030 NF (2 pieces) 1127 NF						1708 NF
235									

230							
225		1131,1140,3099 2615 NF (2 pieces) 6534 NF, 5014 NF (5 pieces)	2316,2318 2735 2615 NF (2 pieces) 2338 NF (2 pieces)		615, 2809 NF	1530 ± 662	593 ± 528
220	1438 NF, 1440 NF						
215				5326 NF (5 pieces)	5326 NF (5 pieces)	3189 NF, 4673 NF (3 pieces)	
210				1207 NF, 1842 NF, 1945 NF	2809 NF, (2 pieces)	208 ± 8	151, 1343 NF (2 pieces)
205				4125 NF (2 pieces) 5059 NF (3 pieces)		5059 NF (5 pieces)	
200					1127 NF, 1460 NF, 1842 NF		1708 NF
195							
190							
185					2809 NF		822 ± 100
180						1153 NF, 1438 NF	
175							
170				1004 NF (2 pieces)			5472 NF (5 pieces)

NOTE—NF means no failure.
No failures were observed below the strength level indicated by the horizontal line.

TABLE 3—*Simulated service environment test results, hours to failure for alloys shown.*

Alloy	Strength Level, ksi	Time, h
Maraging 300	300	110, 110, 110, 132
PH13-8 Mo	230	66, 137, 137, 137, 217
Custom 455	230	1800 NF (3 pieces)
Inconel 718	230	2900 NF (3 pieces)
MP35N	270	1000 NF (5 pieces)
MP159	280	1000 NF (5 pieces)

NOTES—NF means no failure.
All bolts loaded to 75 percent actual ultimate tensile strength.

Discussion

The use of the alternate immersion test as set forth in MIL-STD-1312 to screen alloys and coatings is worth the effort because of the ability to duplicate service failures of high-strength bare-alloy steel bolts in little over 100 h and coated-alloy steel bolts after slightly longer times. The simplicity of the procedure lends itself to many laboratories. However, corrosion resistant alloys normally will not fail before 1000 h and may last 5000 h or more. Therefore, a more aggressive test is required in order to rank them.[5] The use of the simulated service environment test provides a condition observed in aerospace applications. Aluminum skin and structure are fastened normally with various bolting alloys which are not galvanically compatible. Thus, electrochemical reactions can occur which cause the generation of hydrogen and oxygen in localized areas. Cracking can be caused by direct hydrogen embrittlement or hydrogen assisted stress corrosion, initiated by crevice attack and pitting.

From the experience gained in conducting a SCC test program, the most common cause of intergranular cracking failure was deep pitting, initiated by crevice corrosion at interfaces. The same kind of attack has been observed in field failures. Since fasteners have unavoidable interfaces with highly stressed areas, it is inevitable that a material susceptible to crevice attack will ultimately fail because of it. Therefore, it behooves the designer to be aware of the advantages and disadvantages of various materials so that he may select carefully according to his needs.

Experience with coatings on fasteners has shown that sacrificiality is preferable to nobility because of the threat of small breaks or cuts in the surface. A thin noble coating is expected to cause intense and rapid galvanic attack of the substrate because of holidays and porosity. Barrier

---

[5] Dull, D. L. and Raymond, L., *Corrosion*, Vol. 29, No. 5, May 1973.

coatings in the low thickness range, normally dictated by fastener thread requirements, do not provide sufficient pore-free protection to be considered effective. A barrier coating thickness in excess of 0.5 mil can prevent corrosion successfully, if applied properly and resistant to mechanical abuse.

The best solution to longer life for aerospace bolts is by the use of corrosion resistant alloys requiring no protective coating system. Precipitation hardening stainless steels at high-strength levels provide at least 1000 h of alternate immersion test time before cracking failures are recorded. These cracking failures usually are initiated by pitting attack and crevice corrosion.

MP35N and MP159 alloys at the 260 ksi bolting strength level did not exhibit any form of corrosion attack nor did they crack even after 5000 h of alternate immersion testing. Neither alloy is susceptible to crevice corrosion as determined by immersion in 10 percent ferric chloride ($FeCl_3$) solution at room temperature.[6]

Although resistance to SCC is of paramount importance to a bolt's function, there are other properties which are just as important for aerospace applications. For example, even though a material may be resistant to SCC, it is not necessarily resistant to hydrogen embrittlement from cleaning, electroplating, or corrosion. With respect to hydrogen embrittlement, the results of the simulated service environment test strongly indicated the susceptibility of the PH13-8Mo-alloy. Subsequent work with notched specimens showed that hydrogen from plating or charging could severely embrittle the alloy.[6] More recently, the same alloy was shown to be extremely susceptible to both SCC and hydrogen embrittlement when tested more aggressively with an electrochemical method.[4]

Thus, the criteria for selecting bolt alloys should be based on a standardized test method where the cause of faliure may be from SCC or hydrogen embrittlement, depending on the choice of the clamped up aerospace structure in the actual application. Sufficient incubation time should be allowed for crevice corrosion to promote pitting and subsequent fracture so that a relative performance can be easily comprehended. Actual hardware should be used which may show inherent weaknesses due to manufacturing procedures in a particular area.

Acknowledgments

I wish to thank the many people who contributed to this work: in particular, R. A. Hibbert for diligent experimental efforts; C. S. Lin, J. J. Laurilliard, and C. J. Keeney, Jr., for helpful studies; K. M. Kulju for relevant discussions; R. A. Walker and R. L. Sproat for technical support; C. Floros for manuscript services.

---

[6] Patel, S. and Taylor, E., *Metal Progress*, Vol. 100, No. 3, Sept. 1971.

R. S. Kaneko[1] *and R. F. Simenz*[1]

Corrosion Thresholds for Interference Fit Fasteners and Cold-Worked Holes

---

REFERENCE: Kaneko, R. S. and Simenz, R. F., "**Corrosion Thresholds for Interference Fit Fasteners and Cold-Worked Holes,**" *Stress Corrosion—New Approaches, ASTM STP 610,* American Society for Testing and Materials, 1976, pp. 252–266.

ABSTRACT: Empirical relationships were obtained between fastener interference or hole expansion and the stress-corrosion thresholds of aluminum alloys. Tensile and stress-corrosion threshold properties were determined for single heats of 2024-T3, 7075-T6, 7075-T76, and 7050-T76 extruded bar used in the studies. The various fastener and hole expansion systems, with a range of interference levels to over 10 mils, were installed in the principal grain directions of each alloy. Specimens were subjected to 3.5 percent sodium chloride alternate immersion and seacoast exposures, then analyzed by visual and metallographic techniques.

The residual tensile stresses created around the holes appeared to rise sharply with increasing amounts of interference, approaching a theoretical limit. Even low interference fits of a few mils caused stress corrosion under the more susceptible conditions. Crack initiation tended to occur further from the hole as interference increased; wet sealant installation helped to reduce galvanic reactions in the vicinity of the hole. Estimated stress corrosion potential over a range of interference fits in aluminum alloys is presented.

KEY WORDS: stress corrosion, aluminum alloys, fasteners, cold worked holes, residual stress, metallographic examination

The fatigue life improvement of a mechanically fastened joint is accomplished essentially by changes in three basic parameters [*1*][2]:

1. Reducing the peak applied tensile stress by imparting an opposing residual compressive stress in the material.
2. Reducing the magnitude of the fluctuating stress by imparting a residual hoop tensile stress in the material which is the unloaded state of stress.

---

[1] Development engineer and group engineer, respectively, Materials and Processes, Lockheed-California Company, Burbank, Calif. 91520.

[2] The italic numbers in brackets refer to the list of references appended to this paper.

3. Reducing the concentration of stress that occurs at notches (fastener holes) and other geometric discontinuities.

Successful methods for improving the fatigue life of fastened joints largely involve cold working the fastener holes prior to installation or installing interference fitted fasteners. Examples of these effects are shown in Fig. 1. Stress analyses show that these procedures result in residual compressive and tensile stresses around the holes, and the hoop tensile stresses may be considerably higher than the stress-corrosion threshold stresses for many materials [*2*]. The fastened joint or structure thereby is rendered susceptible to stress-corrosion cracking (SCC) and failure.

Tests generally indicate that interference fit fasteners and hole expansion procedures can cause SCC in highly susceptible materials and grain directions, but the effects over a range of conditions are not well defined [*3,4*]. Protective measures such as shot peening, wet sealant installation, and paint or sealant overcoating may be only partially successful.

A desirable means of preventing SCC around interference fit holes is to keep the residual stresses below the stress-corrosion threshold. This can be approached by knowing the approximate stresses produced by each fastener system or hole conditioning process, and knowing the stress-corrosion threshold characteristics of the structural materials in the joint.

Several representative aircraft aluminum alloys, including a new candidate, were chosen to provide varying degrees of stress-corrosion resistance. It is well known that the degree of resistance to stress corrosion exhibited by a given aluminum alloy product and temper varies from lot to lot. Therefore, emphasis was placed on a thorough characterization of the stress-corrosion behavior of the test materials. The various interference fit and hole expansion systems were tested in these materials under accelerated corrosion and seacoast exposures. Stress-corrosion performance was analyzed to correlate the amount of intereference with the threshold properties of the aluminum materials.

Procedure

Characterization of Aluminum Alloys

Extruded 2024-T3511, 7075-T6510, 7075-T76510, 2.0 in. (51 mm) thick by 5.0 in. (127 mm) wide, and 7050-T76510, 1.5 in. (38 mm) thick by 6.0 in. (152 mm) wide, were chosen to obtain a variance in thresholds. A single heat of each alloy was evaluated for grain structure, tensile properties, conductivity, stress-corrosion threshold stresses in the principal grain directions, and also by stress-corrosion crack growth tests on double cantilever beam (DCB) specimens.

Smooth Specimen Alternate Immersion (AI) Stress-Corrosion Tests—Groups of ⅛-in. (3.2-mm) diameter tension specimens from each material

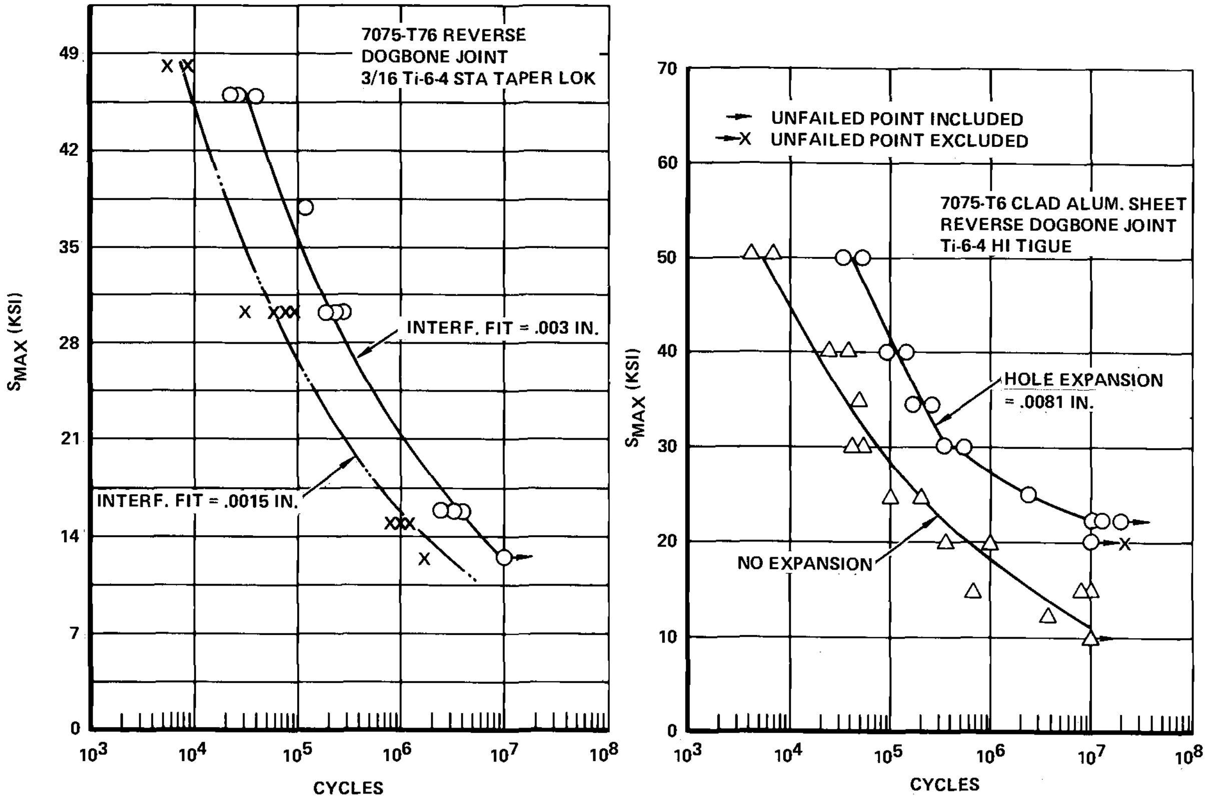

FIG. 1—*Effects of amount of interference fit and hole expansion on fatigue life of joints.*

were stressed in constant deformation type fixtures at different levels to determine approximate threshold values in the short transverse (S), long transverse (T), and longitudinal (L) directions. Test cycles consisted of 10-min immersion in 3.5 percent sodium chloride (NaCl) solution and 50-min air drying each hour, conforming with procedures of FED-STD-151b, Method 823. Test durations were to failure or a maximum of 60 days; the specimens were checked daily. Selected failures were metallographically examined for failure modes.

Stress-Corrosion Crack Growth Tests—SCC susceptibility was also investigated with precracked DCB specimens similar to types used by Boeing and Alcoa [*5,6*]. Specimens were tension precracked by bolt loading to pop-in(s). With bolt end upright, several drops of 3.5 percent NaCl and distilled water solution were placed into the groove three times a day. Crack growth and corresponding deflection (crack opening displacement) were monitored on both sides of the specimens. Specimen orientation was S-L.

Experimental difficulties encountered include crack length measurement (surface corrosion and roughness, surface-subsurface differences, obscure or multiple cracks, branching, symmetry between sides), unknown load increase by corrosion buildup in the crack (especially 2024-T3), and plastic deformation of crack-tip in tension precracking. The calculated K_Q (initial) were high when compared to published values measured on compact tension specimens.

Stress intensity values were calculated from the formula

$$K_I = \frac{vEh[3h(a + 0.6h)^2 + h^3]^{1/2}}{4[(a + 0.6h)^3 + h^2a]} \tag{1}$$

where

v = total deflection of the two arms at the load point (bolt ℄), avg;
E = modulus of elasticity (10.4 × 10^6 psi (71.7 × 10^3 MPa) used for all alloys);
h = ½ specimen height; and
a = crack length from load point, avg.

Residual stress intensity was also determined by measuring the residual load and crack lengths along the fracture face at completion of the test. Stress intensities were computed with the following equation

$$K_I = \left[\frac{P^2}{2b}\left\{\frac{8}{bh^3}\,[3(a + 0.6h)^2 + h^2]\right\}\right]^{1/2} \tag{2}$$

where

P = load,
b = specimen thickness,
h = ½ specimen height, and
a = crack length from load point, avg.

Fastener and Hole Expansion Stress Corrosion Tests

Specimens—Specimens were machined from the extruded bar stock so that holes passed through short transverse-longitudinal, short transverse-long transverse, and long transverse-longitudinal planes (Fig. 2). All holes were a nominal $\frac{3}{16}$ in. (4.8 mm) diameter and $\frac{3}{8}$ in. (9.5 mm) deep. Edge distance and hole spacing were about $2D$ and $4D$, respectively (D = hole diameter). The specimens were sulfuric acid anodized before hole drilling in order to minimize general surface corrosion during exposure. Titanium and steel interference fasteners, aluminum rivets, and plain holes were tested. Expanded holes and solid sleeve expansion were accomplished with special tapered mandrels; the original expansion was 3 to 5 mils (0.08 to 0.13 mm) over the residual (net) interference shown herein. In most cases, duplicate specimens were made in each alloy for accelerated and seacoast exposure. An additional variable was the use of both wet sealant and dry installation.

Environmental Exposures—The 3.5 percent NaCl AI cycling was conducted as previously described, for 60 days. All specimens were checked

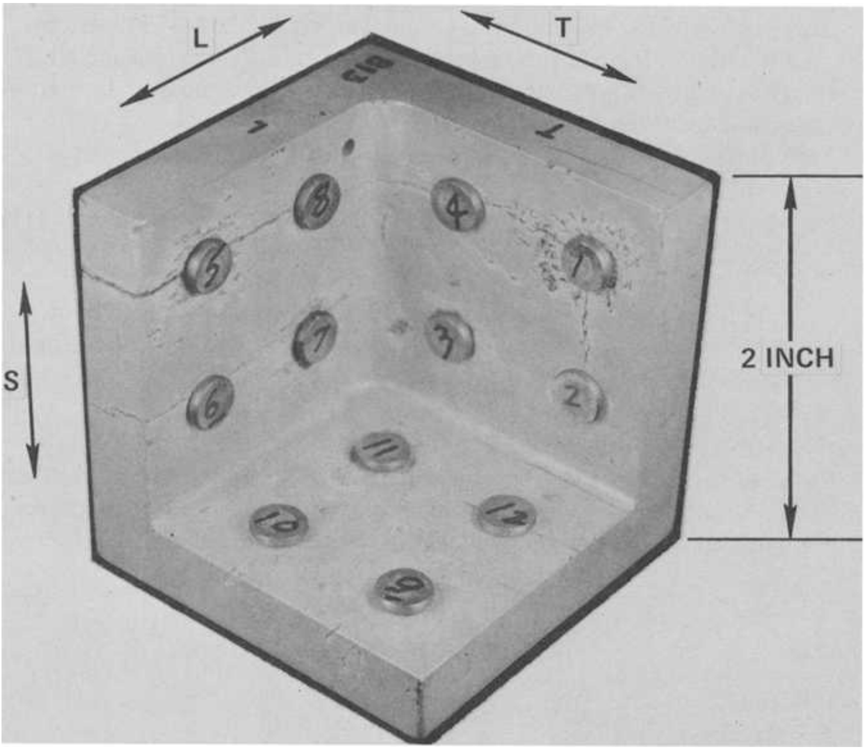

FIG. 2—*Interference fit stress-corrosion specimen after 60 days Al 7075-T6.*

visually under low magnification during the test period without removing corrosion products. After exposure, the specimens were cleaned and then visually and metallographically surveyed to evaluate stress-corrosion behavior. Specimen rivets were removed to verify interference levels. Seacoast exposure is in progress at the Lockheed test site at Point Loma, San Diego, California.

Results

Characterization of Aluminum Alloys

Tensile Properties—Table 1 gives results of tension tests and conductivity measurements. The properties were considered typical for the various alloys.

TABLE 1—*Tension test results of aluminum alloy extruded bar, ⅛-in. (3.2 mm) diameter specimens.*

Alloy-Temper	Electrical Conductivity, % IACS[a]	Grain Direction	F_{tu}, avg, ksi	F_{ty}, avg, ksi	Elongation-½ in., avg. %	Reduction in Area, avg, %
2024-T3	30	S	70.8	47.9	17.0	15.5
2 by 5 in.		L	82.0	58.1	8.0	18.5
7075-T6	33	S	79.9	70.4	7.0	15.5
2 by 5 in.		L	90.6	82.5	6.0	18.5
7050-T76	40	S	81.6	73.2	10.0	20.5
		T	81.9	75.0	11.7	27.5
1.5 by 6 in.		L	86.2	77.0	12.2	36.5
7075-T76	40	S	78.0	64.5	11.0	15.5
2 by 5 in.		L	79.1	70.6	7.5	25.5

[a] IACS = International Annealed Copper Standard.

Grain Structure—Each alloy displayed normal appearing microstructures in which the short transverse structure (most stress corrosion prone) was prominent in the short transverse-longitudinal plane and more equiaxed in the long transverse plane.

Smooth Specimen AI Tests—Threshold determinations are summarized in Fig. 3. The order of increasing resistance to SCC for these heats was concluded as: 2024-T3, 7075-T6, 7050-T76, and 7075-T76. The smooth specimen threshold determination is influenced by length of exposure and interpretation of failure modes. Failures after about 30 days of exposure tended to involve surface pitting and resultant overload.

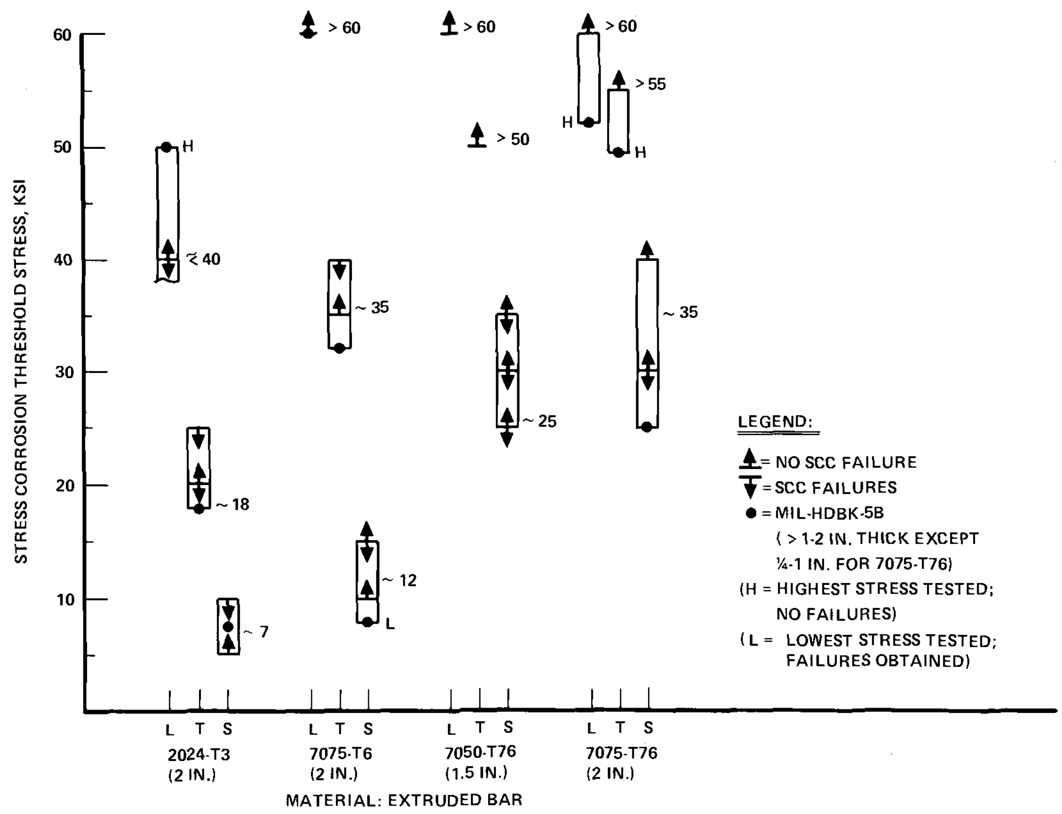

FIG. 3—*Sixty day Al test in 3.5 percent NaCl.*

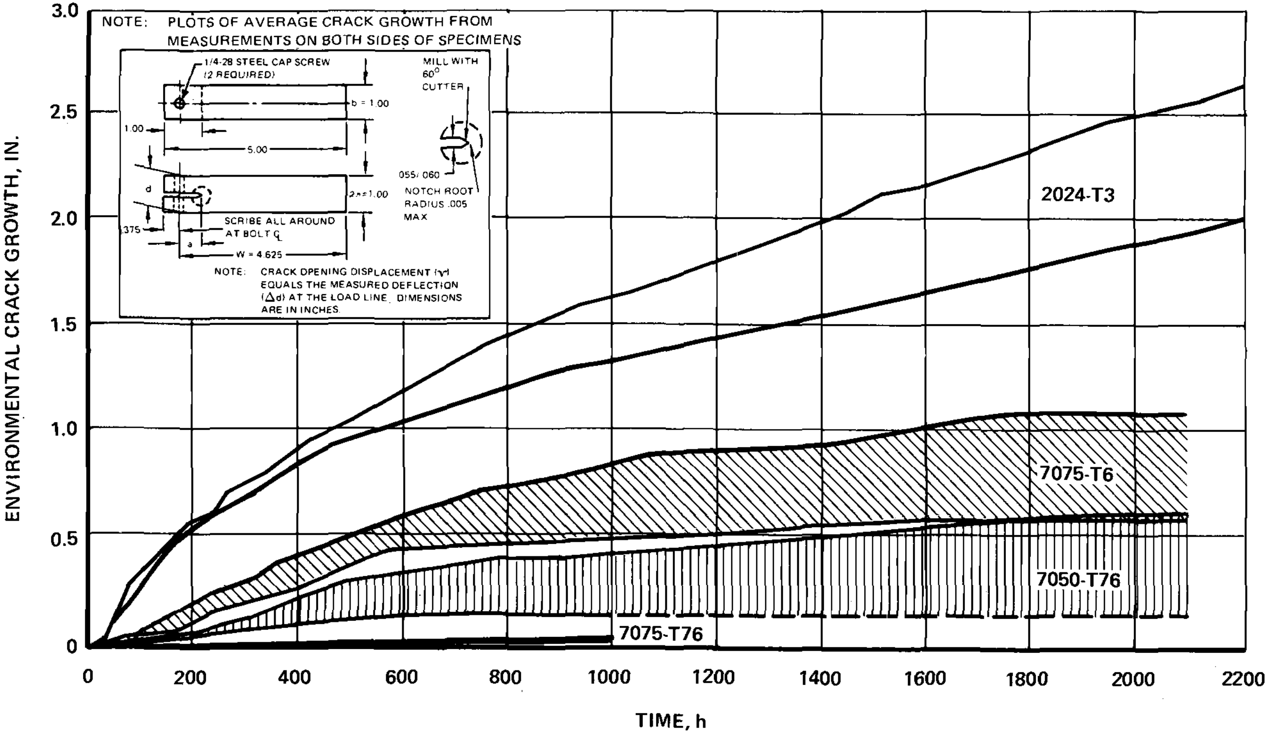

FIG. 4—*Environmental crack growth of (S-L) DCB specimens, 3.5 percent NaCl; 3 times per day.*

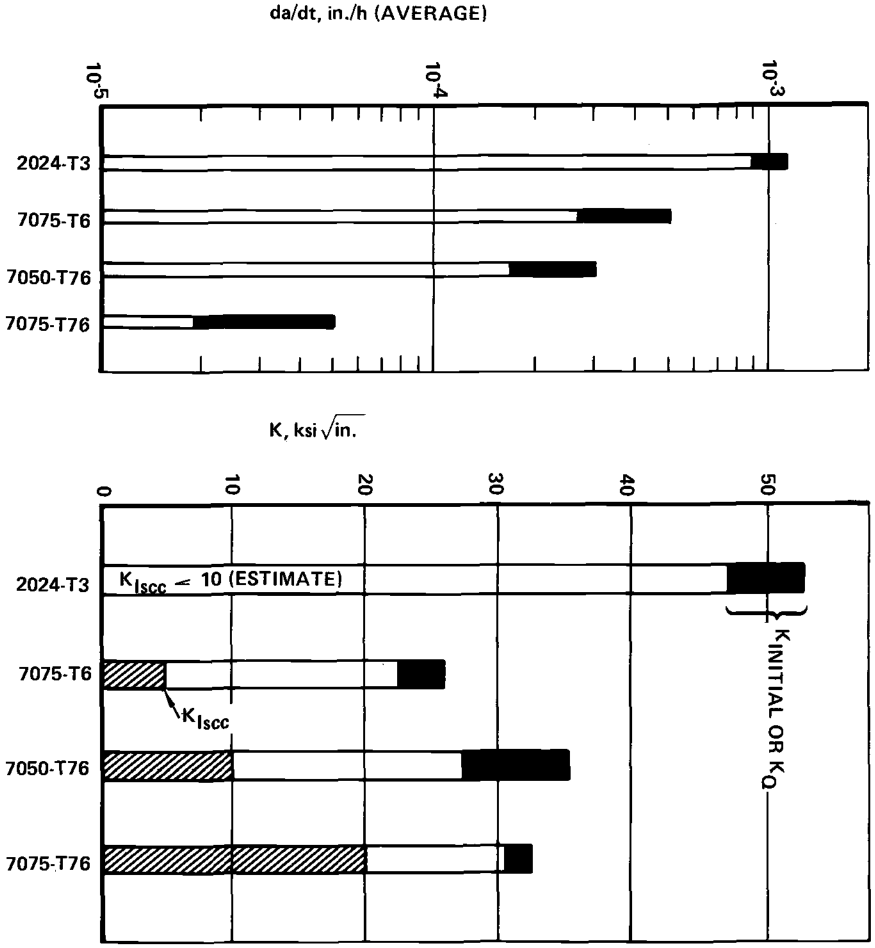

FIG. 5—*Summary of short transverse DCB stress-corrosion test in 3.5 percent NaCl; 3 times per day.*

DCB Stress-Corrosion Crack Growth Tests—Figure 4 compares the crack length versus time bands for three specimens from each alloy. Average crack growth rates and stress intensity data (K_{initial} and K_{Iscc}) are summarized in Fig. 5. These data indicated relative susceptibility among the alloys that correlated with the smooth specimen results. The 2024-T3 had the highest crack velocity; threshold stress intensity (K_{Iscc}) was indeterminate. Next was 7075-T6 which gave $K_{\text{Iscc}} \sim 5$ ksi $\sqrt{\text{in.}}$ The 7050-T76 alloy indicated crack velocity and apparent K_{Iscc} that fell between 7075-T6 and 7075-T76. Alloy 7075-T76 exhibited almost negligible crack growth and the highest threshold stress intensity.

Stress-Corrosion Tests of Fastener and Hole Expansion Specimens

The extent of SCC observed on the various specimens is summarized in Fig. 6. A specimen after testing is shown in Fig. 2. Increasing amounts of interference generally produced more SCC, indicating higher residual tensile stresses around the holes. A similar trend is seen with cold-worked holes. However, at equal levels of net hole expansion, the cold-worked hole probably exhibits less SCC than an interference fit fastener; stress analyses show a hoop stress reduction when the expanded hole relaxes to its residual (net) interference level [*2*]. Increasing the interference fit (up to 4 mils) of an installed fastener in the cold-worked hole appeared only to slightly increase the SCC tendency. (Note that the gross expansion was 3 to 5 mils greater than the residual expansion.) Cracks tended to start further away from the hole as interference increased. This is illustrated by photomacrographs in Fig. 7. Also, SCC was most evident in the S-L plane, especially between the edge (parallel with the short transverse grain) and the adjacent row of holes. Wet sealant installation retarded galvanic reactions around the hole (Fig. 8). It should be noted that at smaller interferences, the peak stresses are theoretically closer to the hole. The base metal immediately next to the hole, such as under the fastener head, is usually less exposed to the corrosive medium.

Figure 9 presents the estimated stress-corrosion potential in terms of the amount of interference versus aluminum alloy threshold stress-to-yield strength ratio. Data from Fig. 6 on interference fit fasteners were used to construct Fig. 9. Mean interference was used for clarity, and the results on cold-worked holes are not included. Figure 9 also indicates that a theoretical limiting residual stress is approached rapidly as interference increases. Results of seacoast exposure tests of duplicate specimens are also being obtained on this program. It is recognized that further substantiating data are needed to firmly establish the stress-corrosion potential of various interference fit fastener systems.

Approximate levels of residual stress were derived for each interference fit fastener or hole expansion system by noting the SCC behavior versus known SCC thresholds for a given alloy and grain direction. The residual stress values for the various interference fit fastener or hole expansion systems determined in this manner were found to be in general agreement with the analytical stress distribution results of Hoffman [*2*] and others.

Conclusions

1. The order of increasing resistance to SCC obtained from 3.5 percent NaCl AI tests on smooth specimens was 2024-T3, then 7075-T6, 7050-T76, and 7075-T76. The estimated threshold stresses of smooth specimens ranged from about 5 ksi (34.5 MPa) to over 60 ksi (413 MPa) depend-

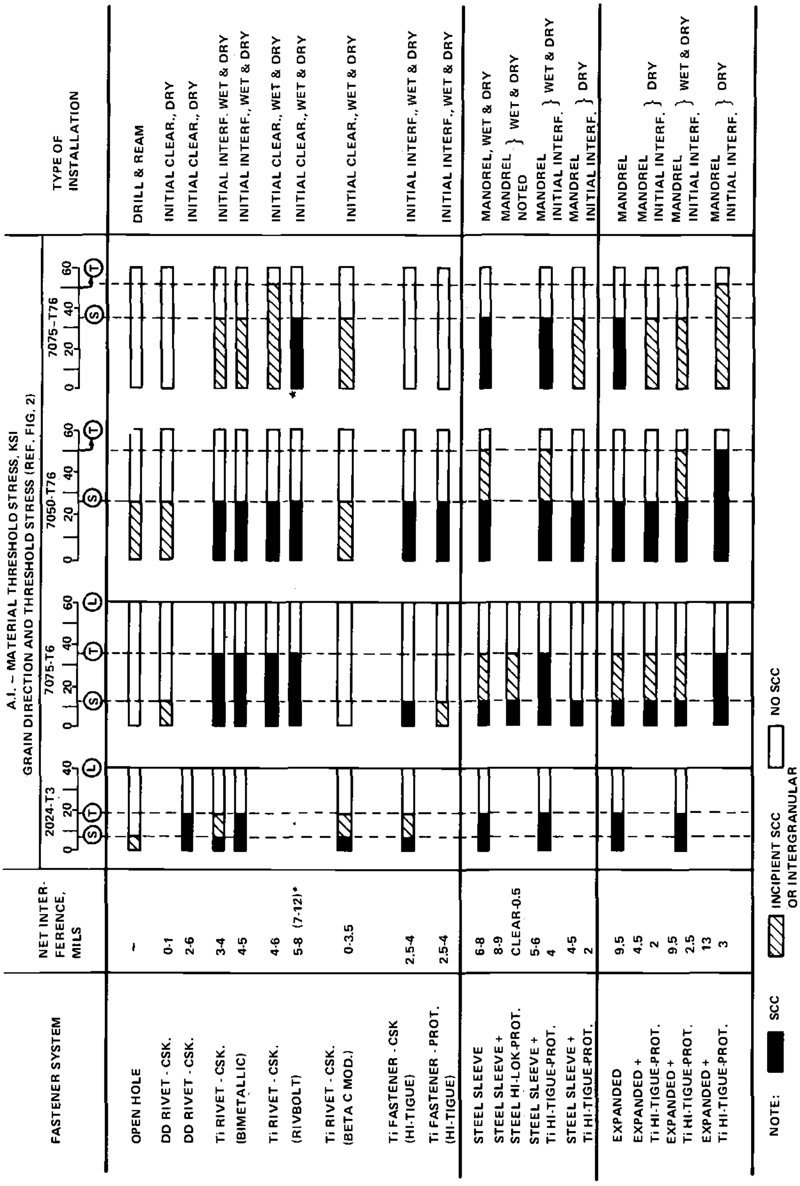

FIG. 6—*Summary of stress-corrosion thresholds versus interference fit fastener systems.*

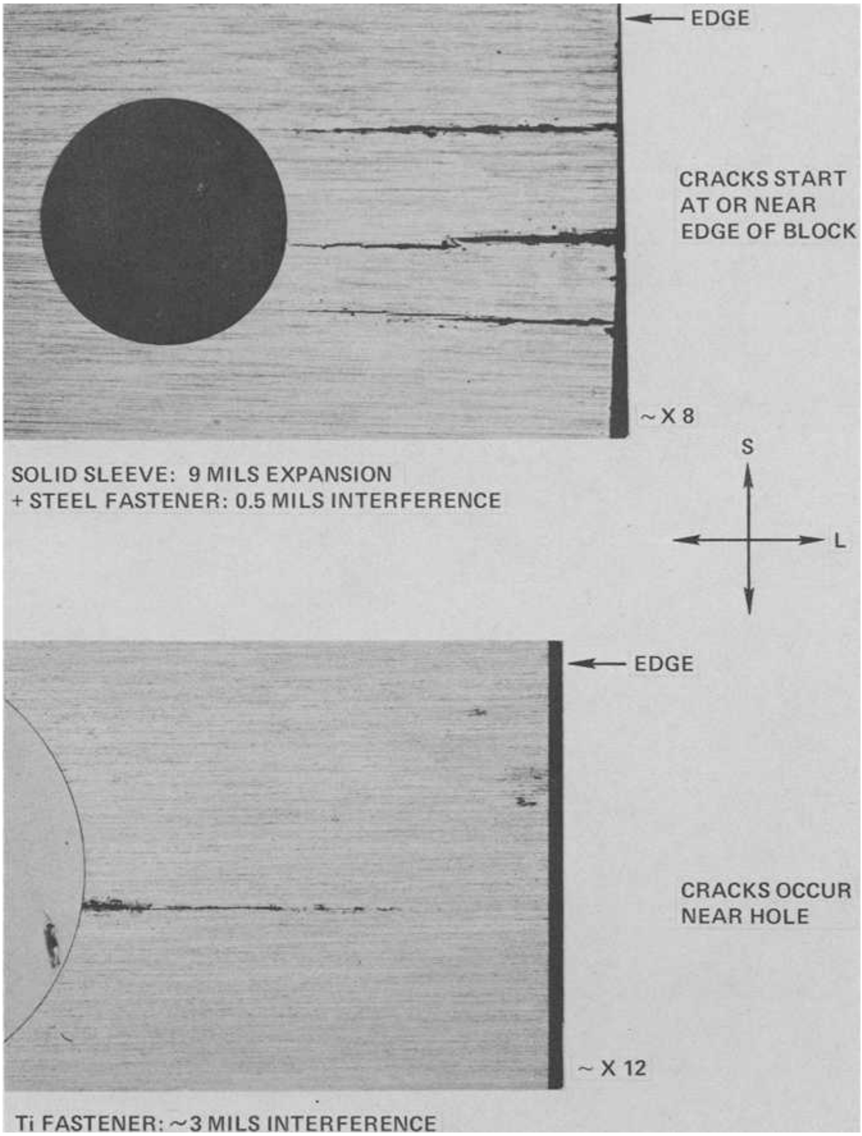

FIG. 7—*SCC after 60 days Al 7075-T6* (top), *2024-T3* (bottom).

ing on alloy and grain direction. Each alloy exhibited normal microstructures and tensile properties. Precracked DCB specimens exposed to 3.5 percent NaCl indicated the same trend as the smooth specimens.

2. Based on stress-corrosion behavior in salt water AI tests, it appears that the residual tensile stresses around the holes rise with increasing

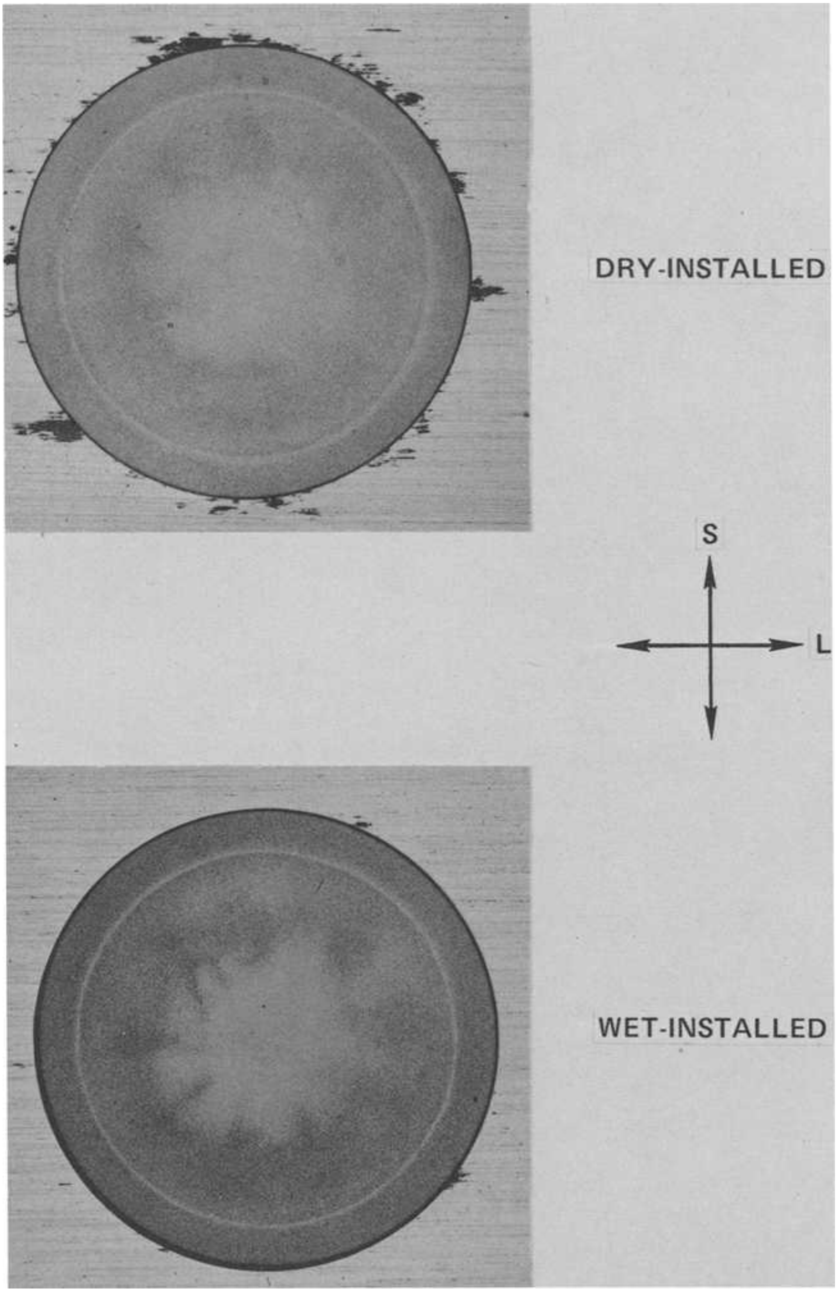

FIG. 8—*Interference titanium fasteners in 7050-T76, 60 days Al exposure. (~ ×9).*

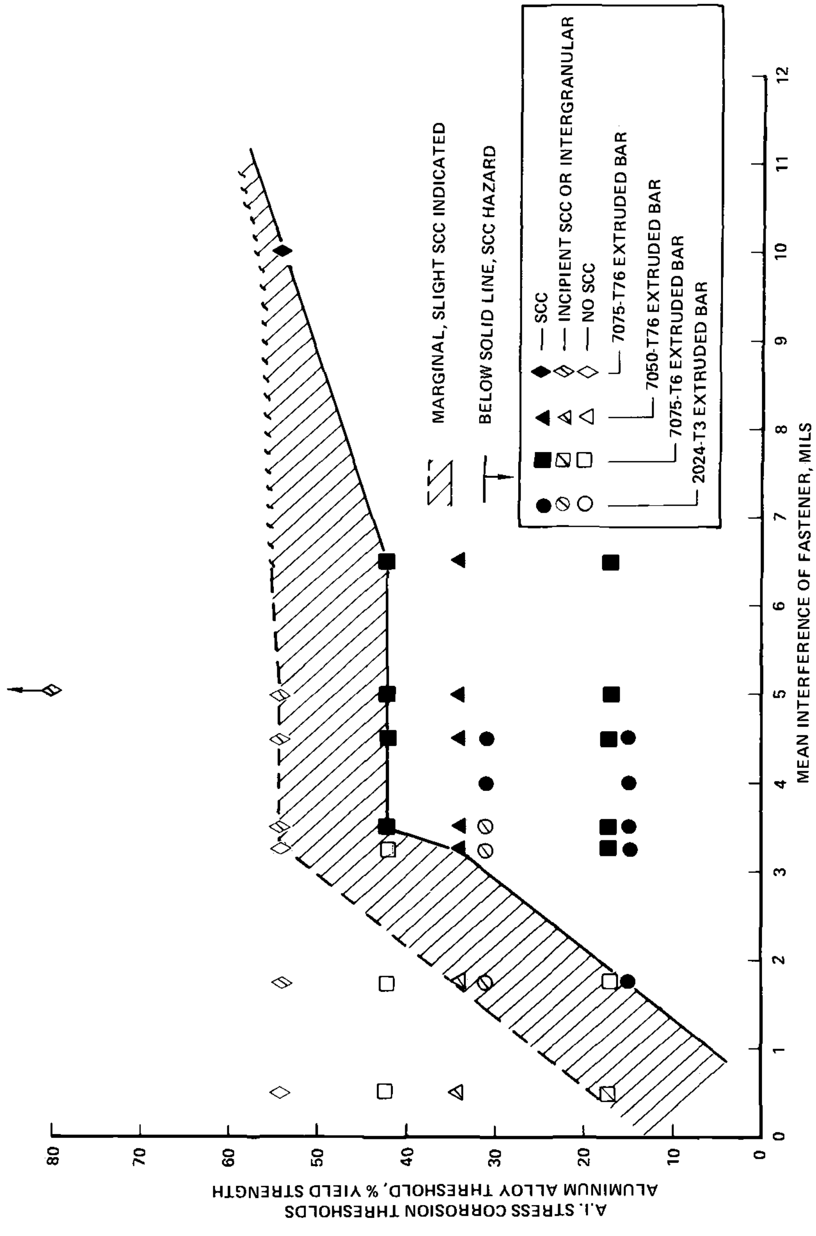

FIG. 9—*Estimated stress-corrosion potential for interference fit fasteners in aluminum alloys.*

amounts of fastener interference or hole expansion, rapidly approaching a theoretical limit.

3. SCC was generally more severe as the fastener interference or hole expansion increased. Even lower interference fits of a few mils caused stress corrosion in the more susceptible materials and grain directions.

4. SCC tended to start further from the hole with increasing fastener interference or hole expansion. Edge distance is especially important where a susceptible grain direciton is open (parallel) to the edge; SCC was prevalent here.

5. The stress-corrosion characteristics of cold-worked (pre-expanded) holes and interference fit holes were similar. However, both analytical and experimental data indicate lesser stress-corrosion tendency due to cold working, when comparing fastener interference versus cold-worked holes at similar net expansion levels.

6. Wet sealant installation may offer more protection at lower interferences where SCC seems to originate closer to the hole.

References

[*1*] Urzi, R. B., "Advanced Methods to Improve the Fatigue Behavior of Fastened Joints." M.S. thesis, California State University, Northridge, Jan. 1975.

[*2*] Hoffman, O., "C5-A Interference Fastener Study, Summary of Analytical Results," private data, presented at the 10 Jan. 1973, meeting of the Lockheed Fracture Mechanics Task Group.

[*3*] Tiffany, C. F., Stewart, R. P., and Moore, T. K., "Fatigue and Stress-Corrosion Test of Selected Fasteners/Hole Processes," Technical Report ASD-TR-72-111, Air Force Dynamics Laboratory, Aeronautical Systems Division, Air Force Materials Laboratory, Wright-Patterson Air Force Base, Ohio, Jan. 1973.

[*4*] Philips, J. L., "Sleeve Coldworking Fastener Holes," Technical Report AFML-TR-74-10, Vol. 1, Boeing Commercial Airplane Company, Feb. 1974.

[*5*] Hyatt, M. V., *Corrosion,* Vol. 26, No. 11, Nov. 1970, pp. 487–503.

[*6*] Sprowls, D. O., Shumaker, M. B., Walsh, J. D., and Coursen, J. W., "Evaluation of Stress-Corrosion Cracking Susceptibility Using Fracture Mechanics Techniques," Contract No. NAS 8-21487, Final Report–Part 1, 31 May, 1973.

S. Hanagud[1] *and A. E. Carter*[1]

Interference Fits and Stress-Corrosion Failure

REFERENCE: Hanagud, S. and Carter, A. E., **"Interference Fits and Stress-Corrosion Failure,"** *Stress Corrosion—New Approaches, ASTM STP 610,* American Society for Testing and Materials, 1976, pp. 267–288.

ABSTRACT: Service failure analysis and theoretical and experimental investigations have been carried out to investigate the stress-corrosion susceptibility of the aluminum alloy structures due to the use of interference fit sleeves and mandrel-coining procedures. A methodology has been discussed for the design of interference fits so that maximum improvement of fatigue life can be attained while the stress-corrosion susceptibility is kept to a minimum.

KEY WORDS: stress corrosion, interference fit sleeves, stress coining, fatigue life, residual stresses

The stress concentration at the fastener holes in aircraft structures has the effect of reducing the fatigue life of the aircraft structure. Interference fit fasteners, interference fit bushings (or sleeves), and other cold-working processes, such as stress coining, are often used [*1–3*][2] at the fastener holes to increase the fatigue life of the structure. The terms "interference fit fastener" and "interference fit bushings" are self-explanatory. The term "stress coining" refers to the cold-working process of drawing an oversized mandrel through the fastener hole.

The objective of the interference fits and other cold-working processes are to create a region of residual compressive stresses surrounding the fastener holes. The residual compressive stresses have the effect of reducing the magnitude of applied tensile stresses at the fastener holes and thus improving the fatigue life of the structure. In addition to creating a region of compressive stresses, residual tensile stresses are also created in the structure as a result of the cold-working processes. These tensile stresses reach their maximum values at a short distance away from the hole. These tensile stresses may cause stress-corrosion cracking (SCC) of the aircraft

---

[1] Professor and graduate student, respectively, School of Aerospace Engineering, Georgia Institute of Technology, Atlanta, Ga. 30332.

[2] The italic numbers in brackets refer to the list of references appended to this paper.

structure. Therefore, any proper design of interference fit fastener, interference fit bushings, or stress coining processes should consider both the stress-corrosion susceptibility and fatigue-life improvement together. This paper discusses the investigations leading to such a methodology in three parts:

1. Service failure analysis of actual aircraft parts are discussed to emphasize the fact that stress-corrosion failure has taken place due to some types of cold-working processes.
2. Laboratory tests have been conducted to show that stress corrosion may result after the use of interference fit bushings in aluminum alloy 7075-T651. Interpretation of the test results are based on the calculation of residual stresses near the fastener hole of the structure. A brief description of the calculation and results are shown in the Appendix.
3. By using the expressions for residual stresses and other available results, an approximate method, for optimum improvement of fatigue life of a structure with fastener holes by cold-working processes, has been discussed.

Service Failure Analysis

The part shown in Fig. 1*a* was milled from aluminum alloy 7075-T651 plate stock and belonged to an aircraft flap. The part had developed fatigue cracks after being in service for approximately ten years. The developed cracks originated from fastener holes that were drilled parallel to the plate short transverse direction. Typical fracture surfaces were as shown in Figs. 1*b* and *c*. As displayed in the figure, the cracks originated at the hole inside diameter. Electron fractography confirmed the fact that the fracture mechanism was fatigue. Well-defined striations and transgranular crack propagation were evident as shown in Fig. 1*d*.

This particular part was replaced by an identical part milled from aluminum alloy 7075-T651 plate stock. However, the replaced part had "cold worked" fastener holes. The objective of the cold working was to improve the fatigue life of the part. The ⅜-in.-diameter holes were cold worked by drawing an oversized mandrel through the bores. The mandrel interference was about 0.004 to 0.006 in. on the diameter.

After a relatively short amount of service of about two years, the newly replaced parts with cold-worked fastener holes developed cracks. Crack origin was no longer at the inner surface of the fastener holes. In fact, the crack originated a short distance away from the hole, as pointed up by arrows in Fig. 2*a*. Corrosion pitting was evident. The fracture origin was identified as stress corrosion by means of electron fractography (Fig. 2*b*). The crack mechanism was intergranular with multiple secondary intergranular cracks and corrosion pitted grain facets as shown in Fig. 2*b*. Evidence of SCC fatigue transition cracks was noted as shown in Fig. 2*c* and

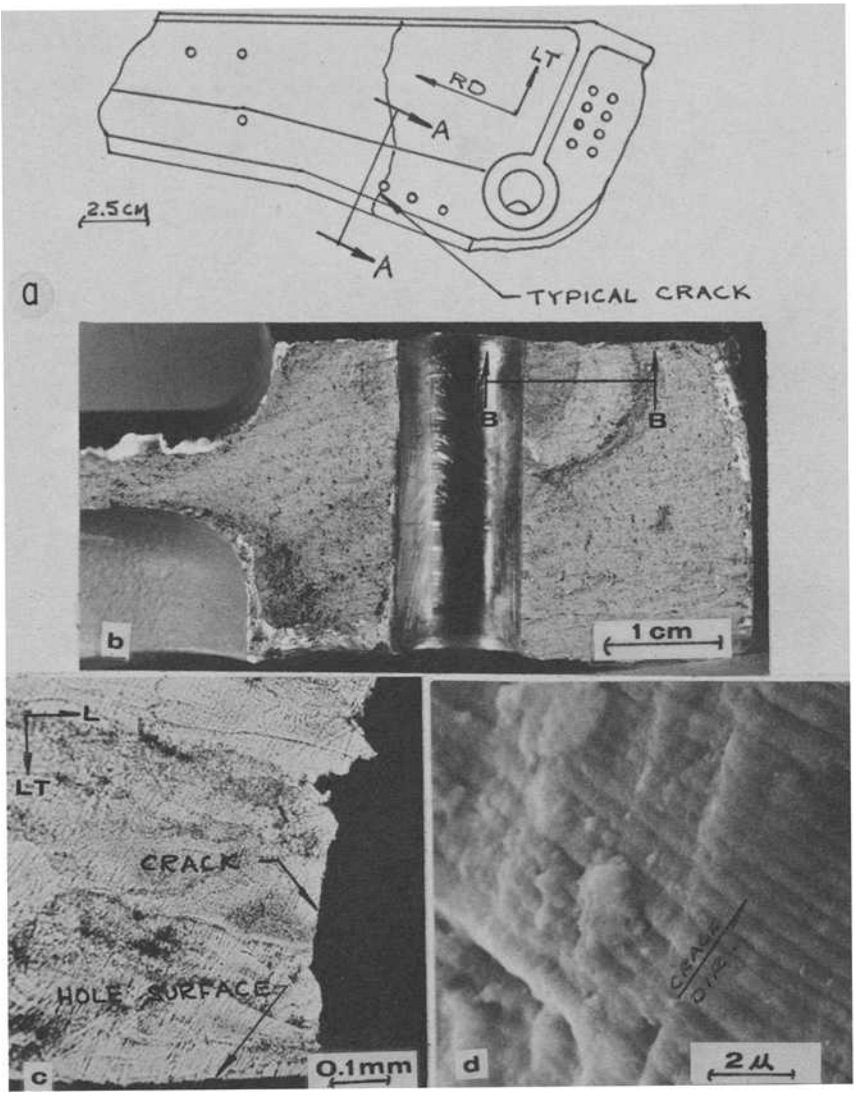

FIG. 1—(a) *Aircraft structural component failure at fastener hole stress concentration.* (b) *View A-A, fracture surface through noncold worked hole.* (c) *Cross section B-B, exhibiting transgranular crack path.* (d) *SEM photomicrograph of crack fatigue striations.*

d. No material abnormalities were found on cross sections. The Brinell hardness averaged 145, corresponding to a yield strength of 69 000 psi. SCC had not been observed in "noncold worked" parts.

It was suspected that the stress-corrosion cracks were caused by the residual tensile stresses resulting from the cold-working process. These residual stresses exceeded the threshold [*4*] and were responsible for the

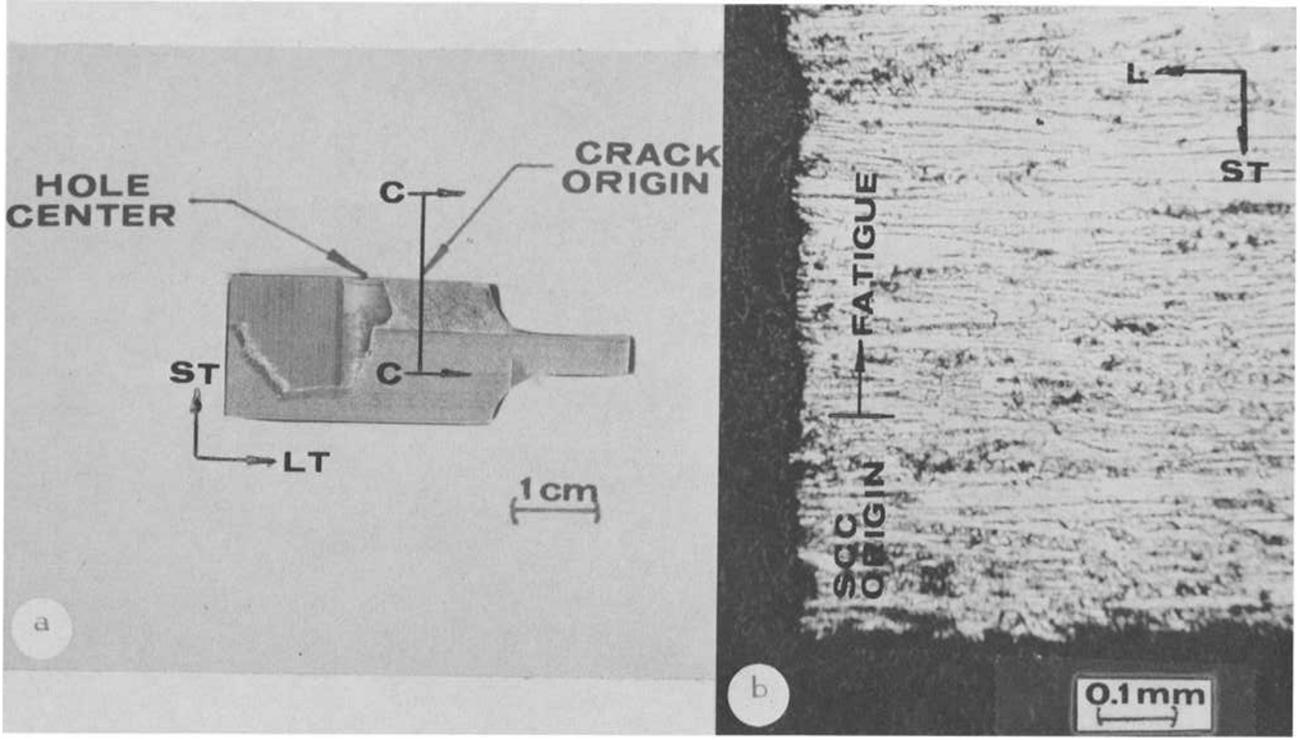

FIG. 2—(a) *Cold-worked fastener hole failure.* (b) *Cross section C-C through crack origin.*

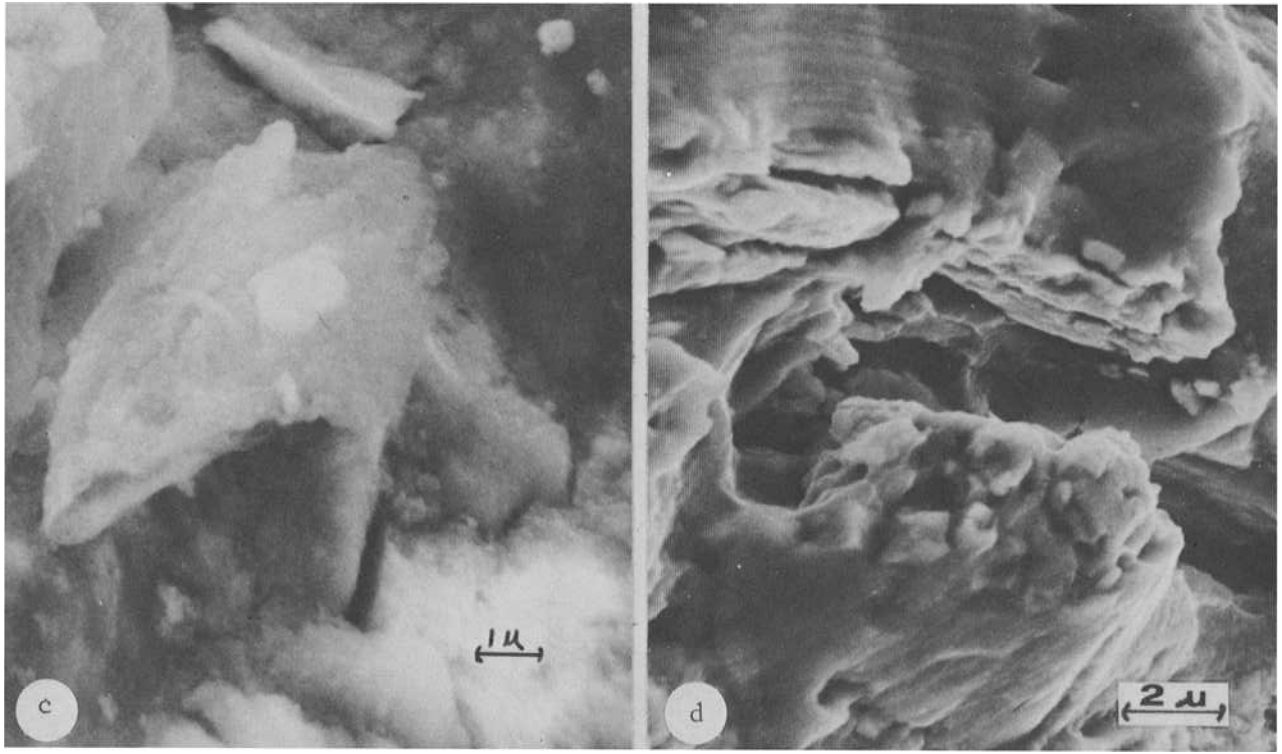

FIG. 2—(c) *Scanning electron photomicrograph of SCC origin.* (d) *Scanning electron photomicrograph of SCC fatigue transition.*

stress-corrosion cracks as explained in Ref *5*. The origin of the crack was at a distance two times the radius of the hole as shown in Ref *5*.

Stress-Corrosion Susceptibility of Cold-Working Interference Fit Bushings

In Ref *5*, the stress-corrosion susceptibility of stress-coining processes has been established by laboratory experiments. In the preceding section of this paper, a service failure analysis established the fact that the stress-corrosion failure due to stress-coining process is indeed a definite possibility in real structures. In order to design the stress-coined fasteners for maximum improvement of fatigue life and minimum stress-corrosion susceptability, a knowledge of the residual stress distribution as a function of the interference resulting from the stress-coining process is necessary. These expressions are derived in Ref *5* for stress-corrosion processes. Similar information on residual stresses due to the use of interference fit fasteners and interference fit sleeves are needed to optimize the design of fasteners with interference fit fasteners or interference fit sleeves. However, no such information on residual stresses is available. The derivation of residual stresses due to the use of interference fit sleeves are discussed in the Appendix of this paper. In this section, laboratory experiments on interference fit sleeves are discussed. These experiments show that the residual stresses calculated in the Appendix can cause SCC. The tests are also conducted to verify the origin of cracks predicted by using the expressions for residual stresses in the Appendix.

Test Specimens

Specimens were machined from 2-in.-thick AISI 7075 T651 plate stock. Grain orientation was longitudinal-short transverse as shown in Fig. 3. Five to eight 0.249/0.250-in. holes were drilled in each of the eight specimens. The hole spacings varied from ½ to 1 in. The inside surface of the holes were honed to 32-rms surface finish.

No external load was applied to the specimens during the test duration. Prior to testing, seven specimens were cold worked by using interference fit sleeves. The amount of interference on the diameter was 0.011 to 0.019 in. This interference corresponded to the additional displacement on the inner diameter of the sleeve or the outer diameter of the cold-working mandrel. These sleeves were made of A286 stainless steel, and a special tool was used to drive the sleeve into the hole. The sleeves were precision formed, thin-wall tubular elements. After expanding the hole by using the special tool, the sleeves were left in place at the hole.

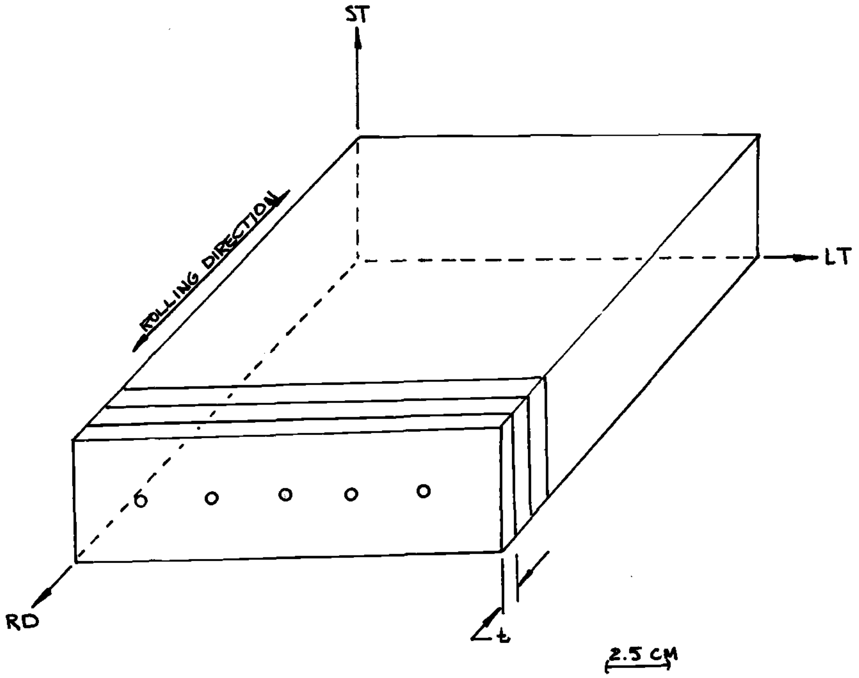

Material: AISI 7075-T651 Plate.
Thickness: 0.25 inch.
Hole Size: 0.25 inch diameter, five holes equally spaced.
Cold Work: 0011 - 0.019 bushing-mandrel diametrical interference.

FIG. 3—*Alternate immersion specimen.*

Test Procedure

Alternate immersion test procedure was used as specified in Ref 6. The cycles were timed for 10-min immersion of the specimen followed by 50-min air drying time. The cycles were controlled by a timer activated solenoid valve which caused the air to enter the reservoir tank containing the salt solution. The rising pressure caused the salt solution to flow into the test chamber. The second timer signal closed the solenoid valve which stopped the airflow into the tank, thus reversing the flow of the salt solution.

The test solution was 3.5 percent sodium chloride (NaCl) by weight dissolved in distilled water. The salinity of the solution was checked each day by using a hydrometer, and distilled water was added to compensate for evaporation. Solution pH was maintained at 6.4 to 7.2. Air temperature

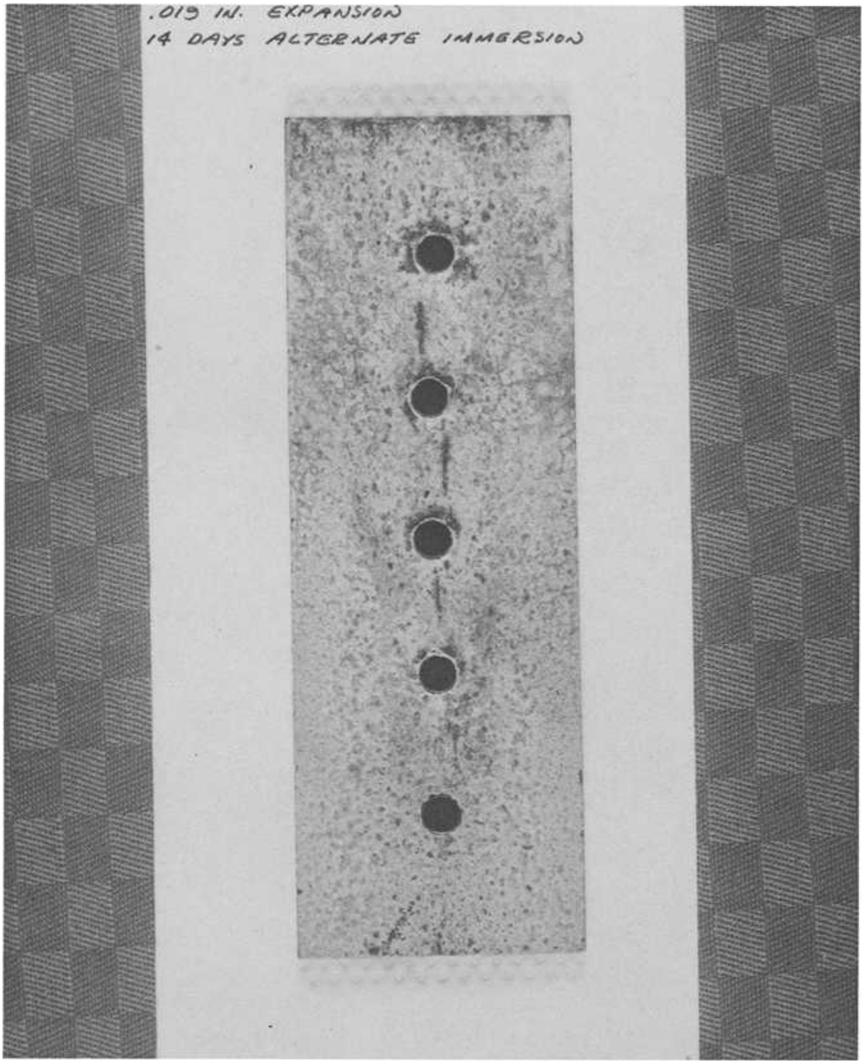

FIG. 4(a)—*Macroscopic view of the specimen after alternate immersion tests* (δ = *0.019 in.*).

in the test chamber was maintained in the range of 78 to 82°F, with a relative humidity of 45 percent. This test solution complied with the requirements of the federal test standard [6] No. 151b, Method 823.

Test Results

All seven specimens, with interference fit sleeves, exhibited corrosion pitting and oxidation. Macrocracking was evident in four of the speci-

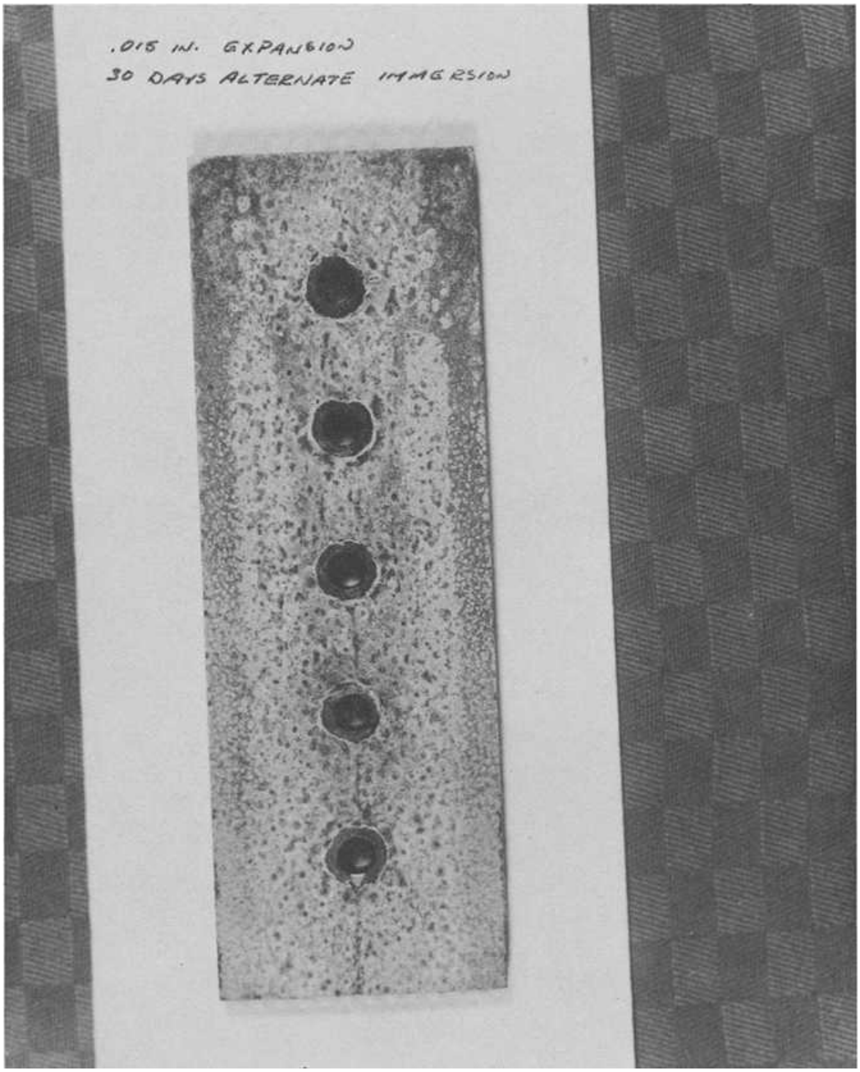

FIG. 4(b)—*Macroscopic view of the specimen after alternate immersion tests* *($\delta = 0.015$ in.).*

mens. The specimens with interference of 0.019-in. interference developed macrocracks, as shown in Fig. *4a*, after 14 days in the alternate immersion test chamber. The specimens with 0.015 interference developed macrocracks after 30 days of alternate immersion testing as shown in Fig. 4*b*. In all specimens, cracks were aligned perpendicular to the specimen short transverse direction. Cross sections through the specimen indicated that cracks had developed throughout the thickness as shown in micrographs of Fig. 5.

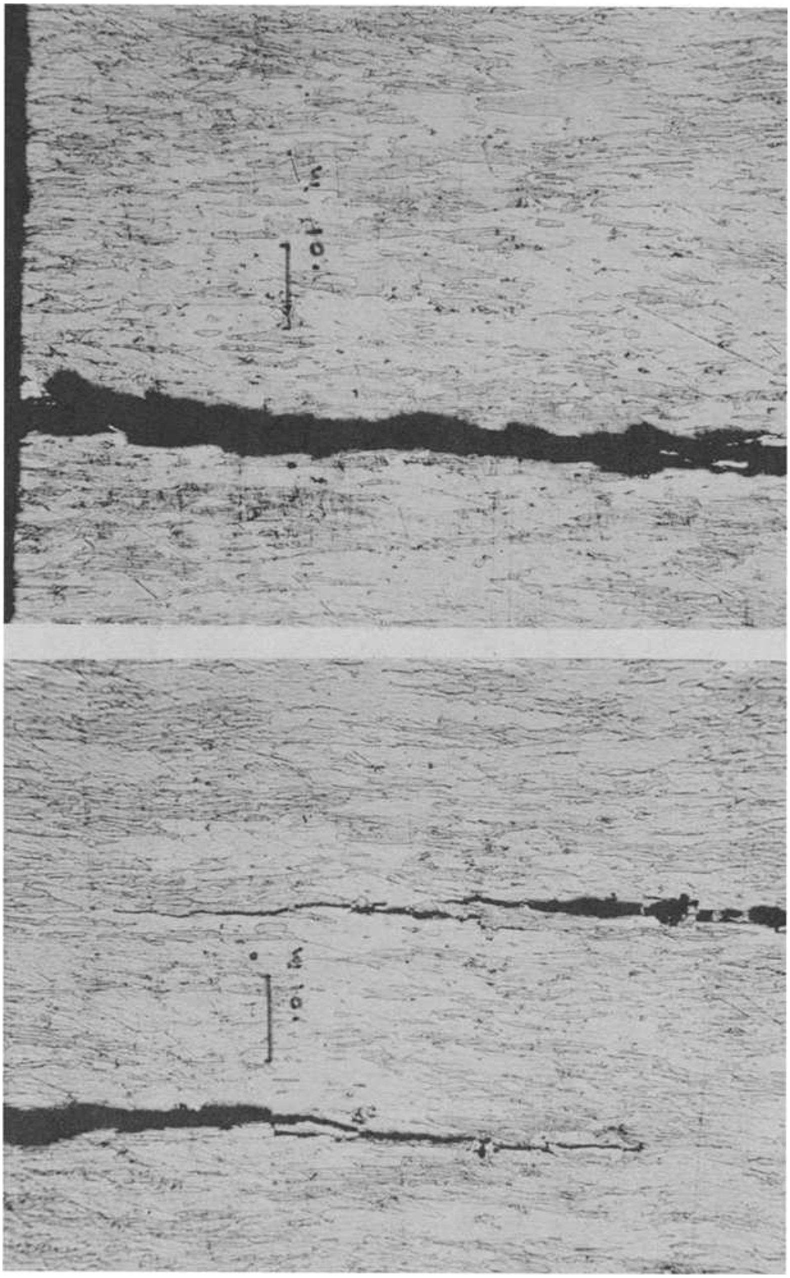

FIG. 5—*Micrographs of the cross section.*

Sectioning of specimens without macrocracks, indicated many microcracks throughout the thickness of the specimen as shown in Fig. 6. Electron fractography confirmed the fact that fracture mechanism was stress corrosion.

Conclusions from Tests

From the calculations of the type described in the Appendix, it can be shown that the residual tensile stresses due to the use of cold-working interference fit sleeves, with interferences of 0.019 and 0.015 in., exceed the stress-corrosion threshold of 7 ksi for the aluminum alloy 7075-T651 in longitudinal-short transverse direction. The alternate immersion tests have confirmed this fact. The crack origins in the tests are near the locations of maximum tensile stress predicted by the calculations and are at a distance of about two times the radius of the hole from the center of the fastener hole.

Optimum Design of the Amount of Interference

The expressions for residual stresses in the plate, due to stress coining [*5*] or interference fit sleeves (see Appendix) can be used to design optimum amount of interferences that would maximize the improvement of fatigue life and minimize the stress-corrosion susceptibility. The needed methodology for the design is explained by considering the case of stress coining.

Stress Formulas

For the case of stress coining, the tangential compressive stress at a fastener hole is given by the following equation [*5*]

$$\sigma_\theta(a) = 2\sigma_y \ln (a/b) \tag{1}$$

where

σ_y = tensile yield stress,
a = radius of the hole, and
b = radius of the elastic-plastic interference.

The quantity b can be obtained by solving the following equation [*5*]

$$\delta = 2u_{oe} + \frac{\sigma_y}{E}\left\{(3 - \nu)\frac{a}{2}\left(\frac{b^2}{a^2} - 1\right) - 2(1 - \nu)a \ln \frac{b}{a}\right\} \tag{2}$$

where

δ = interference (measured on diameter),
ν = Poisson's ratio, and
E = modulus of elasticity.

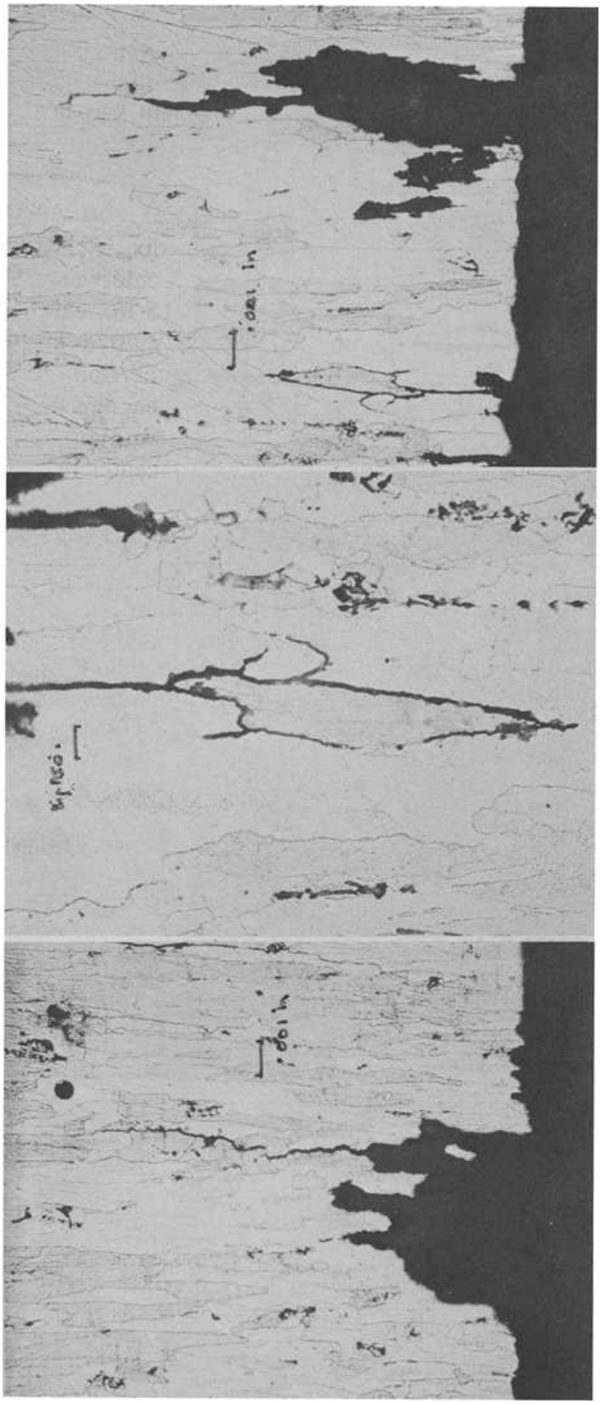

FIG. 6—*Micrographs of the cross section.*

The maximum radial elastic displacement of the hole before incipient yielding occurs in the material is denoted by u_{oe} and can be calculated from the following equation

$$u_{oe} = \sigma_y \frac{(1 + \nu)a}{2E} \tag{3}$$

Maximum tensile stress that can cause stress corrosion is at the elastic-plastic interface and the magnitude is given by the following equation

$$\sigma_\theta(b) = \frac{\sigma_y}{2}\left(1 - \frac{a^2}{b^2}\right) + \sigma_y \frac{a^2}{b^2} \ln \frac{a}{b} \tag{4}$$

Design Methodology

The variation of maximum area stress, with the total life in cycles, for a ¼-in.-thick plate with ¼-in.-diameter hole is shown in Fig. 7. For a given interference δ the residual compressive stress is given by Eq 1. For example, for $\delta = 0.0023$, the compressive stress at the hole is equal to 12.4 ksi. If the operating area stress is 45 ksi, the effect of interference will be to reduce the magnitude of the stress at the hole that includes the stress concentration effects. The reduction can be obtained by solving the combined elastic-plastic problem of residual stresses and the externally applied load. From solution of the problem by numerical methods the new stresses at the hole surface can be obtained.

From the value of new stresses at the hole, the new effective area stress can be estimated by correcting for the stress concentrations. Then, the new fatigue life can be obtained from Fig. 8. For example, for an applied area stress of 40 ksi and interference of 0.004, in a ¼-in.-thick plate and ¼-in.-diameter hole, the new effective area stress is approximately equal to 19.7 ksi. This corresponds to a fatigue life of $10^{5.1}$ cycles. This agrees with the experimental point shown in Fig. 7. By using similar calculations, the variation of the amount of interference with the fatigue life has been plotted for area stress of 45 ksi in Fig. 8. The figure also illustrates the increases in the maximum tensile stress and the limit on the amount of interference that can be used, subject to the threshold of 7 ksi for longitudinal-short transverse direction. These maximum residual tensile stresses were calculated from Eq 4 for ¼-in. plate and ¼-in.-diameter hole in the 7075-T651 alloy.

By plotting such figures, the maximum interference that can be used and the maximum life that can be gained without stress-corrosion susceptibility can be estimated for all needed area stresses.

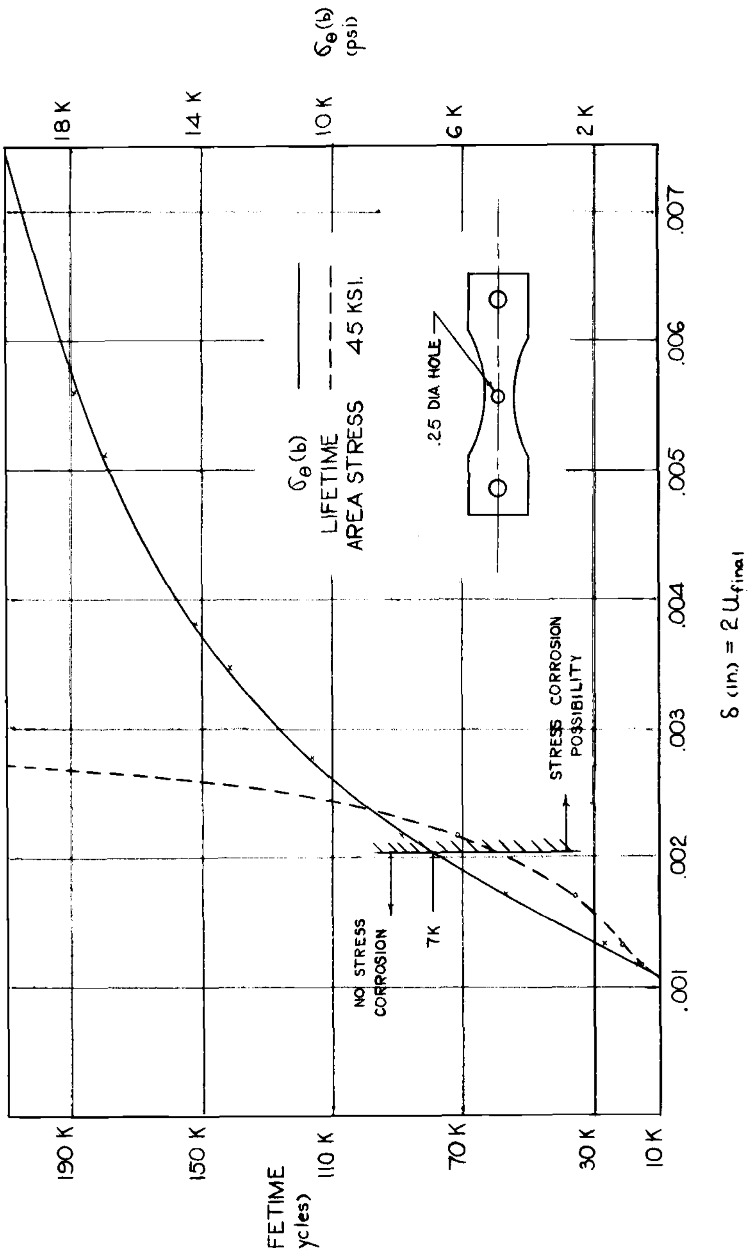

FIG. 7—*SN diagram for ¼-in. plate with ¼-in. holes.*

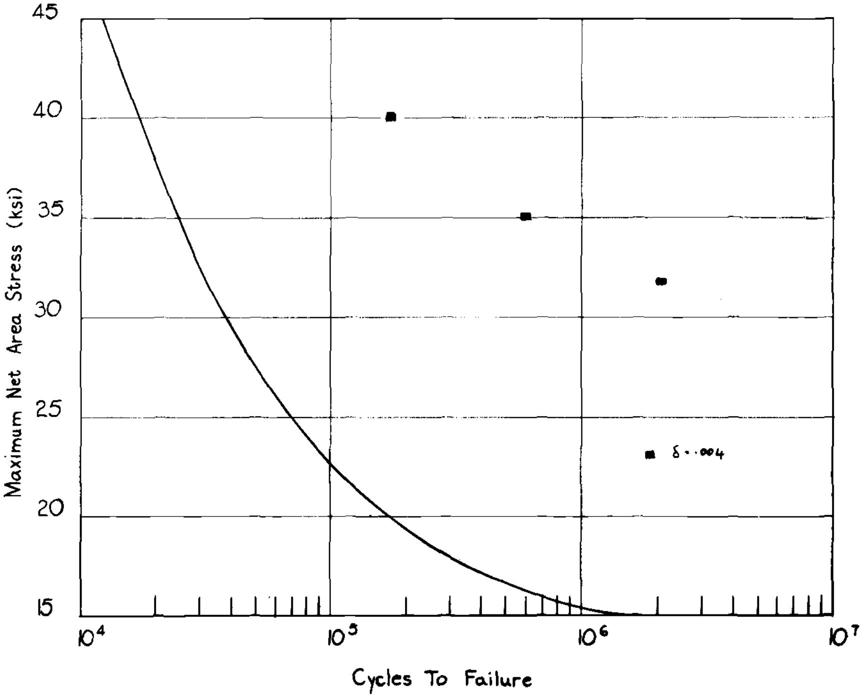

FIG. 8—*Variations of fatigue life and maximum tensile stress with interference.*

Conclusions

This paper has shown that it is possible, in practice, to "overcoin" the fasteners to such an extent that stress-corrosion failure may take place. Such failures are possible during the use of stress coining or interference fit sleeves. This paper has also shown that it should be possible to design the interference for sleeves or mandrel-coining so that stress-corrosion susceptibility is minimized. Even under these limitations, an appreciable amount of gain in fatigue life is expected.

Acknowledgment

Part of this work was supported by NASA Grant NGR-11-002-169.

APPENDIX

For the purpose of stress analysis, the problem of sleeve cold-working process can be stated as follows. A steel sleeve of inner diameter a and outer diameter is surrounded by aluminum alloy 7075-T651. The radius c is the elastic-plastic radius in aluminum. The stresses in steel are assumed to be below the yield stress. A radial displacement $\bar{u}$ (corresponding to the desired interference δ) is applied at the radius $r = a$. This constitutes the loading. After the radial displacement at $r = a$ has reached $\bar{u}$, the system is unloaded. Then the stress at the inner radius $r = a$ is zero. The combination of loading and unloading results in the residual stresses in a region surrounding the fastener hole of initial radius $r = b$.

It is assumed that the plate is thin enough that plane-stress conditions can be assumed. Small displacements are assumed. The elastic-plastic behavior of the aluminum alloy is taken into account by assuming Tresca yield condition and the associated flow rules. The elastic unloading is assumed in the plate.

The loading problem is divided into an elastic loading until incipient yield occurs at $r = b$. Corresponding to a radial displacement $\bar{u}_e$ at $r = a$. For $\bar{u} > \bar{u}_e$, the elastic-plastic problem has been solved. Analysis of the elastic unloading problem following the elastic-plastic loading analysis yields the desired expressions for residual stresses. The analysis is carried out on the assumption of cylindrical symmetry.

Elastic Analysis

It is assumed that the radial displacement at $r = b$ is increased from its value of zero to its final value $\bar{u}_f$ slowly. For a value of $\bar{u}$ less than a certain value $\bar{u}_e$, both the sleeve and the aluminum alloy plate exhibit elastic behavior. At $\bar{u} = \bar{u}_e$, incipient yielding occurs at $r = b$. The purpose of the elastic analysis is to obtain the value of $\bar{u}_e$.

The elastic displacements and stresses in both steel and aluminum alloy are given by the well-known Lamè solutions under plane-stress conditions.

$$u_s = A_1 r + \frac{A_2}{r}, \qquad a < r < b \tag{5}$$

$$\sigma_{rs} = \frac{E_s}{1 - \nu_s^2}\left\{A_1(1 + \nu_s) - \frac{A_2}{r^2}(1 - \nu_s)\right\}, \qquad a < r < b \tag{6}$$

$$\sigma_{\theta s} = \frac{E_s}{1 - \nu_s^2}\left\{A_1(1 + \nu_s) + \frac{A_2}{r^2}(1 - \nu_s)\right\}, \qquad a < r < b \tag{7}$$

$$u_a = A_3 r + \frac{A_4}{r}, \qquad r > b \tag{8}$$

$$\sigma_{ra} = \frac{E_a}{1 - \nu_a^2}\left\{A_3(1 + \nu_a) - \frac{A_4}{r^2}(1 - \nu_a)\right\}, \qquad r > b \tag{9}$$

$$\sigma_{\theta a} = \frac{E_a}{1 - \nu_a^2}\left\{A_3(1 + \nu_a) - \frac{A_4}{r^2}(1 - \nu_a)\right\}, \qquad r > b \tag{10}$$

The quantities u_s, σ_{rs}, $\sigma_{\theta s}$, E_s, and ν_s, with subscripts s, represent radial displacement, radial normal stress, hoop stress, modulus of elasticity, and Poisson's ratio of steel sleeve occupying the region $a < r < b$. The quantity r is the radial coordinate measured from the center of the fastener hole. Similarly, the quantities with subscript a represent the appropriate variables in aluminum alloy occupying the region $r > b$. Shear stresses are zero because of symmetry. The unknown constants A_1, A_2, A_3, and A_4 can be determined from the following boundary conditions

$$r = a, \qquad u_s = \bar{u} \text{ (applied radial displacement)} \tag{11}$$

$$r = b, \qquad u_a = u_s \tag{12}$$

$$r = b, \qquad \sigma_{rs} = \sigma_{ra} \tag{13}$$

$$r \rightarrow \infty, \qquad \sigma_{ra} = 0 \tag{14}$$

The last condition assumes that the dimensions of the plate are large compared to the hole radius. It is also assumed that spacing between the fastener holes are large enough that interference can be neglected. The values of A_1, A_2, A_3, and A_4 are

$$A_2 = \frac{\dfrac{\bar{u}b}{a}\left(1 + \dfrac{E_s}{E_a}\dfrac{1+\nu_a}{1-\nu_s}\right)}{\dfrac{b}{a^2}\left(1 + \dfrac{E_s}{E_a}\dfrac{1+\nu_a}{1-\nu_s}\right) + \dfrac{1}{b}\left(\dfrac{E_s}{E_a}\dfrac{1+\nu_a}{1-\nu_s} - 1\right)} \tag{15}$$

$$A_1 = \frac{\bar{u}}{a} - \frac{A_2}{a^2} \tag{16}$$

$$A_3 = 0 \tag{17}$$

$$A_4 = \frac{\bar{u}}{a} b^2 \left\{ 1 - \frac{\left(1 + \dfrac{E_s}{E_a}\dfrac{1+\nu_a}{1-\nu_s}\right)\left(\dfrac{1}{a^2} - \dfrac{1}{b^2}\right)}{\dfrac{1}{a^2}\left(1 + \dfrac{E_s}{E_a}\dfrac{1+\nu_a}{1-\nu_s}\right) + \dfrac{1}{b^2}\left(\dfrac{E_s}{E_a}\dfrac{1+\nu_a}{1-\nu_s} - 1\right)} \right\} \tag{18}$$

Yielding will occur when Tresca yield condition is satisfied in some region. In this case the Tresca condition results in $(\sigma_{\theta a} - \sigma_{ra})$ attaining the value of the yield stress in tension σ_y at $r = b$ from Eqs 9 and 10.

$$(\sigma_{\theta a} - \sigma_{ra})_{r=b} = \left[2\frac{C_4}{r^2}\frac{E_a}{1+\nu_a}\right]_{r=b} = \sigma_y \tag{19}$$

By substituting for C_4 from Eq 18, it can be determined that yield occurs when $\bar{u}$ attains the following value

$$\bar{u} = \frac{\sigma_y a}{2F_1} \tag{20}$$

where

$$F_1 = \left\{ 1 - \frac{\left(1 + \dfrac{E_s}{E_a}\dfrac{1+\nu_a}{1-\nu_s}\right)\left(\dfrac{1}{a^2} - \dfrac{1}{b^2}\right)}{\dfrac{1}{a^2}\left(1 + \dfrac{E_s}{E_a}\dfrac{1+\nu_a}{1-\nu_s}\right) + \dfrac{1}{b^2}\left(\dfrac{E_s}{E_a}\dfrac{1+\nu_a}{1-\nu_s} - 1\right)} \right\} \frac{E_a}{1+\nu_a} \tag{21}$$

Elastic-Plastic Loading

For $\bar{u} > \bar{u}_e$, there will be a plastic region in the aluminum alloy sheet. This region is denoted by $b < r < c$ in the figure. The region $r > c$ is still elastic. Similarly the region $a < r < b$ of the steel sleeve is elastic because it has been assumed that the yield strength of steel is high enough that yield will not occur in steel. The radius c represents the elastic-plastic boundary. The value of c is an unknown and depends on the applied radial displacement $\bar{u}$ at $r = b$. The relationship between c and $\bar{u}$ will be determined from elastic plastic analysis.

The displacements and stresses in the region $a < r < b$ and $r > c$ are still elastic and are given by the following equations

$$u_s^{ep} = B_1 r + \frac{B_2}{r}, \qquad a < r < b \tag{22}$$

$$\sigma_{rs}^{ep} = \frac{E_s}{1 - \nu_s^2}\left\{B_1(1 + \nu_s) - \frac{B_2}{r^2}(1 - \nu_s)\right\}, \qquad a < r < b \tag{23}$$

$$\sigma_{\theta s}^{ep} = \frac{E_s}{1 - \nu_s^2}\left\{B_1(1 + \nu_s) + \frac{B_2}{r^2}(1 - \nu_s)\right\}, \qquad a < r < b \tag{24}$$

$$u_{ae}^{ep} = B_3 r + \frac{B_4}{r}, \qquad r > c \tag{25}$$

$$\sigma_{rae}^{ep} = \frac{E_a}{1 - \nu_a^2}\left\{B_3(1 + \nu_a) - \frac{B_4}{r^2}(1 - \nu_a)\right\}, \qquad r > c \tag{26}$$

$$\sigma_{\theta ae}^{ep} = \frac{E_a}{1 - \nu_a^2}\left\{B_3(1 + \nu_a) + \frac{B_4}{r^2}(1 - \nu_a)\right\}, \qquad r > c \tag{27}$$

The superscript *ep* identifies the stresses and displacements in elastic-plastic loading phase. The subscript *ae* identifies the stresses and displacements in the elastic region of the aluminum alloy, that is, for $r > c$. The constants B_1, B_2, B_3, and B_4 are to be determined from boundary conditions. The stresses in the plastic region can be determined easily from equilibrium and yield conditions. The displacement analysis needs the flow rules. Equilibrium equation is

$$\frac{\partial \sigma_{rap}^{ep}}{\partial r} + \frac{(\sigma_{rap}^{ep} - \sigma_{\theta ap}^{ep})}{r} = 0 \tag{28}$$

yield condition is

$$\sigma_{\theta ap}^{ep} - \sigma_{rap}^{ep} = \sigma_y \tag{29}$$

The subscript *ap* identifies the stresses and displacements in the plastic region $b < r < c$ of the aluminum alloy. From Eqs 28 and 29 σ_{rap} and $\sigma_{\theta ap}$ can be obtained.

$$\sigma_{rap}^{ep} = \sigma_y \ln r + B_5 \tag{30}$$

$$\sigma_{\theta ap}^{ep} = \sigma_y + \sigma_y \ln r + B_5 \tag{31}$$

The displacement u_{ap}^{ep} will be determined later. The displacement function will contain another constant of integration denoted by *df*. The constants B_1, B_2, B_3, B_4, and B_5, *df*, and the unknown elastic-plastic boundary c can be obtained from the following seven boundary conditions.

$$r \rightarrow \infty, \qquad \sigma_{rae}^{ep} = 0 \tag{32}$$

$$r = c, \qquad \sigma_{rae}^{ep} = \sigma_{rap}^{ep} \tag{33}$$

$$r = c, \qquad u_{ae}^{ep} = u_{ap}^{ep} \tag{34}$$

$$r = c, \qquad \sigma_{\theta ae}^{ep} - \sigma_{rae}^{ep} = \sigma_y \tag{35}$$

$$r = b, \qquad \sigma_{rap}^{ep} = \sigma_{rs}^{ep} \tag{36}$$

$$r = b, \qquad u_{ap}^{ep} = u_s^{ep} \tag{37}$$

$$r = a, \qquad u_s^{ep} = \bar{u} \tag{38}$$

From Eqs 32, 33, 35, 36, and 38, the constants B_1, B_2, B_3, B_4, and B_5 can be evaluated in terms of the unknown elastic-plastic boundary. Then the following expressions can be written

$$\sigma_{rae}^{ep} = -\frac{\sigma_y}{2}\frac{c^2}{r^2}, \qquad r > c \tag{39}$$

$$\sigma_{\theta ae}^{ep} = \frac{\sigma_y}{2}\frac{c^2}{r^2}, \qquad r > c \tag{40}$$

$$u_{ae}^{ep} = \frac{1+\nu_a}{2E_a}\sigma_y\frac{c^2}{r}, \qquad r > c \tag{41}$$

$$\sigma_{rap}^{ep} = \sigma_y \ln\frac{r}{c} - \frac{\sigma_y}{2}, \qquad b < r < c \tag{42}$$

$$\sigma_{\theta ap}^{ep} = \sigma_y \ln\frac{r}{c} + \frac{\sigma_y}{2}, \qquad b < r < c \tag{43}$$

$$u_s^{ep} = \bar{u}\frac{r}{a} + F_1 b^2\left(\frac{1}{r} - \frac{r}{a^2}\right), \qquad a < r < b \tag{44}$$

$$\sigma_{rs}^{ep} = \frac{E_s}{1-\nu_s{}^2}\left\{\left(\frac{\bar{u}}{a} - \frac{b^2}{a^2}F_1\right)(1+\nu_s) - \frac{b^2}{r^2}F_1(1-\nu_s)\right\}, \qquad a < r < b \tag{45}$$

$$\sigma_{\theta s}^{ep} = \frac{E_s}{1-\nu_s{}^2}\left\{\left(\frac{\bar{u}}{a} - \frac{b^2}{a^2}F_1\right)(1+\nu_s) + \frac{b^2}{r^2}F_1(1-\nu_s)\right\}, \qquad a < r < b \tag{46}$$

where

$$F_1 = \frac{\dfrac{E_s}{1-\nu_s}\dfrac{\bar{u}}{a} + \dfrac{\sigma_y}{2} - \sigma_y \ln\dfrac{b}{c}}{\dfrac{E_s}{1-\nu_s}\dfrac{b^2}{a^2} + \dfrac{E_s}{1+\nu_s}} \tag{47}$$

The displacement u_{ap}^{ep} is now determined from the flow rules associated with the Tresca condition. The flow rules can be obtained by using Koiters' generalized plastic potential.[3]

$$d\bar{\epsilon}_{\theta ap}^{ep} = \lambda\, dc; \qquad d\bar{\epsilon}_{\theta ap}^{ep} = \lambda\, dc; \qquad d\bar{\epsilon}_{2ap}^{ep} = 0 \tag{48}$$

The quantity λ is the plastic flow function and dc is the incremental elastic-plastic boundary displacement. The bar has been placed on the strain increment for the following reason. The total strain increment in the plastic region is a combination of plastic strain increment and the elastic strain increment.[3] Then

$$d\epsilon_{rap}^{ep} = d\bar{\epsilon}_{rap}^{ep} + d\bar{\bar{\epsilon}}_{rap}^{ep} \tag{49}$$

The first term on the right hand side is given by Eq 48. The second term is given by the Hook's law

$$d\bar{\bar{\epsilon}}_{rap}^{ep} = \frac{1}{E}\left(d\sigma_{rap}^{ep} - \nu d\sigma_{rap}^{ep}\right) \tag{50}$$

---

[3] Fung, Y. C., *Foundations In Solid Mechanics,* Prentice Hall, Englewood Cliffs, N. J., 1965, p. 146.

Similar equations can be written for $d\epsilon_{ap}^{ep}$. Then, it can be shown by eliminating λ that

$$d\epsilon_{rap}^{ep} + d\epsilon_{\theta ap}^{ep} = \frac{1 - \nu_a}{E_a} (d\sigma_{rap}^{ep} + d\sigma_{\theta ap}^{ep}) \tag{51}$$

From kinematics, it is known that

$$d\epsilon_{rap}^{ep} = \frac{\partial}{\partial r} (du_{pp}^{ep}); \qquad d\epsilon_{\theta ap}^{ep} = \frac{du_{ap}^{ep}}{r} \tag{52}$$

Equations 51 and 52 can be used to obtain the following differential equation for incremental displacement du_{ap}^{ep}

$$\frac{\partial}{\partial r} (du_{ap}^{ep}) + \frac{du_{ap}^{ep}}{r} = -2\sigma_y \frac{1}{c} dc \frac{(1 - \nu_a)}{E_a} \tag{53}$$

Then

$$du_{ap}^{ep} = \frac{df}{r} - \sigma_y \frac{(1 - \nu_a)}{E_a} \frac{r}{c} dc \tag{54}$$

The constant df and the relationship between c and $\bar{u}$ can now be determined from the remaining boundary conditions, Eqs 34 and 37, that have not been used. These boundary conditions can be rewritten as follows

$$r = b, \qquad du_{ap}^{ep} = du_s^{ep} \tag{55}$$

$$r = c, \qquad du_{ap}^{ep} = du_{ae}^{ep} \tag{56}$$

From these two boundary conditions the following equation is obtained

$$\frac{d\bar{u}}{dc} = \frac{1}{F_2} \left\{ \frac{b}{c} F_3 - 2 \frac{c}{b} \right\} \tag{57}$$

where

$$F_2 = \left\{ \frac{E_s}{1 - \nu_s} \left(\frac{b^2/a^2 - 1}{f_1} - 1 \right) \frac{b}{a} \right\} \tag{58}$$

$$f_1 = \frac{E_s}{1 - \nu_s} \frac{b^2}{a^2} + \frac{E_s}{1 + \nu_s} \tag{59}$$

$$F_3 = \frac{\sigma_y}{f_1} \left(1 - \frac{b^2}{a^2} \right) + \sigma_y \frac{(1 - \nu_a)}{E_a} \tag{60}$$

$$F_4 = \frac{(1 + \nu_a)}{E_a} \sigma_y \tag{61}$$

Equation 57 can be integrated from the lower limit $\bar{u}_e$ to the upper limit corresponding to the value of the final value of radial displacement imparted by the mandrel $\bar{u}_f$. Then

$$\bar{u}_f = \bar{u}_e + \frac{1}{F_2} \left\{ F_3 b \ln \frac{c}{b} + F_4 (c^2 - b^2) \frac{1}{b} \right\} \tag{62}$$

Equation 62 provides the elastic-plastic boundary radius corresponding to the maximum radial displacement $\bar{u}_f$ introduced by the mandrel. The next step is the analysis of unloading.

Unloading

For elastic unloading, that is, withdrawing the cold-working mandrel from the sleeve, the stress and displacements can be written as follows

$$u_s^r = u_s^{ep}(r) + C_1 r + C_{2/r}, \qquad a < r < b \tag{63}$$

$$u_{ap}^r = u_{ap}^{ep}(r) + C_3 r + \frac{C_4}{r}, \qquad b < r < C \tag{64}$$

$$u_{ae}^r = u_{ae}^{ep}(r) + C_5 r + \frac{C_6}{r}, \qquad r > C \tag{65}$$

$$\sigma_{rs}^r = \sigma_{rs}^{ep}(r) + \frac{E_s}{1 - \nu_s{}^2}\left\{C_1(1 + \nu_s) - \frac{C_2}{r^2}(1 - \nu_s)\right\}, \qquad a < r < b \tag{66}$$

$$\sigma_{rap}^r = \sigma_{rap}^{ep}(r) + \frac{E_a}{1 - \nu_a{}^2}\left\{C_3(1 + \nu_a) - \frac{C_4}{r^2}(1 - \nu_a)\right\}, \qquad b < r < C \tag{67}$$

$$\sigma_{rae}^r = \sigma_{rae}^{ep}(r) + \frac{E_a}{1 - \nu_a{}^2}\left\{C_5(1 + \nu_a) - \frac{C_6}{r^2}(1 - \nu_a)\right\}, \qquad r > C \tag{68}$$

$$\sigma_{\theta s}^r = \sigma_{\theta s}^{ep}(r) + \frac{E_s}{1 - \nu_s{}^2}\left\{C_4(1 + \nu_s) + \frac{C_2}{r^2}(1 - \nu_s)\right\}, \qquad a < r < b \tag{69}$$

$$\sigma_{\theta ap}^r = \sigma_{\theta ap}^{ep}(r) + \frac{E_a}{1 - \nu_a{}^2}\left\{C_3(1 + \nu_a) + \frac{C_4}{r^2}(1 - \nu_a)\right\}, \qquad b < r < C \tag{70}$$

$$\sigma_{\theta ae}^r = \sigma_{\theta ae}^{ep} + \frac{E_a}{1 - \nu_a{}^2}\left\{C_5(1 + \nu_a) + \frac{C_6}{r^2}(1 - \nu_a)\right\}, \qquad r > C \tag{71}$$

In these equations the superscript r identifies the residual stresses and displacements after the mandrel is withdrawn. The six constants C_1, C_2, C_3, C_4, C_5, and C_6 can be determined from the following boundary conditions.

$$r = a, \qquad \sigma_{rs}^r = 0 \tag{72}$$

$$r = b, \qquad u_{rs}^r = u_{ap}^r \tag{73}$$

$$r = b, \qquad \sigma_{rs}^r = \sigma_{rap}^r \tag{74}$$

$$r = c, \qquad u_{ap}^r = u_{ae}^r \tag{75}$$

$$r = c, \qquad \sigma_{rap}^r = \sigma_{rae}^r \tag{76}$$

$$r \rightarrow \infty, \qquad \sigma_r^r \quad 0 \tag{77}$$

The following values of constants are obtained.

$$C_1 = \frac{C_2}{b^2} F_5 \tag{78}$$

$$C_2 = (1 + \nu_s)\frac{u}{a} - \frac{b^2}{a^2}\,\frac{\dfrac{E_s}{1 - \nu_s}\dfrac{u}{a} + \dfrac{\sigma_y}{2} - \sigma_y \ln\dfrac{b}{c}}{\dfrac{E_s}{1 - \nu_s}\dfrac{b^2}{a^2} + \dfrac{E_s}{1 + \nu_s}}\,\frac{1}{F_6} \tag{79}$$

$$C_3 = 0 \tag{80}$$

$$C_4 = \frac{C_2}{b^2} F_5 \tag{81}$$

$$C_5 = 0 \tag{82}$$

$$C_6 = C_4 \tag{83}$$

and

$$F_5 = \frac{\dfrac{E_s}{E_a}\,\dfrac{1 + \nu_a}{1 - \nu_s} - 1}{\dfrac{E_s}{E_a}\,\dfrac{1 + \nu_a}{1 - \nu_s} - 1} \tag{84}$$

$$F_6 = \frac{1 - \nu_s}{a^2} - \frac{1}{b^2} F_5(1 - \nu_s) \tag{85}$$

Summary

The threshold yielding displacement can be obtained from Eq 20. Then, the radius c of the elastic-plastic boundary corresponding to the applied maximum radial displacement $\bar{u}_f$ by the mandrel can be obtained by solving Eq 60 by trial and error approach. The residual stresses can then be obtained from Eqs 65–70 and 80–85. The maximum hoop stress is tension at the elastic-plastic boundary.

References

[*1*] Smith, C. R., "Preventing Fatigue Failures," *Assembly Engineering,* Hitchcock Publishing Co., Wheaton, Ill., March 1968.

[*2*] Speakman, E. R. in *Achievement of High Fatigue Resistance in Metals and Alloys, ASTM STP 467,* American Society for Testing and Materials, 1970, pp. 209–227.

[*3*] Hills, J. F., "Advantages of Some New Fastener Systems," Society of Automotive Engineers Business Aircraft Meeting, Wichita, Kans., 3–5 April 1968.

[*4*] Brown, R. H., Sprowls, D. O., and Schumaker, M. B. in *Stress Corrosion Cracking of Metals—A State of the Test, ASTM STP 518,* American Society of Testing and Materials, 1972, pp. 116–117.

[*5*] Carter, A. E. and Hanagud, S., "Stress Corrosion Susceptibility of Stress Coined Aluminum Alloy Structures," *Journal American Institute of Aeronautics and Astronautics,* Vol. *13,* No. 7, *1975,* pp. 858–863.

[*6*] "Stress Corrosion Test for Aluminum Alloy Plate, Extrusions, and Forgings by Alternate Immersion," Federal Test Method Standard No. 151b, Method 823, 1967.

C. M. Chen,[1] *M. H. Froning,*[1] *and E. D. Verink, Jr.*[1]

Crevice Corrosion and Its Relation to Stress-Corrosion Cracking

REFERENCE: Chen, C. M., Froning, M. H., and Verink, E. D., Jr., **"Crevice Corrosion and Its Relation to Stress-Corrosion Cracking,"** *Stress Corrosion—New Approaches, ASTM STP 610,* American Society for Testing and Materials, 1976, pp. 289–307.

ABSTRACT: Crevice corrosion of high-strength low-alloy D6AC and Type 316 stainless steel was surveyed using artificial crevice assemblies. A critical potential, referred to as the "crevice protection potential" was found, above which crevice corrosion occurs and below which it does not. The corrosion condition in the crevice is related importantly to the mechanism of cracking, that is, stress-corrosion cracking or hydrogen embrittlement.

KEY WORDS: stress corrosion, stainless steels, crack propagation, hydrogen embrittlement, pitting

Stainless steels are susceptible to crevice corrosion. For example a sheet of austenitic stainless steel can be cut by placing a stretched rubber band around it and then immersing the assembly in seawater [*1*].[2] Several types of crevice and stress-corrosion tests were performed to compare the behavior of Type 316 stainless steel with the high-strength, low-alloy steel D6AC.

Several authors [*1–4*] suggest that crevice corrosion and pitting corrosion propagate by similar mechanisms, that is, hydrolysis of metal ions leads to acidification within the occluded cell to balance charge and cause intensification of attack. Thus, some authors have characterized the process as "autocatalytic." The same autocatalytic process can be thought to occur in stress-corrosion cracking (SCC) at the crack-propagation apex. In this case the electrode potential at the crack apex is also important. If it is below (more active than) the equilibrium potential of the hydrogen electrode, hydrogen embrittlement is possible [*5*]. If the electrode poten-

---

[1] Visiting assistant professor, research engineer, and chairman and professor, Department of Materials Science and Engineering, University of Florida, Gainesville, Fla. 32611.

[2] The italic numbers in brackets refer to the list of references appended to this paper.

tial at the crack apex is more noble than the equilibrium potential of the hydrogen electrode, active path SCC is presumed to occur. Thus, the potential within the occluded cell may be used to differentiate the mechanism of cracking. It is possible for crevice corrosion, pitting corrosion, and SCC to occur "simultaneously" in a test assembly. It is also possible that one mode, say crevice corrosion, will initiate first and suppress pitting or stress corrosion elsewhere on the specimen as the result of providing cathodic protection to the remainder of the exposed area.

Experimental

D6AC high-strength, low-alloy steel and Type 316 stainless steel were used to conduct artificial crevice experiments along with a number of SCC tests. The D6AC was austenitized, quenched, and tempered to a final hardness of HRC 48, and Type 316 stainless steel was in the dead soft condition.

The following is an outline of the tests conducted:

Type I

Occluded Cell Crevice Tests—A number of tests were performed on both D6AC and Type 316 stainless steel using an occluded cell. The cell was adapted by Efird [*6*] from an original design published by Pourbaix [7] (Fig. 1).

Although the occluded cell geometry differs from that of an actual crevice it does present several advantages. The size of the occluded cell, which is separated from the bulk cell by a 4-μm porosity, fritted glass disk, permits measurements of crevice potential, pH, and Cl^- concentration.

Specimen Design—The bulk specimen in the cell consisted of a rectangular specimen with a wire soldered to the back. The front face of the specimen was mechanically polished through 600 grit silicon carbide (SiC). The specimen was then cleaned in acetone, rinsed with distilled water, and brush coated (except for a 6-cm^2 area on the front face) with three coats of Microshield[3] stop-off lacquer.

Preparation of the crevice specimen was identical to that of the bulk specimen except for its smaller size. The exposed area was 0.5 cm^2.

Electrolytes Employed—The bulk solution was 0.1 N sodium chloride (NaCl) + 0.0125 N sodium tetraborate ($Na_2B_4O_7$) adjusted with 1.0 N sodium hydroxide (NaOH) to pH = 10. The solution was saturated with oxygen throughout the test.

The crevice solution consisted of 0.1 N NaCl adjusted with 1.0 N NaOH to pH = 10. The $Na_2B_4O_7$ buffer was not used in the occluded cell.

---

[3] Trademark, Michigan Chrome and Chemical Company.

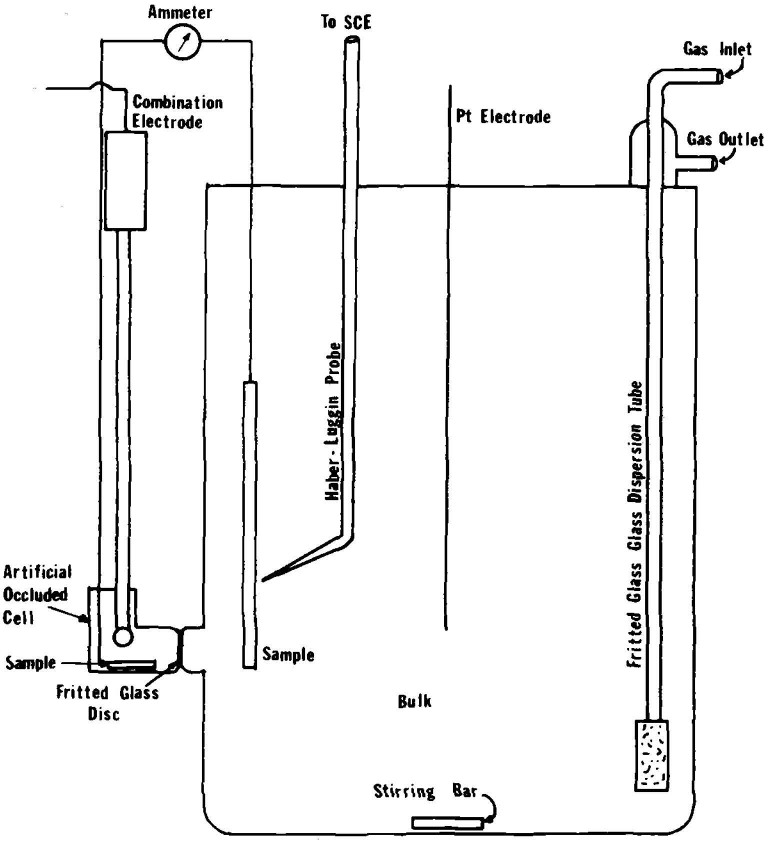

FIG. 1—*Artificial occluded crevice corrosion cell (Type I).*

Tests Conducted—A summary of the experiments performed using the occluded cell (Type I) test assembly is given in Table 1A.

Type II

Simulated Crevice Tests—The Type II crevice assembly shown in Fig. 2, was designed by Wilde [*8*] and consisted of two plates of steel fastened together by a plastic nut and bolt. The assembly is much closer in design to the geometry of an actual crevice; however, it does not provide an easy way to measure potential, pH, and Cl^- concentration inside the crevice.

Specimen Design—Crevices were prepared by mechanically polishing pairs of 2-in. (50.8-mm) long by 1-in. (25.4-mm) wide specimens through 600 grit SiC. (Thickness of the specimens depended on materials available in inventory; D6AC: 0.25 in. (6.25 mm) thick; Type 316 stainless steel:

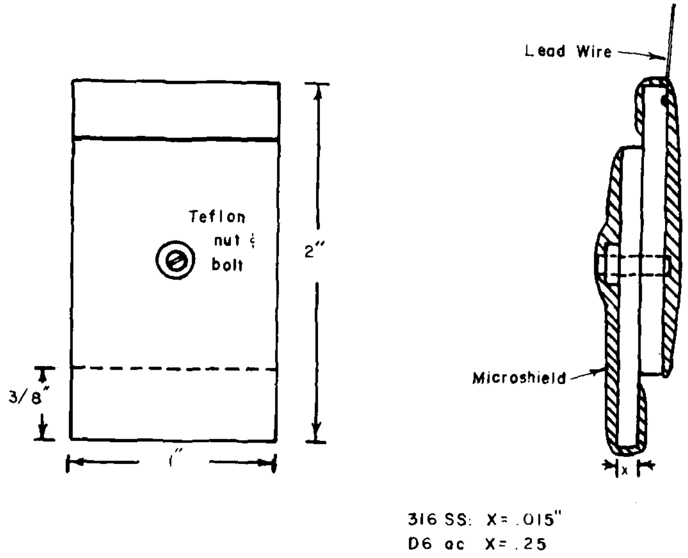

FIG. 2—*Artificial crevice assembly (Type II).*

0.015 in. (0.38 mm). A wire was soldered to the back of one of the specimens to aid in polarizing the crevice assembly. The specimens were cleaned in acetone, rinsed with distilled water, and air dried prior to assembly. The bulk areas of the specimen were then brush coated with three coats of Microshield.

Tests Conducted—A summary of the tests conducted using the Type II test assembly is given in Table 1B.

Type III

U-Bend Crevice/Stress Corrosion Tests—U-bend tests were performed on Type 316 stainless steel thin sheet specimens (4 by ½ by 0.015 in. (101.6 by 12.7 by 0.38 mm)). The specimens were prepared by masking off all but a $\frac{1}{16}$ in. (1.60 mm) wide section in the center with Microshield (Fig. 3*a*). The specimens were then bent into a U-configuration around a ¾-in. (19.1-mm) diameter steel mandrel and their ends restrained inside a ¾-in. (19.1-mm) inside diameter glass-ring fixture (Fig. 3*b*). The resulting applied stress was beyond the elastic limit but not calculated precisely. The specimens were then anodically polarized to various potentials to induce crevice corrosion under the Microshield adjacent to the $\frac{1}{16}$-in. (1.60-mm) wide exposed area. Resulting crevice corrosion, pitting corrosion, intergranular corrosion, and SCC were surveyed using the scanning electron microscope (SEM).

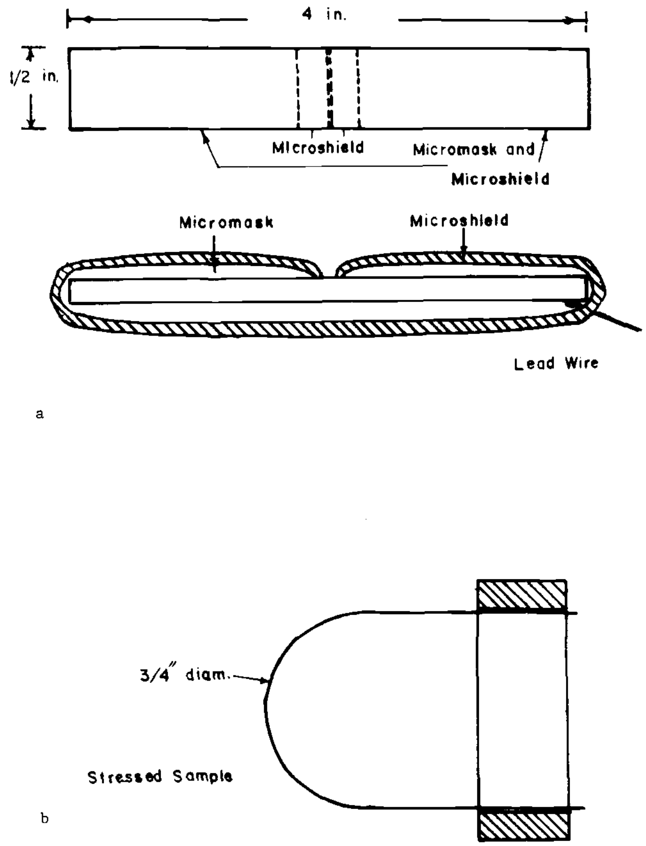

(*a*) Specimen coated with Micromask and Microshield.
(*b*) U-bend specimen in a glass ring fixture.

FIG. 3—*U-bend stress-corrosion specimen (Type III).*

The specimens of Type 316 stainless steel were all annealed under vacuum at 2000°F (1093°C) for 15 min and then given a sensitizing heat treatment for 2 h at either 1500°F (815°C) or 1200°F (649°C) prior to testing.

Results

Type I: Occluded Cell Crevice Tests

D6AC Steel—When the bulk and occluded specimens were not connected electrically in a pH 10 solution of 0.1 N NaCl (Test 1*a*, Table 1) the resulting corrosion potentials of the bulk and crevice specimens were –270 and –450 mV versus saturated calomen electrode (SCE), respectively. A subsequent polarization scan of the bulk specimen (Test 1*a*) resulted in a polarization curve which displayed no hysteresis when the scan direction was reversed.

TABLE 1—(A) *Summary of crevice corrosion tests performed using the occluded cell (Type I) test assembly.*

Test Number	Specimen	Test Description
1*a*	D6AC	free corrosion potentials of the bulk and crevice specimens were recorded after 10 min immersion, and then a polarization scan was obtained for the bulk specimen between −800 and −150 mV SCE; bulk and occluded specimens were not electrically connected
1*b*	D6AC	free corrosion potentials were obtained for both specimens after 10 min immersion; the specimens were then electrically connected to each other, and the current flowing from the crevice specimen to the bulk specimen (crevice current) was recorded; a polarization scan between −800 and −230 mV SCE was then performed on the bulk specimen (Fig. 4); crevice current versus the bulk specimen potential is shown in Fig. 6
2*a*	D6AC	bulk specimen was polarized at −400 mV, and the crevice current versus time was recorded
2*b*	D6AC	bulk specimen was then polarized to −550 mV, and again the crevice current versus time was recorded (Fig. 7)
2*c*	D6AC	electrometer was connected between the crevice specimen and a reference electrode in the occluded cell; the crevice potential versus bulk polarization potential was recorded (Fig. 5)
3	Type 316 stainless steel	a polarization scan between −600 and +460 mV SCE was made on the bulk specimen. A plot of crevice current versus bulk specimen potential was also obtained
4*a*	Type 316 stainless steel	bulk specimen was first polarized to +350 mV SCE to stimulate crevice corrosion, and then the potential was quickly lowered to −50 mV SCE

NOTE—1. Unless otherwise stated bulk and occluded specimens were electrically connected to each other through a zero resistance ammeter.
2. All polarization scans were performed using a scan rate of 600 mV/h.

TABLE 1—(B) *Summary of tests conducted using the Type II simulated crevice.*

Test Number	Specimen	Test Description
5*a*	D6AC	polarization scan in 0.1 N NaCl adjusted with 1.0 N NaOH to pH 10 and saturated with O_2
5*b*	D6AC	polarization scan in 0.1 N NaCl + 0.0125 N $Na_2B_4O_7$ adjusted with 1.0 N NaOH to pH 10 and saturated with O_2
5*c*	D6AC	polarization scan in 0.1 N NaCl + 0.1 N K_2CrO_4 and saturated with O_2 (Fig. 8)
6	Type 316 stainless steel	polarization scan in 0.6 N NaCl saturated with O_2 (Fig. 9)

NOTE—All polarization scans were performed using a scan rate of 600 mV/h.

A similar test was conducted with the bulk and occluded specimens connected through a zero resistance microammeter (Test 1*b*). The electrical connection of the specimens resulted in three notable observations. First, 75 μA of current began flowing from the crevice specimen to the bulk specimen. Second, the corrosion potential of the bulk specimen decreased from −270 to −405 mV SCE. Third, the corrosion potential of the occluded specimen (the crevice specimen) increased from −450 to −425 mV SCE (the remaining 20 mV difference in corrosion potential between the two specimens was attributed to a voltage (IR) drop through the cell). A subsequent polarization scan of the bulk specimen resulted in the polarization curve shown in Fig. 4. A significant hysteresis was observed.

In comparison it was noted that electrical connection of the bulk and occluded specimens resulted in a hysteresis which was associated with crevice corrosion.

Figure 5 (Test 2*c*), which is a plot of the crevice potential versus the bulk polarization potential, shows a pronounced deviation from linearity which increases with the polarization potential. This acts as a driving force for crevice corrosion.

Figure 6 is a plot of the crevice corrosion current (current measured by the microammeter connected between the bulk and occluded specimens) versus the bulk specimen potential. The figure indicates that when the bulk

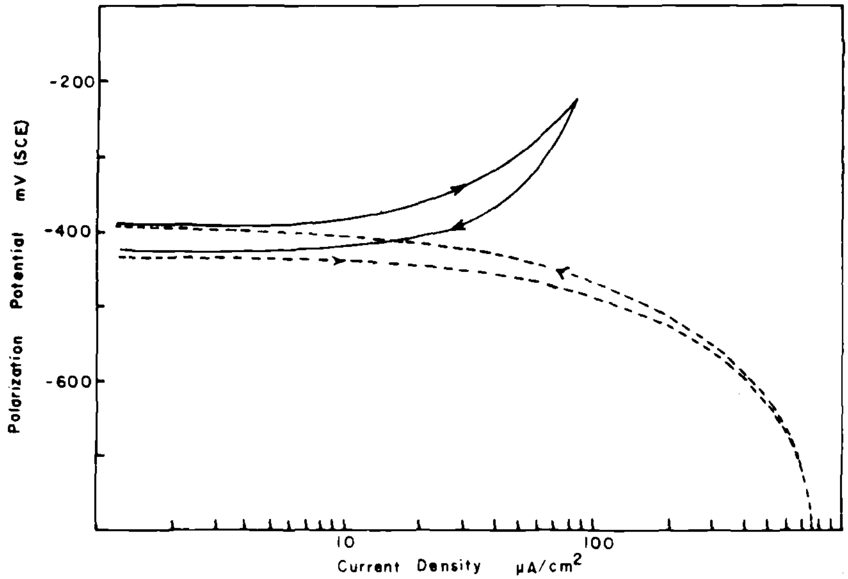

FIG. 4—*Polarization curve for D6AC bulk specimen when the bulk and occluded specimens were electrically connected by a zero resistance ammeter. Hysteresis was observed.*

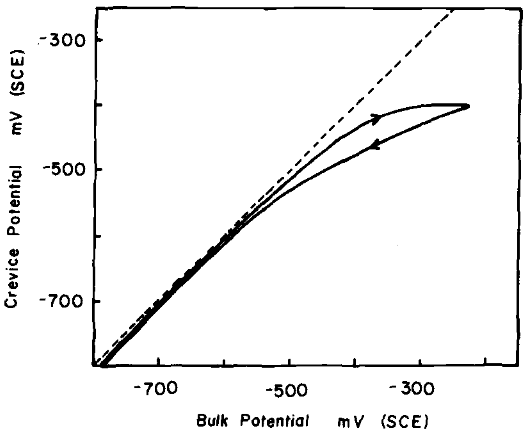

FIG. 5—*Occluded cell potential versus bulk potential for D6AC. Curve deviates from linearity.*

specimen was polarized to a potential more negative than a certain critical potential (approximately −610 mV SCE on Fig. 6) the crevice current changed from positive (corrosion of occluded specimen) to negative (no corrosion of occluded specimen). Also, the corrosion product in the occluded cell changed from bluish-black to brown. Efird and Verink [6], working with copper-nickel alloys, referred to an analogous potential as the "crevice protection potential." This potential, while somewhat influenced by experimental procedures (for example, scan rate, etc.), is reproducible within ±20 mV.

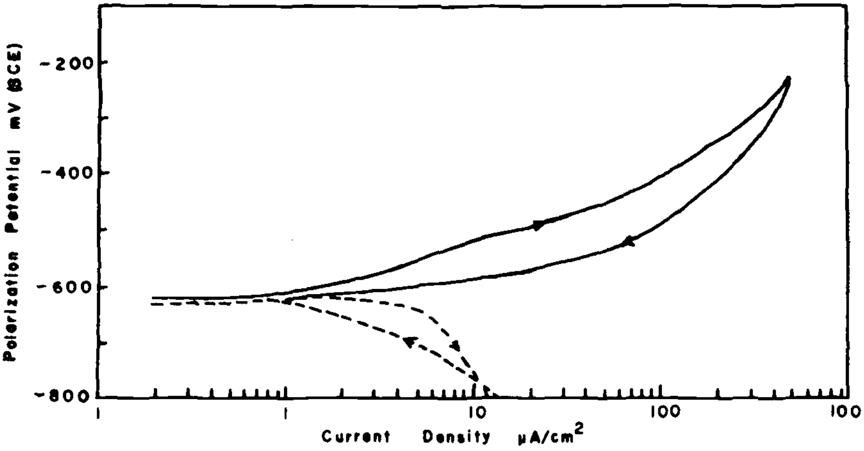

FIG. 6—*Crevice current between the bulk and occluded specimens versus bulk specimen polarization potential for D6AC. Current from crevice specimen changed from positive to negative at approximately −610 mV SCE.*

Additional specimens were potentiostatically polarized to −400 mV (Test 2*a*) and the crevice current monitored as a function of time. Since the potential was considerably more anodic than the critical potential (−610 mV SCE) crevice current continually increased with time. The indication is that once a crevice is initiated, maintenance of the electrode potential considerably more positive than the crevice protection potential will result in propagation of crevice corrosion.

Polarization at −550 mV SCE (Test 2*b*) which is still above but closer to the crevice protection potential resulted in the current versus time plot shown in Fig. 7. After an initial increase in current a maximum was reached followed by a gradual decrease in current and finally a change in current direction (that is, no crevice corrosion). The results thus indicate that the crevice protection potential determined through polarization scans may appear at a somewhat more active potential than the actual protection potential.

As a further verification of the validity of the concept of a crevice protection potential, a series of specimens were polarized and maintained at various potentials below −600 mV SCE. All of the specimens exhibited negative crevice currents (that is, no crevice corrosion), and occluded-cell pH increased to values higher than the bulk solution pH.

Type 316 Stainless Steel—Similar tests employing Type 316 stainless steel (instead of D6AC) were conducted (Tests 3, 4*a*, and 4*b*) and demonstrated that a similar crevice protection potential also exists for Type 316. As with D6AC, when the polarization potential was changed from a value above the crevice protection potential to a value below it, the corrosion product changed color from blue-black to brown.

Type II: Crevice Tests

D6AC—Polarization curves were obtained for D6AC in 0.1 N NaCl, 0.1 N NaCl + 0.125 N $Na_2B_4O_7$ adjusted to pH 10 with 1.0 N NaOH, and 0.1 N NaCl + 0.1 N potassium chromate (K_2CrO_4). All three curves showed severe hysteresis because of the crevice corrosion which occurred. The polarization curve obtained using the chromate solutions is shown in Fig. 8 and is representative of all three curves. The crevice protection potentials obtained from the polarization scans while reproducible, differed somewhat depending on the solution employed; this may have been due to some difference in chemical composition of the electroylte within the crevices.

Type 316 Stainless Steel—A polarization scan was made using a Type II, Type 316 stainless steel crevice specimen to confirm (again) the similarities of crevice corrosion behavior between D6AC and Type 316 stainless steel. Figure 9 shows the same type of hysteresis as obtained with D6AC (Fig. 8).

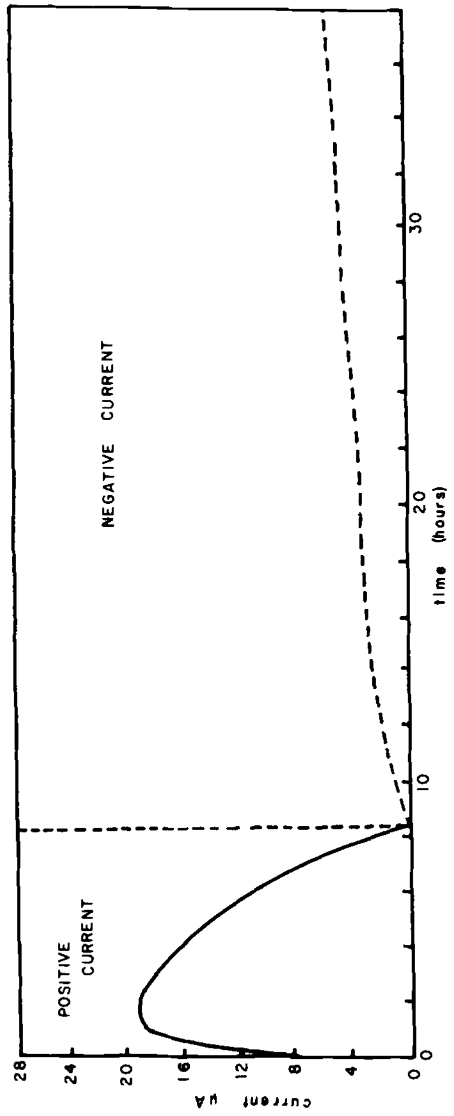

FIG. 7—*Crevice corrosion current between the bulk and occluded specimens versus time for D6AC when the bulk specimen was polarized at −550 mV SCE.*

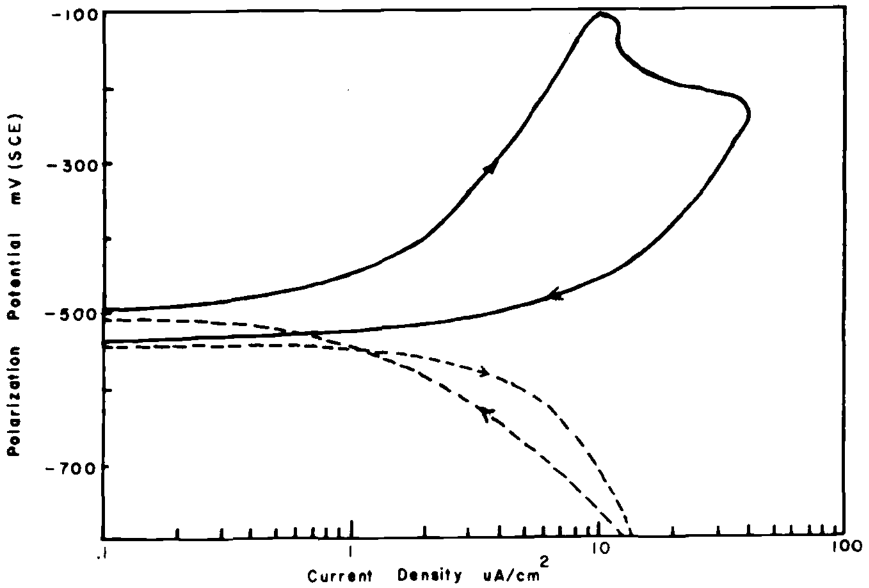

FIG. 8—*Polarization curve of a D6AC Type II crevice specimen in a 0.1 N NaCl + 0.1 N K_2CrO_4 solution.*

Type III: Crevice-Stress-Corrosion Tests

Type 316 Stainless Steel—When crevice corrosion of Type III specimen was induced, gross pitting, intergranular corrosion, and SCC were retarded on the uncoated (exposed) area of the specimen. Although they were not easily visible to the unaided eye, SEM studies revealed all these processes did occur simultaneously inside the crevice.

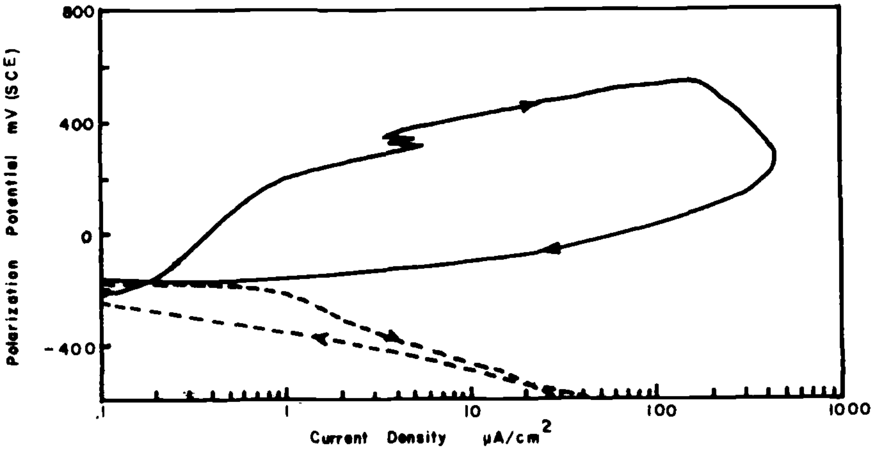

FIG. 9—*Polarization curve of the Type 316 stainless steel Type II crevice assembly in 0.6 N NaCl after immersion in the solution for 42 h.*

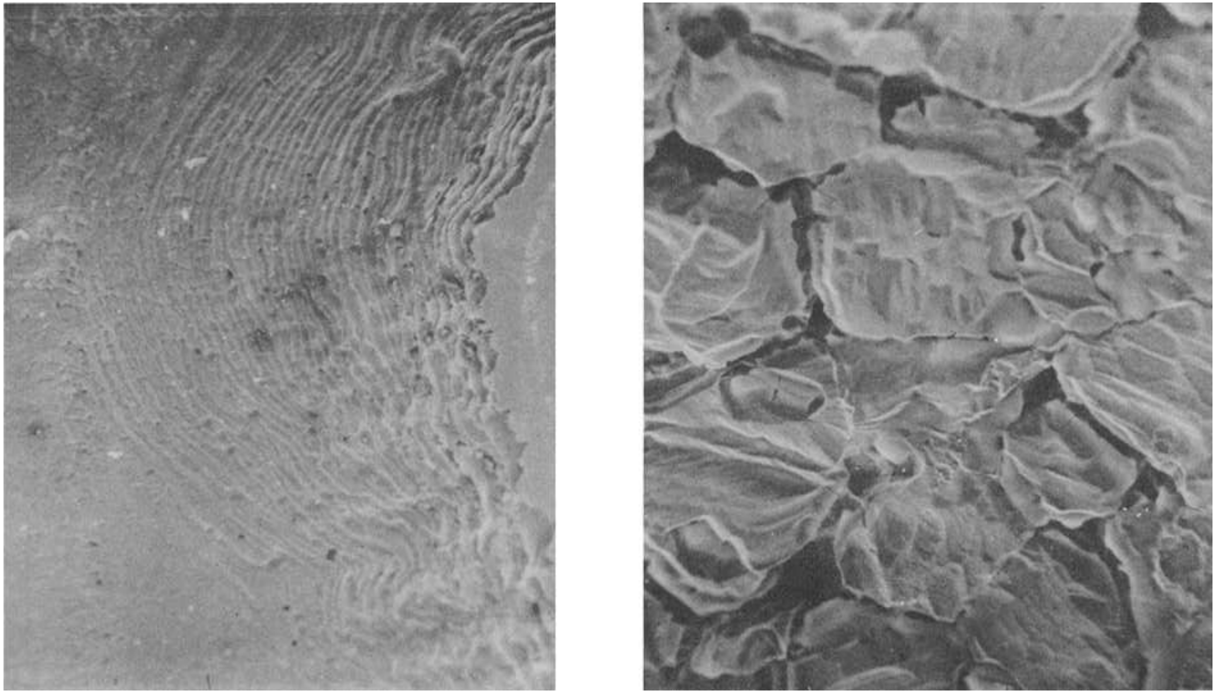

(*a*) Crevice corrosion observed under Microshield coating (×20).
(*b*) Intergranular corrosion, pitting, and general dissolution inside crevice (×200).

FIG. 10—*Scanning electron photographs of crevice corrosion areas on Type III Type 316 stainless steel. Specimens were annealed, then sensitized 2 h at 1200°F (649°C) prior to immersion.*

(*c*) Subcracking in grain boundaries (×450).
FIG. 10—*Continued.*

Figure 10*a* shows the crevice corrosion observed under the Microshield coating, for the annealed Type 316 stainless steel specimens which had been sensitized 2 h at 1200°F (649°C) and water quenched. As is shown in Fig. 10*b*, intergranular corrosion and pitting are apparent in addition to general dissolution within the crevice. Subcracking is visible both in the grain boundaries and inside the pits (Fig. 10*c*).

Annealed specimens sensitized 2 h at 1500°F (815°C and water quenched, showed intergranular corrosion and some intergranular SCC along with the crevice corrosion. Grains were separated almost completely from the specimens.

Discussion

Although the Type I crevice assembly has a geometry which differs from an actual crevice, it simulates many of the characteristics of the latter while retaining the ability to monitor potential, pH, etc. The potentiodynamic polarization data for both D6AC and Type 316 stainless steel provides evidence of the existence of a critical potential called the crevice protection potential above which crevice corrosion occurs and below which crevice corrosion is retarded. The precise value of the crevice protection potential varies somewhat with the manner in which the test is performed, but the conditions of testing used herein appear to place it at a somewhat lower potential (more conservative) than the protection potential against pitting.

In all cases the crevice current flowed from the crevice to the bulk specimen, and the corrosion product was blue-black in color when the bulk polarization potential was above the crevice protection potential; below this potential, the crevice current flowed from the bulk to the crevice specimen, the pH in the crevice increased, and the corrosion product changed to a brown color. X-ray analysis failed to confirm the compositions of the corrosion products.

Similar results were obtained for both D6AC and Type 316 stainless steel from tests employing the Type II crevice assembly, which more closely duplicates the geometry of an actual crevice but which does not permit easy monitoring of potential and pH changes. Such results seem to confirm the validity of the observations from the Type I tests.

When crevice corrosion occurred in the Type I (occluded cell) tests, the potential and pH in the crevice were shifted to values which correspond to the corrosion region (in the Pourbaix diagram for iron) while those of the bulk remained in the passivation region. The potential and pH seemed to be a function of the bulk polarization potential as is shown by Pourbaix for ordinary carbon steel in Fig. 11*a* [*9*]. The tendency of the potential and pH to change shows that the more noble the bulk polarization potential, the lower the pH and the more noble the potential in the crevice. The locus of points which depict the potential and pH of the crevice (Fig. 11*a*) seems to depend on the material, solutions, etc.

In general it seems reasonable to classify the crevice corrosion into three cases as follows:

Case 1

The locus of pH and potential points in the crevice is above the extension of the iron oxide (Fe_2O_3) formation line [*17*] (Fig. 11*b*). Dotted lines 1, 2, 3, 4, 5, 6, and 7 show the corresponding pH and potential points in the crevice and the bulk cell. As the bulk polarization potential decreases in the cathodic direction, the pH increases, and the potential decreases in the crevice as dotted lines 1, 2, and 3 show. The potential in the crevice is more active than that of the bulk, and the crevice current, therefore, flows from the crevice to the bulk specimen. When dotted line 4 hits the Fe_2O_3 formation line [*28*], crevice corrosion is retarded, and the pH in the crevice increases crucially. Further polarization will increase the crevice pH even higher than that of the bulk; the potential in the crevice

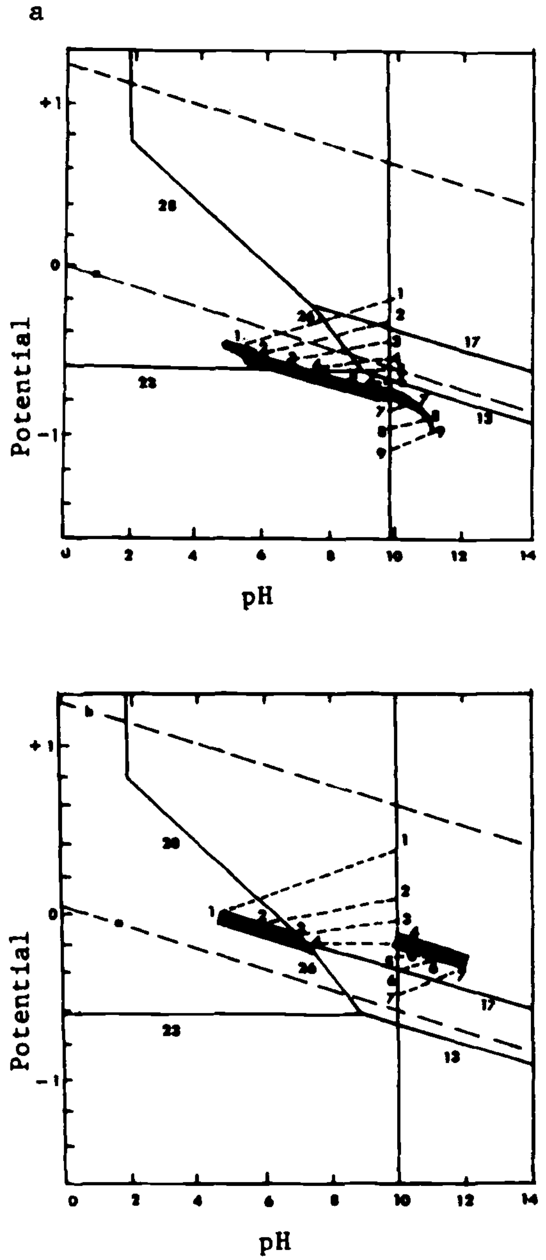

FIG. 11—(a) *Influence of external polarization on the potential* and *pH inside the crevice for an ordinary carbon steel.* (b) *Influence of external polarization on the potential and pH inside the crevice for an austenitic stainless steel.*

is a little more noble than that in the bulk, and the polarity of the crevice current is changed to negative, that is, the crevice corrosion is retarded. Copper and its alloys [*6*] as well as Type 316 stainless steel appear to belong to this category. In the experimentally determined potential pH diagram for Type 316 stainless steel the protection potential is definitely above the equilibrium hydrogen evolution line [*10*]. No hydrogen evolution will occur in the crevice in this case since the potential is above the equilibrium hydrogen line.

Case 2

The locus of pH and potential points in the crevice is below the iron oxide (Fe_3O_4) formation line [*13*], and its extension as shown by Pourbaix [*9*] in Fig. 11*a*. When dotted line 4 hits the immunity line [*23*] at the crevice protection potential, the crevice corrosion becomes negligible. Further cathodic polarization increases the pH inside the crevice. When the potential is below dotted line 7, the potential in the crevice is more noble than that of the bulk, and current polarity is changed to negative; the pH in the crevice becomes higher than that in the bulk. Ordinary carbon steel, and low-alloy, high-strength steel (for example, D6AC) belong to this category. Hydrogen evolution can occur in the crevice in this case since the electrode potential in the crevices is below the potential of the equilibrium hydrogen electrode. This is shown by the experimental potential pH diagram developed by Johnson [*11*]. Care must be exercised in the use of such materials since they are subject to hydrogen embrittlement unless special procedures can be employed to avoid hydrogen entry into the steel (see Parrish et al [*12*]).

Case 3

The locus of pH and potential points in the crevice is between the Fe_2O_3 and Fe_3O_4 formation lines [*13,17*], and their extensions. The locus of pH and potential points in the crevice will hit the Fe_3O_4 formation line [*26*] as the bulk polarization potential is decreased in the cathodic direction. It depends on whether the locus is above (or below) the hydrogen line whether hydrogen evolution will (or will not) occur in the crevice.

Since crevice corrosion, pitting corrosion, and SCC could possibly propagate with a similar mechanism, this concept for crevice corrosion can be applied to the mechanisms for SCC. It is clear that the stress cracking mechanism depends on the location of the locus of the crevice pH and potential in the potential pH diagram. When the crevice corrosion occurs like Case 1 where the locus of pH and potential in the crevice is above the hydrogen evolution line, hydrogen embrittlement is impossible, and the SCC is due mainly to autocatalytic and stress assisted anodic dissolution

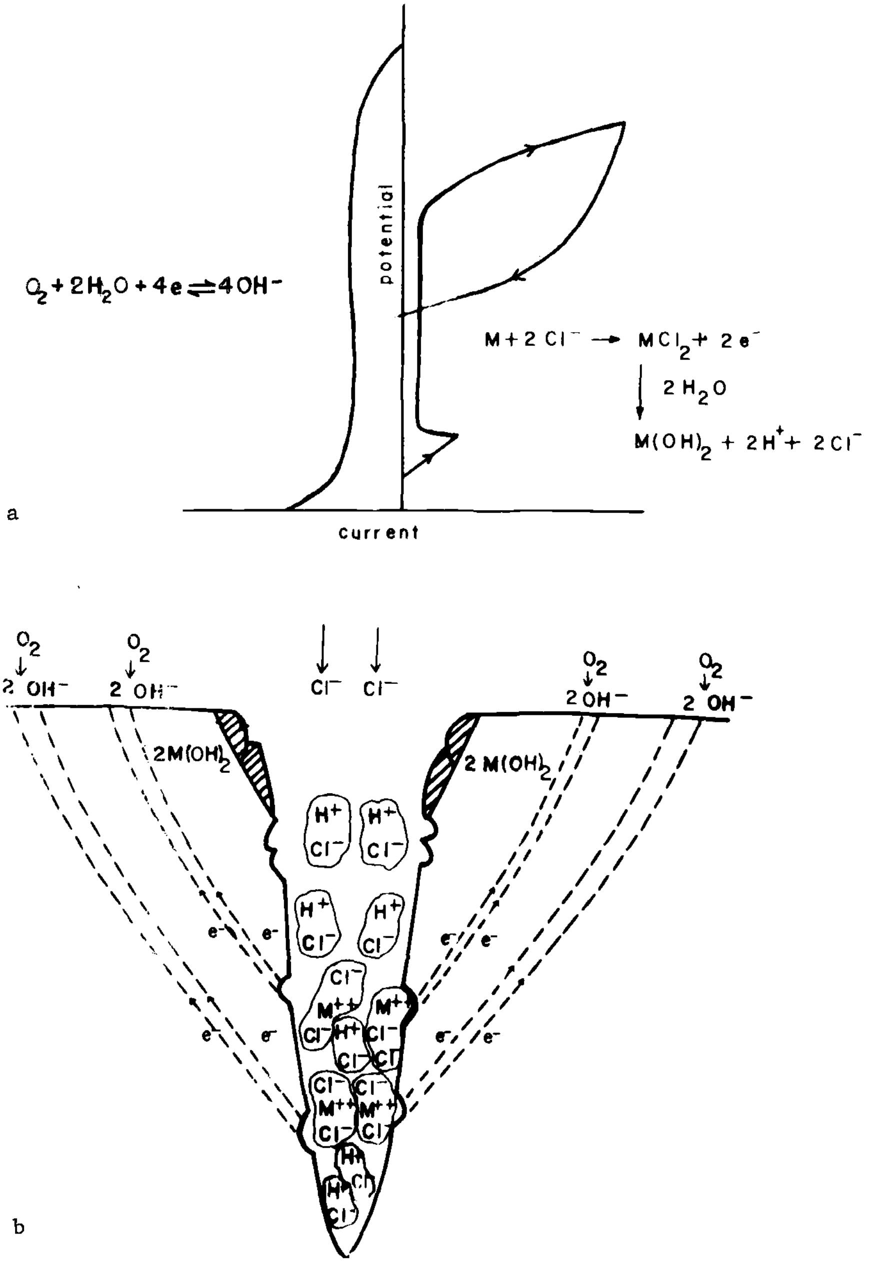

(*a*) Schematic diagram for polarization curve as found in Type 316 stainless steel.
(*b*) Schematic picture for SCC of Type 316 stainless steel.

FIG. 12—*Crevice effect on SCC when crevice condition is above the equilibrium hydrogen evolution line.*

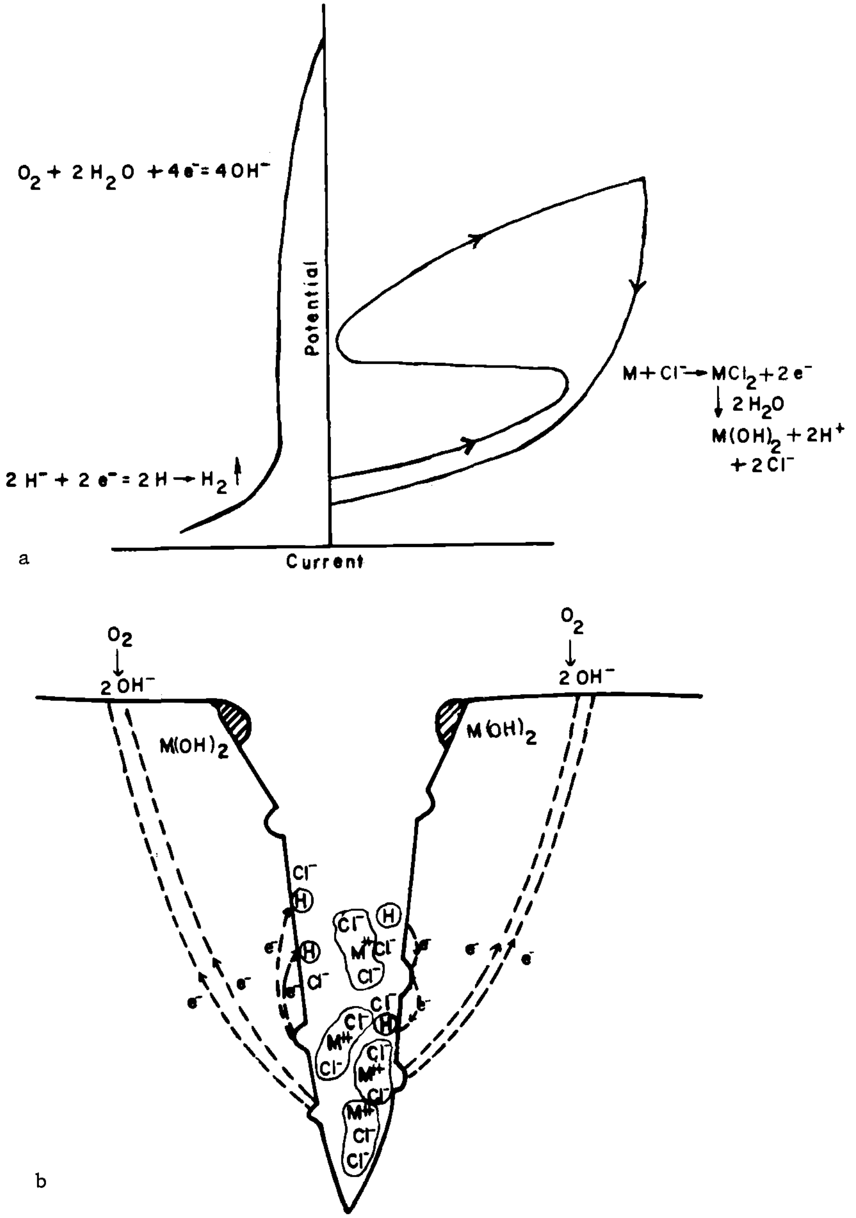

(*a*) Schematic diagram for polarization curve as found in D6AC.
(*b*) Schematic picture for SCC of D6AC.

FIG. 13—*Crevice effect on SCC when crevice condition is below the equilibrium hydrogen evolution line.*

as is shown in Fig. 12. When the crevice corrosion occurs like Case 2 where the locus of pH and potential in the crevice is below the hydrogen evolution line, both hydrogen embrittlement and SCC are possible as is shown in Fig. 13. Case 3 would present a possibility of cracking by either mode, depending on the potential and pH in the crevice and its relation to the potential of the equilibrium hydrogen electrode.

References

[*1*] Fontana, M. G. and Greene, N. D., *Corrosion Engineering,* McGraw-Hill, New York, 1967, p. 39.

[*2*] Rosenfeld, L. and Marshakov, I. K., *Corrosion,* Vol. 20, 1964, p. 115t.

[*3*] Schafer, G. J. and Foster, P. K., *Journal of the Electrochemical Society,* Vol. 106, 1959, p. 468.

[*4*] Schafer, G. J., Gabriel, J. R., and Foster, P. K., *Journal of the Electrochemical Society,* Vol. 107, 1960, p. 1102.

[*5*] Brown, B. F., *Rapports Technique,* Vol. 112 RT 170, 1970, p. 1.

[*6*] Efird, K. D. and Verink, E. D., Jr., submitted for publication in *Corrosion.*

[*7*] Pourbaix, M., *Corrosion,* Vol. 26, 1970, p. 431.

[*8*] Wilde, B. E., *Corrosion,* Vol. 28, 1972, p. 283.

[*9*] Pourbaix, M., *Lectures on Electrochemical Corrosion,* Plenum Press, New York, 1973, p. 274.

[*10*] Froning, M. H., unpublished work, University of Florida, Gainesville, Fla., 1974.

[*11*] Johnson, J. M., "Use of Experimental Potential pH Diagram for D6AC Steel to Interpret Its Corrosion Behavior in Aqueous Media," M.S. thesis, University of Florida, Gainesville, Fla., 1974.

[*12*] Parrish, P. A., "The Retardation of Crack Propagation for High Strength, Low Alloy Steels in Aqueous Media by Addition of Oxidizing Inhibitors," Ph.D. dissertation, University of Florida, Gainesville, Fla., 1974.

S. W. Dean, Jr.[1]

Review of Recent Studies on the Mechanism of Stress-Corrosion Cracking in Austenitic Stainless Steels

REFERENCE: Dean, S. W., Jr., "**Review of Recent Studies on the Mechanism of Stress-Corrosion Cracking in Austenitic Stainless Steels,**" *Stress Corrosion—New Approaches, ASTM STP 610,* American Society for Testing and Materials, 1976, pp. 308–337.

ABSTRACT: A review of the work done to elucidate the mechanism of stress-corrosion cracking of austenitic stainless steels is presented. The major emphasis is placed on the cracking which occurs in chloride environments, although other environments are mentioned. This paper is intended to update earlier reviews and is concerned mainly with works published in the period 1960–1971.

The various studies on the effects of environmental and metallurgical factors on the kinetics of the cracking process are reviewed in detail. Variables such as temperature, chloride concentration, pH, stress, and metallurgical state are discussed. Also, the various studies on the electrochemistry of the system are reviewed.

The major theories on the mechanism of the cracking process are divided into two groups: The electrochemical theories postulate that the effect of tensile stress is to accelerate the localization of the corrosion process at crack sites. These theories include stress assisted segregation of damaging elements in the steel to the crack region, moving crystal imperfections including dislocations, and slip steps. The hydrogen entry theories, such as the formation of an easily corroded hydride phase or eta martensite formation, also fall into this category. The quasi-mechanical theories involve a mechanical fracture step in addition to corrosion. Tunnel pitting, corrosion produced wedging, and reduction of stress energy required to propagate a crack through chemical adsorption are examples of these theories. Finally, some areas of future work are discussed, and questions which need to be resolved are delineated.

KEY WORDS: stress corrosion, austenitic stainless steels, crack propagation, nucleation, residual stresses, plastic strain, magnesium chloride

Stress-corrosion cracking (SCC) is usually defined in terms of a cracking process which requires the simultaneous action of tensile stress and a

---

[1] Formerly, supervisor, Corrosion Group, Metals Research Laboratories, Olin Corp., New Haven, Conn. 06504; presently, senior corrosion engineer, Corporate Engineering Department, Air Products and Chemicals, Inc., Allentown, Pa. 18105.

specific corrosive environment which leads to an early failure of the alloy. It is a serious problem with many alloys. Stainless steels in particular have suffered from this form of failure because their unique corrosion resisting nature has led to their widespread use in a variety of environments. Since this problem was first recognized, there have been many studies of the problem. The results of these studies have been summarized from time to time in a number of excellent review papers [*1–4*].[2]

The purpose of this review is primarily to summarize the published works which pertain to the mechanism of SCC of austenitic stainless steels over the period from 1960–1972. The major emphasis has been placed on the phenomenological aspects of chloride induced cracking to show both what has been learned about this problem and what areas need further work. In addition, there is a discussion of the various environments which cause SCC in austenitic stainless steels together with a discussion of the many theories of stress cracking which have been put forth to explain this phenomenon.

Environments Which Cause Cracking

Hot Chlorides

Probably the most widely encountered form of stress failure occurs in aqueous chloride environments at temperatures above 80°C. In this case, the cracking follows a transgranular path [*1*]. Figure 1 shows a photomicrograph of a typical transgranular crack in section. Because it has been so widely encountered, it has become the most studied type of SCC failure in these alloys. The chloride ion is ubiquitous in aqueous environments, and, as a result, there have been many failures, often in unexpected locations. This has placed a severe limitation on the use of austenitic stainless steel in process equipment.

Much of the experimental work on chloride cracking has been carried out in artificial environments such as boiling magnesium chloride ($MgCl_2$) solutions. Although these solutions cause rapid cracking they do not necessarily simulate the cracking observed in field applications. Therefore, the results and conclusions from laboratory studies must not be extrapolated to plant situations without justification. Moreover, it should be noted that there are other ions besides chloride which can cause cracking. Thus, in field failures, it is necessary to establish which ions in fact caused the failure observed. It is not sufficient to deduce from the fact that transgranular SCC occurred that chloride was present. The hot chloride environment is discussed in greater detail later.

---

[2] The italic numbers in brackets refer to the list of references appended to this paper.

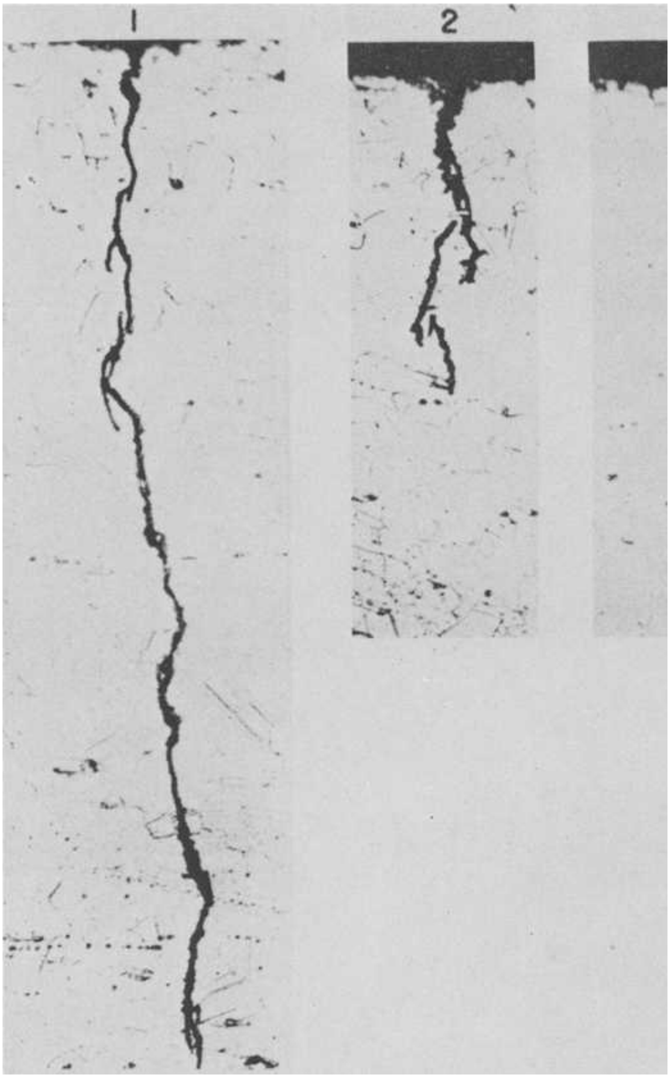

FIG. 1—*Sections of Type 347 stainless steel bent beam specimen exposed to aqueous chloride solution at 204°C (~×350)* [36].

Caustic

Another widely encountered environment which causes stainless steels to crack is hot concentrated caustic. This environment has not received the attention which chlorides have [*5*]. Alkali metal hydroxides are frequently used to adjust the pH of aqueous systems. When water containing these free hydroxides contacts hot stainless steel surfaces, the water evaporates leaving a concentrated caustic electrolyte which can then cause cracking.

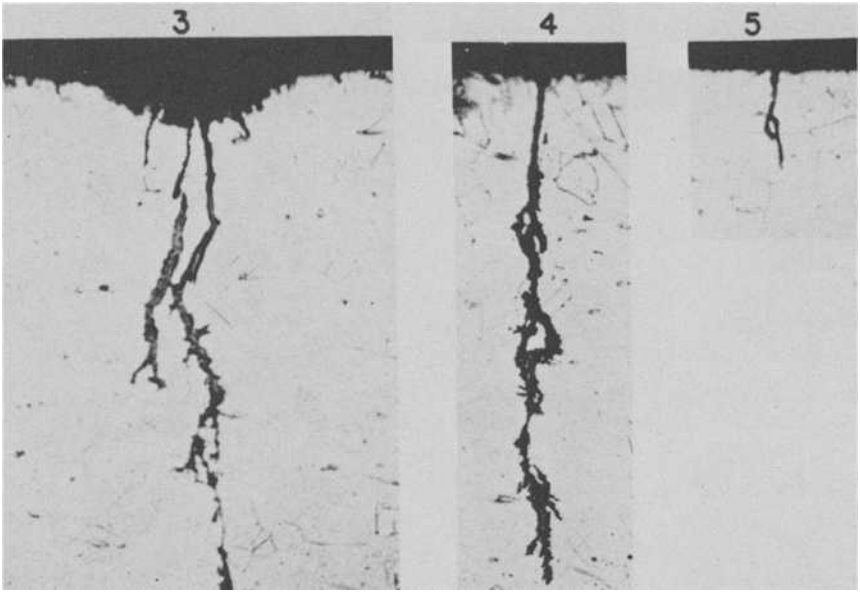

FIG. 1—*Continued.*

Neither water nor oxygen is necessary for caustic cracking [*5*]. In fact, the presence of oxygen may delay or inhibit the cracking process. At temperatures over 300°C caustic concentrations as low as 2 percent have been reported to cause cracking. Alkaline salts, such as sodium carbonate (Na_2CO_3) and sodium phosphate (Na_3PO_4) do not cause cracking so long as there is no free hydroxide present. However, at proper environment and temperature conditions, (especially at high temperatures) Na_2CO_3 can dissociate and form free sodium hydroxide ($NaOH$).

The morphology of the cracking which occurs in caustic is not unique. Both intergranular and transgranular cracks form under various conditions. At lower temperatures and caustic concentrations intergranular cracks are prevalent [*6*]. In these cases sensitizing heat treatments of the alloy tend to accelerate the cracking process. At higher temperatures, namely, around 300°C, the cracking process tends to be transgranular [*7*].

It should be noted that the caustic cracking process is fundamentally different from the chloride cracking which has been so widely studied. Most of the alloys with high nickel contents which successfully resist chloride cracking are prone to rapid cracking failure in caustic. This emphasizes the need for correct diagnosis in analyzing field failures. Exposure to high-temperature caustic usually results in a characteristic blue oxide on stainless steels, and this can be an important clue in diagnosing failures [*8*].

Other Environments

SCC failures have been reported in a variety of other environments. These have not been studied in detail and so will only be mentioned in passing. Acello and Greene [*9*] have reported intergranular SCC in sulfuric acid (H_2SO_4) solutions containing chlorides at room temperatures. This work confirmed observations by others who have noted the tendency for austenitic stainless steels to crack intergranularly in chloride solutions at lower temperatures than is noted normally in transgranular cracking.

Intergranular failures have also been noted in high-temperature water containing oxygen [*10*]. In this case crevices of some type are usually necessary to initiate the corrosion process which precedes the cracking step. Sensitizing heat treatments accelerate this type of cracking. Polythionic acid and other related sulfide environments may cause failures as well under some circumstances. Also situations which cause hydrogen entry into the alloy can cause a type of failure which is more properly treated as hydrogen embrittlement rather than SCC and so is beyond the scope of this paper.

General Observations on the Phenomenonology of Chloride Cracking

The cracking process is considered generally to have two steps, initiation and propagation. During the initiation period, no cracking occurs, but the corrosion process proceeds to develop conditions suitable for the initiation of cracking. Creep rate studies [*11*] have demonstrated that these processes are clearly separate in the sense that the kinetics of each process are different. Kohl's results on this are shown in Fig. 2.

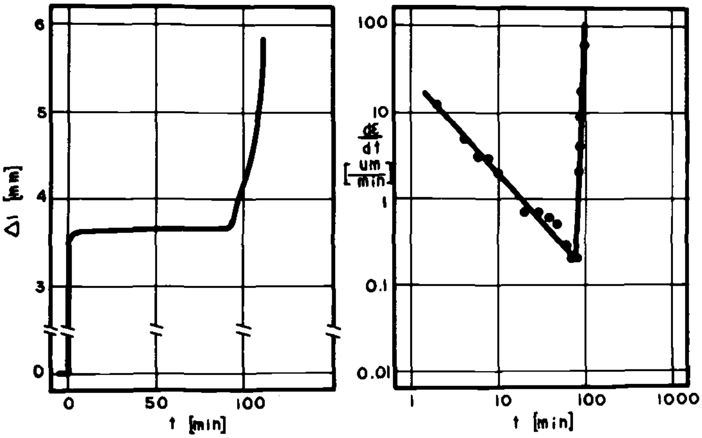

FIG. 2—*Time-elongation curve and time-elongation rate (creep rate) curve of stainless steels in $MgCl_2$ solution showing onset of cracking* [11].

Kinetics

The most widely used concept in describing the kinetics of cracking processes is that of "time to failure" or "time to cracking." This is, at best, an imperfect measure. In some cases, it means the time to develop a visible crack on the surface of a specimen. Here the time reported is roughly equal to the initiation time. This concept has been very useful in alloy development work where the emphasis is on determining whether a particular alloy will crack in an environment. Of course, the results are affected strongly by the type of specimen used and on the technique of examining the specimen.

In other cases, the end point of the tests is the failure of the specimen as determined by a loss of strength or breaking of the piece [*12*]. In these types of specimens, the failure time is a composite of the initiation time plus some additional time for the crack to penetrate through the specimen.

In both of these tests, the result obtained is strongly specimen dependent, and in that sense the results are somewhat qualitative in nature. Other work has shown that the specimen preparation has a significant effect on both the magnitude and reproducibility of cracking time.

The crack initiation process is, in fact, a random process which occurs at points on the stressed surface. Cracks then grow laterally as well as into the specimen. The random nature of the crack initiation process resembles the pit initiation process. The larger the area under stress the more likely it is for an early crack to form. This also points up the reason why initiation time results are determined largely by the type of specimen used. The American Society for Testing and Materials (ASTM) has recognized the importance of specimen preparation in obtaining reproducible results in SCC testing. ASTM Committee G-1 on the Corrosion of Metals has investigated this problem and has standards underway for most of the commonly used types of specimens [*14,15*] including the bent beam, U-bend, direct tension, precracked specimen, and others.

There have been some studies on the crack propagation processes in austenitic stainless steels. The propagation rate has been commonly expressed as a penetration rate and various ranges have been reported. Some of these results are shown in Table 1. The crack propagation rate is clearly a function of numerous environmental and alloy variables, and so it is not surprising that there has been relatively little agreement over the values reported. Furthermore, the cracks do not penetrate the metal in a straight line path but generally show frequent changes in direction and branching as well.

Eckel [*16*] has shown that the crack penetration process is not linear but rather follows a logarithmic law of the form (Fig. 3)

$$\ln \frac{T}{T_0} = \frac{D}{M} \qquad (1)$$

where

T = total exposure time,
T_0 = time to initiate the cracking process,
D = maximum crack depth, and
M = a constant.

The value of M is obtained from the slope of the line obtained by plotting D versus log T. The rate of crack propagation can then be obtained by differentiating Eq 1

$$\frac{dD}{dT} = \frac{M}{T}, \qquad T > T_0 \tag{2}$$

Eckel suggested that this expression is not correct because Eq 1 contains both nucleation and growth rate terms. He proposed that the crack-growth rate should be a function of the time from nucleation rather than the total exposure time, and he suggested the following relationship as being more suitable

$$\frac{dD}{dT} = \frac{M}{T - T_0}, \qquad T > T_0 \tag{3}$$

One objection to this analysis is that Eq 3 predicts an infinite crack-growth rate at the instant of crack nucleation. Moreover, the data presented followed the rule shown in Eq 1 rather than Eq 3. In addition, these data were obtained on U-bend specimens, and there is some question whether other types of specimen loading would behave similarly.

Eckel also reported data for the mean crack depth as a function of exposure time. The mean crack depth leveled out for Type 304 stainless steel after about 80 min, even though the maximum crack depth continued to

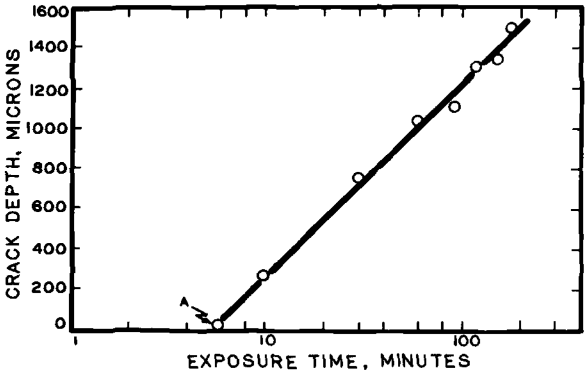

FIG. 3—*Maximum crack depth versus exposure time for stainless steel in boiling MgCl₂* [16].

TABLE 1—*Crack-propagation speed for stress-corrosion cracks in austenitic stainless steels in aqueous chloride environments.*

Reference	Date	Stress, ksi	Specimen Type	Environment		Alloy Type	Rate	
				Temperature, °C	Solution		nm/s	mm/h
Greeley et al [*24*]	1965	10 to 30	DTW	154	$MgCl_2V$	302	18 to 56	0.06 to 0.20
Hawkes et al [*23*]	1963	11 to 65	DTW	154	$MgCl_2V$	316	14 to 35	0.045 to 0.12
Kraft [*19*]	1965	10 to 20	DTW	154	$MgCl_2V$	302	50 to 180	0.18 to 0.65
Staehle [*36*]	1959	3, 7	3PT	264	NaCl	347	19 to 56	0.07 to 0.2
Hoar [*18*]	1956	0 to 60	DTW	154	$MgCl_2L$	various		0.5 to 3

NOTE—DTW = direct tension wire.
3PT = bent beam: 3-point load.
V = vapor.
L = liquid.

grow. This suggests that the new cracks which nucleated later were not growing as fast as the deeper cracks. This is reasonable because the deeper cracks tend to relieve the stress at the surface of the specimen.

Many of the important questions concerning the kinetics of the stress-corrosion process of austenitic stainless steels which were considered in early studies have not been reevaluated in more recent work. For example, the question of the rate of the stress-corrosion process relative to the general-corrosion process has not been considered recently. With the event of rapid chemical analysis techniques, for example, atomic absorption, it would be of interest to know quantitatively how much of the corrosion products of the stress-corrosion process ends up dissolved in the solution relative to that remaining on the crack walls as oxide or other insoluble product. Also, it is of interest to know if there is any evidence for concentration of one or more of the alloy component elements in the surrounding solution. Wilde [*17*] has made some measurements which provide insight into these questions. He found that the chromium content in the $MgCl_2$ solution was lower than would be expected based on the alloy content. This work is discussed later.

Effects of Stress

The existence of tensile stress at the metal surface is a necessary condition for SCC. However, the quantitative effect of stress on the kinetics of the stress-corrosion process is not a simple question in view of the interaction of specimen geometry with the kinetics of the cracking process.

One of the most interesting questions relative to the effect of stress is whether there is a threshold stress below which SCC does not occur. The procedure here is to run tests at various stress levels and obtain data which is then plotted as stress versus time to failure. This is analogous to the technique for handling fatigue data, and so the curves which result have been called static fatigue curves.

There have been many conflicting views on the question of threshold stress. Hoar and Hines [*18*] found in 18-8 alloy wires that fracture occurred at very low stresses on as-received wire. However, in later work with laboratory annealed specimens they reported that there was indeed a threshold stress at about 20 000 psi. The discrepancy here was probably due to residual stresses in the as-received wire. Kraft et al [*19*] verified that residual stresses were sufficient to cause SCC in Types 302 and 316 wire. They did not observe a threshold stress *per se*, but noted that the time to failure and the calculated incubation time increased rapidly at stresses below 10 000 psi. One complicating factor in this work was the development of pits which caused local stress concentrations, and these areas were the sites for crack growth. Therefore, the true local stresses in these areas were much greater than the total applied stress, and this could mask any threshold stress effect. Others have noted that the threshold stress, if it exists at all, is too low to be significant from an engineering viewpoint [*12*].

Maskell and West [*2*] have studied the effect of stress on the cracking of four austenitic stainless steel alloys with increasing nitrogen levels. They found that the failure time could be correlated with the applied stress by means of the expression

$$\log \frac{t}{t_0} = -A \frac{\sigma}{\sigma_y} \tag{4}$$

where

t = failure time,
t_0 = a constant,
A = a constant,
σ = applied stress, and
σ_y = 0.3 percent proof stress.

In the case of the highest nitrogen steel (0.246 percent) there was a break in the curve at low stresses with failure time being much larger than predicted using the above expression in this region. This type of expression, of course, precludes a threshold effect if it is valid over the entire stress spectrum. The constant t_0 is, in fact, the failure time at zero applied stress. This suggests that residual stresses in these specimens were causing cracking even though the specimens were annealed before testing. Annealing usually involves water quenching, and quenching stresses are sufficient to cause cracking.

The linear relationship between stress level and the logarithm of the failure time seems logical inasmuch as the logarithm of time function correlates crack depth and normalizes the statistics of cracking time data in many cases [*21*]. However, many investigators have noted that there is a break in this linear relationship with the failure times increasing strongly at the low stresses [*22,23*], for example, see the cracking time versus stress results in Fig. 4.

This break in the stress versus logarithm of the failure time curve was also reported by Hawkes et al [*23*] for Types 304, 309, and 316 stainless steel. They found that the crack morphology was related to the stress and that there was a lower crack density at lower stresses. Greeley et al [*24*] noted that crack density increased with increasing stress. However, they also noted that the crack-propagation rate was nearly independent of the applied stress in Type 302 stainless steel confirming a similar conclusion made by Uhlig and Lincoln [*12*]. This suggests that the stress concentration effect at the base of a crack is severe, and this region is probably close to the yield stress of the alloy regardless of the applied stress.

The effect of stress on a specimen is to cause strain, and it is this tensile strain which probably causes SCC to occur. Parkins [*2*] has considered

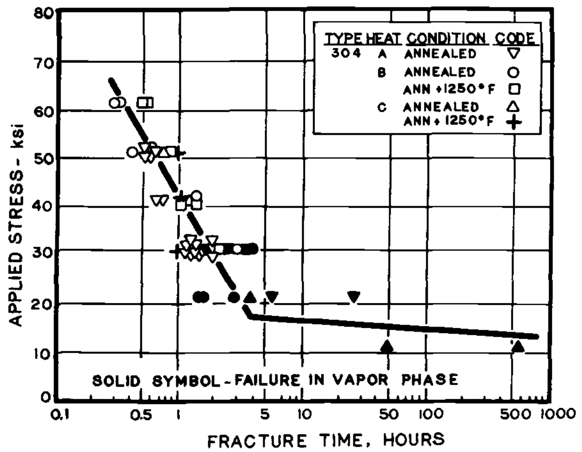

FIG. 4—*Applied stress versus fracture time for Type 304 stainless steel in boiling $MgCl_2$ solution, "static fatigue curve"* [22].

plastic strain as a distinct factor in causing cracking. Plastic strain is the irreversible strain associated with yielding and involves more than a simple extension of the crystal lattice. Most SCC work has been done with loads above the nominal yield point, but the low values reported for threshold stresses in the work just discussed make it appear as if plastic strain is not necessary to the stress-corrosion process. This may be an anomaly resulting from the fact that high local stresses can build up around pits and other regions of stress concentration. Plastic strain can then occur in these regions leading to the onset of cracking which will aggravate the stress concentration effect. However, the question as to whether plastic strain is a necessary condition for the SCC process needs further work to be answered convincingly.

Smialowski and Rychick [*25*] have reported that the failure time for their Types 302 and 304 stainless steels exhibited a minimum and then rose almost tenfold as the stress increased and passed through a maximum (Fig. 5). This effect was more pronounced with Type 302 than Type 304 and was more evident with their tapered specimen than with a conventional uniform cross-section specimen. This behavior is rather unusual; however, it can be rationalized on the basis that conventional specimen configurations are not designed to reveal this type of behavior. Indeed, the bent beam type specimen has a complete range of stresses present from the calculated maximum to no stress. Others have noted that in a limited range of low plastic strain the cracking time increased as the strain increased [*24*].

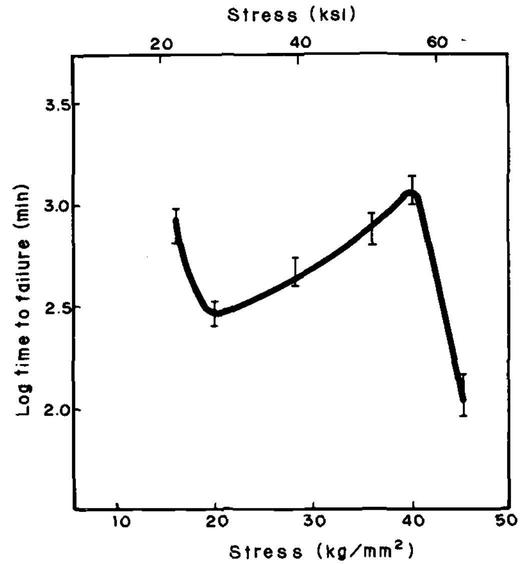

FIG. 5—*Time to failure versus applied stress for Type 304 stainless steel in* $MgCl_2$ *solution showing increase in failure time in the plastic strain region with contour direct tension specimen* [25].

Effect of Environment Variations

The corrosive environment plays an essential role in determining whether SCC occurs. In addition, it is a determining factor on the rate of the cracking process. In the case of the SCC of austenitic stainless steels a number of environmental factors can be identified: temperature, chloride ion concentration, pH, oxygen or other oxidizing agent concentrations or both, corrosion product concentrations, and other action and anion concentrations. The effects of these factors will be discussed briefly next.

Temperature—Kohl [*10*] has studied the effect of temperature on the initiation and cracking times in $MgCl_2$ solutions using a 19 percent chromium, 9 percent nickel alloy loaded in uniaxial tension. He correlated his results with an Arrhenius relationship and calculated the activation energies for both the induction period and the time to failure (Fig. 6). By using a conventional type tension specimen equipped with a recording extensometer, he was able to detect the onset of cracking very accurately.

He obtained activation energies of 13 and 16 kcal/mol for the induction period, 20 and 25 kcal/mol for crack propagation. In each case the smaller activation energy was found in the more dilute solution, (33 to 34 percent by weight, boiling point 123°C), while the higher value refers to the conventional concentration (44 to 45 percent by weight, boiling at

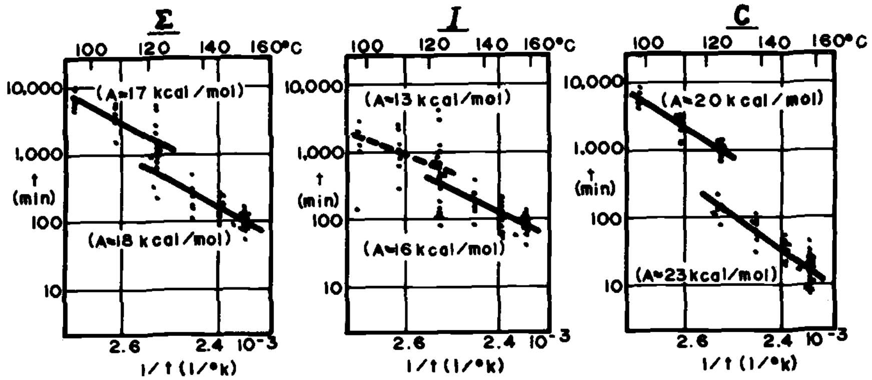

FIG. 6—*Arrhenius plots of time to fracture Σ, induction period I, and crack propagation period C, versus reciprocal temperature* [11].

154°C). Similar observations were also made earlier by Thomas et al [*26*]. Kohl [*11*] also noted variations of a factor of two for the crack initiation period, and a factor of ten for the crack propagation rate at a given temperature, resulting from different chloride ion concentrations.

Solution Composition—There are so many variables in the solution phase that it would be impossible to obtain a complete and comprehensive description of effects of all of these variables on the cracking kinetics. However, there have been many studies of specific solution composition effects and some of these are described next.

$MgCl_2$ solutions have traditionally been used to test stainless alloys for susceptibility SCC. Because it has been recognized that minor differences in the makeup of this test medium can have drastic effects on the cracking time, ASTM Committee G-1 has endeavored to prepare a standard for the preparation and use of $MgCl_2$ in SCC tests [*27,15*]. This recommended practice gives many good suggestions for the conduct of tests in boiling $MgCl_2$.

Many studies have shown that the pH of the chloride solution is an important variable and should be controlled if reproducible results are to be obtained [*28*]. In general, it has been found that lowering the pH of $MgCl_2$ solution accelerates the cracking rate. Baker et al [*29*] have investigated the effect of solution pH on the cracking rate of Type 304 stainless steel in an $MgCl_2$-$FeCl_3$ environment. They found that U-bend specimens cracked very rapidly in this solution when the pH was below 2.5. The number of cracks per unit area was higher at the higher pH but the rate of stress relief was about the same. They discovered that additions of hydrochloric acid (HCl), aluminum chloride ($AlCl_3$), ferric chloride ($FeCl_3$), etc, decreased the pH of the $MgCl_2$ solution and thereby accelerated cracking. Furthermore, they found that the pH of the solution within the cracks was in the range of 1.4 to 1.6 regardless of the pH of the corroding solution. Marak and Hochman [*30*] have also observed similar low pH regions in cracks in Type 304 stainless steel specimens. This behavior was accompanied by the formation of an oxide film rich in iron and chromium on the metal surface.This type of films was also found on the internal crack surfaces. Baker et al [*29*] suggested that the reason for this pH film formation effect was a result of the metal ion, oxide hydrolysis equilibrium

$$2Cr^{+++} + 3H_2O = Cr_2O_3 + 6H^+ \qquad (5)$$

This type of hydrolysis would maintain the low pH in confined regions only if the reduction of hydrogen ions at cathodic areas were sufficiently distant from the anode area. The oxide film then is a result of the hydrolysis reaction. They postulated that this oxide film was somehow necessary to the stress-corrosion process, but its function was not discussed. Wilde [*17*] found that the chromium content in the $MgCl_2$ solution after cracking was significantly lower than the stoichiometric quantity based on corrosion of the alloy. This supports the assumption that Eq 5 occurred during cracking.

The observation that oxide film formation is necessary for the SCC process suggests that the presence of corrosion products is necessary for the process to proceed. The importance of corrosion products in promoting SCC has been demonstrated in other alloy systems, such as brass in ammoniacal solutions [*31*] and nickel-base copper alloys in hydrofluoric acid (HF) solutions [*32*]. This effect gives rise to a phenomenon frequently in SCC situations where the specimens fail in the vapor or splash area over a liquid corrodent. This has also been frequently noted for stainless steels in chloride environments [*24*]. An explanation frequently offered for this is that oxygen availability is responsible; however, the importance of corrosion products should not be overlooked.

Baker et al [*29*] also noted that additions of glycerol, ethylene glycol, and carbitol suppressed cracking although these compounds accelerated the general corrosion process. Others have noted that the rate of cracking is suppressed by various additions. Uhlig and Cook [*33*] found that additions of sodium acetate, nitrate, iodide, or benzoate all partially inhibited the cracking rate of Type 304 stainless steel in $MgCl_2$ solutions at 130°C. They were careful to adjust the pH of the solution after addition of the inhibitor so that the test solution retained a constant pH. However, they did not measure the effect of these additions on the general corrosion rate. Neither did they attempt to determine whether these inhibitors affected the crack initiation and propagation processes equally.

One question of interest has been whether halides other than chloride can cause cracking. Louthan [*34*] found that iodides did not cause SCC of austenitic stainless steels. Rhodes [*35*] found that cracking occurred in magnesium bromide ($MgBr_2$) solutions but at a much reduced rate relative to that observed in $MgCl_2$ solutions under the same conditions.

Staehle et al [*36*] explored the effect of oxygen and chloride concentrations on the SCC of Type 347 stainless steel specimens. They found that at 400°F oxygen was necessary to produce cracking in the sodium chloride (NaCl) solutions which they used. Cracks originated from pits in the specimen, and the vapor zone was made more aggressive than total immersion in the solution if alternate wetting and drying conditions occurred. These observations are particularly interesting because they are in contrast to the observations in concentrated $MgCl_2$ solutions. Here neither oxygen nor pitting was necessary to cause cracking [*12*]. Staehle et al [*36*] also noted that cracking occurred at relatively low chloride levels in the vapor phase, but in the liquid phase cracking did not occur until relatively high concentrations were tried.

The contrast in behavior between the low pH concentrated $MgCl_2$ solutions or similar environments, for example, calcium chloride ($CaCl_2$) and $FeCl_2$-$FeCl_3$ solutions, and the more dilute neutral chloride solutions, such as NaCl, are significant both from the theoretical and the practical standpoint. Clearly, in neutral solutions the cathodic process must play a more important role in driving the localized corrosion processes to develop an environment suitable for the stress-corrosion process. This, no doubt, is one of the events which must occur during the initiation process in these environments. In fact, Uhlig and Lincoln predicted this behavior based on their results in $MgCl_2$ [*12*].

Water is another critical ingredient in the SCC process of austenitic stainless steel. Rhodes [*35*] reported that transgranular cracking did not occur in anhydrous chloride melts. However, others have noted intergranular cracking in anhydrous $AlCl_3$, KCl, and $FeCl_3$ melts. It should be noted that this is an important distinction between chloride cracking and caustic cracking because caustic cracking does occur in truly anhydrous melts, for example, ones in equilibrium with metallic sodium. This suggests that hydrogen may play a critical role in causing transgranular cracking because hydrogen is present in anhydrous caustic but not in anhydrous chlorides.

The cation species may also be important. Thomas et al [*26*] found that at constant pH lithium chloride (LiCl) was less effective than $MgCl_2$ in causing rapid cracking.

Howard and Pyle [*37*] have suggested that solution viscosity may be a factor. They have interpreted the cracking process in terms of slip line spacing.

Electrochemical Observations

There have been many experimental studies in which electrochemical measurements have been made in conjunction with cracking rate kinetics.

These have included the measurement of corrosion potentials during stress cracking, measurement of polarization curves in stress-cracking environments, and determination of the effects of polarization on SCC kinetics. Many of the observations which have been made are seemingly contradictory, although, considering the diversity in experimental conditions, this is not surprising.

Measurement of the corrosion potential of stressed specimens versus time during the cracking process have been made by many investigators. The earlier work of Hoar and Hines [*18*] has been more recently confirmed and extended by Anderson [*38*] and Cochran and Staehle [*13*]. These papers showed that the stress-corrosion process was accompanied by a characteristic shift in potential. Initially, the potential holds at a relatively active level, and then after a period it becomes more noble, passing through a maximum and then moving in the active direction before failure occurs, Fig. 7. This behavior has been attributed to the various stages of the cracking process, namely, initiation, fine crack formation, and open crack development.

Barnartt and Van Rooyen [*28*], however, have shown that this variation in potential occurred both when stress was present and when it was absent, although it tended to be greater in susceptible alloys when tensile stress was present. This makes the interpretation of these shifts in terms of the cracking process very doubtful. Barnartt and Van Rooyen argued that this shift in potential is due to the development of an oxide film on the electrode surface which inhibits the anodic dissolution process.

The oxide film which forms in $MgCl_2$ solutions is not a passive film in the sense that it forms and becomes stable at more noble potentials. Many

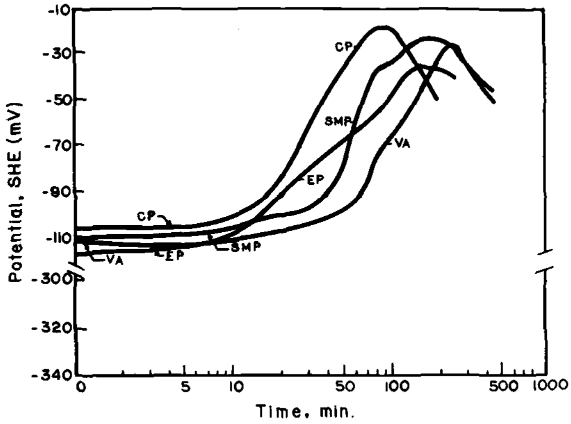

FIG. 7—*Open circuit potential versus exposure time for stressed vacuum annealed Type 310 stainless steel specimens having various surface preparation treatments. Specimens in boiling $MgCl_2$ (154°C). CP = chemical polish, EP = electropolish, VA = vacuum anneal, SMP = smooth mechanical polish* [13].

investigators have noted this, for example, Smialowski and Rychcik [*25*]. It is apparent from Uhlig and Lincoln's [*12*] measurements that this film does reduce the overall corrosion rate. Uhlig and Sava's [*39*] work on Type 310 stainless steel indicates that this film does not impede the cracking process. On the other hand, Wilde [*17*] has shown evidence that a classic passivity does occur for Type 304 stainless in a boiling $MgCl_2$ environment. His results indicate that the active region occurs at a potential substantially more active, that is, 400 mV, than the normal corrosion potential. His work suggests that the normal corrosion potential of stainless steels in this environment is, in fact, above the critical pitting potential for the alloy. However, his results must be viewed with caution because of the assumptions he made in his calculations. Furthermore, his similar experiments in boiling LiCl solutions did not confirm these results.

It has been frequently noted [*12,25*] that the SCC process in austenitic stainless steels could be delayed or prevented by the application of cathodic current, that is, cathodic protection. On the other hand, the effect of anodic polarization has not been as clear cut. Uhlig and Lincoln [*12*] reported that anodic polarization up ot 0.01 mA/cm^2 did not affect the cracking kinetics. In contrast, Barnartt and Van Rooyen's data [*28*] indicated that some acceleration of the cracking process could be achieved with anodic polarization. Kohl [*11*] noted that potentiostatic testing reduced the scatter in both the initiation and crack-propagation rate. Furthermore, he determined that potentiostatic anodic polarization reduced the initiation time tenfold or more but had a much smaller effect on the crack-propagation rate in concentrated $MgCl_2$ solutions (44 percent). In more dilute solutions (33 percent), anodic polarization reduced both the initiation and crack-propagation reactions. He found further that anodic polarization significantly reduced the activation energy of the initiation process from 16 to 4 kcal/g mole. A smaller reduction in activation energy, that is, from 23 to 17 kcal/g mole was noted for the propagation reaction.

These observations shed some light on why seemingly contradictory conclusions have been reached on the effect of anodic polarization. In cases where little or no effect was found it is likely that the failure time was controlled by the crack-propagation reaction, while the investigators who noted the acceleration of cracking by anodic polarization were seeing a reduction in initiation time. This is true for $MgCl_2$ solutions boiling at 154°C. However, at lower temperatures or in other environments the conclusion would no doubt be different.

Metallurgical Effects

Alloy Composition—The effect of alloy composition has been widely studied, and the effects of many alloying elements have been determined. Basically, the addition of alloying elements can either be detrimental,

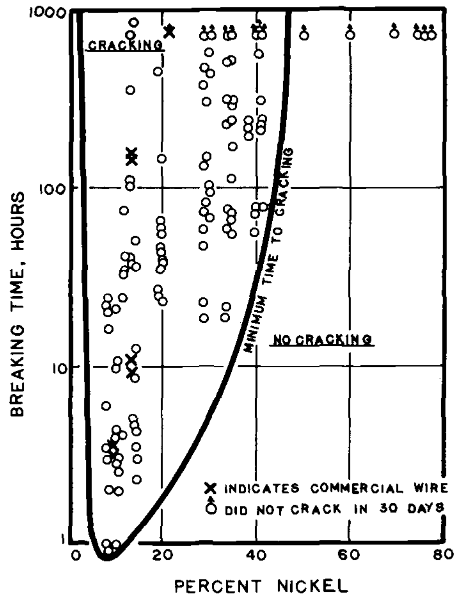

FIG. 8—*Failure time for iron, 18 percent chromium, nickel alloys wires in boiling 42 percent $MgCl_2$ versus nickel content* [41].

beneficial, or have no significant effect on the susceptibility of the alloy [*40*]. Care must be exercised in drawing conclusions from some of this work because the 18 percent chromium, 8 percent nickel composition will readily transform to ferrite under the influence of minor alloying additions, and this complicates interpretation of the results.

Copson [*41*] has reported that nickel increases the resistance of stainless steels to SCC. He found that alloys containing 40 percent nickel did not crack in more than 1000 h in boiling $MgCl_2$ solutions. The minimum time to cracking for his direct loaded wire specimens was found to follow a U-shaped curve with a minimum near 10 percent nickel, Fig. 8. Uhlig and White [*42*] reported that carbon, silicon, and cobalt were beneficial in reducing cracking rates. Lang [*40*] examined a number of alloying elements in an 18 percent chromium, 20 percent nickel, base alloy using U-bend specimens in boiling $MgCl_2$. She confirmed that carbon and silicon additions were beneficial. Alloys containing 0.1 percent carbon or 2 percent silicon did not crack in 30-day tests.

Lang also noted that many elements appear to be detrimental to the stress-corrosion resistance. In particular, the Group V elements of the Periodic Table, namely: nitrogen, phosphorus, arsenic, antimony, and bismuth, were especially harmful. Ruthenium and aluminum were also found to cause cracking in a short time. This work confirmed Uhlig and White's [*42*] observation that nitrogen accelerates cracking. Van Rooyen

[*42*] had reported also that molybdenum was harmful. Subsequently, the effect of nitrogen has been studied in greater detail [*20,44*].

Denhard [*22*] noted that chromium variations from 11 to 23 percent had little influence. Van Rooyen [*42*] observed that manganese had little effect. Lang [*40*] found that sulphur, tin, boron, titanium, columbium, zirconium, and cerium had little effect over the range studied. Wilde and Armijo [*45*] also confirmed that sulfur had no effect on the cracking rate of a 14 percent chromium, 14 percent nickel composition in boiling $MgCl_2$ solution.

The fact that many of the elements causing accelerated cracking fall in Group V of the Periodic Table suggests that the role of these elements is chemical rather than metallurgical. Two of the beneficial elements, carbon and silicon, on the other hand, fall in Group IV, and this provides additional support for this contention.

Graf [*46*] has studied the effect of alloy composition on the transgranular SCC of binary solid solution alloys and has concluded that cracking can only occur when the more noble element is less than 50 atomic percent. Copson [*41*] interpreted his findings on the effect of the nickel on the cracking of stainless steels in boiling $MgCl_2$ solutions in terms of this theory. He also presented some electrode potential data for various alloys in a room temperature $FeCl_2$ solution which indicated that nickel is noble to stainless steel in this environment. Graf proposed that there is enrichment of the more noble element at the crack wall. An area for future study would be the use of modern electron probe scans over crack surfaces to determine if enrichment in fact occurs.

Effect of Thermal and Structural Treatments—The effects of other metallurgical factors such as plastic strain, grain size, second phase constituents, and partial transformation have not been extensively reported, although the literature contains a wide variety of comments on these effects. Strain has been discussed earlier under the effect of stress.

Plastic strain or cold work appears to decrease the failure time with a minimum occurring around 10 percent reduction in area. This effect has been reported in many studies [*23,24,25,47*]. However, improvement in stress-corrosion resistance with increasing cold work is not substantial and may reverse when the strain level is high [*25*].

Plastic strain can cause low nickel stainless steel to partially transform from austenitic to martensite. This transformation may in some cases explain the variations in cracking behavior noted for various amounts of strain [*24*]. Uhlig and White's work [*42*] suggests that stainless steels which have transformed to martensite by deformation may be more resistant. Birley and Tromans [*48*] have found evidence for the presence of a body-centered-cubic (bcc) martensite at the fracture surface and crack tip of Type 304L stainless steel cracked in boiling $MgCl_2$. Furthermore, they found that this phase occurred only in conjuction with the SCC process. Ductile fractures did not produce this phase. Martensitic and ferritic steel are also subject to classic hydrogen embrittlement, and this makes experimental studies on the stress corrosion susceptibility of such alloys substantially more difficult especially in the area of interpretation of results.

Other metallurgical effects have not been studied in any detail. Denhard [*22*] included commercial alloys such as Armco 17-14 Cu Mo and Armco 17-10 P in both annealed and aged conditions. The Armco 17-14 Cu Mo alloy showed a more rapid failure of the annealed material at lower stress. The other alloy, Armco 17-10 P, showed no significant differences between annealed and annealed plus aged conditions. Also, sensitizing heat treatments, that is, heating in the vicinity of 1200°F did not cause any significant effects in Types 304, 304L, or 347. This treatment causes precipitation of chromium carbides in the grain boundaries and makes the alloy subject to intergranular corrosion in some environments.

Crack Morphology

The stress-corrosion cracks which develop in austenitic stainless steels are generally transgranular in nature, that is, they penetrate through the grains rather than following grain boundaries. However, it is frequently observed that cracks change direction when passing through grain boundaries. In addition, cracks frequently branch both within grains and at grain boundaries.

There have been cases reported where intergranular cracking has accompanied transgranular cracking [*30*]. This occurs even more frequently in caustic cracking. This should not be surprising because grain boundaries are frequently sites for preferential corrosive attack in many alloy systems. In stainless steels, sensitizing heat treatments (holding in the 900 to 1400°F region) cause susceptibility to intergranular attack due to chromium carbide ($Cr_{23}C_6$) formation in grain boundaries with subsequent chromium depletion in adjacent areas. This type of occurrence may direct some cracks along grain boundaries. It has also been observed that cracking occasionally transforms from intergranular at the outset of the cracking process to transgranular deeper within the metal structure [*49*]. This probably reflects a change in the chemistry of the corrosion process which occurs in the growing cracks, similar to the initiation of transgranular cracks from pits.

Many investigators have noted that the cracks follow the (111) family of planes. Louthan [*34*], for example, found that incipient cracks were aligned with ±2 deg of the (111) direction. Tromans and Nutting [*50*] also noted this. Louthan noted that some grains had as many as five or six incipient cracks, while adjacent grains had none. From this he inferred that the susceptibility to crack initiation was very dependent upon the relationship between the grain orientation and direction of applied stress. This could also account for the fact that cracks tend to change direction as they pass from grain to grain. However, as the crack propagation process proceeds, the cracks seem less affected by the grain orientation.

Electron microscopy on thin-foil specimens of austenitic stainless steel has revealed that tunnel pitting occurs in these alloys when exposed to boiling $MgCl_2$ environments. These tunnel pits have been proposed as precursors for the cracking process by a number of investigators [*33,52*]. These tunnel pits follow the (111) direction [*51*] and may be influenced by stress [*52*]. An example of tunnel pitting is shown in Fig. 9.

Theories on the Mechanism of Cracking

During the past decade, there has been a large number of studies on the various factors which affect the SCC of austenitic stainless steels with the aim of developing a logical mechanism of the process. There have been a number of proposals for such a theory but none has been widely accepted. Dix [*53*] proposed an electrochemical mechanism for SCC of aluminum alloys. This theory assumed that there existed continuous paths within the alloy which were suscepitble to selective corrosion. Aluminum alloys almost always crack along intergranular paths so that this assumption is quite justified. However, austenitic stainless steels crack transgranularly so

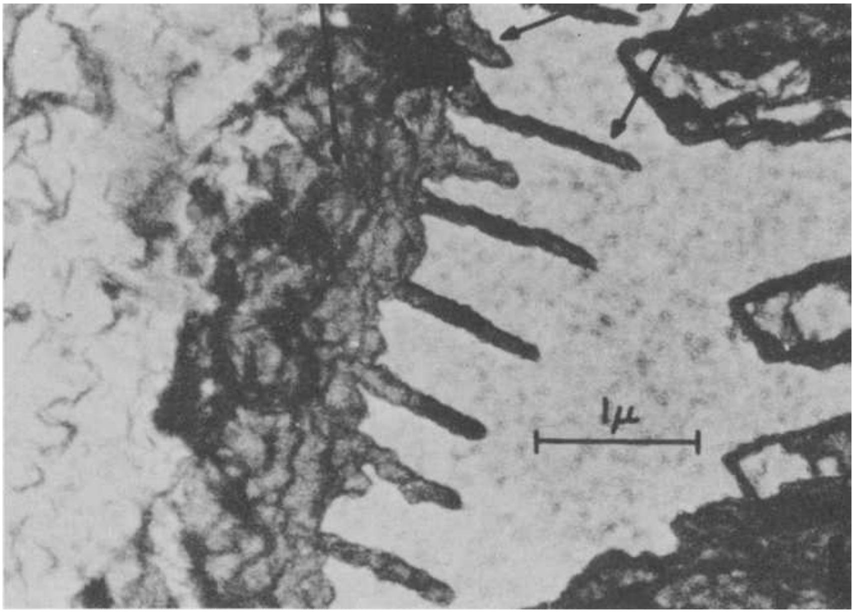

FIG. 9—*Oxide replica of Type 304 stainless steel stressed above yield point and exposed to boiling $MgCl_2$ showing corrosion tunnels* [52].

that the assumption of preexisting continuous susceptible paths does not appear to be justified.

This has led to two types of theories [*54*] assuming either of the following:

1. The active path forms at the crack tip as a result of the combined action of stress and the environment.
2. The cracking process is partially mechanical in nature.

There are, in fact, a number of theories associated with both of these concepts and these will be discussed further.

Electrochemical Theories

Effect of Stress on Potentials—It is well known in thermodynamics that the application of stress can cause reversible or irreversible changes in the internal energy of the stressed phase. These changes should in turn cause a variation in the electrode potential of a metal under stress according to the expression

$$\Delta E = \frac{\sigma^2 M}{2 Y \rho n F} \tag{6}$$

where

ΔE = change in electrode potential from applied stress,
σ = applied stress,
Y = modulus of elasticity (Young's modulus),
ρ = density,
M = atomic weight for the metal,
n = number of electrons associated with the electrochemical reaction, and
F = electrochemical equivalent (Faraday's number).

In fact, this expression has been questioned by Clarke [*55*] who points up that the strain induced potential can only exist as a transient in a reversible electrode situation. It should be noted that this equation gives the same change in potential regardless of whether the applied stress is compressive or tensile.

Dean [*56*] has measured the change in potential which occurred when various types of austenitic stainless steels were stressed in boiling 42 percent $MgCl_2$. He found that the more susceptible types showed larger potential shifts than resistant alloys, namely, 25 mV for Type 304 versus 10 mV for a relatively resistant grade. However, it is difficult to postulate that local potential variations could give rise to the localized corrosion rates necessary to account for the cracking velocities which are reported.

Effect of Stress on Kinetics—A more realistic explanation is that stress somehow affects the electrochemical kinetic factors which govern the reaction process. More specifically the rate of an electrochemical reaction in one direction can be written in the form following

$$i = i_0 \exp \frac{-\alpha nF(E - E_0)}{RT} \tag{7}$$

where

i = current density associated with the reaction, that is, the rate of reaction,
i_0 = exchange current density, that is, the rate of the reaction at equilibrium,
α = a constant known as the symmetry factor,
$E - E_0$ = potential displacement from equilibrium or overvoltage,
n and F = definitions under Eq 6, and
R and T = gas constant and absolute temperature, respectively.

Stresses would be expected to cause variations in both i_0 and α. Furthermore, this type of variation is probably a function of crystal orientation; thus, the observation that stress-corrosion crack-growth rates are a function of crystal orientation is consistent with this hypothesis.

Static Crystal Sites—A variety of proposals have been put forth as to what metallurgical factors affect the electrochemical kinetic parameters. Robertson and Tetelman [*57*] proposed that static imperfections could be responsible. Uhlig and Sava [*39*] noted that heat treatment of Type 310 stainless steels at temperatures in the vicinity of 150°C caused a significant decrease in the cracking time. This suggested that segregation of damaging elements, such as nitrogen under the influence of stress and temperature, was occurring which subsequently caused cracking. Eckel and Clevinger [*44*], in their discussion of the aging of stainless steels containing nitrogen, have provided further insight on the nature of static crystal sites responsible for SCC in these alloys.

Moving Imperfections—Scully and Hoar [*58*], on the other hand, were unable to obtain evidence for any change in the electrochemical kinetic parameters until plastic deformation or yielding of the metal occurred. This suggests that moving crystal imperfections may be responsible. Hoar noted that the solution in the vicinity of the yielding of electrode must be flowing at a relatively high velocity in order to see this effect.

Dislocation Arrays: Planar versus Tangled—Swann [*59*] found that the dislocation patterns in susceptible stainless steels tended to form planar arrays, whereas in resistant alloys the dislocation patterns were cellular or tangled, Fig. 10. The planar arrays of dislocation may then show a greater i_0 than the surrounding metal. The major objection to this theory is that high nickel alloys (16 percent chromium, 7 percent iron) which show tangled or cellular dislocation arrays and are completely resistant to SCC in chloride environments, show cracking both in hot aqueous solutions containing lead and in hot caustic environments. Austenitic stainless steels, which crack readily in chloride solutions and have planar dislocation arrays, resist cracking in these hot aqueous lead solutions [*10*]. The relationships between dislocations, stacking faults, and SCC have been discussed further by Douglass et al [*60*].

Slip-Step Emergence—Smith and Staehle [*61*] suggested a theory based on slip-step emergence. They pointed up that slip step emergence was not a sufficient condition for cracking since pure iron and nickel show slip-step emergence when stress is applied. It is necessary to have a specific interaction between some factor in the environment and the slip steps which will then increase i_0 or decrease α. Scully [*62*] has also discussed the question of slip-step emergence in some detail.

Stress-Aging Microsegregation—Another possibility was put forth by Swann and Pickering [*63*]. They noted that in the stress aging of austenitic stainless steels jerky plastic flow occurred, Fig. 11. This phenomenon, known as the Portevin-Le Chatelier effect, is associated with the microsegregation of solute atoms to dynamic defects in the crystal structure.

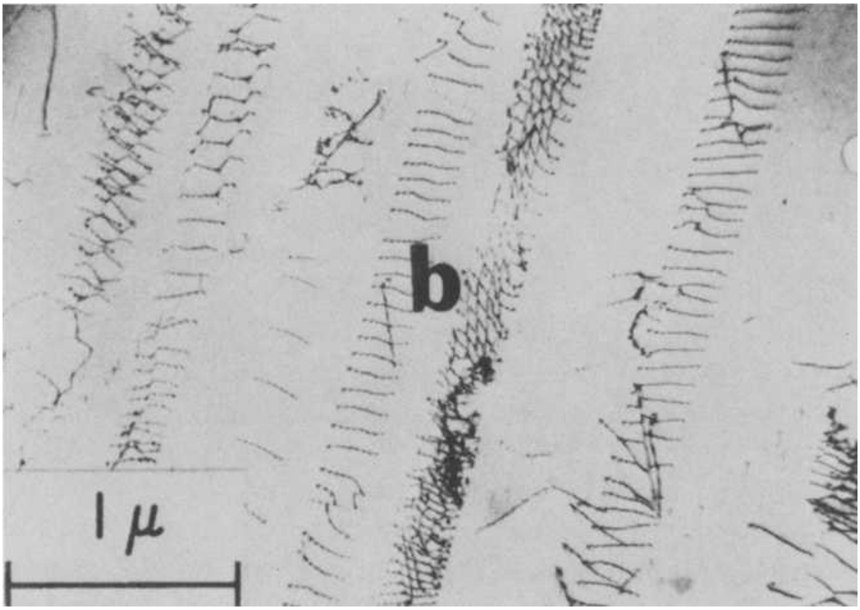

FIG. 10—*Electron micrographs of thin-foil specimens of austenitic stainless steels showing dislocation arrays.* (b) *12.8 percent nickel, 0.12 percent nitrogen steel showing deformed, planar array;* (c) *20 percent nickel, 0.1 percent carbon steel deformed 10 percent showing cellular tangled array* [59].

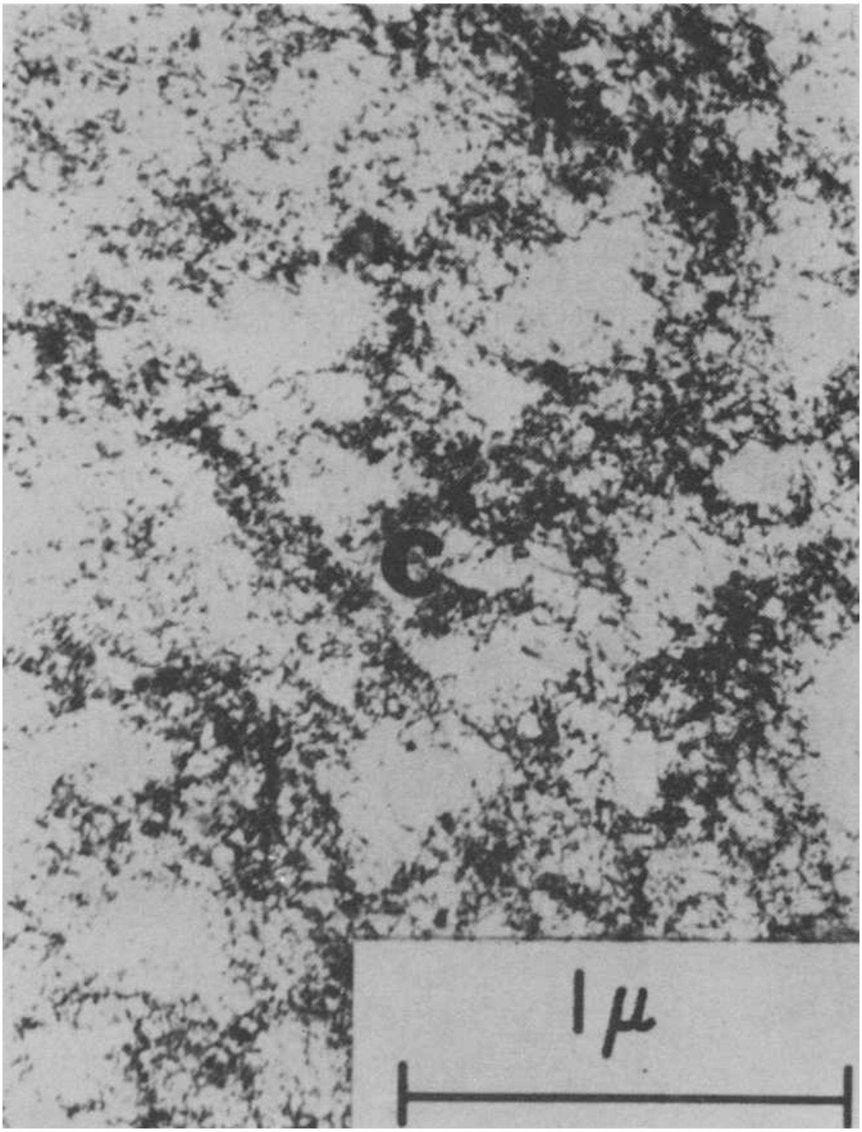

FIG. 10—*Continued.*

They proposed that this type of segregation could account for transgranular SCC behavior. In this case, the cracking rate could be limited by the solute diffusion rate as well as the electrochemical polarization.

Hydride Formation—Hydrogen has been linked to the stress corrosion phenomena by a number of investigators. Vaughan et al [*64*] noted that hydrogen entering into Type 304 stainless steels formed a phase which

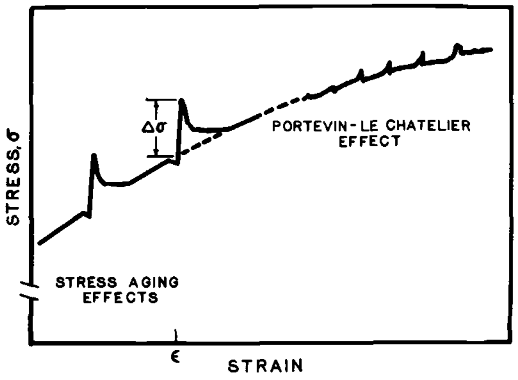

FIG. 11—*Schematic of stress-strain curve of face-centered-cubic alloy showing stress aging, jerky plastic flow (Portevin Le Chatelier effect)* [63].

they postulated to be a hydride. However, later work by Birley and Tromans [*48*] suggested that this phase was η-martensite. They postulated that this phase was susceptible to selective attack. Vaughan et al noted that under the influence of stress, this phase diffused into stringers normal to the direction of stress. In the more resistant varieties of stainless steel, this "hydride phase" did not diffuse under stress. The hydrogen entry in this case was produced by cathodic charging in H_2SO_4 saturated with arsenic. Lattice expansion accompanied the entry of hydrogen. A major objection to this mechanism is that the driving force for entry of hydrogen in this work, for example, 5 V, was substantially greater than that in corrosive environments.

Hydrogen Induced Martensite Transformation—Rhodes [*35*] proposed a somewhat different mechanism based on hydrogen. He found that neither hydroxyl nor chloride ions caused cracking in the absence of water. Although later observations have contradicted this in the case of hydroxyl ions [*5*], Rhodes proposed that cathodic hydrogen is necessary for crack initiation. Crack propagation occurs through preferential dissolution of a hydrogen induced corrosion path, that is, hydrogen entry causes an increased value of i_0. There is a buildup of hydrogen ions in the cracks due to precipitation of the hydroxide form of corrosion products. The hydrogen induced path he believed to be martensite platelets. Another possibility he proposed is the mechanical cracking of the steel due to hydrogen embrittlement. A major problem with this theory is that it does not explain the crack morphology or kinetics inasmuch as hydrogen induced martensite platelets should occur randomly.

Shively et al [*65*] presented evidence for the entry of hydrogen into stainless steels. They found that even anodic polarization does not suppress the entry of hydrogen in chloride environments. They used mass spectrometric methods with deuterium to identify the entry of hydrogen.

Quasi-Mechanical Theories

An alternative to the electrochemical mechanism is the possibility that a mechanical tearing or fracture step occurs in the cracking process. This is an attractive alternative because it explains the transgranular nature of the cracking process, inasmuch as mechanical failure mechanisms are generally transgranular. The problem with this assumption is then to rationalize the interaction of the corrosion process occurring only in certain selected environments which causes slow crack growth at stresses well below the ultimate stress.

Tunnel Pitting-Tearing—One theory which has been proposed is that tunnel pitting occurs in planar arrays during the cracking process, and then the metal between the pits fails by a mechanical tearing or ductile fracture. Pickering and Swann [*66*] proposed this as a general mechanism for SCC for a number of alloys. These tunnel pits have been observed by Nielsen [*51*] using oxide replica techniques. Dean et al [*52*] studied the formation of tunnel pits in iron-nickel-chromium alloys. They concluded that a tensile stress is required before tunnel pitting will occur. Furthermore, they found that tunnels occurred in Types 304 and 310 and in nickel alloy 800 (iron, 22 percent chromium, 35 percent nickel) but not in nickel alloy 600 (nickel, 16 percent chromium, 7 percent iron). Dislocations, however, were not found to be reactive in the $MgCl_2$ environment used in their tests. Their conclusion was that tunnels propagated trench formation rather than a mechanical failure of the walls.

Corrosion Product Wedging—Another mechanical failure mechanism involves the buildup of corrosion products in existing cracks which then exert a wedging action. Pickering et al [*67*] demonstrated that corrosion products can build up and exert stress in at least some circumstances. This mechanism, in fact, may operate in some cases to further the crack propagation process, but it does not provide an explanation of crack initiation.

Specific Adsorption: Bond Weakening—Uhlig [*68*] has proposed that chloride ion adsorption in conjunction with the corrosion process reduces the stress necessary to propagate a crack, that is, it reduces the surface energy through a process of weakening of the metallic bonds. This mechanism is similar to the mechanism of failure which causes stress cracking of plastics in solvents and detergents. Uhlig and Cook [*33*] found that ions such as acetate, nitrate, iodide, etc., which adsorb preferentially on stainless steel surfaces, tend to inhibit the SCC process. An unresolved question on this theory is why ions such as acetate, etc., which adsorb more strongly than chloride, do not weaken the metallic bonds more effectively than chloride, and cause cracking in their own right. It should be noted that this theory does not require a corrosion process and is, therefore, completely mechanical.

Outlook

In the past decade, the phenomenon of SCC in austenitic stainless steels has been studied in much greater detail than earlier. A variety of environments have been discovered which cause cracking in addition to the traditional $MgCl_2$ system. A number of excellent studies have been made on the phenomenology of the cracking process. A variety of theories of the cracking mechanism have been put forth, but to date there does not seem to be sufficient data to positively confirm or disprove any of these.

Developments of particular significance in this period have included the use of the electron microscope to examine crack nucleation and growth. Another valuable technique has been the use of cryogenics to freeze the specimen and then break it open to examine the crack and its environment with a minimum of disturbance to the environment. The work to standardize test methods and specimen design should be very helpful to future investigators in planning and carrying out experiments.

Areas which require more work would now appear to be a critical examination of the kinetics of the crack nucleation and growth process in a variety of specimens. With the help of rapid analytical tools, such as atomic absorption, it should be possible to define the electrode processes in detail. This would be very helpful in determining whether mechanical crack growth proceeds by strictly electrochemical processes or whether mechanical steps are occurring. Finally, the use of new and sophisticated methods may provide the additional information necessary to explain the cracking process. The scanning electron microscope and microprobe should be extremely helpful in determining compositional variations in the vicinity of cracks as well as showing the topography and structure in these areas. Also, methods such as inelastic neutron scattering spectroscopy and ion probe analysis may be very valuable in defining the role of hydrogen and other light elements in the cracking process.

References

[1] Harwood, J. J. in *Report on Stress Corrosion Cracking of Austenitic Chromium Nickel Stainless Steels, ASTM STP 264,* American Society for Testing and Materials, 1960, pp. 22–24, 63–67.
[2] Parkins, R. N., *Metallurgical Reviews,* Vol. 9, No. 35, 1964, pp. 201–259.
[3] Nielson, N. A., *Journal of Materials,* Dec. 1970, pp. 794– 829.
[4] Latanision, R. M. and Staehle, R. W., "Stress Corrosion Cracking of Iron-Nickel-Chromium Alloys," Proceedings of Conference on Fundamental Aspects of Stress Corrosion Cracking, Ohio State University, 1967, National Association of Corrosion Engineers, 1969.
[5] Dillon, C. P., *Materials Protection and Performance,* Vol. 11, No. 48, June 1972.
[6] Evans, U. R. in *Stress Corrosion Cracking and Embrittlement,* W. D. Robertson, Ed., Wiley, New York, 1956, pp. 158–162.
[7] Wanklyn, J. N. and Jones, D., *Chemistry and Industry,* 1958, pp. 888–889.
[8] Williams, W. L., *Corrosion,* Vol. 13, 1957, pp. 539t–545t.

[9] Acello, S. J. and Greene, N. D., *Corrosion,* Vol. 18, 1962, pp. 286t–290t.

[10] Copson, H. R. and Dean, S. W., *Corrosion,* Vol. 21, 1965, pp. 1–8.

[11] Kohl, H., *Corrosion,* Vol. 23, 1967, pp. 39–49.

[12] Uhlig, H. H., and Lincoln, J., Jr., *Journal of the Electrochemical Society,* Vol. 105, 1958, pp. 325–332.

[13] Cochran, R. W. and Staehle, R. W., *Corrosion,* Vol. 24, 1968, pp. 369–378.

[14] ASTM G.30-72, "Recommended Practice for Making and Using the U-Bend Stress Corrosion Test Specimen," and ASTM G.39-73, "Standard Method for Preparation and Use of Bent Beam Stress Corrosion Specimens," *1975 Annual Book of ASTM Standards,* Part 10, pp. 703–711, 760–769, American Society for Testing and Materials, Philadelphia, 1975.

[15] Craig, H. L., Jr., Sprowls, D. O., and Piper, D. E. in *Handbook on Corrosion Testing and Evaluation,* W. H. Ailor, Ed., Wiley, New York, 1971, pp. 231–290.

[16] *Eckel, J. F., Corrosion,* Vol. 18, 1962, pp. 270t–276t.

[17] Wilde, B. E., *Journal of the Electrochemical Society,* Vol. 118, 1971, pp. 1717–1725.

[18] Hoar, T. P. and Hines, J. G., *Journal of the Iron and Steel Institute,* 1956, pp. 124–143.

[19] Kraft, G. H. G., Amacker, J. Z., Saxer, R. K., and Meyers, J. R., *Corrosion,* Vol. 21, 1965, pp. 188–195.

[20] Maskell, R. V. and West, J. M., *British Corrosion Journal,* Vol. 6, 1971, pp. 10–16.

[21] Booth, F. F., Tucker, G. E. G., and Goddard, H. P., "Statistical Distribution of Stress Corrosion Endurance," *Corrosion,* Vol. 19, 1963, pp. 390t–395t.

[22] Denhard, E. E., Jr., *Corrosion,* Vol. 16, 1960, pp. 359t–369t.

[23] Hawkes, H. P., Beck, F. H., and Fontana, M. G., *Corrosion,* Vol. 19, 1963, pp. 247t–253t.

[24] Greeley, P. J., Russo, V. J., Saxer, R. K., and Meyers, J. R., *Corrosion,* Vol. 21, 1965, pp. 327–331.

[25] Smialowski, M. and Rychcik, M., *Corrosion,* Vol. 23, 1967, pp. 218–221.

[26] Thomas, K. C., Ferrari, H. M., and Allio, R. J., *Corrosion,* Vol. 20, 1964, pp. 89t–92t.

[27] ASTM G.36-73, "Recommended Practice for Performing Stress Cracking Tests in a Boiling Magnesium Chloride Solution," *1975 Annual Book of ASTM Standards,* Part 10, pp. 739–746, American Society for Testing and Materials, Philadelphia, 1975. This standard is based on: M. A. Streicher and A. J. Sweet, "Apparatus for Stress Corrosion Test in Boiling Magnesium Chloride Solutions," *Corrosion,* Vol. 25, 1969, pp. 1–6.

[28] Barnartt, S. and Van Rooyen, D., *Journal of the Electrochemical Society,* Vol. 108, 1961, pp. 222–229.

[29] Baker, H. R., Bloom, M. C., Bolster, R. N., and Singleterry, C. R., "Film and pH Effects in the Stress Corrosion Cracking of Type 304 Stainless Steel," *Corrosion,* Vol. 26, 1970, pp. 420–426.

[30] Marek, M. and Hochman, R. F., *Corrosion,* Vol. 26, 1970, pp. 5–6.

[31] Mattsson, E., *Electrochimica Acta,* Vol. 3, 1961, pp. 279–291.

[32] Graf, L., Laconi, H. L., Richter, W., and Wittich, W., *Zeitschrift für Metallkunde,* Vol. 54, 1963, pp. 406–416.

[33] Uhlig, H. H. and Cook, E. W., Jr., *Journal of the Electrochemical Society,* Vol. 116, 1967, pp. 173–177.

[34] Louthan, M. R., Jr., *Corrosion,* Vol. 21, 1965, pp. 288–294.

[35] Rhodes, P. R., *Corrosion,* Vol. 25, 1969, pp. 462–472.

[36] Staehle, R. W., Beck, F. H., and Fontana, M. G., *Corrosion,* Vol. 15, 1959, pp. 373t–381t.

[37] Howard, D. and Pyle, T., *British Corrosion Journal,* Vol. 3, 1968, pp. 301–304.

[38] Anderson, B., *Corrosion,* Vol. 18, 1962, pp. 425t–432t.

[39] Uhlig, H. H. and Sava, J. P., "Origin of Delay Time in Stress Corrosion Cracking of Austenitic Stainless Steels," Proceedings of the Second International

Congress on Metallic Corrosion, National Association of Corrosion Engineers, 1963, pp. 211–215.

[40] Lang, F. S., *Corrosion,* Vol. 18, 1962, pp. 378t–382t.

[41] Copson, H. R. in *Physical Metallurgy of Stress Corrosion Fracture,* T. N. Rhodin, Ed., Interscience, New York, 1959, pp. 247–267.

[42] Uhlig, H. H. and White, R. A., *Transactions,* American Society for Metals, Vol. 52, 1970, pp. 830–847.

[43] Van Rooyen, D., "Some Aspects of Stress Corrosion Cracking in Austenitic Stainless Steels," First International Congress on Metallic Corrosion, Butterworth, London, 1962, pp. 309–318.

[44] Eckel, J. F. and Clevinger, G. S., *Corrosion,* Vol. 26, 1970, pp. 251–255.

[45] Wilde, B. E. and Armijo, J. S., *Corrosion,* Vol. 23, 1967, pp. 208–214.

[46] Graf, L., *Stress Corrosion Cracking and Embrittlement,* W. D. Robertson, Ed., Wiley, New York, 1956.

[47] Hines, J. G., *Corrosion Science,* Vol. 1, 1961, pp. 2–20.

[48] Birley, S. S. and Tromans, D., *Corrosion,* Vol. 27, 1971, pp. 63–71.

[49] Ohtani, H. and Dodd, R. A., *Corrosion,* Vol. 21, 1965, pp. 161–172.

[50] Tromans, D. and Nutting, J., *Corrosion,* Vol. 21, 1965, pp. 143–160.

[51] Nielsen, N. A., *Corrosion,* Vol. 20, 1964, pp. 104t–110t.

[52] Dean, M. F., Beck, F. H., and Staehle, R. W., *Corrosion,* Vol. 23, 1967, pp. 192–201.

[53] Dix, E. H., *Transactions of the American Institute of Mining and Metallurgical Engineers,* Vol. 137, No. 11, 1940.

[54] Bates, J. F., *Industrial and Engineering Chemistry,* Vol. 58, 1966, pp. 18–29.

[55] Clarke, M., *Corrosion Science,* Vol. 10, 1970, pp. 671–678.

[56] Dean, S. W., Jr., "Studies on the Mechanism of Stress Corrosion Cracking in Austenitic Stainless Steels in Particular Electrode Potential Considerations," SB thesis, Massachusetts Institute of Technology, Cambridge, Mass., 1958.

[57] Robertson, W. D. and Tetelman, A. S., *Strengthening Mechanisms in Solids,* American Society for Metals, Metals Park, Ohio, 1960, p. 218.

[58] Scully, J. C. and Hoar, T. P., "Mechanochemical Anodic Dissolution of Fe-Ni Alloys in Hot Chloride Solution at Controlled Electrode Potential," Proceedings of Second International Congress on Metallic Corrosion, National Association of Corrosion Engineers, 1963, pp. 184–187.

[59] Swann, P. R., *Corrosion,* Vol. 19, 1963, pp. 102t–112t.

[60] Douglass, D. L., Thomas, G., and Roser, W. R., *Corrosion,* Vol. 20, 1964, pp. 15t–27t.

[61] Smith, T. J. and Staehle, R. W., *Corrosion,* Vol. 23, 1967, pp. 117–129.

[62] Scully, J. C., *Corrosion Science,* Vol. 7, 1967, pp. 197–207.

[63] Swann, P. R. and Pickering, H. W., *Corrosion,* Vol. 19, 1963, pp. 369t–372t.

[64] Vaughan, D. A., Phalen, D. I., Peterson, C. L., and Boyd, W. K., *Corrosion,* Vol. 19, 1963, pp. 315t–326t.

[65] Shively, J. H., Hehemann, R. F., and Troiano, A. R., *Corrosion,* Vol. 23, 1967, pp. 215–217.

[66] Pickering, H. W. and Swann, P. R., *Corrosion,* Vol. 19, 1963, pp. 373t–389t.

[67] Pickering, H. W., Beck, F. H., and Fontana, M. G., *Corrosion,* Vol. 18, 1962, pp. 230t–239t.

[68] Uhlig, H. H. in *Physical Metallurgy of Stress Corrosion Fracture,* T. N. Rhodin, Ed., Interscience, New York, 1959, pp. 1–15.

Susumu Takemura,[1] *Masao Onoyama,*[1] *and Takayuki Ooka*[1]

Stress-Corrosion Cracking of Stainless Steels in Hydrogen Sulfide Solutions

REFERENCE: Takemura, Susumu, Onoyama, Masao, and Ooka Takayuki, **"Stress-Corrosion Cracking of Stainless Steels in Hydrogen Sulfide Solutions,"** *Stress-Corrosion—New Approaches, ASTM STP 610,* American Society for Testing and Materials, 1976, pp. 338–348.

ABSTRACT: The environment causing stress-corrosion cracking (SCC) at the top of a distillation tower in a crude oil refinery was reproduced in the laboratory. It was an acidified hydrogen sulfide solution with a pH value up to 3.5 at 80°C. In the solution, austenitic stainless steels such as AISI Type 304 or 316 failed because of SCC; however, modified ferritic stainless steels showed good corrosion resistance.

KEY WORDS: stress corrosion, cracking (fracturing), hydrogen sulfide, solutions, crude oil, refineries, distillation equipment, austenitic stainless steels, ferritic stainless steels, corrosion resistance, susceptibility

Austenitic stainless steels are known to undergo stress-corrosion cracking (SCC) in chloride solutions [*1,2*].[2] Solutions containing chloride ions generally are used for testing. For example, high silicon austenitic stainless steel has been reported to have a resistance to cracking in a 42 percent magnesium chloride ($MgCl_2$) solution [*3,4*]. Sensitized austenitic stainless steels undergo intergranular SCC in high temperature, pressurized water having very low chloride ion concentrations (several tens to several hundreds part per million. As for nonchloride solutions, the occurrence of intergranular SCC of sensitized stainless steels in polythionic acid has been reported [*5,6*].

Also, at the top of a distillation tower in an oil refinery, general corrosion and SCC occurs with austenitic stainless steels [*7,8*]. Chloride ions are reported to have been the cause. This present study was made in an effort to provide the similar environment at the top of a distillation tower in the laboratory, for the ultimate purpose of finding steels having sufficient cor-

---

[1] Researcher, researcher, and manager of Research Laboratory, respectively, Hikari Works, Nippon Steel Corporation, Yamaguchi, Japan.

[2] The italic numbers in brackets refer to the list of references appended to this paper.

rosion resistance in such an environment. The study at the same time served to identify the substances causing SCC at the top of the tower.

A laboratory test procedure was first developed and evaluated, after which the corrosion resistance of various types of stainless steels was determined by using the test procedure thus established.

Test Procedure

A water-cooled condenser was attached to a 1000-ml glass flask, and 600 ml of test solution was put in the flask and maintained at 80°C in a hot water bath. During the test, hydrogen sulfide (H_2S) gas was injected into the solution continuously at 2 litre/h through the bottom of the flask in order to saturate the solution.

Types, chemical compositions, and tensile properties of the stainless steels used for the test are shown in Table 1. Of these commercial stainless steels, 434-Mod and 19Cr-2Mo are intended to diminish susceptibility to intergranular corrosion at the weld metal or heat-affected zone by lowering their carbon and nitrogen contents and adding titanium and columbium, while retaining their corrosion resistance as ferritic stainless steels. The steels were cold rolled to a thickness of 1.5 mm, cut into specimens 15 mm wide by 100 mm long, and heat treated. The heat-treated specimens were dry ground with emery paper up to grade 240 and bent into U-shapes in parallel with the rolling direction with a radius of 10 mm. For the SCC test, the specimens were U-bent and fixed by jigs. Two such specimens of the same stainless steel were immersed in the solution.

Other specimens were gained as follows: after the tension test, specimens 1.5 mm thick by 25 mm wide by 200 mm gage length (GL) were strained up to 10 percent elongation, they were then cut into specimens 1.5 by 15 by 100 mm, ground with emery paper up to grade 240, and bent into U-shapes.

After specified test duration periods, the specimens were rinsed and dried and their surfaces inspected either visually or with a ×200 magnification using an optical microscope. Then cracking depths of the sections at these parts where corrosion (or cracking) was the greatest were measured using the microscope. The factors and applied ranges which were studied and the recommended test conditions obtained from the experimental results are shown in Table 2.

Experimental Results

Effect of Hydrogen Sulfide

Table 3 shows the results of experiments on Type 304 stainless steel. No cracking was caused in the solution either saturated with H_2S or acidi-

TABLE 1—*Chemical compositions and tensile properties of the tested materials.*

Materials	Chemical Compositions, weight %								0.2% Proof Stress, kg/mm²	Tensile Strength, kg/mm²	Total Elongation, %
	C	Si	Mn	P	S	Ni	Cr	Others			
Austenitic stainless steels:											
AISI Type 304	0.06	0.9	1.1	0.03	0.01	8.6	18.5	...	27.8	66.4	54.0
AISI Type 304L	0.02	0.7	1.1	0.03	0.01	10.7	18.1	...	26.9	60.3	54.0
AISI Type 316	0.04	0.6	1.0	0.03	0.01	13.2	16.6	Mo2.2	27.6	60.1	53.0
AISI Type 321	0.04	0.6	1.2	0.02	0.01	9.5	17.6	Ti0.3	28.5	63.6	51.0
Ferritic stainless steels:											
AISI Type 430	0.06	0.6	0.5	0.02	0.01	...	16.4	...	30.9	48.0	32.0
AISI Type 434	0.08	0.5	0.5	0.02	0.01	...	16.2	Mo1.0	35.7	55.2	28.0
AISI Type 434-Mod	0.01	0.5	0.5	0.02	0.01	...	16.6	Mo1.0: Cb0.3: Ti0.2	36.9	54.1	27.0
19Cr-2Mo steel	0.007	0.1	0.1	0.02	0.008	...	19.1	Mo2.0: Cb0.3: Ti0.2	35.0	51.2	33.5

TABLE 2—*Test conditions.*

Factors	Applied Ranges of the Test Conditions	Recommended Test Condition
H_2S gas	0 or 2 litre/h/600 ml	2 litre/h/600 ml
Cl^- ion	0 to 6.7 % (as 10 % NaCl)	36 ppm
H^+ ion	initial pH 1.0 to 7.0	initial pH 3.0
Temperature	80°C	80°C
Stress application	U bended with a radius of 10 mm and restricted, or strained by tension to 10 % elongation	U bended with a radius of 10 mm and restricted
Restriction jig	titanium, AISI Type 304 or Teflon jig	titanium jig
Test duration	3 to 15 days	15 days

fied with hydrochloric acid (HCl). Cracking caused in the solution acidified with HCl and then saturated with H_2S. Cracking occurred transgranularly only at the bent parts for solution-treated specimens, and over the surface for elongated and bent specimens. Figures 1 and 2 show cracks on both surfaces and sections.

Effect of Chloride Ions

Table 3(2) shows the results of tests made by using HCl and sulfuric acid (H_2SO_4) for adding hydrogen ions. It became evident that chloride

TABLE 3—*Effects of H_2S, HCl, and chloride ion on the SCC susceptibility of AISI Type 304.*

(1) Coeffect of H_2S and HCl

Conditions of the Specimens	H_2S Saturated Water	HCl Acidified Water, pH 1.0	HCl Acidified (pH 1.0) and H_2S Saturated Solution
As solution treated	○ ○	○ ○	○ ○
U-bend	○ ○	○ ○	● ● (200 μm)
10 % strained and U-bend	○ ○	○ ○	● ● (150 μm)

(2) Comparison of Chloride and Sulfate Ion

Conditions of the Specimens	HCl: pH 3.0	H_2SO_4: pH 3.0
As solution treated	○ ○	○ ○
U-bend	● ● (200 μm)	● ● (120 μm)
10 % strained	● ● (150 μm)	● ● (60 μm)
10 % strained and U-bend	● ● (150 μm)	● ● (100 μm)

○ Not cracked at 80°C, 15 days.

● Cracked at the same condition, the values bracketed are the maximum crack depths in 2 specimens.

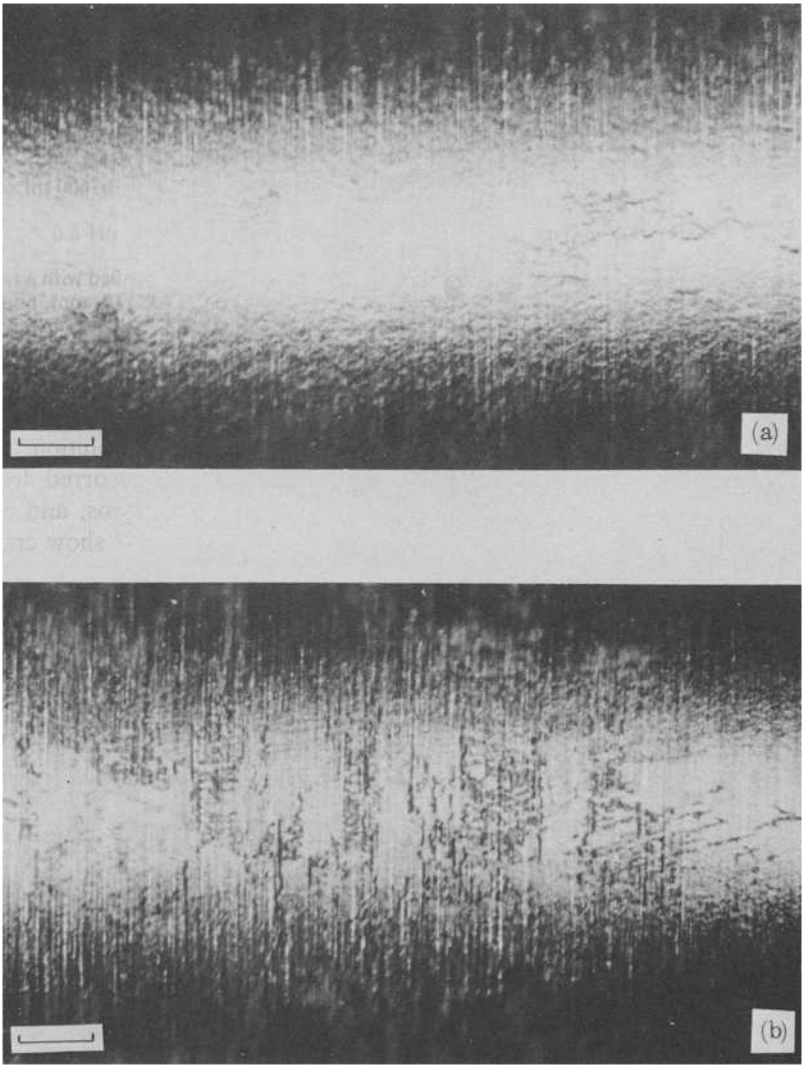

(*a*) AISI Type 304 (scale mark indicates 1 mm).
(*b*) AISI Type 434 (scale mark indicates 1 mm).

FIG. 1—*Surface of the U-bend specimen corroded in H_2S saturated solution (pH 3.0 with HCl, 80°C, 15 days).*

ions were not always necessary for the occurrence of cracking because it occurred even in H_2SO_4 solutions.

Effect of Hydrogen Ion Concentration

Table 4 shows the occurrence or nonoccurrence of cracking when the pretest pH values of solutions were changed within a range of 1.0 to 7.0

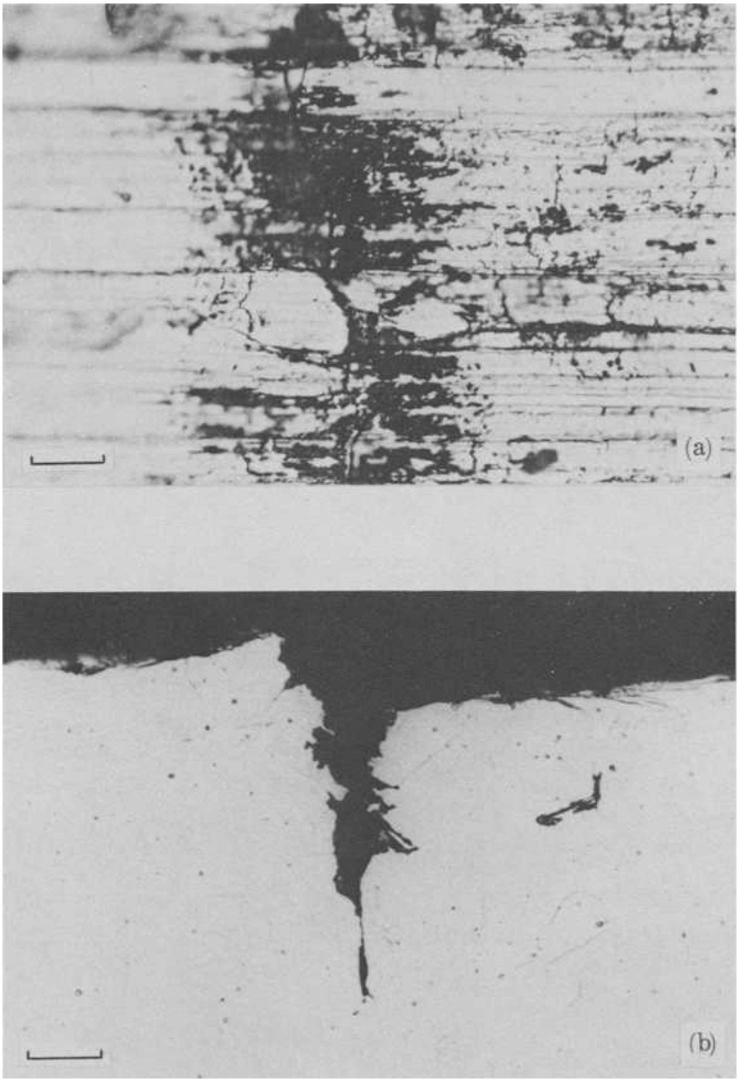

(*a*) Surface (scale mark indicates 20 μm).
(*b*) Longitudinal section (scale mark indicates 20 μm).

FIG. 2—*Stress corrosion cracking of AISI Type 304 in H_2S saturated solution (pH 3.0 with HCl, 80°C, 15 days).*

by adding HCl or sodium hydroxide (NaOH). Figure 3 shows the observed relationship between the lapse of time and changes in pH values. In the cases of solutions with the initial pH value of 7.0, their pH values decreased 5.2 to 5.4 five hours after the start of H_2S injection, and to about 4.1 fifteen days thereafter, without causing cracking. In the cases of solution with an initial pH value of 3.0, their pH values scarcely changed

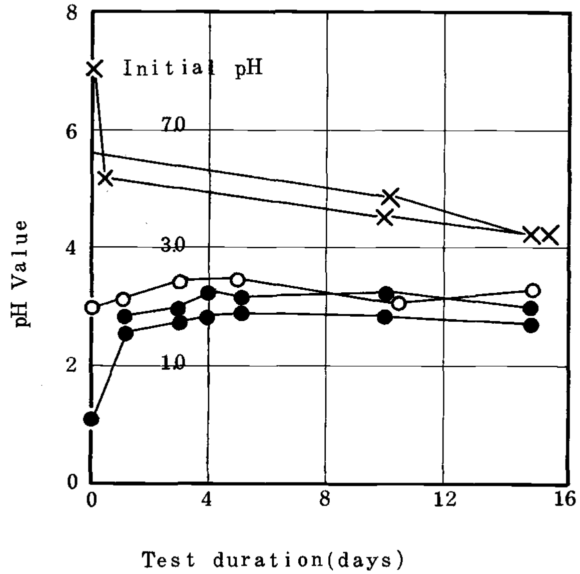

FIG. 3—*Changes in pH of H_2S saturated solution during testing (80°C).*

throughout the test duration and cracking occurred. In the cases with the initial pH value of 1.0, the pH values increased to 2.5 after 24 h, and continued to increase gradually thereafter until they reached about 3.1 on the 15th day after the start of injection. In this case, cracking also occurred.

TABLE 4—*Effect of hydrogen ion concentration on the SCC susceptibility of AISI Type 304 in H_2S saturated solution (80°C, 15 days).*

Conditions of the Specimens	pH Value Prepared with HCl		
	pH 1.0	pH 3.0	pH 7.0
As solution treated	○ ○	○ ○	○ ○
U-bend	● ● (200 μm)	● ● (180 μm)	○ ○
10 % strained	● ● (150 μm)	● ● (70 μm)	○ ○
10 % strained and U-bend	● ● (150 μm)	● ● (120 μm)	○ ○

○ Not cracked.
● Cracked at the same condition, the values bracketed are the maximum crack depths of 2 specimens.

Table 5 shows the result of more detailed tests on solution-treated Types 304 and 316 and annealed Type 434, which was conducted to find the initial pH values of solutions causing cracking. Cracking occurred in Type 304 when the pH value was below 3.0 and in Type 316 where it was 3.5 or below. Only shallow pitting corrosion occurred in Type 434 when the pH values were below 4.0.

TABLE 5—*Effect of hydrogen ion concentration on the SCC susceptibilities of AISI Types 304, 316, and 434 in H_2S saturated solution (U-bend, 80°C, 15 days).*

Initial pH Value Prepared with HCl	Steels		
	AISI Type 304	AISI Type 316	AISI Type 434
pH 3.0	● ● (140 μm)	● ● (230 μm)	△ △ (25 μm)
pH 3.5	○ ○	○ ● (300 μm)	△ △ (25 μm)
pH 4.0	○ ○	○ ○	△ △ (25 μm)
pH 4.5	○ ○	○ ○	○ ○
pH 5.0	○ ○	○ ○	○ ○

○ Not corroded.
● Cracked, the values bracketed are the maximum crack depths in 2 specimens.
△ Pitting corroded, the values bracketed are the maximum pit depths in 2 specimens.

Effect of Jigs

In the preceding tests, titanium jigs were always used to restrict the specimens. In another test, polyfluoroethylene fiber (Teflon) or Type 316 stainless steel were used as materials for the restriction jigs for comparison with the titanium jigs. In all cases, however, cracking occurred. As there was no necessity for considering the electrochemical effect of the jigs, titanium bolts and nuts were used thereafter as holding jigs.

Test Duration

As shown in Table 6, Type 304 stainless steel started to crack on the fifth day. Though there was not any clear relationship between the depth of cracking and the duration of the test, the depth of cracking was greater when the test was continued for 15 days. In the case of Type 434, cracking did not occur, and only shallow pitting corrosion was evident after 15 days.

TABLE 6—*Effect of the test duration on the SCC susceptibilities of AISI Types 304 and 434 in H_2S saturated solution (U-bend, pH 3.0 with HCl, 80°C).*

	Test Duration, days			
Steels	3	5	9	15
AISI Type 304	○ ○	● ● (85 μm)	● ● (70 μm)	● ● (140 μm)
AISI Type 434	○ ○	○ ○	○ ○	△ △ (25 μm)

○ Not corroded.
● Cracked, the values bracketed are the maximum pit depths in 2 specimens.
△ Pitting corroded, the values bracketed are the maximum pit depths in 2 specimens.

Evaluation of the Various Types of Stainless Steels

As a result of the foregoing tests, the test condition shown in Table 2 was used as a recommended one. The results of the cracking susceptibility tendencies of the various stainless steels evaluated under these recommended conditions are shown in Table 7. All austenitic stainless steels were cracked transgranularly in the solution-treated state and intergranularly cracked in the sensitized state. No ferritic stainless steel showed cracking susceptibility in the annealed state. Sensitized Type 434 was intergranularly cracked. In spite of being heated up to 1220°C and cooled, 434-Mod and 19Cr-2Mo were not sensitized and thus did not crack. Figure 4 shows microphotographs of the intergranular cracking of the sensitized Types 304 and 434, and the pitting attack of Type 434-Mod.

TABLE 7—*Susceptibilities of some stainless steels to SCC in H_2S saturated solution (U-bend, pH 3.0 with HCl, 80°C, 15 days).*

	Conditions	
Steels	Annealed	Sensitized[a]
Austenitic:		
AISI Type 304	transgranular cracking	transgranular and intergranular cracking
AISI Type 304L	transgranular cracking	not tested
AISI Type 316	transgranular cracking	not tested
AISI Type 321	transgranular cracking	not tested
Ferritic:		
AISI Type 430	pitting	not tested
AISI Type 434	pitting	intergranular cracking
AISI Type 434-Mod	pitting	pitting
19Cr-2Mo steel	slight pitting	slight pitting

[a] Sensitized at 650°C for 2 h for austenitic steels and at 1220°C for 5 min for ferritic steels and air cooled.

Discussion

The intended laboratory reproduction of transgranular SCC that had been experienced in stainless steels at the top of a distillation tower [*8*] is believed to have been achieved. Insufficient experimental data are available for hypothesizing a mechanism to explain the cracking in this environment. The morphologies of cracking were the same as those appearing at the tower top of an oil refinery, although the depth of cracking was shallower in this study than at the refinery top.

It will be necessary to compare the cracking behavior of carbon steels or high-strength alloy steels in acidified H_2S solutions, with the observed behavior of the stainless steels. In the present study, the surfaces of the

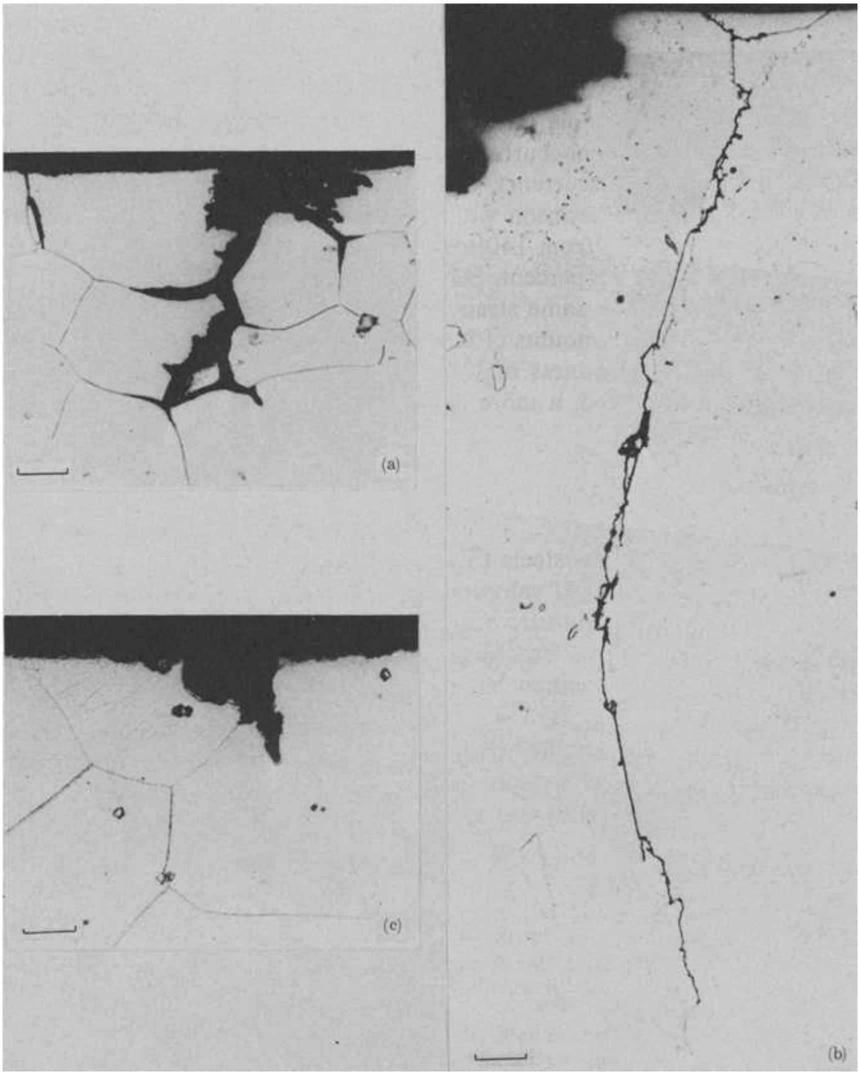

(a) AISI Type 304 sensitized at 650°C for 2 h (scale mark indicates 20 μm).
(b) AISI Type 434 sensitized at 1220°C for 3 min (scale mark indicates 50 μm).
(c) AISI Type 434-Mod sensitized at 1220°C for 3 min (scale mark indicates 20 μm).

FIG. 4—*Stress corrosion cracking and pitting of the sensitized stainless steels in H_2S saturated solution (U-bend, pH 3.0 with HCl, 80°C, 15 days).*

specimens retained their metallic gloss almost unchanged from the original state and only the cracked parts and their immediate vicinities turned blackish, revealing that the extent of corrosion is small. Cathodic polarization resulted in the nonoccurrence of cracking, whereas anodic polarization resulted in the occurrence of cracking. However, this point will be discussed on another occasion with sufficient experimental data. Hardness of Type 304 increases from 140 to 150 Vickers hardness number (VHN) for a tensile strain of 6 percent. Hardness of Type 316 increases from 140 to 150 VHN after the same strain. Cracking occurs in both as shown in Table 4. Data on the amounts of ferrite as measured by a ferrite meter and the changes in the hardness of U-bend specimens are still lacking. After these data are collected, a more detailed discussion will be made on the cracking behavior.

Conclusions

1. Austenitic stainless steels (Types 304, 316, etc.) are subject to SCC in 80°C solutions with pH values adjusted to below 3.0 by the addition of hydrochloric acid (or sulfuric acid) and saturated with hydrogen sulfide.
2. The test conditions described in (1) are considered to provide the similar corrosive environment at the top of a distillation tower of an oil refinery.
3. Stainless steels capable of withstanding exposure to such an environment are ferritic stainless steels improved in intergranular corrosion susceptibility (Type 434-Mod and 19Cr-2Mo).

References

[1] Kohl, H., *Corrosion,* Vol. 23, No. 2, 1967, pp. 39–49.
[2] Rhodes, P. R., *Corrosion,* Vol. 25, No. 11, 1969, pp. 462–472.
[3] Ueda, M. et al, Technical Report No. 2, Nippon Steel Corporation, Tokyo, Japan, 1973, pp. 66–74
[4] Davis, J. A., *Corrosion,* Vol. 26, No. 3, 1970, pp. 95–98.
[5] Uto, Y., *Corrosion Engineering,* Vol. 19, No. 3, 1970, pp. 117–125.
[6] Brophy, A. J., *Materials Performance,* Vol. 13, No. 15, 1974, pp. 9–15.
[7] Couper, A. S., *Materials Protection,* Vol. 8, No. 10, 1969, pp. 17–22.
[8] Ooka, T. et al, *Journal of the Japan Petroleum Institute,* Vol. 11, No. 11, 1968, pp. 845–851.

C. G. Interrante[1] *and G. E. Hicho*[1]

Removal of Iron-Sulfide Deposits from Fracture Surfaces

REFERENCE: Interrante, C. G. and Hicho, G. E., "**Removal of Iron-Sulfide Deposits from Fracture Surfaces,**" *Stress Corrosion—New Approaches, ASTM STP 610,* American Society for Testing and Materials, 1976, pp. 349–365.

ABSTRACT: Steels are most commonly used at moderate strength levels at which they have high ductility and resistance to subcritical crack growth due to hydrogen. Thus, in testing the susceptibility to hydrogen damage of these steels, severe charging conditions are commonly used, and hydrogen sulfide is often used in low-pH solutions to obtain the desired high fugacity for the test. The fracture faces of specimens tested in this type of solution become covered with iron and other sulfides that are difficult to remove without affecting the underlying metal as well. The removal of these sulfide deposits from the fracture surfaces is a prerequisite to fractographic analysis of the failure mode, and it was attempted by various methods. Hydrogen reduction of the sulfides at elevated temperatures followed by ultrasonic cleaning in alcohol was found to be much more successful than the other methods studied. This is true principally because the hydrogen-reduction treatment did not attack the fracture surface. Procedures for four different cleaning treatments are described, and they are rated in terms of their relative capability for cleaning sulfide-contaminated fracture surfaces without affecting the underlying metal. Evaluations of these methods for double-cantilever-beam and Charpy V-notch specimens of a 2¼Cr-1Mo steel with fracture surfaces that were created at various stress-intensity levels provides information needed for studying the cracking mechanism under severe sulfide exposure conditions.

KEY WORDS: stress corrosion, crack propagation, ductility, hydrogen, failure, fracture tests, steels, fractography

When the most commonly used steels of moderate strength levels are subject to tests of susceptibility to hydrogen damage in laboratory experiments, high-fugacity environments containing hydrogen sulfide (H_2S) frequently are used. In these environments, the fracture surfaces become contaminated with sulfides. This contamination precludes meaningful fractographic studies needed for understanding the mechanism by which failure occurred.

---

[1] Metallurgists, National Bureau of Standards, Washington, D. C. 20234.

Steels are used most commonly at moderate strength levels at which they have high ductility and resistance to subcritical crack growth due to hydrogen. The tensile strength levels of the steels in question are in the range, of 108 ksi (745 MPa) to 130 ksi (895 MPa). This strength-level range corresponds to a hardness level range of HRC 20 to 30, in which resistance to hydrogen damage is relatively good. Steels at the low end of this range can even be used in refinery process streams which contain H_2S or cyanide environments known to be particularly severe in respect to hydrogen damage and charging effects.

The suitability of various steels for a given industrial application is determined either by field experience, or by laboratory tests in a simulation of the environment in question. For steels of moderate strength levels, tests of the susceptibility to hydrogen damage and subcritical crack growth often must be conducted under severe charging conditions. In laboratory tests, the desired high hydrogen-fugacity levels needed to characterize the susceptibility are often obtained using aqueous low-pH solutions containing H_2S. However, when steels are subject to sulfide environments, they become covered with deposits of iron sulfides. The thickness of these deposits increases with time of exposure, and the original fracture face can be chemically attacked by extended exposures. In industrial failures, the exposure time is so long that the fracture faces from these failures are commonly so badly deteriorated that they are of little value for fractographic studies. Sulfide deposits form on all exposed surfaces, even on regions near the tip of a tight crack in a laboratory specimen that has had only several days exposure to aqueous environments containing sulfides. Thus, sulfide deposits on the surfaces of fractures are an impediment to the development of an understanding of the fracture mode (and hence the mechanism) of failures of steels in sulfide environments.

Our understanding of the mechanism of hydrogen damage has received much attention, particularly for steels of higher strength levels. Work on steels with moderate levels of strength is receiving increased attention, and fractography is important in these efforts because it is needed to understand the failure mode. To this end, experimentalists must have available fracture surfaces that have been cleaned so that they are free of contaminants applied after failure. Even these clean surfaces will not provide the needed information if they have been deteriorated by chemical attack which can occur from either exposure to aggressive cleaning agents or to extended exposure to sulfide environments. Accordingly, a program of tests was undertaken to determine suitable methods for removal of sulfide deposits from the surfaces of fractures of steels of moderate strength. The steel used in this test program was a 2¼Cr-1Mo steel tempered to hardness levels of from HRC 20 to 30.

Experimental Procedure

Four methods for the removal of sulfide deposits from fracture surfaces were studied using fracture-toughness type specimens that had been exposed for five days to an acetic acid solution saturated with H_2S. These methods used various cleaning agents: (1) aqueous solution of ammonium citrate, (2) electrolytic, alkaline solution with sodium cyanide, (3) electrolytic, sulfuric acid solution containing an organic inhibitor, and (4) hydrogen gas at elevated temperatures. In addition, replica stripping, using an acetate replicating tape, was used in the earlier phases of this study as an attempt to remove sulfides.

The fracture surfaces that were used in these sulfide removal studies had been exposed to sulfide solutions using either of two experimental conditions. One condition gave a variable time of exposure to the solution and the other gave a constant exposure to the solution. The variable exposure condition was obtained using a double-cantilever-beam (DCB) specimen that was loaded with a wedge and placed in the solution where it was cracked very slowly by the action of the solution on the loaded specimen. The fracture surface of this type of specimen has a crack initiation area called a chevron, and this area received the longest time of exposure to the sulfide solution. The other end of the fracture surface is the crack tip, and this area received the shortest exposure to the sulfide environment. The other type of exposure used a Charpy V-notch (CVN) specimen that had been completely fractured before being placed in the sulfide environment.

All specimens tested were exposed for five days in the sulfide environment. Thus, it was expected the CVN specimens would be coated with a heavy coating of sulfides, because these fracture surfaces were exposed for the full five days, whereas the fracture surfaces of the DCB specimens received a variable exposure of from three to five days depending on the location along the fracture length. The effectiveness of a sulfide removal technique was judged by scanning electron microscope (SEM) fractography. However, preliminary judgments were made by observation by eye and with the light microscope at low magnifications. These preliminary judgments were used to screen completely unacceptable cleaning treatments.

The test solution for these exposures was an acetic acid solution that was initially set at a pH level of 3.5, purged with nitrogen to remove oxygen from the solution, and then saturated with H_2S at 1 atm, and resaturated once daily until the last day of exposure. As the five-day exposure time elapsed, the pH increased to a level of about 4.5. At the end of this exposure, the specimens were removed from the solution and then cleaned by one of the four methods studied:

Method 1—A solution of 10 g of ammonium citrate in 100 ml of distilled water was heated to 30°C (86°F), and this solution was applied to the fracture surface by mildly stroking with a bristle brush until the specimen appeared clean. Following brushing, the specimen was sprayed with ethyl alcohol and dried with hot air before the surface was examined on the SEM.

Method 2—A proprietary oxidizing, alkaline solution containing sodium cyanide was heated to and maintained at 49°C (120°F) during an electrolytic cleaning operation. Initially, the specimen was the cathode, and a graphite rod, the anode. After 7 s, polarity was reversed so that the specimen alternated being the cathode and then the anode, for a total of 14 s. One entire cleaning cycle consisted of 12 current reversals (84 s) at a predetermined level of current. After each of five successive cleaning cycles that were studied, an optical microscope was used to examine the fracture surface for cleanliness. After the last of these cycles, the specimen was considered clean enough for use in SEM studies.

The initial current value tried was 1.25 amp for a current density of about 20 A/dm^2 for times up to 18 min. The fracture surface was not cleaned adequately with this technique, and the current was increased to about 2 amp for a second (more intensive) cleaning cycle on a second specimen. This process was repeated using current values of about 4, 5, and finally 7 amp on this second specimen. After each cycle, the fracture surface was sprayed with ethyl alcohol, dried with hot air, and then examined optically. After the 7-amp cleaning cycle, the fracture surface was judged to be reasonably clean, and it was used for studies of the fracture mode on the SEM.

Method 3—A sulfuric acid solution with an organic inhibitor was used according to a procedure given by ASTM Committee G-1, as reported in[2] ASTM Recommended Practice for Preparing, Cleaning, and Evaluating Corrosion Test Specimens (G 1-72). In this procedure, a steel specimen is electrolytically cleaned with sulfuric acid, containing an organic inhibitor, diorthotolyl thiourea, (0.5 g/litre).

Prior to the electrolytic cleaning, the fracture surface was stroked mildly with a bristle brush dipped in ethyl alcohol. This removed any loose material. During the electrolytic cleaning, the specimen was the cathode and a graphite rod, the anode. The temperature of the solution was about 75°C (167°F). The specimen was kept in the solution for approximately 2 min[2] at a current density of about 20 A/dm^2. Then the specimen was removed from the solution, sprayed with ethyl alcohol, dried with hot air, and observed on the SEM.

Method 4—Several techniques using hydrogen gas were studied. Specimens were exposed to hydrogen gas for various times at temperatures of 510°C (950°F), 625°C (1157°F), 680°C (1256°F), and 760°C (1400°F). These temperatures were all considered to be below the A_1 temperature[3] for this steel. These elevated-temperature exposures to hydro-

---

[2] Three minutes is recommended in ASTM Recommended Practice G 1-72.

[3] Unpublished measurements and calculations by Professor A. W. Pense of Lehigh University indicated that the A_1 on heating is about 807°C (1485°F) for this steel.

gen gas resulted in the formation of H_2S by a reaction between the H_2 and the sulfides on the steel. Other workers[4] have used this technique for determinations of the amount of iron sulfide (FeS) present in or on the surface of steel. As FeS was found to be a major constituent of the sulfide deposits covering the fracture surfaces of the DCB specimens used in the present study, the Bandi method was considered to be potentially useful for this work.

Hydrogen reduction of the sulfides was accomplished by placing sulfide contaminated specimens in an alumina boat, and then inserting the boat into a VYCOR tube furnace. The furnace was sealed, and argon was introduced into the furnace at a rate of 300 ml/min, while the furnace was heated to 200°C (392°F). After 45 min from the start of this heating cycle, hydrogen gas was substituted for the argon (at the same 300 ml/min rate) and the temperature was increased to the reduction temperature. The furnace was maintained for a fixed time at the reduction temperature and then cooled to 250°C (482°F). At this temperature, an argon atmosphere was substituted for the hydrogen; and the furnace was then cooled to about 38°C (100°F) before the specimen was removed for examinations.

The rate of removal of sulfides from the fracture surface was monitored qualitatively by monitoring precipitation of cadmium sulfide (CdS) in a cadmium chloride ($CdCl_2$) solution placed at the exit duct of the tube furnace. The effluent gas from the furnace contained H_2S. This gas was bubbled through an aqueous solution of $CdCl_2$ which was contained in a transparent jar. This was done principally to transform the H_2S into a precipitate so as to prevent the escape of this poisonous gas into the laboratory. In the jar, one could observe the formation of a yellow precipitate of CdS, and as the rate of precipitation decreased with time, the reaction, which removed sulfides from the fracture surface, was considered to be approaching completion.

Upon removal of the specimen from the furnace, the specimen was cleaned ultrasonically in alcohol for a minimum time of 30 min, hot air dried, and then observed with the SEM.

The required time at temperature was determined arbitrarily by examination of specimens in the SEM after various reduction times. If the fracture surface had too much contamination and the fracture mode could not be determined, it was returned for additional exposure at the same temperature. The times reported in Table 1 are cumulative times used for the specimens that were rated. These times varied from 3½ h at 680°C (1256°F) to 4 days at 510°C (950°F).

During the SEM examinations of the cleaned fracture surfaces fractographs were taken at select locations within the chevron, and at sites near

---

[4] Private communications with W. R. Bandi of U.S. Steel Research Laboratories, Monroeville, Pa.

TABLE 1—*Results of ratings of fracture surfaces cleaned by various methods.*

Cleaning Method	Specimen Number	Type of Fracture Surface Rated	Rating No. for Various Locations			Comments
			Chevron or CVN[a]	Midlength or Branch[b]	Crack Tip[c]	
Method 1: Aqueous solution of ammonium citrate	15C	DCB branch crack	not applicable	3 to 4	3 to 4	rated 3 to 4 for attack on steel and 2 to 3 for removal of sulfides
Method 2: Electrolytic, alkaline solution with sodium cyanide	10C	Charpy crack	4	not applicable	not applicable	84 s at 112 A/dm^2; rated 4 on attack on steel and 2 for removal of sulfides
	19C	DCB main crack	5	5	2	1½ min at approximately 20 A/dm^2; sulfides not adequately removed
			5	5	2	18 min at approximately 20 A/dm^2; sulfides not adequately removed
Method 3: Electrolytic, acid solution with organic inhibitor	1C	DCB main crack	4	not rated	4	steel was badly attacked during cleaning

Method 4: Hydrogen reduction temperature, time						
760°C (1400°F), 1½ h	1B	DCB main crack	2	2	1	rating of 2 is due to original sulfide attack
680°C (1256°F), 2 h	22A	DCB main crack	4	3	2	this specimen received a 6-day exposure to sulfides; others had 5 days of exposure
680°C (1256°F), 14 h	22A	DCB main crack	3	2 to 3	2	after 7 h in H_2, specimen was judged to be nearly the same as after 2 h in H_2
680°C (1256°F), 3½ h	10C-B/2	DCB main crack	not rated	2 to 3	1	
625°C (1157°F), 24 h	1B	DCB main crack	3	2 to 3		
510°C (950°F), 4 days	10C-A/2	DCB main crack	4	2	not rated	this treatment was judged to be better than that of the 680°C, 3½ h treatment
510°C (950°F), 4 days	1A	DCB branch crack	not applicable	2	1	
510°C (950°F), 4 days	1C-B	DCB main crack	not applicable	2	1	
510°C (950°F), 4 days	1C	DCB main crack	3 to 4	2	1	
Replica stripping with no other cleaning	24B	DCB main crack	5	3	2	not recommended, except possibly for crack tip region

[a] Exposure time—approximately 5 days.
[b] Exposure time—approximately 3 to 4 days.
[c] Exposure time—approximately 2 to 3 days.

the crack tip but on the sulfide exposed side of the crack tip, and at a position midway between these two sites. These fractographs were rated for their usefulness in studies of the fracture mode. The arbitrary rating system used was based on a scale of five with a rating of five being the worst rating given, and with lesser ratings representing varying degrees of usefulness according to the following definitions:

1. Appearance is similar to uncontaminated and unattacked fracture surface.
2. Removal of contaminants was adequate for fracture-mode determinations, and attack of cleaning agents was considered minimal.
3. Removal of contaminants was marginal to adequate for fracture mode determination, and attack may be more than considered desirable for fracture-mode studies.
4. The cleaning treatment removed some or all of the contaminants, but attack on fracture surface grains or grain boundaries or both was very pronounced so that fracture mode could not be determined.
5. The cleaning treatment removed little or none of the contaminant although it may have attacked grain boundaries.

Results and Discussion

After specimens were removed from the sulfide test solution, the severity of the sulfide contamination on the fracture surface was rated before and after cleaning. This was done by inspection of the fracture faces with an optical microscope and with the SEM. The SEM was used for preparing fractographs and sulfur X-ray area scans.

The inspections revealed that prior to cleaning the CVN specimens and the chevron area of the DCB specimens had similarly full sulfide coverages. Coverage around the midlength position of the DCB specimens was similar to that near the start of the branch cracks examined. This level of sulfide buildup was almost as severe but not as thick as that observed on the chevron area and on the CVN fractures. The crack-tip region of either a branch crack or a main crack was affected markedly less by the sulfide solution; this region had local sites of individual grains that contained little or no apparent contamination, along with the contaminated sites. From the uncontaminated grains at a crack tip, one could determine the fracture mode from fractographs, at least at selected sites of least contamination.

The appearances of the specimens after exposure to the sulfide solution are shown in Figs. 1 and 2. In Fig. 1*a*, a low magnification SEM fractograph is shown for a DCB specimen. Most of this fractograph shows the fracture surface of a branch crack. The balance of the fractograph shows other parts of the specimen, which also had been exposed to the test solution:

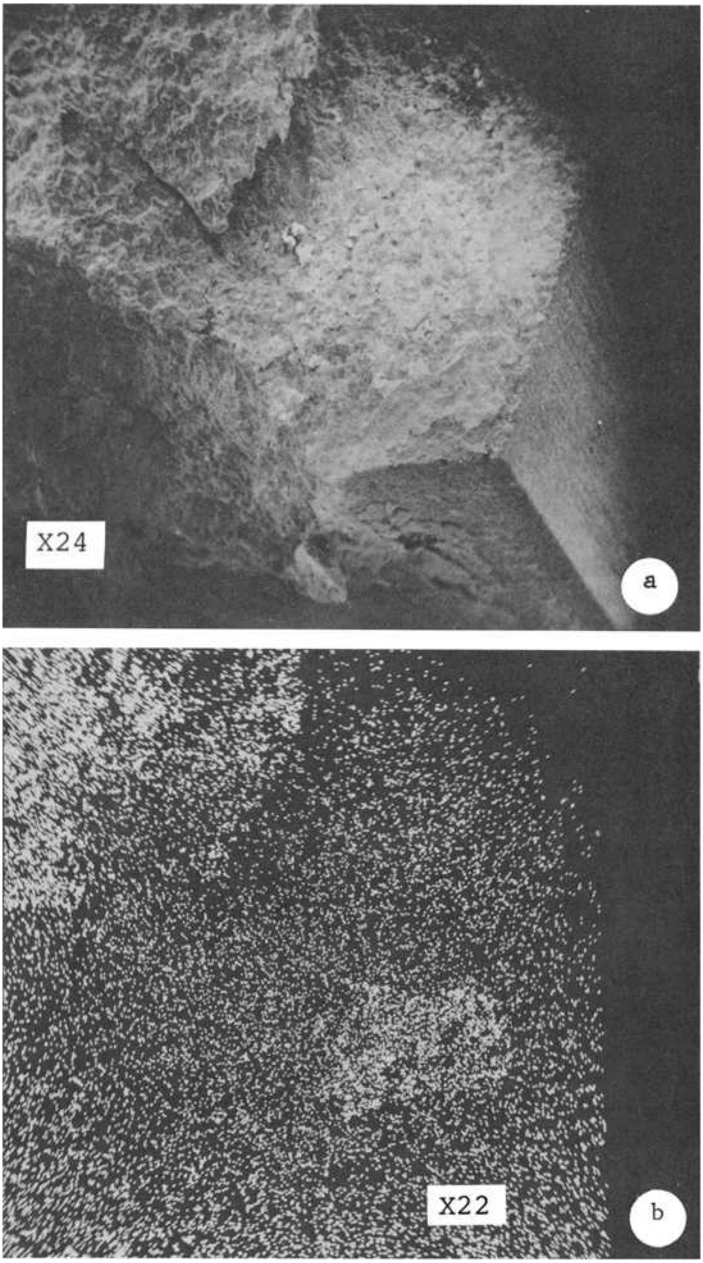

FIG. 1—*Scanning electron microscope fractograph* (a) *and sulfur X-ray area scan of this same location* (b) *showing that after exposure to the test solution, sulfides are present on branch crack, main crack, and machined surfaces.*

At the bottom of the fractograph is a main crack from which the branch crack developed, and the flat parts on the right side (and on the bottom right) are machined surfaces of the specimen. Figure 1*b* is a sulfur X-ray area scan taken at the same specimen location and magnification as those used for Fig. 1*a*. It shows that sulfides are present on all of the exposed surfaces—even on the machined surfaces—and that, on the branch crack, some areas have higher buildup of sulfides (as indicated by the density of white dots). In Fig. 2, these sulfide deposits are shown with fractographs taken at higher magnifications. Sulfide coverage of the fracture in the chevron area, (Fig. 2*a*) is pronounced, whereas coverage on the crack-tip area (Fig. 2*b*) is only moderate.

The results of the ratings of specimens after cleaning by various treatments are given in Table 1. In general, these ratings indicated that replica stripping gave poor results, and it is not recommended except possibly for mild cleaning in crack-tip regions. The ratings further indicated that during cleaning by Methods 1, 2, and 3, the removal of sulfides was generally slow in comparison with the rate of attack on the steel of the fracture surface, and that by Method 4, sulfide removal was accomplished without attack on the steel.

The effect of Method 1 treatment, using a solution of ammonium citrate, is shown in Fig. 3 taken at the tip of a branch crack. The exposed steel grains were attacked badly by the cleaning treatment, and there still remained many areas with sulfide deposits on the fracture surface, so that a rating of three to four was given due to attack on the metal. Furthermore, at locations closer to the main crack, the surface of this branch crack rated three to four because very little of the sulfide deposit had been removed from the surface.

The electrolytic cleaning methods gave results similar to the results obtained with Method 1. However, the appearance of the attack on the metal was different for each of the three methods. For Method 2, a specimen cleaned at 20 A/dm^2 was rated five because it had little or no sulfide removal. A CVN specimen that was cleaned at 112 A/dm^2 had severe grain boundary attack (rated four), and metal removal from the grains was observed in regions that still contained sulfides. A fractograph of this later specimen is shown as Fig. 4.

Electrolytic cleaning by Method 3, with the acid solution containing an organic inhibitor, resulted in severe pitting attack on the metal. This is shown in the fractograph of Fig. 5 taken at the tip of a crack in a DCB specimen. This attack was observed even in regions where there were sulfides remaining on the fracture surface. Accordingly, the treatment was rated four and was judged to have marginal applicability for cleaning surfaces similar to the main crack examined.

Cleaning by Method 4, using hydrogen reduction at various temperatures, resulted in fracture surfaces that were rated two to four at the chev-

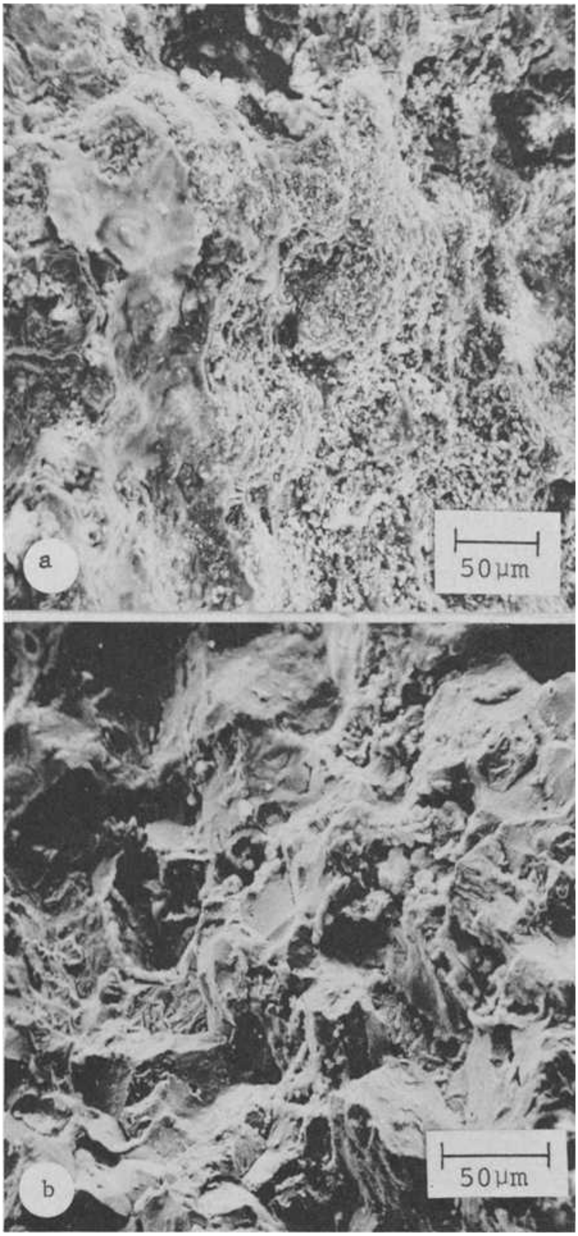

FIG. 2—*Fractographs showing that after exposure, sulfide coverage in the chevron region is pronounced* (a) *whereas that at a crack tip* (b) *is only moderate.*

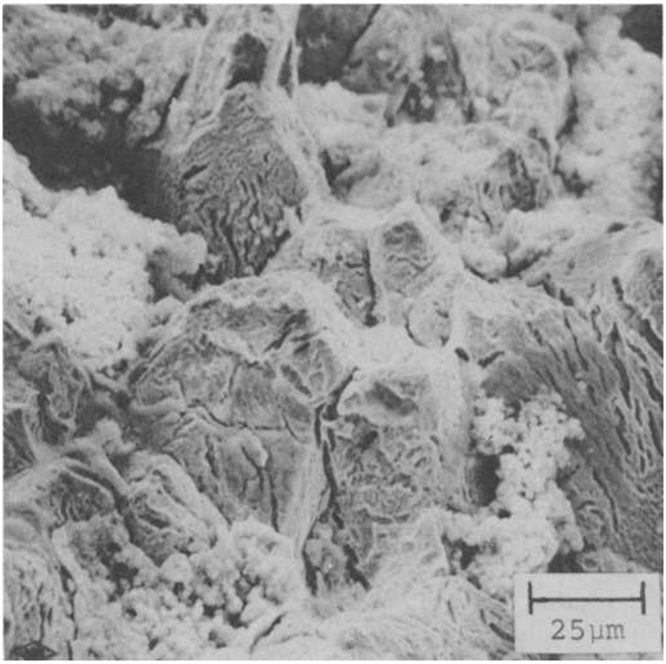

FIG. 3—*Fractograph taken at the tip of a branch crack after cleaning with ammonium citrate, showing incomplete sulfide removal and severe attack on the metal.*

ron area, two to three at midlength areas, and one to two at crack-tip areas. DCB specimen 1B, treated at 760°C (1400°F), was held in the reduction furnace until the reaction between the effluent gas and the $CdCl_2$ solution no longer produced a yellow precipitate. The appearance of this specimen, after ultrasonic cleaning, is shown in Fig. 6, and it was judged to be as good as or better than that of any other specimen examined in this study. The removal of sulfides was nearly complete on most of the fracture face. The removal was complete over regions large enough for determinations of the fracture mode on all parts of the fracture, even in the chevron area. This is shown in Fig. 6*a* taken in the chevron area, which is the area with the most tenacious sulfide deposits. This figure shows that the grains are not as smooth as the grains of the crack-tip region shown as Fig. 6b. For reasons that follow, this rough appearance is believed to be due to a deterioration of the metal in the chevron area caused by the prior action of the sulfide environment on the metal. The formation of sulfides has apparently destroyed parts of the original fracture face. This deterioration was much less pronounced at the midlength position on this specimen, and at the crack-tip region (Fig. 6*b*) there was

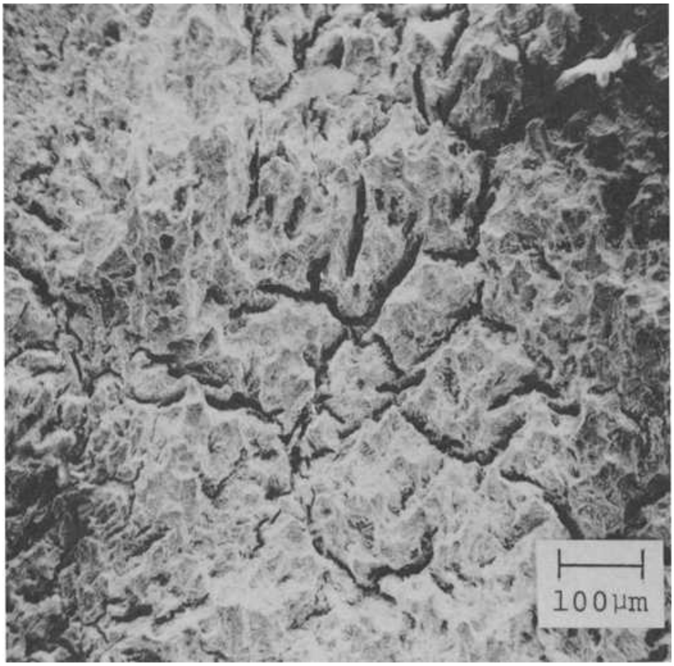

FIG. 4—*Fractograph taken on the fracture surface of a CVN specimen after cleaning by Method 2 (oxidizing electrolytic solution) at a current density of 112 A/cm*^{2}*, showing pronounced grain-boundary attack and incomplete sulfide removal.*

little or no noticeable deterioration of the original fracture. Thus, it seems clear that the action of the sulfides, rather than that of the hydrogen reduction reaction, is responsible for the deterioration. Furthermore, the pressure of hydrogen gas required to attack steel is known[5] to be much greater than the pressure of 1 atm used in this reduction treatment.

The ratings of three and four, which are marginal and unsatisfactory, were given for selected locations on some of the hydrogen-reduced specimens. These ratings were due to the incompleteness of the sulfide removal from these locations. If the reduction reaction were to have been brought to completion (as it was for specimen 1B treated at 760°C for 1½ h) with sufficient time at temperature, any of the temperatures from 510°C to 760°C (950°F to 1400°F) would have removed sulfides sufficiently for a rating of two. Thus, when complete removal of the sulfides is needed, the reaction should be monitored by observing the $CdCl_2$ solution during the reduction treatment, and the treatment should not be terminated until

---

[5] Nelson, G. A., Welding Research Council Bulletin 145, Section II, "Action of Hydrogen on Steel at High Temperature and High Pressure," Oct. 1969.

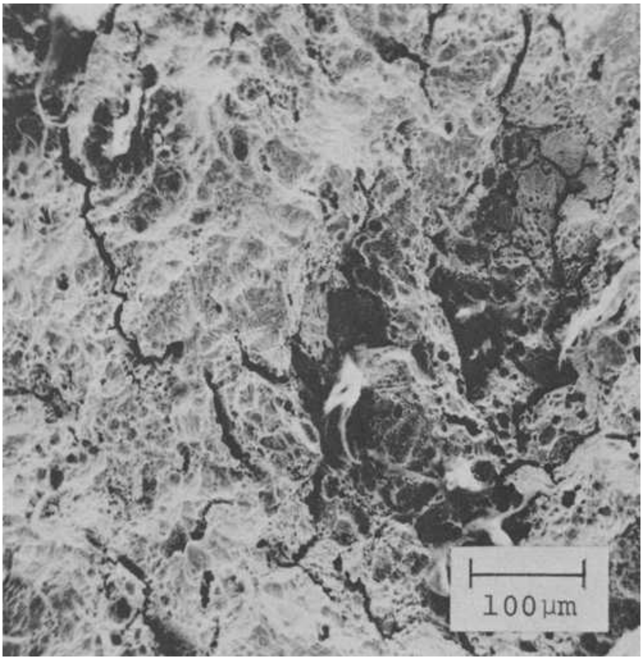

FIG. 5—*Fractograph taken near the tip of a crack in a DCB specimen after cleaning by Method 3 (acid electrolyte with inhibitor), showing attack of the metal and pitting.*

the yellow CdS precipitate is no longer being formed in this solution. The lower temperatures are recommended only when laboratory facilities limit the temperature that can be used for the hydrogen reduction treatment.

The importance of the ultrasonic cleaning treatment is demonstrated in Fig. 7. Figure 7*a* shows the crack-tip region of a DCB branch crack after ultrasonic cleaning of a specimen that had been treated at 510°C (950°F) for four days. The fracture surface is clean and free of the residue that is shown in Fig. 7*b* taken before the ultrasonic cleaning but after the reduction treatment. This residue was much more pronounced in regions that were covered more heavily with sulfides, and so the ultrasonic treatment was found to be even more important for removal of this residue in regions that had a heavy sulfide deposit.

Summary

The results of ratings of fractographs, which show the SEM appearances of fracture surfaces that had been contaminated with sulfide deposits and then cleaned by four different methods, indicated that hydrogen reduction

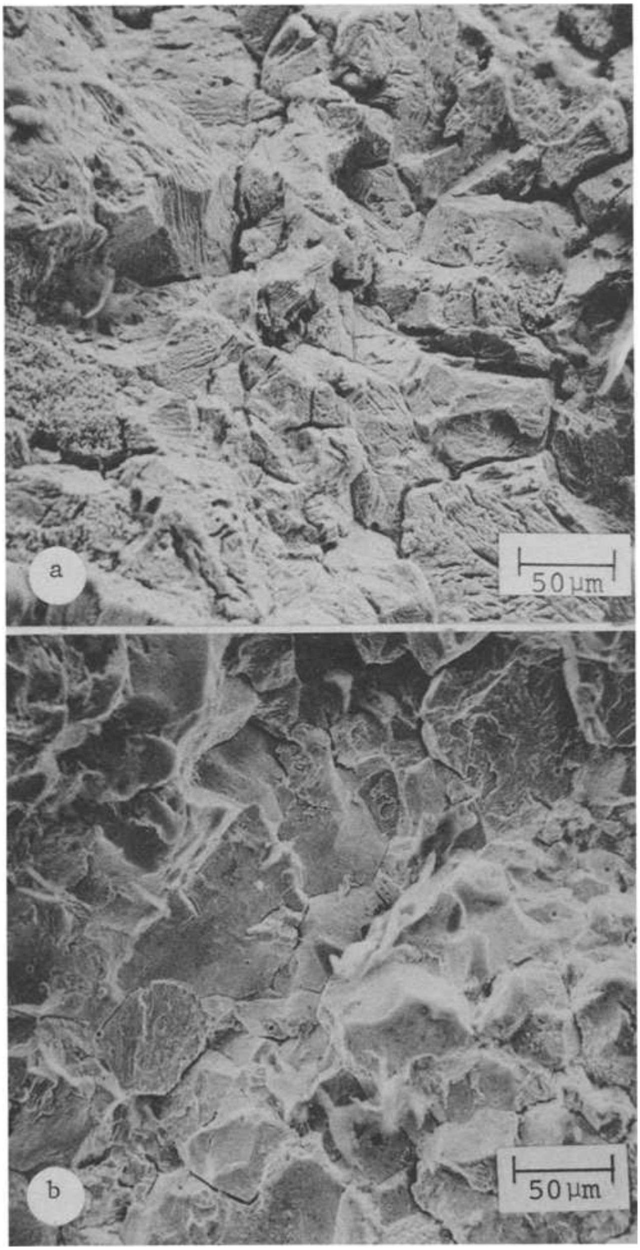

FIG. 6—*Fractographs taken at the chevron* (a) *and crack tip* (b) *areas of a DCB specimen cleaned by hydrogen reduction at 760°C (1400°F), showing nearly complete sulfide removal.*

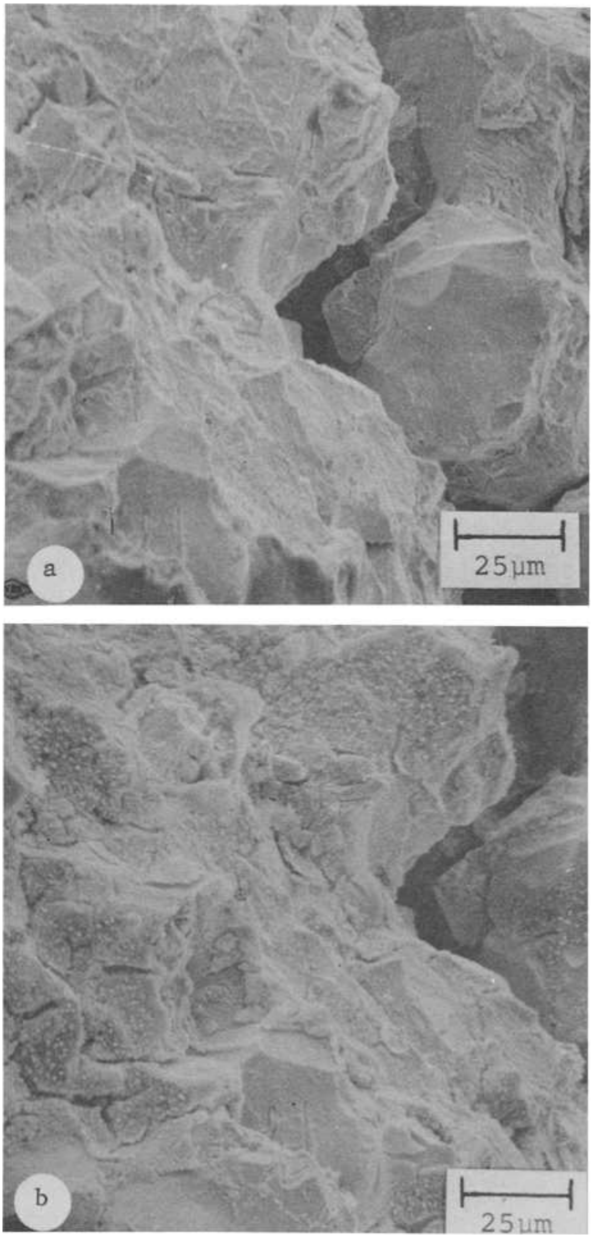

FIG. 7—*Fractographs taken at a crack tip of a DCB branch crack cleaned by hydrogen reduction at 510°C (950°F) showing the ultrasonically cleaned surface* (a) *and the residue* (b) *from hydrogen reduction, that was later removed ultrasonically.*

below the A_1 temperature was more satisfactory than cleaning with any of the three types of aqueous solutions used in this study. These solutions included one containing ammonium citrate and two electrolytic solutions, one acid and one alkaline. With the aqueous solutions, the removal of sulfides was generally slow in comparison with the rate of attack on the fracture surface, with the result that by the time sufficient removal of the sulfides had been accomplished, the attack on the metal was considered to be sufficiently extensive so that characterization of the mode of fracture became questionable or completely unfeasable. On the other hand, the hydrogen-reduction treatments did not attack the steel, and they removed sulfide deposits adequately for studies of the fracture mode. The fracture surfaces of hydrogen-reduced specimens that had been exposed to sulfide environments for extended times did show deterioration, particularly on surfaces that had been exposed for extended times of about four to five days to aqueous sulfide environments. However, this deterioration was believed to have been the result of prior sulfide attack.

Juri Kolts[1]

Hydrogen Induced Delayed Failure of Type 310 Stainless Steel Foils

---

REFERENCE: Kolts, Juri, "**Hydrogen Induced Delayed Failure of Type 310 Stainless Steel Foils,**" *Stress-Corrosion—New Approaches, ASTM STP 610,* American Society for Testing and Materials, 1976, pp. 366–380.

ABSTRACT: Hydrogen has been generally dismissed as playing a significant role in the mechanism of stress corrosion cracking of stable austenitic stainless steels because of the absence of brittle, delayed failures under cathodic charging conditions. In this investigation, 5-μm-thick foils of T310 (25Cr-20Ni) stainless steel have been embrittled with the application of cathodic potentials. Static delayed failures were observed in 1 N sulfuric acid (H_2SO_4) at ambient temperatures. Increased cathodic polarization resulted in decreased times to failure. The presence of 5-ppm arsenic greatly reduced the time to failure at a given applied potential. At a given current density, the time to failure for foils was considerably longer in solutions with pH 6 than in 1 N H_2SO_4.

Scanning electron microscopy of fracture surfaces from cathodically charged specimens demonstrated a severe loss in ductility. The fracture mode following hydrogen charging was planar and was distinctively different from the ductile mode of failure in the absence of hydrogen.

Classical hydrogen embrittlement of high-strength steels may be shown to be a reversible phenomenon by alternate hydrogen charging and degassing for many cycles. This results in a long total charging time with no concomitant permanent damage. In the present experiments, this was demonstrated for the T310 stainless steel by application of the proper potentials. The ductility of hydrogen charged specimens was recovered after baking at 400°F for 4 h.

The hydrogen content of foils was found to exceed 4000-ppm hydrogen after charging in arsenic poisoned acid solutions. Charging times, high-hydrogen content and embrittlement of the stainless steel foils were related.

KEY WORDS: hydrogen embrittlement, stress corrosion, cracking (fracturing), austenitic stainless steels, cleavage, solubility

Hydrogen induced brittle delayed failures have not been observed in austenitic stainless steel, although measurable changes in ductility, elongation, and fracture stresses are well documented [*1–9*].[2] Surface cracking of

---

[1] Senior research corrosion engineer, Research and Technology, Armco Steel Corporation, Middletown, Ohio 45043.

[2] The italic numbers in brackets refer to the list of references appended to this paper.

austenitic stainless steels has been observed by numerous investigators [*10–13*]. The absence of hydrogen induced brittle delayed failures, and the magnitude of the ductility changes in the stable stainless steels have been cited as major objections to warrant serious consideration of a hydrogen-stress corrosion cracking (SCC) model.

The hydrogen induced ductility losses of T304 stainless steel have been the subject of intensive study. This material is susceptible to transformation to α'-martensite. Consequently, many models have incorporated the martensite transformation into effects of hydrogen on SCC. These models cannot explain embrittlement in alloys such at T310 stainless steel where the α'-martensite transformation has not been observed. In addition, extremely high electrolytic cathodic charging currents (0.1 to 0.5 A/cm^2) have been previously utilized to embrittle the stainless steels. These currents are considered excessively high to be related to actual conditions existing inside stress corrosion cracks.

Therefore, in this investigation, thin foils of T310, a stable austenitic stainless steel, were examined at potentials which would be expected inside propagating stress corrosion cracks. The delayed failures and fracture phenomena have been studied in hopes of providing more insight into the effects of hydrogen during SCC.

Hydrogen contents were measured and reversibility experiments were performed to demonstrate that the embrittlement was indeed due to hydrogen and not to other phenomena such as corrosion fatigue, stress assisted corrosion, or intergranular attack.

Procedure

Type 310 stainless steel with the following analysis was employed in this investigation:

C	Mn	Si	P	S	Cr	Ni
0.062	1.40	0.52	0.027	0.010	24.36	19.58

The initial thickness of 50 μm was cold rolled with an ultrathin rolling mill to 13 μm, hydrogen annealed, and again rolled to the final thickness of 5 μm. The steel was then annealed continuously as a strip in dry hydrogen at 1070°C (1950°F) and rapidly cooled in hydrogen. Prior to testing the foils were degreased with 1,1,1-trichloroethane and rinsed with deionized water. Figure 1 shows the microstructure of the final processed steel. The resulting material had an ASTM grain size of approximately 11 in the plane of rolling. All solutions were prepared from reagent grade chemicals and high-purity water. Arsenic additions were made as sodium arsenite.

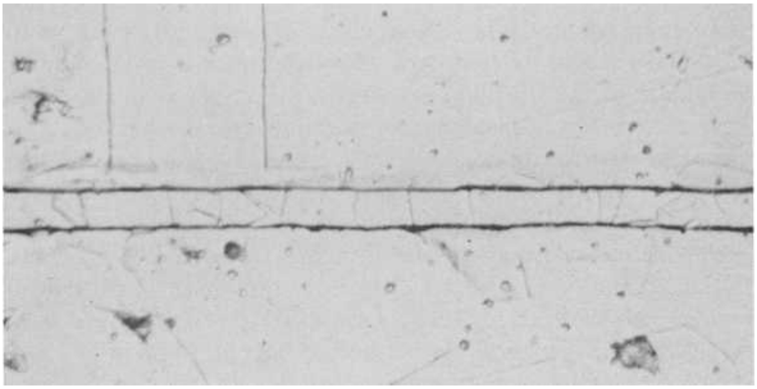

FIG. 1—*Microstructure of 5-μm-thick T310 stainless steel foil, electrolytic oxalic acid etch (×1000).*

The delayed failure testing apparatus is displayed schematically in Fig. 2. Electrical contact to the specimens was made by an epoxy coated stainless steel bolt at the base of the fixture. The specimen had a gage length of 1.9 cm (0.75 in.) and gage width of 1.27 cm (0.5 in.) with a total surface area of approximately 40 cm^2. The load was applied as adjustable weights on a cantilever beam. The potential was controlled with respect to a saturated calomel electrode by a potentiostat, as shown in Fig. 2. No

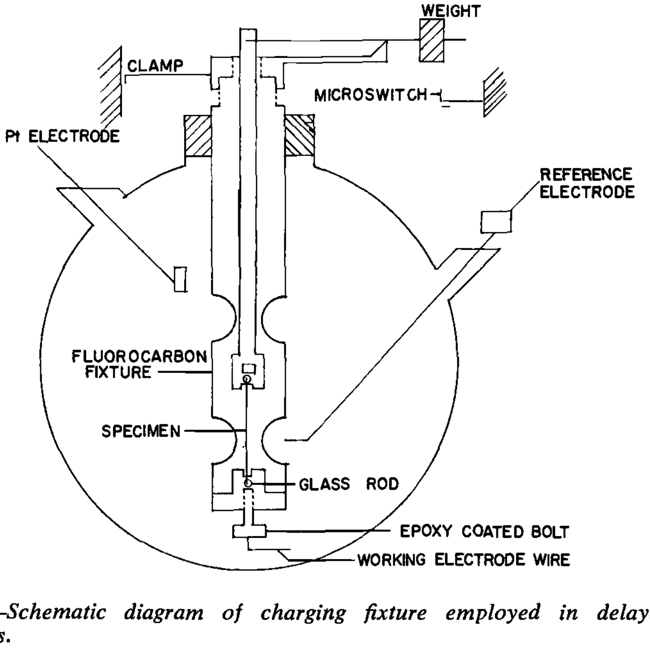

FIG. 2—*Schematic diagram of charging fixture employed in delayed failure experiments.*

corrections were made for polarization resistance or liquid junction potentials. Also, no special efforts to deaerate the solution were made.

Hydrogen charging experiments to correlate hydrogen contents with embrittlement were performed in the following manner: The 5-μm foil specimens were electrolytically charged in 1 N sulfuric acid (H_2SO_4) or 0.5 *M* sodium sulfate (Na_2SO_4), 5-ppm arsenic at 25°C. The specimens were preweighed, degreased, and placed into a specimen holder that would permit quick specimen removal and quenching into liquid nitrogen (N_2). After charging for the specified period of time, the foils were rinsed in 10 percent nitric acid (HNO_3), then in deionized water, and then quenched into liquid N_2 where they were stored until ready for hydrogen analysis. The times between charging and the liquid N_2 quench were of the order of 15 to 30s. Immediately before analysis, the specimens were rinsed in acetone, air dried, and placed into the analysis chamber.

Hydrogen analysis was performed by a Leco hydrogen analyzer. The principle employed in this technique has been described previously [*14*]. Hydrogen is degassed from the specimen in a vacuum at 1200°C. A mercury diffusion pump is used to transport the gases which have evolved from the specimen into a chamber of known volume. With the use of a McLeod gage, pressure measurements are made before and after the gases are recirculated over hot catalytic copper oxide to convert H_2 to water (H_2O) and through a magnesium perchlorate collector to adsorp the water. Hydrogen contents can then be calculated. National Bureau of Standards (NBS) 352 unalloyed titanium calibration standards containing 32-ppm hydrogen were used as checks to assure accuracy.

Results

Delayed Failure Results

In this investigation, hydrogen induced delayed failures of austenitic stainless steels have been produced. Failures occur at potentials and charging current densities which could be expected inside propagating crevices, pits, and stress-corrosion cracks [*15,16*]. Figure 3 displays the times to failure of the T310 foils as a function of applied potential in 1 N H_2SO_4 with and without arsenic additions. Arrows indicate points where no fracture occurred. As in the case for classical hydrogen embrittlement, increasing cathodic polarizations result in decreasing times to failure. No failures were experienced at small anodic polarizations. No failures occurred in the H_2SO_4 at the corrosion potential or when the specimen was stressed in air in the absence of electrolyte. High-anodic polarization resulted in excessive loss of metal by anodic dissolution, as expected, and are not reported here.

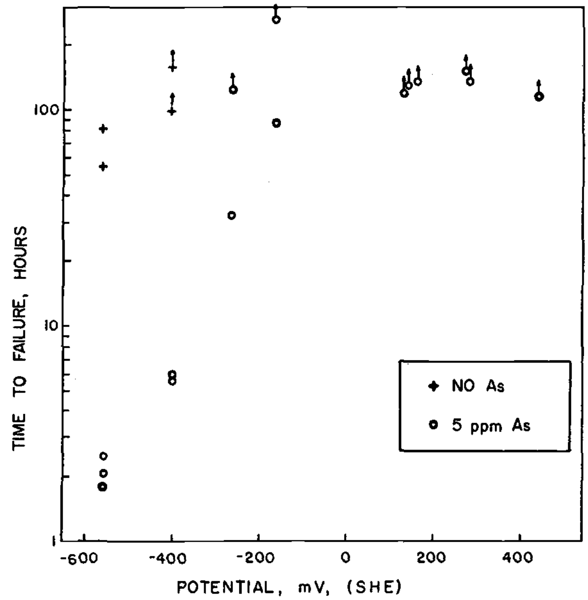

FIG. 3—*Time to failure of 5-μm T310 stainless steel foils as a function of applied potential in 1 N H_2SO_4 at 25°C, initial stress 30 000 psi.*

The addition of only 5-ppm arsenic greatly reduced the time to failure under cathodic charging conditions. Times to failure decreased from greater than 50 h to approximately 2 h with arsenic additions at the lowest charging potential investigated. This is consistent with the known effect of arsenic [*17,18*] as a cathodic poison in promoting hydrogen entry into steel.

The failures at −0.160 and −0.260 V standard hydrogen electrode (SHE) occurred at the crevice between the specimen and specimen holder making the local potential at the fracture site somewhat uncertain. All the other failures occurred in the gage sections. Even if the data at −0.160 and −0.260 SHE are disregarded (since local currents and potentials in the crevice are not known), failures at −0.400 SHE occurred at cathodic current densities of approximately 100 $\mu A/cm^2$. Such low current densities are surely in the range expected for propagating stress-corrosion cracks. Also, the extremely high arsenic concentrations such as 0.1 to 1 percent are not necessary as only 5-ppm arsenic is sufficient to affect the delayed failure behavior.

Figure 4 demonstrates the times to failure for the 1 N H_2SO_4 and the 0.5 *M* Na_2SO_4 (pH of approximately 6). The two failures that did occur in 0.5 *M* Na_2SO_4 were not at the highest charging currents investigated. At the highest charging current (6 mA/cm^2) failures in acid occurred in

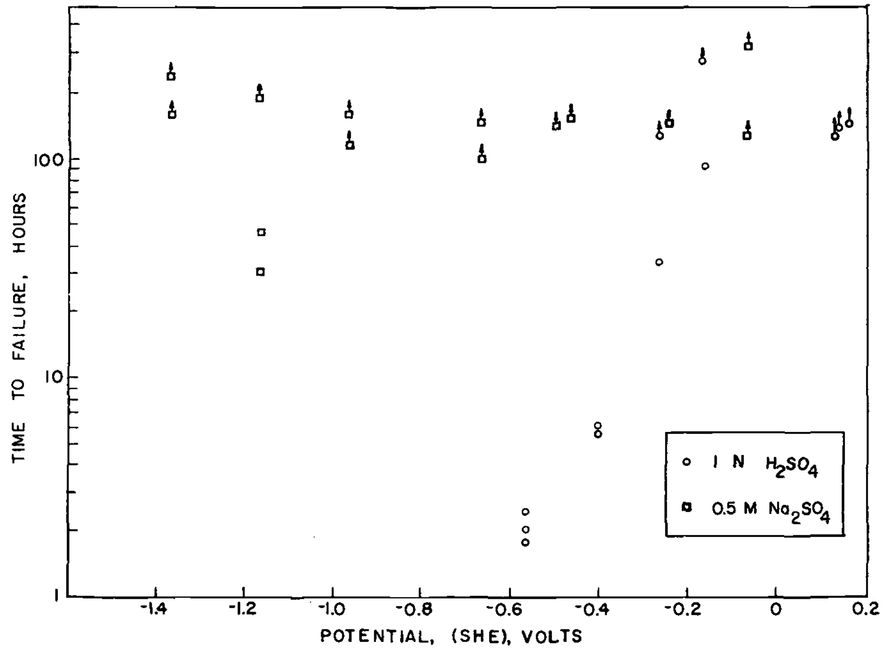

FIG. 4—*Time to failure of 5-μm T310 stainless steel foils as a function of applied potential in solutions with 5-ppm arsenic at 25°C, initial stress 30 000 psi.*

approximately 2 h, whereas no failures were seen in the Na_2SO_4 solutions at times exceeding 170 h.

Cracking and Fracture Morphology

The delayed failures under cathodic charging conditions are extremely brittle and typical of cleavage fractures. While cleavage fractures are common in martensitic steel and titanium alloys, such fracture morphologies in austenitic stainless steels have been observed only in SCC experiments [*19*].

Numerous secondary cracks were observed when charging at 6 mA/cm^2. At the lower cathodic current densities (higher positive potentials) no secondary cracks were observed. Because of the small grain, it is somewhat difficult to determine the fracture path. However, both transgranular and intergranular paths are evident.

Scanning electron photomicrographs of fracture surfaces are shown in Fig. 5. The specimen fractured in air by overstressing in the absence of charging (Fig. 5*a*) shows the typical ductile failure associated with a large reduction in area. The specimens which exhibited delayed failures are extremely brittle showing essentially zero ductility. A cleavage type planar


b
a

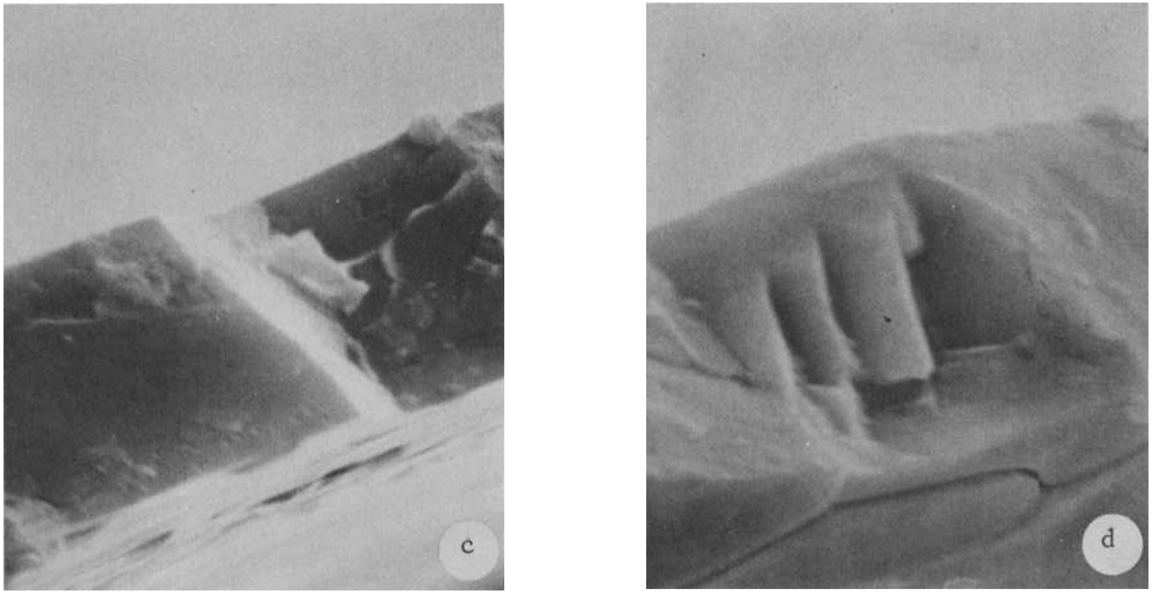

(*a*) Fractured in air.
(*b*) Delayed failure (126 min) after charging in 1 N H_2SO_4, 5-ppm arsenic at −0.560 V SHE (−6 mA/cm^2).
(*c*) Same as *b*.
(*d*) Delayed failure (5.7 h) after charging in 1 N H_2SO_4, 5-ppm arsenic at −0.160 V SHE (−100 μA/cm^2).

FIG. 5—*Scanning electron photomicrographs of fracture surface of T310 stainless steel foils (×5000).*

fracture morphology is observed with regions exhibiting steps possibly delineating crystallographic planes. Previously, changes in fracture mode have been reported in hydrogen affected regions, but such large areas of planar, featureless cleavage fracture surfaces have not been seen.

The above brittle fracture surfaces have been obtained in specimens charged under uniaxial tension. Brittle behavior was also noticed when specimens were charged in 1 N H_2SO_4 in the absence of intentionally applied stresses and then deformed. Figure 6 represents a fracture surface of a specimen that was charged and then fractured in air by crumbling the foil. In this case the stresses were not expected to be uniaxial. This fracture surface resembles a quasi-cleavage type of fracture with features no longer as flat and planar as in specimens charged under uniaxial tension.

In summary, analysis of the fracture surfaces has shown that the failure under cathodic charging conditions was indeed brittle with little or no associated ductility, and the failure mode closely resembles cleavage fractures.

Reversibility Experiments

The reversibility of hydrogen embrittlement in high-strength steels is a well-documented phenomenon [*20*]. Reversibility experiments were per-

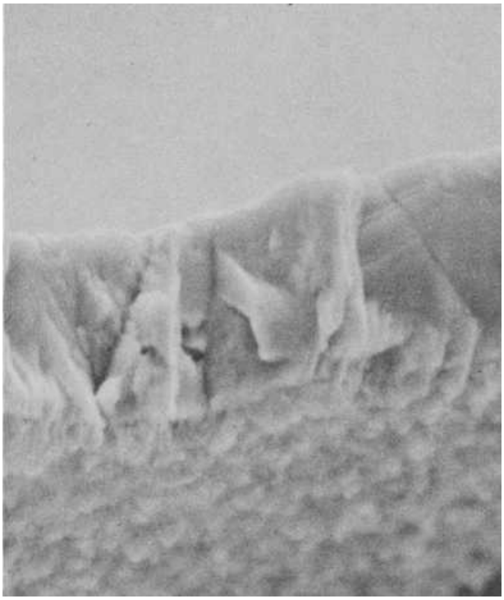

FIG. 6—*Scanning electron photomicrograph of fracture surface of T310 stainless steel cathodically charged in 1 N H_2SO_4, 5-ppm arsenic, rinsed, dried, and fractured in air (×2000).*

formed on the T310 foils to demonstrate that the steel was indeed embrittled by hydrogen in a manner typical of the high-strength steels. The films were stressed to 30 000 psi and charged galvanostatically in arsenic poisoned in 1 N H_2SO_4. The current was alternated every 10 min between -6.25 and $+0.02$ mA/cm^2. The cathodic current corresponds to the range of potentials where delayed failure occurred in approximately 2 h. It was expected that the anodic cycle would permit degassing of the specimen and thus prolong the time to failure. This was indeed the case as the time to failure was extended beyond 6.7 h of cathodic charging time. A similar experiment with 5 min charging at -6.25 mA/cm^2 and 10 min at $+0.20$ mA/cm^2 extended the failure to 12.8 h of cathodic charging time.

It might be argued that the delayed failures during cathodic charging resulted from fatigue by evolving gas bubbles, by active path dissolution, or perhaps by stress assisted corrosion. All of the foregoing would result in damage while in solution. The above could not occur after removal of the electrolyte, while embrittlement by hydrogen would occur after electrolyte removal. Finally damage by the above three mechanisms would be permanent and not recoverable by annealing at low temperatures.

To show that hydrogen was indeed the cause of embrittlement, specimens were charged without applied stresses for 4 h in arsenic poisoned 1 N H_2SO_4. Specimens were then rinsed in 10 percent HNO_3, deionized water, and acetone, and air dried. The specimens were still extremely brittle and could be easily broken simply by crumbling (see Fig. 7). Brittle fractures occurred in the absence of an electrolyte after charging. Scanning electron microscopy (SEM) confirmed the fractures to be brittle with little or no associated ductility. After aging (degassing) similarly charged specimens in air at 400°F for 4 h, the specimens were no longer brittle and could be easily handled without crumbling.

Hydrogen Contents of Charged Specimens

Since the embrittlement of thick specimens of austenitic stainless steels is limited to thin-surface layers as evidenced by only surface cracking, these surface layers may be expected to contain higher hydrogen contents than the bulk. Consequently, a hydrogen analysis of the ultrathin T310 stainless foils would be representative of the outer layers in bulk charged specimens.

Hydrogen contents (Table 1) exceeding 4000 ppm or approximately 20 atomic percent were found in specimens charged at 6 mA/cm^2 in 1 N H_2SO_4 for times of 2 h or greater. These measured hydrogen contents are far in excess of any reported for austenitic stainless steels [*21,22*]. These data demonstrate that only a small surface layer is affected by hydrogen in charging experiments with thick specimens.

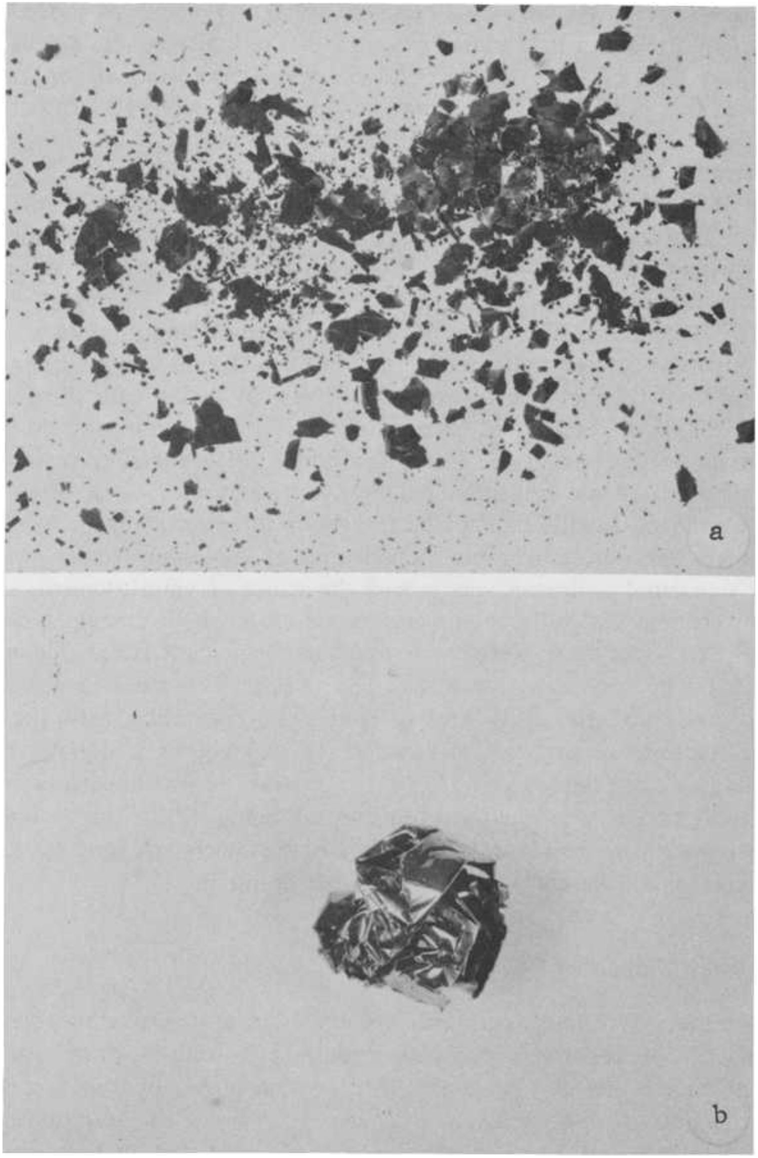

(*a*) Immediately after charging.
(*b*) After annealing 4 h at 205°C (400°F).

FIG. 7—*T310 stainless steel cathodically charged in 1 N H_2SO_4, 5-ppm arsenic in absence of stress, rinsed, dried, and crumbled between fingers (×3).*

TABLE 1—*Hydrogen content of 5 μm, T310 foils after charging in solutions with 5-ppm arsenic, 25°C, 6 mA/cm^2.*

		1 N H_2SO_4		0.5 *M* Na_2SO_4	
Charging Time, h		ppm H	Brittle	ppm H	Brittle
Vacuum annealed 1950, 15 min	0	13	no	...	...
As processed	0	39	no	...	...
	0.5	2190	no	610	no
	1	2880	no	840	no
	2	4880	yes	960	no
	4	4050	yes	1050	no

Some uncertainty might exist whether the extremely high hydrogen contents were associated with surface occluded hydrogen such as hydrides of arsenic rather than absorbed hydrogen. It is unlikely that the hydrogen was present as adsorbed hydrogen on the surface because increasing charging times resulted in increases in hydrogen contents, and the time to reach saturation of adsorbed hydrogen would certainly be expected to occur in a much shorter time than 2 h. To determine whether the hydrogen was associated with arsenic surface contaminants, X-ray fluorescent analyses of the charged specimens were made. No arsenic peaks were observed indicating that the hydrogen was not associated with surface hydrides of arsenic.

Table 1 demonstrates that charging from acid solutions results in substantially higher hydrogen contents than charging from neutral solutions. Correspondingly, the steel was not brittle following charging in the Na_2SO_4 solutions. Specimens were considered brittle if they would fracture into bits when crumbled between the fingers.

It appears that the high-hydrogen contents of approximately 4000 ppm are necessary for the through embrittlement of the stainless steels. A charging time of 2 h corresponds to that required to produce embrittlement as evidenced by the ease of crumbling in these charging experiments (Table 1). In the delayed failure experiments, charging currents in arsenic poisoned H_2SO_4 of 6 mA/cm^2 corresponds to failure times of approximately 2 h.

Discussion

This investigation presents new phenomena which may have a strong bearing on present mechanisms of SCC in austenitic stainless steels. Delayed failures under cathodic charging conditions have been observed, strong evidence of cleavage fractures has been seen, reversible hydrogen damage has been noted, and extremely high-hydrogen contents of 4000 ppm have been related to the brittle behavior of T310 stainless steel.

Attempts to date have been made to relate the influence of hydrogen during SCC to the formation and embrittlement of martensite [*23,24*]. Although this may occur in less stable steels such as T304, T310 does not undergo such a transition. The results from the current investigation indicate that α'-martensite formation is not necessary in order for hydrogen to play a role in a SCC model of austenitic steels. However, this is not to infer that second phase formation plays no role in the embrittlement of T310 stainless steel. The hexagonal phase as described by numerous investigators [*11,25,26*] is certainly known to occur upon cathodic charging austenitic stainless steel, including T310, and may play a significant role in the embrittlement phenomenon.

The cathodic current densities previously employed to demonstrate the effect of hydrogen on mechanical properties have been considered excessively high to be encountered in propagating cracks. This investigation has shown that hydrogen embrittlement occurs at very low cathodic currents (100 $\mu A/cm^2$) which could be expected in the cracks.

Any model which incorporates hydrogen as playing a significant role in the SCC of stainless steel must explain why thick specimens do not exhibit delayed failures upon cathodic charging and why SCC rates increase with anodic polarizations. During cathodic charging, hydrogen enters uniformly into the steel over the entire surface. Delayed failures in bulk specimens would then occur by cathodic charging only if the entire specimen is embrittled. Due to the slow diffusion of hydrogen in austenitic stainless steels, complete embrittlement in thick specimens is unlikely.

If a crack or fissure should occur on the surface during cathodic charging, hydrogen is less likely to enter at the crack tip. Certainly in the absence of cathodic charging, the feasibility of hydrogen entry during stress corrosion in the vicinity of a propagating stress-corrosion crack has been demonstrated [*15,23*]. However, when the surface is polarized cathodically, experimental evidence [*27–30*] has shown that the pH in a crack or crevice will increase to high values, even from bulk acid electrolytes. Increased pH has been shown in this investigation to reduce the influx of hydrogen into steel and thus reduce the embrittlement of the steel. Possibly the surface films formed at higher pH values may be sufficiently impermeable to hydrogen to retard hydrogen entry as shown by Piggott and Jiarkowski [*31*].

If SCC cracking occurs by a hydrogen embrittlement mechanism, then the hydrogen must enter in the vicinity of the crack tip. From the pH dependence of hydrogen entry and embrittlement and from knowledge of pH and potential conditions inside cracks with externally applied anodic currents, hydrogen is more likely to enter in the vicinity of the crack tip during external anodic polarizations. According to the foregoing hypothesis, the effect of external cathodic polarizations on the retardation of SCC is consistent with a hydrogen-SCC mechanism.

Certainly, corrosion is necessary in a propagating stress corrosion crack to maintain the anolyte composition and potential conditions conducive to hydrogen entry. Transitions from pitting corrosion to SCC are known to occur in stainless steels. Since anolyte compositions and potentials inside pits and stress corrosion cracks are similar, it is difficult to explain such transitions. Perhaps further investigations of the effects of hydrogen and of the conditions under which hydrogen entry occurs could further elucidate this phenomenon.

Conclusions

1. Type 310 stainless steel was embrittled by hydrogen during cathodic charging in 1 N H_2SO_4 at ambient temperatures. Delayed failures under static load occurred; increasing cathodic polarizations resulted in decreased time to failure.
2. The fracture surfaces of cathodically charged specimens exhibiting delayed failure were planar, cleavage type failures, and exhibited essentially zero ductility.
3. The saturation hydrogen content of brittle T310 has been measured to be ~4000-ppm hydrogen. Embrittlement and high-hydrogen content were related.
4. Additions of 5-ppm arsenic to 1 N H_2SO_4 greatly reduced the time to failure of cathodically charged thin foils of T310 stainless steel.
5. Embrittlement of charged specimens occurred after specimens were removed from the electrolyte. Degassing the hydrogen charged, brittle specimens reduced the embrittlement.

Acknowledgments

I wish to acknowledge R. L. Swigert and C. A. VanScoy for performing the hydrogen analysis, D. Lentz for work on the scanning electron microscope, and J. A. Peterson and D. M. Smith for their valuable contributions through numerous discussions throughout the course of this work.

References

[*1*] Whiteman, M. B. and Troiano, A. R., *Corrosion*, Vol. 21, 1965, p. 53.
[*2*] Thompson, A. W. in *Hydrogen in Metals*, I. M. Bernstein and A. W. Thompson, Eds., American Society for Metals, 1974, p. 91.
[*3*] Vennett, R. M. and Ansell, G. S., *Transactions*, American Society for Metals, Vol. 62, 1969, p. 1007.
[*4*] Vennett, R. M. and Ansell, G. S., *Transactions*, American Society for Metals, Vol. 60, 1967, p. 242.
[*5*] Walter, R. J., Jewett, R. P., and Chandler, W. T., *Materials Science and Engineering*, Vol. 5, 1969/1970, p. 98.

[6] Louthan, R., Jr., Caskey, G. R., Jr., Donovan, J. A., and Rawl, D. E., Jr., *Materials Science Engineering*, Vol. 10, 1972, p. 357.
[7] Benson, R. Jr., Dann, R. K., and Roberts, L. W., Jr., *Transactions*, American Institute of Mining, Metallurgical, and Petroleum Engineers, Vol. 242, 1968, p. 2199.
[8] Louthan, M. R., Jr., Donovan, J. A., and Rawl, D. E., *Corrosion*, Vol. 29, 1973, p. 108.
[9] Louthan, M. R., Jr., in *Hydrogen in Metals*, I. M. Bernstein and A. W. Thompson, Eds., American Society for Metals, 1974, p. 53.
[10] Maulik, P. and Burke, J., *Scripta Metallurgica*, Vol. 9, 1975, p. 17.
[11] Okada, H., Hosai, Y., and Abe, S., *Corrosion*, Vol. 26, 1970, p. 183.
[12] Holzworth, M. L., *Corrosion*, Vol. 25, 1969, p. 107.
[13] Lagneborg, R., *Journal of the Iron and Steel Institute*, Vol. 207, 1969, p. 363.
[14] McLellan, R. B. and Oates, W. A., *Acta Metallurgica*, Vol. 21, 1973, p. 181.
[15] Smith, J. A., Peterson, M. H., and Brown, B. F., *Corrosion*, Vol. 26, 1970, p. 539.
[16] Pickering, H. W. and Frankenthal, P. R., *Localized Corrosion*, National Association of Corrosion Engineers, Houston, Tex., 1971, p. 261.
[17] Newman, J. F. and Shreir, L. L., *Corrosion Science*, Vol. 9, 1969, p. 631.
[18] McCright, R. D. and Staehel, R. W., *Journal of the Electrochemical Society*, Vol. 121, 1974, p. 609.
[19] Scully, J. C. in *The Theory of Stress Corrosion Cracking in Alloys*, NATO, Brussels, 1971, p. 125.
[20] Elsen, A. R. and Fletcher, E. A., DMIC Report No. 196, Defense Metals Information Center, Battelle Memorial Institute, Columbus, Ohio, 20 Jan. 1964.
[21] Shively, J. H., Hehemann, R. F., and Troiano, A. R., *Corrosion*, Vol. 22, 1966, p. 253.
[22] Powell, G. W., Braun, J. D., Chaney, K. F., and Downs, G. L., *Corrosion*, Vol. 26, 1970, p. 223.
[23] Rhodes, P. R., *Corrosion*, Vol. 25, 1969, p. 462.
[24] Birley, S. S. and Tromans, D., *Corrosion*, Vol. 27, 1971, p. 63.
[25] Vaughan, D. A., Phalen, D. I., Peterson, C. L., and Boyd, W. K., *Corrosion*, Vol. 19, 1963, p. 315t.
[26] Vaughan, D. A. and Phalen, D. I., *Metallurgical Engineering Quarterly*, American Society for Metals, Vol. 5, No. 4, 1965, p. 39.
[27] Pourbaix, M., *Localized Corrosion*, National Association of Corrosion Engineers, Houston, Tex., 1971, p. 12.
[28] Lennox, T. L., Jr., and Peterson, M. H., *Localized Corrosion*, National Association of Corrosion Engineers, Houston, Tex., 1971, p. 173.
[29] Peterson, M. H., Lennox, T. S., Jr., and Groover, R. E., *Materials Protection*, Vol. 9, No. 1, 1970, p. 23.
[30] Davis, J. A., *Localized Corrosion*, National Association of Corrosion Engineers, Houston, Tex., 1971, p. 168.
[31] Piggott, M. R. and Jiarkowski, A. C., *Journal of the Iron and Steel Institute*, Vol. 210, No. 12, 1972, p. 901.

F. H. Beck,[1] *J. Juppenlatz,*[2] *and P. F. Wieser*[3]

Effects of Ferrite and Sensitization on Intergranular and Stress-Corrosion Behavior of Cast Stainless Steels

REFERENCE: Beck, F. H., Juppenlatz, J., and Wieser, P. F., "**Effects of Ferrite and Sensitization on Intergranular and Stress-Corrosion Behavior of Cast Stainless Steels,**" *Stress Corrosion—New Approaches, ASTM STP 610,* American Society for Testing and Materials, 1976, pp. 381–398.

ABSTRACT: Cast stainless steels of the CF grades (19Cr, 9Ni), which find widespread application in the chemical, petrochemical, and power generating industry, were subjected to intergranular corrosion tests (Huey) and stress-corrosion tests (vapor phase of aqueous 875-ppm sodium chloride (NaCl) solution at 477 K [400°F]) to evaluate the effect of ferrite in the range of 0 to 40 ferrite numbers, in the solution-annealed and in the sensitized condition.

The intergranular corrosion tests demonstrated beneficial effects of ferrite for all the alloys tested in the solution-annealed condition and for the molybdenum-free cast steel grades in the sensitized condition. Ferrite increased the sensitization effects on intergranular corrosion for the molybdenum-bearing grades. Highest corrosion rates in Huey tests, based upon weight loss measurements, do not necessarily mean deepest intergranular attack. Intergranular attack was found to terminate at ferrite-austenite grain boundaries. The intergranular corrosion test results would indicate that ferrite numbers exceeding 10 offer greater operating safety for cast, corrosion resistant grades, CF-3, CF-3M, CF-8, and CF-8M in the solution-annealed condition and also, in the event of sensitization, for cast corrosion-resistant grades CF-3 and CF-8.

Significantly increased resistance to stress-corrosion cracking with increasing ferrite content was observed for cast steels in the solution-annealed and in the sensitized condition. These stress-corrosion cracking tests would indicate that ferrite numbers of 10 or more offer greater operating safety for cast corrosion-resistant CF grades in the solution-annealed as well as in the sensitized condition.

KEY WORDS: stress corrosion, cracking (fracturing), castings, stainless steels, corrosion tests, ferrite, sensitizing

---

[1] Professor, Department of Metallurgical Engineering, Ohio State University, Columbus, Ohio 43210.

[2] Chief metallurgist, Quaker Alloy Casting Company, Myerstown, Pa. 17067.

[3] Research director, Steel Founders' Society of America, Rocky River, Ohio 44116.

Cast corrosion-resistant steel grades may be grouped by their metallurgical structure. Thus, there are fully austenitic grades such as Type CN-7M (20Cr, 29Ni), martensitic grades such as CA-15 and CA-6NM (13Cr and 13Cr, 4Ni, respectively) and grades with a duplex austenitic-ferritic structure. There are two principal alloy types among the steels with duplex structures. One of these is Type CD-4MCu (26Cr, 5Ni), which can be hardened by aging. The other type is represented by the widely used CF Grades (19Cr, 9Ni). CF-3 type steels contain typically 10 to 20 percent ferrite, while CF-8 types usually have about 10 percent ferrite. The amount of ferrite varies with composition [*1,2*].[4] Higher tensile strength properties are promoted by ferrite [*1*]. Controlled ferrite grades CF-3A and CF-8A, with superior strength properties, therefore, are recognized by the American Society for Testing and Materials (ASTM).

The duplex austenite-ferrite structure of these solution-annealed CF-type (19Cr, 9Ni) cast stainless steels promotes superior corrosion resistance through anodic polarization of the ferrite phase [*3*] in boiling acetic acid ($C_2H_4O_2$) (99.7 and 75 percent), in boiling phosphoric acid (H_3PO_4) (88 and 40 percent), and in 15 percent sulfuric acid (H_2SO_4) at ambient temperatures. Ferrite has also been shown [*3*] to be beneficial by enhancing the resistance of solution-annealed CF-type stainless castings to intergranular corrosion, and of CF- and CE-type (28Cr, 9Ni) stainless steel castings to stress-corrosion resistance.

Ferrite-bearing stainless cast steel grades are of vital importance in the chemical and electric power industries because of the improved combination of strength and corrosion resistance offered by duplex-austenite-ferrite structures. Failure of cast stainless steel components due to intergranular or stress corrosion is rare. Intergranular corrosion, however, may occur in nitric acid (HNO_3) environments when stainless steel is sensitized. Sensitization may result from fabrication or repair welding, hard facing, or improper heat treatment.

There is little, if any, published information on the stress-corrosion susceptibility of stainless steel castings upon sensitization, or on the effects of ferrite in the sensitized condition. The lack of this information and the concern over sensitization effects on operation and safety of power generating equipment [*4*] has led to the study reported here.

Materials

Twenty-three different cast alloy compositions were used in this investigation. These alloys and their compositions are presented in three major groups in Table 1. The first group contains static castings of alloy Types CF-3, CF-8, CF-3M, and CF-8M of three ferrite levels. Each alloy is

---

[4] The italic numbers in brackets refer to the list of references appended to this paper.

identified by alloy type, letter, or number or all three. The letters are simply a code system, and the numbers refer to the ferrite content in terms of ferrite numbers [2,5]. These ferrite numbers correspond closely to the actual ferrite contents (volume percent) of the cast steels. The wide range in ferrite contents, for instance, ferrite numbers 0 to 37 for CF-3 in Group I, was prepared deliberately and occasionally resulted in slight compositional deviations from ASTM standards. For example, CF-3 alloy A, with a ferrite number of 0, contained 16.97 percent chromium and 13.35 percent nickel as compared to an ASTM minimum chromium level of 17 percent and an ASTM maximum nickel level of 12 percent. All alloys in the first group were supplied as standard Alloy Casting Institute (ACI) keel bars in the solution-annealed condition.

The second group of alloys are static and centrifugal castings from four heats, that is, high-nitrogen CF-8, CF-3M, CF-20, and CF-8C. The coding system for these alloys contains both a number and the letters S or C which refer to the statically or centrifugally cast specimens, respectively, from each heat. The letters (HN) identify the high-nitrogen heats, and the last set of numbers gives the ferrite number. Static portions of each heat were cast into standard ACI keel bar molds of silica molding sand. Centrifugally cast portions were cast into pipes 56.5 cm (22.3 in.) long by 25.4 cm (10 in.) outside diameter with a wall thickness of 2.22 cm (0.88 in.). All test material was supplied in the solution-annealed condition.

The third group of alloys, wrought materials, were supplied in annealed sheet or plate.

Specimen Preparation and Testing

All of the materials except for the high-nitrogen CF-8 heat which was solution-treated for 2 h at 1366 K (2000°F) were solution heat treated for 2 h at 1394 K (2050°F) and water quenched. All of the sensitizing heat treatments were for 1 h at 922°K (1200°F) followed by water quenching. Subsequent to heat treating the specimens were polished on wet No. 120 grit abrasive cloth, degreased in acetone, and placed in test.

The susceptibility to intergranular attack associated with chromium carbide (Cr_xC_y) and sigma-phase was evaluated in Huey tests (ASTM Recommended Practices for Detecting Susceptibility to Intergranular Attack in Stainless Steel (A 262-64T, Practice C)). These tests consisted of exposing 2.5 by 2.5 by 0.64-cm specimens (1 by 1 by 0.25-in.) to boiling 65 weight percent aqueous HNO_3 for five consecutive 48-h periods. Weight loss was measured after each period and converted to corrosion rates in mils per year (mpy) or millimeters per year (mmpy). Experience indicates that alloys are prone to intergranular corrosion if the corrosion rate increases rapidly or exceeds 0.43 mmpy (18 mpy) for wrought alloys or 0.76 mmpy (30 mpy) for cast alloys.

TABLE 1—*Chemical analysis of test materials.*

Alloy			Percent Composition										
Type	OSU Code	Ferrite, volume %	C	Mn	Si	Cr	Ni	Mo	N	Cu	S	P	Cb
GROUP I. STATIC CASTINGS													
CF3	A	0	0.02	0.78	1.20	16.97	13.35	...	0.030	...	...	...	...
CF3	K	20	0.023	0.84	1.21	20.36	8.25	...	0.013	...	...	...	...
CF3	C	37	0.02	0.83	1.50	21.81	7.68	...	0.056	...	...	...	...
CF8	D	0	0.08	0.74	1.22	18.08	12.20	...	0.050	...	...	...	...
CF8	E	5	0.07	0.84	1.25	19.99	9.38	...	0.062	...	...	...	...
CF8	F	16	0.08	0.78	1.28	21.37	8.08	...	0.077	...	...	...	...
CF3M	L	0	0.026	1.28	0.90	17.16	13.46	2.48	...	...	...	...	...
CF3M	M	20	0.026	0.91	1.43	20.31	10.86	2.59	...	...	...	...	...
CF3M	N	39	0.021	0.77	1.14	21.59	9.50	2.78	...	...	...	...	...
CF8M	G	0	0.08	0.85	1.12	16.72	15.02	2.51	0.042	...	...	...	...
CF8M	J	15	0.07	0.79	1.39	20.17	9.55	2.40	0.064	...	...	...	...
CF8M	O	38	0.05	0.82	0.27	21.87	9.64	2.65	0.035	...	...	...	...

GROUP II. STATIC AND CENTRIFUGAL CASTINGS

CF8	4S[a](HN)[b]	11	0.067	0.78	1.05	20.57	8.52	...	0.086	...	0.014	0.019	...
CF8	4C(HN)	9											
CF3M	6S(HN)	9	0.03	0.87	0.62	19.55	10.74	2.35	0.13	...	0.028	0.024	...
CF3M	6C(HN)	10											
CF20	8S	12	0.15	0.65	1.64	21.67	8.15	...	0.025	...	0.022	0.018	...
CF30	8C	11											
CF8C	12S	12	0.069	1.04	1.08	19.31	8.80	...	0.037	...	0.012	0.020	0.479
CF8C	12C	7											

GROUP III. WROUGHT MATERIALS

304[c]			0.066	1.05	0.63	18.44	8.47	0.19	...	0.15	0.015	0.016	...
304[d]			0.07	1.29	0.37	18.88	9.14	0.97	...	0.08	0.012	0.024	...
304L[e]			0.022	1.06	0.48	18.13	9.29	...	...	...	0.014	0.021	...
316[c]			0.056	1.80	0.35	18.20	12.71	2.31	...	0.19	0.010	0.018	...
316[d]			0.07	1.58	0.50	18.36	13.22	2.40	...	0.04	0.008	0.025	...
316L[c]			0.023	1.70	0.37	17.30	13.84	2.44	...	...	0.013	0.021	...
316L[d]			0.022	1.22	0.41	17.25	13.28	2.50	...	0.08	0.015	0.012	...

NOTE—OSU = Ohio State University.

[a] S = static portion of split heat.
C = centrifugal portion of split heat.

[b] HN = high nitrogen.

[c] Stress corrosion specimens.

[d] Huey specimens.

[e] Stress corrosion and Huey specimens.

The susceptibility to stress corrosion cracking (SCC) was evaluated by the stress required to produce cracking in specimens exposed for 8 h to the vapor phase over an 875-ppm sodium chloride (NaCl) solution (aqueous) at 477 K (400°F). This test was selected because it correlates well with actual service problems; it was developed originally to evaluate materials for condenser tube applications and represents a severe, accelerated test. The stress-corrosion specimens were stressed in bending by three-point loading. The specimens measured approximately 3.3 cm (1.3 in.) long by 1 cm (0.4 in.) wide by 0.25 cm (0.1 in.) thick. One of the large faces of these specimens (face to be placed in tension during test) was polished on No. 500 grit abrasive cloth to facilitate examination for stress-corrosion cracks upon completion of the tests.

All of the specimens subjected to the boiling HNO_3 test (Huey) were sectioned subsequent to testing. The cross sections were polished metallographically and etched to reveal the nature and the extent of corrosion. Photomicrographs of the cross sections were made on all specimens at a magnification of ×100. The as-corroded surfaces of selected specimens were also examined under the scanning electron microscope (SEM), and scanning electron micrographs of typical structures were recorded at a magnification of ×100.

Etching reagents for the ordinary metallography varied with the alloys being examined. Those compositions containing ferrite in the microstructures were etched in Villela's reagent (10-ml hydrochloric acid (HCl), 100-ml methyl alcohol (CH_4O) 1-g picric acid ($C_6H_3N_3O_7$) immersion); the fully austenitic cast alloys were etched in either Villela's or Marble's (4-g cupric sulfate ($CuSO_4$), 20-ml HCl, 20-ml water (H_2O) immersion) reagents, while the wrought alloys were etched in chromic acid (H_2CrO_4) solution (10-g H_2CrO_4, 100-ml H_2O electrolytic).

Results and Discussion

Huey Test

Corrosion rate data determined from measured weight loss indicate reduced sensitivity to intergranular corrosion with increasing ferrite content in the solution-annealed condition (Table 2, Group I). CF-8M type steel (alloys G, J, and O) for example, exhibited a weight loss of 0.63 mmpy (25 mpy) at a ferrite number of 0, 0.41 mmpy (16 mpy) at a ferrite number of 15, and 0.33 mmpy (14 mpy) at a ferrite number of 38. The maximum depth of intergranular attack (measured on polished cross sections of tested Huey specimens) was comparable for the different ferrite levels of solution-annealed Group I steels (Table 2).

After being sensitized, the alloys exhibited higher corrosion rates than the solution-annealed specimens. Sensitization effects were minimized by lower carbon contents in cast molybdenum-free CF alloys and in wrought Types 316 and 304 steels. The corrosion rate of CF-20, for example, with 0.15 percent carbon, increased by 2.4 and 9 mmpy due to sensitization; for CF-8, with 0.08 percent carbon, the increase was 0.13 to 0.83 mmpy, and for CF-3, with 0.02 percent carbon, the increase was only 0.10 to 0.21 mmpy. Carbon had similar effects in wrought steels Types 304 and 316. The opposite effects of carbon, however, were noted for cast molybdenum-bearing grades.

The data on maximum depth of intergranular attack of tested Huey specimens reveal some discrepancies with weight loss measurements in the sensitized condition. For example, CF-8 cast steel (Table 2, Specimens D-0, E-5, and F-16) exhibited a weight loss in the sensitized condition corresponding to 0.46, 0.73, and 1.1 mmpy (18, 29, and 42 mpy) at ferrite numbers of 0, 5, and 16, respectively. The maximum depth of intergranular attack, however, decreased with ferrite from 0.33 mm (13 mils) at a ferrite number of 0, to 0.18 mm (7 mils) at a ferrite number of 5, and to 0.20 mm (8 mils) at a ferrite number of 16. Another example of this difference concerns the sensitized CF-3 (Table 1, specimens A-0, K-20, and C-37). The maximum depth of intergranular attack of sensitized CF-3 steels also decreases with ferrite (from 0.051 mm or 2 mils at a ferrite number of 37 to 0.28 mm or 11 mils at a ferrite number of 0). Comparable corrosion rates, however, were observed based upon weight loss measurements.

The effect of ferrite appears to be that of introducing additional grain boundaries. Photomicrographs in Fig. 1 illustrate this behavior for CF-8 steel. Intergranular attack appears to be arrested at the austenite/ferrite grain boundaries. Scanning electron micrographs further show the selective attack that eventually leads to loss of entire grains (Fig. 2). This loss of grains, resulting in the conventionally measured weight loss, is further observed in the granular appearance of the surface of sensitized Types 316 and 316L after completion of the Huey test (Fig. 3).

The overall effects of ferrite on intergranular corrosion of solution-annealed and sensitized cast steels are illustrated in Fig. 4 in terms of the maximum depth of intergranular attack observed on tested Huey specimens. Ferrite enhances the resistance to intergranular attack of solution-annealed molybdenum-bearing as well as molybdenum-free alloys (CF-3, CF-8, CF-3M, CF-8M). Sensitized molybdenum-bearing steels (CF-3M, CF-8M) and the higher carbon steels (CF-20) exhibit increased intergranular attack with higher ferrite levels.

Cast steel components are not employed in the sensitized condition when properly heat treated or weld fabricated. Sensitization results in higher

TABLE 2—*Huey test penetration data (weight loss and measured).*

Alloy			Rates from Weight Loss Data				Penetration Measured at End of Test			
			Solution Annealed		Sensitized		Solution Annealed		Sensitized	
Type	OSU Code	Ferrite, volume %	mmpy	mpy	mmpy	mpy	mm	mils	mm	mils
					GROUP I. STATIC CASTINGS					
CF3	A	0	0.33	13	0.43	17	0.051	2	0.28	11
CF3	K	20	0.25	10	0.46	18	0.025	1	0.076	3
CF3	C	37	0.23	9	0.41	16	0.025	1	0.051	2
CF8	D	0	0.33	13	0.46	18	0.025	1	0.330	13
CF8	E	5	0.28	11	0.73	29	0.025	1	0.180	7
CF8	F	16	0.28	11	1.1	42	0.051	2	0.200	8
CF3M	L	0	0.38	15	0.38	15	0.076	3	0.051	2
CF3M	M	20	0.41	16	7.3	290	0.025	1	0.610	24
CF3M	N	39	0.30	12	16.0	640	0.025	1	0.330	13
CF8M	G	0	0.63	25	0.61	24	0.025	1	0.025	1
CF8M	J	15	0.41	16	3.6	140	0.051	2	0.53	21
CF8M	O	38	0.33	14	7.6	300	0.051	2	0.43	17

				GROUP II. STATIC AND CENTRIFUGAL CASTINGS						
CF8	4S(HN)	11	0.25	10	0.58	23	0.051	2	0.13	5
CF8	4C(HN)	9	0.30	12	0.96	38	0.051	2	0.18	7
CF3M	6S(HN)	9	0.18	7	12.0	480	0.051	2	1.1	44
CF3M	6C(HN)	10	0.18	7	15.0	600	0.10	4	1.0	40
CF20	8S	12	2.4	95	4.8	190	0.63	25	0.53	21
CF20	8C	11	2.0	77	11.0	420	0.38	15	1.1	44
CF8C	12S	12	0.30	12	0.61	24	0.076	3	0.051	2
CF8C	12C	7	0.18	7	0.41	16	0.076	3	0.13	5
				GROUP III. WROUGHT MATERIALS						
304			0.15	6	0.81	32	0.20	8	0.28	11
304L			0.15	6	0.15	6	0.051	2	0.051	2
316			0.20	8	4.8	190	0.025	1	0.38	15
316L			0.18	7	0.35	14	0.10	4	0.25	10

NOTE—OSU = Ohio State University.
mils = 0.001 inch.
mpy = mils per year.
mm = millimetre.
mmpy = millimetres per year.

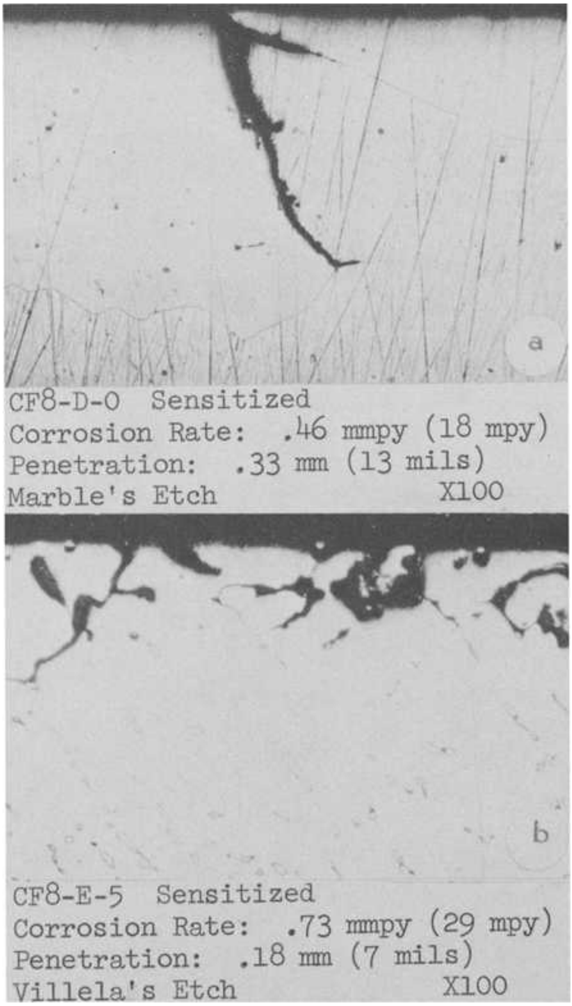

FIG. 1—*Cross sections of sensitized CF-8 specimens showing nature and extent of attack in Huey test.*

intergranular attack. However, these effects are minimized by ferrite in molybdenum-free cast grades CF-3 and CF-8.

Stress Corrosion

The resistance to SCC of cast stainless steels in NaCl vapor increased with the ferrite content in the solution-annealed and in the sensitized condition (Fig. 5, data of Group I steels). The bars in Fig. 5 show the stress

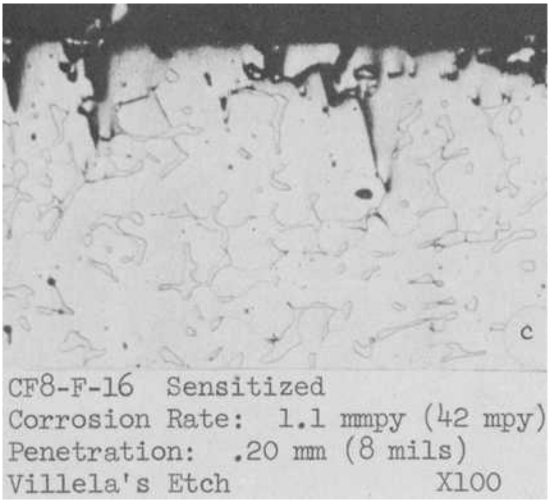

FIG. 1—*Continued.*

required to cause cracking for cast and wrought alloys. Results of previous studies [*3*] on solution-annealed material are in good agreement with these data.

An increase in stress-corrosion resistance with ferrite content is noted in spite of variations in the resistance to SCC of different lots of the same grade; for instance, between CF-8 with normal nitrogen contents and CF-8 to which deliberate nitrogen additions were made (OSU Code, Lots E and F versus OSU Code, Lots 4S and 4C). CF-20 steels, containing 11 and 12 percent ferrite, which proved highly sensitive to intergranular corrosion measured in the Huey test, displayed good resistance to SCC. Low resistance to SCC was observed for the columbium-stabilized grade CF-8C. Edeleanu [*6*] reported similar results for 18 percent chromium, 8 percent nickel steels with 0.6 percent titanium containing up to 10 percent ferrite. His studies were conducted using a boiling 42 percent magnesium chloride ($MgCl_2$) solution and indicated lower susceptibility with increased ferrite content. Edeleanu also reported that ferrite does not usually crack and in fact seems to hinder cracking.

The SCC data for the wrought alloys are also included in Fig. 5. Except for Type 316 stainless steel which shows moderate resistance to cracking, the wrought alloys show a very low resistance comparable to ferrite-free or low ferrite-containing cast alloys.

A summary graph of the effect of ferrite on resistance to SCC and yield strength is presented in Fig. 6. All data from this and a previous investigation [*3*] were combined. Thus, data points include cast CF-type steels discussed here as well as fully austenitic cast CN-7M (28Ni, 20Cr), cast

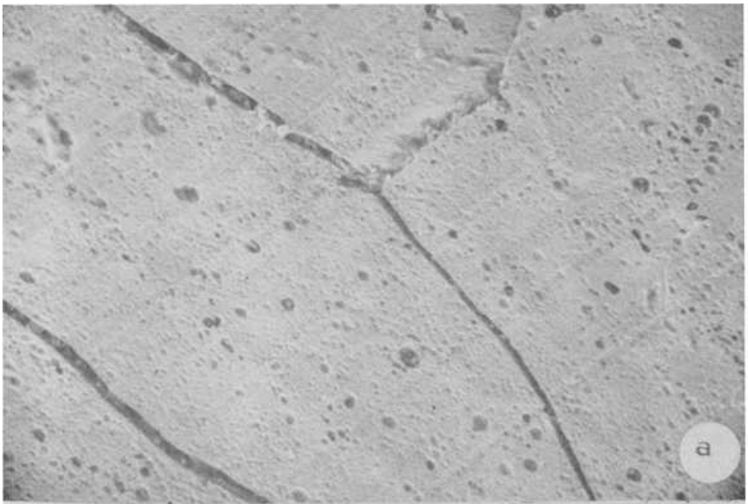

CF8-D-0 Sensitized X100
Corrosion Rate: .46 mmpy (18 mpy)

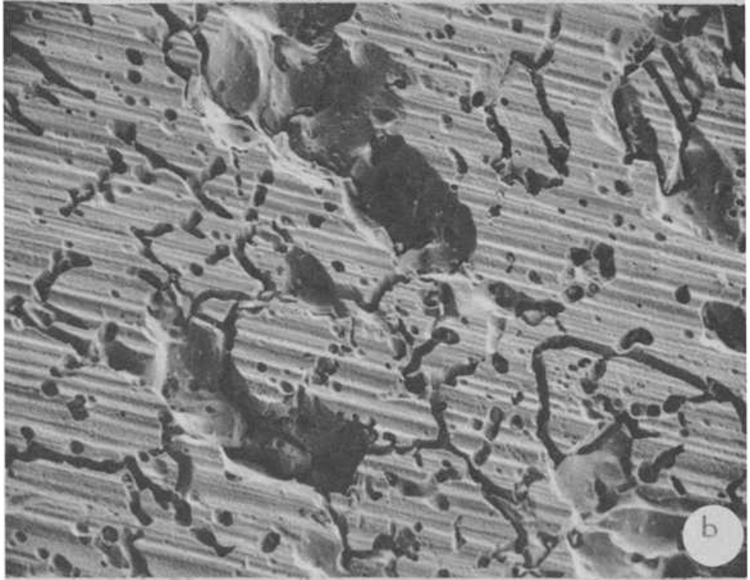

CF8-E-5 Sensitized X100
Corrosion Rate: .73 mmpy (29 mpy)

FIG. 2—*Scanning electron micrographs of surfaces of sensitized CF-8 specimens illustrated in Fig. 1.*

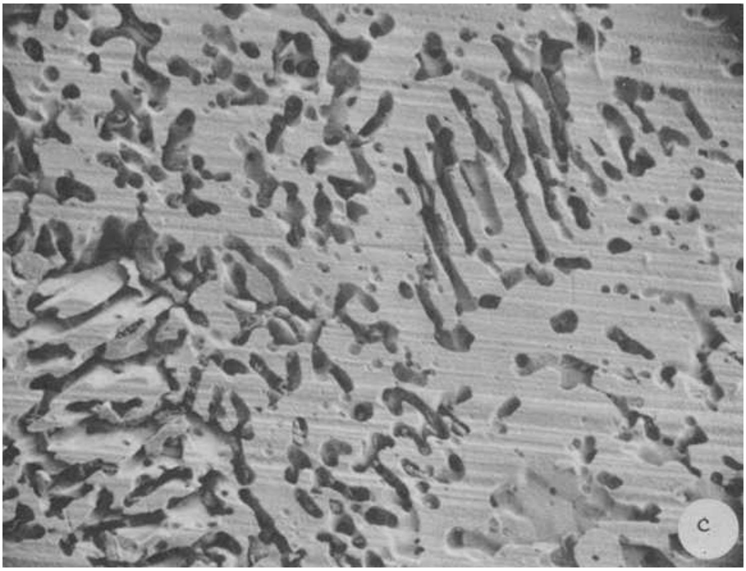

FIG. 2—*Continued.*

CE-type (28Cr, 9Ni), and the age-hardenable CD-4MCu (26Cr, 5Ni, 3Cu) with 65 percent ferrite. Conservative trend lines are shown for the lowest stress at which cracking may be expected and for the yield strength. The large number of data combined in Fig. 6 gives considerable confidence in the beneficial effect of ferrite above 10 percent, with regard to stress-corrosion resistance and above 5 percent with regard to strength.

Summary and Conclusions

Only limited or no published information exists on cast stainless steels with regard to the effect of ferrite content on their resistance to intergranular corrosion and their susceptibility to SCC in the solution-annealed and the sensitized condition. Failures of cast stainless components due to intergranular or stress corrosion are rare but concern exists especially in the power generating industry [*4*] due to sensitization that may occur primarily in welding and weld facing operations. Cast alloys of the CF grades (19Cr, 9Ni), which find widespread application in the chemical, petrochemical, and power generating industry, were subjected, therefore, to intergranular corrosion tests (Huey) and stress-corrosion tests (vapor phase of aqueous 875-ppm NaCl solution at 477 K (400°F)) to evaluate

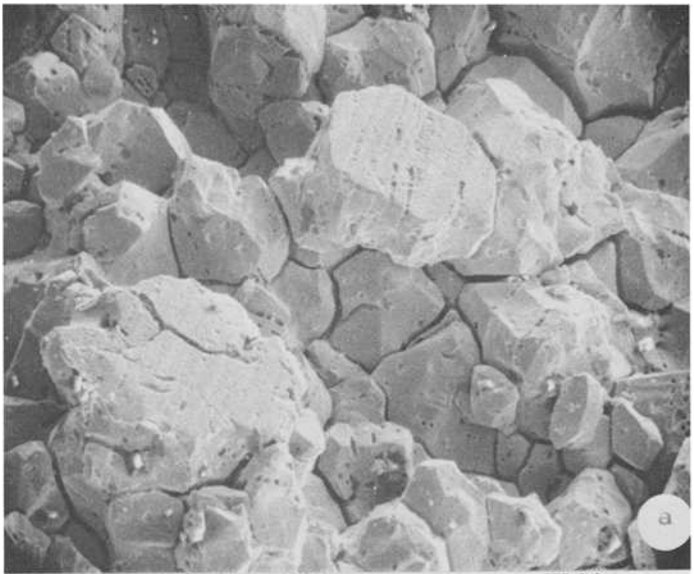

Type 316 Sensitized X100
Corrosion Rate: 4.8 mmpy (190 mpy)

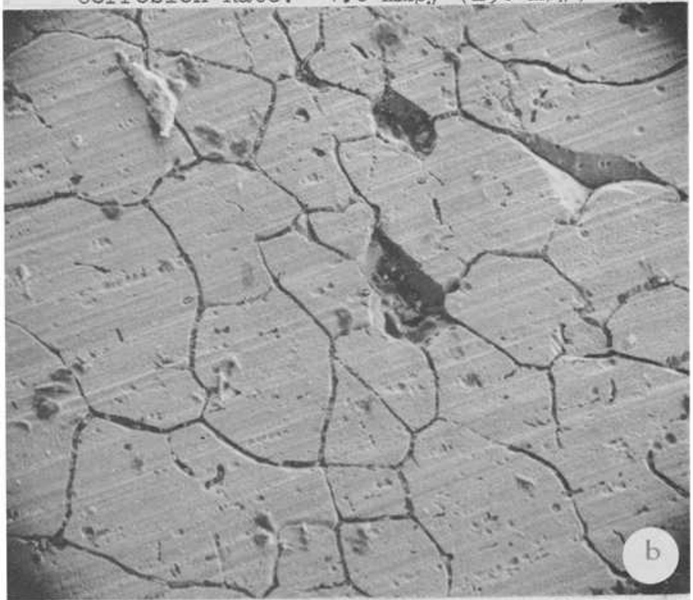

Type 316L Sensitized X100
Corrosion Rate: .35 mmpy (14 mpy)

FIG. 3—*Scanning electron micrographs of surfaces of sensitized Types 316 and 316L specimens.*

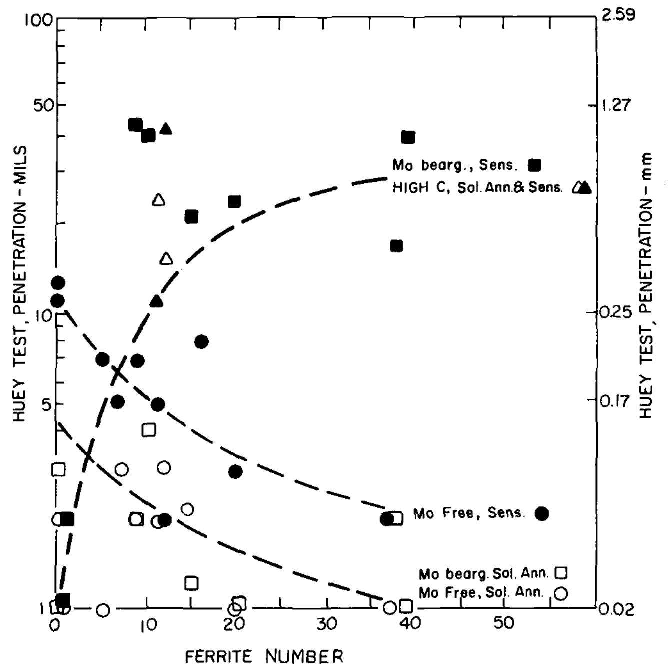

FIG. 4—*Effect of ferrite on maximum depth of intergranular attack and penetration, measured metallographically on Huey test specimens, cast CF-type stainless steels.*

the effect of ferrite in the range of 0 to 40 ferrite numbers, in the solution-annealed and in the sensitized condition.

The intergranular corrosion tests demonstrated beneficial effects of ferrite for all the alloys tested in the solution-annealed condition and for the molybdenum-free cast steel grades in the sensitized condition. Ferrite increased the sensitization effects on intergranular corrosion for molybdenum-bearing grades. Highest corrosion rates in Huey tests, based upon weight loss measurements, do not necessarily mean deepest intergranular attack. Intergranular attack was found to terminate at ferrite/austenite grain boundaries. These metallographic observations are explained on the basis of a disconnected distribution of carbide in sensitized, ferrite-containing alloys (that is, in discrete ferrite pools) as compared to a continuous grain boundary network in fully austenitic castings of the same carbon level. The intergranular corrosion tests results would indicate that ferrite numbers exceeding 10 would offer greater operating safety for cast corrosion resistant grades CF-3, CF-3M, CF-8, and CF-8M in the solution-annealed condition and also in the event of sensitization for cast corrosion resistant grades CF-3 and CF-8.

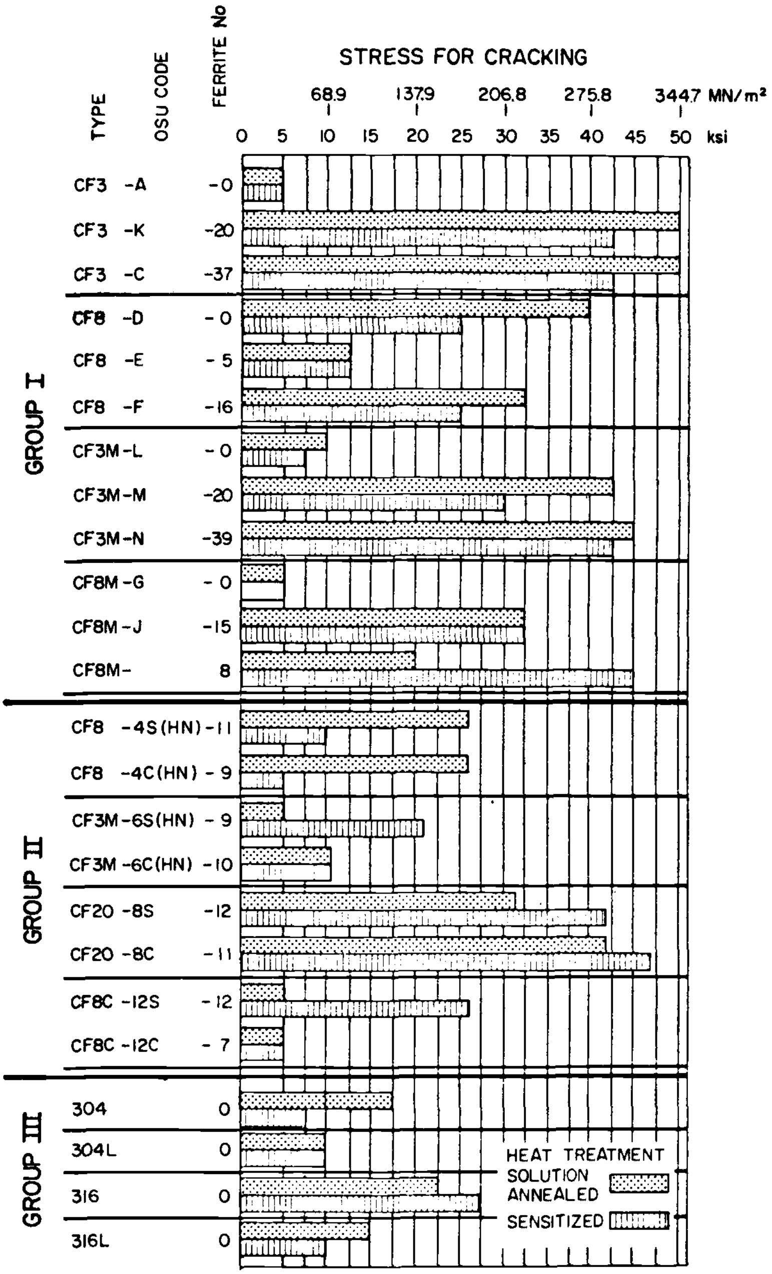

FIG. 5—*Effect of sensitizing on the stress required to induce SCC in 8 h in the vapor phase over aqueous 875-ppm NaCl solution at 477K (400°F).*

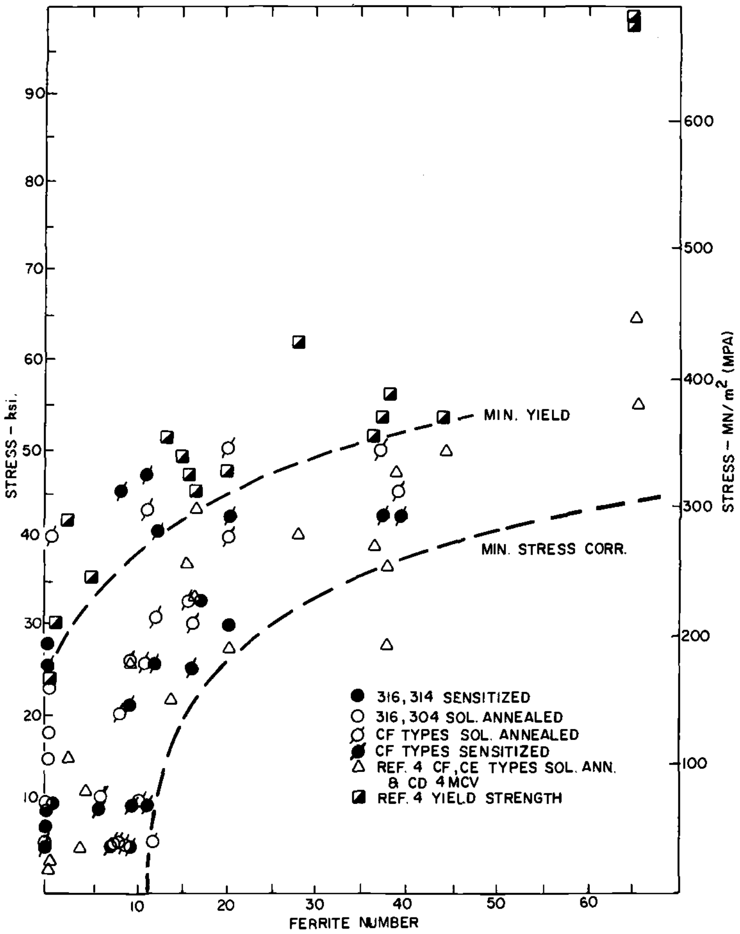

FIG. 6—*Effect of ferrite on yield strength and stress-corrosion susceptibility of cast stainless steels 8 h test in vapor of 875-ppm NaCl aqueous solution at 477K (400°F).*

The SCC tests in the severe vapor phase environment of a 477 K (400°F), aqueous 875-ppm NaCl solution demonstrated a significant increase in the resistance to SCC with increasing ferrite content. The beneficial effects of ferrite were noted for cast steels in the solution-annealed and in the sensitized condition. These SCC test results indicate that ferrite contents of 10 or more ferrite numbers would offer greater operating safety for cast corrosion resistant CF grades in the solution-annealed as well as in the sensitized condition.

Acknowledgment

The authors express appreciation for the guidance provided by the High Alloy Technical Research Committee of the Steel Founders' Society of

America and member company contributions. Special thanks go to Professor M. G. Fontana, head of Metallurgical Engineering Department, Ohio State University, for his contributions to this research and to A. V. Barthof, who conducted the work described in this report. The SEM contribution was made by R. Farrar. Cast materials were prepared by Leroy Finch and Harold Rose of ESCO Corporation, Portland, Oregon. E. A. Schoefer assisted in the design of proper alloy chemistries to yield desired ferrite contents.

References

[1] Beck, F. H., Schoefer, E. A., Flowers, J. W., and Fontana, M. G. in *Advances in the Technology of Stainless Steel and Related Alloys, ASTM STP 369*, American Society for Testing and Materials, 1965.
[2] Schoefer, E. A., "A Diagram for Estimation of Ferrite Content in Stainless Steel Castings," Appendix to "Mossbauer-Effect Examination of Ferrite in Stainless Steel Welds and Castings," by L. J. Schwartzgruber, L. H. Bennett, E. A. Schoefer, W. T. DeLong, and H. C. Campbell, *Welding Journal*, Vol. 53, No. 1, Research Supplement, 1974, pp. 1-S to 10-S.
[3] Flowers, J. W., Beck, F. H., and Fontana, M. G., "Corrosion and Age Hardening Studies of Some Cast Stainless Alloys Containing Ferrite," *Corrosion, Journal of Science and Engineering*, National Association of Corrosion Engineers, May 1963.
[4] "ACRS Looking at Sensitized Steel; NSP Changing Over at Monticello," *Nucleonics Week*, Vol. 11, No. 19, 14 May 1970, p. 1.
[5] "Calibration Procedure for Instruments to Measure the Delta Ferrite Content of Austenitic Stainless Steel Weld Metal." WRC Publication of 1 July 1972.
[6] Edeleanu, C. in *Stress Corrosion Cracking and Embrittlement*, W. D. Robertson, Ed., Wiley, New York, 1956, p. 126.

Teruhisa Ohki,[1] *Masayuki Tanimura,*[1] *Kazuhisa Kinoshita,*[1]
and Gennosuke Tenmyo[1]

Effect of Inclusions on Sulfide Stress Cracking

REFERENCE: Ohki, Teruhisa, Tanimura, Masayuki, Kinoshita, Kazuhisa, and Tenmyo, Gennosuke, **"Effect of Inclusions on Sulfide Stress Cracking,"** *Stress Corrosion—New Approaches, ASTM STP 610,* American Society for Testing and Materials, 1976, pp. 399–419.

ABSTRACT: Sulfur was taken as a residual element in steel for investigating the sulfide stress-cracking characteristics. The tests were performed by controlling the shape and the amount of the sulfide inclusions by adding rare earth metal (REM) and varying the sulfur content from 0.002 to 0.019 percent. Susceptibility to sulfide stress cracking was found to be correlated to the sulfur content and also to the shape of the inclusions.

Detailed observation of crack nucleation showed that though precracks nucleate and grow from elongated sulfide inclusions to form large cracks in conventional steels, the nucleation can be suppressed by controlling the shape of sulfide inclusions to the globular type.

The results of this work suggest that controlling the shape of sulfide inclusions by adding an optimum amount of REM is so effective that it would completely minimize the detrimental effect of sulfur against hydrogen sulfide stress cracking.

KEY WORDS: stress corrosion, microstructure, compositions, sulfur, sulfide stress cracking, shape control, inclusions, rare earth metals, environments, embrittlement, delayed fracture, absorption, hydrogen, hydrogen sulfide, crack nucleation, crack propagation, toughness, ductility, stresses, cathodic charging

A number of studies have been reported on the properties of steel exposed to environments containing hydrogen sulfide used for investigating the chemical and physical factors, knowing that strong correlation exists between the strength of the steel and its cracking resistance. Also the microstructure and chemical composition have considerably large effects, although there are some exceptions. In studying the properties of steel exposed in hydrogen sulfide (H_2S) atmosphere, it is necessary to take into account the strength, structure, and composition of the steel. Regarding

---

[1] Researcher, manager, manager, and general manager, respectively, Steel Products Section, Technical Research Center, Nippon Kokan Kabushiki Kaisha, Kawasaki, Japan.

strength, the National Association of Corrosion Engineers (NACE) Committee Report [*1*][2] recommends tempering above 1150°F (620°C) for getting hardness number HRC equal or less than 22. Though this hardness is considered the maximum to ensure safety against corrosion cracking, in some cases still higher hardness is allowed depending on the environment where the steel is used.

It has been observed that the high-temperature tempered martensite structure with uniform distribution of spheroidized carbides has the highest cracking resistance, while untempered martensite structure is the most favorable for cracking, and the structure with coarse spheroidized carbides and lamellar carbides formed by slow cooling, normalizing, and isothermal transformation falls in between the preceding two kinds of structures [*2*]. Regarding the chemical composition, studies have been conducted on carbon, manganese, nickel, molybdenum, etc., and, although there are some differences in opinion on their effects, all just about agree on the detrimental effects of manganese and nickel. Of the residual elements, sulfur is considered the most detrimental because it assists absorption of hydrogen into the steel; consequently, the steel with higher sulfur content is more favorable for stress cracking [*2–6*].

Though the effects of such residual elements are considered great for getting a wide scattering of H_2S stress-corrosion cracking characteristics for constant strength, structure, and chemical composition levels, the role of sulfur in the steel to the cracking characteristics is not yet obvious. Therefore, the authors became interested in sulfur as a residual element in steel and investigated the relationship of sulfur content and sulfide shape to sulfide stress-cracking characteristics.

Test Methods

Specimen Steel

The steel for testing was melted in an induction furnace, cast to 50-kg ingot, and rolled into a plate 12 mm thick. The commercial heat was melted in a 50-ton basic oxygen furnace, rolled into 170-mm-diameter billets, and finally into a 7-in. diameter seamless pipe.

Heat Treatment

After austenitizing at 880°C for half an hour, all the specimens were water quenched and tempered to obtain the prescribed strength level (530 to 650°C). The specimens were all of a tempered martensite structure.

---

[2] The italic numbers in brackets refer to the list of references appended to this paper.

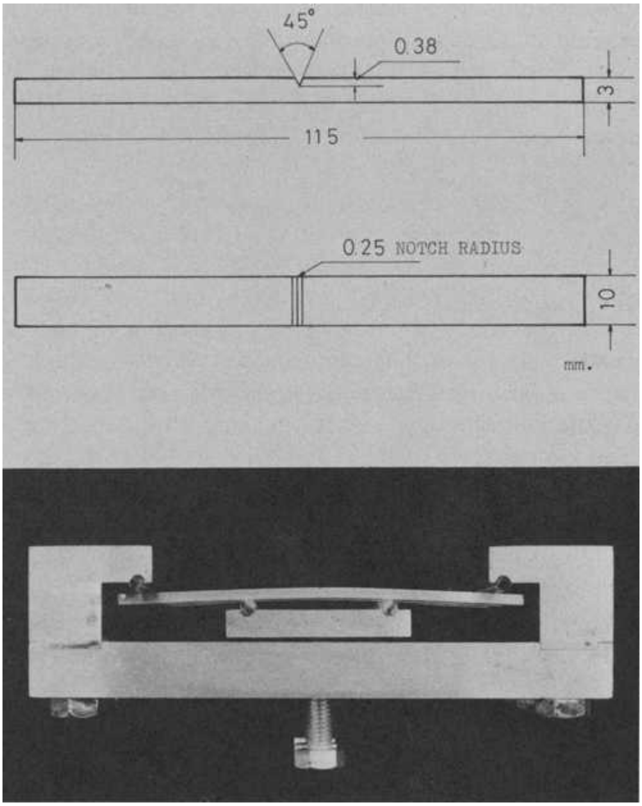

FIG. 1—*Specimen configuration and view of assembled holder.*

Shape of the Specimen and Loading Technique

A notched beam corrosion specimen was adopted for the purpose of centralizing the stress on the specimen. Figure 1 shows the specimen and its test holder. The stress was applied to the specimen by four-point bending. Using a 20-ton Instron type tensile machine, four-point bending tests were performed, and a load-deflection curve was obtained for each steel. The deflection corresponding to the yield strength was taken as the first point of departure from linearity in the load-deflection curve.

Corrosion Test

After determining the deflection corresponding to the yield strength, stress was applied in various ratios at 10 percent intervals against the yield deflection by a fixed-strain four-point bending jig. The specimens, after polishing with emery paper, were degreased and then immersed in an 0.5

percent aqueous solution of acetic acid. The solution was purged with nitrogen to remove the oxygen before adding H_2S. All tests were run with approximately 3000-ppm H_2S dissolved in the solution, which was achieved by continuously bubbling H_2S through the cells. The specimens were inspected every day; the total test period was 21 days.

Laboratory Tests

Effects of Sulfur

For studying the effects of sulfur, the chemical composition, strength level, and heat treatment of the specimens were kept constant. The standard chemical composition for oil well pipes for sour gas was taken as a basis with different amounts of sulfur, and the structure was fully quenched and tempered.

For studying the effects of the shape of sulfide inclusions, REM was added to some specimens for controlling the shape. The addition of REM had been found to be most effective among various alloying elements for controlling the shape of sulfides in a previous work.

The chemical compositions and mechanical test values are shown in Table 1. Sulfide cracking test results are shown in Fig. 2. The figure shows

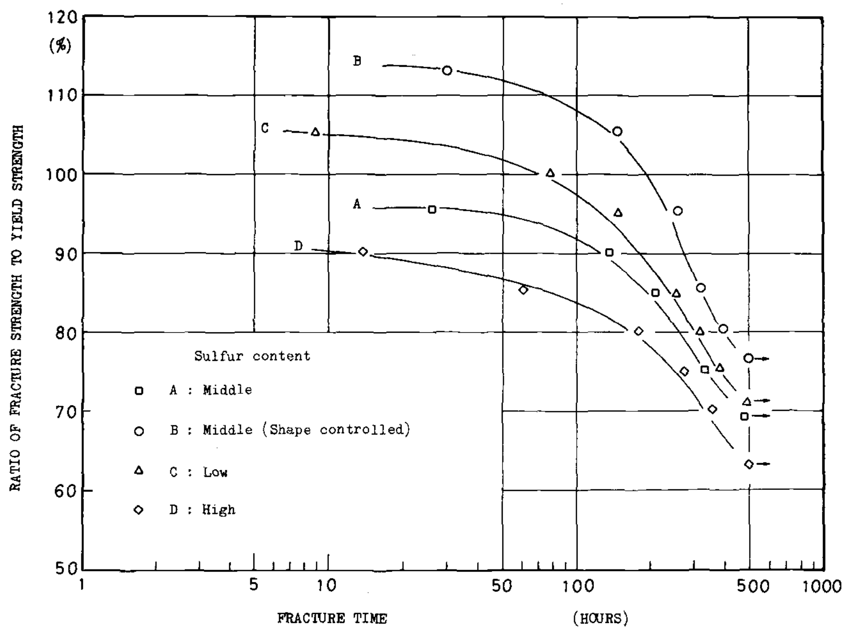

FIG. 2—*Results of sulfide stress cracking test for laboratory heats with various amounts of sulfur.*

TABLE 1—*Chemical composition and mechanical test values of the steels tested* (*1*).

Alloy Type	C	Si	Mn	P	S	REM		0.2% Offset Stress, kg/mm²	Tensile Strength, kg/mm²
						Ce	La		
A	0.32	0.39	1.21	0.009	0.011	. . .	. . .	58.0	71.2
B	0.32	0.29	1.34	0.016	0.011	0.025	0.008	60.2	72.7
C	0.32	0.28	1.42	0.016	0.002	. . .	. . .	60.1	71.3
D	0.32	0.31	1.32	0.016	0.030	. . .	. . .	55.8	68.5

that the fracture time at the higher applied stress side are extended into the longer time side as the sulfur content becomes lower. Since the yield strength of Steel D is slightly lower than that of Steels A and C, the apparent difference is small, but it is evident that sulfide cracking is dependent strongly on the sulfur content. For Steels A and B the sulfur content is the same, but, for Steel B, the shape of sulfide inclusions was changed to a globular form by adding REM. It is apparent that shape controlling of sulfide is also effective in reducing sulfide cracking. That is, shape controlling of sulfide inclusions, together with reducing the sulfur content, is an effective means for lowering sulfide crack susceptibility.

Effects of Shape Controlling of MnS Inclusions

The effects of the shape change of manganese sulfide (MnS) inclusions on the susceptibility to stress cracking for constant sulfur content were studied in the next step. The shape of MnS inclusions was controlled by changing the amount of REM added, resulting in an optimum amount of REM for the best corrosion characteristics. An example of the results is shown in Table 2 and Fig. 3.

For Steel A no shape controlling of MnS was made, for Steels B and C an optimum and excessive amount of REM, respectively, was added. That is, Steel A contains MnS inclusions (ASTM Type A), Steel B

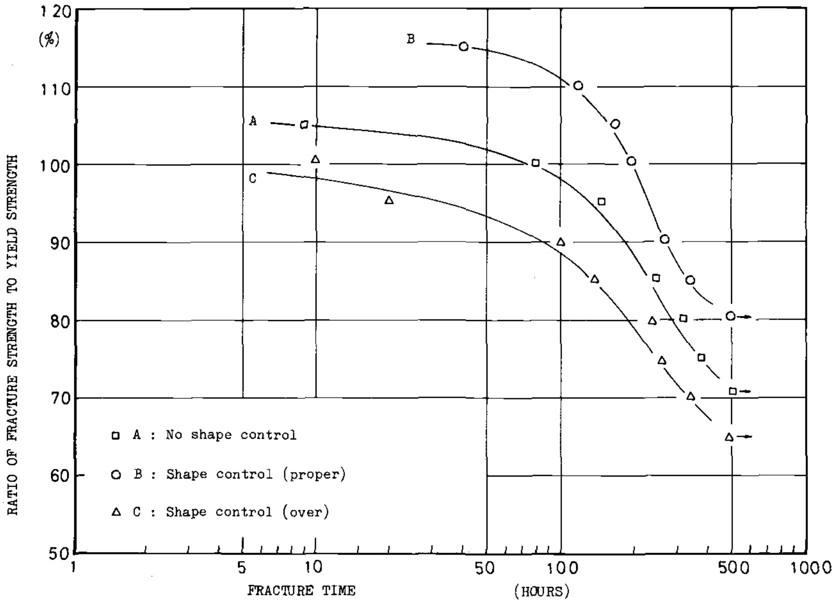

FIG. 3—Effects of inclusion-shape control on sulfide stress cracking characteristics.

TABLE 2—*Chemical composition and mechanical test values of the steels tested* (*2*).

Alloy Type	C	Si	Mn	P	S	REM		0.2% Offset Stress, kg/mm^2	Tensile Strength, kg/mm^2
						Ce	La		
A	0.32	0.28	1.42	0.016	0.002	. . .	. . .	60.1	71.3
B	0.31	0.31	1.31	0.015	0.003	0.010	0.003	65.0	76.8
C	0.30	0.35	1.31	0.016	0.003	0.025	0.008	67.1	78.6

spheroidized sulfide inclusions, and Steel C globular (ASTM Type D) and alumina (ASTM Type B) inclusions in bandform without any MnS inclusions. The figure shows that the resistance to stress cracking becomes the greatest when the MnS inclusions are spheroidized completely (Steel B).

The foregoing results show that the spheroidization of sulfide inclusions, together with lowering of sulfur content itself, is most effective against sulfide stress cracking.

Effects of Sulfur Content and Shape Controlling

The effects of sulfur content on those that are inclusion-shape controlled and those not controlled are shown in Fig. 4, the base chemical composition of the specimens being the same. The sulfur content was varied from 0.002 to 0.019 percent, in which inclusion-shape controlling was done on the specimens with sulfur content between 0.003 and 0.009 percent. In order to obtain clear distinction between the shape controlled and uncontrolled cases, the yield strength was raised about 75 kg/mm^2 for increasing the crack susceptibility. The tests show that when the sulfide is spheroidized, even when the sulfur content is low, the fracture stress shifts over to the higher stress side. Although these laboratory heats had relatively small reduction ratio and short MnS extension, the effect of shape controlling is apparent. Consequently, the effects of spheroidizing the sulfide inclusions, together with reducing sulfur content for commercial heats, would greatly lower the susceptivility to sulfide stress cracking.

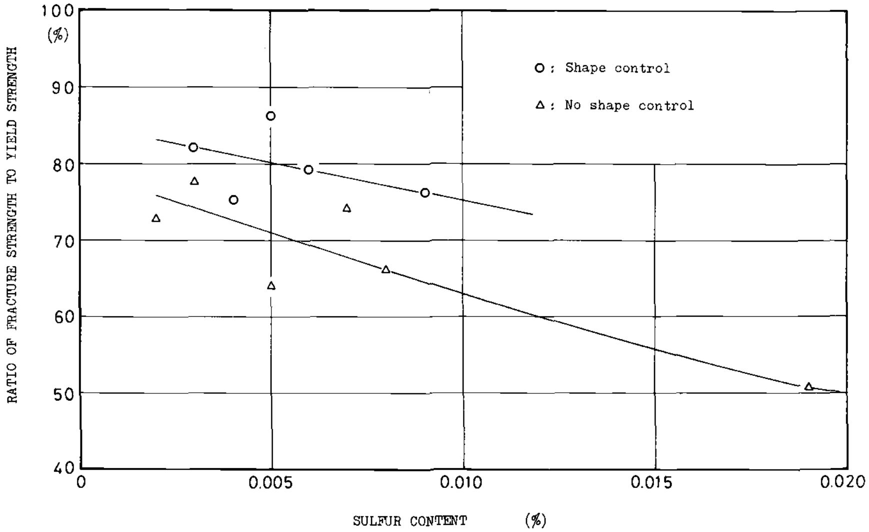

FIG. 4—*Relationship between sulfur content and stress level for fracture in 200 h.*

TABLE 3—*Chemical composition and mechanical test values of commercial heats.*

Alloy Type	C	Si	Mn	P	S	REM		0.2% Offset Stress, kg/mm^2	Tensile Strength, kg/mm^2
						Ce	La		
A	0.34	0.28	1.17	0.011	0.003	0.012	0.004	76.5	88.8
B	0.35	0.28	1.06	0.014	0.003	...	...	76.1	89.9
C	0.30	0.28	1.21	0.015	0.019	...	...	75.6	86.0

Tests at Production Scale

Since the tests at laboratory scale showed that controlling the sulfide shape, together with lowering the sulfur content, was most effective against sulfide stress cracking, the tests were conducted at a production scale by manufacturing seamless pipes. Table 3 shows the chemical composition of the steels tested. Steel A contains low sulfur in which the shape of sulfides was controlled by adding REM. Steel B contains ultralow sulfur. Steel C contains a normal amount of sulfur.

Cleanliness

Table 4 shows the cleanliness measurements (percent in area) of the billet specimens for the middle position of the ingot. The cleanliness measurement for other positions of the ingot are almost the same as those for the middle positions. In both the low-sulfur (B) and conventional (C) steels, sulfide, alumina, and globular inclusions are present, and, especially in the conventional steel, a large amount of sulfide inclusions can be noted. When REM is added for controlling the shape of sulfides, sulfide inclusions can be hardly observed, but considerable amount of globular inclusions and a few alumina inclusions are seen.

Shapes of Inclusions

The typical shapes of inclusions observed are shown in Fig. 5. In conventional steel, a large number of MnS inclusions are observed extending in the rolled direction and forming into groups. In low-sulfur steel, the MnS inclusions exist in isolated form, and no grouping like in the conventional steel are observed. Where the shape of sulfide is controlled, evenly distributed spheroidized REM sulfide can be observed.

Sulfide Stress Cracking Test

A typical example of the results of sulfide stress-cracking tests is shown in Fig. 6. Each plotted point indicates the average fracture time of three

TABLE 4—*Cleanliness measurements (percent in area) of commercial heats.*

Type of Inclusions / Alloy Type	Sulfide Type Inclusions (ASTM Type-A)	Alumina Type Inclusions (ASTM Type-B)	Globular Type Inclusions (ASTM Type-D)	Total
REM addition (Steel A)	0	0	0.03	0.03
Low S (Steel B)	0.03	0.01	0.01	0.05
Conventional (Steel C)	0.13	0.01	0.01	0.15

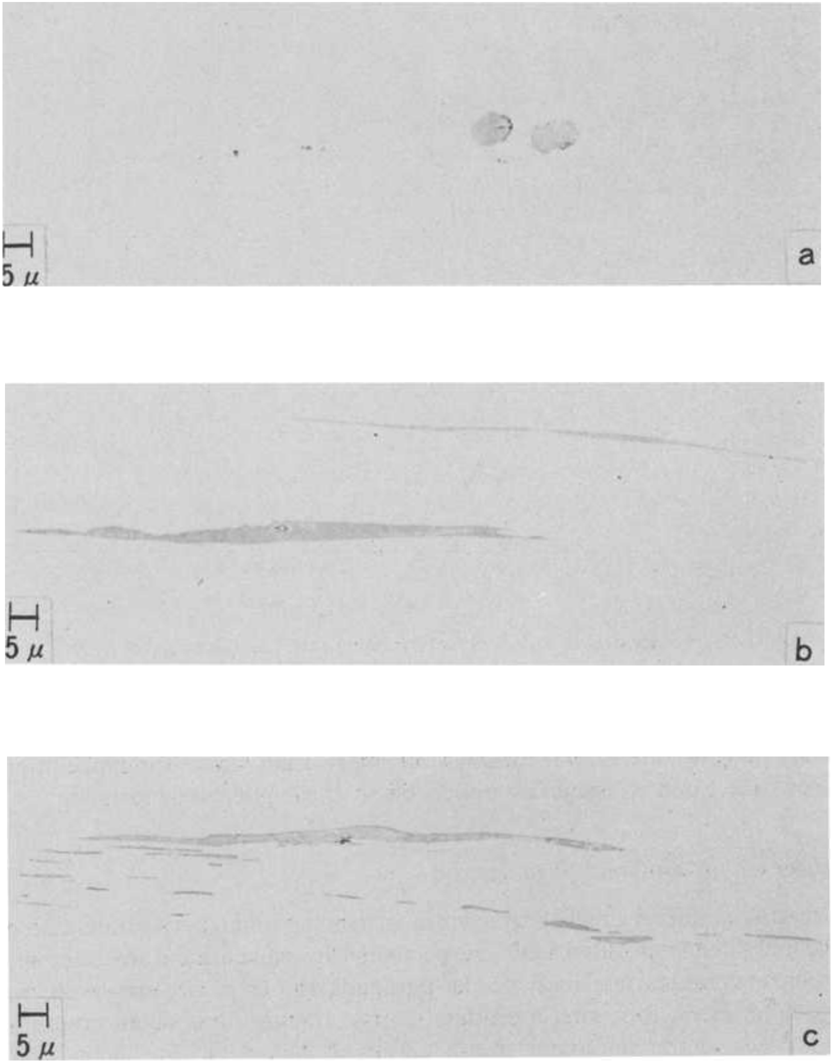

FIG. 5—*Sulfide inclusions in the steels tested (commercial heats):* (a) *with REM addition (Steel A),* (b) *low S (Steel B), and* (c) *conventional (Steel C).*

specimens. From the figure it is evident that lowering the sulfur content causes substantial rise in threshold stress and that the inclusion-shape controlling causes the fracture time for higher applied stress to become longer. Figure 7 shows the changes of fracture stress when the strength of steels are changed. Each curve shows that there exists an inversely proportional relationship between the yield strength and fracture stress, and that by

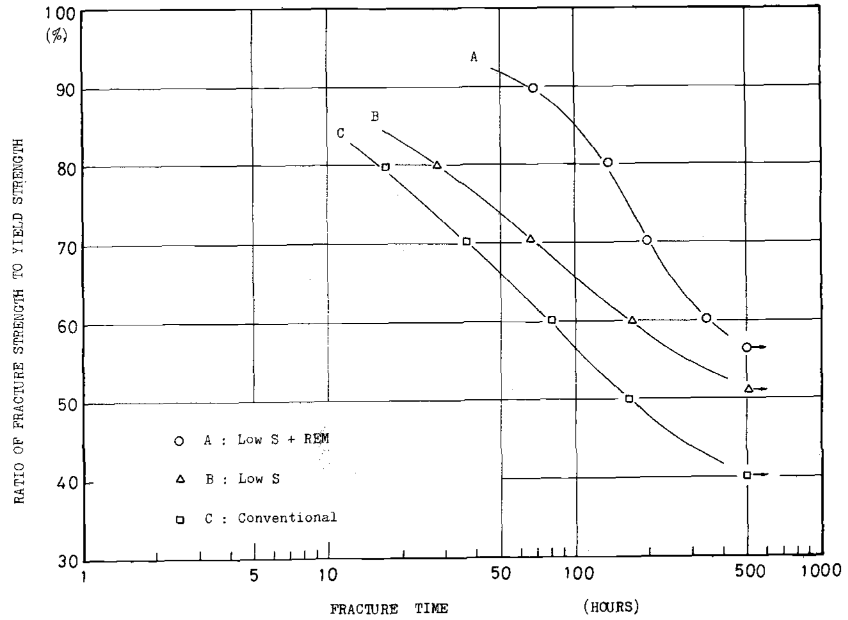

FIG. 6—*Results of sulfide stress cracking tests for commercial heats.*

lowering the sulfur content and controlling the shape of sulfide inclusions raises the fracture stress considerably more than those for conventional steel. The trend is especially noticeable at the higher yield strength.

Observations on Crack Propagation

Figure 8 shows crack propagation in conventional, low-sulfur, and inclusion-shape controlled steels, respectively. In conventional steel, the main crack and numerous small cracks perpendicular to it are observed, with the main crack following a crooked course tracing these small cracks. At the crack ends, microcracks are observed ahead of the main crack. Numerous MnS inclusions, extended in a rolled direction, exist at these small cracks with defects occurring at the interface between matrix and MnS. This would indicate that the microcracks ahead of the main crack grow into small perpendicular cracks and that the main crack propagates into these. In sulfide-shape controlled steel, the main crack forms at the notch bottom, grows out from the pit, and propagates in a straight line, none of the small cracks being perpendicular to the main crack as observed in conventional steel. In the scope of this work, cracks which propagated from globular inclusions were not observed. In the low-sulfur steels, relatively linear cracks propagate, but some cracks are observed to prop-

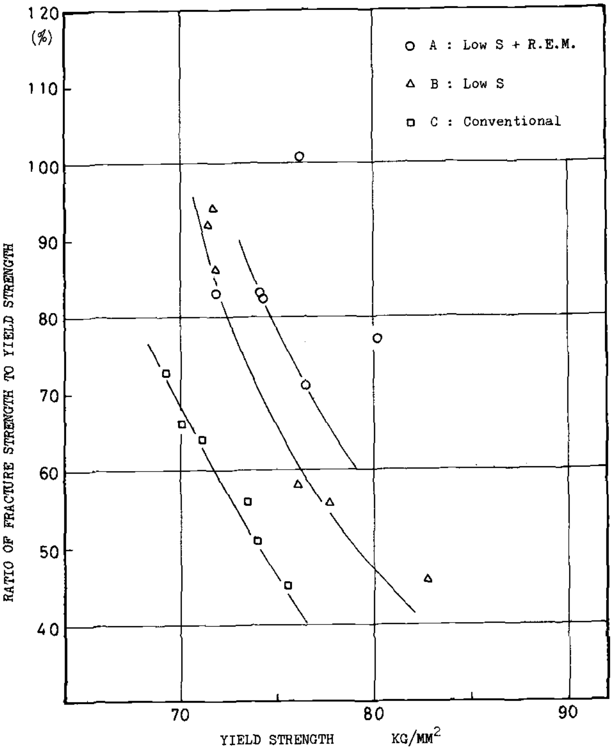

FIG. 7—*Relationship between yield strength (0.2 percent flow stress in tension test) and stress level for fracture in 200 h.*

agate from the points torn off at the MnS inclusions. Although not as noticeable as in conventional steel, small cracks perpendicular to the main cracks are observed. These results show that even for low sulfur content, if sulfide inclusions are present, they become the sites for cracks.

Observations of Cracking Along Immersion Time

The results just mentioned show that there is a difference in the formation of cracks in conventional steel and in inclusion-shape controlled steel. Therefore, for studying the progress of cracking, the test was carried out applying the load at a fixed value (60 percent of yield strength) during the immersion of the specimens in a corrosive solution. The specimens were taken out every 50 h for investigating the changes in notched parts.

Figure 9 shows the results for conventional steel.

1. After 50 h, the MnS existing in the vicinity of the notch starts to corrode.

2. After 75 h, a small crack forms at the MnS inclusions at the notch bottom. The interface between the elongated MnS and matrix is torn off.
3. After 150 h, the notched bottom is corroded considerably together with the formation of several cracks under the notch bottom which show noticeable growth. Figure 9*b* shows the torn-off cracks near the crack tips making it evident that these formed to connect the MnS inclusions.
4. The fractured state shows that a large number of crack traces are present under the notch bottom. The main crack propagates by connecting these cracks.

Figure 10 shows the results for inclusion-shape controlled steel. The corrosion at the notch bottom grows more severely with the passage of immersion time in a corrosive solution, but no torn-off cracks are observed in the interior of the steel. A view of the fractured state shows that the main crack is formed linearly from one pit at the notch bottom, and that the crack shape is relatively more linear than that without inclusion-shape control. Remaining inclusions were detected in the main crack. No other crack formation was observed in the interior of the steel.

From the results just shown, it is concluded that when inclusion-shape control is not applied, the specimen, when immersed in the corrosive solution, begins to develop torn-off cracks at the MnS sites existing under the notch bottom after a short period of time. To induce small cracks results in early fracture. When inclusion-shape control is applied, the spheroidized sulfides have less stress concentration than the MnS inclusions extending in the rolled direction, making it difficult for the cracks to develop. When the sulfur content is lowered, there is less chance for formation of torn-off cracks to appear under the notch bottom. Therefore, very few of the main cracks are induced by torn-off cracks at inclusions, and many propagate through the elastic-plastic strain interfaces determined by stress distribution in the matrix.

Discussion

It is shown that sulfide crack susceptibility is interrelated with sulfur content and also bears a relationship with the shape and distribution of sulfide inclusions. Usually the MnS inclusions are presently extended in a rolled direction in the steel, and, if the sulfur content is increased, a large number of localized groups of MnS inclusions begin to appear. When a stress-applied specimen is exposed in a corrosive hydrogen sulfide atmosphere, the hydrogen generated by corrosion diffuses in the steel, when trapped by the elongated MnS inclusions present under the bottom of the notch where the stress is the greatest. As suggested by Tetelman [7], the hydrogen is deposited on the nucleus of microcracks and microvoids at the three-dimensional stress field, then the interface between the elongated

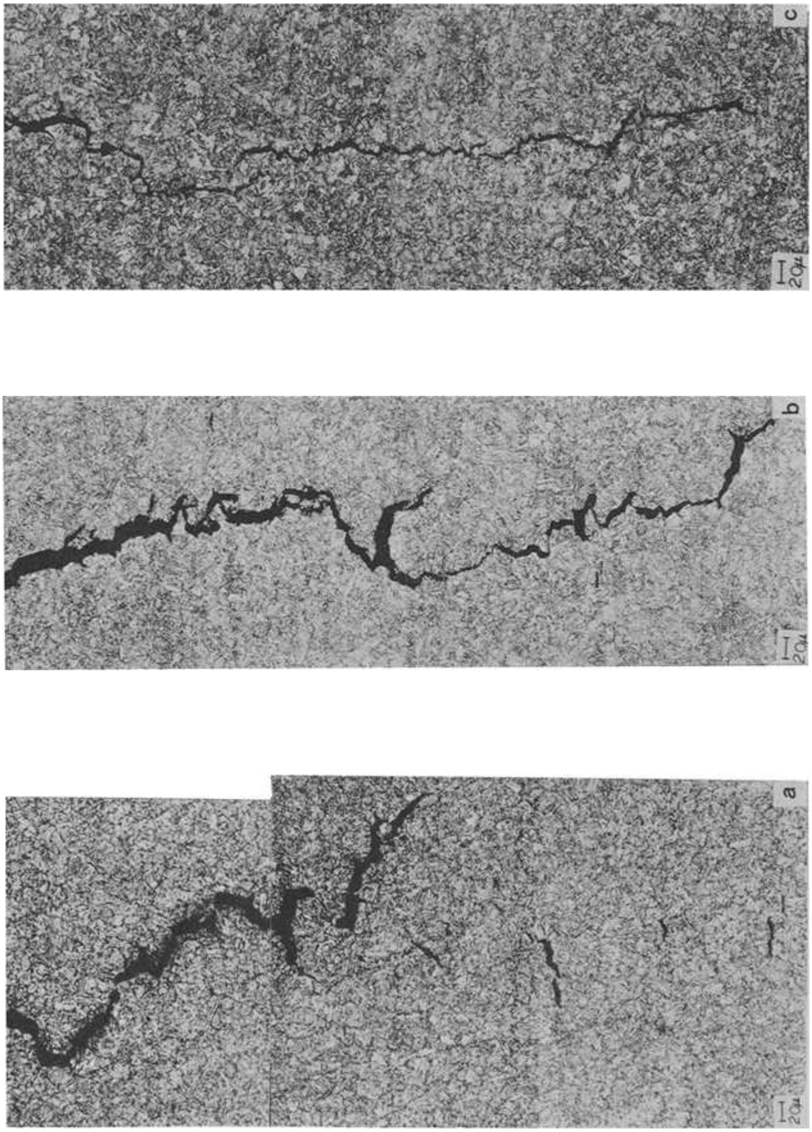

FIG. 8—*View of crack propagation: (a) conventional steel (Steel C), (b) low sulfur steel (Steel B), and (c) REM added steel (Steel A).*

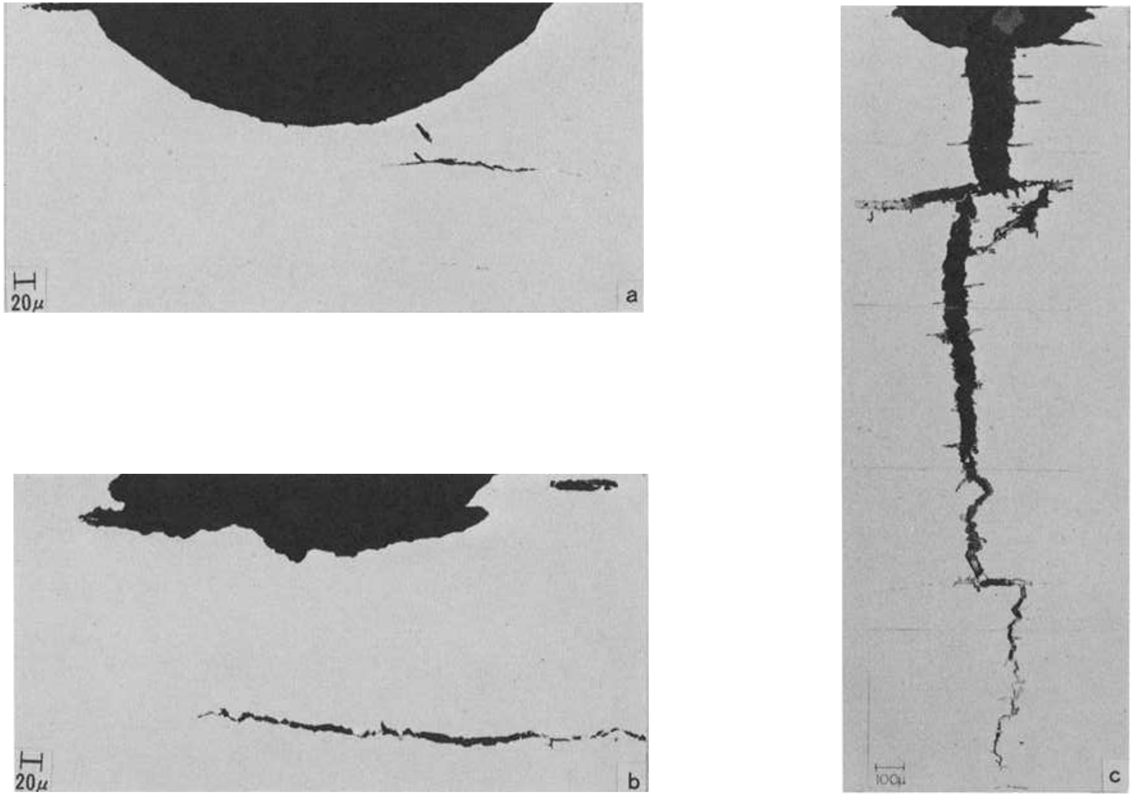

FIG. 9—*Formation of cracks at the notch bottom in conventional steel:* (a) *75 h,* (b) *150 h, and* (c) *view of the fractured crack.*

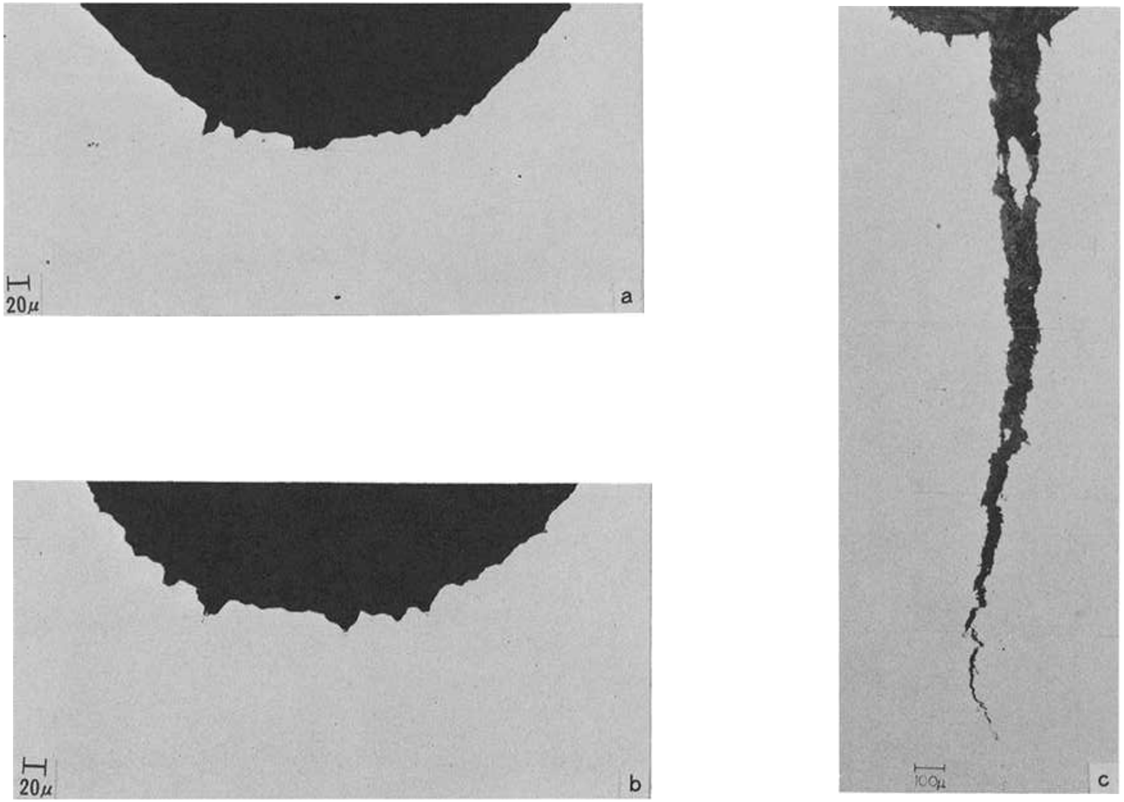

FIG. 10—*Formation of cracks at the notch bottom in inclusion-shape controlled steel:* (a) *50 h,* (b) *200 h, and* (c) *view of the fractured crack.*

MnS and matrix is torn off. The torn-off crack grows with time, and when it grows to a certain size determined by the applied stress and strength of the steel, it connects to the notch bottom and becomes a main crack that propagates. The crack propagation advances due to repetition of the following mechanism:

1. Microcracks form under the notch bottom and start to grow.
2. The pit formed at the notch bottom connects to the microcracks ahead.
3. Microcracks form ahead of the main crack with MnS inclusions as nuclei.
4. The main crack connects to these and propagates.

The following drawings show the schematics of the mechanism just mentioned.

(1)

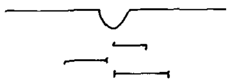

(2)

(3)

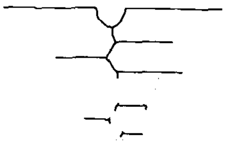

(4)

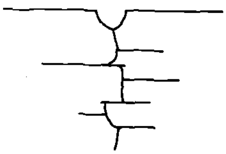

Figure 11 shows the fractured surface under the notch bottom as seen by the scanning electrode microscope (SEM). These would agree with the cracking mechanism just described. Therefore, lowering the sulfur content would reduce the MnS inclusions extending in the rolled direction and would lessen the chances for presence of the inclusions that become the sites for microcracks which would induce a main crack at the notch bottom. Spheroidizing the MnS inclusions will prevent tearing off the interface between the inclusion and the matrix and reduce the chance for propagation of the main crack.

A number of observations have been reported showing that the inclusions, carbides, and the like become the origins for the propagation of cracks in sulfide stress cracking or delayed fracture [*8–15*]. Though it is not obvious because of the many different ideas proposed for the causes of cracking, it is considered to be true that the hydrogen absorbed in the steel collects at the interface between the matrix and the inclusions to make the matrix brittle and, consequently, that the deformation of inclusions, their distribution, and the shape and size of the defects at the interface between the inclusions and matrix affect the cracking characteristics.

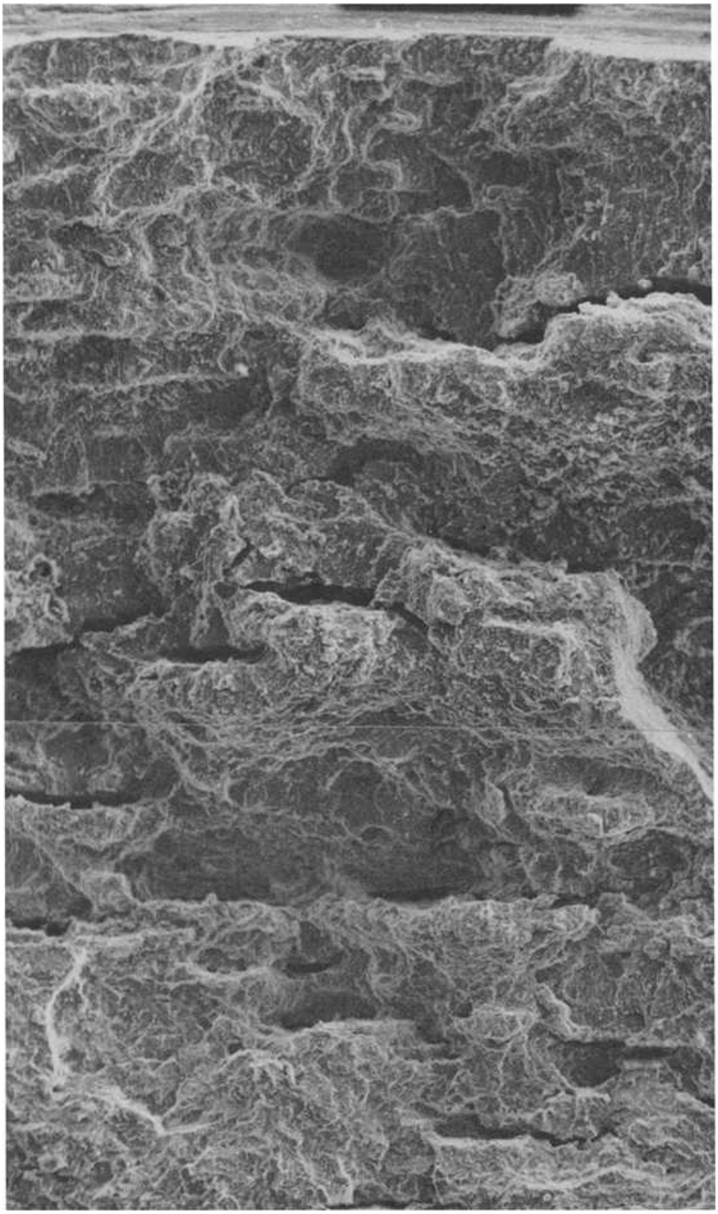

FIG. 11—*SEM image of fractured surface.*

That is, when the sulfur content is increased, a large number of elongated MnS inclusions are distributed in the steel to trap the hydrogen diffused in the steel making the vicinity of the inclusions brittle. Increase in the amount of MnS causes numerous local embrittled places to exist in the steel, and the precracks, formed at each of these places, make it extremely easy for the main crack to propagate. Increasing the sulfur content also allows blisters and corrosion pits to form readily, while assisting the corrosive reaction itself. On the other hand, spheroidizing the elongated MnS inclusions would cause less stress concentration than the elongated one because smaller amounts of hydrogen trapped at the inclusion and matrix interfaces make precracks difficult to form. That is, spheroidizing the elongated inclusions produces the same effect on sulfide cracking susceptibility as reducing the sulfur content to a very low value. (Figure 4 shows that the steel with spheroidized sulfides of 0.006 percent sulfur is equivalent to that with 0 percent sulfur without shape control.)

Conclusion

Susceptibility to sulfide stress cracking has intimate correlation with the sulfur content. The shape, amount, and distribution of sulfide inclusions have the greatest effect on cracking susceptibility.

The results of this work suggest that controlling the shape of sulfide inclusions by adding optimum amount of REM is so effective that it minimizes the detrimental effect of sulfur in promoting hydrogen sulfide stress cracking.

References

[1] National Association of Corrosion Engineers Committee Report, *Materials Protection*, Vol. 5, 1966, p. 81.
[2] Snape, E., *Corrosion*, Vol. 24, 1968, p. 261.
[3] Schuetz, A. E. and Robertson, W. D., *Corrosion*, Vol. 13, 1957, p. 437t.
[4] Uhlig, H. H., *Metallurgical Progress*, Vol. 57, 1950, p. 486.
[5] Lorenz, K. and Medewar, G., *Erdol und Kohle*, Vol. 17, 1964, p. 1015.
[6] Hayness, A. G. and Blower, R., *British Iron and Steel Research Association—Iron and Steel Institute Special Report*, Vol. 76, 1962, p. 33.
[7] Tetelman, A. S., *Proceedings of Conference on Fundamental Aspects of Stress Corrosion Cracking*, Ohio State University, 1976, p. 446.
[8] Farrell, K. and Quarrell, A. G., *Journal of the Iron and Steel Institute*, Vol. 202, 1964, p. 1002.
[9] Boniszewski, T. and Moreton, J., *British Welding Journal*, Vol. 14, 1967, p. 321.
[10] Tetelman, A. S. and McEvily, A. J., *Fracture of Structural Materials*, Wiley, New York, 1967.
[11] Kawashima, A., Takano, M., Hashimoto, K., and Shimodaira, S., *Journal of the Japanese Institute of Metals*, Vol. 38, 1974, p. 254.
[12] Tokuda, A. and Ohnishi, K., "Toward Improved Ductility and Toughness," Symposium Proceedings, 1971, Climax Molybdenum, Japan.
[13] Evans, G. M. and Rollasor, E. C., *Journal of the Iron and Steel Institute*, Vol. 207, 1969, p. 1484.

[*14*] Dahl, W., Stoffels, H., Hengstenberg, H., and Düren, C., *Stahl und Eisen,* Vol. 87, 1967, p. 125.

[*15*] Zubko, A. A., Malkin, V. I., Medvedev, E. A., Pokidyshev, V. V., Khoklov, S. F., and Shnol, E. M., *Metallovedenie i Termicheskaia Abrabotha Metallov,* 1973, p. 52.

Summary

It is inevitable that a multi-faceted problem such as stress corrosion would elicit the diverse approaches found in these pages. One is forced to look hard for common elements. Certainly the biggest advance in the past decade has been the application of linear elastic fracture mechanics to the design of precracked specimens. While it is true that the stress-intensity factor K_{Iscc}, has found common usage and wide acceptance, it is unfortunate that the apparently equally useful ratio analysis diagram (RAD) is still reported only by its originators, the Naval Research Laboratory. Such a diagram makes it possible to compare a wide range of alloys against a combined standard of yield strength and toughness, two priorities of prime interest to designers, and the limitations imposed by environmental cracking.

At least, some reconciliation has been made between the data established using smooth specimens for threshold values of stress-corrosion susceptibility and the plateau velocity of crack-growth rates using precracked specimens. This naturally suggests that kinetic factors are more significant than so-called material constants (thermodynamic or state properties) like the stress-intensity factor. Here is an echo of a fundamental teaching of corrosion science, that the polarization behavior of a metal (a kinetic value) is far more significant towards its behavior than its electrochemical potential—the thermodynamic analog of K_I.

Several authors have addressed themselves to the wider use of kinetic parameters in these studies. The constant strain rate method is one which overcomes the problem of discontinuous crack growth, which is a troublesome fact of life for those of us who would study crack-growth rates. In another work, K_I is held constant, to better define the role of mechanical energy in the stress-corrosion process, as contrasted to the diffusion of aggressive species which lower the material's properties.

Continued examination of fracture mechanics test methods, and their applicability to stress-corrosion studies has led to the use of slow loading rate, rising load toughness testing to reveal a metal's susceptibility to stress-corrosion cracking. Short-term tests, on the order of minutes, replace the conventional test durations lasting hundreds of hours. However, the authors fail to recognize that K_{Iscc} is not a purely material constant but is strongly influenced by the environment. Using thermodynamic terminology, if K_{Ic} represents a standard state, just as E° represents the standard electrochemical potential, then K_{Iscc} may have any value, depending on the magnitude of the state functions which define the environment in equilibrium with the crack tip. Hydrogen in its various forms will produce different K_{Iscc} values, if it is the rate determining species in the corrosion reaction pathway.

Several authors did attempt to look at the crack tip and adjacent crack surfaces, using chemical and electrochemical theory and experimentation. They are to be complimented on these efforts, but they would be the first ones to admit that only the barest start has been made in this endeavor. The next symposium will surely contain papers reflecting extensions of these, and even as yet untried, methods for reaching into the crack, where the metal meets the corrosive millieu.

Other papers dealt with statistical approaches, large, prototype specimens, bolts, weldments, and real life artifacts. Some authors are concerned about compositional effects, metallurgical variables, and residual stresses. It is hoped that the level of sophistication revealed in these papers reflects the best science and engineering that can be applied to the serious problem of stress-corrosion cracking.

H. Lee Craig, Jr.
School of Marine and Atmospheric Science, University of Miami, Miami, Fla. 33149; symposium chairman and editor of this publication.

Index

Key to Abbreviations Used in Index

T = table
D = definition
F = figure
[ ] = see this subject under this listing